UNIVERSITY OF CALIFORNIA

Santa Barbara

Applications of Fe Complexes and Nanoparticles as Catalysts in Water

A dissertation submitted in partial satisfaction of the

requirements for the degree Doctor of Philosophy

in Chemistry

by

Haobo Pang

Committee in charge:

Professor Bruce Lipshutz, Chair

Professor Javier Read de Alaniz

Professor Armen Zakarian

Professor Trevor Hayton

September 2020

The dissertation of Haobo Pang is approved.

Javier Read de Alaniz

Armen Zakarian

Trevor Hayton

Bruce Lipshutz, Committee Chair

August 2020

Applications of Fe Complexes and Nanoparticles as Catalysts in Water

Copyright © 2020

by

Haobo Pang

ACKNOWLEDGEMENTS

First and foremost, I’d like to express my deepest gratitude to my advisor, Bruce H. Lipshutz. I still remember that I was attracted by him and his research directions after the first time he introduced his environmentally friendly and sustainable chemistry. Before that communication, I had never thought about replacing organic solvent with water for reactions, especially for organic reactions. It was him who opened another door in organic chemistry for me to see a vast field of green chemistry. I am impressed with his enthusiasm, rich experience, hard work, approach to problem solving, and exceptional writing skills. As an international student, with the help of him, I gradually learned to use academic words to elaborate on our projects and discoveries. During my five-year doctoral program, he not only enlightened me in chemistry, but also inspired me in life. I still remember that he comforted me when I met with setbacks and failure, as well as he taught me how to get along with each other. Now, I am going to complete my PhD program, and thanks to his help, which pushed me to get better. I feel so fortunate to have him as my advisor during my PhD program.

Additionally, I also thank my parents. In these five years, they provide unwavering support and unconditional love. I chat with them every week and talked about my research and daily life. They did not major in chemistry, but every time I communicated with them about my work or the issue I met in my daily life, they listened patiently and gave me their advice based on their experience. Moreover, they have never put any pressure on me. On the contrary, they usually relieve me when I'm stressed out. I really appreciate their patience and understanding.

Moreover, I would like to thank Dr. Ye Wang. When I first entered the group, I was not familiar with the processes of doing research including how to design control experiments, optimize the nanocatalysts, refine the reaction conditions, and organize academic reports. And he usually discussed with me about my project, and gave me his advice about the problems I met based on his rich experience in research. With the help of him, I was gradually familiar and even mastered those techniques, which made me able to do the project independently. In addition, during the discussion with him, I also learned a lot about organic chemistry, especially the research projects of our group. Moreover, he also helped me to be familiar with the surrounding area, and gave me a ride to Santa Barbara, Outlets and Los Angeles, which made me adapt to the life of the United States as soon as possible. Hence, I really thank him for helping me a lot during my PhD program.

Furthermore, I would like to thank Bo Jin, Nicholas Lee, and Landstrom Danial. I have discussed with them a lot about the issues I met in my research, and I could usually get so many suggestions and advice from them, which helped me a lot in my projects. And I still want to thank Yuting Hu and Julie Yu. They helped me to complete my final project, the nanocatalyst for Heck coupling reactions. And, finally, I would like to thank all the mates in our research group for their support and encouragement in the past five years.

VITA OF HAOBO PANG
August 2020

EDUCATION

Bachelor of Science in Chemistry, Nanjing University, June 2014

Doctor of Philosophy in Organic Chemistry, University of California, Santa Barbara, August 2020 (expected)

PROFESSIONAL EMPLOYMENT

2015-2020: Teaching Assistant, Department of Chemistry and Biochemistry, University of California, Santa Barbara

PUBLICATIONS

(1) Pang, H.; Gallou, F.; Sohn, H.; Camacho-Bunquin, J.; Delferro, M.; Lipshutz, B. H. Synergistic effects in Fe nanoparticles doped with ppm levels of (Pd + Ni). A new catalyst for sustainable nitro group reductions. *Green Chem.* **2018**, *20*, 130.

(2) Pang, H.; Wang, Y.; Gallou, F.; Lipshutz, B. H. Fe-catalyzed reductive couplings of terminal (hetero)aryl alkenes and alkyl halides under aqueous micellar conditions. *J. Am. Chem. Soc.* **2019**, *141*, 17117.

(3) Lee, N. R.; Cortes-Clerget, M.; Wood, A. B.; Lippincott, D. J.; Pang, H.; Moghadam, F. A.; Gallou, F.; Lipshutz, B. H. Coolade. A Low-Foaming Surfactant for Organic Synthesis in Water. *ChemSusChem* **2019**, *12*, 3159.

(4) Pang, H.; Jin, B. and Lipshutz, B. H., Pentafluorophenylboronic Acid (first updated). *eEROS*, article.

(5) Pang, H.; Hu, Y.; Yu, T. and Lipshutz, B. H. Water-Sculpting of a Heterogeneous Nanoparticle Pre-catalyst into an Active Catalyst for Heck Couplings Under Micellar Catalysis Conditions. (*in preparation*)

(6) Yu, T.; Pang, H.; Cao, Y.; Gallou, F.; Lipshutz, B. H. Safe, Scalable, Inexpensive, and Mild Nickel-Catalyzed Magita-like C-S Cross-Couplings in Recyclable Water. (*in preparation*)

ABSTRACT

Applications of Fe Complexes and Nanoparticles as Catalysts in Water

by

Haobo Pang

Given the importance of amine as intermediates for fine chemicals, agrochemicals, pharmaceuticals, dyes and polymers, selective reduction of nitro-containing aromatics and heteroaromatics to the corresponding amines represents an essential methodology. In the previous work of our group, it was found that commercial sources of $FeCl_3$ with only part per million (ppm) levels of Pd, after processing into nanoparticles (NPs), could be used to catalyze reduction of nitroarenes in water at room temperature. Initial research of mine was dedicated to enhancing the activity of such nanoparticle catalysts. In this project, the original Fe/ppm Pd nanoparticles were doped with ppm levels of Ni, which resulted in a significant enhancement of the rates of reductions of nitro-containing aromatics and heteroaromatics in aqueous micellar media at room temperature by three to eight times. A remarkable synergistic effect was uncovered between ppm levels of Pd and Ni embedded within iron nanoparticles. $NaBH_4$ serves as the source of inexpensive hydride. Broad substrate scope is documented, along with several other features including: low catalyst loading (80 ppm Pd and 1600 ppm Ni), low residual metal in the products, and recycling of the catalyst and reaction medium, which together highlight the green nature of this new technology. Such a nanocatalyst was thoroughly characterized by transmission electron microscopy (TEM) and

energy-dispersive x-ray (EDX), which showed the content of each element in the nanoparticles. In addition, such synergistic effects were also explained in terms of the structure of the nanoparticles by X-ray absorption spectroscopy (XAS), extended X-ray absorption fine structure (EXAFS) and X-ray absorption near edge structure (XANES).

Csp^3-Csp^3 bond formation significantly extends the available routes for well-known complicated molecular constructions, which undoubtedly has profound implications for preparing pharmaceuticals. Rather than forming Csp^3-Csp^3 bonds directly, the reductive coupling of a vinyl-substituted aromatic or heteroaromatic and an alkyl bromide or iodide provided an alternate methodology for Csp^3-Csp^3 bond formation. A commercially available Fe salt was used as catalyst precursor, coordinated by 3,4,7,8-tetramethyl-1,10-phenanthroline. The new C–C bond is regiospecifically formed, at room temperature, at the β-position of the alkene in the presence of Zn as reductant. Such a discovery provided a novel idea for the formation of Csp^3-Csp^3 carbon bonds in total synthesis. Apart from broad substrate scope (50 samples), including diverse functional groups and heterocycles, this process could be both scaled up and applied to the synthesis of a precursor of a SphK inhibitor, which illustrated the potential application in the pharmaceutical area. Recycling of the reaction medium and an associated low E Factor (< 5) reflect the sustainability of such chemistry. The coupling process was shown to only occur in an aqueous micellar medium, where a radical process is likely, supported by control experiments, deuterium trapping experiments, and radical clock tests. A mechanism based on these data is proposed.

As a third project, novel nanoparticles were developed, derived by reduction of $FeCl_3$ doped with ppm level Pd, for application to Heck couplings in aqueous micellar media. Using nanoparticle catalysis dramatically enhanced the activity of the catalyst, thus the catalytic Pd loading for these couplings was reduced from 2% to 0.1 mol %. It is worth mentioning that such reactions were run between room temperature and 45 °C, which is much lower than the temperature associated with traditional Heck reactions (typically performed at over 100 °C). In addition to broad substrate scope (26 samples), with educts containing various substituents and heterocycles, the process is highlighted by several other key features, including: low residual Pd (Pd = 0 ppm) in the products, recycling of the reaction medium, and low E Factor (<5). These couplings could also be scale up, and two tandem processes in one pot, provided a strong indication for drug manufacturing.

The nanocatalyst was thoroughly characterized by high angle annular dark-field scanning transmission electron microscopy (HAADF-STEM), EDX elemental mapping, and transmission electron cryo-microscopy (cryo-TEM), which revealed the morphology change of the nanocatalyst before and after exposure to water. X-ray photoelectron spectroscopy (XPS) and inductively coupled plasma mass spectrometry (ICP-MS) provided an explanation of such a change in morphology in terms of elemental content. More research of such nanocatalysts is still in process.

TABLE OF CONTENTS

I. Synergistic Effects in Fe Nanoparticles doped with ppm levels of (Pd + Ni)............1

- General Introduction: Nitro Group Reduction..2
  - Metal-free nitro group reduction 3
  - Metal-based nitro group reductions...9
  - References...17
- Results and discussion 20
  - Synthesis and optimization of Fe/B/Ni NPs 21
  - Synthesis and optimization of Fe/ppm Ni NPs....................................24
  - Synthesis and optimization of Fe/ppm (Pd + Ni) NPs.........................31
  - Comparisons with reported catalysts...34
  - Characterization of Fe/ppm (Pd + Ni) NPs..37
  - Discussion on substrate scope 41
  - E Factor, Recycling, and Residual Metals in the products..................46
  - One-pot sequences 52
  - Studies on the mechanism of nitro group reductions...........................55
  - Conclusions..60
  - References..61
- Appendix...65
  - General Remarks 65
  - Final Optimized Preparation of Fe/ppm (Pd + Ni) Nanoparticles.......66
  - Preparation of substrates...67

General Procedure for Nitro Group Reduction 69

One-pot study 70

E Factor and recycle studies 72

Residual palladium, nickel, and iron in products 75

Analytical data 77

References 95

NMR spectra 97

II. Fe-catalyzed reductive couplings of terminal aryl alkenes and alkyl halides 130

General Comments on Hydrocarbonation 131

Hydroarylation 131

Hydroalkylation 146

References 157

Results and Discussion 159

Optimization of reaction conditions for hydroalkylation 159

Scope of the hydroalkylation 168

Further research on reaction medium 174

Hydroalkylation of alkenes using alkyl iodides and alkyl chlorides 176

Recycling and E Factors 178

Potential manufacturing applications 179

Mechanistic Studies 180

Conclusions 189

References 191

Appendix 194

General Remarks 194

Optimized General Procedure for Coupling Reactions 195

Preparation of substrates 196

Selectivity on 1-phenylbutadiene 202

E Factor and Recycle Studies 203

Reaction at the gram scale 204

Synthesis of the precursor to a SphK inhibitor 204

Mechanistic studies 205

Analytical data 214

References...251

NMR spectra 252

III. Water-sculpting of a pre-catalyst into an active catalyst for Heck couplings 316

General Introduction on Heck-Mizoroki coupling reactions..................317

References...332

Results and discussion 334

Optimization of Fe/ppm Pd NPs...335

Optimization of reaction conditions 341

Characterization of the NPs 344

Scope of HM coupling reaction..354

Comparisons between reported catalysts..356

Recycle, E Factor, and scale up reaction 357

Residual Pd in products from HM reactions.....................................358

1-Pot sequences 359

Conclusions...360

References...362

Appendix.......366

- General Remarks.......366
- Final Optimized Preparation of Fe/ppm Pd Nanoparticles.......367
- Comparison between Pd catalyst and Fe/ppm Pd NPs.......368
- Titration of MeMgCl solution by LiCl-I_2.......369
- Analysis of the nanoparticle.......370
- General Procedure for HM reaction.......397
- Control experiments for Fe/ppm Pd NPs in HM reaction.......398
- E Factor, residual palladium, and recycling reaction.......401
- Scale-up reaction.......406
- 1-Pot sequence of reactions.......407
- Analytical data for products.......410
- References.......428
- NMR spectra.......429

I. Synergistic Effects in Fe Nanoparticles doped with ppm levels of (Pd + Ni)

Reproduced with permission from

Pang, H.; Gallou, F.; Sohn, H.; Camacho-Bunquin, J.; Delferro, M.; Lipshutz, B. H. Synergistic effects in Fe nanoparticles doped with ppm levels of (Pd + Ni). A new catalyst for sustainable nitro group reductions. *Green Chem.* **2018**, *20*, 130.

Copyright 2018 Royal Society of Chemistry.

General Introduction: Nitro Group Reduction

Aromatic and heteroaromatic amines represent a class of intermediates that are especially useful for preparation of pharmaceuticals, agrochemicals, polymers, and dyes.[1] Hence, reduction of nitro group to form amines has been the focus of chemists for a long time. In general, optimized reductions of nitroarenes falls into two broad categories: metal-free methods and metal-based methods.[2] The mechanism of the reduction of nitroarenes via intermediate nitroso and hydroxylamines has been well-studied, as shown in Scheme 1.[3] The hydroxylamine formed can be reduced to the corresponding aniline directly. On the other hand, the hydroxylamine can also condense with the nitroso intermediate to form an azoxy species. The azoxy intermediate can be easily reduced to generate a diazo compound, which can be further hydrogenated to form a hydrazine. It has been believed that the formed hydrazine could then be reduced to the aniline. However, according to research from our group, only trace quantities of an azoxy species are reduced to the corresponding diazo derivative, and no conversion of a diazo compound to a hydrazine was detected during the reduction process by Fe/ppm Pd nanoparticles.[4] Hence, avoiding the formation of hydroxylamine is crucial for the overall conversion to the desired product.

Scheme 1: Mechanism of nitro group reduction

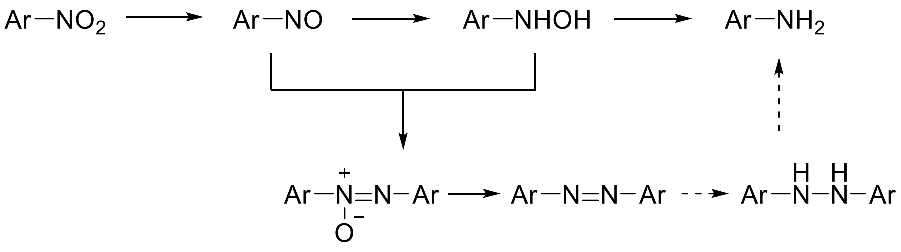

Metal-free nitro group reduction

In the 1950s, it was reported selected nitroarenes could be reduced by sodium hydrosulfite[5] or sodium sulfide[6] (shown in Scheme 2). Both techniques were achieved in hot water. However, recovery of the aniline product was not efficient for both, totaling only about 70%. In order to further enhance the conversion and broaden the generality of nitro group reduction to cope with the increasing requirements of synthesis and industry, many techniques were investigated, discovered, and developed without metal catalysts.

Scheme 2: Representative nitro group reduction with $Na_2S_2O_4$ and Na_2S

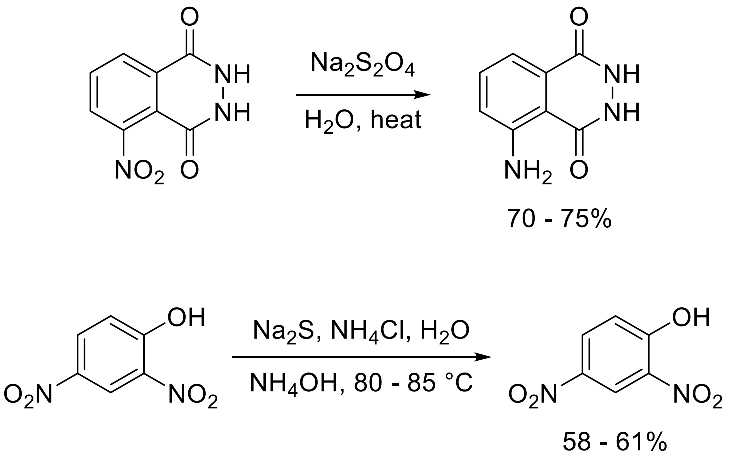

Xu's group from Nanjing University proposed a method that achieves hydrogenation of aromatic nitro compounds by features use of fullerene for activating molecular hydrogen (Scheme 3).[7] According to their research, reduction of nitroarenes could be achieved using fullerene with high yields using light irradiation and H_2 (1 atm) as hydrogen source at room temperature. Moreover, they also found that there is a synergetic effect between C_{60} and C_{60}^{-}. The mixture of C_{60}:C_{60}^{-} = 2:1 could also catalyze hydrogenation of nitro compounds in excellent yields under an atmosphere of H_2 (4 – 5 MPa) at 120 – 160 °C even without light irradiation. Although the exact mechanism is not well known, the author supposed that it might involve a synergistic exciplex. Compared with traditional stoichiometric reductions of nitro compounds facilitated by Fe/HCl or Na_2S, this approach not only decreased the heavy-metal waste pollution, but also lowered the cost of the overall process. However, such research did not provide an extensive substrate scope with diverse functional groups. Hence, whether such a technique works well on substrates with multiple substituents or heterocycles needs to be further studied.

Scheme 3: Xu's nitro group reduction with fullerene

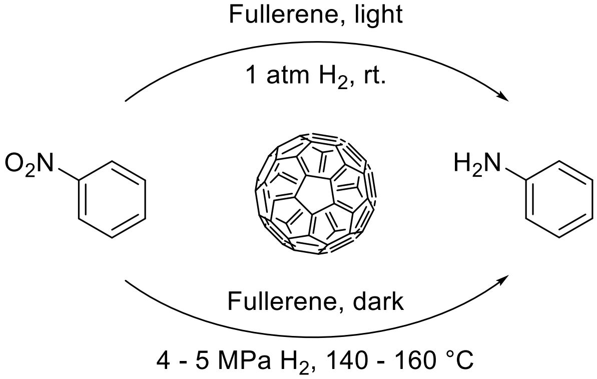

Plant-derived natural products can be used as environmentally friendly alternatives for metal-based catalysts. Moreover, because of its sustainability, stability, selectivity, and economy, such an approach is getting more attention. In 2014, Kumar's group discovered vasicine, a quinazoline alkaloid from the leaves of Adhatoda vasica, that could be used as reductant for hydrogenation of nitroarenes in water at 120 °C (Scheme 4).[3] This technique has good functional group tolerance, including ketones, nitriles, acids and could lead to relatively high yields for some heterocyclic nitroarenes. According to their investigation of the mechanism, vasicinone and quinazoline were observed as the major by-products after the reduction, which showed that the hydrogen on the produced aniline should be from vasicine.

Scheme 4: Kumar's nitro group reduction by vasicine

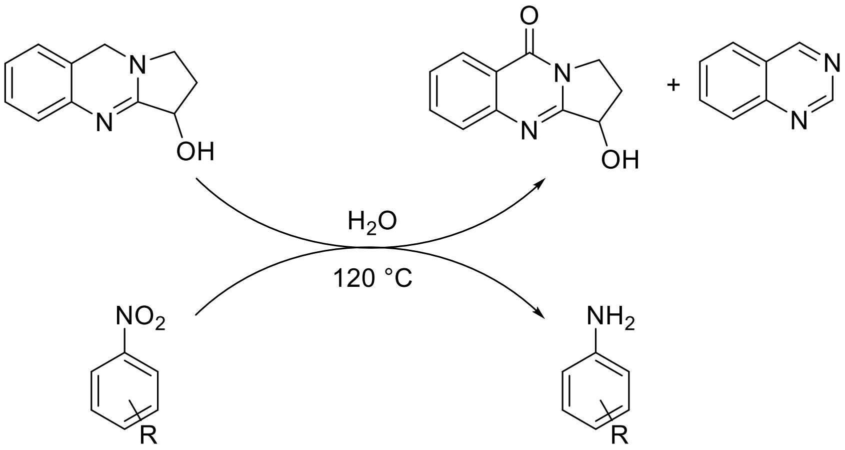

In 2015, Benaglia's group developed a novel technique which achieved hydrogenation of aliphatic or aromatic nitro compounds to the corresponding amines by $HSiCl_3$ combined with *N*-ethyl-*N*-isopropylpropan-2-amine (DIPEA) in acetonitrile at 0 °C or room temperature (Scheme 5).[8] According to studies by Bernstein[9] and Lerner,[10] $R_3NH^+/SiCl_3^-$ forms from this combination of $HSiCl_3$ and R_3N, which can also generate $SiCl_2$ in situ though an equilibrium, as shown in Scheme 5. Hence, Benaglia and co-workers proposed two plausible mechanisms based on $SiCl_3^-$ and $SiCl_2$ separately (Scheme 5). In the first pathway, $SiCl_3^-$ as a nucleophile might attack the nitrogen atom. However, in the other one, $SiCl_2$ may react with N=O bonds through a cheletropic mechanism.

Scheme 5: Benaglia's nitro group reduction by $HSiCl_3$ combined with R_3N

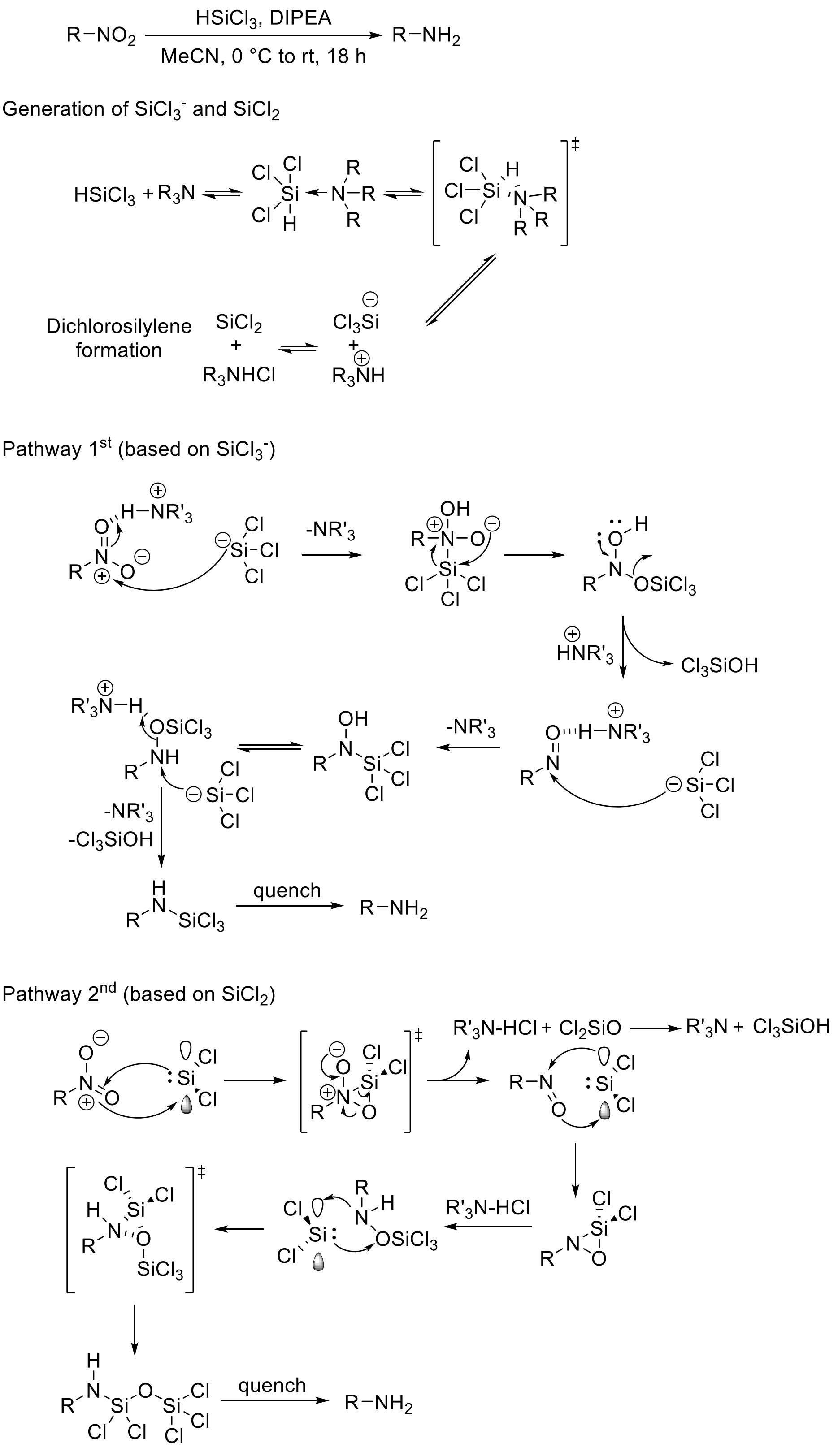
R−NO2
HSiCl3, DIPEA
MeCN, 0 °C to rt, 18 h
R−NH2
Generation of SiCl3- and SiCl2
HSiCl3 + R3N
‡
Dichlorosilylene formation
SiCl2 + R3NHCl
Cl3Si + R3NH
Pathway 1st (based on SiCl3-)
-NR'3
HNR'3
Cl3SiOH
-NR'3
-NR'3
-Cl3SiOH
quench
R−NH2
Pathway 2nd (based on SiCl2)
‡
R'3N-HCl + Cl2SiO
R'3N + Cl3SiOH
R'3N-HCl
‡
quench
R−NH2

In a subsequent report, Cozzi and co-workers further investigated the mechanism of the reduction of nitro groups by the combination of $HSiCl_3$ and R'_3N through competition reactions and calculations.[11] According to the correlation between experimental activation energy $\Delta\Delta G^{\neq}$ (kcal/mol) and Hammett constants σ_H in reductions of electron-poor and electron-rich nitro groups, they found that the electron-poor nitro groups cases were reduced faster, which suggested that a nucleophile was involved in the mechanism. Besides, the activation Gibbs free energy calculated by M06-2X, wB97XD and MP2 indicated that compared with $SiCl_3^-$ and free $SiCl_2$, R_3N-$SiCl_2$ is the preferred structure generated from $HSiCl_3$ and R'_3N. With further calculations, Cozzi's group proposed a convincing reaction sequence proceeding in three steps, as shown in Scheme 6.

Scheme 6: Gibbs free energy profile for nitro group reduction by $HSiCl_3$ and R'_3N

Step 1st: From nitro to nitroso derivative

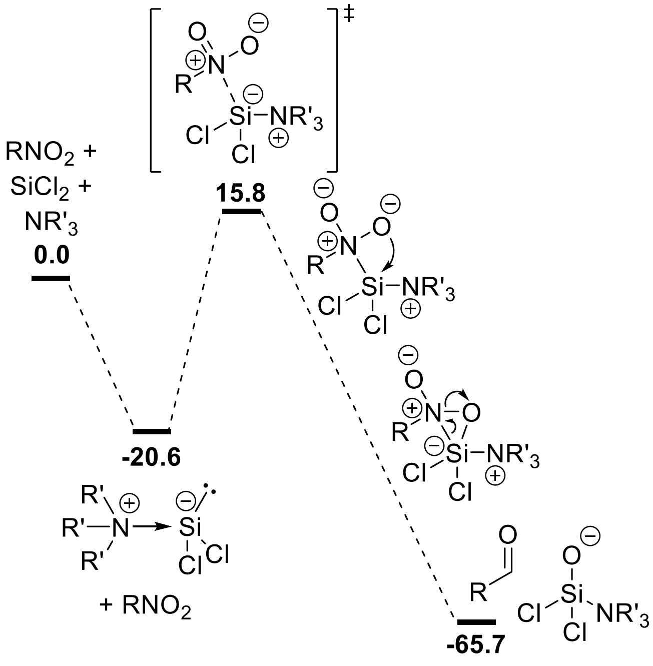

Step 2nd: From nitroso to cyclic hydroxylamine analogue

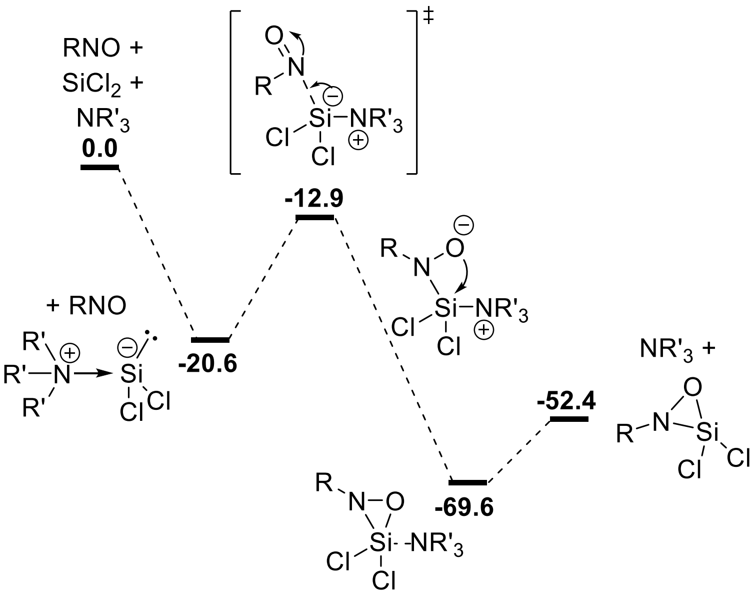
RNO +
SiCl2 +
NR'3
0.0
-12.9
+ RNO
-20.6
-69.6
-52.4
NR'3 +

Step 3rd: From silylated cyclic hydroxylamine

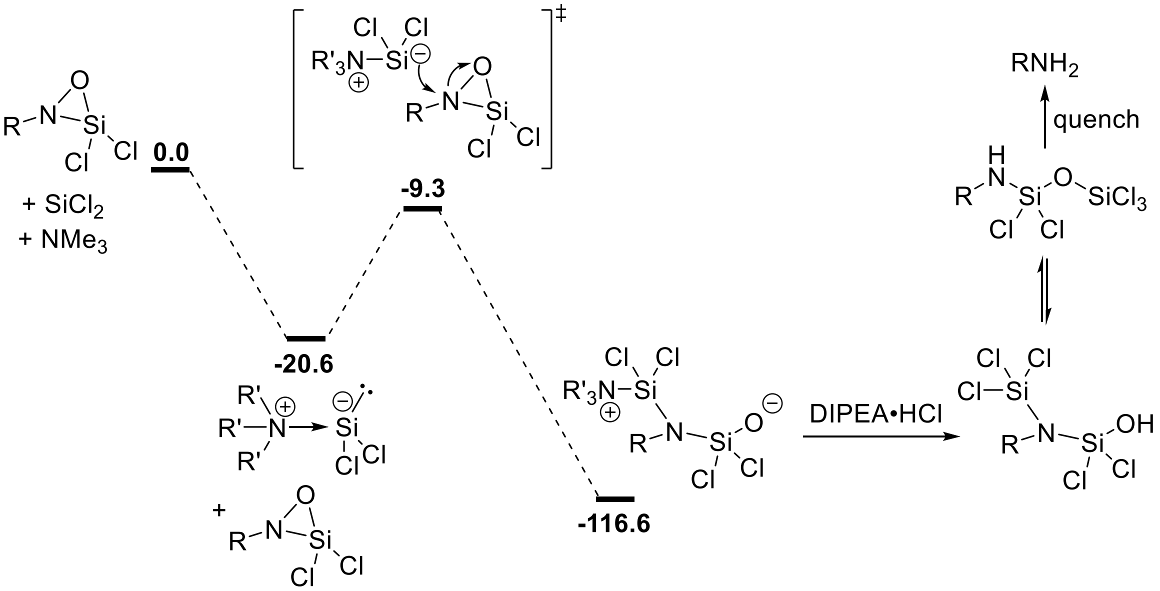
0.0
+ SiCl2
+ NMe3
-9.3
-20.6
-116.6
DIPEA•HCl
RNH2
quench

Furthermore, Wu's group developed another metal-free technique for hydrogenation of nitro groups in 2016. In their process, aromatic nitro compounds could be reduced by the combination of B_2pin_2 and KO-*t*-Bu to the corresponding anilines in isopropanol at 110 °C.[12] 2-Isopropoxy-4,4,5,5-tetramethyl-1,3,2-dioxaborolane (*i*-PrOBpin) was discovered as by-product through ^{11}B NMR and GC-MS after the reduction. Based on this outcome, the author proposed a plausible mechanism for the total process shown in Scheme 7.

Scheme 7: Wu's nitro group reduction by B_2pin_2 and KO*t*-Bu and mechanism

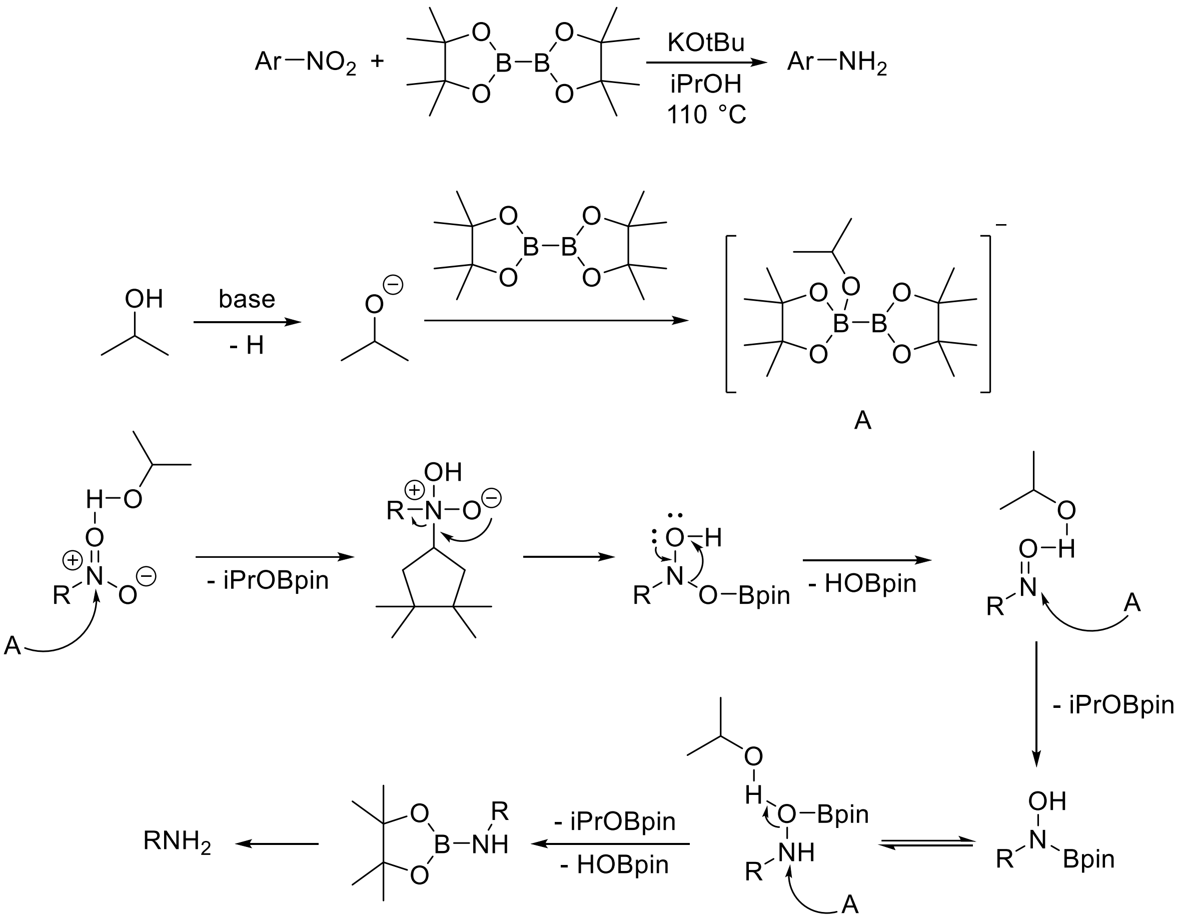
Ar−NO2 +
KOtBu
iPrOH
110 °C
Ar−NH2
OH
base
- H
A
- iPrOBpin
- HOBpin
- iPrOBpin
OH
R
Bpin
A
- iPrOBpin
- HOBpin
RNH2

Metal-based nitro group reductions

Compared with the metal-free hydrogenation of nitro group, reductions of nitro compounds with metal or metal catalysts were developed long ago. In 1854, French chemist Antoine Béchamp discovered that the reduction of aromatic nitro groups could be accomplished using iron powder and hydrochloride acid.[13] Such methods usually take place under mild conditions with good functional group tolerance. However, this method required the reaction vessel to have relatively high acid resistance. Since then, chemists have paid more attention to preparing metal catalysts with strong reductive activity by simple methods, such as Raney nickel[14] or palladium-on-carbon[15], and achieved reduction of nitroaromatics by those catalysts with hydrogen as reductant. Nowadays, with advances in the field of catalysis and materials, more and more catalysts synthesized using various metals have been applied to catalyzing hydrogenation of compounds containing nitro groups.

In 2013, Beller and co-workers developed a new catalyst based on cobalt (see Scheme 8).[16] To prepare the catalyst, cobalt(II) acetate tetrahydrate and 1,10-phenanthroline were stirred in ethanol followed by addition of carbon powder. After refluxing for four hours, the mixture was dried under vacuum. The leftover material was ground and heated to 800 °C to get the Co-phenanthroline/C as catalyst. A loading of 1 mol % catalyst was needed for catalyzing the reduction of nitroaromatics under a hydrogen atmosphere (50 bar) in THF at 110 °C. Furthermore, this methodology showed impressive chemoselectivity and broad functional group tolerance (alkene, alkyne, iodide, ketone and aldehyde). However, the drawback to this method is also obvious. High pressures and temperatures limit its applications. Moreover, in 2015, Beller's group developed another novel catalyst based on iron.[17] Similar to the former method, $Fe(OAc)_2$ and 1,10-phenanthroline were stirred in ethanol followed by addition of carbon powder and further stirring at 60 °C for 12 – 15 hours. The mixture was cooled and ethanol was removed in vacuo and the residual material was totally dried. The catalyst Fe_2O_3/NGr@C was obtained after being pyrolyzed at 800 °C. Catalyzed by this new material, aromatic nitro compounds could be reduced to aniline with HCOOH–Et_3N in THF at 120 °C. Nitro heterocyclic substrates were also prepared using this technique.

Scheme 8: Beller's nitro group reduction

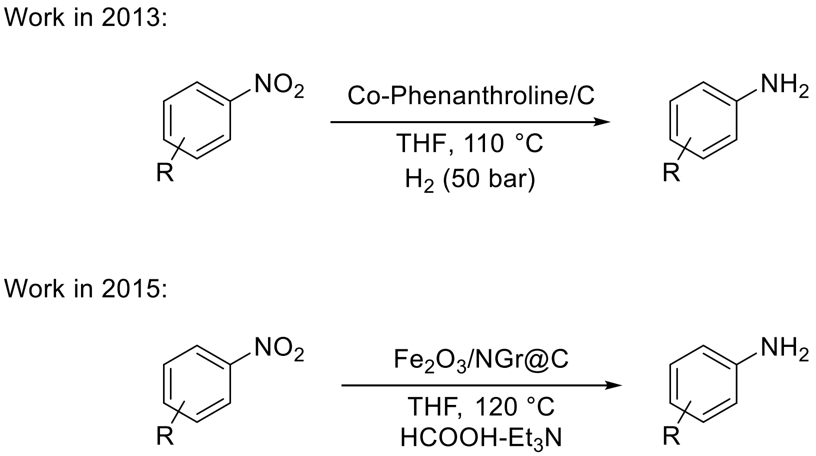

Singh's group developed Co nanoparticles as well as Ni nanoparticles by reducing the metal chloride in a poly(vinylpyrrolidone) (PVP)-stabilized aqueous-phase with $NaBH_4$.[18] Both types of nanoparticles achieved reductions of compounds containing nitro groups in water at room temperature with hydrazine monohydrate as reductant. However, this technique needs 20 mol % catalyst loading. On the other hand, Llusar's group synthesized a new diamino cluster, $[Mo_3S_4Cl_3(dnbpy)_3](PF_6)$ by refluxing a mixture of $[Mo_3S_4(tu)_8(H_2O)]Cl_4 \cdot 4H_2O$ and 4,4'-dinonyl-2,2'-bi-pyridine in CH_3CN, which could also catalyze reductions of nitroarenes to the corresponding anilines in methanol at 70 °C under a hydrogen atmosphere (20 bar).[19]

Zhan's group developed a new type of phosphorus-doped porous organic polymer, POL-Ph_3P, which could serve as both support and ligand for palladium nanoparticles for nitro group reductions.[20] To prepare catalyst POL-Ph_3P, PCl_3 was added to (4-vinylphenyl)magnesium bromide followed by quenching to afford tris(4-vinylphenyl)phosphane. 1,3,5-Tribromobenzene, tris(4-vinylphenyl)phosphane, $Pd(PPh_3)_4$ and K_2CO_3 were dissolved in dry DMF and the mixture was stirred at 120 °C for 72 hours. The POL-Ph_3P was obtained after washing as a gray solid, which was stirred with $PdCl_2$ in

MeCN for five hours to get yellow Pd/POL-Ph_3P nanoparticles. This nanocatalyst could be used with only 0.5 mol % Pd loading for reductions of nitroaromatics to anilines under hydrogen (1 atm) in ethanol at room temperature. Moreover, Martin's group developed another type of Pd nanoparticles, PVP-Pd nanoparticles, which were electrochemically reduced on a polycrystalline Pt disc electrode employing an aqueous solution of H_2PdCl_4 and KNO_3 containing poly-(N-vinyl-2-pirrolydone) polymer as the stabilizing agent by application of a constant current pulse.[21] The resulting material has relatively high activity for reduction of nitroaromatics in EtOH/H_2O at room temperature with $NaBH_4$ as reductant.

Since early research on bimetallic catalysts, carried out by Exxon Research and Engineering in the 1960s, more and more bimetallic catalysts have been investigated and developed. As novel materials, bimetallic catalysts usually exhibit higher activity and selectivity due to their different electronic and chemical properties from that of the parent metals. Therefore, on the basis of mono-metal materials for catalysis (hydrogenation), more and more chemists have begun to pay attention to bimetallic catalysts for nitro group reductions. Fan and co-workers developed a novel nanocatalyst, Au/TiO_2-VS (Scheme 9).[22] They added TiO_2 to an aqueous solution of $[Au(en)_2]Cl_3$ with pH = 9.4. After being aged for two hours and washed by deionized water, the samples were dried under vacuum followed by being reduced in 5% H_2/Ar to get the Au/TiO_2-VS nanocatalyst. Such nanomaterial could be used to catalyze the reduction of nitro compounds in EtOH/H_2O with 1 mol % Au loading under CO atmosphere at room temperature. This catalyst worked for both aromatic and aliphatic nitro compounds. In terms of the mechanism of reduction, the author believed that ultra-small Au nanoparticles supported on titania could form Au-H bonds, which had a high activity for nitro group reduction.

Scheme 9: Fan’s nitro group reduction by Au/TiO_2-VS (2009)

$$\mathrm{R{-}NO_2} \xrightarrow[\substack{\mathrm{EtOH/H_2O\ (2{:}1\ v/v)} \\ \mathrm{CO\ (5\ atm),\ 25\ °C}}]{\mathrm{Au/TiO_2\text{-}VS\ (1\ mol\%\ Au)}} \mathrm{R{-}NH_2}$$

Lu’s group from Shanghai University developed a bimetallic catalyst, Ni-6.0% MoO_3/CN@SBA-15 (Scheme 10).[23] SBA-15 was added into water–ethanol solution of $Ni(NO_3)_2·6H_2O$ and $(NH_4)_6Mo_7O_{24}·4H_2O$ and the mixture was dried and calcined at 400 °C to get the final catalyst. Nitroaromatics could be reduced in ethanol at 40 °C by this catalyst in the presence of hydrazine monohydrate as reductant. The authors believe that the high catalytic performance of Ni-6.0% MoO_3/CN@SBA-15 catalysts could be attributed to the synergistic effect of both Ni and MoO_3. The hydrazine was absorbed mainly on the Mo sites and cleaved into two active H* species on the surface. The H* reacted with the nitroaromatics which may have weak interactions with Ni on the surface of catalyst.

Scheme 10: Lu’s nitro group reduction by Ni-6.0% MoO_3/CN@SBA-15

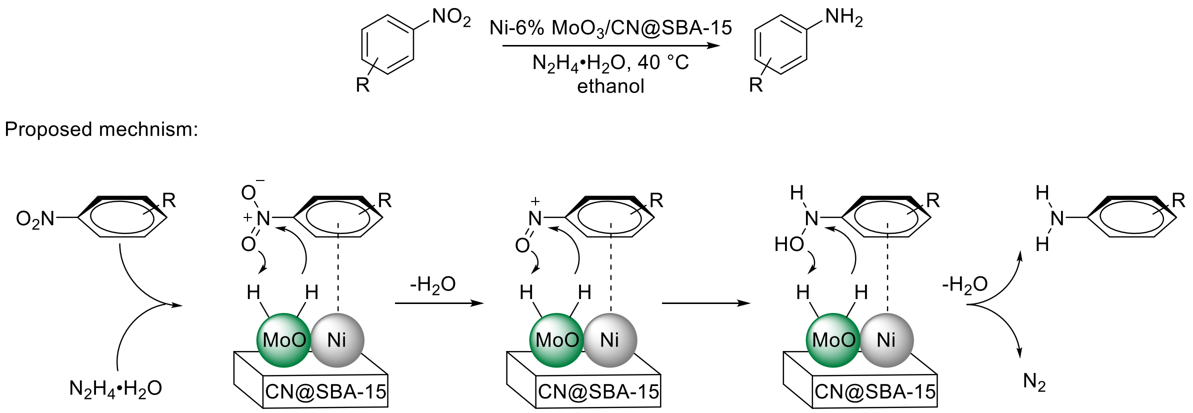

Apart from Ni-6.0% MoO_3/CN@SBA-15, Zhou’s group developed another bimetallic nanocatalyst, Pt-SnO_2/Al_2O_3, with a core-shell structure as illustrated in Scheme 11.[24] They injected a solution containing $NaBH_4$/ethyl alcohol into a mixture of chloroplatinic(IV) acid (H_2PtCl_6), tin(II) 2-ethylhexanoate, ethylene glycol, and polyvinylpyrrolidone at 50 °C. They detected that the yellow-brown solution changed to a dark colloid during this reduction.

The mixture was further centrifuged with acetone to collect a black powder of Pt@Sn followed by redispersion in ethanol with added alumina. The resulting mixture was heated at 50 °C after which ethanol was then removed. The Pt-SnO_2/Al_2O_3 was collected after further being calcined at 500 °C. Although this catalyst did not show excellent activity for reduction of nitroaromatics, the efficiency of Pt-SnO_2/Al_2O_3 was shown to be enhanced significantly compared with Pt/Al_2O_3. In terms of the explanation for the improvement, theoretical calculations using Density Functional Theory were performed by the authors. According to their calculations, compared with the Pt surface alone, the Pt surface with SnO_2 has stronger absorption ability for hydrogen and nitroaromatics, but weaker absorption ability for anilines, which indicates that the starting material can be captured quickly on the Pt surface with SnO_2, while the product can be released more easily, leading to the effective utilization of the catalyst's surface.

Scheme 11: Zhou's nitro group reduction by Pt-SnO_2/Al_2O_3

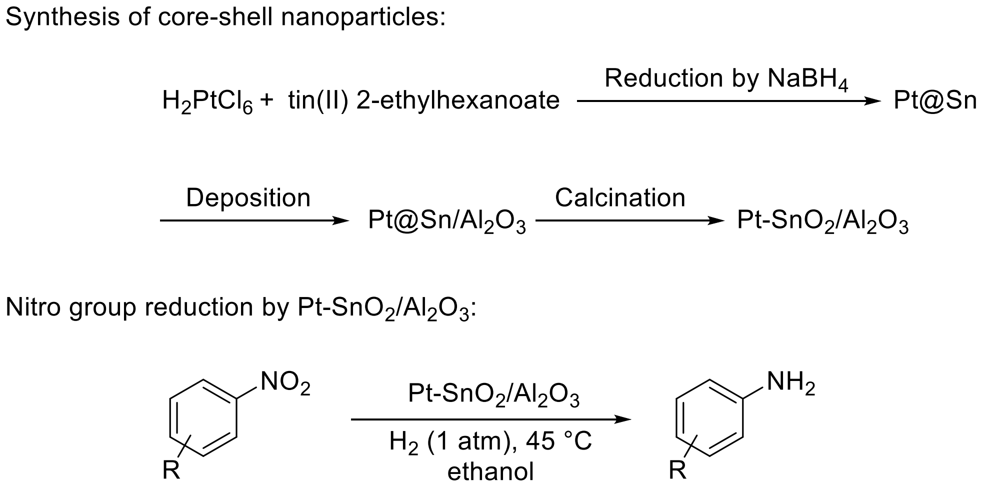
Synthesis of core-shell nanoparticles:
H2PtCl6 + tin(II) 2-ethylhexanoate
Reduction by NaBH4
Pt@Sn
Deposition
Pt@Sn/Al2O3
Calcination
Pt-SnO2/Al2O3
Nitro group reduction by Pt-SnO2/Al2O3:
NO2
R
Pt-SnO2/Al2O3
H2 (1 atm), 45 °C
ethanol
NH2
R

In 2017, Corma and co-workers discovered and developed a novel nanolayered molybdenum disulfide cobalt-promoted materials (Co-Mo-S), which can be used as a chemo-selective catalyst for the reduction of nitroaromatics under hydrogen atmosphere (11 bar) in toluene at 150 °C.[25] This material was prepared via reduction of ammonium molybdate [$(NH_4)_6Mo_7O_{24}\cdot 4H_2O$] together with elemental sulfur and cobalt acetate [$Co(OAc)_2\cdot 4H_2O$] in a mixture in distilled water by hydrazine with heat (150 °C). This technique has good chemoselectivity for the hydrogenation of nitroarenes. Substrates containing easily reducible functional groups such as ketone, nitrile, aldehyde, acid, alkene and alkyne are also tolerated during the reaction.

Our group also developed in 2016 a different nanocatalyst, “Fe/ppm Pd” nanoparticles.[26] The catalyst was prepared via reduction of a combination of $FeCl_3$ and $Pd(OAc)_2$ in THF solution by MeMgCl, which could be used for nitro group reductions where only 80 ppm Pd are needed, performed in 2 wt % TPGS-750-M/H_2O at room temperature with $NaBH_4$ as hydrogen source. The technology uses water as the reaction medium, which avoids the introduction of organic solvents, thus greatly reducing the organic waste from the reaction. With a simple method of synthesis of catalyst, a wide substrate scope, low catalyst loading, and mild reaction conditions, this novel process has advantages over other methods in literature. Nonetheless, there is still room for improvement. For instance, Fe/ppm Pd nanoparticles could still be further improved in terms of catalytic activity.

The development of new technologies for chemoselective hydrogenation of nitro compounds is a continuously evolving area. Due to the importance of amines as precursors and intermediates in agricultural and pharmaceutical chemistry, a considerable number of new techniques have appeared over the last few decades in the search for more sustainable and environmentally friendly methods. Metal-free processes have drawn chemists’ attention because there were no toxic or harmful heavy metals involved in the overall process. However, since the organic byproducts after the reaction can be difficult to remove, extensive applications of these techniques have yet to be found. On the other hand, with the rise and innovation of nanomaterials, the technologies based on metal catalysts, such as Pd, Co and Fe are changing with each passing day. Lower and lower metal loadings in catalysts have been applied to hydrogenations. Furthermore, due to the synergistic effects involving electronic and/or geometrical interactions among different metals, bimetallic nanoparticles show better activity and selectivity compared with monometallic counterparts. In conclusion, there is every reason to believe that there will be new developments in this field as improvements in materials science and new catalyst design emerge.

References

1. (a) Birch, A. M.; Groombridge, S.; Law, R.; Leach, A. G.; Mee, C. D.; Schramm, C. Rationally Designing Safer Anilines: The Challenging Case of 4-Aminobiphenyls. *J. Med. Chem.* **2012**, *55*, 3923. (b) Downing, R. S.; Kunkeler, P. J.; van Bekkum, H. Catalytic syntheses of aromatic amines. *Catal. Today* **1997**, *37*, 121. (c) Blaser, H.-U.; Steiner, H.; Studer, M. Selective Catalytic Hydrogenation of Functionalized Nitroarenes: An Update. *ChemCatChem* **2009**, *1*, 210.

2. Orlandi, M.; Brenna, D.; Harms, R.; Jost, S.; Benaglia, M. Recent Developments in the Reduction of Aromatic and Aliphatic Nitro Compounds to Amines. *Org. Process Res. Dev.* **2018**, *22*, 430.

3. Sharma, S.; Kumar, M.; Kumar, V.; Kumar, N. Metal-Free Transfer Hydrogenation of Nitroarenes in Water with Vasicine: Revelation of Organocatalytic Facet of an Abundant Alkaloid. *J. Org. Chem.* **2014**, *79*, 9433.

4. Gabriel, C. M.; Parmentier, M.; Riegert, C.; Lanz, M.; Handa, S.; Lipshutz, B. H.; Gallou, F. Sustainable and Scalable Fe/ppm Pd Nanoparticle Nitro Group Reductions in Water at Room Temperature. *Org. Process Res. Dev.* **2017**, *21*, 247.

5. Redemann, C. T.; Redemann, C. E. 5-Amino-2,3-Dihydro-1,4-Phthalazinedione. *Org. Synth.* **1949**, *29*.

6. Hartman, W. W.; Silloway, H. L. 2-Amino-4-Nitrophenol. *Org. Synth.* **1945**, *25*.

7. Li, B.; Xu, Z. A Nonmetal Catalyst for Molecular Hydrogen Activation with Comparable Catalytic Hydrogenation Capability to Noble Metal Catalyst. *J. Am. Chem. Soc.* **2009**, *131*, 16380.

8. Orlandi, M.; Tosi, F.; Bonsignore, M.; Benaglia, M. Metal-Free Reduction of Aromatic and Aliphatic Nitro Compounds to Amines: A $HSiCl_3$-Mediated Reaction of Wide General Applicability. *Org. Lett.* **2015**, *17*, 3941.

9. Bernstein, S. C. Mechanism of interaction between tertiary amines and trichlorosilane. *J. Am. Chem. Soc.* **1970**, *92,* 699.

10. Meyer-Wegner, F.; Nadj, A.; Bolte, M.; Auner, N.; Wagner, M.; Holthausen, M. C.; Lerner, H.-W. The Perchlorinated Silanes Si_2Cl_6 and Si_3Cl_8 as Sources of $SiCl_2$. *Chem. Eur. J.* **2011**, *17*, 4715.

11. Orlandi, M.; Benaglia, M.; Tosi, F.; Annunziata, R.; Cozzi, F. $HSiCl_3$-Mediated Reduction of Nitro-Derivatives to Amines: Is Tertiary Amine-Stabilized $SiCl_2$ the Actual Reducing Species? *J. Org. Chem.* **2016**, *81*, 3037.

12. Lu, H.; Geng, Z.; Li, J.; Zou, D.; Wu, Y.; Wu, Y. Metal-Free Reduction of Aromatic Nitro Compounds to Aromatic Amines with B_2pin_2 in Isopropanol. *Org. Lett.* **2016**, *18*, 2774.

13. Béchamp, A. De l'action des protosels de fer sur la nitronaphtaline et la nitrobenzine. nouvelle méthode de formation des bases organiques artificielles de Zinin. *Annales de chimie et de physique*. **1854**, *42*, 186.

14. Allen, C. F. H.; VanAllan, J. 2-Amino-p-Cymene. *Org. Synth.* **1942**, *22*.

15. Bavin, P. M. G. 2-Aminofluorene. *Org. Synth.*, **1960**, *40*.

16. Westerhaus, F. A.; Jagadeesh, R. V.; Wienhöfer, G.; Pohl, M.-M.; Radnik, J.; Surkus, A.-E.; Rabeah, J.; Junge, K.; Junge, H.; Nielsen, M.; Brückner, A.; Beller, M. Heterogenized cobalt oxide catalysts for nitroarene reduction by pyrolysis of molecularly defined complexes. *Nat. Chem.* **2013**, *5*, 537.

17. Jagadeesh, R. V.; Natte, K.; Junge, H.; Beller, M. Nitrogen-Doped Graphene-Activated Iron-Oxide-Based Nanocatalysts for Selective Transfer Hydrogenation of Nitroarenes. *ACS Catal.* **2015**, *5*, 1526.

18. Rai, R. K.; Mahata, A.; Mukhopadhyay, S.; Gupta, S.; Li, P.-Z.; Nguyen, K. T.; Zhao, Y.; Pathak, B.; Singh, S. K. Room-Temperature Chemoselective Reduction of Nitro Groups Using Non-noble Metal Nanocatalysts in Water. *Inorg. Chem.* **2014**, *53*, 2904.

19. Pedrajas, E.; Sorribes, I.; Gushchin, A. L.; Laricheva, Y. A.; Junge, K.; Beller, M.; Llusar, R. Chemoselective Hydrogenation of Nitroarenes Catalyzed by Molybdenum Sulphide Clusters. *ChemCatChem* **2017**, *9*, 1128.

20. Ding, Z.-C.; Li, C.-Y.; Chen, J.-J.; Zeng, J.-H.; Tang, H.-T.; Ding, Y.-J.; Zhan, Z.-P. Palladium/Phosphorus-Doped Porous Organic Polymer as Recyclable Chemoselective and Efficient Hydrogenation Catalyst under Ambient Conditions. *Adv. Synth. Catal.* **2017**, *359*, 2280.

21. Uberman, P. M.; García, C. S.; Rodríguez, J. R.; Martín, S. E. PVP-Pd nanoparticles as efficient catalyst for nitroarene reduction under mild conditions in aqueous media. *Green Chem.* **2017**, *19*, 739.

22. He, L.; Wang, L.-C.; Sun, H.; Ni, J.; Cao, Y.; He, H.-Y.; Fan, K.-N. Efficient and Selective Room-Temperature Gold-Catalyzed Reduction of Nitro Compounds with CO and H_2O as the Hydrogen Source. *Angew. Chem., Int. Ed.* **2009**, *48*, 9538.

23. Huang, H.; Wang, X.; Li, X.; Chen, C.; Zou, X.; Ding, W.; Lu, X. Highly chemoselective reduction of nitroarenes over non-noble metal nickel-molybdenum oxide catalysts. *Green Chem.* **2017**, *19*, 809.

24. Liu, M.; Tang, W.; Xie, Z.; Yu, H.; Yin, H.; Xu, Y.; Zhao, S.; Zhou, S. Design of Highly Efficient Pt-SnO_2 Hydrogenation Nanocatalysts using Pt@Sn Core–Shell Nanoparticles. *ACS Catal.* **2017**, *7*, 1583.

25. Sorribes, I.; Liu, L.; Corma, A. Nanolayered Co–Mo–S Catalysts for the Chemoselective Hydrogenation of Nitroarenes. *ACS Catal.* **2017**, *7*, 2698.

26. Feng, J.; Handa, S.; Gallou, F.; Lipshutz, B. H. Safe and Selective Nitro Group Reductions Catalyzed by Sustainable and Recyclable Fe/ppm Pd Nanoparticles in Water at Room Temperature. *Angew. Chem., Int. Ed.* **2016**, *55*, 8979.

Results and discussion

As discussed in the Introduction, improvements in the activity of this Fe/ppm Pd nanocatalyst in hydrogenation of nitro reactions are to be expected. As one of the most commonly used metals in modern metal catalysis, nickel has been found to be active in numerous processes, especially in hydrogenation reactions. Moreover, as one of the most abundant transitional metals on earth, nickel only costs 11.9 dollars per kilogram right now, which is only 1/4500 of the price of palladium. Because nickel is highly active in catalytic hydrogenation and its price is far less than that compared with palladium, we focused at the outset on forming a Ni-Fe alloy nanocatalyst so that further improve catalytic activity for hydrogenations through synergistic effects between iron and nickel in catalyst, and to lower the cost for synthesis of the nanocatalyst.

Initially, 4-chloronitrobenzene was chosen as starting material for optimization of a new, multi-metal nanocatalyst. Since the original work by Feng[1] showed that only two hours were needed for hydrogenation of 4-chloronitrobenzene, our first aim was to complete the reduction in less time. At the outset, we continued to use the original method to synthesize nanocatalysts. That is, $Ni(OAc)_2·4H_2O$ (0.033 mol) and $FeCl_3$ (0.1 mmol) were reduced using MeMgCl (0.133 mmol) in dry THF at room temperature. After evaporation of THF in vacuo, the nanocatalyst was stored in a vial under a blanket of argon. Use of only 0.6 mol % Ni nanocatalyst to catalyze the hydrogenation of 4-chloronitrobenzene with 1.5 equivalents of $NaBH_4$ as hydrogen source in 2 wt % TPGS-750-M/H_2O (0.5 M) at room temperature for two hours did not afford any corresponding aniline in the reaction mixture. At that time, another publication from our group appeared in which the authors used $NaBH_4$ to reduce $Pd(OAc)_2$ in TPGS-750-M/H_2O directly to make a Pd nanocatalyst, which was then used to effect stereoselective semi-hydrogenation of alkynes. This led to a change of reducing agents, from MeMgCl as to $NaBH_4$ as reductant for synthesizing the Fe/Ni nanoparticles for eventual use in water.

Synthesis and optimization of Fe/B/Ni NPs

The appropriate quantity of $NaBH_4$ was added to an aqueous solution containing $FeCl_3$ and $Ni(OAc)_2{\cdot}4H_2O$. The mixture was stirred for twenty minutes followed by filtration to obtain a black powder. After being totally dried under vacuum, the powder was stored in a vial under argon. Afterward, the black powder was used as catalyst for reduction of 4-chloronitrobenzene with $NaBH_4$ as reductant in 2 wt % TPGS-750-M at room temperature. The conversion and selectivity were determined by GC-MS, as shown in Table 1.

The initial ratio of nickel to iron was 1:3. With 0.6 mol % Ni present, there was no aniline detected in the mixture after a two-hour reaction time using 1.5 equivalents of $NaBH_4$ (Entry 1). Furthermore, although the amount of $NaBH_4$ was increased with each reaction (from 1.5 to 3 equivalents), neither a 1:3 nor 1:4 nickel:iron ratio afforded better selectivity (Entries 2 and 3). Further increasing the precent Ni from 0.6 to 2 mol % helped improve the extent of conversion, but the selectivity was marginal (ca. 10%; Entry 5). Based on the GC-MS of the final mixture, most nitro compounds were consumed; however, only about 10% aniline had been generated. Most starting material converted into (*Z*)-1,2-bis(4-chlorophenyl)diazene 1-oxide or (*E*)-1,2-bis(4-chlorophenyl)diazene. Moreover, between Entries 3 and 4, the nanocatalyst with a 1:4 nickel:iron ratio generated more by-product compared with the nanocatalyst containing a 1:3 nickel:iron ratio. Additionally, the nanocatalyst with 1:1 nickel:iron ratio showed significant improvement in selectivity, up to 68% (Entry 6). Even in the reaction over one hour, the selectivity was 61% (Entry 11). In order to enhance the activity for the catalyst, the nickel:iron ratio was increased from 1:1 to 2:1, 4:1 and 10:1, and correspondingly, the loading of nickel in each reaction was increased to 5.3%, 6.4 and 7.2%. However, it was surprising to find that there was a dramatic decline in selectivity (Entries 7, 8 and 9). Subsequently, pure nickel nanoparticles as black powder could be obtained by reducing $Ni(OAc)_2 \cdot 4H_2O$ directly in water with $NaBH_4$ without using $FeCl_3$. Fortunately, this nanocatalyst with 8% nickel loading in the reaction showed excellent selectivity on hydrogenation of 4-chloronitrobenzene, which was reduced up to 99% (Entry 10). However, all efforts to lower the nickel loading within these nanoparticles failed. Even with a 4% nickel loading, the selectivity was only 15% (Entry 13). Finally, attempts to optimize the nickel/iron nanocatalyst in terms of nickel source led to the observation that NPs from $Ni(NO_3)_2 \cdot 6H_2O$ seemed to work better compared those made with $Ni(OAc)_2 \cdot 4H_2O$ and $NiCl_2$ (Entries 16, 17 and 18). In summary, using the same nickel loading in these reactions, the nanocatalyst with a 1:1 nickel:iron ratio worked the best in reductions of nitroarenes. However, the reactions remained incomplete even after two hours and hence, the aim of improving nanocatalyst activity had not yet been achieved.

Table 1: Optimization of Fe/B/Ni nanoparticles for nitro group reductions

$$Ni(OAc)_2{\bullet}4H_2O + FeCl_3 \xrightarrow[H_2O]{NaBH_4} \text{Fe/B/Ni NPs}$$

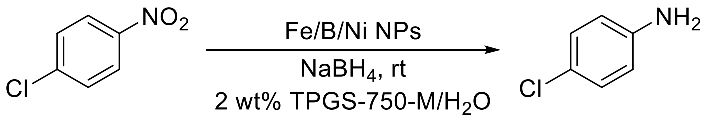

Entry	Ni:Fe	Ni%	$NaBH_4$ equiv	Reaction time (h)	Conversion (%)	Selectivity (%)
1	1:3	0.6	1.5	2	7	n.d
2	1:3	0.6	3	0.75	5	1
3	1:4	0.6	3	0.75	27	1
4	1:4	2	3	2	95	5
5	1:3	2	3	2	87	11
6	1:1	4	3	2	97	68
7	2:1	5.3	3	1	97	11
8	4:1	6.4	3	1	97	9
9	10:1	7.2	3	1	94	6
10	pure Ni	8	3	1	99	99
11	pure Ni	0.8	3	1.5	73	6
12	pure Ni	1.6	3	1.5	78	7
13	pure Ni	4	3	1.5	94	15
14	1:1	4	3	1	83	61
15	1:5	1.3	3	1	62	26
16	1:5	0.72	3	1	11	2
17[a]	1:5	0.72	3	1	14	3
18[b]	1:5	0.72	3	1	27	13

[a] $NiCl_2$ instead of $Ni(OAc)_2{\bullet}4H_2O$; [b] $Ni(NO_3)_2{\bullet}6H_2O$ instead of $Ni(OAc)_2{\bullet}4H_2O$.

Synthesis and optimization of Fe/ppm Ni NPs

Although for the hydrogenation of nitro compounds attempts to make nanoparticles via reduction of a nickel and iron salt mixture with $NaBH_4$ failed, the higher the nickel loading for each reaction, or the higher the nickel:iron ratio in the nanoparticle, the better the selectivity of the reduction. Thus, it seemed that nickel and iron needed an appropriate ratio to catalyze the reduction. Hence, re-examination of the route used to prepare the nanocatalyst was carried out by reducing mixtures of $FeCl_3$ and nickel salt with MeMgCl in dry THF. The nickel salt (0.04 mmol) and $FeCl_3$ (0.5 mmol) were added to a flask under an atmosphere of dry argon. The flask was then covered with a septum and 5 mL dry THF was added by syringe. The reaction mixture was stirred for 20 minutes at room temperature. While maintaining a dry atmosphere at room temperature, a 1 M solution of MeMgCl in THF was very slowly (1 drop/2 sec) added to the reaction mixture (about 0.6 mL, 0.6 mmol). After addition, a 0.1 M solution of MeMgCl in THF was added very slowly (1 drop/2 sec) to the reaction mixture (about 0.3 mL, 0.03 mmol). After complete addition of the Grignard reagent, the mixture was stirred for an additional twenty minutes at room temperature. Appearance of a yellow-brown color was indicative of generation of nanomaterial. After twenty minutes, the mixture was quenched with pentane (containing traces of water). THF was then evaporated under reduced pressure at room temperature. Removal of THF was followed by triturating the mixture with pentane to provide yellow-brown colored nanomaterial as a powder (trituration was repeated three to four times). The Fe/ppm Ni nanocatalyst obtained was dried under reduced pressure at room temperature and stored in a vial protected by argon.

Optimization of the nickel within the resulting nanoparticles was carried out as shown in Table 2 (isolated yields shown). The rationale here was based on prior research on Fe/B/Ni nanoparticles, where the Fe/ppm Ni nanocatalyst made from different nickel salts may show different activities on hydrogenation of nitroaromatics. During this optimization, it was discovered:

1) Using 10% THF as cosolvent increases the activity of the reaction catalyst.

2) The order in which the starting material and catalyst are added is crucial to the activity of the resulting catalyst. The nanocatalyst needed to be added to the vial containing aqueous TPGS-750-M solution followed by reduction by $NaBH_4$. During this process, the color of the solution changed from yellow-brown to black, accompanied by a large quantity of bubbling, which meant that the catalyst had already been activated. Finally, nitro compounds were added followed by covering the vial with a cap.

3) Compared with $Ni(AcO)_2 \cdot 4H_2O$, $NiCl_2$ and $Ni(acac)_2$, the nanocatalyst made from $NiBr_2$ and $Ni(NO_3)_2 \cdot 6H_2O$ as nickel sources worked better in the hydrogenation of nitro groups with the same nickel loading (0.16 mol %). Hence, the following research was based on the nanocatalyst prepared from $NiBr_2$ or $Ni(NO_3)_2 \cdot 6H_2O$ as nickel source.

Table 2: Optimization the source of nickel in Fe/ppm Ni nanoparticles

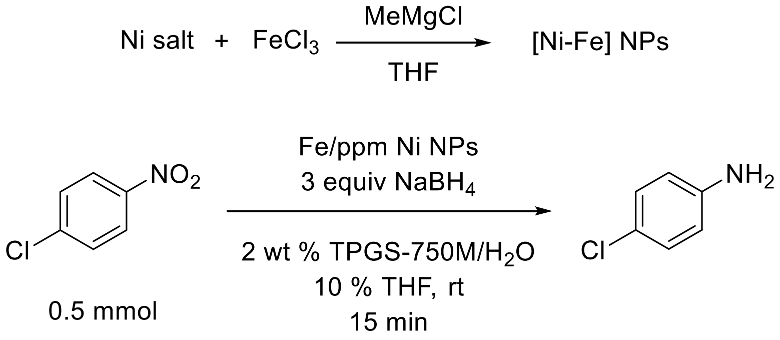
Ni salt + FeCl3
MeMgCl
THF
[Ni-Fe] NPs
NO2
Cl
0.5 mmol
Fe/ppm Ni NPs
3 equiv NaBH4
2 wt % TPGS-750M/H2O
10 % THF, rt
15 min
NH2
Cl

Entry	Ni source	Ni %	Yield
1	$Ni(AcO)_2•4H_2O$	0.16	27 %
2	$NiCl_2$	0.16	21 %
3	$Ni(acac)_2$	0.16	24 %
4	**$NiBr_2$**	**0.16**	**41 %**
5	**$Ni(NO_3)_2•6H_2O$**	**0.16**	**43 %**

In making these nanoparticles, the quantity of MeMgCl used for the reduction of the Ni salt and $FeCl_3$ mixture was found to also impact the activity of the resulting nanocatalyst. Hence, precise control over the quantity of MeMgCl used during making nanoparticles was essential in determining the most appropriate ratio. Tables 3 and 4 show optimization of the quantity of MeMgCl and nickel loading used to make the nanocatalyst with $Ni(NO_3)_2·6H_2O$ and $NiBr_2$ as nickel sources.

Table 3: Optimization on the quantity of MeMgCl and the nickel loading of the nanocatalyst with $Ni(NO_3)_2 \cdot 6H_2O$ as nickel source

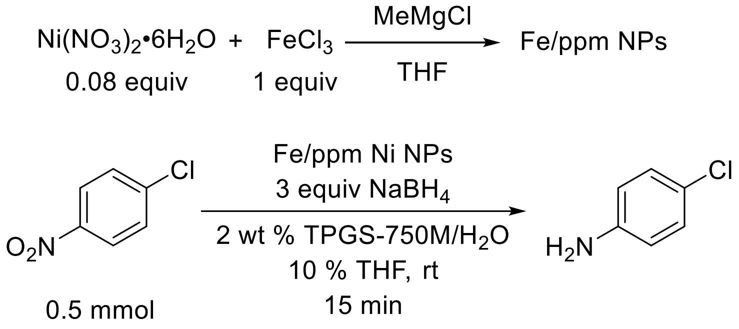

Ni(NO3)2•6H2O + FeCl3
0.08 equiv
1 equiv
MeMgCl
THF
Fe/ppm NPs
Cl
O2N
0.5 mmol
Fe/ppm Ni NPs
3 equiv NaBH4
2 wt % TPGS-750M/H2O
10 % THF, rt
15 min
Cl
H2N

Entry	MeMgCl equiv[a]	Ni %	Yield (%)
1	1.25	0.16	44
2	1.27	0.16	43
3	1.3	0.16	28
4	1.5	0.16	26
5	2	0.16	7
6	1.27	0.04	4
7	1.27	0.08	9
8	1.27	0.12	21
9	1.27	0.20	57
10[b]	1.27	0.16	79
11	**1.27**	**0.32**	**93**
12	1.27	0.64	94
13	1.27	1.28	94

[a]Amount relative to $FeCl_3$; [b]12 h

Use of $Ni(NO_3)_2 \cdot 6H_2O$ was tested for nanoparticle formation by reducing it with different amounts of MeMgCl. The results from hydrogenation of 4-chloronitrobenzene indicated that the nanocatalysts produced by reduction with 1.25 and 1.27 equivalents of MeMgCl had better catalytic activity in hydrogenation of nitro groups, compared with 1.3 to 2 equivalents of same Grignard reagent (Table 3, Entries 1 to 5). Moreover, although the nanocatalyst produced by reduction with 1.25 equivalents of MeMgCl showed somewhat better activity towards hydrogenation of nitroarenes than the counterpart reagent with 1.27 equivalents, the resulting nanoparticles were also more hygroscopic. The nanoparticles would become wet and even form a yellow liquid during collection or weighting such that it was hard to use and store these in air. Further optimization focused on proper nickel loading for each reaction. With the same nanocatalyst derived from $Ni(NO_3)_2 \cdot 6H_2O$, hydrogenation of 4-chloronitrobenzene was complete using 0.32 mol % nickel loading (Entry 11). In attempt to lower the nickel loading, from 0.32 mol % to 0.16 mol %, even extending the reaction time to twelve hours, the hydrogenation remained incomplete (Entry 10).

Table 4: Optimization of the nanocatalyst based on the quantity of MeMgCl used with NiBr$_2$ as the source of nickel

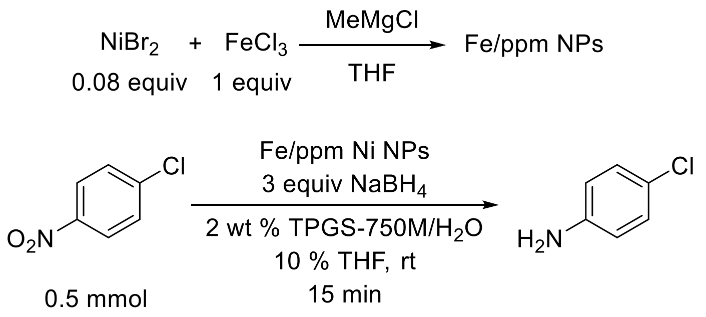
NiBr2
0.08 equiv
+
FeCl3
1 equiv
MeMgCl
THF
Fe/ppm NPs
Cl
O2N
0.5 mmol
Fe/ppm Ni NPs
3 equiv NaBH4
2 wt % TPGS-750M/H2O
10 % THF, rt
15 min
Cl
H2N

Entry	MeMgCl equiv[a]	Ni %	Yield
1	1.1	0.16	22 %
2	1.2	0.16	26 %
3	1.25	0.16	34 %
4	1.3	0.16	41 %
5	1.35	0.16	60 %
6	1.4	0.04	19 %
7	1.4	0.08	38 %
8	1.4	0.12	61 %
9	**1.4**	**0.16**	**96 %**
10	**1.4**	**0.2**	**97 %**
11	1.5	0.04	5 %
12	1.5	0.08	13 %
13	1.5	0.12	29 %
14	1.5	0.16	83 %
15	**1.5**	**0.2**	**95 %**
16	1.7	0.16	77 %
17	2.0	0.16	79 %

[a] Amount relative to $FeCl_3$

On the other hand, both the number of equivalents of MeMgCl and the nickel loading on the anoparticle derived from $NiBr_2$ could be optimized as well (Table 4). The result of reduction of 4-chloronitrobenzene showed that the reaction would go to completion when catalyzed by nanoparticles containing only 0.16 mol % nickel loading produced by reduction with 1.4 equivalents of MeMgCl (Entry 10). Any further increase or decrease in the quantity of MeMgCl used for the preparation of this nanocatalyst, or lowering of the nickel loading in these hydrogenation reactions led to a reduction in the yield of the aniline.

On the basis of these early results, it appeared that new nanoparticles containing ppm level of Ni, along with Fe, had been found, which together could effect hydrogenation of 4-chloronitrobenzene in 2 wt % TPGS-750-M/H_2O at room temperature in fifteen minutes. The reaction time was significantly reduced compared with the two hours needed for Feng’s Fe/ppm Pd nanoparticles to catalyze the same substrate. It was apparent that the Fe/ppm Ni nanoparticles seemed to have higher catalytic activity for reduction of nitroaromatics than the original nanoparticles containing palladium. However, attempting hydrogenation of two other simple nitroarenes (1-nitronaphthalene and 1-chloro-4-nitro-2-(trifluoromethyl)benzene) catalyzed with the same Fe/ppm Ni nanocatalyst did not lead much better results in terms of the rates for reduction for these two substrates (Table 5). Hence, another nanocatalyst needed to be developed to fully satisfy the original aim of improving the catalytic activity of nanoparticles towards hydrogenation of diverse nitroarenes.

Table 5: Comparison between Fe/ppm Ni NPs and NPs of Fe/ppm Pd NPs

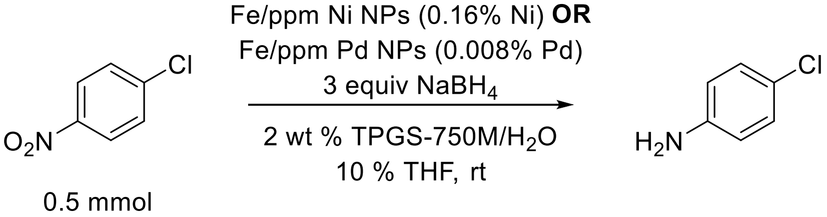
Fe/ppm Ni NPs (0.16% Ni) OR
Fe/ppm Pd NPs (0.008% Pd)
3 equiv $NaBH_4$
2 wt % TPGS-750M/H_2O
10 % THF, rt
0.5 mmol
Cl
O_2N
H_2N

Substrates	Fe/ppm Pd NPs		Fe/ppm Ni NPs	
	Reaction time (h)	Yield (%)	Reaction time (h)	Yield (%)
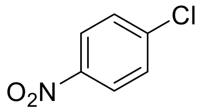	2	90	0.25	96
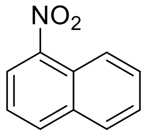	2	94	0.5	61
			1	79
			1.5	93
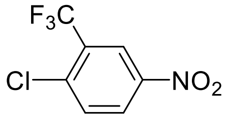	2	98	0.5	71
			1	86
			1.5	95

Synthesis and optimization of Fe/ppm (Pd + Ni) NPs

In previous work, Fe/ppm Ni nanoparticles had been found to have good catalytic activity for use in hydrogenations of nitroarenes. However, a catalyst containing a single metal still did not meet our requirements for activity. Moreover, from earlier discussion herein, it was clear that the bimetallic catalyst, as a novel material, often has synergistic effects arising from both electronic and/or geometrical interactions between the multi-metals, and this was usually found to be more advantageous in terms of selectivity and activity. This led to the notion of adding small amount of palladium (e.g., 80 ppm) to the original iron-nickel nanoparticles to see if it would significantly improve the catalytic activity of the nanoparticles towards nitro group reductions. To better compare the activity of the bi-metal-containing nanocatalyst with the mono-metal counterpart, iron nanoparticles containing only palladium were prepared using $Pd(OAc)_2$ (0.002 mmol) and $FeCl_3$ (0.5 mmol). In the THF solution, the mixture of $Pd(OAc)_2$ and $FeCl_3$ was reduced using 0.635 mmol of MeMgCl, being added slowly (1 drop/2 sec), followed by stirring for an additional twenty minutes at room temperature. After quenching and evaporating the THF, the obtained nanocatalyst was used for hydrogenation of nitro compounds with only 80 ppm Pd loading in each reaction. The results of hydrogenation of 4-chloronitrobenzene are shown in Table 6. Using only 1.5 equivalents of $NaBH_4$ relative to the quantity of 4-chloronitrobenzene, a 66% yield as determined by GC-MS was observed after reaction for two hours (Entry 1). When the quantity of $NaBH_4$ was increased from 1.5 to 3 equivalents, the GC-MS yield reached 74% (Entry 2). Further augmentation of $NaBH_4$ from 3 to 5 equivalents, requiring only one hour, led to 87% yield (Entry 3), which indicated that the quantity of $NaBH_4$ in the reaction is crucial for controlling the extent of reduction. Subsequently, 0.02 equivalents of $Ni(NO_3)_2 \cdot 6H_2O$ were added for the preparation of the Fe/ppm (Pd+Ni) nanoparticles. With the same Pd loading, quantity of $NaBH_4$, and reaction time, the yield increased to 98%, having been catalyzed be this new bimetallic nanocatalyst. With further increases of Ni loading and decreases in reaction time, the reduction of 4-chloronitrobenzene could be driven to completion using 0.16 mol % Ni and 0.008 mol % Pd loading at room temperature within only fifteen minutes. Additional studies focused on reducing the quantity of $NaBH_4$ used in the reaction were then conducted. When the equivalents of $NaBH_4$ were reduced from five to three, there was no obvious influence on yield. However, any further lowering of the quantity of $NaBH_4$ resulted in lowering of the final yield (Entries 6 to 10).

Table 6: Optimization of the Fe/ppm (Pd + Ni) NPs

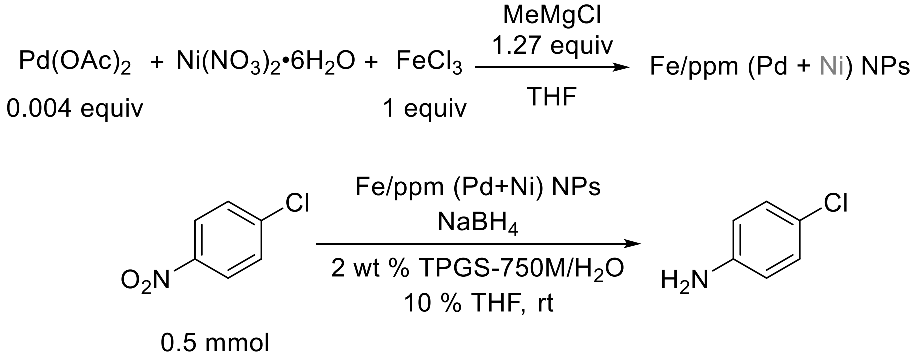

Pd(OAc)2 + Ni(NO3)2•6H2O + FeCl3
0.004 equiv
1 equiv
MeMgCl
1.27 equiv
THF
Fe/ppm (Pd + Ni) NPs
Cl
O2N
0.5 mmol
Fe/ppm (Pd+Ni) NPs
NaBH4
2 wt % TPGS-750M/H2O
10 % THF, rt
Cl
H2N

Entry	$Ni(NO_3)_2$•$6H_2O$ equiv	$NaBH_4$ (equiv)	Ni%	Pd%	Time (h)	Yield (%)[a]
1	0	1.5	0	0.008	2	66
2	0	3	0	0.008	2	74
3	0	5	0	0.008	1	87
4	0.02	5	0.04	0.008	1	98
5	0.04	5	0.08	0.008	0.75	91
6	0.08	5	0.16	0.008	0.25	99 (98)
7	0.08	4	0.16	0.008	0.25	97
8	0.08	3	0.16	0.008	0.25	98 (96)
9	0.08	2	0.16	0.008	0.25	88
10	0.08	1	0.16	0.008	0.25	59

[a] Yield is from GC-MS, isolated yield is in parenthesis

In order to verify that the novel nanocatalyst has enhanced catalytic activity for the hydrogenations of nitro-containing compounds relative to that described earlier by Feng, more starting materials with different structures were tested for comparison purposes (Table 7). These comparisons indicated that under the same set of conditions (3 equivalents $NaBH_4$, room temperature, 2 wt % TPGS-750-M/H_2O), the new Fe/ppm (Pd + Ni) NPs could catalyze the complete hydrogenation of nitroarenes within a much shorter timeframe, indicative a generally higher catalytic activity then the original catalyst containing only 80 ppm Pd.

Table 7: Comparison between Fe/ppm (Pd + Ni) NPs and NPs of Fe/ppm Pd NPs (without Ni)

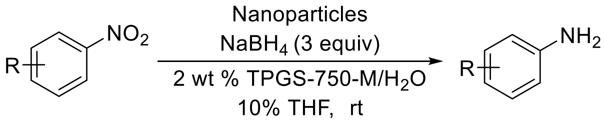

Catalyst / Product	**Fe/ppm Pd + Ni^a NPs**		Fe/ppm Pd NPs	
	Time	Yield^b	Time	Yield^b
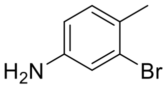	30 min	98 %	90 min	96 %
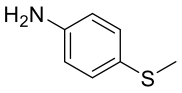	2 h	88 %	12 h	72 %
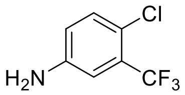	30 min	98 %	2 h	94 %
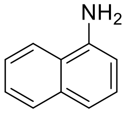	30 min	99 %	2 h	98 %
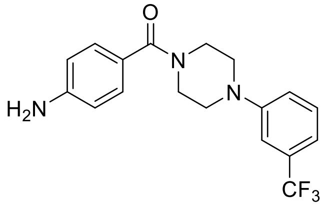	2 h	88 %	8 h	90 %

^{a}Ni source: $Ni(NO_3)_2•6H_2O$, MeMgCl: 1.27 equiv (relative to $FeCl_3$); ^{b}Isolate Yield

Comparisons with reported catalysts

In order to highlight the advantages of this novel technology based on a newly developed nanocatalyst for hydrogenation of nitroaromatics, broader comparisons were undertaken with reductions of 4-chloronitronbenzene, 1-nitronaphthalene and morpholino-(4-nitrophenyl)methanone as starting materials (Table 8 to 10).

Table 8: Comparison reductions of the nitro groups in 4-chloronitrobenzene to 4-chloroaniline with alternative reported catalysts

Catalyst	Amount of Catalyst	H source	Reaction condition	Time	Yield (%)[a]	Ref.
Fe/ppm Pd + Ni NPs	**0.008% Pd** **0.16% Ni** **2 mol% Fe**	$NaBH_4$ (3 equiv)	**2% wt. TPGS-750-M, 10 % THF, rt**	**15 min**	**>99 (96)**	**our work**
3 wt% Co-L_1/C	1 mol%	50 bar H_2	THF/H_2O 110 °C	6 h	95	2
Pd-pol	1.75% Pd	$NaBH_4$ (10 equiv)	H_2O, rt	5 h	57	3
Pd/ZrP	0.4% Pd	HCOOH	EtOH, 60 °C	16 h	93	4
$Fe(OTf)_3$	10 mol% Fe	$NaBH_4$ (20 equiv)	EtOH, r.t	4 h	80 (47)	5
Fe-phenanthroline/C	1 mol% Fe	N_2H_4-H_2O (4 equiv)	THF, 100 °C	10 h	96 (96)	6
KOtBu	1.2 equiv	B_2pin_2 (3.1 equiv)	*i*PrOH, 110 °C	2 h	95 (86)	7
Au/TiO_2-VS	1 mol% Au	CO/H_2O	EtOH	30 min	99	8
$FeBr_2$-PPh_3	10 mol% Fe	$PhSiH_3$ (2.5 equiv)	toluene 110 °C	16 h	99	9
Pd^0-AmP-MCF	1 mol% Pd	H_2 (1 atm)	EtOAc, rt	7 h	97	10
$[Mo_3S_4Cl_3(dnbpy)_3](PF_6)$	5 mol%	20 bar H_2	MeOH, 70 °C	18 h	92 (80)	11
Fe	5 equiv	Fe/HCl	10 equiv HFIP, 2 N HCl, rt	30 min	84	12
$Pd(OAc)_2$	1%	N_2H_4-H_2O (5 equiv)	H_2O, 50 °C	8 h	97	13
Pd_9Ag_1-N-doped-MOF-C	0.5 mol%	formic acid	EtOH/H_2O, HCOOK, 30 °C	6 h	91	14
$NiCl_2$-$6H_2O$	0.25 mol%	$NaBH_4$	0.01 wt % nanocellulose/H_2O, rt	2 h	84	15
Pt-SnO_2/Al_2O_3	0.5 wt % Pt	0.1 MPa H_2	EtOH, 45 °C	1 h	87	16
Co-Mo-S-0.39-180	5 mol% Co, 8 mol% Mo	11 bar H_2	toluene, 180 °C	7 h	99 (90)	17
PVP-Pd NPs	0.1 mol%	$NaBH_4$	EtOH/H_2O, rt	1 h	90	18
Ni-MoO_3/SBA-15	6 mol%	N_2H_4-H_2O	EtOH, 40 °C	30 min	99	19
0.75-500-γ-Fe_2O_3/MC	43 wt %	N_2H_4-H_2O	EtOH, 80 °C	1 h	100	20
FeS_2	0.8 equiv	50 bar H_2	H_2O-THF, 120 °C	18 h	100	21
7 wt% Pd NPs @ POL-2	0.5 mol%	1 atm H_2	EtOH, 60 °C	3 h	91	22
Co@NC-800	4.2 mol%	3 MPa H_2	EtOH, 110 °C	6 h	97	23

[a] Isolated yield in parentheses.

Table 9: Comparison reductions of the nitro groups in 1-nitronaphthalene to corresponding aniline with alternative reported catalysts

Catalyst	Amount of Catalyst	H source	Reaction condition	Time	Yield (%)[a]	Ref.
Fe/ppm Pd + Ni NPs	**0.008% Pd 0.16% Ni 2 mol% Fe**	**$NaBH_4$ (3 equiv)**	**2% wt. TPGS-750-M, 10 % THF, rt**	**30 min**	**99**	**our work**
Pd/ZrP	0.4% Pd	HCOOH	EtOH, 40 °C	16 h	93	4
Fe-phenanthroline/C	1 mol% Fe	N_2H_4/H_2O (4 equiv)	THF, 100 °C	10 h	99	6
Pd^0-AmP-MCF	1 mol% Pd	H_2 (1 atm)	EtOAc, rt	7 h	97	10
Fe	5 equiv	Fe/HCl	10 equiv HFIP, 2 N HCl, rt	30 min	60	12
Pd_9Ag_1-N-doped-MOF-C	0.5 mol%	formic acid	$EtOH/H_2O$, HCOOK, 30 °C	6 h	91	14
7 wt% Pd NPs @ POL-2	0.5 mol%	1 atm H_2	EtOH, rt	1 h	98	22
Ni-PVAm/SBA-15	10 mol% Ni	$NaBH_4$ (4 equiv)	H_2O, rt	42 min	98	24
Ni NPs	20 mol% Ni	N_2H_4/H_2O	H_2O, rt	60 min	96	25
Co NPs	20 mol% Co			90 min	97	
$[Pd_2(bpnp)(\mu\text{-}OH)(CF_3CO_2)_2](CF_3CO_2)$	0.5 mol%	1 atm H_2	MeOH, 50 °C	12 h	100	26
NAP-Mg-Pd(0)PS	1.98 mol%	PMHS	H_2O, Et_3N, 80 °C	5 h	91	27
$NiS_{2+x}/g\text{-}C_3N_4$	9 wt %	$NaBH_4$	H_2O, rt	1 h	94	28
PdNPs@Cell-N-GQD	0.56 mol%	$NaBH_4$	H_2O/EtOH, rt	2 h	90	29

Table 10: Comparison reductions of the nitro groups in morpholino-(4-nitrophenyl)methanone to corresponding aniline with alternative reported catalysts

Catalyst	Amount of Catalyst	H source	Reaction condition	Time	Yield (%)[a]	Ref.
Fe/ppm Pd + Ni NPs	**0.008% Pd 0.16% Ni 2 mol% Fe**	$NaBH_4$ (3 equiv)	**2% wt. TPGS-750-M, 10 % THF, rt**	**30 min**	**99**	**our work**
$Fe(OTf)_3$	10 mol% Fe	$NaBH_4$ (20 equiv)	EtOH, r.t	4 h	80 (32)	5
KOtBu	1.2 equiv	B_2pin_2 (3.1 equiv)	*i*PrOH, 110 °C	2 h	93 (80)	7
$[Mo_3S_4Cl_3(dnbpy)_3](PF_6)$	5 mol%	20 bar H_2	MeOH, 70 °C	18 h	88	11
Fe_2O_3/NGr@C	5 mol% Fe	HCOOH-Et_3N (1.75 equiv)	THF, 120 °C	20-24 h	95	30
Co_3O_4-NGr/C	2 mol% Co	HCOOH-Et_3N (3.5 equiv)	THF, 100 °C	15 h	95	31

[a]Isolated yield in parentheses.

From these three comparisons, it was found that for all cases, due to the higher activity of the new nanocatalyst compared with other methods in the literature, hydrogenation of nitroarenes could now be run using lower metal loadings (1600 ppm Ni and 80 ppm Pd), shorter reaction times, and far milder reaction conditions (room temperature). Moreover, using $NaBH_4$ as reductant was much safer compared to use of high-pressures of hydrogen. Even more importantly, the reduction process was carried out in water as the reaction medium, which is more environmentally friendly than organic solvents.

Characterization of Fe/ppm (Pd + Ni) NPs

Two samples were prepared for TEM analysis. For the first sample, Fe/ppm (Pd + Ni) nanoparticles (6 mg) were added to an oven dried 4 mL microwave reaction vial containing a PTFE-coated magnetic stir bar. After addition, 1 mL of aqueous solution of 2 wt % TPGS-750-M was added via syringe. The mixture was stirred at room temperature for five minutes to obtain a yellow solution, as shown in Figure 1A. For the second sample, Fe/ppm (Pd + Ni) nanoparticle (6 mg) was added to an oven dried 4 mL microwave reaction vial containing a PTFE-coated magnetic stir bar. After addition, 1 mL aqueous solution of 2 wt. % TPGS-750-M followed by $NaBH_4$ (10 mg) was added to the vial. The mixture was stirred at room temperature for one minute to obtain a black suspension, as shown in Figure 1B.

Figure 1: Nanoparticles in aqueous TPGS-750-M solution without $NaBH_4$ (A) and with $NaBH_4$ (B)

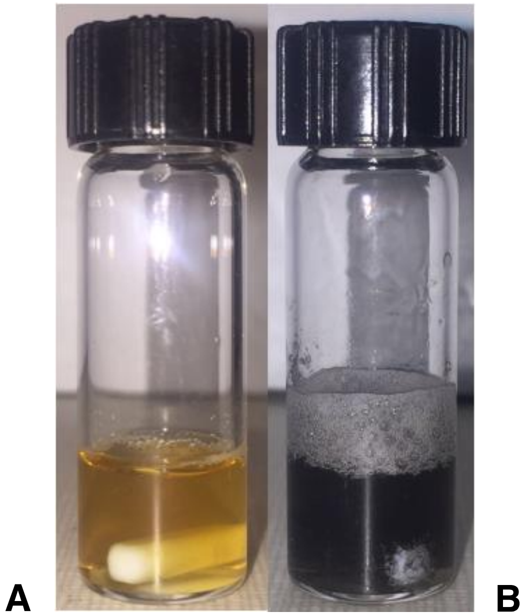

Both samples were prepared on 200 mesh copper grids and analyzed using FEI Tecnai G2 Sphera 200kV EDX as shown in Figures 2 and 3. For the first sample, without $NaBH_4$ added, NPs could be identified as ca. 5 nanometer powders with irregular shapes distributed in the liquid phase (Figure 2). In addition, the Fe (but not Ni) on these powders could be identified base on Energy-dispersive X-ray spectroscopy (EDX) spectra. However, after $NaBH_4$ had been added, the TEM images were totally different compared with the former images. That is, now black nanoclusters of ca. 10 nanometers were found to be distributed in the liquid phase (Figure 3). Moreover, EDX analysis indicated that both Fe and Ni could be identified within these back nanoclusters. Nevertheless, the quantity of palladium was too low to be observed in either of the EDX spectra. Hence, it was presumed that the nanomaterial prepared was only a pre-catalyst. Before $NaBH_4$ was added to the mixture in aqueous micellar media, the nickel might dissolve in the liquid phase, instead of attaching to the nanopowders. Moreover, after the addition of NaBH4, the nickel could be reduced and combine with the Fe and Pd to form the real, active catalyst, which could then be used for hydrogenation of nitroaromatics. This also explained why the reaction required activation of the nanocatalyst with $NaBH_4$ first to obtain the best reactivity.

Figure 2: TEM and EDX analysis of nanoparticles in aqueous TPGS-750-M solution (without $NaBH_4$)

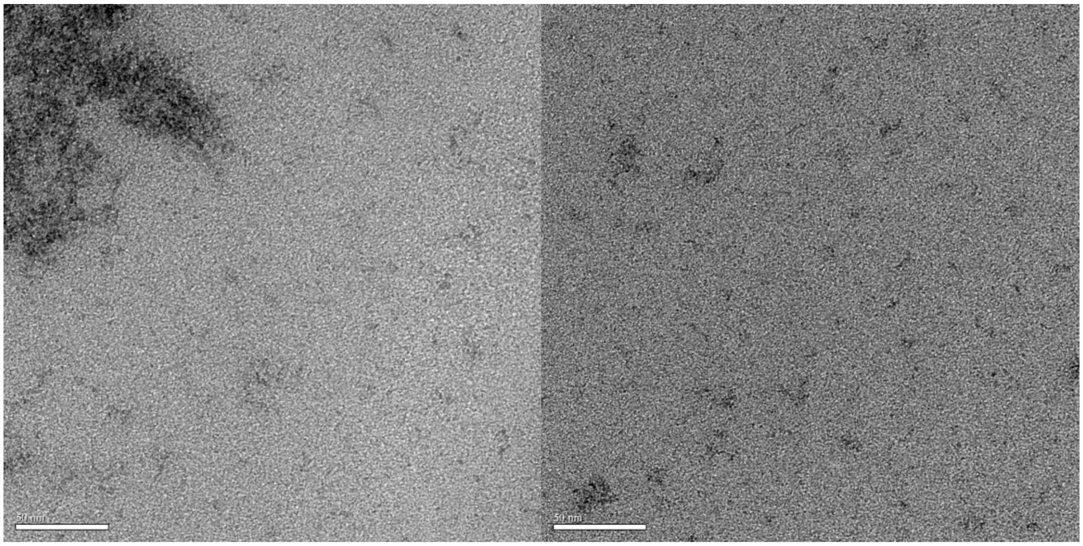

Scale bar: 50 nm.

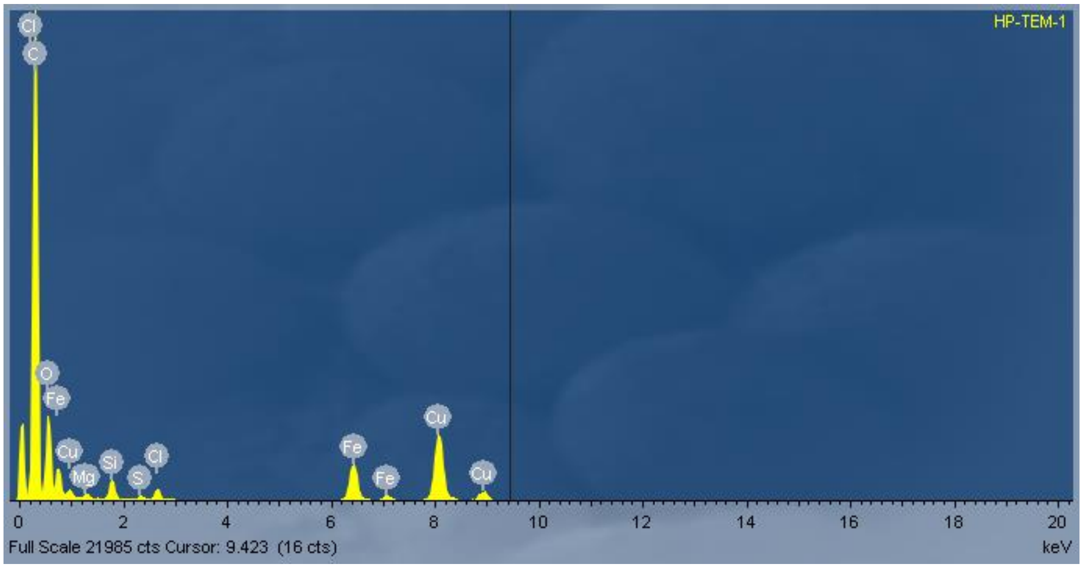

Figure 3: TEM and EDX analysis of nanoparticles in aqueous TPGS-750-M solution (with $NaBH_4$)

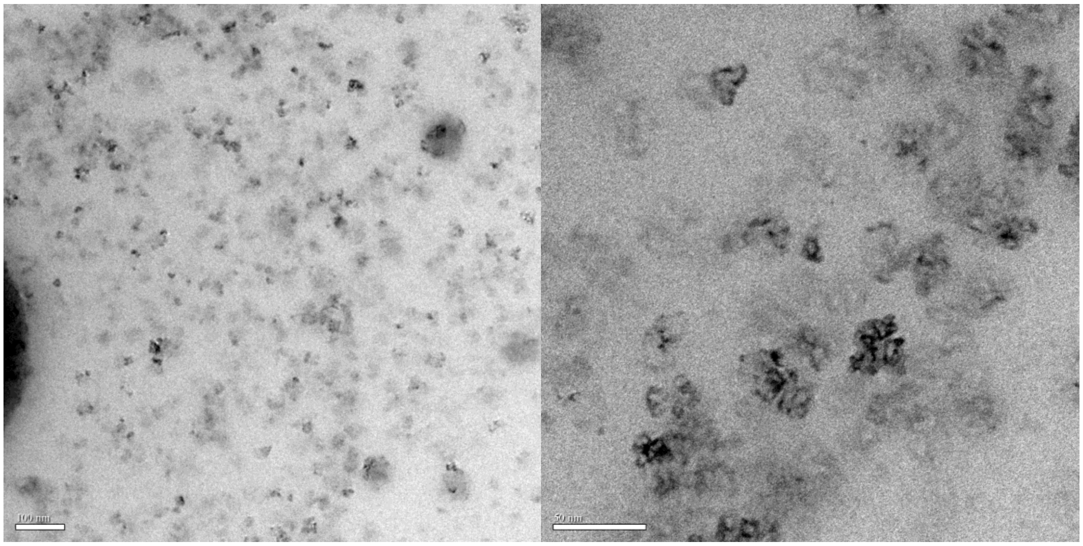

Scale bar: (1) 100 nm; (2) 50 nm.

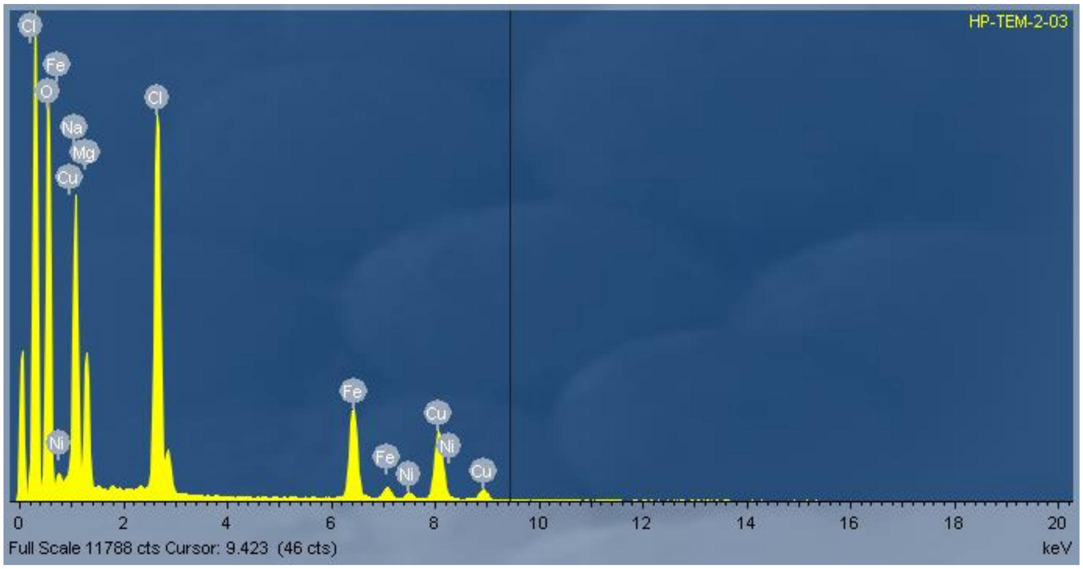

Discussion on substrate scope

To assess the scope of this technology, an expansive study was undertaken examining several types of nitroarenes and -heteroarenes. Under standard conditions (i.e., 2 wt % TPGS-750-M/H_2O, $NaBH_4$ (3 equiv), 10% THF co-solvent at room temperature), most reactions took place quite smoothly and in excellent yields. Products containing substituents on the aromatic/hetroaromatic ring, including fluoro- (**10**), chloro- (**1**, **4**), bromo- (**2**, **7**, **10**, **14**), trifluoromethyl- (**12**, **17**, **18**), chlorodifluoromethoxy- (**23**), were formed without incident. Reduction in the presence of other functionality, such as ester (**25**, **26**), amide (**6**, **11**, **12**, **13**, **14**, **16**, **19**, **21**, **25**), sulfonyl- (**15**), thio- (**3**, **24**), hydrazinyl- (**22**, **27**), as well as C-C double bonds (**25**), likewise, occurred smoothly. Heterocycles including pyridine (**7**, **18**), isoxazole (**19**), quinoline (**13**), piperazine (**12**), piperidine (**20**), morpholine (**21**) were all tolerated, strongly suggesting potential applications to targets in the pharmaceutical and agrochemical arenas. By contrast, reactions run under identical conditions but in pure THF were extremely slow, with 4-chloronitrobenzene affording the targeted product to the extent of only 27% after 16 hours.

Table 11: Representative hydrogenation of nitroarenes

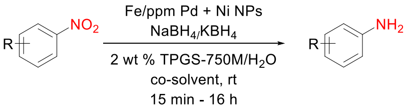

R
NO_2
Fe/ppm Pd + Ni NPs
$NaBH_4$/KBH_4
2 wt % TPGS-750M/H_2O
co-solvent, rt
15 min - 16 h
R
NH_2

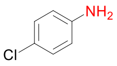

1 15 min, 96 %

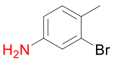

2 30 min, 98 %

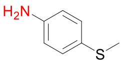

3 2 h, 88 %

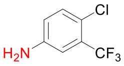

4 30 min, 98 %

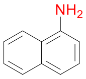

5 30 min, 99 %

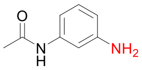

6 30 min, 98 %

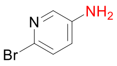

7 15 min, 94 %

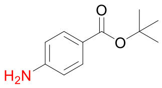

8 2 h, 98 %

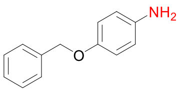

9 10 h, 86 %
16 h, 96 %

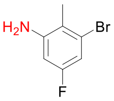

10 4 h, 90 %

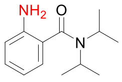

11 2 h, 98 %[c]

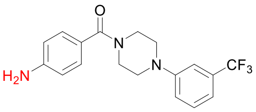

12 2 h,88 %

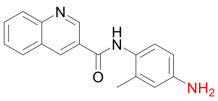

13 16 h, 80 %[d]

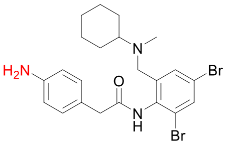

N
H_2N
Br
O
N
H
Br

14 2 h, 84 %[e]

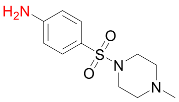

15 16 h, 98 %[f]

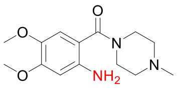

16 16 h, 83 %[g]

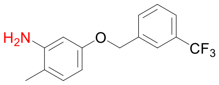

17 16 h, 96 %[h]

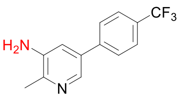

18 6 h, 74 %[i]
16 h, 86 %

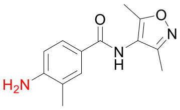

19 6 h, 96 %[d]

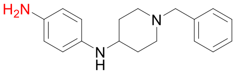

20 16 h, 92 %[j]

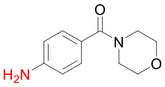

21 30 min, 99 %

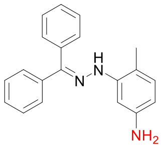

22 16 h, 95 %[k]

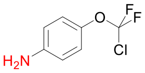

23 30 min, 91 %

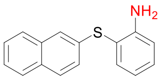

24 16 h, 92 %[l]

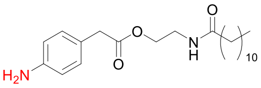

O
O
N
H
O
10
H_2N

25 8 h, 92 %[m]

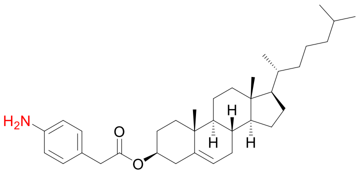

26 4 h, 95 %[n]

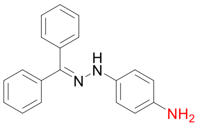

27 16 h, 99 %[o]

[a]Reaction conditions: nitro compound (0.5 mmol), Fe nanoparticles (6 mg, 2% Fe, 80 ppm Pd, 1600 ppm Ni), $NaBH_4$ (1.5 mmol), 2 wt % TPGS-750-M/H_2O (1 mL), THF (0.1 mL); [b]Isolated yield; [c]nitro compound (0.125 mmol), Fe nanoparticles (3 mg), $NaBH_4$ (0.375 mmol), 2 wt % TPGS-750-M/H_2O (1 mL), THF (0.1 mL); [d]DMSO (0.25 mL); [e]nitro compound (0.125 mmol), Fe nanoparticles (3 mg), $NaBH_4$ (0.375 mmol), 2 wt % TPGS-750-M/H_2O (1 mL), THF (0.3 mL); [f]nitro compound (0.25 mmol), Fe nanoparticles (3 mg), $NaBH_4$ (0.75 mmol), TPGS-750-M/H_2O (1 mL), THF (0.1 mL); [g]nitro compound (0.25 mmol), Fe nanoparticles (3 mg), $NaBH_4$ (0.75 mmol), TPGS-750-M/H_2O (1 mL), CH_3OH (0.25 mL); [h]nitro compound (0.5 mmol), Fe nanoparticles (12 mg), $NaBH_4$ (3 mmol), 2 wt % TPGS-750-M/H_2O (1 mL), DCM (0.1 mL); [i]THF (0.25 mL); [j]nitro compound (0.5 mmol), Fe nanoparticles (12 mg), KBH_4 (3 mmol), 2 wt % TPGS-750-M/H_2O (1 mL), THF (0.25 mL); [k]nitro compound (0.125 mmol), Fe nanoparticles (1.5 mg), KBH_4 (0.375 mmol), 2 wt % TPGS-750-M/H_2O (1 mL), DMSO (0.25 mL); [l]nitro compound (0.125 mmol), Fe nanoparticles (2.5 mg), KBH_4 (0.75 mmol), 2 wt % TPGS-750-M/H_2O 1 mL, DMSO 0.25 mL; [m]nitro compound (0.25 mmol), Fe nanoparticles (2.5 mg), KBH_4 (0.75 mmol), 2 wt % TPGS-750-M/H_2O (1 mL), THF (0.25 mL); [n]nitro compound (0.25 mmol), Fe nanoparticles (3 mg), $NaBH_4$ (0.75 mmol), 2 wt % TPGS-750-M/H_2O (1 mL), DCM (0.3 mL); [o]nitro compound (0.125 mmol), Fe nanoparticles (1.5 mg), KBH_4 (0.75 mmol), 2 wt % TPGS-750-M/H_2O (1 mL), THF (0.25 mL).

Several of the examples studied (Table 11) presented special challenges due to the nature of nitro compounds that can be highly crystalline, and/or flocculent solids and therefore, slow to gain entry to the inner micellar cores. This usually happened for substrates with higher molecular mass. During the hydrogenation process, these substrates often brought up some practical issues, such an adherence to the stir bar, or formation of insoluble gums. Varying amounts of a co-solvent, as well as changing the reaction concentration were frequently applied as solutions to those problems. Some hydrogenations of nitroaromatics led to higher yields with varying percentages of THF, such as for products **14**, **18**, **20**, **25** and **27**. For some insoluble or much more polar substrates, using more polar co-solvents such as MeOH (see **16**) and DMSO (see **13**, **19**, **22**, **24**) were found to also lead to clean overall primary amine formation. It was worth noting that not only the water-miscible organic solvents but also water-immiscible counterparts could still be used as co-solvent in these reactions. For compounds **17** and **26**, it was shown that compared with THF, DMSO and MeOH, dichloromethane was the best co-solvent for these nitro group reductions. Furthermore, lowering the global concentration from 0.5 to 0.25, or even to 0.125 M also occasionally was beneficial (see **11**, **14**, **15**, **16**, **22**, **24**, **25**, **26**, **27**). Typically, $NaBH_4$ was used to generate the Pd-H species, although on occasion, KBH_4 led to a more effective reduction, as noted previously by Gallou and co-workers.[32] During expansion of the substrate scope, these nanoparticles were found to not lose their activity for several months when stored at room temperature and without protection from air. Should these NPs turn from yellow-brown to orange upon exposure to air over time, there is no loss in activity since the $NaBH_4$ in the pot quickly converts them back to their active form.

Although these NPs have high activity towards hydrogenation of nitroarenes, along with broad functional group tolerance, no reaction is perfect, and there are limitations to these reductions as well. Firstly, due to their high activity towards hydrogenation, some reducible functional groups, such as alkynes, are not tolerated in this process. Several attempts to reduce prop-2-yn-1-yl 3-methyl-4-nitrobenzoate to the corresponding aniline, gave a messy reaction. After isolation, only 23% of propyl 4-amino-3-methylbenzoate was obtained. Clearly, the alkynes were reduced during the hydrogenation of the nitro groups.

Secondly, these reactions require excess $NaBH_4$ as reductant in the aqueous phase, which leads to relatively strongly basic media. Some functional groups which could be hydrolyzed in base, such as certain esters, also would not survive such conditions. An attempt to reduce 4-cyanophenyl 2-(4-nitrophenyl)acetate did not afford the corresponding aniline. Instead, 4-hydroxybenzonitrile, resulting from hydrolysis of starting material was isolated. Similar results were found upon exposure of 7-(benzyloxy)naphthalen-2-yl 2-nitrobenzoate as starting material. Clearly, the ester group is not stable in such reactions.

In addition, in cases where the nitro group was part of a conjugated network such that it has added electron density nearby (e.g., by an electron-rich functional group attached at an adjacent site), the activity of the catalyst towards hydrogenation is greatly diminished (Scheme 1). An attempt to hydrogenate 8-bromo-6-chloro-3-nitroimidazo[1,2-a]pyridine catalyzed by Fe/ppm (Pd + Ni) NPs (80 ppm Pd, 1600 ppm Ni) at room temperature in 2 wt % TPGS-750-M/H_2O and 15% THF with three equivalents of $NaBH_4$ gave only a 21% yield of product after a four hour period. Even with an extended reaction time up to sixteen hours, only 23% of corresponding aniline was obtained. From resonance associated with 8-bromo-6-chloro-3-nitroimidazo[1,2-a]pyridine, the nitro group is located where the electron density is relatively high. In addition, 4-(5-isopropoxy-2-methyl-4-nitrophenyl) pyridine, a compound from Novartis, met the same fate. Attempts to improve the yield by extending the reaction time, increasing $NaBH_4$ loading, using KBH_4, lowering the reaction concentration, and changing the co-solvent were all of no consequence. As for the structure for this starting material, the isopropoxy residue at the *ortho*-position relative to the nitro group is a relatively strong electron-donating group, which increases electron density at the nitro group. Therefore, regardless of conditions, the nanocatalyst was ineffective at reducing this substrate. As for why the Fe/ppm (Pd + Ni) NPs shows different activity on catalysis of hydrogenation towards electron-deficient and electron-rich nitroarenes, this analysis will be presented later along with a discussion on the mechanistic aspects associated with this nanocatalytic system.

Scheme 1: Failed hydrogenations on electron-rich nitro compounds

8-Bromo-6-chloro-3-nitroimidazo[1,2-a]pyridine:

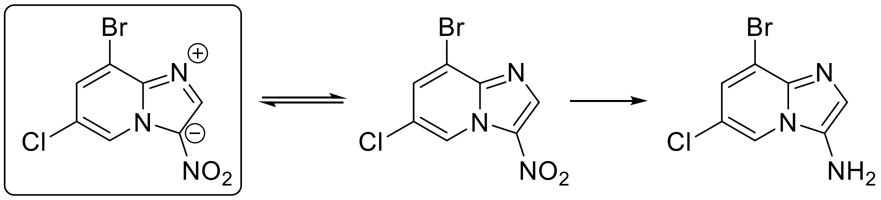

1. Fe-ppm (80 ppm Pd, 1600 ppm Ni), 3 equiv $NaBH_4$, 4 h, 15% THF.
Yield: 21%.
2. Fe-ppm (80 ppm Pd, 1600 ppm Ni), 3 equiv $NaBH_4$, 16 h, 15% THF.
Yield: 23%.

4-(5-Isopropoxy-2-methyl-4-nitrophenyl) pyridine:

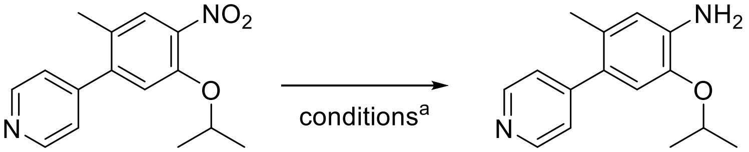

Entry	Modified conditions	Yield[b]
1	None	19
2	Extend the time to 4 hours	21
3	Extend the time to 6 hours	20
4	Extend the time to 16 hours	23
5	6 equiv $NaBH_4$ instead of 3 equiv	24
6	3 equiv KBH_4 instead of $NaBH_4$	23
7	Lower the reaction concentration to 0.25 M	13
8	DMSO as co-solvent	19
9	MeOH as co-solvent	17
10	DMF as co-solvent	21

[a]Original conditions: nitro compounds (0.5 mmol, 1 equiv), Fe/ppm (Pd + Ni) (6 mg, 80 ppm Pd, 1600 ppm Ni), $NaBH_4$ (1.5 mmol, 3 equiv), 2 wt% TPGS-750-M/H_2O 1 mL, 10% THF for 2 h; [b]Yield from GC-MS.

E Factor, Recycling, and Residual Metals in the products

Green chemistry was advanced by Anastas at the US Environmental Protection Agency (EPA), and Warner in the 1990's.[33] These ideas were formulated to help focus attention on the many environmental problems resulting from generation of chemical products and the processes by which they are produced. These concepts were embodied in the 12 Principles of Green Chemistry, including: (1) waste prevention; (2) atom economy; (3) less hazardous chemical synthesis; (4) designing safer chemicals; (5) safer solvents & auxiliaries; (6)

design for energy efficiency; (7) use of renewable feedstocks; (8) reduce derivatives; (9) catalysis; (10) design for degradation; (11) real time pollution prevention; (12) safer chemistry for accident prevention. These Principles are mutually interlinked. In general, the aim is to achieve efficient use of raw materials to manufacture chemical products directly. In this process, energy and resources are conserved, waste is eliminated, and toxic or dangerous reagents and solvents are avoided. In order to assess the environmental acceptability of a manufacturing processes, Sheldon and co-workers proposed the E(nvironmental) Factor in 1992, which is equal to the mass of waste divided by the mass of the product.[34] A higher E Factor means more pollution. On the contrary, a lower E Factor means less waste; consequently, a more environmentally friendly process. In the original research on the E Factors, solvent was assumed to be recovered and reused by distillation. However, in the following tests, chemists found out that the use of diverse organic solvents in various steps made isolation of pure solvents difficult owing to cross contamination, so that the cost of recycling was greatly increased. Moreover, according to an investigation by the ACS Green Chemistry Institute (GCI) Pharmaceutical Round Table, organic solvents are the major contributing item to the determination of E Factors in pharmaceutical manufacturing processes (see the Green Chemistry Institute website). However, there is one exception to these numbers in that water generally excluded from the calculation of E Factors. Since water can oftentimes be used to such a large degree during workup, its inclusion in the determination of E Factors tends to skew these numbers to such a degree that Sheldon chose to ignore water. Sheldon said ‘The best solvent is no solvent and if a solvent (diluent) is needed then water has much to offer: it is non-toxic, non-inflammable, abundantly available and inexpensive.’[35] There is little doubt that our use of aqueous micellar media lowers E Factors in all of its uses, including the hydrogenation process. In order to determine the E Factor associated with this new chemistry, where no organic solvent is involved, 1-chloro-4-nitro-2-(trifluoromethyl)benzene was chosen as starting material to be used at a global concentration of one molar (Scheme 2). For the calculation of an E Factor without water in the equation, only the ethyl acetate for extraction purposes was considered to be part of the equation. The E Factor, therefore, based on organic solvent(s) used is only 3.9, which is quite low and reflects the limited solvent needed to remove the product from the reaction mixture. Even with water counted, the E Factor is only 9.2.

Scheme 2: E Factor of such reaction

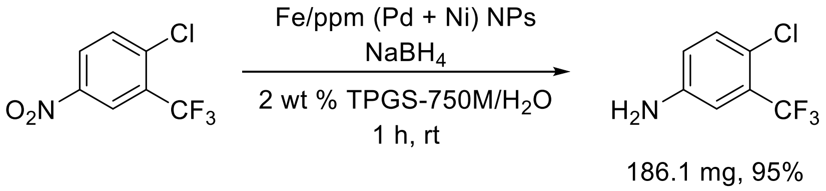

E factor calculation (without water)

$$\text{E factor} = \frac{\text{Mass of organic waste}}{\text{Mass of pure product}} = \frac{\text{Mass of EtOAc}}{\text{Mass of pure product}} = \frac{721\ \text{mg}}{186.1\ \text{mg}} = 3.9$$

E factor calculation (with water)

$$\text{E factor} = \frac{\text{Mass of (organic waste + water)}}{\text{Mass of pure product}} = \frac{\text{Mass of (EtOAc + water)}}{\text{Mass of pure product}} = \frac{721\ \text{mg} + 1000\ \text{mg}}{186.1\ \text{mg}} = 9.2$$

It is notable that this approach is a combination of a heterogeneous catalyst being used in an aqueous phase reaction. The products could be easily extracted by organic solvent with the nanocatalyst left in the aqueous layer. It is also the advantage of heterogeneous catalysis compared with homogeneous catalysis, in that the catalyst and the reaction products can be separated easily. Hence, the nanocatalyst can also be recovered to some extent in a relatively active form, even though the possibility exists for activity lowering owing to leaching of the catalytic metal and degradation of the total catalyst. On the other hand, due to water as the reaction medium, it can easily be reused, along with the dissolved surfactant, after extraction of the product by an organic solvent, such as ethyl acetate (EtOAc) or methyl *tert*-butyl ether (MTBE). In studying recycling of this new reagent, 1-chloro-4-nitro-2-(trifluoromethyl)benzene was selected as substrate. Initially, EtOAc was chosen as the solvent for extraction of product, as done previously. However, by even adding excess fresh nanocatalyst, subsequent next recycle reactions could not be driven to completion. Hence, a control experiment was conducted: 1.0 mL of an aqueous solution of 2 wt % TPGS-750-M was added in a 4 mL microwave reaction vial containing a magnetic stir bar followed by addition of 0.5 mL of EtOAc. After stirring for one minute, the organic layer on the top was then separated (with the aid of a centrifuge, if needed), after which it was removed via pipette. The same extraction procedure was repeated three times. At that time, it was found that the clear aqueous TPGS-750-M solution had become a cloudy emulsion. Subsequently, the formed emulsion was used as reaction medium for a fresh hydrogenation of nitroarene with nanocatalyst. The yield was greatly reduced, even under the same reaction conditions. This indicated that there was some EtOAc left in the aqueous phase after extraction because EtOAc is slightly soluble in water (8.3 g/100 mL at 20 °C), which may compete with the substrate for occupancy inside the micelle structure, leading to reduced levels of conversion of the same time frame. Hence, MTBE was chosen as solvent for extraction instead of EtOAc owing to its lower solubility in water (2.6 g/100 mL). This time, after stirring and separation, the solvent was still clear without formation of an emulsion formed, leading to no obvious effect on yield reduced nitroarene. Based on this result, MTBE was chosen as the solvent for extraction for the study on recycling.

After solving the issue of which solvent to use for extraction, a recycling study was initiated. To begin with, the intention was to recover and reuse 100% of the nanocatalyst, meaning that no additional fresh nanocatalyst was to be added in each recycle. Unfortunately, the yield was found to decrease with each recycle, which indicated that the activity of the nanocatalyst was lowered, although the reasons for these observations remain unclear. One possibility is leaching of the catalytic metal and/or degradation of the initially formed catalyst. To guarantee efficiency of reaction in each recycle, some fresh nanocatalyst was introduced before each additional reaction. After optimization regarding the quantity of nanocatalyst re-added in each recycle, and with reaction times extended, one third of the initial amount of nanocatalyst was recharged with each recycle, leading to complete hydrogenation of nitroaromatics under the same reaction conditions (Scheme 3).

Scheme 3: Study of recycle

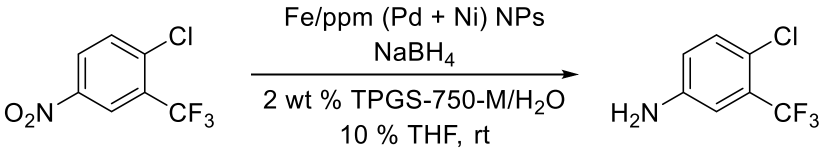

Reaction	Isolated Yield (mg)	Percent Yield (%)
Initial reaction[a]	95.7	98
1st recycle[b]	94.8	97
2nd recycle[b]	93.1	95
3rd recycle[b]	93.3	96
4th recycle[b]	94.5	97

[a]Nitro compounds (0.5 mmol), Fe/ppm (Pd + Ni) (5.7 mg, 80 ppm Pd, 1600 ppm Ni), $NaBH_4$ (1.5 mmol), 2 wt% TPGS-750-M/H_2O (1 mL), THF (0.1 mL) for 0.5 h; [b]Nitro compounds (0.5 mmol), Fe/ppm (Pd + Ni) (5.7 mg, 80 ppm Pd, 1600 ppm Ni), $NaBH_4$ (1.5 mmol), THF (0.1 mL) for 1 h.

Another important aspect of this protocol concerns the amounts of residual metal to be expected in the product from reductions of nitroarenes. Established guidelines for allowable levels of transition metal impurities vary as a function of levels of toxicity. Residual Fe is considered relatively innocuous (limit: 1300 ppm), while limits for both Ni (25 ppm) and especially Pd (10 ppm) are far more rigorous.[36] Metal impurties that exceed these levels require additional time, effort, and cost to have them removed or at least, reduced to allowable levels.

Analyses were conducted on several products resulting from Fe/ppm (Pd + Ni) NP-catalyzed nitro group reductions by inductively coupled plasma mass spectrometry (ICP-MS). Results showed residual palladium to be below 10 ppm, while residual nickel was below 1 ppm (Table 12). Residual iron was also measured and found to be below 5 ppm, implying in the composite that release of any metal from these NPs is minimal.

Table 12: Pd, Ni and Iron residue in the product

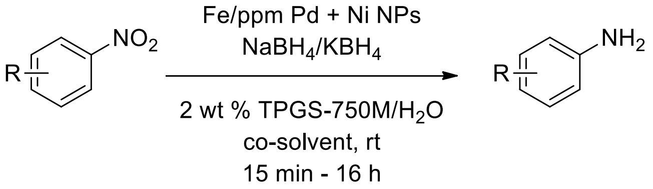

substrate	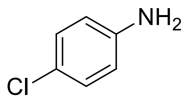	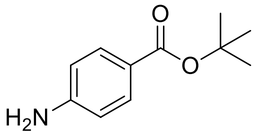	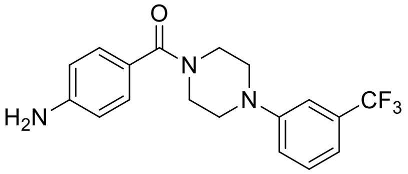
Pd Residue	=< 10 ppm	---	---
Ni Residue	=< 1 ppm	1 ppm	1 ppm

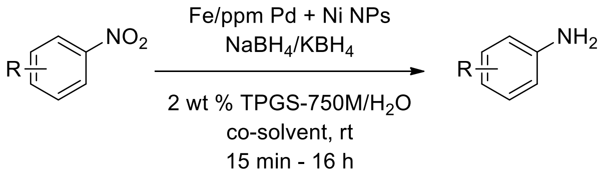

substrate	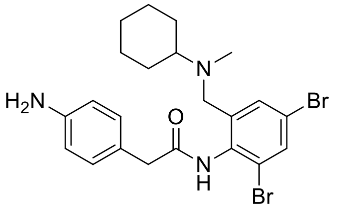	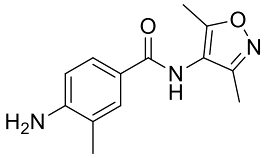
Fe Residue	=< 5 ppm	=< 5 ppm

One-pot sequences

In the 12 Principles of Green Chemistry, waste prevention and design for energy efficiency are two important aspects. On the other hand, multi-step synthesis is widely used in the manufacturing and pharmaceutical industry. Given the increasing number of key synthetic transformations that can now be run under mild conditions in aqueous media using micellar technology,[24] in order to save the reaction medium and reduce the separation cost, one-pot reaction sequences can be planned that take advantage of the commonality of this reaction medium. Initially, attempted hydrogenation of 1-(diphenylmethylene)-2-(2-methyl-5-nitrophenyl)hydrazine with Fe/ppm (Pd + Ni) NPs was to arrive at the corresponding aniline, followed by use of the Cbz group to protect the amine, and thence Fishier indole reaction to get the indole derivative. From the first and second step run under aqueous micellar conditions, the product was obtained in excellent yield (>95%). However, subsequent trials to form benzyl (3-(2-(diphenylmethylene)hydrazineyl)-4-methylphenyl)-carbamate together with 4-methylhexanone (1.1 equivalent) in order to arrive at the corresponding indole derivative (catalyzed by H_2SO_4; 5 equivalents at 80 °C for 14 hours), none of the product was obtained. According to TLC, what remained was a significant amount of benzyl (3-(2-(diphenylmethylene)hydrazineyl)-4-methylphenyl)carbamate in the reaction mixture. Based on the mechanism, as shown in Scheme 4, the concentration of sulfuric acid or 4-methylhexanone may have been too low to get the reaction to move forward. Hence, the amount of 4-methylhexanone was increased from 1.1 to 5 equivalents, the amount of H_2SO_4 from 5 to 20 equivalents, the reaction time was also increased from 14 hours to 48 hours. However, no improvement in the reaction was found. Therefore, it was a possibility that indolization might not take place in aqueous micelles. In order to verify if the aqueous phase could accommodate the indole reaction, a control experiment was run with the same starting materials catalyzed by 10 equivalents 4-methylbenzenesulfonic acid (TsOH) at 78 °C in EtOH over 12 hours. After the reaction, the (3-(2-(diphenylmethylene)hydrazineyl)-4-methylphenyl)carbamate had been consumed, but the main product was only benzophenone and no indole derivative was detected. This result indicated that the (3-(2-(diphenylmethylene)hydrazineyl)-4-methylphenyl)carbamate could not form the corresponding indole even in organic solvent under typical cyclization conditions. Perhaps steric hindrance associated with the -NHCbz was too great; that it might prevent the Fishier indole reaction from happening.[37] Hence, a sterically smaller acetyl group was used to protect the amino group. Nonetheless, the desired indole derivative with N-(3-(2-(diphenylmethylene)hydrazineyl)-4-methylphenyl)acetamide as the starting material in organic solvent (THF) could not be obtained. This necessitated closer scrutiny of the structure of (3-(2-(diphenylmethylene)hydrazineyl)-4-methylphenyl)carbamate.

Scheme 4: Mechanism of Fishier indole step

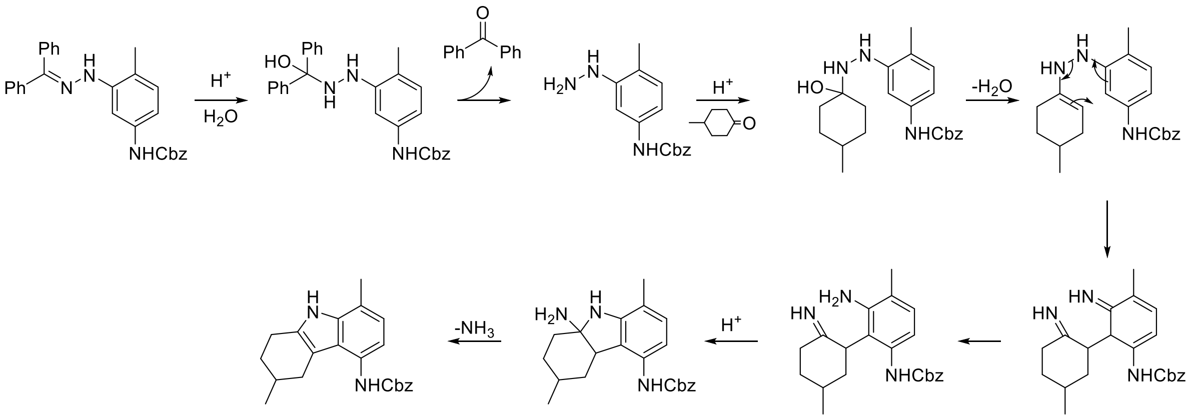

Since the hydrazine residue is on position 3 and the methyl group is on position 4, the indole can only form at position 2. But with the amino group on position 1, independent of the protection group placed on the amine, there is always steric hinderance gaining access to position 2, and hence, preventing indole formation. Use of 1-(diphenylmethylene)-2-(4-nitrophenyl)hydrazine as starting material, on the other hand, where the formed amino group is located at the *para*-position of the hydrazine moiety, there are no substituents on the two *ortho*-positions. So, steric hindrance on the indole reaction is completely eliminated. The sequence, therefore, was designed as shown in Scheme 5. The first step and the second step could still run smoothly in aqueous micelles. The third step, however, only gave a 23% yield of the desired indole derivative, with >60% benzyl (4-(2-(diphenylmethylene)-hydrazineyl)phenyl)carbamate remaining after a 12-hour reaction period, even with five equivalents of 4-methylhexanone present. Further extension of time or changes to the type of the acid were not helpful for conversion. Raising the temperature from 70 °C to 85 °C was attempted, but the carbamate group was not stable in hot water with pH = 1. In view of these failures, it was concluded that the Fishier indole reaction does not work well in aqueous micellar media. Therefore, before the third step, the water was removed from the reaction mixture and THF was added as the solvent for the third step, leading to the targeted indole in 70% overall yield.

Scheme 5: The alternative first 1-pot sequence

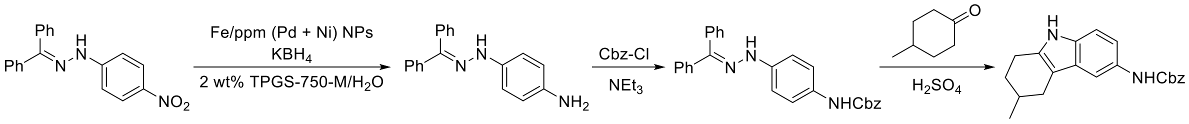
Fe/ppm (Pd + Ni) NPs
KBH_4
2 wt% TPGS-750-M/H_2O
Cbz-Cl
NEt_3
H_2SO_4
Ph
H
N
NO_2
NH_2
NHCbz

The second one-pot sequence was planned in Scheme 6. Initially, converts 4-chloronitorbenzene to its aniline derivative. And the obtained aniline could be used as nucleophile in the subsequent S_NAr addition followed by a Suzuki-Miyaura coupling to afford the final product. The first and second step ran smoothly without any problem in the aqueous micellar media. For the third step, optimizations palladium source, palladium loading and boronic acid equivalent led to the target compound in 94% overall yield.

Scheme 6: The second 1-pot sequence

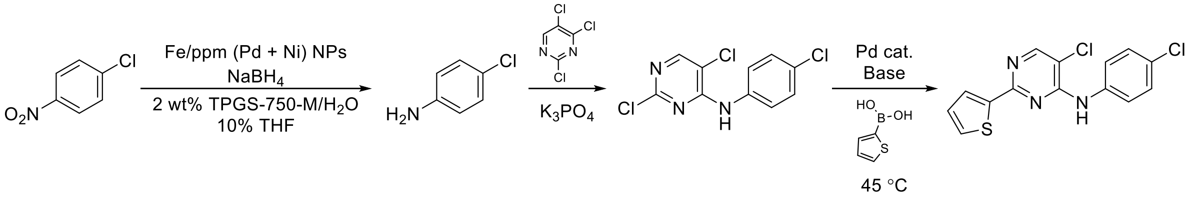
Fe/ppm (Pd + Ni) NPs
$NaBH_4$
2 wt% TPGS-750-M/H_2O
10% THF
K_3PO_4
Pd cat.
Base
HO B-OH
45 °C
O_2N
H_2N
Cl
N
H
S

Studies on the mechanism of nitro group reductions

The mechanism for reductions of nitroarenes has been fully investigated, as discussed in the Introduction. However, the explanation as to why the activity of these nanoparticles could be improved upon doping with nickel still needed to be further elucidated. Before discussing the mechanism of this hydrogenation, some additional details which may provide insight include: 1) when $NaBH_4$ was added to activate the nanocatalyst, a lot of hydrogen gas was generated quickly; 2) during the hydrogenation process, the obtained yield was reduced if the reaction vessel was not sealed well; 3) this chemistry worked better on electron-deficient nitro groups than on electron-rich nitro groups. In addition to these details, X-ray absorption spectroscopy (XAS) was utilized to detect the interaction between Pd and Ni atoms in the amorphous nanomaterial. Two nanomaterials were prepared by reduction of Fe/ppm Pd NPs or Fe/ppm (Pd + Ni) NPs with excess $NaBH_4$ in water. After evaporation and drying under vacuum, the obtained black powders were sent to Argonne National Labs to obtain data by XAS analyses (X-ray Absorption Spectroscopy).

XAS experiments were performed at the insertion device (Sector 10 BM) of the Materials Research Collaborative Access Team (MR-CAT) at the Advanced Photon Source of Argonne National Laboratory. A Si (111) monochromator with a cryo-cooled first crystal and a 250 mm long second crystal were used to provide Pd K edge energy (24350 eV). Harmonic interference was removed by using a 60 cm long flat harmonic rejection mirror with Pt and Rh coatings. Due to the ppm level of Pd loading of the samples, all XAS measurements were done using a 19-element solid-state detector in fluorescence mode. The samples were first finely ground inside an Argon glovebox with/without addition of boron nitride as a diluent to obtain close to an edge step of 1. The mixture was then pressed into a fluorescence sample holder. The sample holder was then transferred to a 10-inch quartz tube (1 in ID) sealed with Kapton windows by two Ultra-Torr fittings attached to three-way valves. The sample tube was then moved to the beamline hutch and flushed with 50 ml/min He prior to the XAS measurement. The beamline was calibrated using a Pd foil and the foil spectrum was collected simultaneously with the samples to correct the edge energies of each sample. Background removal and normalization procedures were carried out using the Athena and Artemis software package to obtain k and r space of the sample spectra.

X-ray absorption near edge structure (XANES) spectra of the samples (activated by $NaBH_4$) were also collected at the Pd-K edge, as shown in Figure 4, which can help determine the oxidation state of Pd. The Pd edge energies of the PdFe and PdFeNi systems were observed to be close to that of Pd Foil (Pd^0), indicating that all the Pd sites are in their most reduced state after activation with $NaBH_4$.

Figure 4: XANES of the Fe/ppm Pd material and Fe/ppm (Pd + Ni) material

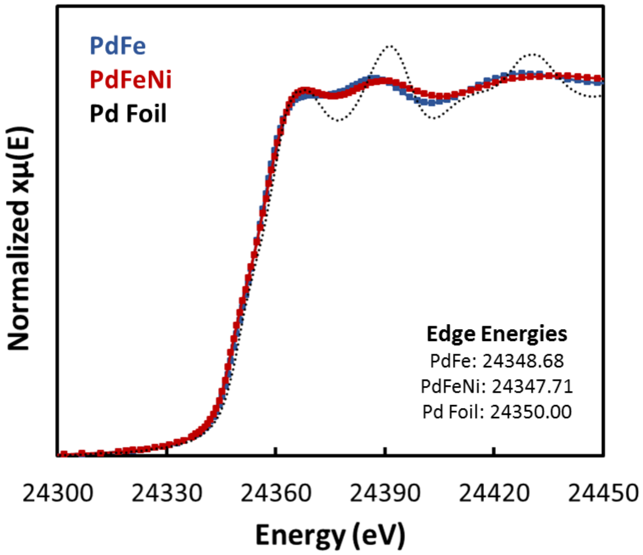

Extended X-ray Absorption Fine Structure (EXAFS) spectra of the samples (activated by $NaBH_4$) collected at the Pd-K edge compared to (a) Pd Foil (b) Pd-Pd single scattering at 2.69 Å. These figures show the presence of a Pd-Pd EXAFS feature in PdFe and the absence of this feature in the presence of Ni. This suggests that the Pd and Ni may form Pd-Ni combination instead of Pd-Pd in the activated Fe/ppm Pd + Ni reagent.

Figure 5: EXAFS of the Fe/ppm Pd material and Fe/ppm (Pd + Ni) material

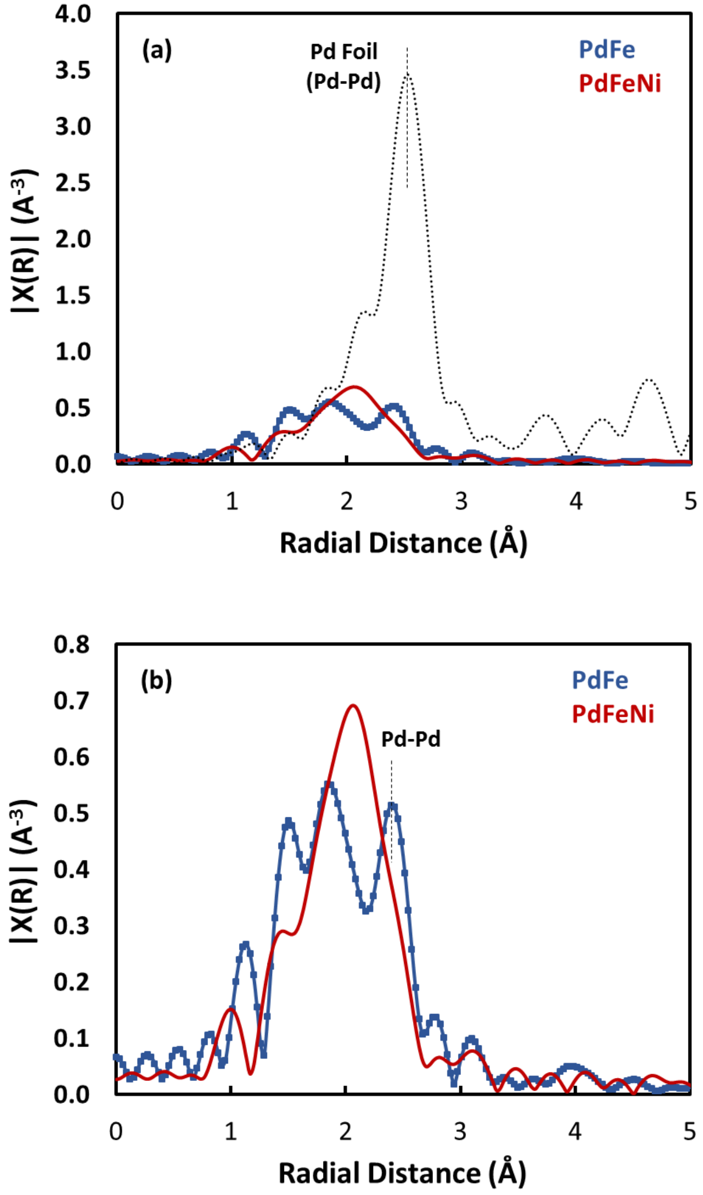

Scheme 7: Proposed mechanism

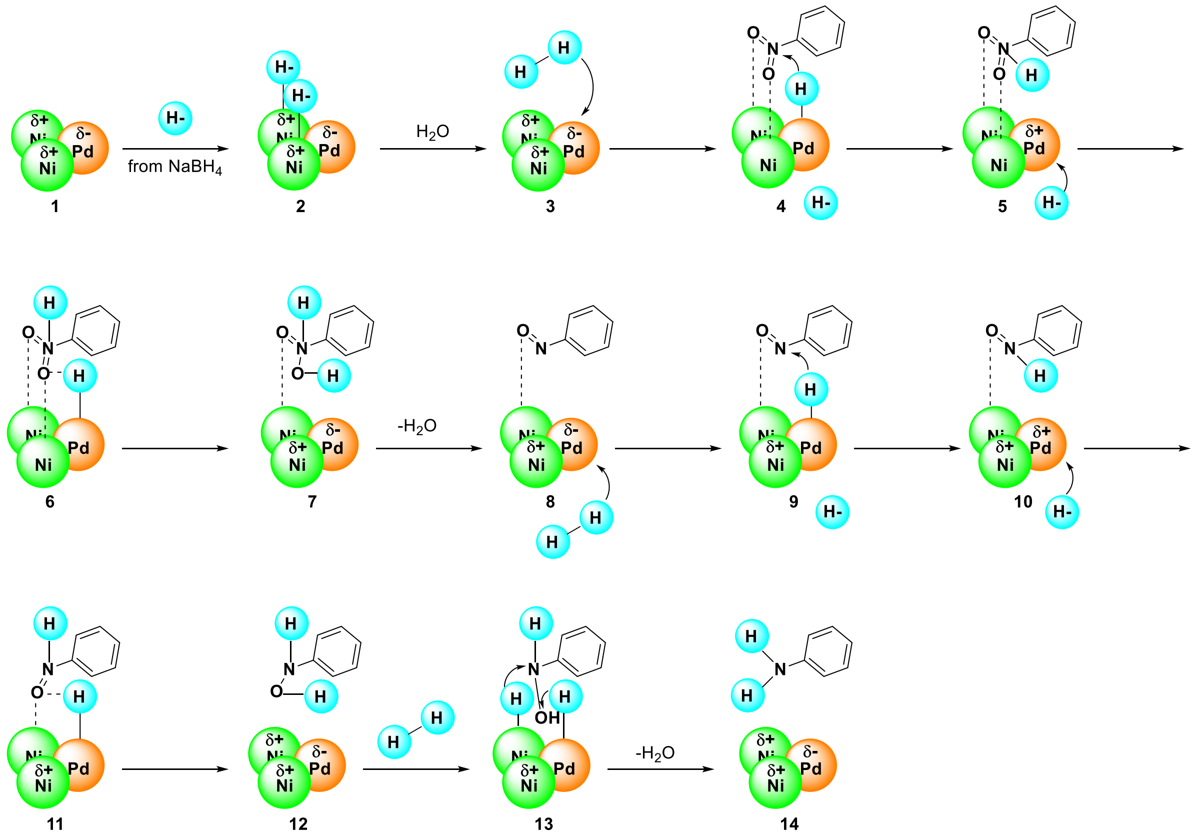

Based on research by Lee and co-workers,[38] the proposed mechanism is shown in Scheme 7. The δ^+/δ^- signs in the illustration represent the localized electron charge in the molecules or bimetallic structure. From **1** to **3**, there was a large quantity of hydrogen formed from $NaBH_4$ being added to the nanoparticles in an aqueous medium. In the following steps, the nitroarene which can be absorbed is reduced to obtain intermediate nitroso (**8**) and hydroxylamine (**12**), which can be further reduced to the corresponding aniline (**14**) directly. Nickel-doped Fe/ppm Pd nanoparticles show greater reactivity on hydrogenation of nitro compounds than the original counterpart, which may be accounted for based on the following reasons:

1) From **1** to **3**, the localized electron charge in the bimetallic nanoparticle is helpful for the generation of hydrogen, which may be the actual reductant in these reactions. This can also explain why the reaction needs to be run in a well-sealed system.
2) From **4** to **6**, the localized positive charge on the Ni in the bimetallic system has electronic interactions with a nitro group, as shown in the Scheme, so that adjacent nitro groups can be easily absorbed on the surface of the nanocatalyst to facilitate the ensuing reduction.
3) In **4** and **9**, using the reduction process of the nitroarene and nitroso derivative, the nitrogen atom can be attacked by the H^- attached to palladium. Hence, this step can be deactivated if the electron cloud on the nitrogen in the nitro group has greater density, which can also explain why the electron-deficient nitro group reduces far more readily than an electron-rich nitro group.

Conclusions

In summary, a new catalyst useful for nitro group reductions in water has been uncovered that contains ppm levels of both Pd and Ni that work in harmony to afford greater reactivity than that observed using related catalysts based on either individual metal. The process is safe, takes place in water under mild conditions, and allows for facile in-flask product isolation as well as recycling of the entire aqueous reaction mixture. The mechanism was proposed to explain the higher reactivity of the bimetallic nanocatalyst towards hydrogenation of nitroaromatics. Very low levels of residual metals are found in the isolated products, further enhancing the attractiveness of this environmentally responsible technology.

References

1. Feng, J.; Handa, S.; Gallou, F.; Lipshutz, B. H. Safe and Selective Nitro Group Reductions Catalyzed by Sustainable and Recyclable Fe/ppm Pd Nanoparticles in Water at Room Temperature. *Angew. Chem., Int. Ed.* **2016**, *55*, 8979.

2. Westerhaus, F. A.; Jagadeesh, R. V.; Wienhöfer, G.; Pohl, M.-M.; Radnik, J.; Surkus, A.-E.; Rabeah, J.; Junge, K.; Junge, H.; Nielsen, M.; Brückner, A.; Beller, M. Heterogenized cobalt oxide catalysts for nitroarene reduction by pyrolysis of molecularly defined complexes. *Nat. Chem.* **2013**, *5*, 537.

3. Dell'Anna, M. M.; Intini, S.; Romanazzi, G.; Rizzuti, A.; Leonelli, C.; Piccinni, F.; Mastrorilli, P. Polymer supported palladium nanocrystals as efficient and recyclable catalyst for the reduction of nitroarenes to anilines under mild conditions in water. *J. Mol. Catal. A: Chem.* **2014**, *395*, 307.

4. Tuteja, J.; Nishimura, S.; Ebitani, K. Base-free chemoselective transfer hydrogenation of nitroarenes to anilines with formic acid as hydrogen source by a reusable heterogeneous Pd/ZrP catalyst. *RSC Advances* **2014**, *4*, 38241.

5. MacNair, A. J.; Tran, M.-M.; Nelson, J. E.; Sloan, G. U.; Ironmonger, A.; Thomas, S. P. Iron-catalysed, general and operationally simple formal hydrogenation using $Fe(OTf)_3$ and $NaBH_4$. *Org. Biomol. Chem.* **2014**, *12*, 5082.

6. Jagadeesh, R. V.; Wienhöfer, G.; Westerhaus, F. A.; Surkus, A.-E.; Pohl, M.-M.; Junge, H.; Junge, K.; Beller, M. Efficient and highly selective iron-catalyzed reduction of nitroarenes. *Chem. Commun.* **2011**, *47*, 10972.

7. Lu, H.; Geng, Z.; Li, J.; Zou, D.; Wu, Y.; Wu, Y. Metal-Free Reduction of Aromatic Nitro Compounds to Aromatic Amines with B_2pin_2 in Isopropanol. *Org. Lett.* **2016**, *18*, 2774.

8. He, L.; Wang, L.-C.; Sun, H.; Ni, J.; Cao, Y.; He, H.-Y.; Fan, K.-N. Efficient and Selective Room-Temperature Gold-Catalyzed Reduction of Nitro Compounds with CO and H_2O as the Hydrogen Source. *Angew. Chem., Int. Ed.* **2009**, *48*, 9538.

9. Junge, K.; Wendt, B.; Shaikh, N.; Beller, M. Iron-catalyzed selective reduction of nitroarenes to anilines using organosilanes. *Chem. Commun.* **2010**, *46*, 1769.

10. Verho, O.; Gustafson, K. P. J.; Nagendiran, A.; Tai, C.-W.; Bäckvall, J.-E. Mild and Selective Hydrogenation of Nitro Compounds using Palladium Nanoparticles Supported on Amino-Functionalized Mesocellular Foam. *ChemCatChem* **2014**, *6*, 3153.

11. Pedrajas, E.; Sorribes, I.; Gushchin, A. L.; Laricheva, Y. A.; Junge, K.; Beller, M.; Llusar, R. Chemoselective Hydrogenation of Nitroarenes Catalyzed by Molybdenum Sulphide Clusters. *ChemCatChem* **2017**, *9*, 1128.

12. Chen, X.-L.; Ai, B.-R.; Dong, Y.; Zhang, X.-M.; Wang, J.-Y. Hexafluoro-2-propanol-assisted quick and chemoselective nitro reduction using iron powder as catalyst under mild conditions. *Tetrahedron Lett.* **2017**, *58*, 3646.

13. Xu, Z.-b.; Lu, G.-p.; Cai, C. Palladium nanoparticles stabilized by aqueous vesicles self-assembled from a PEGylated surfactant ionic liquid for the chemoselective reduction of nitroarenes. *Catal. Commun.* **2017**, *99*, 57.

14. Liu, Z.; Dong, W.; Cheng, S.; Guo, S.; Shang, N.; Gao, S.; Feng, C.; Wang, C.; Wang, Z. Pd_9Ag_1-N-doped-MOF-C: An efficient catalyst for catalytic transfer hydrogenation of nitro-compounds. *Catal. Commun.* **2017**, *95*, 50.

15. Prathap, K. J.; Wu, Q.; Olsson, R. T.; Dinér, P. Catalytic Reductions and Tandem Reactions of Nitro Compounds Using in Situ Prepared Nickel Boride Catalyst in Nanocellulose Solution. *Org. Lett.* **2017**, *19*, 4746.

16. Liu, M.; Tang, W.; Xie, Z.; Yu, H.; Yin, H.; Xu, Y.; Zhao, S.; Zhou, S. Design of Highly Efficient Pt-SnO_2 Hydrogenation Nanocatalysts using Pt@Sn Core–Shell Nanoparticles. *ACS Catal.* **2017**, *7*, 1583.

17. Sorribes, I.; Liu, L.; Corma, A. Nanolayered Co–Mo–S Catalysts for the Chemoselective Hydrogenation of Nitroarenes. *ACS Catal.* **2017**, *7*, 2698.

18. Uberman, P. M.; García, C. S.; Rodríguez, J. R.; Martín, S. E. PVP-Pd nanoparticles as efficient catalyst for nitroarene reduction under mild conditions in aqueous media. *Green Chem.* **2017**, *19*, 739.

19. Huang, H.; Wang, X.; Li, X.; Chen, C.; Zou, X.; Ding, W.; Lu, X. Highly chemoselective reduction of nitroarenes over non-noble metal nickel-molybdenum oxide catalysts. *Green Chem.* **2017**, *19*, 809.

20. Tian, M.; Cui, X.; Yuan, M.; Yang, J.; Ma, J.; Dong, Z. Efficient chemoselective hydrogenation of halogenated nitrobenzenes over an easily prepared γ-Fe_2O_3-modified mesoporous carbon catalyst. *Green Chem.* **2017**, *19*, 1548.

21. Morse, J. R.; Callejas, J. F.; Darling, A. J.; Schaak, R. E. Bulk iron pyrite as a catalyst for the selective hydrogenation of nitroarenes. *Chem. Commun.* **2017**, *53*, 4807.

22. Ding, Z.-C.; Li, C.-Y.; Chen, J.-J.; Zeng, J.-H.; Tang, H.-T.; Ding, Y.-J.; Zhan, Z.-P. Palladium/Phosphorus-Doped Porous Organic Polymer as Recyclable Chemoselective and Efficient Hydrogenation Catalyst under Ambient Conditions. *Adv. Synth. Catal.* **2017**, *359*, 2280.

23. Sun, X.; Olivos-Suarez, A. I.; Oar-Arteta, L.; Rozhko, E.; Osadchii, D.; Bavykina, A.; Kapteijn, F.; Gascon, J. Metal–Organic Framework Mediated Cobalt/Nitrogen-

Doped Carbon Hybrids as Efficient and Chemoselective Catalysts for the Hydrogenation of Nitroarenes. *ChemCatChem* **2017**, *9*, 1854.

24. Kalbasi, R. J.; Nourbakhsh, A. A.; Babaknezhad, F. Synthesis and characterization of Ni nanoparticles-polyvinylamine/SBA-15 catalyst for simple reduction of aromatic nitro compounds. *Catal. Commun.* **2011**, *12*, 955.

25. Rai, R. K.; Mahata, A.; Mukhopadhyay, S.; Gupta, S.; Li, P.-Z.; Nguyen, K. T.; Zhao, Y.; Pathak, B.; Singh, S. K. Room-Temperature Chemoselective Reduction of Nitro Groups Using Non-noble Metal Nanocatalysts in Water. *Inorg. Chem.* **2014**, *53*, 2904.

26. Yang, S.-T.; Shen, P.; Liao, B.-S.; Liu, Y.-H.; Peng, S.-M.; Liu, S.-T. Catalytic Reduction of Nitroarenes by Dipalladium Complexes: Synergistic Effect. *Organometallics* **2017**, *36*, 3110.

27. Damodara, D.; Arundhathi, R.; Ramesh Babu, T. V.; Legan, M. K.; Kumpaty, H. J.; Likhar, P. R. Polymethylhydrosiloxane derived palladium nanoparticles for chemo- and regioselective hydrogenation of aliphatic and aromatic nitro compounds in water. *RSC Advances* **2014**, *4*, 22567.

28. Zhang, Y.-N.; Li, X.-H.; Cai, Y.-Y.; Gong, L.-H.; Wang, K.-X.; Chen, J.-S. Bio-inspired noble metal-free reduction of nitroarenes using NiS_{2+x}/g-C_3N_4. *RSC Adv.* **2014**, *4*, 60873.

29. Keshipour, S.; Adak, K. Pd(0) supported on N-doped graphene quantum dot modified cellulose as an efficient catalyst for the green reduction of nitroaromatics. *RSC Advances* **2016**, *6*, 89407.

30. Jagadeesh, R. V.; Natte, K.; Junge, H.; Beller, M. Nitrogen-Doped Graphene-Activated Iron-Oxide-Based Nanocatalysts for Selective Transfer Hydrogenation of Nitroarenes. *ACS Catal.* **2015**, *5*, 1526.

31. Jagadeesh, R. V.; Banerjee, D.; Arockiam, P. B.; Junge, H.; Junge, K.; Pohl, M.-M.; Radnik, J.; Brückner, A.; Beller, M. Highly selective transfer hydrogenation of functionalised nitroarenes using cobalt-based nanocatalysts. *Green Chem.* **2015**, *17*, 898.

32. Gabriel, C. M.; Parmentier, M.; Riegert, C.; Lanz, M.; Handa, S.; Lipshutz, B. H.; Gallou, F. Sustainable and Scalable Fe/ppm Pd Nanoparticle Nitro Group Reductions in Water at Room Temperature. *Org. Process Res. Dev.* **2017**, *21*, 247.

33. Anastas, P. T.; Warner, J. C. *Green Chemistry: Theory and Practice*. Oxford University Press, Oxford, 1998.

34. Sheldon, R. A. Organic Synthesis: Past, Present and Future. *Chem. Ind. (London),* **1992**, 903.

35. Sheldon, R. A. The E Factor: fifteen years on. *Green Chem.* **2007**, *9*, 1273.

36. Committee For Medicinal Products For Human Use (CHMP), *Guideline On The Specification Limits For Residues Of Metal Catalysts Or Metal Reagents*. London: European Medicines Agency, 2008.

37. Wagaw, S.; Yang, B. H.; Buchwald, S. L. A Palladium-Catalyzed Strategy for the Preparation of Indoles: A Novel Entry into the Fischer Indole Synthesis. *J. Am. Chem. Soc.* **1998**, *120*, 6621.

38. Nguyen, L. T. M.; Park, H.; Banu, M.; Kim, J. Y.; Youn, D. H.; Magesh, G.; Kim, W. Y.; Lee, J. S. Catalytic CO_2 hydrogenation to formic acid over carbon nanotube-graphene supported PdNi alloy catalysts. *RSC Advances* **2015**, *5*, 105560.

Appendix

General Remarks

A solution of 2 wt % TPGS-750-M/H_2O solution was prepared by dissolving TPGS-750-M in degassed HPLC grade water, and was stored under argon. TPGS-750-M was made as previously described[1] and is available from Sigma-Aldrich (catalog number 733857). $FeCl_3$ was purchased from Alfa Aesar. $NaBH_4$ was purchased from Acros Organics. All commercially available reagents were used without further purification. All reactions were carried out in a sample vial (4 mL) equipped with a Teflon-coated magnetic stir bar. Thin layer chromatography (TLC) was done using Silica Gel 60 F254 plates (0.25 mm thick), purchased from Merck. Column chromatography was done in glass columns using Silica gel 60 (EMD, 40-63 μm) or with pre-packed 25-gram KP-Sil Biotage$^{\Theta}$ SNAP Cartridges on the Biotage$^{\Theta}$ Isolera Prime autocolumn. GC-MS data was recorded on an Agilent Technologies 7890A GC system coupled with Agilent Technologies 5975C mass spectrometer using HP-5MS column (30 m × 0.250 mm, 0.25 μ) purchased from Agilent Technologies. ^{1}H and ^{13}C NMR spectra were obtained in $CDCl_3$ or DMSO-d_6 using 400 MHz or 500 MHz Varian NMR spectrometer. Chemical shifts in ^{1}H NMR spectra are reported in parts per million (ppm) on the δ scale from an internal standard of residual $CDCl_3$ (7.26 ppm) or the central peak of DMSO-d_6 (2.50 ppm). Data are reported as follows: chemical shift, multiplicity (s = singlet, d = doublet, t = triplet, q = quartet, quin = quintet), integration, and coupling constant in Hertz (Hz). Chemical shifts in ^{13}C NMR spectra are reported in ppm on the δ scale from the central peak of residual $CDCl_3$ (77.16 ppm) or the central peak of DMSO-d_6 (39.52 ppm). IR data was collected on a Perkin Elmer Spectrum Tow UATR FT-IR

Spectrometer and peaks were described according to relative intensity and resolution as follows: s = strong, m = medium, w = weak, br = broad.

Final Optimized Preparation of Fe/ppm (Pd + Ni) Nanoparticles

In an oven dried round-bottomed flask, anhydrous 99.99% pure $FeCl_3$ (162.2 mg, 1 mmol), $Pd(OAc)_2$ (0.9 mg, 0.004 mmol) and $Ni(NO_3)_2 \cdot 6H_2O$ (23.2 mg, 0.08 mmol) was added under an atmosphere of dry argon. The flask was covered with a septum, and 5 mL dry THF was added via syringe. The reaction mixture was stirred for twenty minutes at room temperature. While maintaining a dry atmosphere at room temperature, a 1 M solution of MeMgCl in THF was very slowly (1 drop/2 sec) added to the reaction mixture (about 1.2 mL, 1.2 mmol). After addition, a 0.1 M solution of MeMgCl in THF was very slowly (1 drop/2 sec) added to the reaction mixture (about 0.7 mL, 0.07 mmol). After complete addition of the Grignard reagent, the mixture was stirred for an additional twenty minutes at room temperature. Appearance of a yellow-brown color was indicative of generation of nanomaterial.

After 20 minutes, the mixture was quenched with pentane (containing traces of water). THF was then evaporated under reduced pressure at room temperature. Removal of THF was followed by triturating the mixture with pentane to provide yellow-brown colored nanomaterial as a powder (trituration was repeated 3 to 4 times). The Fe nanoparticles obtained were dried under reduced pressure at room temperature for ten minutes yielding 0.6 g Fe/ppm (Pd + Ni) nanoparticles. The material was used as such for subsequent reactions under micellar conditions.

Preparation of substrates

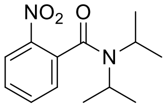

A

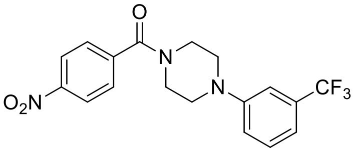

B

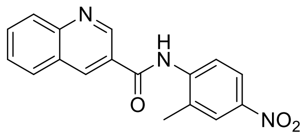

C

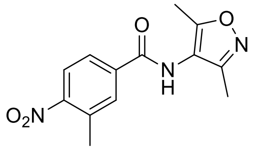

D

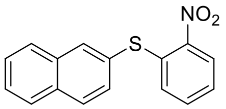

E

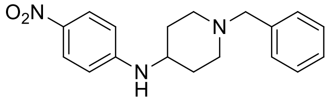

F

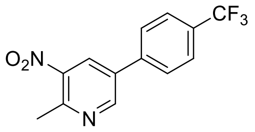

G

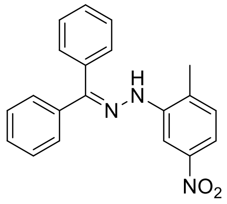

H

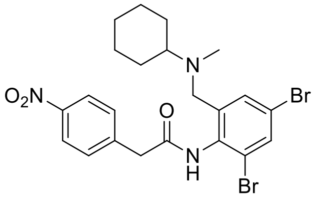

I

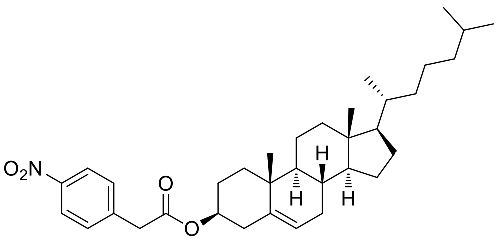

J

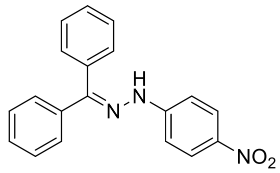

K

Substrates **A** – **D** were synthesized using the general procedure 1 (vide infra); Substrates **E** and **F** were synthesized according to literature;[2] Substrate **G** was synthesized using a Suzuki-Miyaura coupling;[3] Substrates **H** and **K** were synthesized using general procedure 2 (vide infra); Substrates **I** and **J** were synthesized using general procedure 3 (vide infra).

General procedure 1[4]

In an oven-dried 50 mL round bottom flask containing a PTFE-coated magnetic stir bar, aryl carboxylic acid (5 mmol, 1 equiv), DMF (0.05 mL) and CH_2Cl_2 (10 mL) were added.

The mixture was cooled to 0 °C and oxalyl chloride (1.2 equiv) was added in a few portions. The mixture was stirred at room temperature for 1.5 hours. The DCM was then removed via rotary evaporation. Dry CH_2Cl_2 (10 mL), Et_3N (6.6 equiv) and amine (6 mmol) were then added. The mixture was stirred at room temperature until TLC showed completion. The solution was washed with saturated aqueous NH_4Cl (2 × 25 mL), $NaHCO_3$, and brine (2 × 30 mL). The organic layer was separated and dried over anhydrous Na_2SO_4. Volatiles were removed under reduced pressure to obtain crude product that was purified by flash chromatography on silica gel with a gradient elution using hexanes and EtOAc.

General procedure 2

In an oven-dried 25 mL round bottom flask containing a PTFE-coated magnetic stir bar, $[Pd(\pi\text{-allyl})Cl]_2$ (0.01 equiv), cBRIDP (0.02 equiv) and dry THF 1 mL were added under an atmosphere of dry argon. The mixture was stirred under argon at 45 °C for 5 minutes. (Diphenylmethylene)hydrazine (5.25 mmol, 1.05 equiv) and bromonitrobenzene (5 mmol, 1 equiv) and 10 mL aqueous solution of 2 wt % TPGS-750-M were added. The mixture was stirred at 45 °C until the TLC control showed completion. The solution was extracted by CH_2Cl_2. The organic layer was washed with saturated aqueous NH_4Cl (2 × 25 mL), $NaHCO_3$, and brine (2 × 30 mL). The organic layer was separated and dried over anhydrous Na_2SO_4. Volatiles were removed under reduced pressure to obtain crude product which was purified by flash chromatography on silica gel with a gradient eluent using hexanes and EtOAc.

General procedure 3[5]

In an oven-dried 50 mL round bottom flask containing a PTFE-coated magnetic stir bar, aryl carboxylic acid (5 mmol, 1 equiv), amine or alcohol (5 mmol, 1 equiv), EDC·HCl (1.1 equiv), DMAP (15 mg) and CH_2Cl_2 (10 mL) were added. The mixture was stirred under reflux until the TLC control showed completion. The solution was washed with saturated aqueous NH_4Cl (2 × 25 mL), $NaHCO_3$, and brine (2 × 30 mL). The organic layer was separated and dried over anhydrous Na_2SO_4. Volatiles were removed under reduced pressure to obtain crude product which was purified by flash chromatography on silica gel with a gradient eluent using hexanes and EtOAc.

General Procedure for Nitro Group Reduction

Fe/ppm Pd + Ni nanoparticle (6 mg, 2 mol % Fe, 80 ppm Pd, 1600 ppm Ni) was added to an oven dried 4 mL microwave reaction vial containing a PTFE-coated magnetic stir bar. After addition, 1 mL aqueous solution of 2 wt % TPGS-750-M was added via syringe. The mixture was stirred at room temperature for 30 s. After stirring, 120 μL THF was added as co-solvent after which $NaBH_4$ (57.0 mg, 1.50 mmol) was added to the reaction mixture. During addition of $NaBH_4$, the reaction mixture turned black with evolution of hydrogen gas. The mixture was stirred at room temperature for 3 s or until all the mixture turned black. The nitro group-containing substrate (0.5 mmol) was then added quickly to the catalyst suspension. The reaction vial was covered again with a rubber septum and stirred vigorously at room temperature. Progress of the reaction was monitored by TLC.

After complete consumption of starting material, the septum was removed. Minimal amounts of organic solvent (EtOAc, DCM, Et_2O, etc.) were added, and the mixture was stirred *gently* for one minute. Stirring was stopped and the organic layer was then allowed to separate, after which it was removed via pipette. The same extraction procedure was repeated, and the combined organic extracts were dried over anhydrous Na_2SO_4. Volatiles were evaporated under reduced pressure and semi-pure product was purified by flash chromatography over silica gel.

One-pot study

1-Pot 3-step reduction/amine protection/Fischer indole synthesis

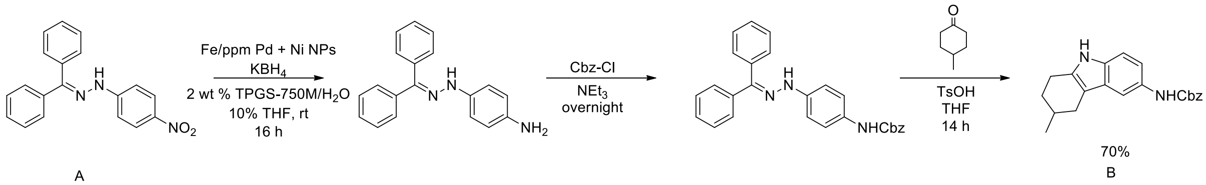

Fe/ppm Pd + Ni nanoparticle (2.6 mg, 2 mol % Fe, 80 ppm Pd, 1600 ppm Ni) was placed into an oven dried 8 mL microwave reaction vial containing a PTFE-coated magnetic stir bar. An aqueous solution (2 mL) of 2 wt % TPGS-750-M was added via syringe, and the mixture was stirred at room temperature for 30 sec. KBH_4 (81 mg, 1.5 mmol) was then added slowly to the reaction mixture. During addition of KBH_4, the reaction mixture turned black with evolution of hydrogen gas. 1-(Diphenylmethylene)-2-(4-nitrophenyl)hydrazine (79.3 mg, 0.25 mmol) was then added to the catalyst suspension, and then 0.5 mL THF was added as co-solvent. The reaction vial was covered again and the mixture was vigorously stirred for 16 hours until complete consumption of starting material. The resulting mixture was neutralized with 4 M HCl. Benzyl chloroformate (107.3 mg, 0.625 mmol) and Et_3N (76 mg, 3 mmol) were then added. The reaction vial was covered again and the mixture was vigorously stirred overnight. The resulting mixture was neutralized with 4 M HCl. After that, most of the water in the mixture was removed by rotary evaporation. THF (2 mL) was added as solvent, along with 4-methylcyclehexanone (140.2 mg 1.25 mmol) and 4-methylbenzenesulfonic acid (475.6 mg, 2.5 mmol). The reaction vial was covered again and the contents were vigorously stirred at 75 °C for 12 hours. After the reaction, the mixture was neutralized by addition of saturated Na_2CO_3 and the mixture was extracted with DCM. The organic extracts were removed by rotary evaporation and purified by flash chromatography over silica gel with Et_2O/hexane (15/85) to obtain pure benzyl (3-methyl-2,3,4,4a,9,9a-hexahydro-1H-carbazol-6-yl) carbamate as a faint yellow semi-solid (58.7 mg, 0.17 mmol, 70%).

^{1}H NMR (500 MHz, $CDCl_3$) δ 7.76 (m, 1 H), 7.48 (m, 6 H), 7.34 (m, 1 H), 7.13 (d, *J* = 8.5 Hz, 1 H), 7.03 (m, 1 H), 6.76 (s, 1 H), 5.27 (s, 2 H), 2.80 (dd, *J* = 4.5, 1 H), 2.69 (m, 2 H), 2.23 (m, 1 H), 1.93 (m, 2 H), 1.55 (m, 1 H), 1.14 (d, *J* = 6 Hz, 3 H).

^{13}C NMR (125 MHz, $CDCl_3$) δ 154.2, 136.5, 136.1, 133.2, 129.6, 128.6, 128.24, 128.19, 128.0, 114.3, 110.5, 110.1, 109.0, 66.8, 31.3, 29.6, 29.3, 22.9, 21.7.

HRMS(ESI): Calcd. For $C_{21}H_{22}O_2N_2Na$ $[M+Na]^+$ 357.1579. Found: 357.1563.

1-Pot 3 step reduction, S$_N$Ar reaction, and Suzuki-Miyaura reaction

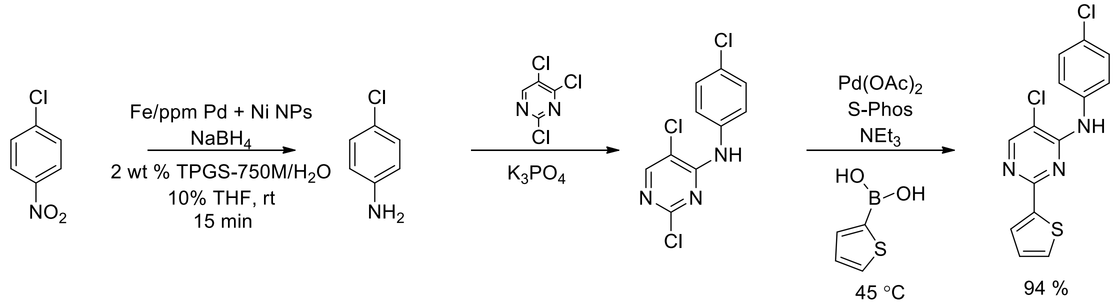

Fe/ppm Pd + Ni nanoparticle (5.2 mg, 2 mol % Fe, 80 ppm Pd, 1600 ppm Ni) were placed into an oven dried 4 mL microwave reaction vial containing a PTFE-coated magnetic stir bar. An aqueous solution (2 mL) of 2 wt % TPGS-750-M was added via syringe, and the mixture was stirred at room temperature for 30 seconds. After stirring, $NaBH_4$ (57 mg, 1.5 mmol) was slowly added to the reaction mixture. During addition of $NaBH_4$, the reaction mixture turned black with evolution of hydrogen gas. 4-Chloronitrobenzene (78.8 mg, 0.5 mmol) was then added to the catalyst suspension, and then 0.1 mL THF was added as co-solvent. The reaction vial was covered again and the mixture was vigorously stirred for ca. fifteen minutes until complete consumption of starting material. The resulting mixture was neutralized with 4 M HCl. 2,4,5-Trichloropyrimidine (91.7 mg, 0.5 mmol) and K_3PO_4 (127.3

mg, 0.6 mmol) were then added. The reaction vial was covered again and the mixture was vigorously stirred overnight. After the reaction, thiophen-2-ylboronic acid (96 mg 0.75 mmol), NEt_3 (151.8 mg, 1.5 mmol), $Pd(AcO)_2$ (2.2 mg, 0.01 mmol) and SPhos (8.2 mg, 0.02) were then added. The reaction vial was covered again and the contents were vigorously stirred at 45 °C for 16 hours. After the reaction, the mixture was extracted with EtOAc. The organic extracts were removed by rotary evaporation and purified by flash chromatography over silica gel with Et_2O/hexane (15/85) to obtain pure 5-chloro-N-(4-chlorophenyl)-2-(thiophen-2-yl)pyrimidin-4-amine as white solid (150.6 mg, 0.47 mmol, 94%).

^{1}H NMR (500 MHz, DMSO-d_6) δ 9.22 (s, 1 H), 8.49 (s, 1 H), 8.21 (d, *J* = 3 Hz, 1 H), 7.82 (d, *J* = 8.5 Hz, 2 H), 7.66 (d, *J* = 5 Hz, 1 H), 7.61 (m, 1 H), 7.46 (d, *J* = 9 Hz, 2 H).

^{13}C NMR (125 MHz, DMSO-d_6) δ 158.6, 155.8, 154.9, 141.2, 137.9, 128.69, 128.67, 127.9, 127.50, 127.48, 124.3, 112.5.

HRMS(CI): Calcd. For $C_{14}H_9Cl_2N_3S$ [M^+] 320.9894. Found: 320.9890.

E Factor and recycle studies

Procedure for determination of E Factors

Fe/ppm Pd + Ni nanoparticle (11.4 mg, 2 mol % Fe, 80 ppm Pd, 1600 ppm Ni) was placed into an oven dried 5 mL microwave reaction vial containing a PTFE-coated magnetic stir bar. The reaction vial was covered with a rubber septum and 1.0 mL aqueous solution of 2 wt % TPGS-750-M was added via syringe. The mixture was stirred at room temperature for 10 sec. The septum was opened and $NaBH_4$ (114 mg, 3 mmol) was added to the reaction mixture. During addition of $NaBH_4$ reaction mixture was turned black with evolution of hydrogen gas. 1-Chloro-4-nitro-2-(trifluoromethyl)benzene (225 mg, 1 mmol) was then added and the vial was again covered. The contents were stirred vigorously until complete consumption of the starting material (about 1 h). The resulting mixture was extracted with

EtOAc (0.4 mL × 2). The organic layer was then separated (with the aid of centrifuge, if needed) and dried over anhydrous Na_2SO_4, after which the volatiles were removed under reduced pressure and purified by flash chromatography over silica gel with EtOAc/hexanes to obtain 4-chloro-3-(trifluoromethyl)aniline. (186.1 mg, 0.95 mmol, 95%)

Procedures for recycle studies

Initial reaction: Fe/ppm Pd + Ni nanoparticle (5.7 mg, 2 mol % Fe, 80 ppm Pd, 1600 ppm Ni) was placed into an oven dried 5 mL microwave reaction vial containing a PTFE-coated magnetic stir bar. The reaction vial was covered with a rubber septum and 1.0 mL aqueous solution of 2 wt % TPGS-750-M was added via syringe. The mixture was stirred at room temperature for 10 sec. THF (0.1 mL) was added via syringe as co-solvent. The septum was opened and $NaBH_4$ (57 mg, 3 mmol) was added to the reaction mixture. 1-Chloro-4-nitro-2-(trifluoromethyl)benzene (112.5 mg, 0.5 mmol) was then added and the vial was again covered. The contents were stirred vigorously until complete consumption of the starting material (about 1 h). The resulting mixture was extracted with MTBE (0.4 mL × 3). The organic layer was then separated (with the aid of a centrifuge, if needed) and dried over anhydrous Na_2SO_4, after which the volatiles were removed under reduced pressure and purified by flash chromatography over silica gel with EtOAc/hexanes to obtain 4-chloro-3-(trifluoromethyl)aniline (95.7 mg, 0.49 mmol, 98%).

1st recycle: Three drops of 4 M aqueous hydrochloric acid were added to neutralize the aqueous layer. The vial was charged with fresh Fe nanoparticles (2 mg), and THF (0.1 mL). 1-Chloro-4-nitro-2-(trifluoromethyl)benzene (112.5 mg, 0.5 mmol) and $NaBH_4$ (57 mg, 3 mmol) were then added and the vial was again covered. The contents were stirred vigorously until complete consumption of the starting material (about 1 h). The resulting mixture was extracted with MTBE (0.4 mL × 3). The organic layer was then separated (with the aid of centrifuge, if needed) and dried over anhydrous Na_2SO_4, after which the volatiles were removed under reduced pressure and purified by flash chromatography over silica gel with EtOAc/hexanes to obtain 4-chloro-3-(trifluoromethyl)aniline. (94.8 mg, 0.49 mmol, 97%).

2nd recycle: Three drops of 4 M aqueous hydrochloric acid were added to neutralize the aqueous layer. The vial was charged with fresh Fe nanoparticles (2 mg), and THF (0.1 mL). 1-Chloro-4-nitro-2-(trifluoromethyl)benzene (112.5 mg, 0.5 mmol) and $NaBH_4$ (57 mg, 3 mmol) were then added and the vial was again covered. The contents were stirred vigorously until complete consumption of the starting material (about 1 h). The resulting mixture was extracted with MTBE (0.4 mL × 3). The organic layer was then separated (with the aid of centrifuge, if needed) and dried over anhydrous Na_2SO_4, after which the volatiles were removed under reduced pressure and purified by flash chromatography over silica gel with EtOAc/hexanes to obtain 4-chloro-3-(trifluoromethyl)aniline. (93.1 mg, 0.48 mmol, 95%).

3rd recycle: Three drops of 4 M aqueous hydrochloric acid solution was added to neutralize the aqueous layer. The vial was charged with fresh Fe nanoparticles (2 mg), and THF (0.1 mL). 1-Chloro-4-nitro-2-(trifluoromethyl)benzene (112.5 mg, 0.5 mmol) and $NaBH_4$ (57 mg, 3 mmol) were then added and the vial was again covered. The contents were stirred vigorously until complete consumption of the starting material (about 1 h). The resulting mixture was extracted with MTBE (0.4 mL × 3). The organic layer was then separated (with the aid of centrifuge, if needed) and dried over anhydrous Na_2SO_4, after which the volatiles were removed under reduced pressure and purified by flash chromatography over silica gel with EtOAc/hexanes to obtain 4-chloro-3-(trifluoromethyl)aniline. (93.3 mg, 0.48 mmol, 96%).

4th recycle: Three drops of 4 M aqueous hydrochloric acid solution was added to neutralize the aqueous layer. The vial was charged with fresh Fe nanoparticles (2 mg), and

THF (0.1 mL). 1-Chloro-4-nitro-2-(trifluoromethyl)benzene (112.5 mg, 0.5 mmol) and $NaBH_4$ (57 mg, 3 mmol) were then added and the vial was again covered. The contents were stirred vigorously until complete consumption of the starting material (about 1 h). The resulting mixture was extracted with MTBE (0.4 mL × 3). The organic layer was then separated (with the aid of centrifuge, if needed) and dried over anhydrous Na_2SO_4, after which the volatiles were removed under reduced pressure and purified by flash chromatography over silica gel with EtOAc/hexanes to obtain 4-chloro-3-(trifluoromethyl)aniline. (94.5 mg, 0.49 mmol, 97%).

Residual palladium, nickel, and iron in products

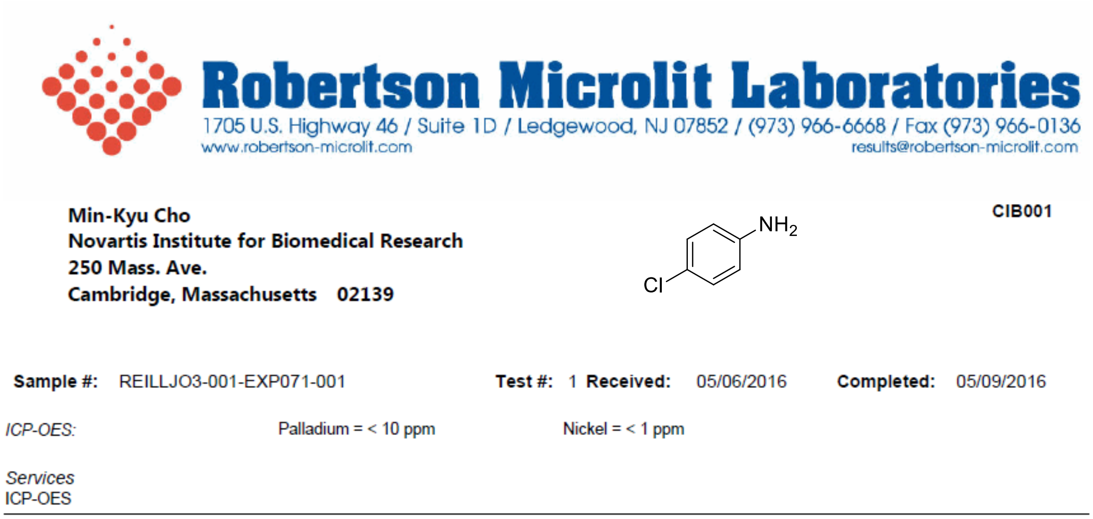

Robertson Microlit Laboratories

1705 U.S. Highway 46 / Suite 1D / Ledgewood, NJ 07852 / (973) 966-6668 / Fax (973) 966-0136

www.robertson-microlit.com

results@robertson-microlit.com

Min-Kyu Cho
Novartis Institute for Biomedical Research
250 Mass. Ave.
Cambridge, Massachusetts 02139

CIB001

Sample #: REILLJO3-001-EXP071-001 **Test #:** 1 **Received:** 05/06/2016 **Completed:** 05/09/2016

ICP-OES: Palladium = < 10 ppm Nickel = < 1 ppm

Services
ICP-OES

Robertson Microlit Laboratories
1705 U.S. Highway 46 / Suite 1D / Ledgewood, NJ 07852 / (973) 966-6668 / Fax (973) 966-0136
www.robertson-microlit.com
results@robertson-microlit.com

Min-Kyu Cho
Novartis Institute for Biomedical Research
250 Mass. Ave.
Cambridge, Massachusetts 02139

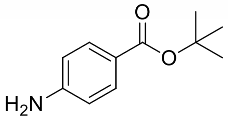

CIB001

Sample #: REILLJO3-001-EXP077-001 **Test #:** 1 **Received:** 08/01/2016 **Completed:** 08/02/2016

ICP-MS: Nickel = 1 ppm

Services
ICP-MS

Robertson Microlit Laboratories
1705 U.S. Highway 46 / Suite 1D / Ledgewood, NJ 07852 / (973) 966-6668 / Fax (973) 966-0136
www.robertson-microlit.com
results@robertson-microlit.com

Min-Kyu Cho
Novartis Institute for Biomedical Research
250 Mass. Ave.
Cambridge, Massachusetts 02139

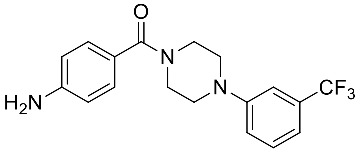

CIB001

Sample #: REILLJO3-001-EXP076-001 **Test #:** 1 **Received:** 08/01/2016 **Completed:** 08/02/2016

ICP-MS: Nickel = 1 ppm

Services
ICP-MS

Robertson Microlit Laboratories
1705 U.S. Highway 46 / Suite 1D / Ledgewood, NJ 07852 / (973) 966-6668 / Fax (973) 966-0136
www.robertson-microlit.com
results@robertson-microlit.com

Min-Kyu Cho
Novartis Institute for Biomedical Research
250 Mass. Ave.
Cambridge, Massachusetts 02139

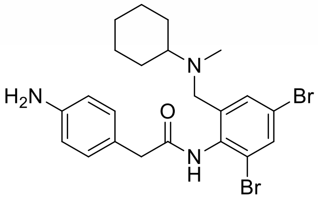

CIB001

Sample #: REILJO3-001-EXP089 **Test #:** 1 **Received:** 05/30/2017 **Completed:** 06/01/2017

ICP-OES: Iron = < 5 ppm

Services
ICP-OES

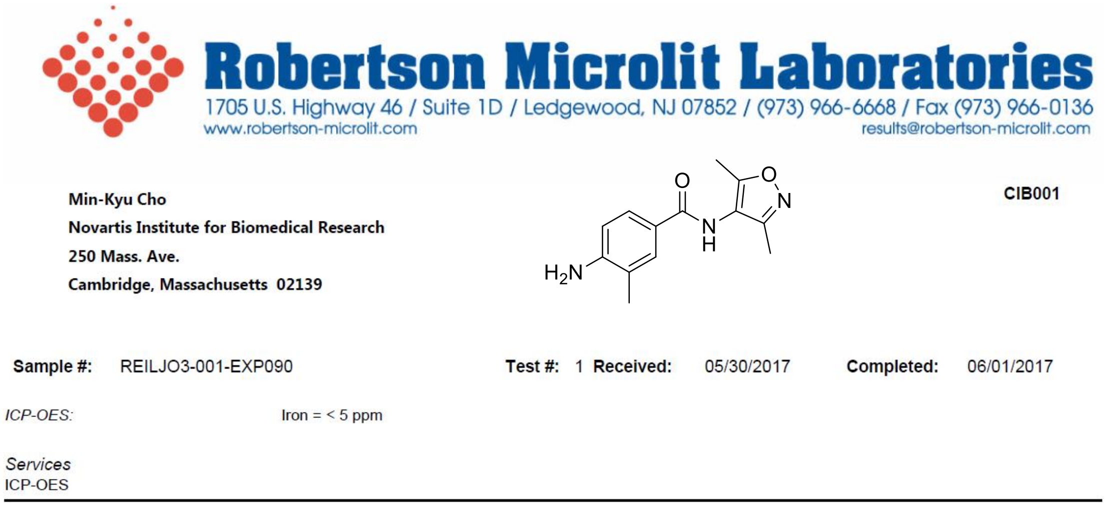

Robertson Microlit Laboratories

1705 U.S. Highway 46 / Suite 1D / Ledgewood, NJ 07852 / (973) 966-6668 / Fax (973) 966-0136

www.robertson-microlit.com results@robertson-microlit.com

Min-Kyu Cho
Novartis Institute for Biomedical Research
250 Mass. Ave.
Cambridge, Massachusetts 02139

CIB001

Sample #: REILJO3-001-EXP090 **Test #:** 1 **Received:** 05/30/2017 **Completed:** 06/01/2017

ICP-OES: Iron = < 5 ppm

Services
ICP-OES

Analytical data

4-Chloroaniline (1) CAS: 106-47-8

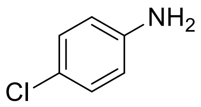

1-Chloro-4-nitrobenzene (78.8 mg, 0.5 mmol), Fe nanoparticles (6 mg), and $NaBH_4$ (57 mg, 1.5 mmol) in 1.0 mL 2 wt % TPGS/H_2O with 0.1 mL THF as co-solvent were reacted at room temperature for 15 minutes yielding 61.5 mg (96%) of 4-chloroaniline as a pale yellow solid (hexane/EtOAc : 80/20).

Spectral data matched that reported in the literature.[6]

^{1}H NMR (500 MHz, $CDCl_3$) δ 7.11 (d, *J* = 10 Hz, 2 H), 6.61 (d, *J* = 5 Hz, 2 H), 3.48 (s, br, 2 H).

^{13}C NMR (125 MHz, $CDCl_3$) δ 145.1, 129.3, 123.4, 116.5.

GC-MS, *m/z*: 127 [M^+].

3-Bromo-4-methylaniline (2) CAS: 7745-91-7

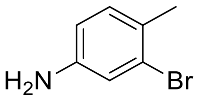

2-Bromo-1-methyl-4-nitrobenzene (108 mg, 0.5 mmol), Fe nanoparticles (6 mg), and $NaBH_4$ (57 mg, 1.5 mmol) in 1.0 mL 2 wt % TPGS/H_2O with 0.1 mL THF as co-solvent were reacted at room temperature for 30 minutes yielding 91.2 mg (98%) of 3-bromo-4-methylaniline as white crystals (hexane/EtOAc : 80/20).

Spectral data matched that reported in the literature.[7]

^{1}H NMR (500 MHz, $CDCl_3$) δ 7.00 (d, *J* = 10 Hz, 1 H), 6.90 (d, *J* = 5 Hz, 1 H), 6.55 (m, 1 H), 3.48 (s, br, 2 H), 2.28 (s, 3 H).

^{13}C NMR (125 MHz, $CDCl_3$) δ 145.6, 131.3, 127.5, 125.3, 118.9, 114.6, 21.9.

GC-MS, *m/z*: 184 [M^+].

4-(Methylthio)aniline (3) CAS: 104-96-1

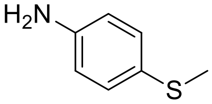

Methyl(4-nitrophenyl)sulfane (84.6 mg, 0.5 mmol), Fe nanoparticles (6 mg), and $NaBH_4$ (57 mg, 1.5 mmol) in 1.0 mL 2 wt % TPGS/H_2O with 0.1 mL THF as co-solvent were reacted at room temperature for 2 hours yielding 61.1 mg (88%) of 4-(methylthio)aniline as a yellow oil (hexane/EtOAc : 70/30).

Spectral data matched that reported in the literature.[8]

^{1}H NMR (500 MHz, $CDCl_3$) δ 7.17 (d, *J* = 10 Hz, 2 H), 6.62 (d, *J* = 10 Hz, 2 H), 3.54 (s, br, 2 H), 2.41 (s, 3 H).

^{13}C NMR (125 MHz, $CDCl_3$) δ 145.2, 131.2, 125.9, 115.8, 18.9.

GC-MS, *m/z*: 139 [M^+].

4-Chloro-3-(trifluoromethyl)aniline (4) CAS: 320-51-4

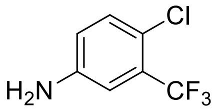

1-Chloro-4-nitro-2-(trifluoromethyl)benzene (112.8 mg, 0.5 mmol), Fe nanoparticles (6 mg), and $NaBH_4$ (57 mg, 1.5 mmol) in 1.0 mL 2 wt % TPGS/H_2O with 0.1 mL THF as co-solvent were reacted at room temperature for 30 minutes yielding 95.9 mg (98%) of 4-chloro-3-(trifluoromethyl)aniline as a yellow oil (hexane/EtOAc : 80/20).

Spectral data matched that reported in the literature.[9]

^{1}H NMR (500 MHz, $CDCl_3$) δ 7.22 (d, *J* = 9 Hz, 1 H), 6.96 (d, *J* = 3 Hz, 1 H), 6.73 (m, 1 H), 3.83 (s, br, 2 H).

^{13}C NMR (125 MHz, DMSO-d_6) δ 145.3, 132.2, 128.8 (q, $J_{(C\text{-}F)}$ = 31 Hz), 123.0 (q, $J_{(C\text{-}F)}$ = 271 Hz), 120.3, 118.8, 113.7 (q, $J_{(C\text{-}F)}$ = 5 Hz).

GC-MS, *m/z*: 195 [M^+].

Naphthalen-1-amine (5) CAS: 132-32-7

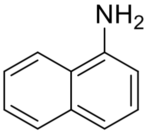

1-Nitronaphthalene (86.6 mg, 0.5 mmol), Fe nanoparticles (6 mg), and $NaBH_4$ (57 mg, 1.5 mmol) in 1.0 mL 2 wt % TPGS/H_2O with 0.1 mL THF as co-solvent were reacted at room temperature for 30 minutes yielding 71.2 mg (99%) of naphthalen-1-amine as white crystals (hexane/EtOAc : 80/20).

Spectral data matched that reported in the literature.[10]

^{1}H NMR (500 MHz, $CDCl_3$) δ 7.82 (m, 2 H), 7.48 (m, 2 H), 7.31 (m, 2 H), 6.80 (m, 1 H), 4.15 (s, br, 2 H).

^{13}C NMR (100 MHz, $CDCl_3$) δ 142.2, 134.5, 128.6, 126.4, 125.9, 124.9, 123.8, 120.9, 119.1, 109.8.

GC-MS, *m/z*: 143 [M^+].

N-(3-Aminophenyl)acetamide (6) CAS: 102-28-3

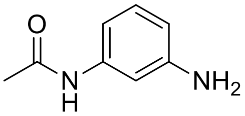

N-(3-Nitrophenyl)acetamide (90.1 mg, 0.5 mmol), Fe nanoparticles (6 mg), and $NaBH_4$ (57 mg, 1.5 mmol) in 1.0 mL 2 wt % TPGS/H_2O with 0.1 mL THF as co-solvent were reacted at room temperature for 30 minutes yielding 73.8 mg (98%) of N-(3-aminophenyl)acetamide as a white oil (DCM/MeOH : 95/5).

Spectral data matched to the reported in literature.[11]

^{1}H NMR (500 MHz, $CDCl_3$) δ 8.17 (s, 1 H), 7.03 (t, *J* = 10 Hz, 2 H), 6.77 (d, *J* = 10 Hz,1 H), 6.37 (d, *J* = 5 Hz, 1 H), 3.68 (s, br, 2 H), 2.06 (s, br, 3 H).

^{13}C NMR (100 MHz, $CDCl_3$) δ 169.1, 147.2, 139.1, 129.6, 111.1, 110.1, 106.9, 24.4.

GC-MS, *m/z*: 150 [M^+].

6-Bromopyridin-3-amine (7) CAS: 13534-97-9

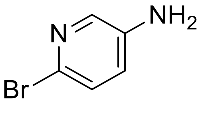

2-Bromo-5-nitropyridine (101.5 mg, 0.5 mmol), Fe nanoparticles (6 mg), and $NaBH_4$ (57 mg, 1.5 mmol) in 1.0 mL 2 wt % TPGS/H_2O with 0.1 mL THF as co-solvent were reacted at room temperature for 15 minutes yielding 81.1 mg (94%) of 6-bromopyridin-3-amine as white crystals (hexane/EtOAc : 70/30).

Spectral data matched that reported in the literature.[12]

^{1}H NMR (500 MHz, $CDCl_3$) δ 7.83 (d, *J* = 5 Hz, 1 H), 7.21 (m, 1 H), 6.88 (m, 1 H), 3.49 (s, br, 2 H).

^{13}C NMR (100 MHz, $CDCl_3$) δ 142.3, 137.1, 129.6, 127.9, 124.9.

GC-MS, *m/z*: 172 [M^+].

t-Butyl 4-aminobenzoate (8) CAS: 18144-47-3

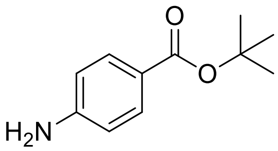

t-Butyl 4-nitrobenzoate (111.6 mg, 0.5 mmol), Fe nanoparticles (6 mg), and $NaBH_4$ (57 mg, 1.5 mmol) in 1.0 mL 2 wt % TPGS/H_2O with 0.1 mL THF as co-solvent were reacted at room temperature for 2 hours yielding 94.9 mg (98%) of *tert*-butyl 4-aminobenzoate as white crystals (hexane/EtOAc : 80/20).

Spectral data matched that reported in the literature.[13]

^{1}H NMR (500 MHz, DMSO-d_6) δ 7.58 (d, *J* = 10 Hz, 2 H), 6.55 (d, *J* = 5 Hz, 2 H), 5.84 (s, br, 2 H), 1.49 (s, 9 H).

^{13}C NMR (125 MHz, DMSO-d_6) δ 165.3, 153.0, 130.9, 117.8, 112.5, 78.8, 28.0.

GC-MS, *m/z*: 193 [M^+].

4-(Benzyloxy)aniline (9) CAS: 6373-46-2

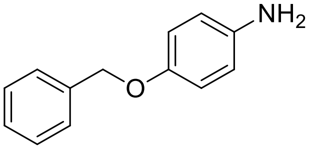

1-(Benzyloxy)-4-nitrobenzene (114.6 mg, 0.5 mmol), Fe nanoparticles (6 mg), and $NaBH_4$ (57 mg, 1.5 mmol) in 1.0 mL 2 wt % TPGS/H_2O with 0.1 mL THF as co-solvent were reacted at room temperature for 10 hours yielding 85.4 mg (86%) of 4-(benzyloxy)aniline as yellow crystals (hexane/EtOAc : 80/20).

Spectral data matched that reported in the literature.[14]

^{1}H NMR (500 MHz, $CDCl_3$) δ 7.47 (m, 2 H), 7.42 (m, 2 H), 7.36 (m, 1 H), 6.86 (d, *J* = 10 Hz, 2 H), 6.66 (d, *J* = 5 Hz, 2 H), 5.03 (s, 2 H), 3.37 (s, br, 2 H).

^{13}C NMR (125 MHz, $CDCl_3$) δ 151.9, 140.3, 137.6, 128.5, 127.8, 127.5, 116.37, 116.1, 70.8.

GC-MS, *m/z*: 199 [M^+].

3-Bromo-5-fluoro-2-methylaniline (10) CAS: 502496-36-8

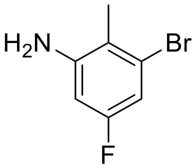

1-Bromo-5-fluoro-2-methyl-3-nitrobenzene (117 mg, 0.5 mmol), Fe nanoparticles (6 mg), and $NaBH_4$ (57 mg, 1.5 mmol) in 1.0 mL 2 wt % TPGS/H_2O with 0.1 mL THF as co-solvent were reacted at room temperature for 4 hours yielding 92.3 mg (90%) of 3-bromo-5-fluoro-2-methylaniline as a faint yellow liquid (hexane/EtOAc : 80/20).

^{1}H NMR (500 MHz, $CDCl_3$) δ 6.73 (dd, *J* = 8.5 Hz, *J* = 2.5 Hz, 1 H), 6.35 (dd, *J* = 10 Hz, *J* = 2.5 Hz, 1 H), 3.82 (s, br, 2 H), 2.20 (s, 3 H).

^{13}C NMR (100 MHz, $CDCl_3$) δ 162.5, 160.0, 146.6, 146.5, 125.3, 125.2, 117.6, 109.7, 109.4, 101.2, 100.9, 16.3.

^{19}F NMR (376 MHz, $CDCl_3$) δ -115.9.

HRMS(CI): Calcd. For C_7H_7BrFN [M^+] 202.9746. Found: 202.9745.

2-Amino-*N,N*-diisopropylbenzamide (11) CAS: 103794-66-7

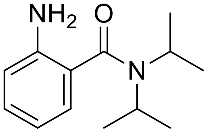

N,N-Diisopropyl-2-nitrobenzamide (31.3 mg, 0.125 mmol), Fe nanoparticles (3 mg), and $NaBH_4$ (14.3 mg, 0.375 mmol) in 1.0 mL 2 wt % TPGS/H_2O with 0.1 mL THF as co-solvent were reacted at room temperature for 2 hours yielding 27.0 mg (98%) of 2-amino-*N,N*-diisopropylbenzamide as a colorless oil (hexane/EtOAc : 80/20).

Spectral data matched that reported in the literature.[15]

^{1}H NMR (500 MHz, $CDCl_3$) δ 7.12 (m, 1 H), 7.00 (m, 1 H), 6.71 (m, 2 H), 4.03 (s, 2 H), 3.74 (s, br, 2 H), 1.35 (s, 12 H).

^{13}C NMR (100 MHz, $CDCl_3$) δ 170.3, 144.3, 129.4, 125.9, 123.8, 117.6, 116.5, 48.4, 20.9.

GC-MS, *m/z*: 220 [M^+].

(4-Aminophenyl)(4-(3-(trifluoromethyl)phenyl)piperazin-1-yl)methanone (12) CAS: 747351-56-0

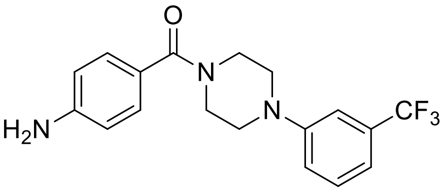

(4-Nitrophenyl)(4-(3-(trifluoromethyl)phenyl)piperazin-1-yl)methanone (189.7 mg, 0.5 mmol), Fe nanoparticles (6 mg), and $NaBH_4$ (57 mg, 1.5 mmol) in 1.0 mL 2 wt % TPGS/H_2O with 0.1 mL THF as co-solvent were reacted at room temperature for 2 hours yielding 153.4 mg (88%) of (4-aminophenyl)(4-(3-(trifluoromethyl)phenyl) piperazin-1-yl)-methanone as a white solid liquid (DCM/MeOH : 95/5).

Spectral data matched that reported in the literature.[16]

^{1}H NMR (500 MHz, DMSO-d_6) δ 7.43 (m, 1 H), 7.24 (m, 1 H), 7.18 (m, 3 H), 7.10 (m, 1 H), 6.57 (d, *J* = 5 Hz, 2 H), 5.57 (s, br, 2 H), 3.63 (s, 4 H), 3.26 (s, 4 H).

^{13}C NMR (125 MHz, DMSO-d_6) δ 170.1, 151.1, 150.6, 130.3 (q, $J_{(C-F)}$ = 30 Hz), 128.5, 127.6, 125.5 (q, $J_{(C-F)}$ = 270 Hz), 122.1, 119.5, 115.04 (q, $J_{(C-F)}$ = 4 Hz), 112.8, 111.8, 111.4 (q, $^3J_{(C-F)}$ = 4 Hz), 48.3.

GC-MS, *m/z*: 349 [M^+].

_N_-(4-Amino-2-methylphenyl)quinoline-3-carboxamide (13)

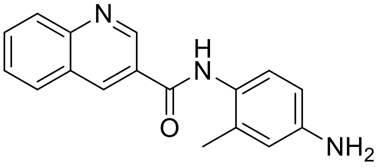

N-(2-Methyl-4-nitrophenyl)quinoline-3-carboxamide (153.7 mg, 0.5 mmol), Fe nanoparticles (6 mg), and $NaBH_4$ (57 mg, 1.5 mmol) in 1.0 mL 2 wt % TPGS/H_2O with 0.25 mL DMSO as co-solvent were reacted at room temperature for 16 hours yielding 110.5 mg (80%) of N-(4-amino-2-methylphenyl)quinoline-3-carboxamide as a yellow oil (hexane/EtOAc : 70/30).

^{1}H NMR (500 MHz, DMSO-d_6) δ 9.92 (s, 1 H), 9.37 (s, 1 H), 8.93 (s, 1 H), 8.13 (t, *J* = 5 Hz, 2 H), 7.90 (t, *J* = 5 Hz, 1 H), 7.72 (t, *J* = 5 Hz, 1 H), 6.99 (d, *J* = 10 Hz, 1 H), 6.49 (s, 1 H), 6.44 (d, *J* = 10 Hz, 1 H), 5.00 (s, br, 2 H), 2.13 (s, 3 H).

^{13}C NMR (125 MHz, DMSO-d_6) δ 164.0, 149.1, 148.5, 147.2, 136.7, 134.6, 131.1, 129.1, 128.8, 127.7, 127.4, 126.6, 124.5, 115.3, 111.6, 18.1.

HRMS(CI): Calcd. For $C_{17}H_{16}N_3O$ $[M+H]^+$ 278.1293. Found: 278.1288.

2-(4-Aminophenyl)-*N*-(2,4-dibromo-6-((cyclohexyl(methyl)amino)methyl)phenyl)acetamide (14)

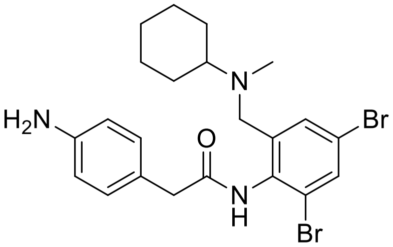

N-(2,4-Bibromo-6-((cyclohexyl(methyl)amino)methyl)phenyl)-2-(4-nitrophenyl)acetamide (67.4 mg, 0.125 mmol), Fe nanoparticles (3 mg), and $NaBH_4$ (14.3 mg, 0.375 mmol) in 1.0 mL 2 wt % TPGS/H_2O with 0.3 mL THF as co-solvent were reacted at room temperature for 2 hours yielding 53.3 mg (84%) of 2-(4-aminophenyl)-N-(2,4-dibromo-6-((cyclohexyl(methyl)- amino)methyl)phenyl)acetamide as a pale yellow solid (DCM/MeOH : 95/5).

^1H NMR (500 MHz, DMSO-d_6) δ 9.58 (s, 1 H), 7.75 (s, 1 H), 7.61 (s, 1 H), 7.03 (d, *J* = 10 Hz, 2 H), 6.51 (d, *J* = 10 Hz, 2 H), 4.91 (s, br, 2 H), 3.44 (s, 2 H) , 3.30 (s, 2 H), 2.26 (m, 1 H), 2.00 (s, 3 H), 1.72 (m, 2 H), 1.65 (m, 2 H), 1.55 (m, 1 H), 1.12 (m, 5 H).

^{13}C NMR (125 MHz, DMSO-d_6) δ 169.8, 147.3, 142.7, 134.6, 132.3, 130.4, 129.5, 123.7, 122.5, 120.0, 113.8, 62.3, 53.1, 41.7, 37.4, 28.1, 25.9, 25.5.

HRMS(CI): Calcd. For $C_{22}H_{28}Br_2ON_3$ $[M+H]^+$ 508.0599. Found: 508.0609.

4-((4-Methylpiperazin-1-yl)sulfonyl)aniline (15) CAS: 21623-68-7

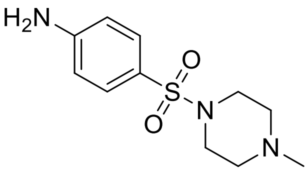

1-Methyl-4-((4-nitrophenyl)sulfonyl)piperazine (71.3 mg, 0.25 mmol), Fe nanoparticles (3 mg), and $NaBH_4$ (28.5 mg, 0.75 mmol) in 1.0 mL 2 wt % TPGS/H_2O with 0.1 mL THF as co-solvent were reacted at room temperature for 16 hours yielding 62.6 mg (98%) of 4-((4-methylpiperazin-1-yl)sulfonyl)aniline as a white soild (DCM/MeOH : 95/5).

^{1}H NMR (500 MHz, DMSO-d_6) δ 7.29 (d, *J* = 5 Hz, 2 H), 6.61 (d, *J* = 10 Hz, 2 H), 6.01 (s, 2 H), 2.73 (s, 4 H), 2.28 (s, 4 H), 2.07 (s, 3 H).

^{13}C NMR (125 MHz, DMSO-d_6) δ 153.2, 129.6, 119.3, 112.7, 53.6, 45.7, 45.3.

HRMS(CI): Calcd. For $C_{11}H_{18}SO_2N_3$ $[M+H]^+$ 256.1120. Found: 256.1118.

(2-Amino-4,5-dimethoxyphenyl)(4-methylpiperazin-1-yl)methanone (16) CAS: 926269-05-8

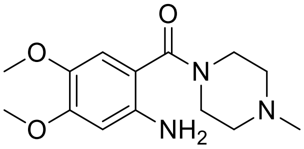

(4,5-Dimethoxy-2-nitrophenyl)(4-methylpiperazin-1-yl)methanone (77.3 mg, 0.25 mmol), Fe nanoparticles (3 mg), and $NaBH_4$ (28.5 mg, 0.75 mmol) in 1.0 mL 2 wt % TPGS/H_2O with 0.25 mL CH_3OH as co-solvent were reacted at room temperature for 16 hours yielding 57.7 mg (83%) of (2-amino-4,5-dimethoxyphenyl)(4-methylpiperazin-1-yl)methanone as a yellow oil (DCM/MeOH : 90/10).

Spectral data matched that reported in the literature.[17]

^{1}H NMR (500 MHz, $CDCl_3$) δ 6.63 (s, 1 H), 6.24 (s, 1 H), 4.21 (s, br, 2 H), 3.82 (s, 3 H), 3.77 (s, 3 H), 3.62 (m, 4 H), 2.41 (m, 4 H), 2.29 (s, 3 H).

^{13}C NMR (125 MHz, $CDCl_3$) δ 170.1, 151.6, 141.2, 141.1, 112.4, 110.4, 101.0, 56.9, 55.8, 55.3, 46.1, 45.0 (br).

GC-MS, *m/z*: 279 [M^+].

2-Methyl-5-((3-(trifluoromethyl)benzyl)oxy)aniline (17)

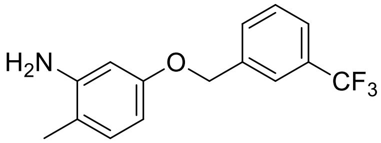

1-Methyl-2-nitro-4-((3-(trifluoromethyl)benzyl)oxy)benzene (155.6 mg, 0.5 mmol), Fe nanoparticles (12 mg), and $NaBH_4$ (114 mg, 3 mmol) in 1.0 mL 2 wt % TPGS/H_2O with 0.1 mL DCM as co-solvent were reacted at room temperature for 16 hours yielding 135.2mg (96%) of 2-methyl-5-((3-(trifluoromethyl)benzyl)oxy)aniline as pale yellow crystals (hexane/EtOAc : 80/20).

^1H NMR (500 MHz, $CDCl_3$) δ 7.72 (s, 1 H), 7.61 (m, 2 H), 7.50 (m, 1 H), 6.99 (d, *J* = 10 Hz), 6.36 (m, 2 H) 5.06 (s, 2 H), 3.64 (s, br, 2 H), 2.13 (s, 3 H).

^{13}C NMR (125 MHz, $CDCl_3$) δ 157.99, 146.7, 138.6, 131.3 (q, $J_{(C\text{-}F)}$ = 32.5 Hz), 131.1, 130.6, 129.1, 127.5 (q, $J_{(C\text{-}F)}$ = 271 Hz), 124.7 (q, $J_{(C\text{-}F)}$ = 3.75 Hz), 124.0 (q, $J_{(C\text{-}F)}$ = 3.75 Hz), 115.6, 104.5, 102.0, 69.2, 16.5.

^{19}F NMR (376 MHz, $CDCl_3$) δ -62.66.

HRMS(EI): Calcd. For $C_{15}H_{14}NOF_3$ [M^+] 281.1027. Found: 281.1019.

2-Methyl-5-(4-(trifluoromethyl)phenyl)pyridin-3-amine (18)

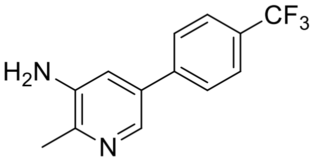

2-Methyl-3-nitro-5-(4-(trifluoromethyl)phenyl)pyridine (141.1 mg, 0.5 mmol), Fe nanoparticles (6 mg), and $NaBH_4$ (57 mg, 1.5 mmol) in 1.0 mL 2 wt % TPGS/H_2O with 0.25 mL THF as co-solvent were reacted at room temperature for 16 hours yielding 108 mg (86%) of 2-methyl-5-(4-(trifluoromethyl)phenyl)pyridin-3-amine as white crystals (hexane/EtOAc : 70/30).

^{1}H NMR (500 MHz, DMSO-d_6) δ 8.02 (s, 1 H), 7.80 (s, 4 H), 7.22 (s, 1 H), 5.23 (s, 2 H), 2.32 (s, 3 H).

^{13}C NMR (100 MHz, DMSO-d_6) δ 143.2, 142.5, 142.3, 134.6, 132.5, 128.4 (q, $J_{(C\text{-}F)}$ = 270.76 Hz), 128.4 (q, $J_{(C\text{-}F)}$ = 32 Hz), 127.2, 125.9 (q, $J_{(C\text{-}F)}$ = 4 Hz), 117.5, 20.4.

^{19}F NMR (376 MHz, DMSO-d_6) δ -61.05.

HRMS(EI): Calcd. For $C_{13}H_{11}N_2F_3$ [M^+] 252.0874. Found: 252.0871.

4-Amino-N-(3,5-dimethylisoxazol-4-yl)-3-methylbenzamide (19)

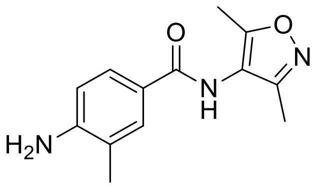

N-(3,5-Dimethylisoxazol-4-yl)-3-methyl-4-nitrobenzamide (137.6 mg, 0.5 mmol), Fe nanoparticles (6 mg), and $NaBH_4$ (57 mg, 1.5 mmol) in 1.0 mL 2 wt % TPGS/H_2O with 0.25 mL DMSO as co-solvent were reacted at room temperature for 6 hours yielding 117.9 mg (96%) of 4-amino-*N*-(3,5-dimethylisoxazol-4-yl)-3-methylbenzamide as a pale yellow solid (hexane/EtOAc : 70/30).

^{1}H NMR (500 MHz, DMSO-d_6) δ 10.3 (s, 1 H), 7.63 (s, 1 H), 7.60 (dd, *J* = 8 Hz, *J* = 2.5 Hz,1 H), 6.64 (d, *J* = 10 Hz, 1 H), 1.92 (s, br, 2 H), 2.16 (s, 3 H), 2.10 (s, 3 H), 1.79 (s, 3 H).

^{13}C NMR (125 MHz, DMSO-d_6) δ 164.7, 161.3, 158.3, 151.1, 130.6, 127.6, 120.0, 119.1, 112.7, 112.7, 113.3, 17.5, 10.4, 6.9.

HRMS(EI): Calcd. For $C_{13}H_{15}O_2N_3$ [M^+] 245.1159. Found: 245.1164.

_N_-1-(1-Benzylpiperidin-4-yl)benzene-1,4-diamine (20) CAS: 1039820-98-8

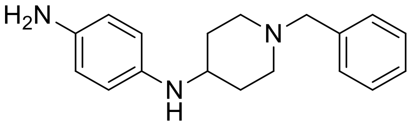

1-Benzyl-*N*-(4-nitrophenyl)piperidin-4-amine (155.7 mg, 0.5 mmol), Fe nanoparticles (12 mg), and KBH_4 (161.8 mg, 3 mmol) in 1.0 mL 2 wt % TPGS/H_2O with 0.25 mL THF as co-solvent were reacted at room temperature for 16 hours yielding 129.8 mg (92%) of *N*-1-(1-benzylpiperidin-4-yl)benzene-1,4-diamine as a deep red solid (DCM/MeOH : 90/10).

^1H NMR (500 MHz, $CDCl_3$) δ 7.34 (m, 4 H), 7.27 (m, 1 H), 6.60 (d, 2 H), 6.51 (d, 2 H), 3.64 (s, 1 H), 3.57 (s, 2 H), 3.19 (m, 3 H), 2.88 (m, 2 H), 2.18 (t, J = 10 Hz, 2 H), 2.02 (m, 2 H), 1.50, (m, 2 H).

^{13}C NMR (100 MHz, $CDCl_3$) δ 139.9, 137.9, 137.4, 129.3, 128.3, 127.3, 116.8, 115.8, 70.5, 62.8, 52.2, 32.3.

HRMS(CI): Calcd. For $C_{18}H_{23}N_3$ [M^+] 281.1892. Found: 281.1899.

(4-Aminophenyl)(morpholino)methanone (21) CAS: 51207-86-4

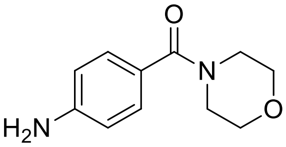

Morpholino(4-nitrophenyl)methanone (118.1 mg, 0.5 mmol), Fe nanoparticles (6 mg), and $NaBH_4$ (57 mg, 1.5 mmol) in 1.0 mL 2 wt % TPGS/H_2O with 0.1 mL THF as co-solvent were reacted at room temperature for 30 minutes yielding 102.4 mg (99%) of (4-aminophenyl)(morpholino)methanone as a pale yellow solid (DCM/MeOH : 70/30).

Spectral data matched that reported in the literature.[14]

^{1}H NMR (500 MHz, $CDCl_3$) δ 7.26 (m, 2 H), 6.64 (m, 2 H), 3.92 (s, br, 2 H), 3.68 (m, 8 H).

^{13}C NMR (100 MHz, $CDCl_3$) δ 170.9, 148.7, 129.3, 124.0, 114.0, 66.8.

GC-MS, *m/z*: 206 [M^+].

3-(2-(Diphenylmethylene)hydrazinyl)-4-methylaniline (22)

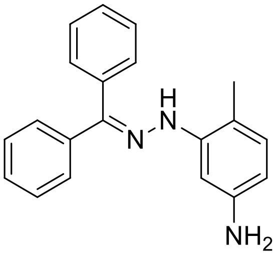

1-(Diphenylmethylene)-2-(2-methyl-5-nitrophenyl)hydrazine (41.4 mg, 0.125 mmol), Fe nanoparticles (1.5 mg), and $NaBH_4$ (14.3 mg, 0.375 mmol) in 1.0 mL 2 wt % TPGS/H_2O with 0.25 mL DMSO as co-solvent were reacted at room temperature for 16 hours yielding 35.7 mg (95%) of 3-(2-(diphenylmethylene)hydrazinyl)-4-methylaniline as an orange solid (hexane/EtOAc : 70/30).

^{1}H NMR (500 MHz, $CDCl_3$) δ 7.59 (m, 4 H), 7.52 (m, 1 H), 7.42 (s, 1 H), 7.34 (m, 5 H), 7.29 (d, *J* = 3 Hz, 1 H), 6.79 (d, *J* = 8 Hz, 1 H), 6.17 (dd, *J* = 8 Hz, *J* = 2.5 Hz, 1 H), 3.63 (s, br, 2 H), 1.75 (s, 3 H).

^{13}C NMR (125 MHz, $CDCl_3$) δ 147.0, 145.1, 143.1, 138.5, 133.1, 131.0, 129.8, 129.4, 129.0, 128.3, 128.1, 126.6, 110.9, 116.9, 99.7, 15.7.

HRMS(EI): Calcd. For $C_{20}H_{19}N_3$ [M^+] 301.1579. Found: 301.1572.

4-(Chlorodifluoromethoxy)aniline (23) CAS: 39065-95-7

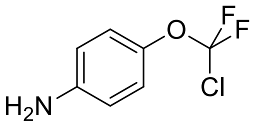

1-(Chlorodifluoromethoxy)-4-nitrobenzene (111.8 mg, 0.5 mmol), Fe nanoparticles (6 mg), and $NaBH_4$ (57 mg, 1.5 mmol) in 1.0 mL 2 wt % TPGS/H_2O with 0.1 mL THF as co-solvent were reacted at room temperature for 30 minutes yielding 88.4 mg (91%) of 4-(chlorodifluoromethoxy)aniline as a yellow liquid (hexane/EtOAc : 70/30).

^{1}H NMR (500 MHz, $CDCl_3$) δ 7.03 (d, *J* = 10 Hz, 2 H), 6.66 (s, 2 H), 3.71 (s, br, 2 H).

^{13}C NMR (125 MHz, $CDCl_3$) δ 146.5, 142.6, 125.8, 122.9, 115.5.

^{19}F NMR (376 MHz, DMSO-d_6) δ -25.77.

HRMS(CI): Calcd. For $C_7H_6ClF_2NO$ [M^+] 193.0106. Found: 193.0104.

2-(Naphthalen-2-ylthio)aniline (24) CAS: 859330-37-3

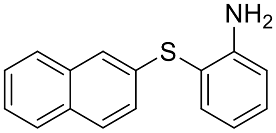

Naphthalen-2-yl(2-nitrophenyl)sulfane (35.2 mg, 0.125 mmol), Fe nanoparticles (2.7 mg), and KBH_4 (40.5mg, 0.75 mmol) in 1.0 mL 2 wt % TPGS/H_2O with 0.25 mL DMSO as co-solvent were reacted at room temperature for 16 hours yielding 28.9 mg (92%) of 2-(naphthalen-2-ylthio)aniline as a yellow solid (hexane/EtOAc : 70/30).

Spectral data matched to the reported in literature.[18]

^{1}H NMR (500 MHz, $CDCl_3$) δ 7.77 (d, *J* = 10 Hz, 1 H), 7.72 (d, *J* = 10 Hz, 1 H), 7.66 (d, *J* = 10 Hz, 1 H), 7.53 (m, 2 H), 7.45 (p, *J* = 10 Hz, 2 H), 7.28 (m, 2 H), 6.83 (m, 2 H), 4.31 (s, br, 2 H).

^{13}C NMR (125 MHz, $CDCl_3$) δ 149.0, 137.5, 134.3, 133.9, 131.7, 131.3, 128.8, 127.9, 127.1, 126.7, 125.6, 125.3, 124.5, 118.9, 115.6, 114.5.

GC-MS, *m/z*: 251 [M^+].

2-Dodecanamidoethyl 2-(4-aminophenyl)acetate (25)

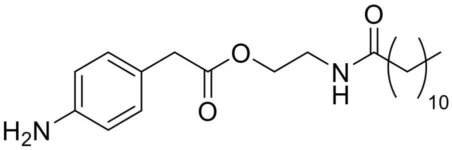

2-Dodecanamidoethyl 2-(4-nitrophenyl)acetate (101.6 mg, 0.25 mmol), Fe nanoparticles (3 mg), and KBH_4 (40.5 mg, 0.75 mmol) in 1.0 mL 2 wt % TPGS/H_2O with 0.25 mL THF as co-solvent were reacted at room temperature for 8 hours yielding 86.9 mg (92%) of 2-dodecanamidoethyl 2-(4-aminophenyl)acetate as a pale yellow solid (DCM/MeOH : 90/10).

^1H NMR (500 MHz, DMSO-d_6) δ 7.87 (s, 1 H), 6.89(d, *J* = 5 Hz, 8 H), 6.50 (d, *J* = 8 Hz, 2 H), 4.95 (s, 2 H), 4.00 (t, *J* = 5.5 Hz, 2 H), 3.41 (s, 2 H), 3.28 (q, *J* = 6 Hz, 2 H), 2.07 (t, *J* = 12.5 Hz, 2 H), 1.47 (m, 2 H), 1.23 (m, 16 H), 0.863 (t, *J* = 7 Hz, 3 H).

^{13}C NMR (125 MHz, $CDCl_3$) δ 172.4, 171.7, 147.4, 129.7, 120.9, 113.8, 62.7, 39.5, 37.5, 35.4, 31.3, 29.1, 29.0, 28.9, 28.8, 28.7, 28.6, 25.2, 22.1, 13.9.

HRMS(CI): Calcd. For $C_{22}H_{37}O_3N_2$ $[M+H]^+$ 377.2804. Found: 377.2804.

(3S,8S,9S,10R,13R,14S,17R)-10,13-Dimethyl-17-((R)-6-methylheptan-2-yl)-2,3,4,7,8,9,10,11,12,13,14,15,16,17-tetradecahydro-1H-cyclopenta[a]phenanthren-3-yl 2-(4-nitrophenyl)acetate (26)

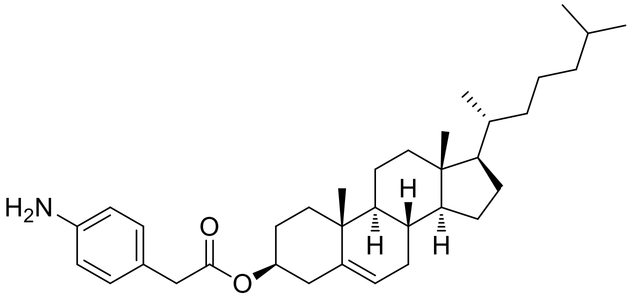

(3S,8S,9S,10R,13R,14S,17R)-10,13-Dimethyl-17-((R)-6-methylheptan-2-yl)-2,3,4,7,8,9,10,11,12,13,14,15,16,17-tetradecahydro-1H-cyclopenta[a]phenanthren-3-yl 2-(4-nitro- phenyl)acetate (137.4 mg, 0.25 mmol), Fe nanoparticles (3 mg), and $NaBH_4$ (28.5 mg, 0.75 mmol) in 1.0 mL 2 wt % TPGS/H_2O with 0.3 mL DCM as co-solvent were reacted at room temperature for 4 hours yielding 123.2 mg (95%) of (3S,8S,9S,10R,13R,14S,17R)-10,13-dimethyl-17- ((R)-6-methylheptan-2-yl)-2,3,4,7,8,9,10,11,12,13,14,15,16,17 tetradecahydro-1H-cyclopenta[a]-phenanthren-3-yl 2-(4-nitrophenyl)acetate as a white solid (hexane/EtOAc : 80/20).

^1H NMR (500 MHz, $CDCl_3$) δ 7.08 (d, *J* = 10 Hz, 2 H), 6.66 (d, *J* =10 Hz, 2 H), 5.35 (d, *J* = 4 Hz, 1 H), 4.60 (m, 1 H), 3.47 (s, 2 H), 3.16 (s, br, 2 H), 3.29 (m, 2 H), 1.99 (m, 2 H), 1.93 (m, 3 H), 1.12 (m, 20 H), 1.01 (s, 4 H), 0.92 (d, 3 H), 0.87 (dd, *J* = 7 Hz, *J* = 2 Hz, 6 H), 0.67 (s, 3 H).

^{13}C NMR (125 MHz, $CDCl_3$) δ 171.7, 146.3, 139.8, 130.2, 124.4, 122.7, 115.4, 74.4, 56.8, 56.3, 50.1, 42.4, 41.0, 39.9, 39.7, 38.2, 37.1, 36.7, 36.3, 35.9, 32.0, 31.9, 28.3, 28.1, 27.9, 24.4, 24.0, 23.0, 22.7, 21.2, 19.5, 18.9, 12.0.

HRMS(EI): Calcd. For $C_{35}H_{53}O_2N$ [M^+] 519.4076. Found: 519.4078.

4-(2-(Diphenylmethylene)hydrazinyl)aniline (27) CAS: 1194714-06-1

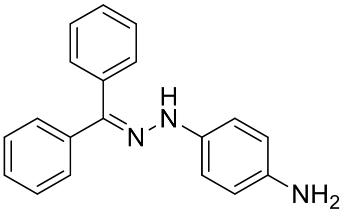

1-(Diphenylmethylene)-2-(4-nitrophenyl)hydrazine (39.7 mg, 0.125 mmol), Fe nanoparticles (1.5 mg), and KBH_4 (40.5 mg, 0.75 mmol) in 1.0 mL 2 wt % TPGS/H_2O with 0.25 mL THF as co-solvent were reacted at room temperature for 16 hours yielding 35.5 mg (99%) of 4-(2-(diphenylmethylene)hydrazinyl)aniline as a dark brown solid (hexane/EtOAc : 70/30).

^{1}H NMR (500 MHz, $CDCl_3$) δ 7.59 (m, 4 H), 7.52 (m, 1 H), 7.34 (m, 6 H), 6.97 (d, *J* = 8.5 Hz, 2 H), 6.71 (d, *J* = 8.5 Hz, 2 H), 3.83 (s, br, 2 H).

^{13}C NMR (125 MHz, $CDCl_3$) δ 148.0, 138.8, 138.7, 138.2, 133.1, 129.7, 129.3, 129.2, 128.2, 127.7, 126.3, 117.0, 114.3.

HRMS(ESI): Calcd. For $C_{19}H_{17}N_3Na$ $[M+Na]^+$ 310.1320. Found: 310.1316.

References

1. Lipshutz, B. H.; Ghorai, S.; Abela, A. R.; Moser, R.; Nishikata, T.; Duplais, C.; Krasovskiy, A.; Gaston, R. D.; Gadwood, R. C. TPGS-750-M: A Second-Generation Amphiphile for Metal-Catalyzed Cross-Couplings in Water at Room Temperature. *J. Org. Chem.* **2011**, *76*, 4379.

2. Isley, N. A.; Linstadt, R. T. H.; Kelly, S. M.; Gallou, F.; Lipshutz, B. H. Nucleophilic Aromatic Substitution Reactions in Water Enabled by Micellar Catalysis. *Org. Lett.* **2015**, *17*, 4734.

3. Handa, S.; Wang, Y.; Gallou, F.; Lipshutz, B. H. Sustainable Fe–ppm Pd nanoparticle catalysis of Suzuki-Miyaura cross-couplings in water. *Science* **2015**, *349*, 1087.

4. Wencel-Delord, J.; Nimphius, C.; Patureau, F. W.; Glorius, F. [RhIIICp*]-Catalyzed Dehydrogenative Aryl-Aryl Bond Formation. *Angew. Chem., Int. Ed.* **2012**, *51*, 2247.

5. Hackl, M. W.; Lakemeyer, M.; Dahmen, M.; Glaser, M.; Pahl, A.; Lorenz-Baath, K.; Menzel, T.; Sievers, S.; Böttcher, T.; Antes, I.; Waldmann, H.; Sieber, S. A. Phenyl Esters Are Potent Inhibitors of Caseinolytic Protease P and Reveal a Stereogenic Switch for Deoligomerization. *J. Am. Chem. Soc.* **2015**, *137*, 8475.

6. Kelly, S. M.; Lipshutz, B. H. Chemoselective Reductions of Nitroaromatics in Water at Room Temperature. *Org. Lett.* **2014**, *16*, 98.

7. Chen, S.; Lu, G.; Cai, C. Iridium-catalyzed transfer hydrogenation of nitroarenes to anilines. *New J. Chem.* **2015**, *39*, 5360.

8. Sathitsuksanoh, N.; Holtman, K. M.; Yelle, D. J.; Morgan, T.; Stavila, V.; Pelton, J.; Blanch, H.; Simmons, B. A.; George, A. Lignin fate and characterization during ionic liquid biomass pretreatment for renewable chemicals and fuels production. *Green Chem.* **2014**, *16*, 1236.

9. Wang, H.; Wen, K.; Nurahmat, N.; Shao, Y.; Zhang, H.; Wei, C.; Li, Y.; Shen, Y.; Sun, Z. Regioselective chlorination and bromination of unprotected anilines under mild conditions using copper halides in ionic liquids. *Beilstein J. Org. Chem.* **2012**, *8*, 744.

10. Rathore, P. S.; Patidar, R.; Shripathi, T.; Thakore, S. Magnetically separable core–shell iron oxide@nickel nanoparticles as high-performance recyclable catalysts for chemoselective reduction of nitroaromatics. *Catal. Sci. Technol.* **2015**, *5*, 286.

11. Cantillo, D.; Baghbanzadeh, M.; Kappe, C. O. In Situ Generated Iron Oxide Nanocrystals as Efficient and Selective Catalysts for the Reduction of Nitroarenes using a Continuous Flow Method. *Angew. Chem., Int. Ed.* **2012**, *51*, 10190.

12. Kasparian, A. J.; Savarin, C.; Allgeier, A. M.; Walker, S. D. Selective Catalytic Hydrogenation of Nitro Groups in the Presence of Activated Heteroaryl Halides. *J. Org. Chem.* **2011**, *76*, 9841.

13. Sultane, P. R.; Mete, T. B.; Bhat, R. G. Chemoselective N-deacetylation under mild conditions. *Org. Biomol. Chem.* **2014**, *12*, 261.

14. Lu, H.; Geng, Z.; Li, J.; Zou, D.; Wu, Y.; Wu, Y. Metal-Free Reduction of Aromatic Nitro Compounds to Aromatic Amines with B_2pin_2 in Isopropanol. *Org. Lett.* **2016**, *18*, 2774.

15. Tezuka, N.; Shimojo, K.; Hirano, K.; Komagawa, S.; Yoshida, K.; Wang, C.; Miyamoto, K.; Saito, T.; Takita, R.; Uchiyama, M. Direct Hydroxylation and Amination of Arenes via Deprotonative Cupration. *J. Am. Chem. Soc.* **2016**, *138*, 9166.

16. Feng, J.; Handa, S.; Gallou, F.; Lipshutz, B. H. Safe and Selective Nitro Group Reductions Catalyzed by Sustainable and Recyclable Fe/ppm Pd Nanoparticles in Water at Room Temperature. *Angew. Chem., Int. Ed.* **2016**, *55*, 8979.

17. Chakravorty, S.; Klein, H. F.; Hodson, L. E.; Rabillier, M.; Fang, Z.; Richters, A.; Pelly, S. C.; Rauh, D.; Van Otterlo, W. A. L. Synthesis of Novel Piperazine-linked Anthranilic Acids as Potential Small Molecule Kinase Inhibitors. *South Afr. J. Chem.* **2014**, *67*, 71.

18. Yang, D.; Yan, K.; Wei, W.; Zhao, J.; Zhang, M.; Sheng, X.; Li, G.; Lu, S.; Wang, H. Metal-Free Iodine-Catalyzed Direct Arylthiation of Substituted Anilines with Thiols. *J. Org. Chem.* **2015**, *80*, 6083.

NMR spectra

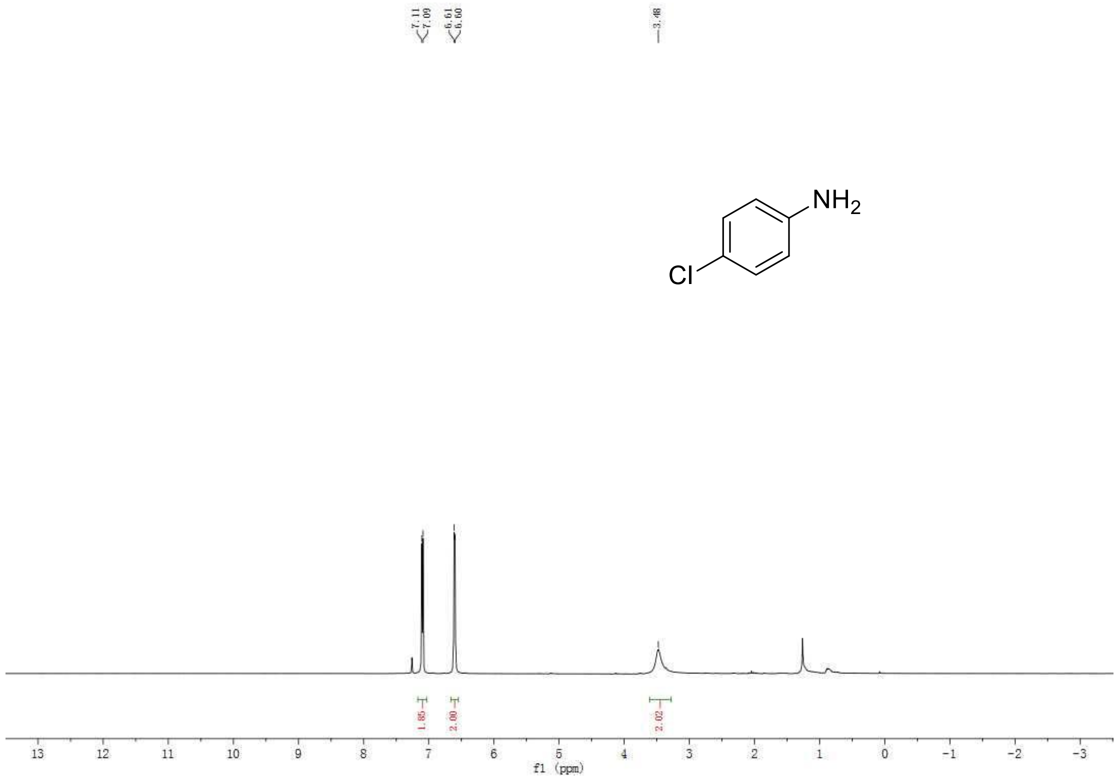
7.11
7.09
6.61
6.60
3.48
NH$_2$
Cl
1.85
2.00
2.02
13 12 11 10 9 8 7 6 5 4 3 2 1 0 -1 -2 -3
f1 (ppm)

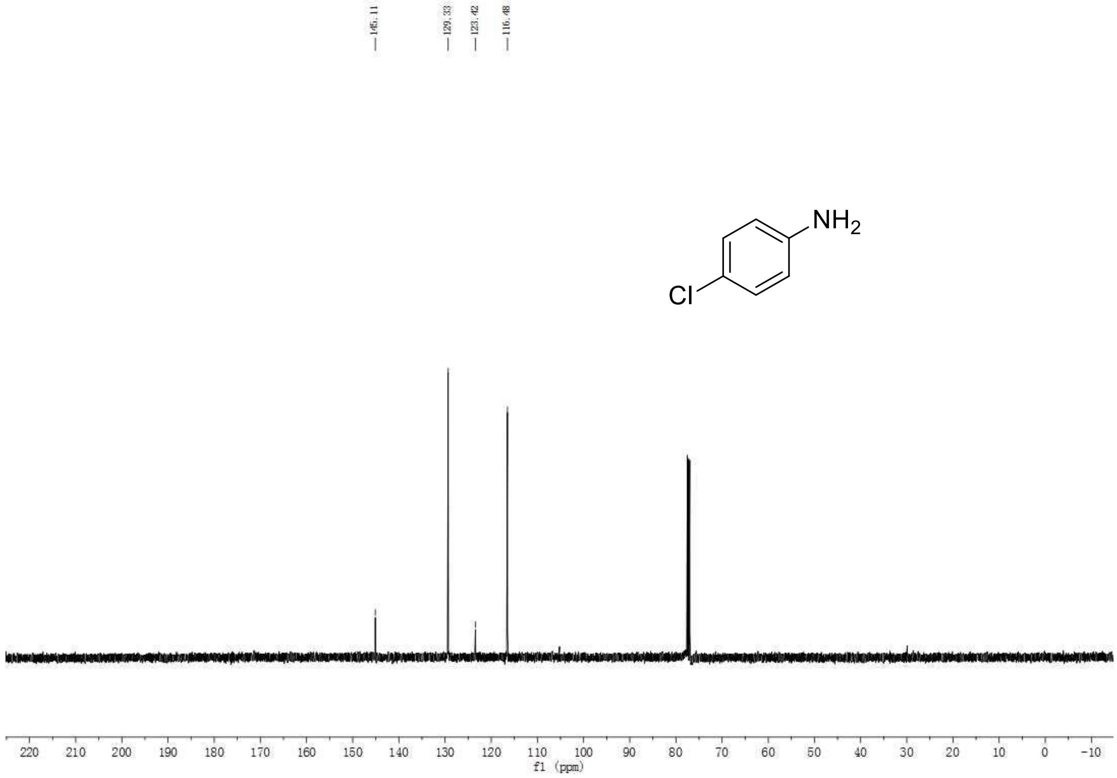
145.11
129.33
123.42
116.48
NH$_2$
Cl
220 210 200 190 180 170 160 150 140 130 120 110 100 90 80 70 60 50 40 30 20 10 0 -10
f1 (ppm)

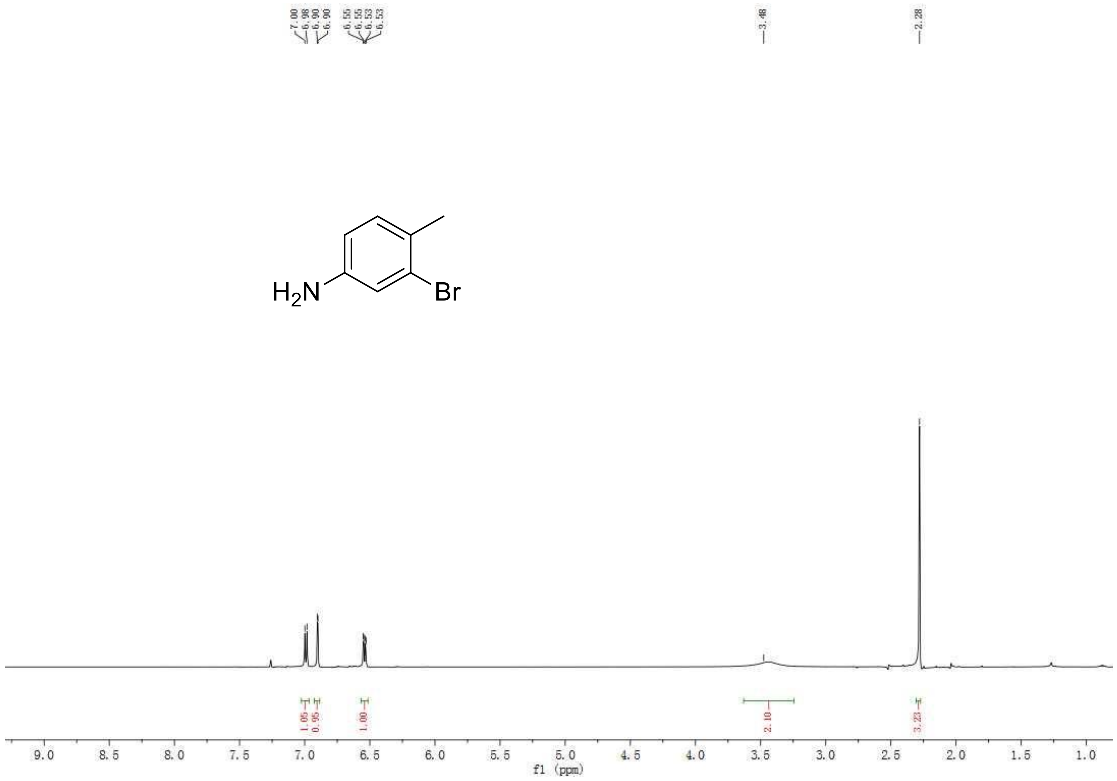
7.00
6.98
6.90
6.90
6.55
6.55
6.53
6.53
3.48
2.28
H2N
Br
1.05
0.95
1.00
2.10
3.23
9.0
8.5
8.0
7.5
7.0
6.5
6.0
5.5
5.0
4.5
4.0
3.5
3.0
2.5
2.0
1.5
1.0
f1 (ppm)

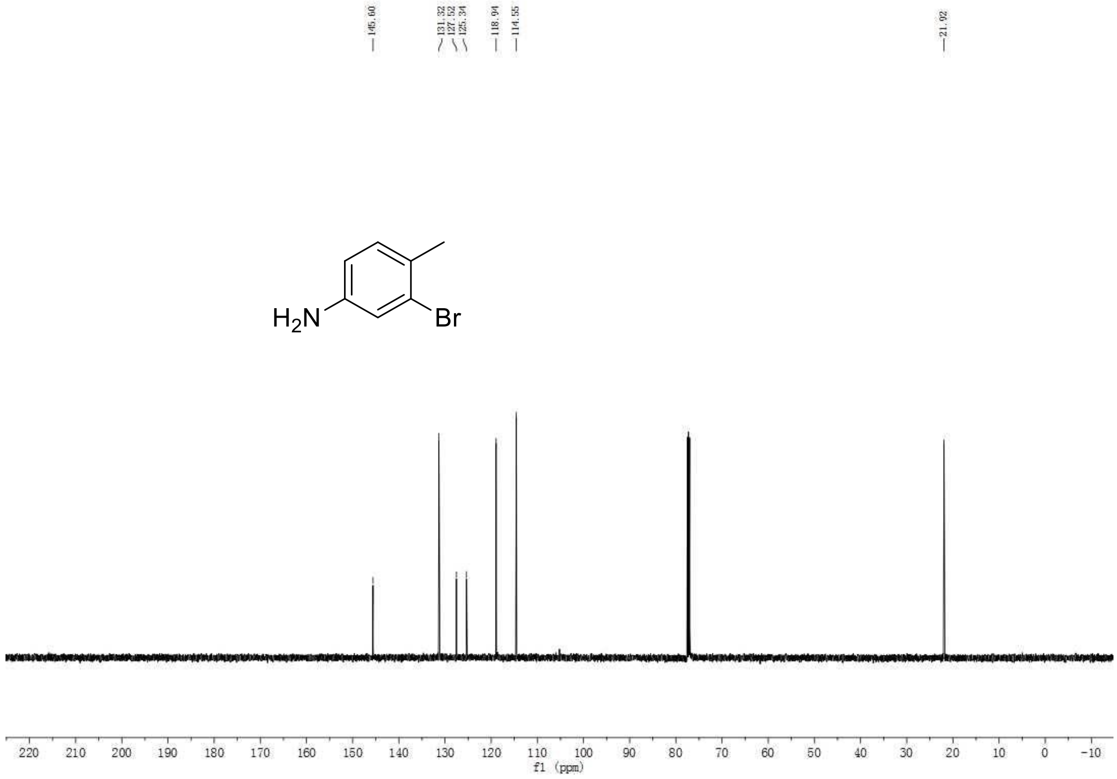
145.60
131.32
127.52
125.34
118.94
114.55
21.92
H2N
Br
220
210
200
190
180
170
160
150
140
130
120
110
100
90
80
70
60
50
40
30
20
10
0
-10
f1 (ppm)

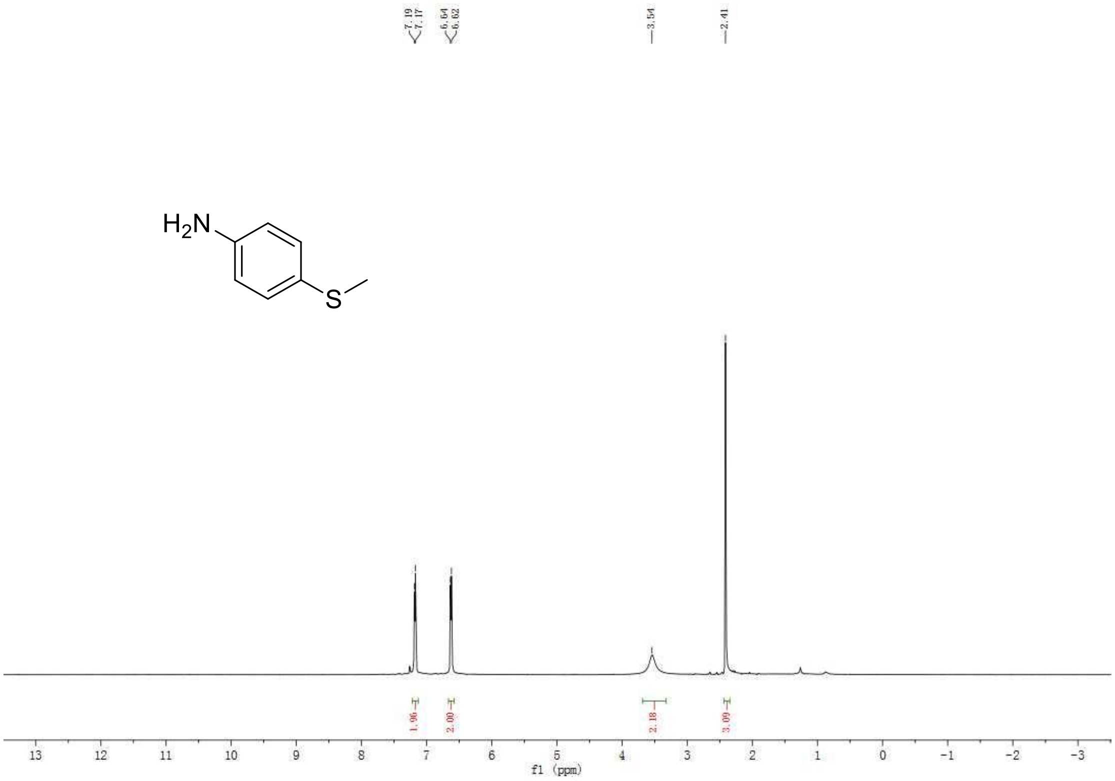
7.19
7.17
6.64
6.62
3.54
2.41
H_2N
S
1.96
2.00
2.18
3.09
13 12 11 10 9 8 7 6 5 4 3 2 1 0 −1 −2 −3
f1 (ppm)

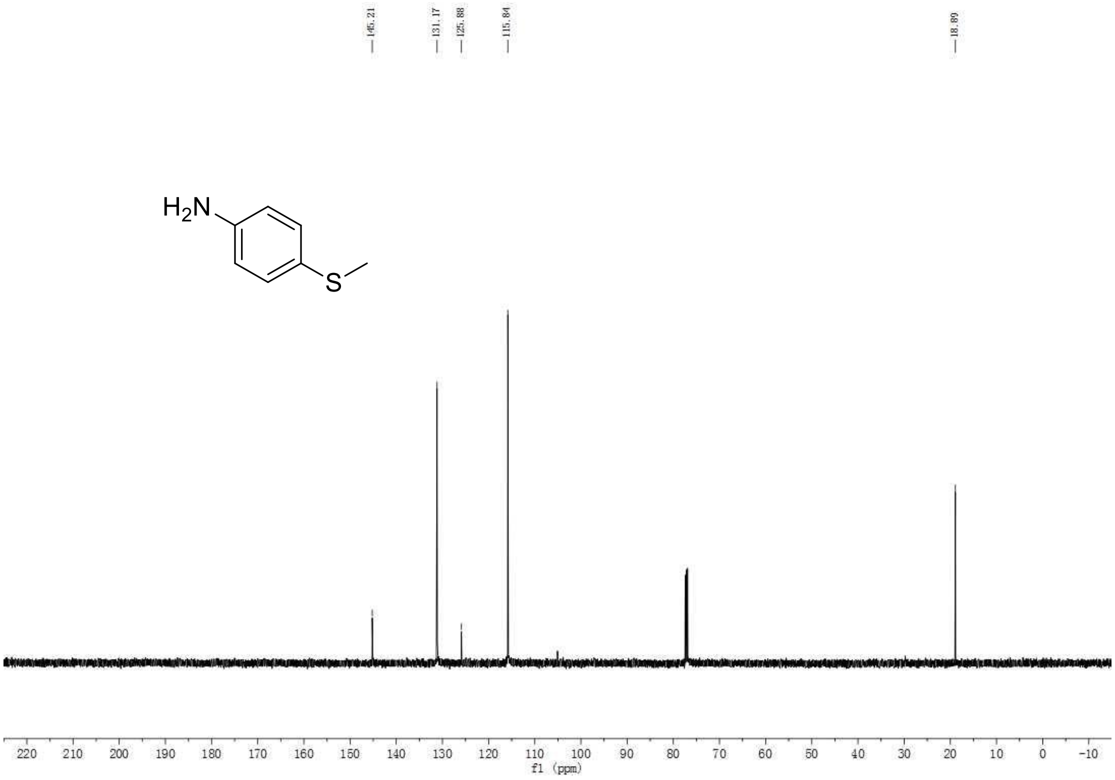
145.21
131.17
125.88
115.84
18.89
H_2N
S
220 210 200 190 180 170 160 150 140 130 120 110 100 90 80 70 60 50 40 30 20 10 0 −10
f1 (ppm)

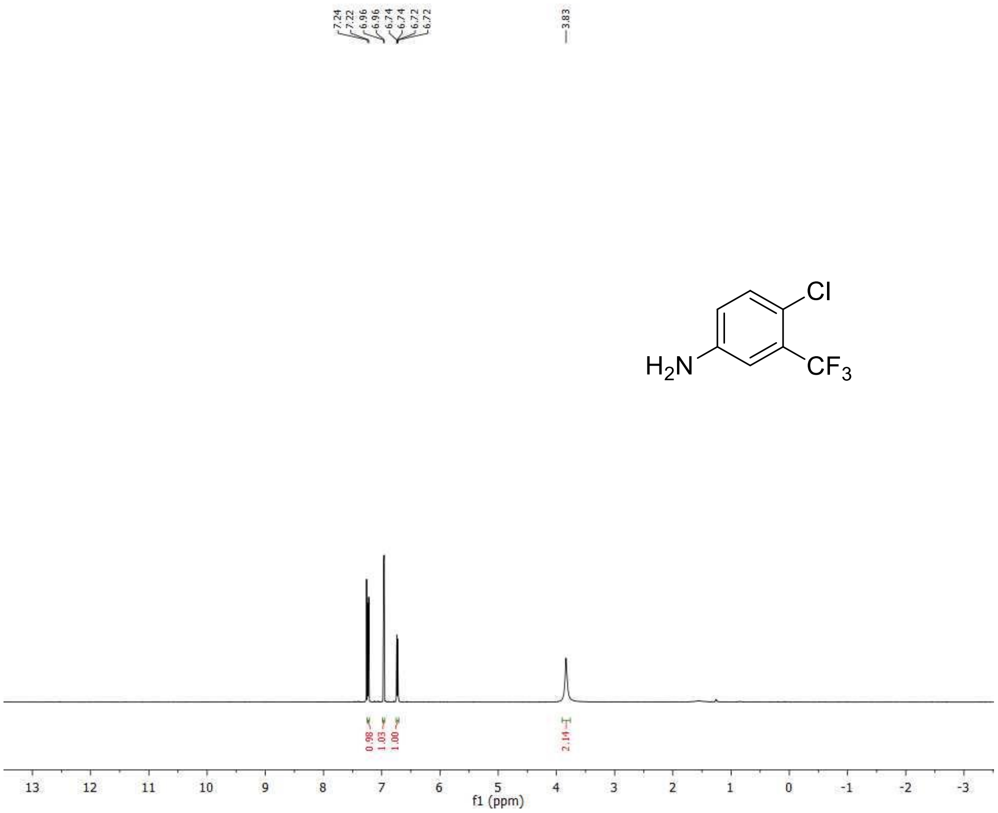

7.24
7.22
6.96
6.96
6.74
6.74
6.72
6.72
3.83
Cl
H2N
CF3
0.98
1.03
1.00
2.14
13
12
11
10
9
8
7
6
5
4
3
2
1
0
-1
-2
-3
f1 (ppm)

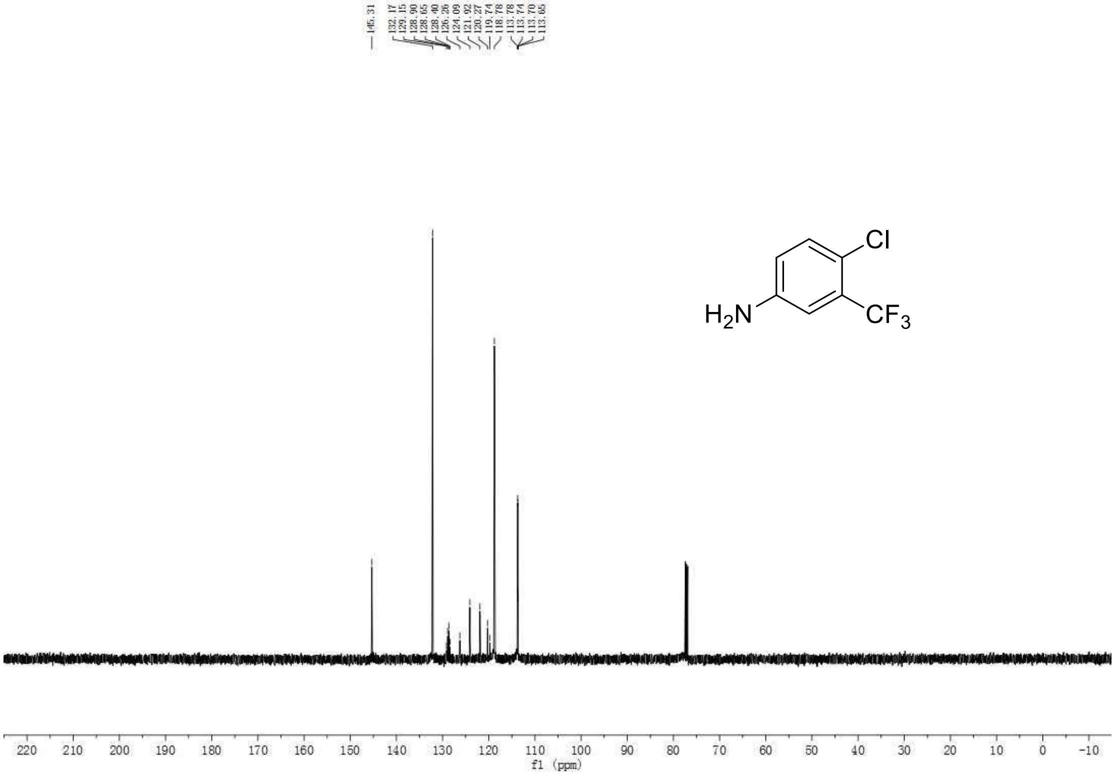

145.31
132.17
129.15
128.90
128.65
128.40
126.26
124.09
121.92
120.27
119.74
118.78
113.78
113.74
113.70
113.65
Cl
H2N
CF3
220
210
200
190
180
170
160
150
140
130
120
110
100
90
80
70
60
50
40
30
20
10
0
-10
f1 (ppm)

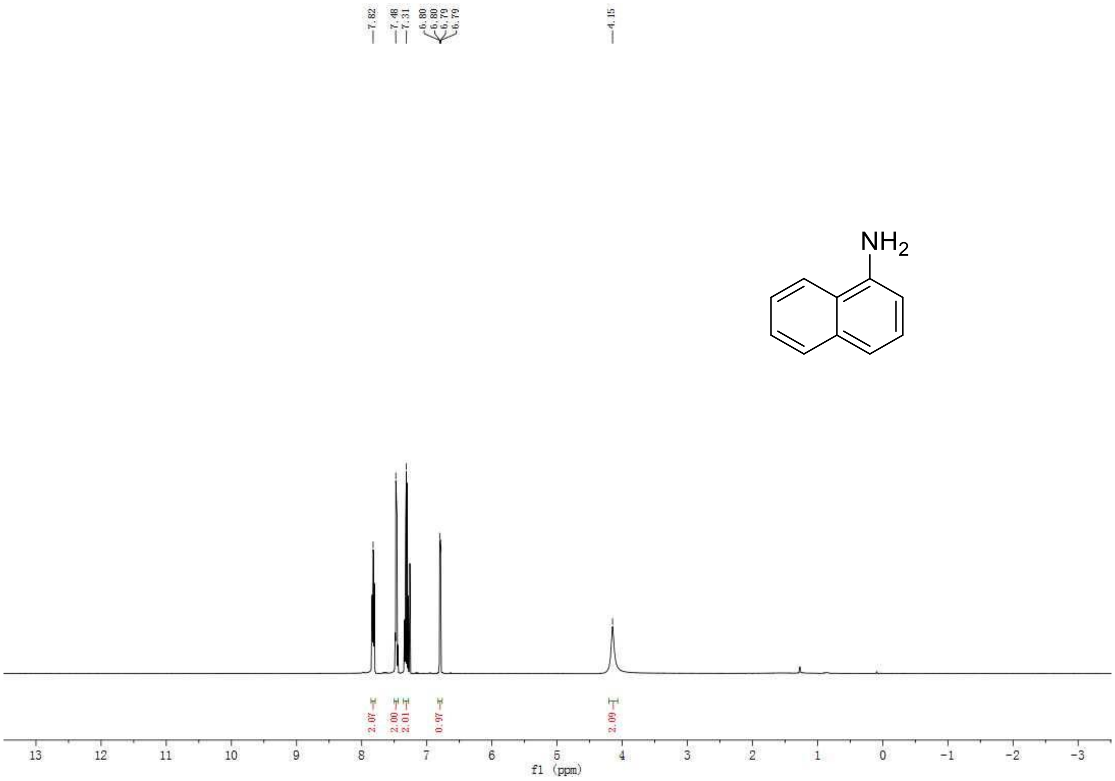
7.82
7.48
7.31
6.80
6.80
6.79
6.79
4.15
NH2
2.07
2.00
2.01
0.97
2.09
13
12
11
10
9
8
7
6
5
4
3
2
1
0
-1
-2
-3
f1 (ppm)

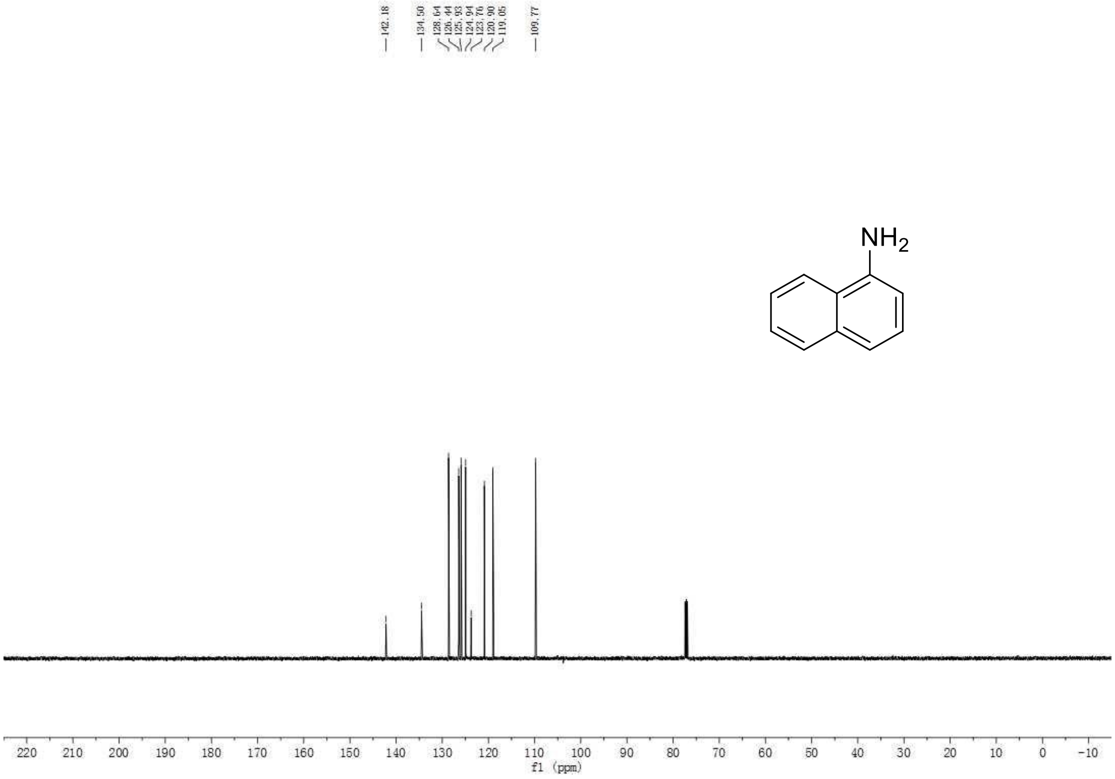
142.18
134.50
128.64
126.44
125.93
124.94
123.76
120.90
119.05
109.77
NH2
220
210
200
190
180
170
160
150
140
130
120
110
100
90
80
70
60
50
40
30
20
10
0
-10
f1 (ppm)

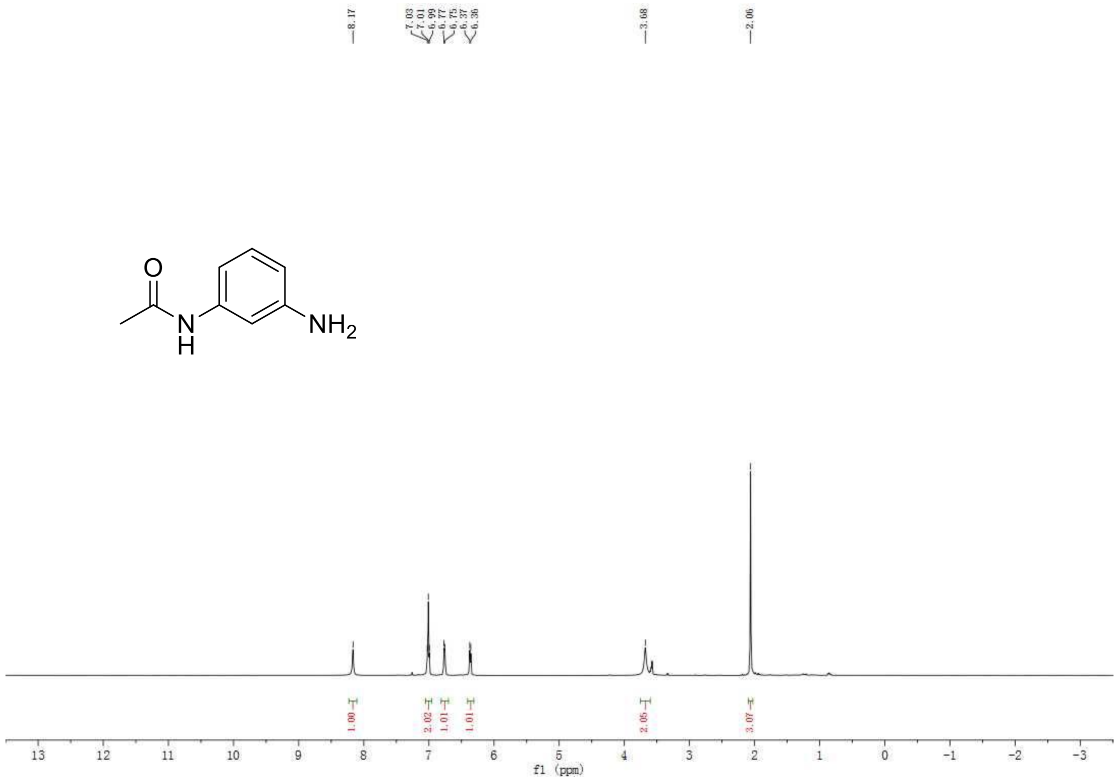
8.17
7.03
7.01
6.99
6.77
6.75
6.37
6.36
3.68
2.06
O
N
H
NH2
1.00
2.02
1.01
1.01
2.05
3.07
13
12
11
10
9
8
7
6
5
4
3
2
1
0
-1
-2
-3
f1 (ppm)

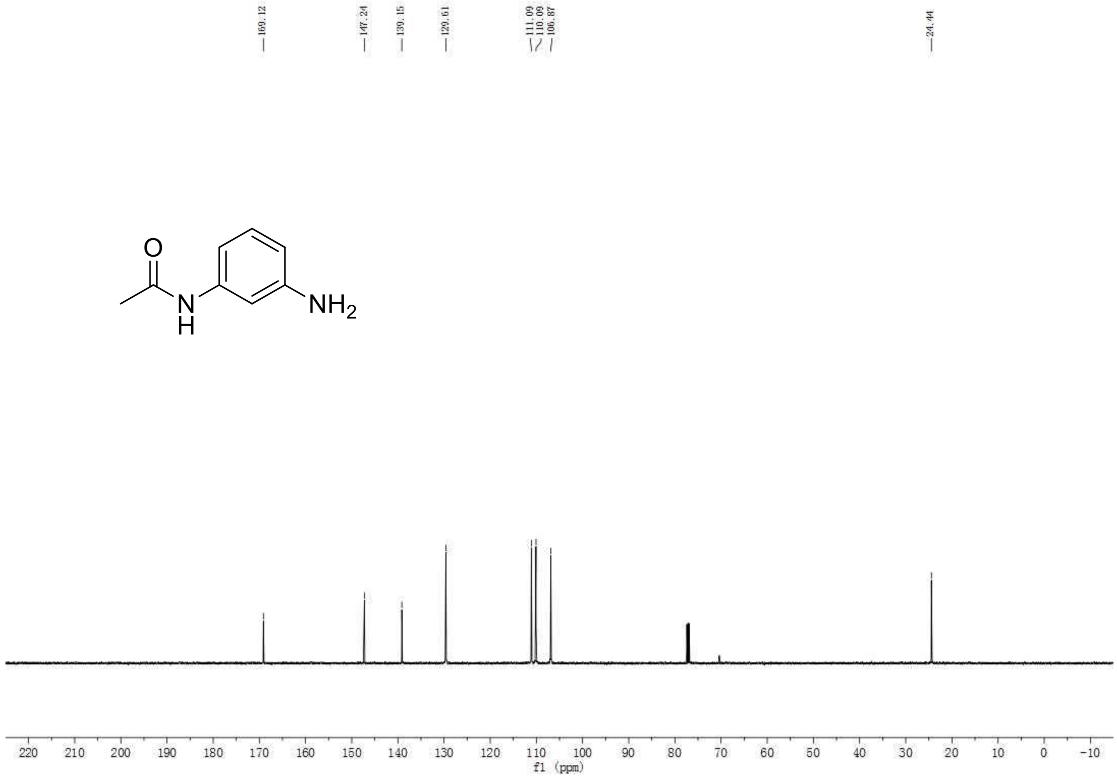
169.12
147.24
139.15
129.61
111.09
110.09
106.87
24.44
O
N
H
NH2
220
210
200
190
180
170
160
150
140
130
120
110
100
90
80
70
60
50
40
30
20
10
0
-10
f1 (ppm)

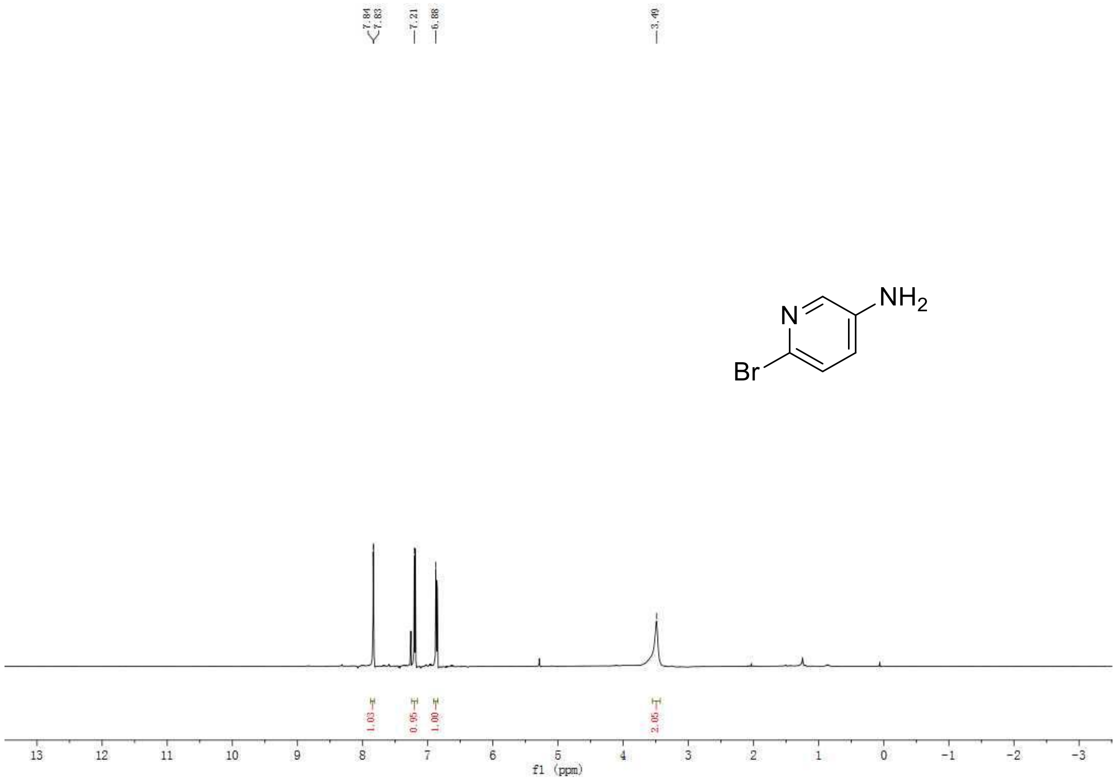

7.84
7.83
7.21
6.88
3.49
NH$_2$
N
Br
1.03
0.95
1.00
2.05
13 12 11 10 9 8 7 6 5 4 3 2 1 0 -1 -2 -3
f1 (ppm)

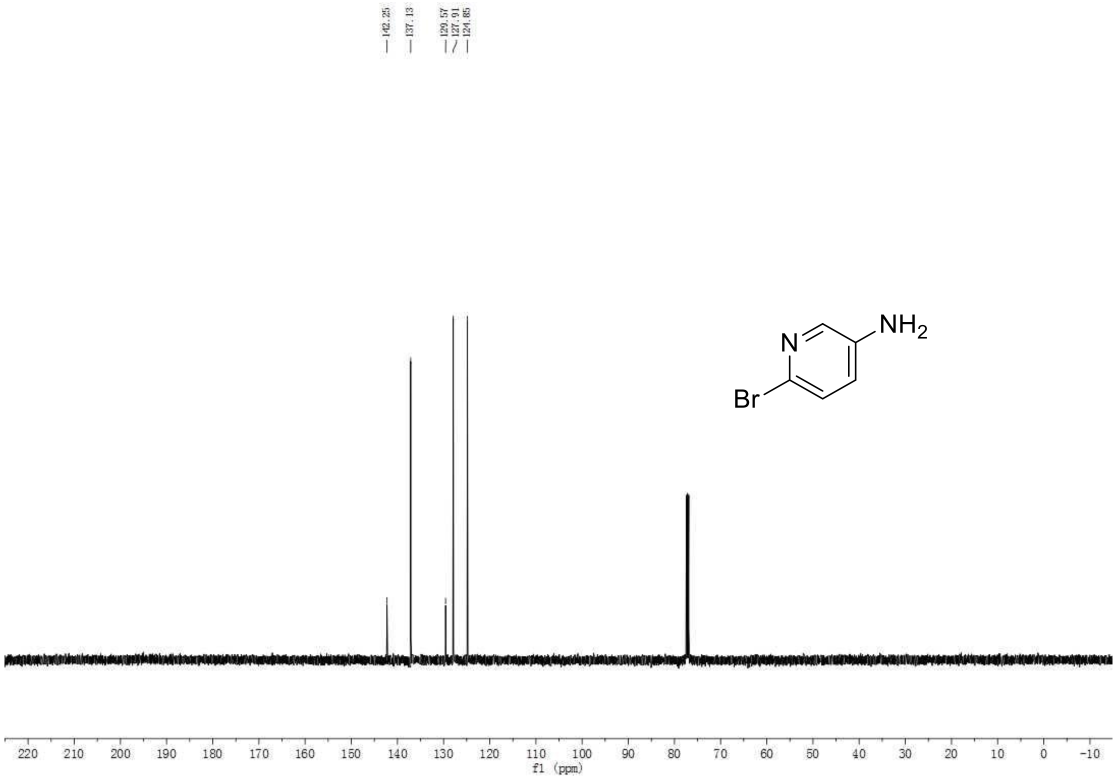

142.25
137.13
129.57
127.91
124.85
NH$_2$
N
Br
220 210 200 190 180 170 160 150 140 130 120 110 100 90 80 70 60 50 40 30 20 10 0 -10
f1 (ppm)

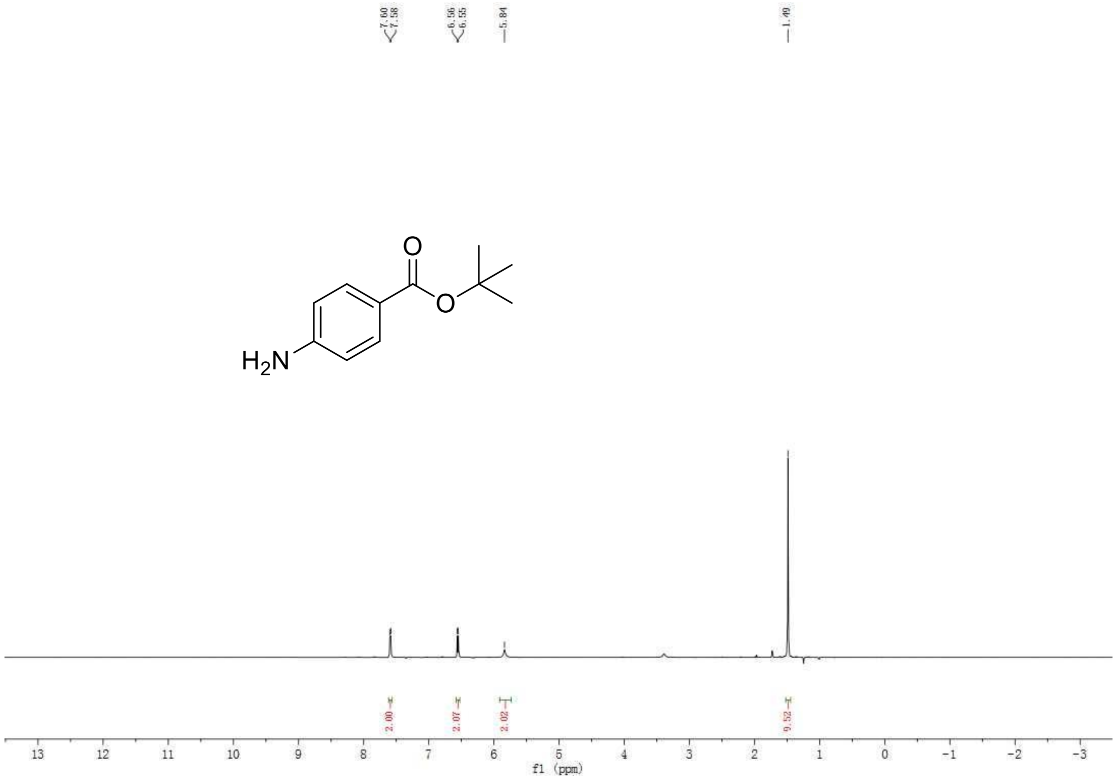

7.60
7.58
6.56
6.55
5.84
1.49
O
O
H2N
2.00
2.07
2.02
9.52
13
12
11
10
9
8
7
6
5
4
3
2
1
0
-1
-2
-3
f1 (ppm)

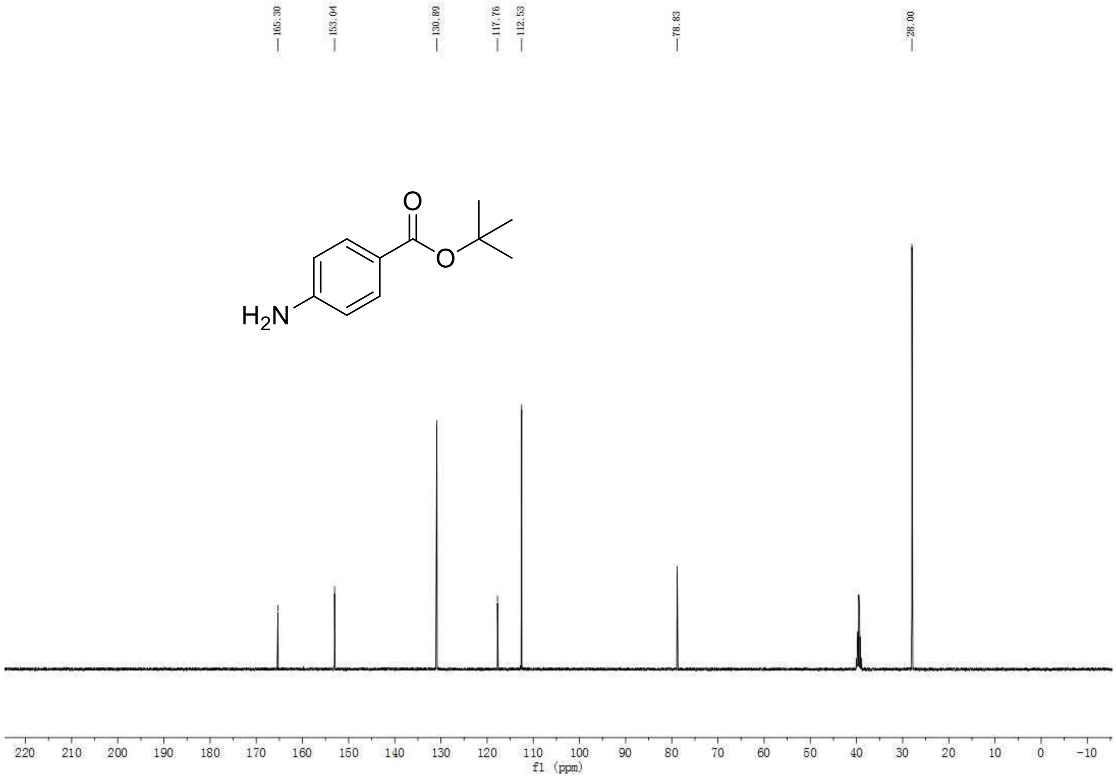

165.30
153.04
130.89
117.76
112.53
78.83
28.00
O
O
H2N
220
210
200
190
180
170
160
150
140
130
120
110
100
90
80
70
60
50
40
30
20
10
0
-10
f1 (ppm)

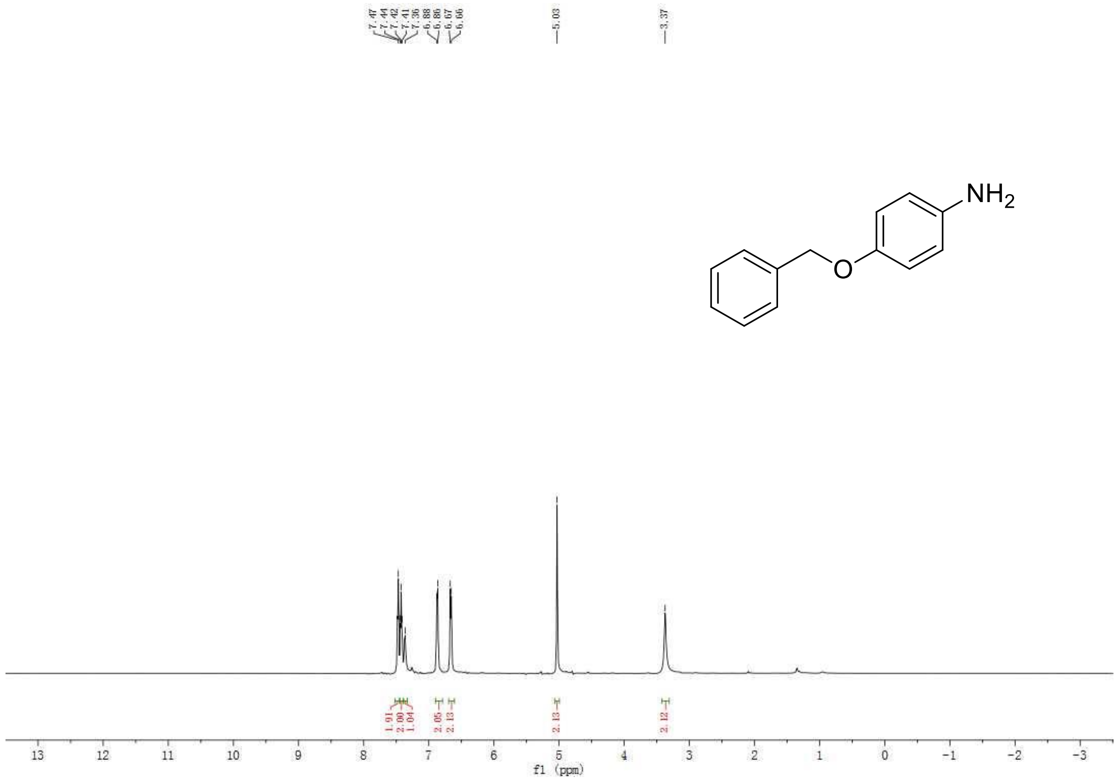
7.47
7.44
7.42
7.41
7.36
6.88
6.86
6.67
6.66
5.03
3.37
NH2
O
1.91
2.00
1.04
2.05
2.13
2.13
2.12
13
12
11
10
9
8
7
6
5
4
3
2
1
0
-1
-2
-3
f1 (ppm)

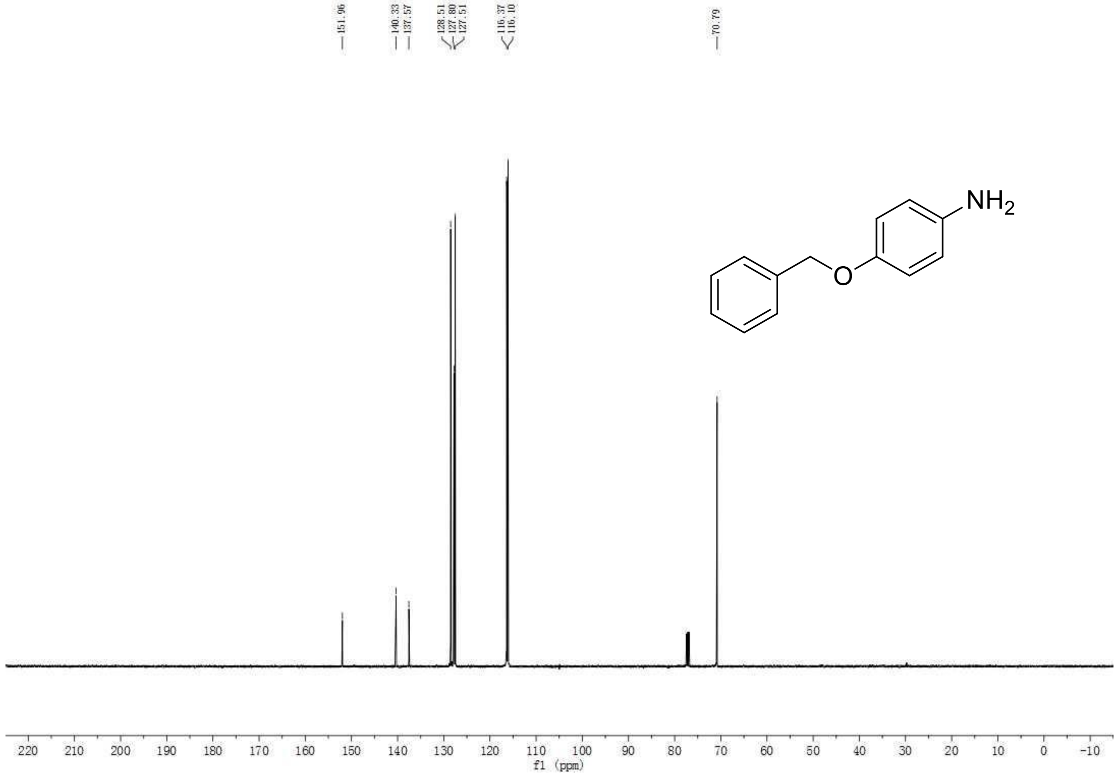
151.96
140.33
137.57
128.51
127.80
127.51
116.37
116.10
70.79
NH2
O
220
210
200
190
180
170
160
150
140
130
120
110
100
90
80
70
60
50
40
30
20
10
0
-10
f1 (ppm)

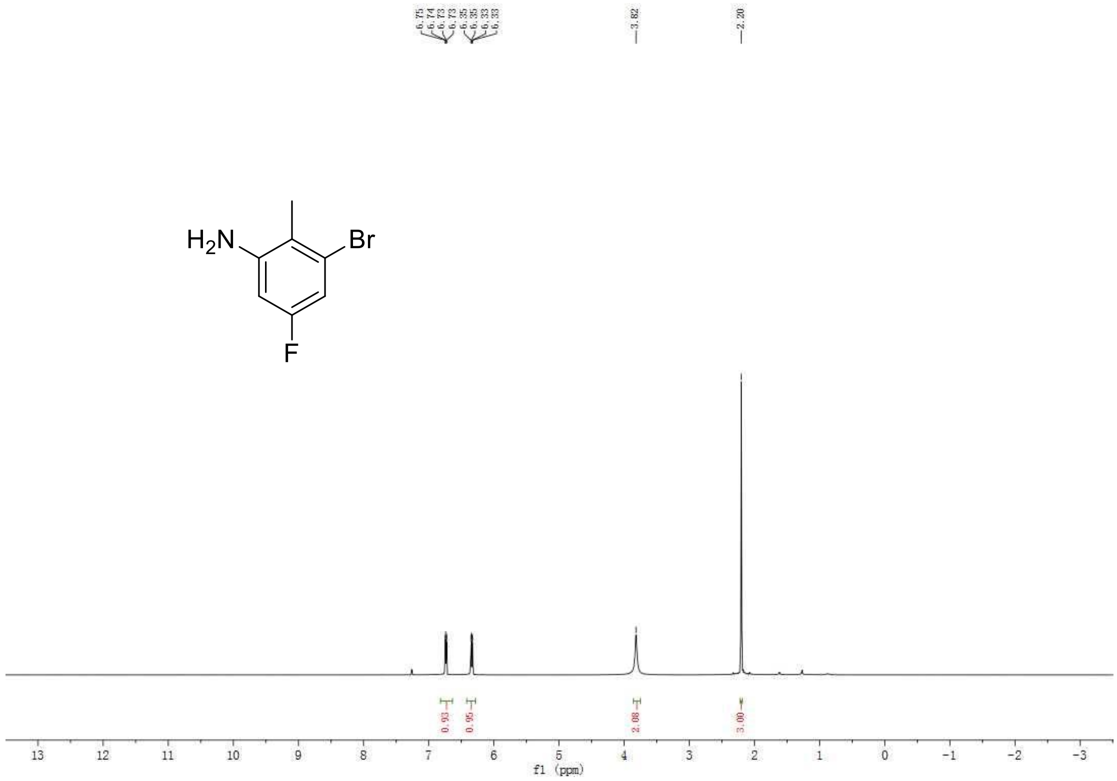
6.75
6.74
6.73
6.73
6.35
6.35
6.33
6.33
3.82
2.20
H2N
Br
F
0.93
0.95
2.08
3.00
13
12
11
10
9
8
7
6
5
4
3
2
1
0
-1
-2
-3
f1 (ppm)

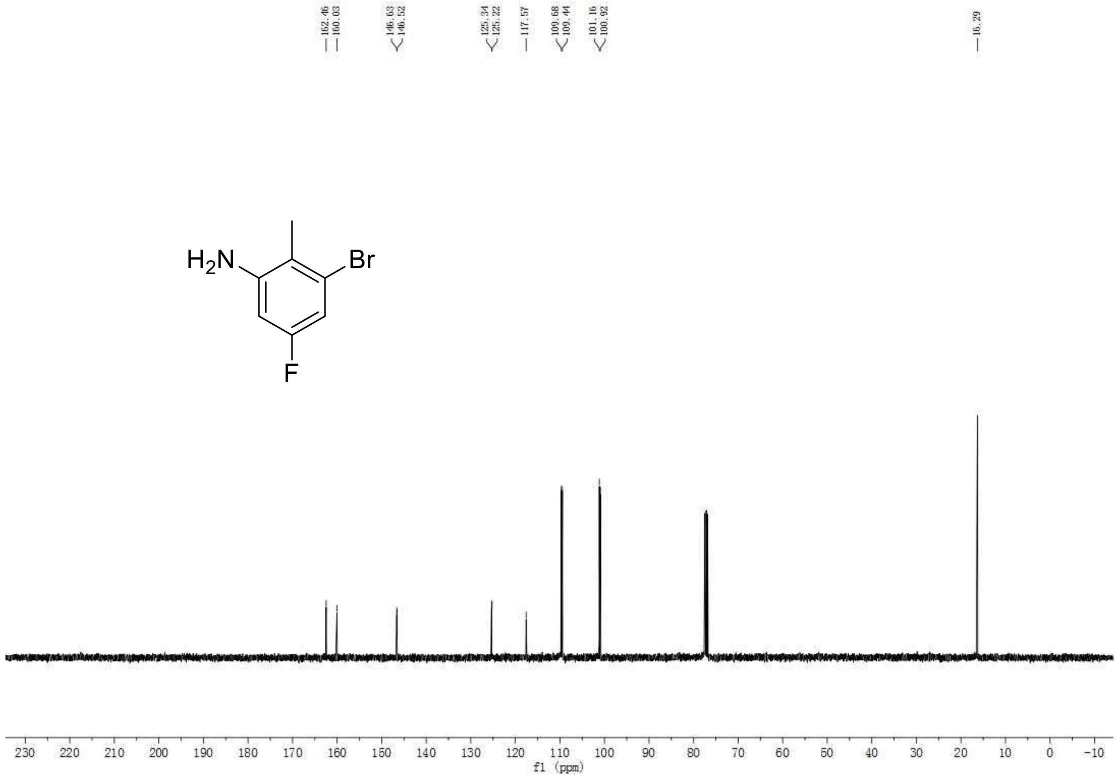
162.46
160.03
146.63
146.52
125.34
125.22
117.57
109.68
109.44
101.16
100.92
16.29
H2N
Br
F
230
220
210
200
190
180
170
160
150
140
130
120
110
100
90
80
70
60
50
40
30
20
10
0
-10
f1 (ppm)

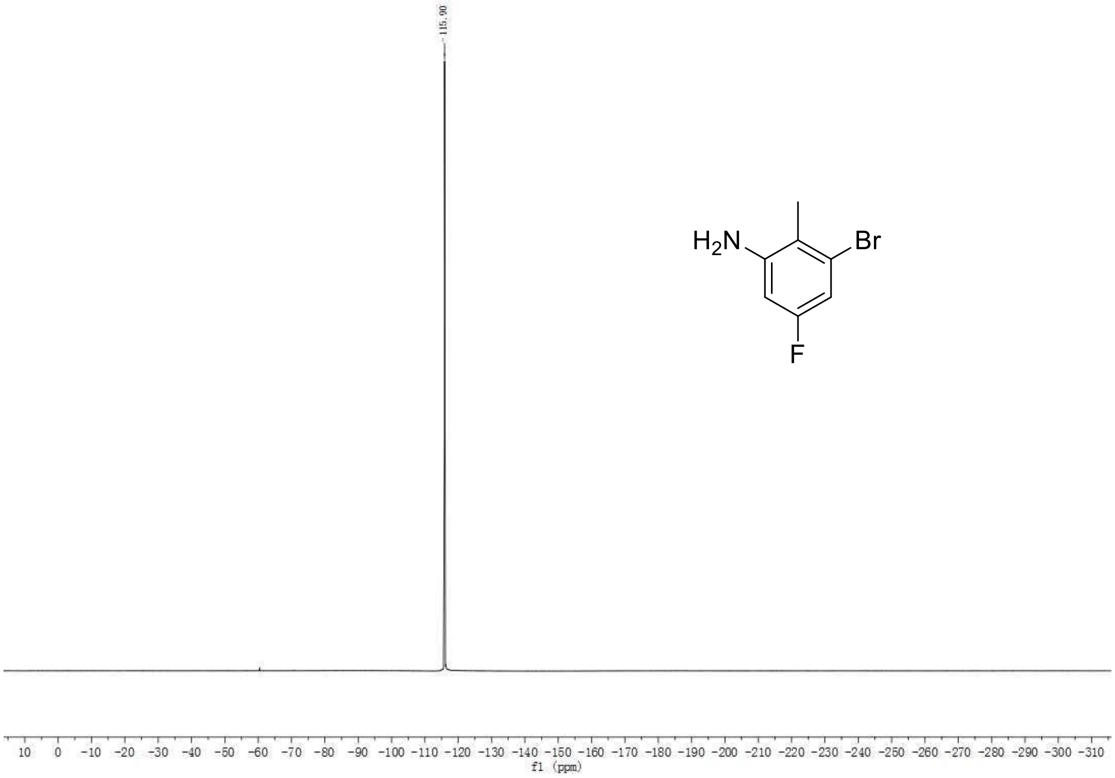
-115.90
H$_2$N
Br
F
10 0 -10 -20 -30 -40 -50 -60 -70 -80 -90 -100 -110 -120 -130 -140 -150 -160 -170 -180 -190 -200 -210 -220 -230 -240 -250 -260 -270 -280 -290 -300 -310
f1 (ppm)

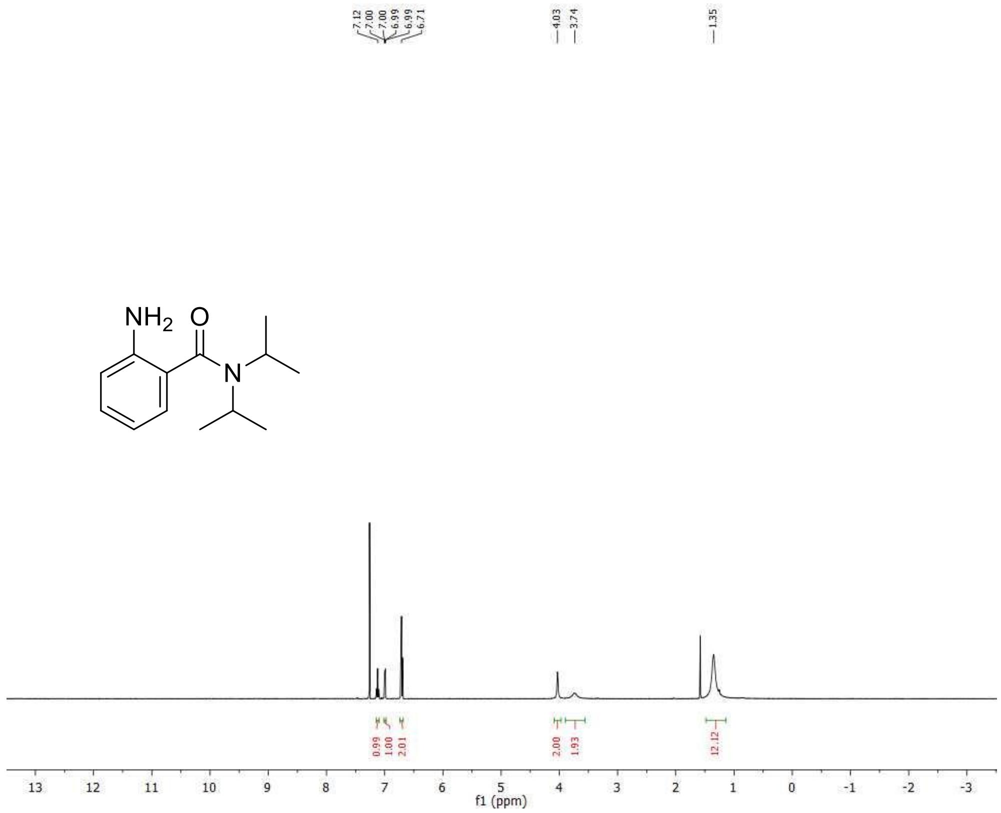
7.12
7.00
7.00
6.99
6.99
6.71
4.03
3.74
1.35
NH2
O
N
0.99
1.00
2.01
2.00
1.93
12.12
13
12
11
10
9
8
7
6
5
4
3
2
1
0
-1
-2
-3
f1 (ppm)

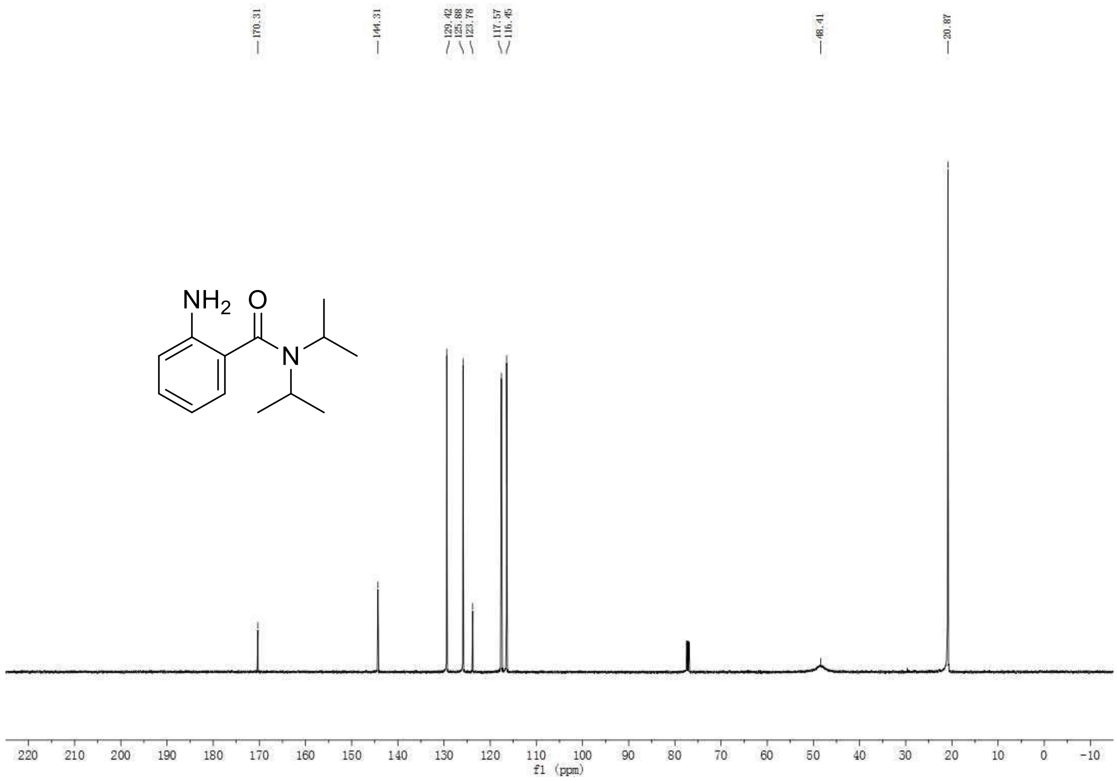
170.31
144.31
129.42
125.88
123.78
117.57
116.45
48.41
20.87
NH2
O
N
220
210
200
190
180
170
160
150
140
130
120
110
100
90
80
70
60
50
40
30
20
10
0
-10
f1 (ppm)

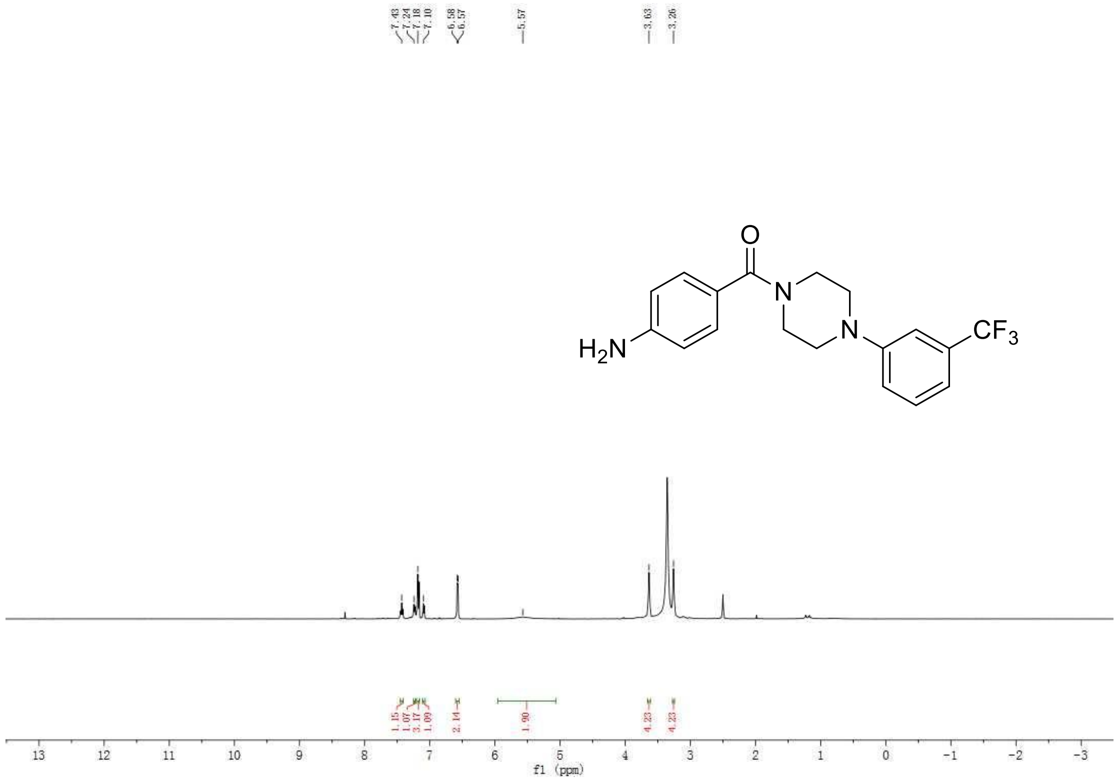
7.43
7.24
7.18
7.10
6.58
6.57
5.57
3.63
3.26
O
N
N
H_2N
CF_3
1.15
1.07
3.17
1.09
2.14
1.90
4.23
4.23
13
12
11
10
9
8
7
6
5
4
3
2
1
0
-1
-2
-3
f1 (ppm)

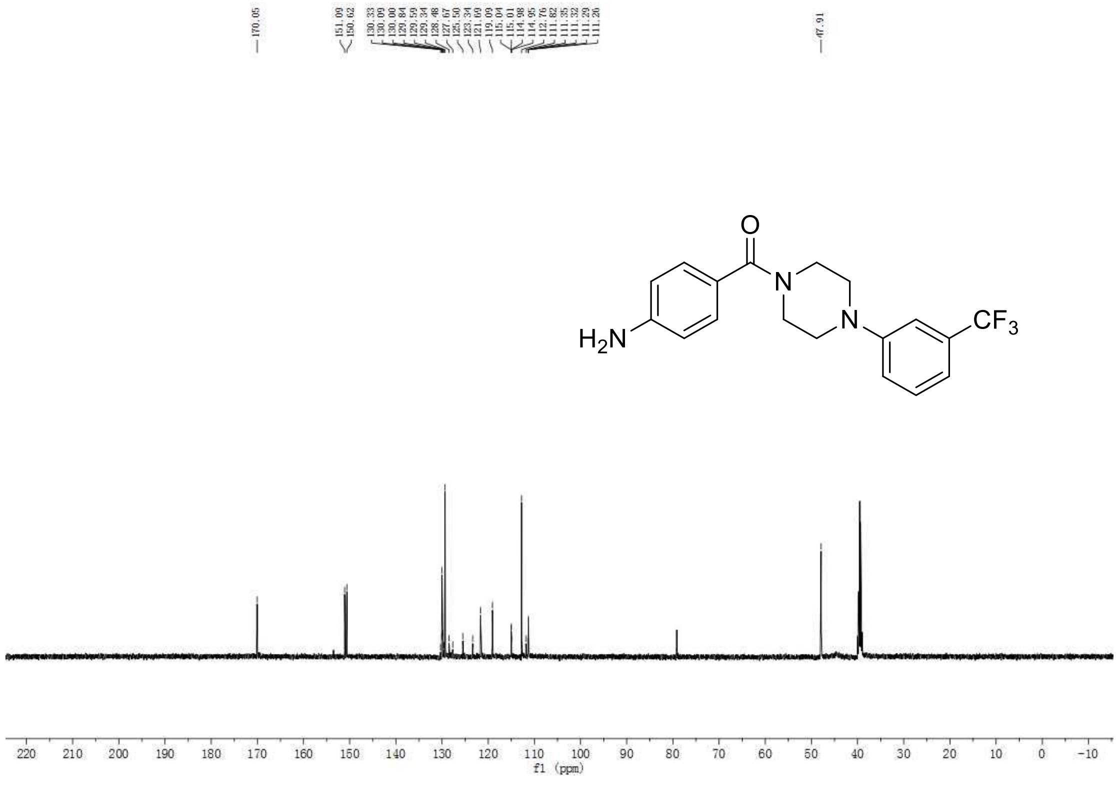
170.05
151.09
150.62
130.33
130.09
130.00
129.84
129.59
129.34
128.48
127.67
125.50
123.34
121.69
119.09
115.04
115.01
114.98
114.95
112.76
111.82
111.35
111.32
111.29
111.26
47.91
O
N
N
H_2N
CF_3
220
210
200
190
180
170
160
150
140
130
120
110
100
90
80
70
60
50
40
30
20
10
0
-10
f1 (ppm)

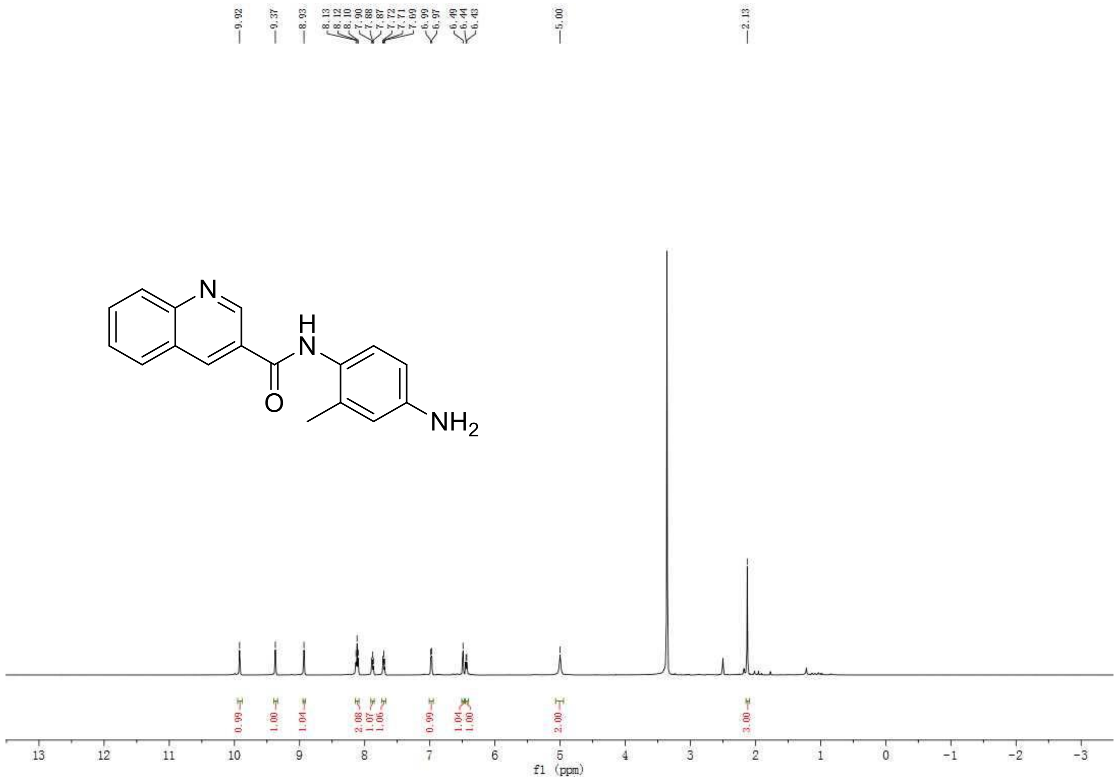
9.92
9.37
8.93
8.13
8.12
8.10
7.90
7.88
7.87
7.72
7.71
7.69
6.99
6.97
6.49
6.44
6.43
5.00
2.13
N
H
N
O
NH2
0.99
1.00
1.04
2.08
1.07
1.06
0.99
1.04
1.00
2.00
3.00
13
12
11
10
9
8
7
6
5
4
3
2
1
0
-1
-2
-3
f1 (ppm)

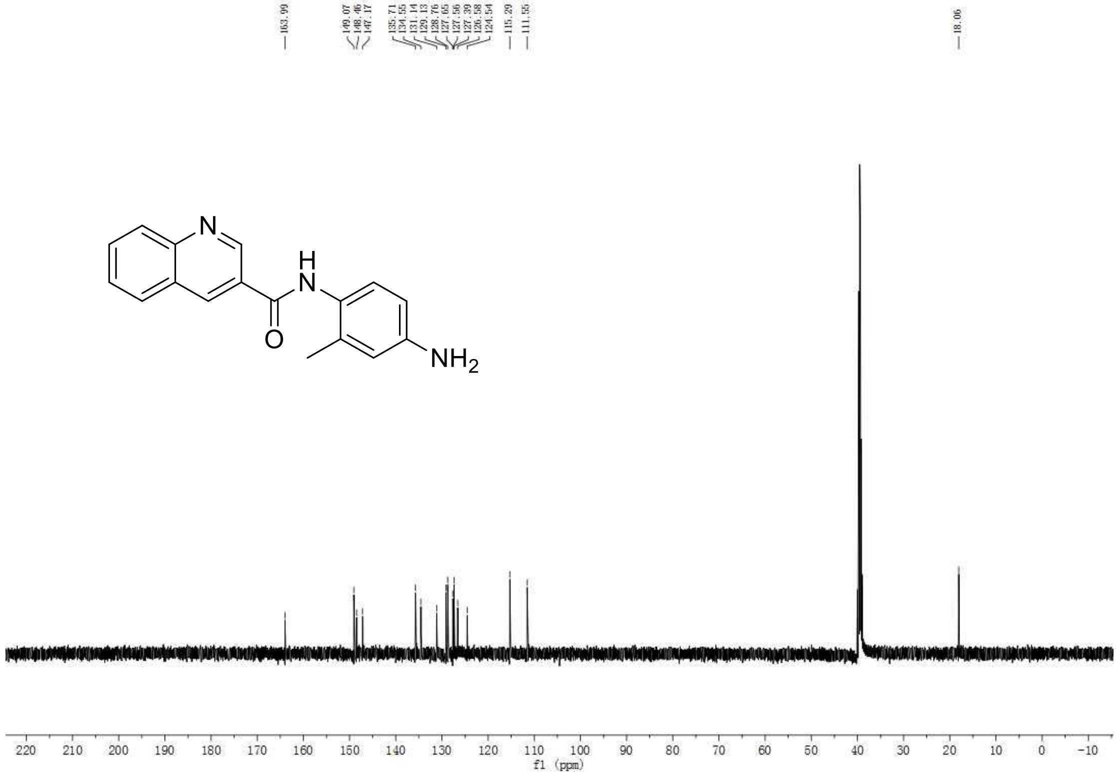
163.99
149.07
148.46
147.17
135.71
134.55
131.14
129.13
128.76
127.65
127.56
127.39
126.58
124.54
115.29
111.55
18.06
N
H
N
O
NH2
220
210
200
190
180
170
160
150
140
130
120
110
100
90
80
70
60
50
40
30
20
10
0
-10
f1 (ppm)

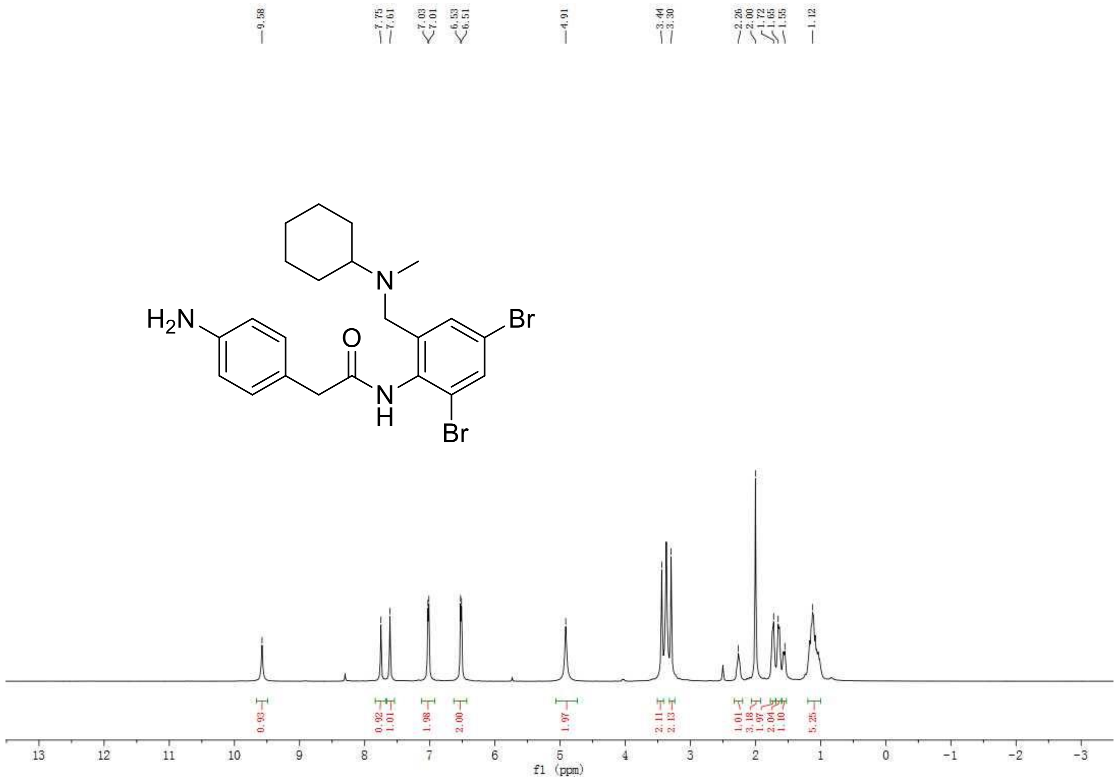
9.58
7.75
7.61
7.03
7.01
6.53
6.51
4.91
3.44
3.30
2.26
2.00
1.72
1.65
1.55
1.12
H₂N
O
N
H
N
Br
Br
0.93
0.92
1.01
1.98
2.00
1.97
2.11
2.13
1.01
3.18
1.97
2.04
1.10
5.25
13
12
11
10
9
8
7
6
5
4
3
2
1
0
-1
-2
-3
f1 (ppm)

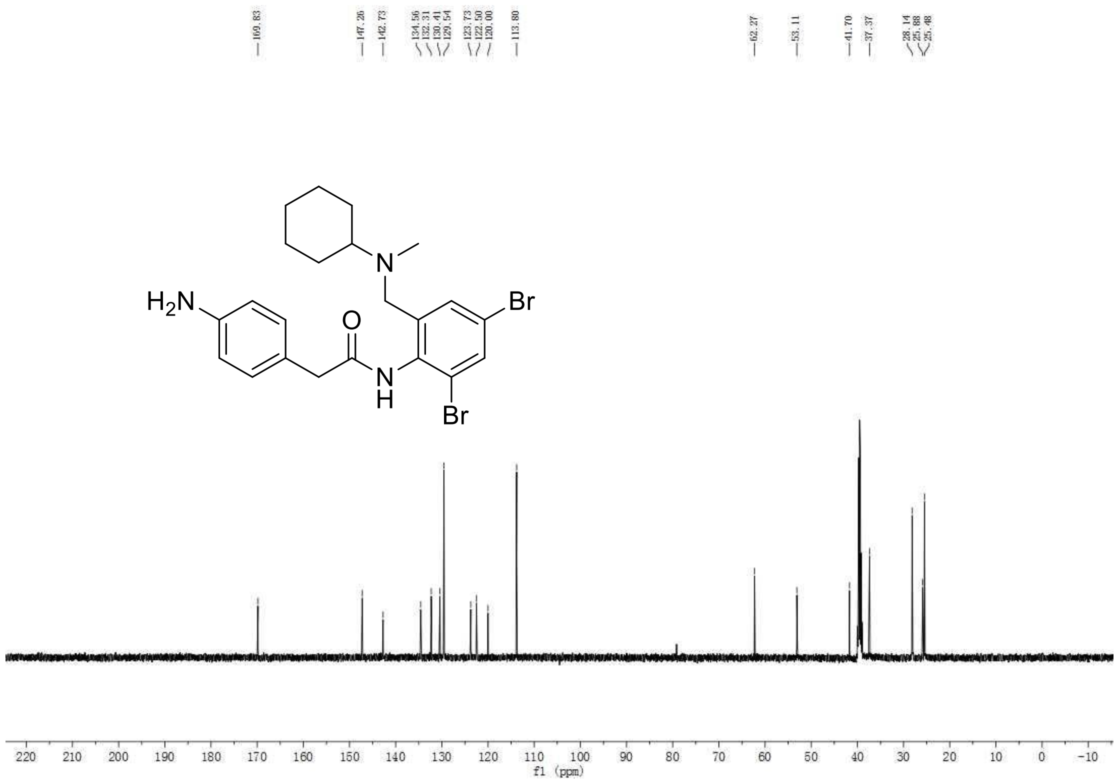
169.83
147.26
142.73
134.56
132.31
130.41
129.54
123.73
122.50
120.00
113.80
62.27
53.11
41.70
37.37
28.14
25.88
25.48
H₂N
O
N
H
N
Br
Br
220
210
200
190
180
170
160
150
140
130
120
110
100
90
80
70
60
50
40
30
20
10
0
-10
f1 (ppm)

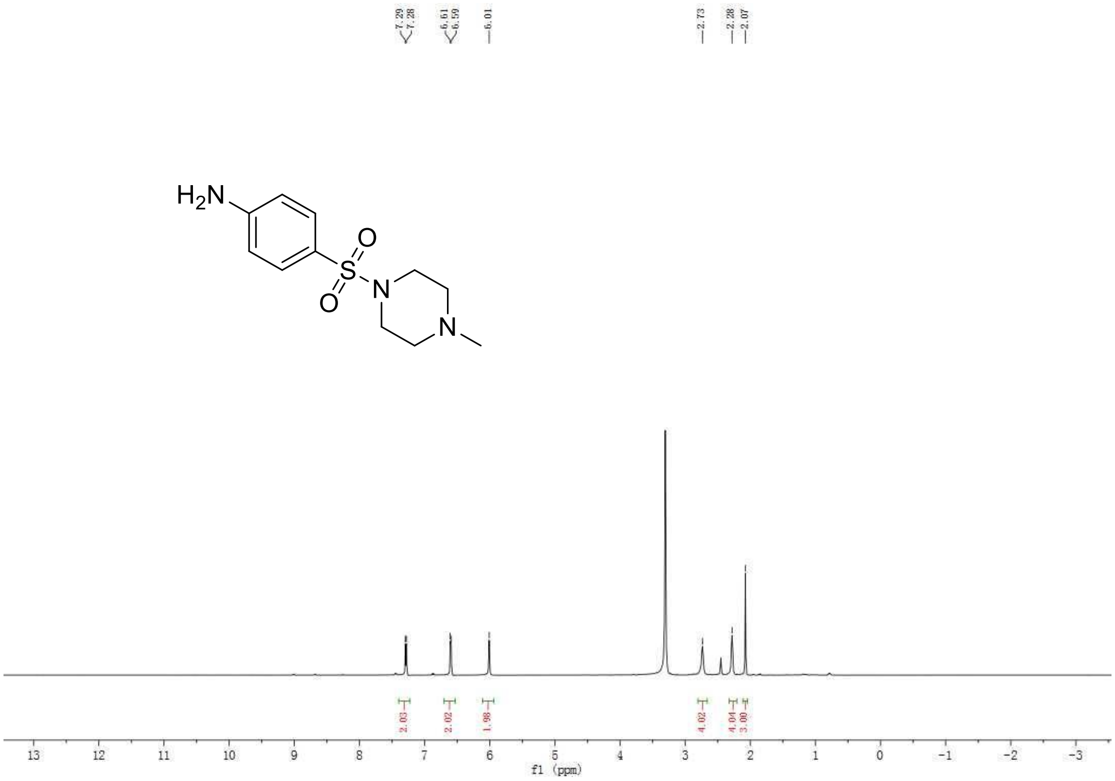
7.29
7.28
6.61
6.59
6.01
2.73
2.28
2.07
H2N
O
S
O
N
N
2.03
2.02
1.98
4.02
4.04
3.00
13
12
11
10
9
8
7
6
5
4
3
2
1
0
-1
-2
-3
f1 (ppm)

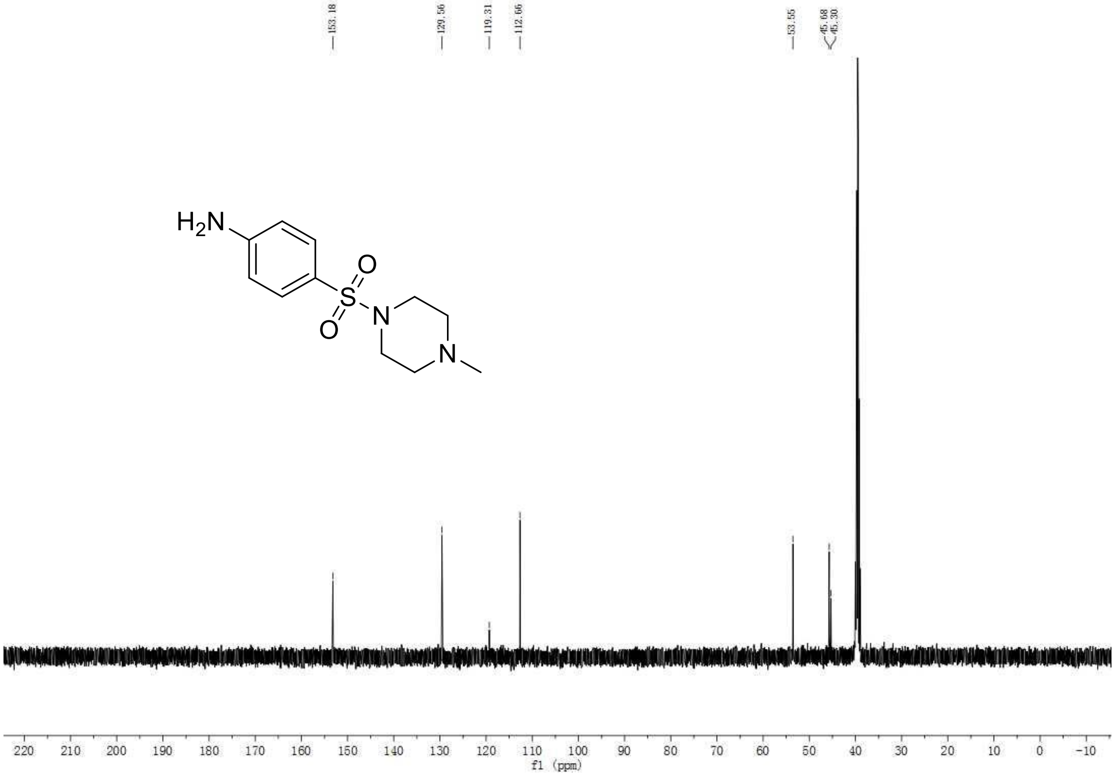
153.18
129.56
119.31
112.66
53.55
45.68
45.30
H2N
O
S
O
N
N
220
210
200
190
180
170
160
150
140
130
120
110
100
90
80
70
60
50
40
30
20
10
0
-10
f1 (ppm)

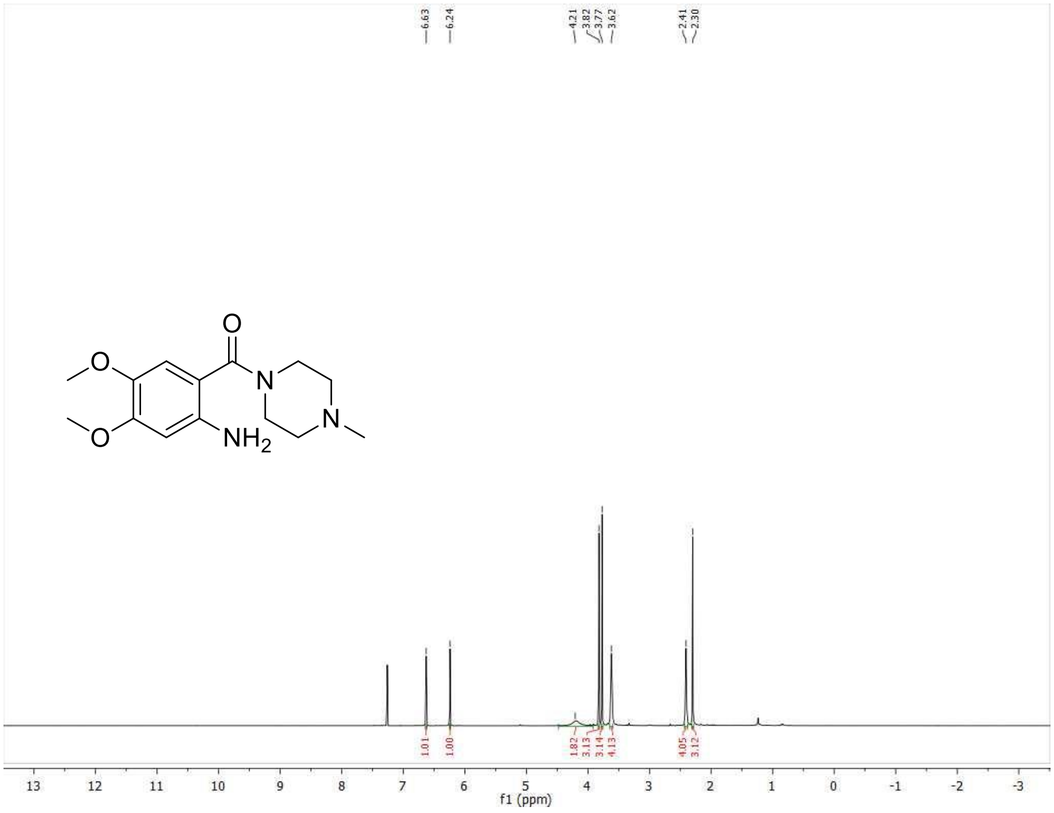
6.63
6.24
4.21
3.82
3.77
3.62
2.41
2.30
O
O
O
N
N
NH2
1.01
1.00
1.82
3.13
3.14
4.13
4.05
3.12
13
12
11
10
9
8
7
6
5
4
3
2
1
0
-1
-2
-3
f1 (ppm)

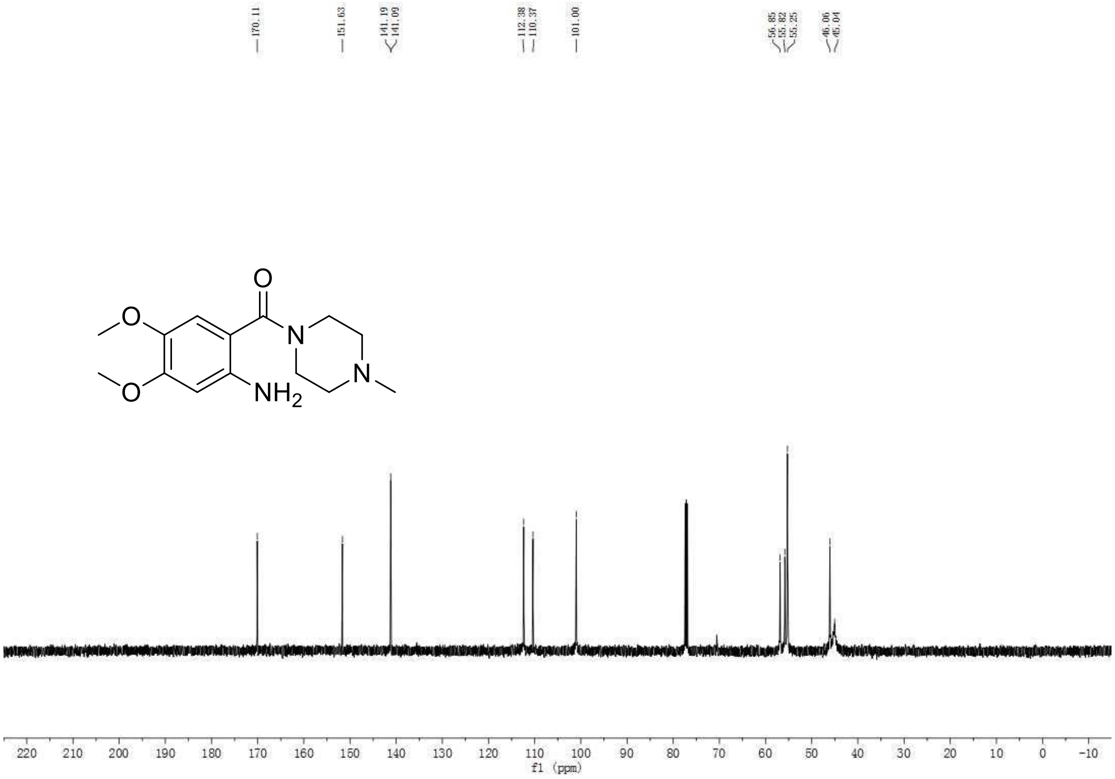
170.11
151.63
141.19
141.09
112.38
110.37
101.00
56.85
55.82
55.25
46.06
45.04
O
O
O
N
N
NH2
220
210
200
190
180
170
160
150
140
130
120
110
100
90
80
70
60
50
40
30
20
10
0
-10
f1 (ppm)

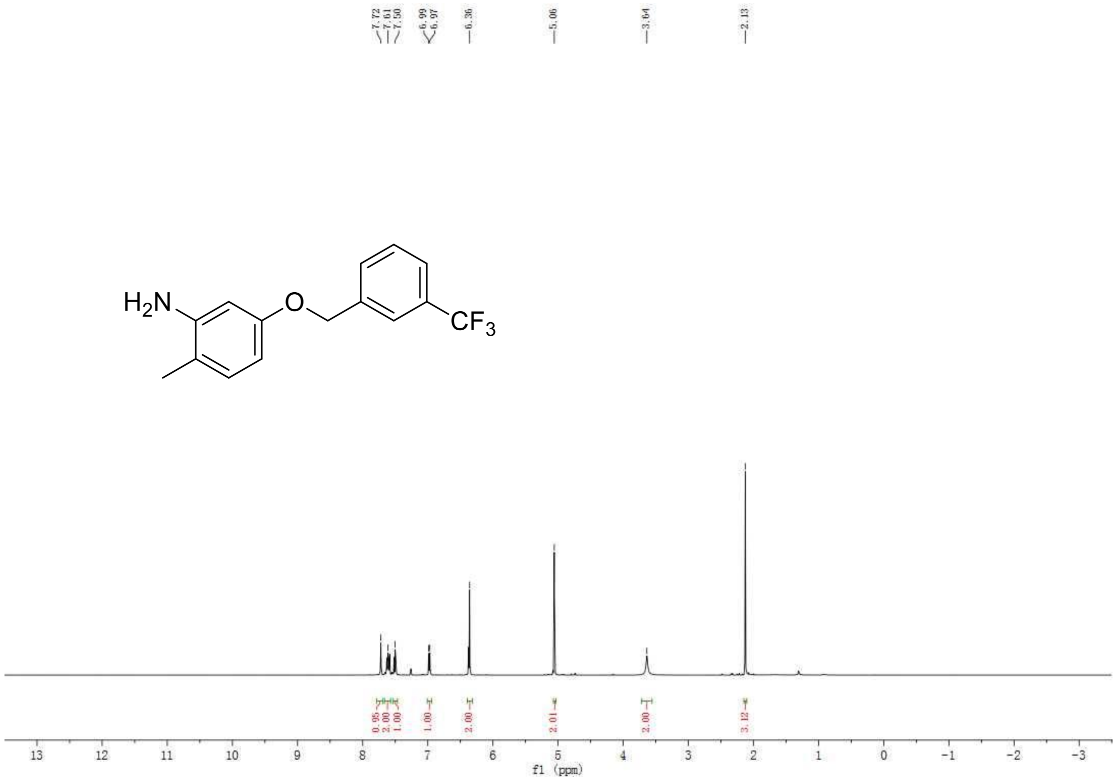
7.72
7.61
7.50
6.99
6.97
6.36
5.06
3.64
2.13
H2N
O
CF3
0.95
2.00
1.00
1.00
2.00
2.01
2.00
3.12
13
12
11
10
9
8
7
6
5
4
3
2
1
0
-1
-2
-3
f1 (ppm)

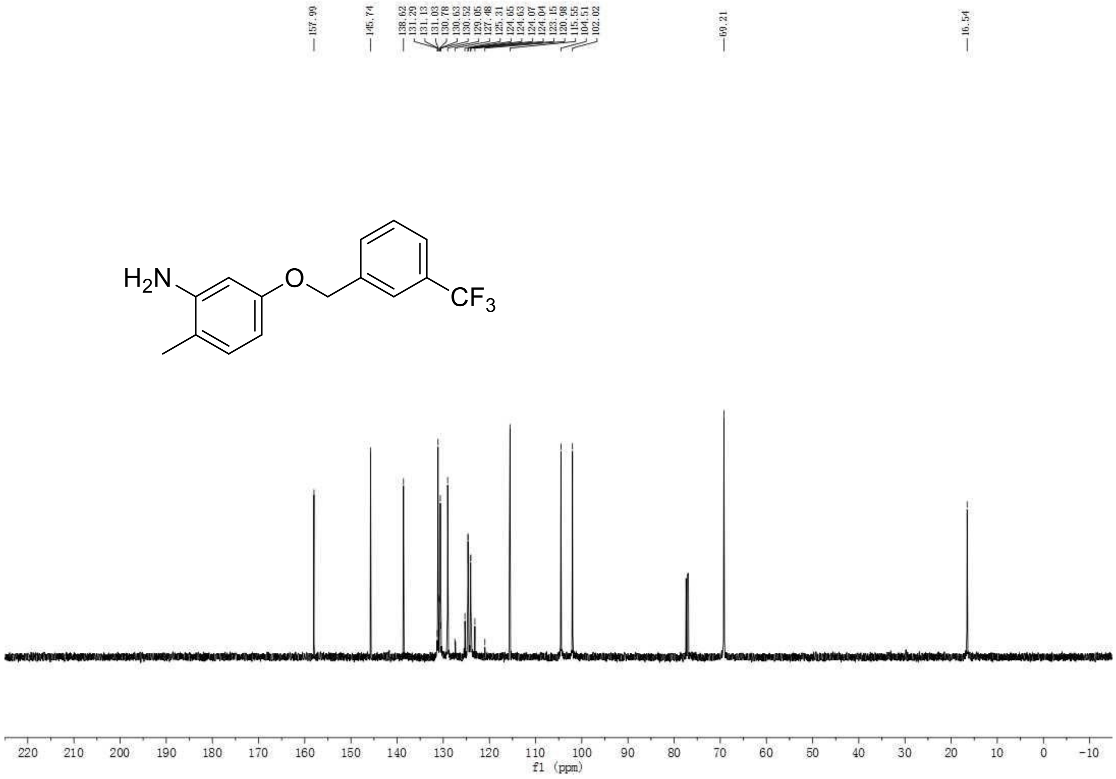
157.99
145.74
138.62
131.29
131.13
131.03
130.78
130.63
130.52
129.05
127.48
125.31
124.65
124.63
124.07
124.04
123.15
120.98
115.55
104.51
102.02
69.21
16.54
H2N
O
CF3
220
210
200
190
180
170
160
150
140
130
120
110
100
90
80
70
60
50
40
30
20
10
0
-10
f1 (ppm)

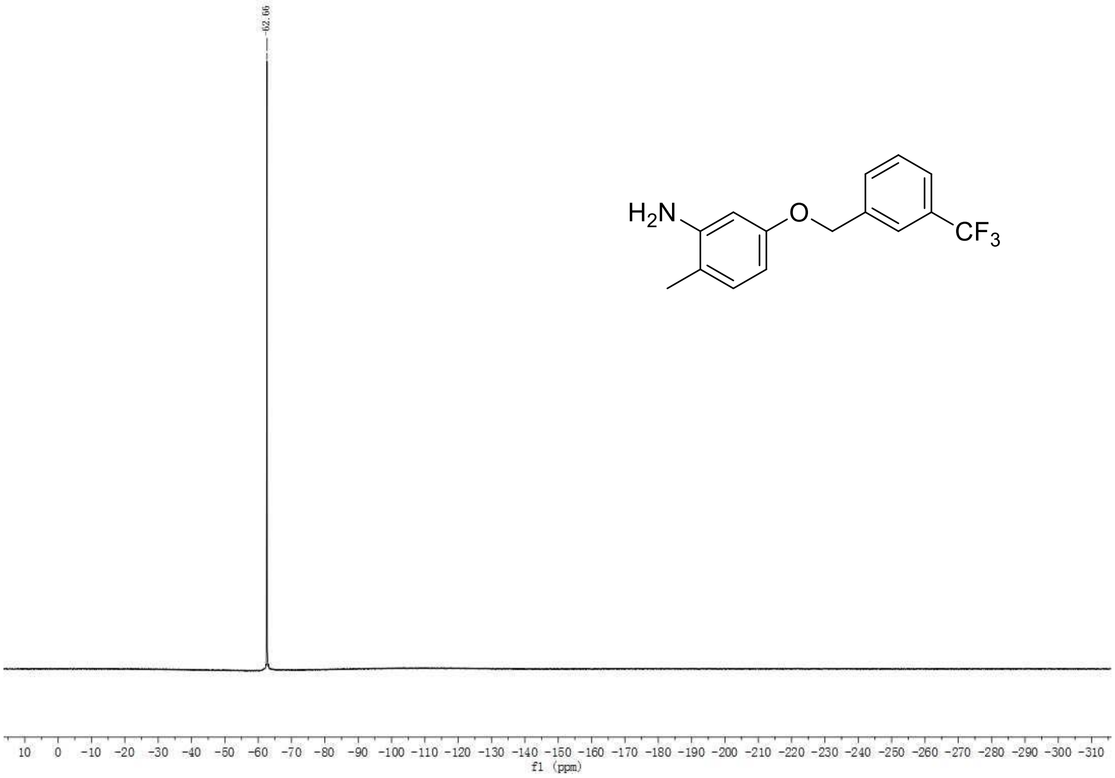
-62.66
H2N
O
CF3
10 0 -10 -20 -30 -40 -50 -60 -70 -80 -90 -100 -110 -120 -130 -140 -150 -160 -170 -180 -190 -200 -210 -220 -230 -240 -250 -260 -270 -280 -290 -300 -310
f1 (ppm)

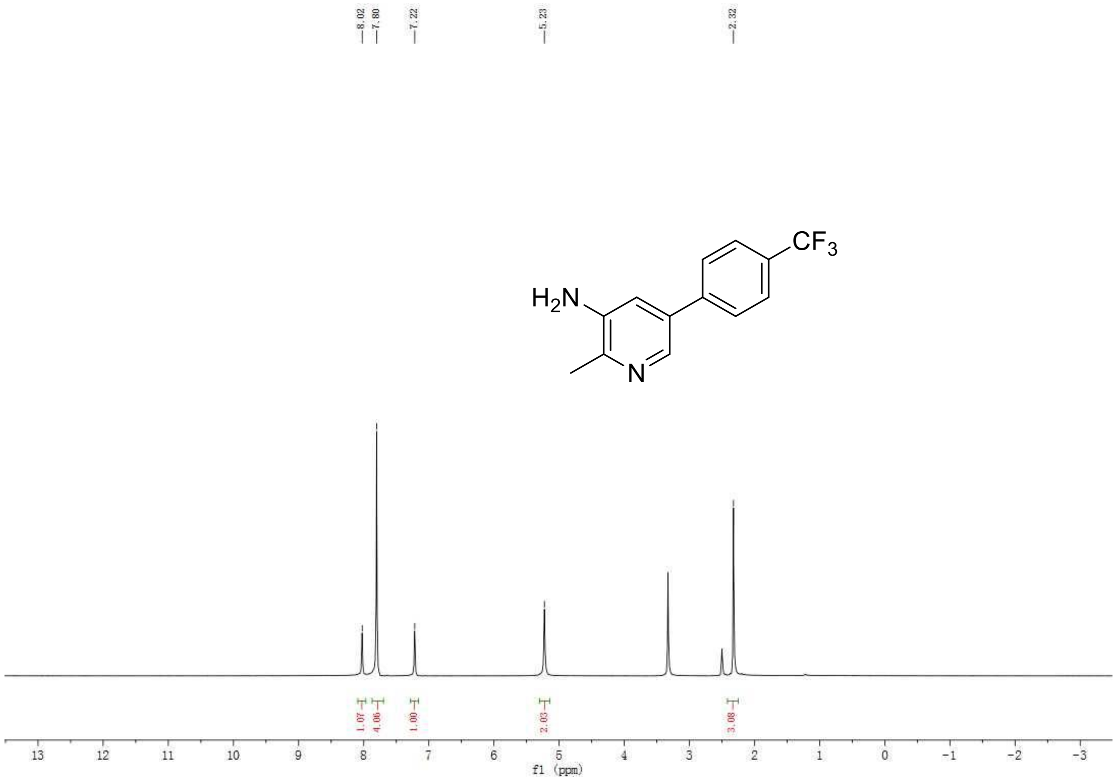
8.02
7.80
7.22
5.23
2.32
CF3
H2N
N
1.07
4.06
1.00
2.03
3.08
13
12
11
10
9
8
7
6
5
4
3
2
1
0
−1
−2
−3
f1 (ppm)

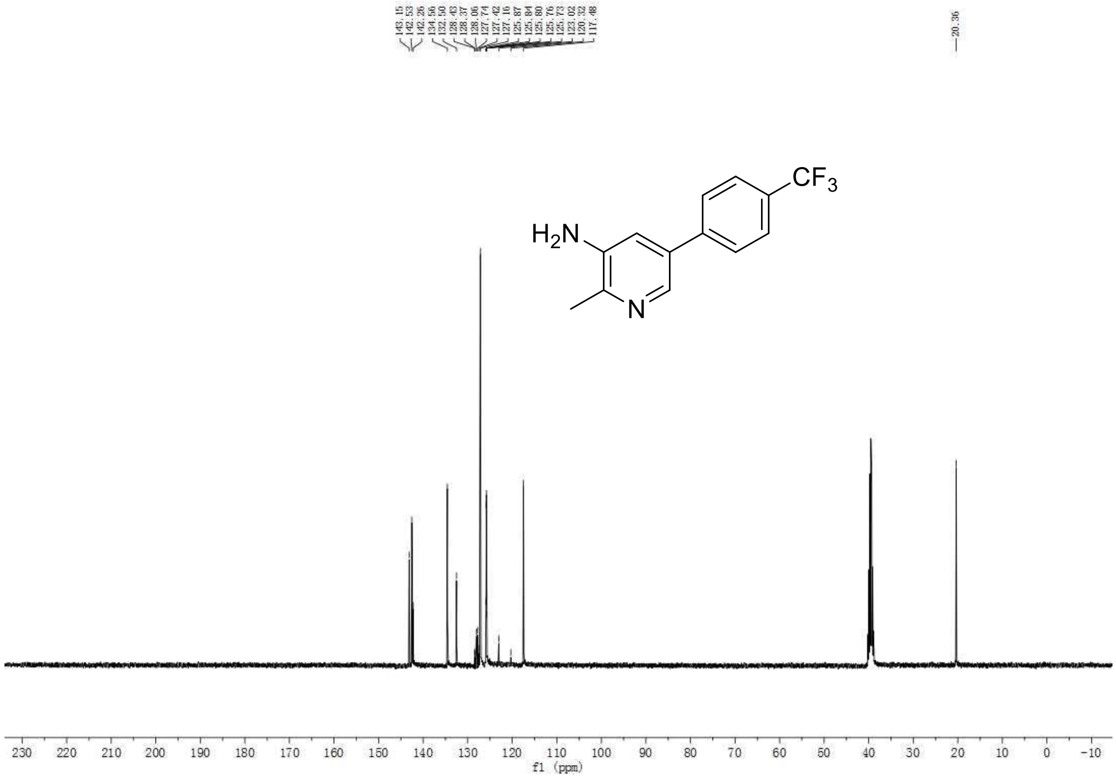
143.15
142.53
142.26
134.56
132.50
128.43
128.37
128.06
127.74
127.42
127.16
125.87
125.84
125.80
125.76
125.73
123.02
120.32
117.48
20.36
CF3
H2N
N
230
220
210
200
190
180
170
160
150
140
130
120
110
100
90
80
70
60
50
40
30
20
10
0
−10
f1 (ppm)

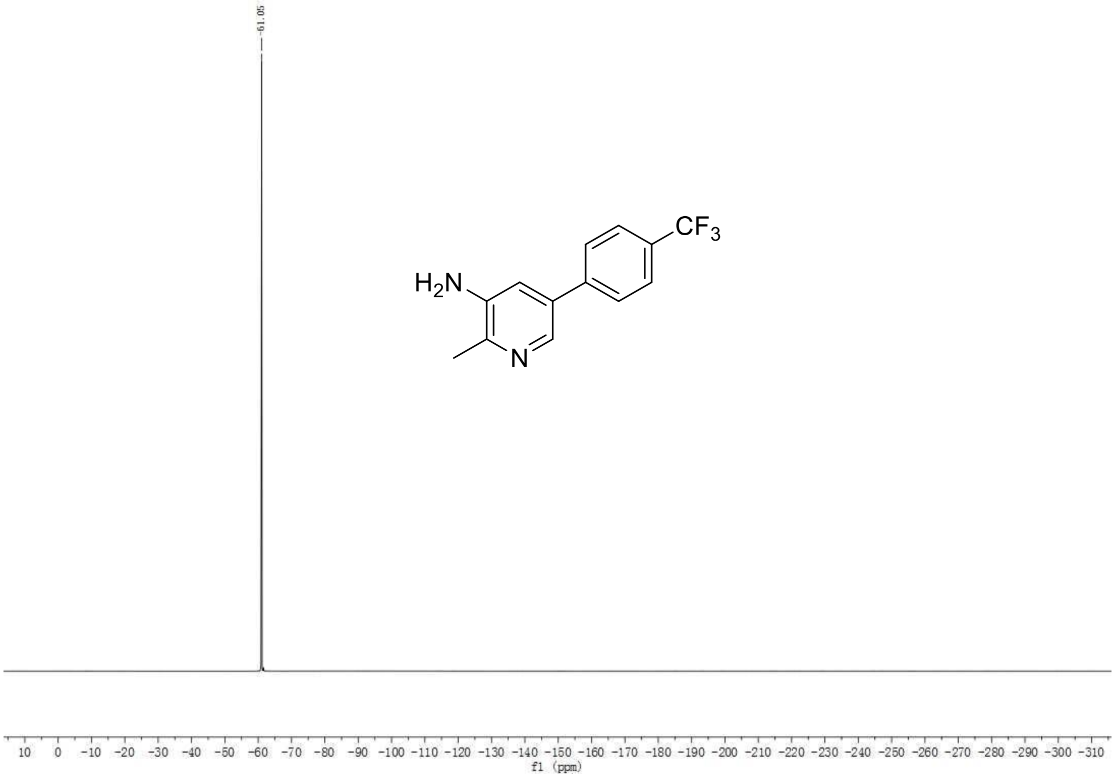
-61.05
H2N
N
CF3
10 0 −10 −20 −30 −40 −50 −60 −70 −80 −90 −100 −110 −120 −130 −140 −150 −160 −170 −180 −190 −200 −210 −220 −230 −240 −250 −260 −270 −280 −290 −300 −310
f1 (ppm)

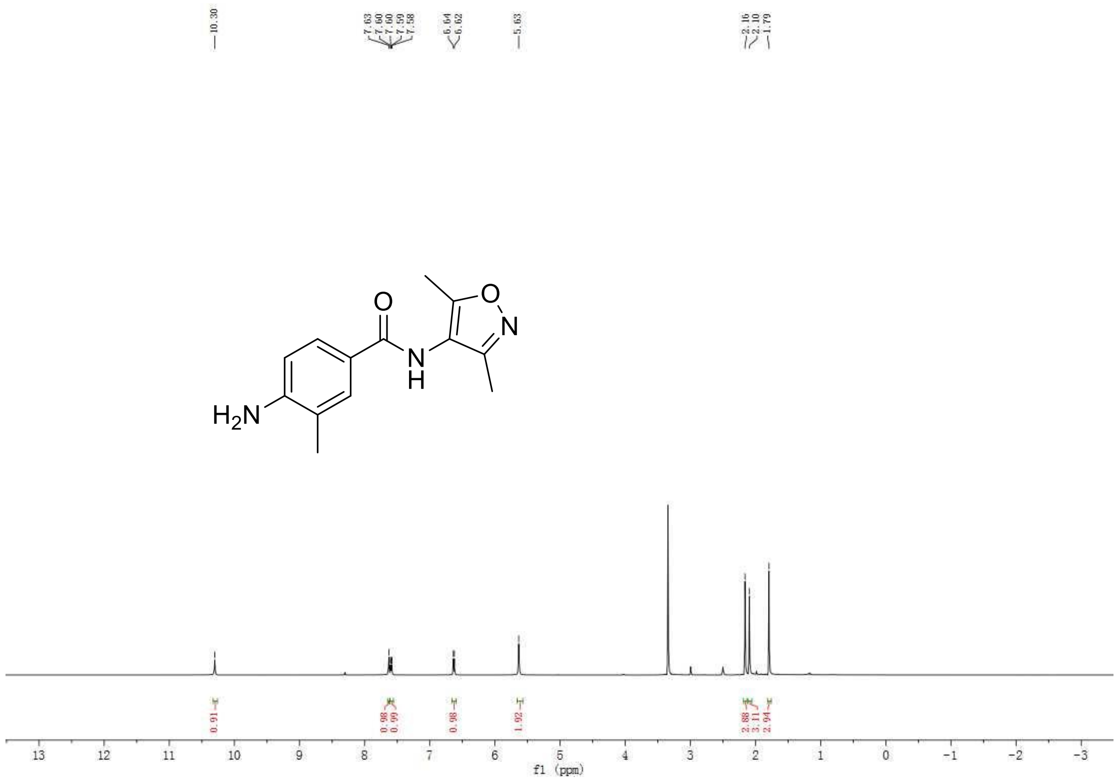
10.30
7.63
7.60
7.60
7.59
7.58
6.64
6.62
5.63
2.16
2.10
1.79
O
O
N
N
H
H₂N
0.91
0.98
0.99
0.98
1.92
2.88
3.11
2.94
13
12
11
10
9
8
7
6
5
4
3
2
1
0
-1
-2
-3
f1 (ppm)

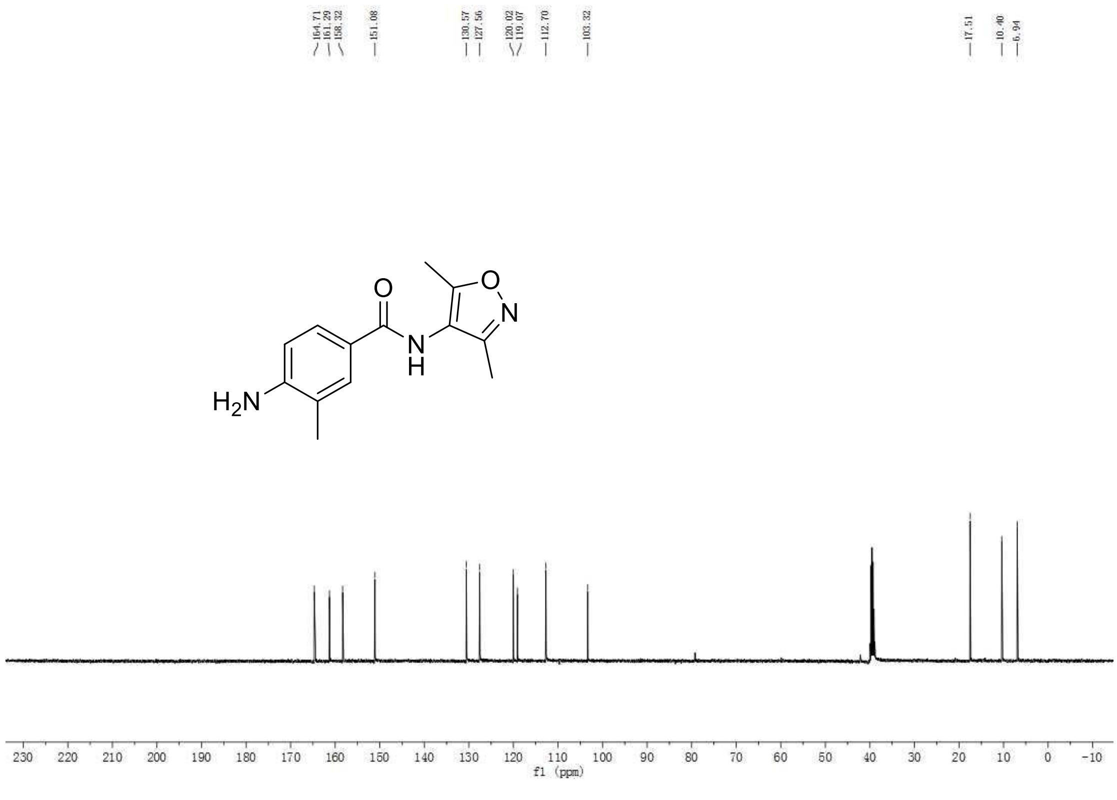
164.71
161.29
158.32
151.08
130.57
127.56
120.02
119.07
112.70
103.32
17.51
10.40
6.94
O
O
N
N
H
H₂N
230
220
210
200
190
180
170
160
150
140
130
120
110
100
90
80
70
60
50
40
30
20
10
0
-10
f1 (ppm)

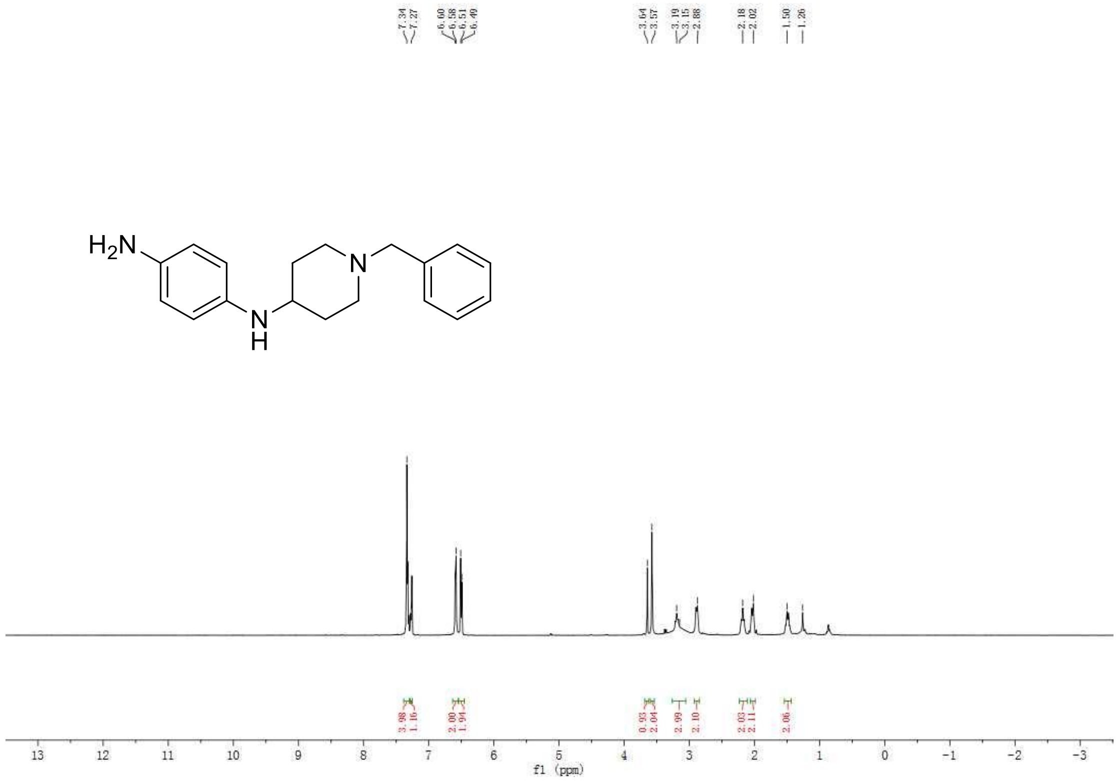
7.34
7.27
6.60
6.58
6.51
6.49
3.64
3.57
3.19
3.15
2.88
2.18
2.02
1.50
1.26
H2N
N
N
H
3.98
1.16
2.00
1.94
0.93
2.04
2.99
2.10
2.03
2.11
2.06
13
12
11
10
9
8
7
6
5
4
3
2
1
0
-1
-2
-3
f1 (ppm)

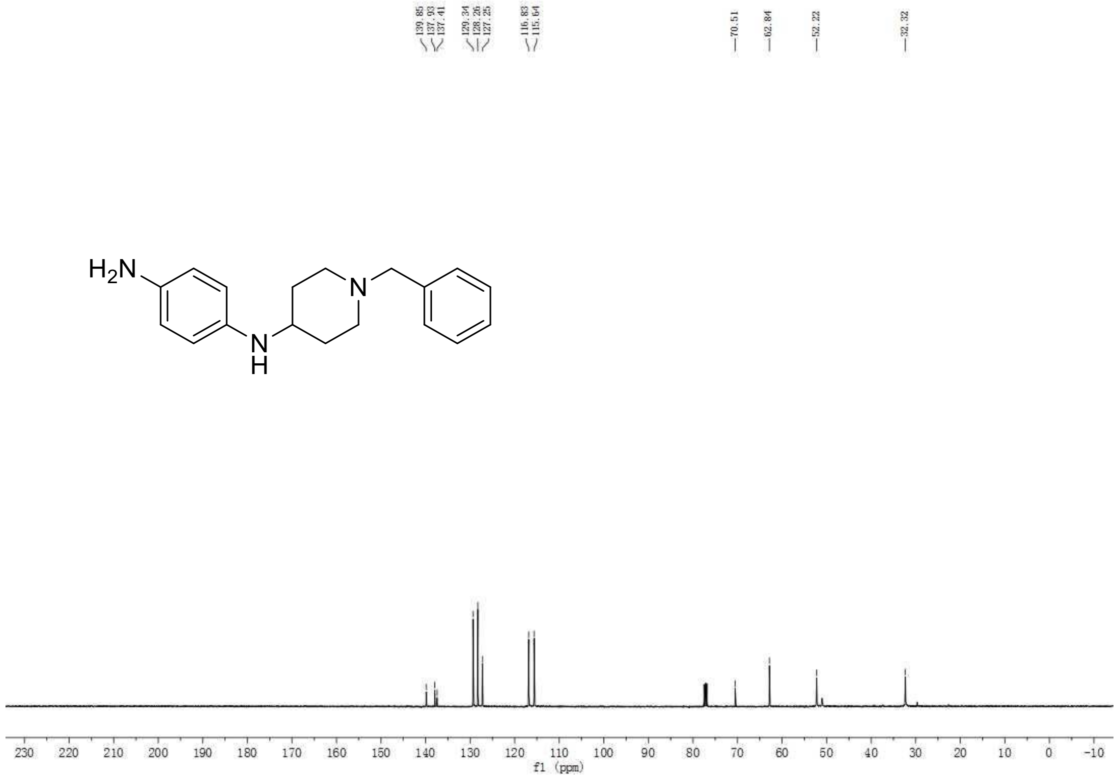
139.85
137.93
137.41
129.34
128.26
127.25
116.83
115.64
70.51
62.84
52.22
32.32
H2N
N
N
H
230
220
210
200
190
180
170
160
150
140
130
120
110
100
90
80
70
60
50
40
30
20
10
0
-10
f1 (ppm)

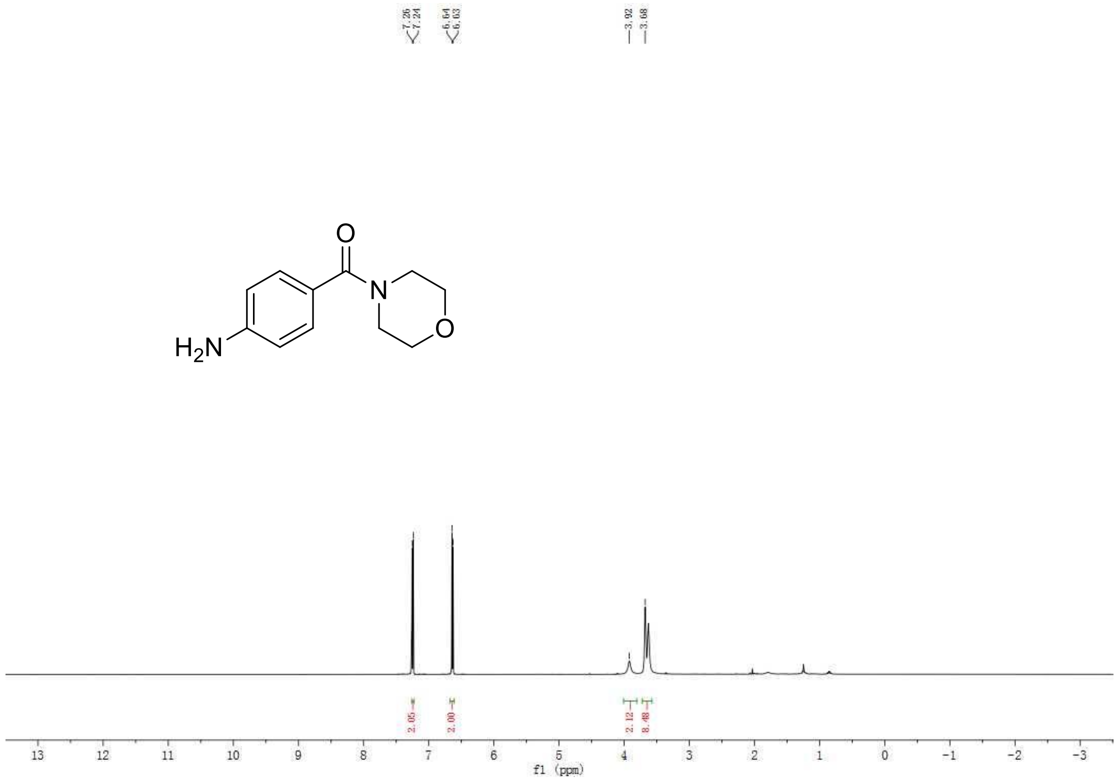
7.26
7.24
6.64
6.63
3.92
3.68
O
N
O
H2N
2.05
2.00
2.12
8.48
13
12
11
10
9
8
7
6
5
4
3
2
1
0
−1
−2
−3
f1 (ppm)

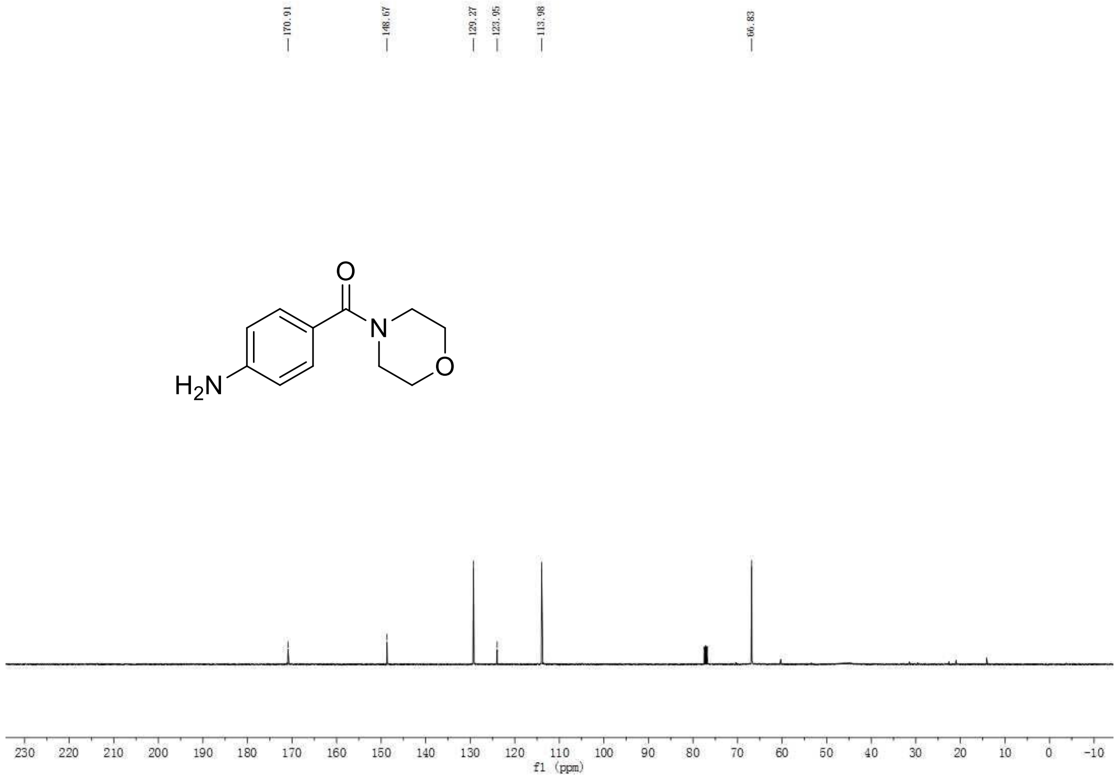
170.91
148.67
129.27
123.95
113.98
66.83
O
N
O
H2N
230
220
210
200
190
180
170
160
150
140
130
120
110
100
90
80
70
60
50
40
30
20
10
0
−10
f1 (ppm)

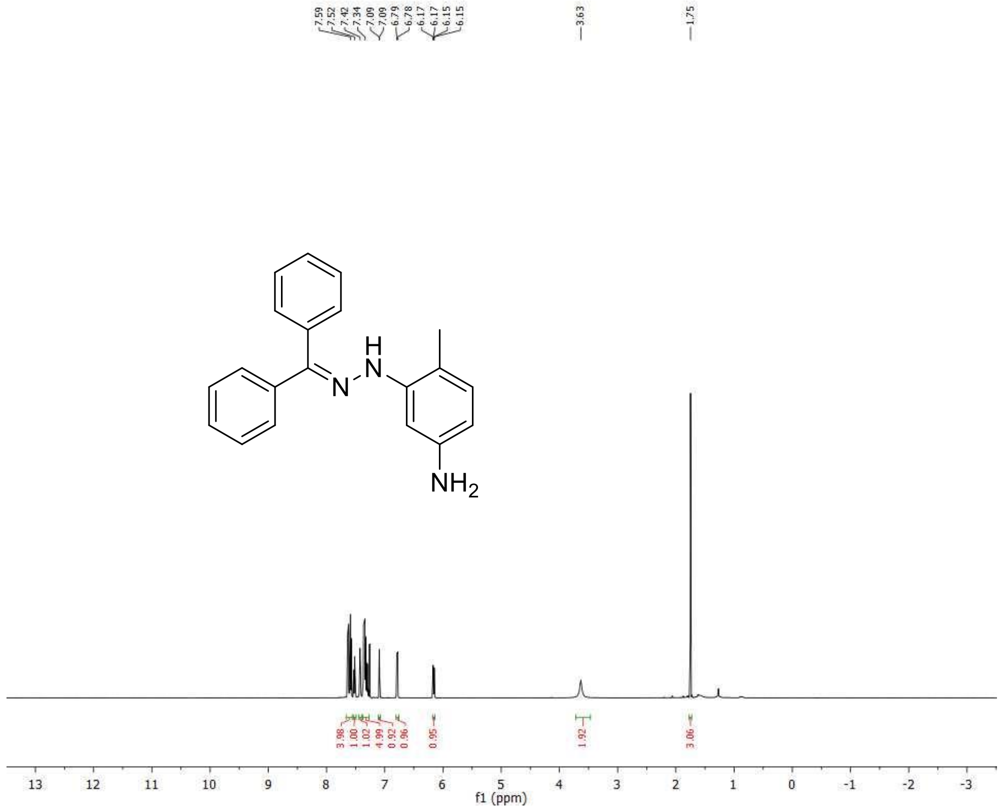
7.59
7.52
7.42
7.34
7.09
7.09
6.79
6.78
6.17
6.17
6.15
6.15
3.63
1.75
H
N
N
NH2
3.98
1.00
1.02
4.99
0.92
0.96
0.95
1.92
3.06
13
12
11
10
9
8
7
6
5
4
3
2
1
0
-1
-2
-3
f1 (ppm)

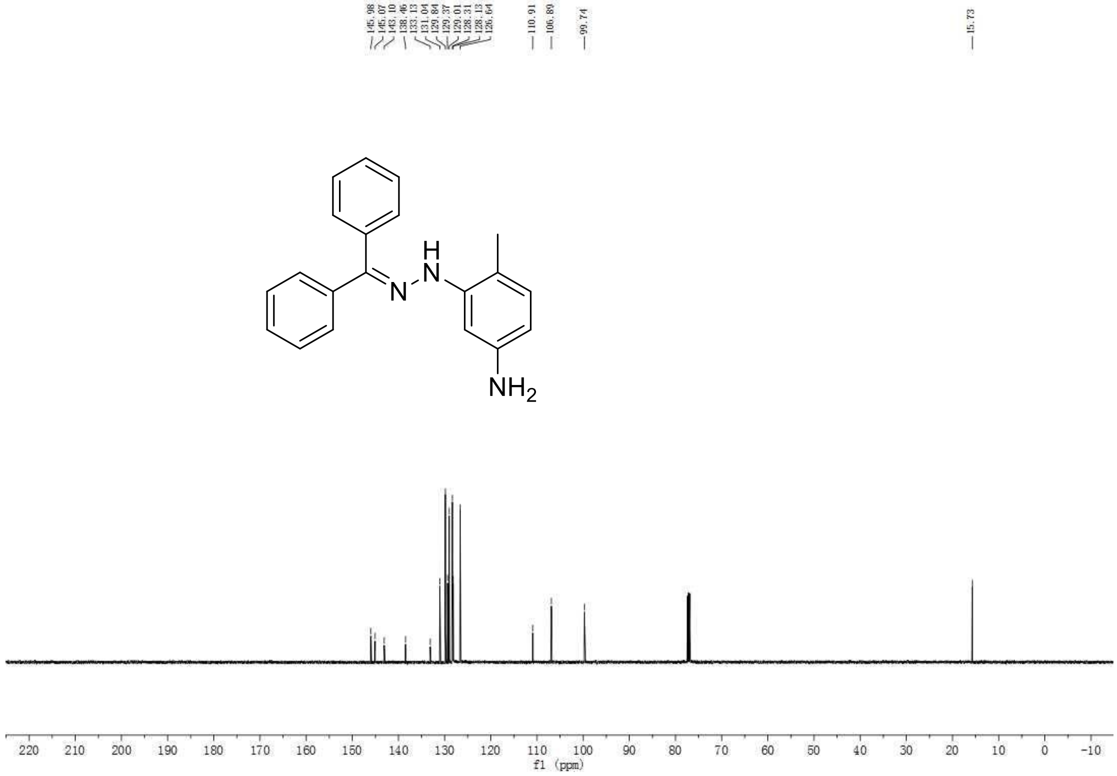
145.98
145.07
143.10
138.46
133.13
131.04
129.84
129.37
129.01
128.31
128.13
126.64
110.91
106.89
99.74
15.73
H
N
N
NH2
220
210
200
190
180
170
160
150
140
130
120
110
100
90
80
70
60
50
40
30
20
10
0
-10
f1 (ppm)

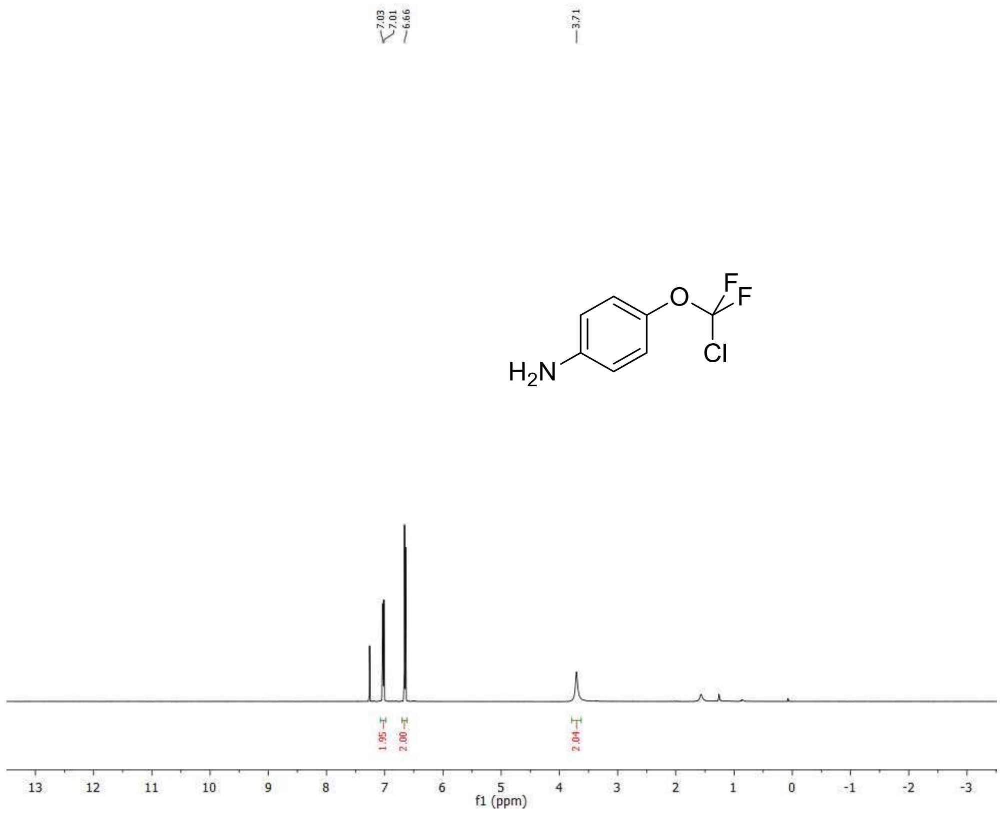
7.03
7.01
6.66
3.71
O
F
F
Cl
H2N
1.95
2.00
2.04
13
12
11
10
9
8
7
6
5
4
3
2
1
0
-1
-2
-3
f1 (ppm)

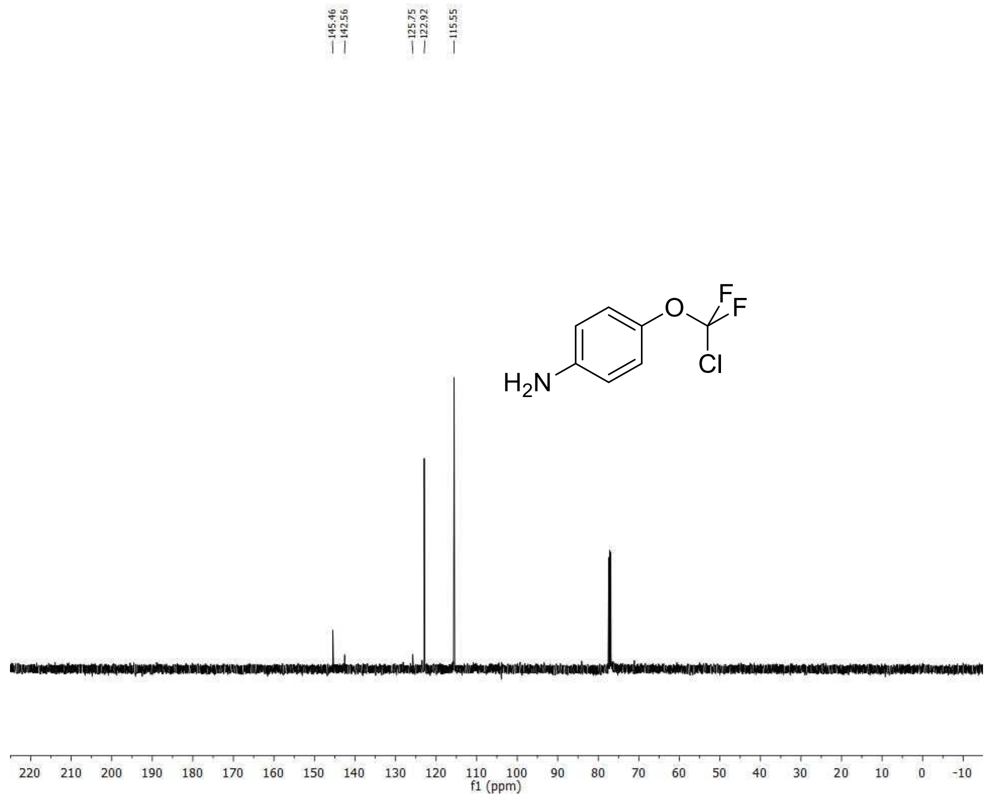
145.46
142.56
125.75
122.92
115.55
O
F
F
Cl
H2N
220
210
200
190
180
170
160
150
140
130
120
110
100
90
80
70
60
50
40
30
20
10
0
-10
f1 (ppm)

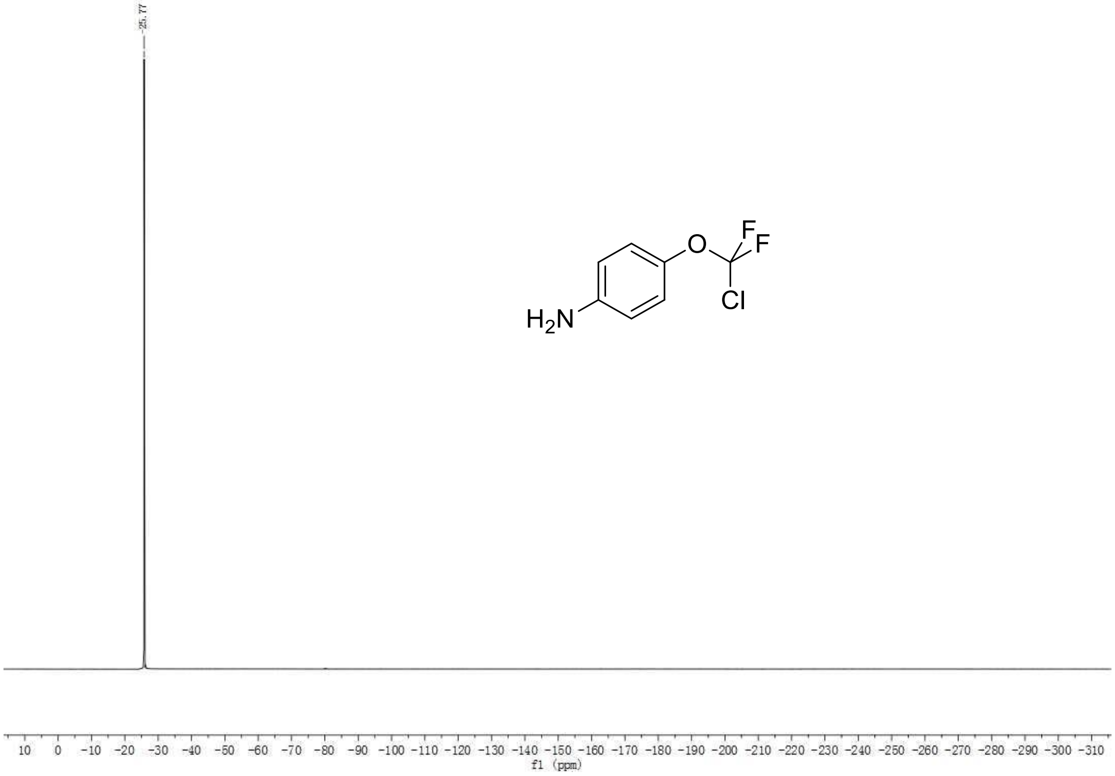
-25.77
H2N
O
F
F
Cl
10 0 -10 -20 -30 -40 -50 -60 -70 -80 -90 -100 -110 -120 -130 -140 -150 -160 -170 -180 -190 -200 -210 -220 -230 -240 -250 -260 -270 -280 -290 -300 -310
f1 (ppm)

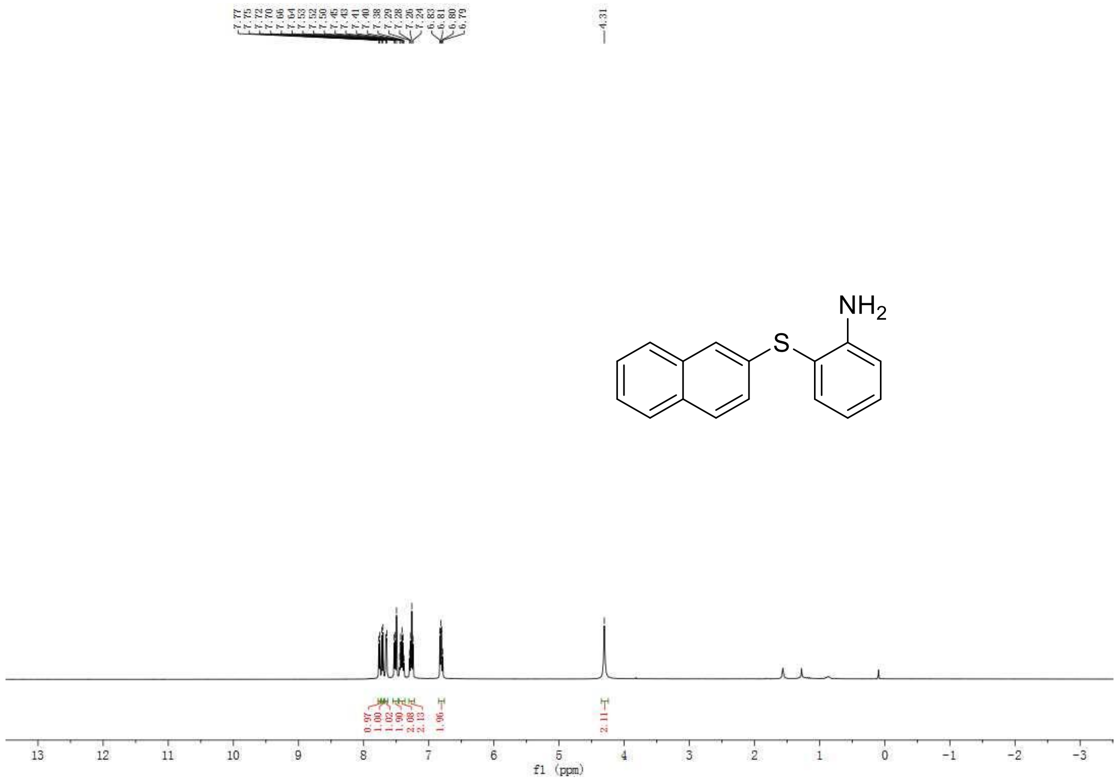
7.77
7.75
7.72
7.70
7.66
7.64
7.53
7.52
7.50
7.45
7.43
7.41
7.40
7.38
7.29
7.28
7.26
7.24
6.83
6.81
6.80
6.79
4.31
NH2
S
0.97
1.00
1.02
1.90
2.08
2.13
1.96
2.11
13
12
11
10
9
8
7
6
5
4
3
2
1
0
-1
-2
-3
f1 (ppm)

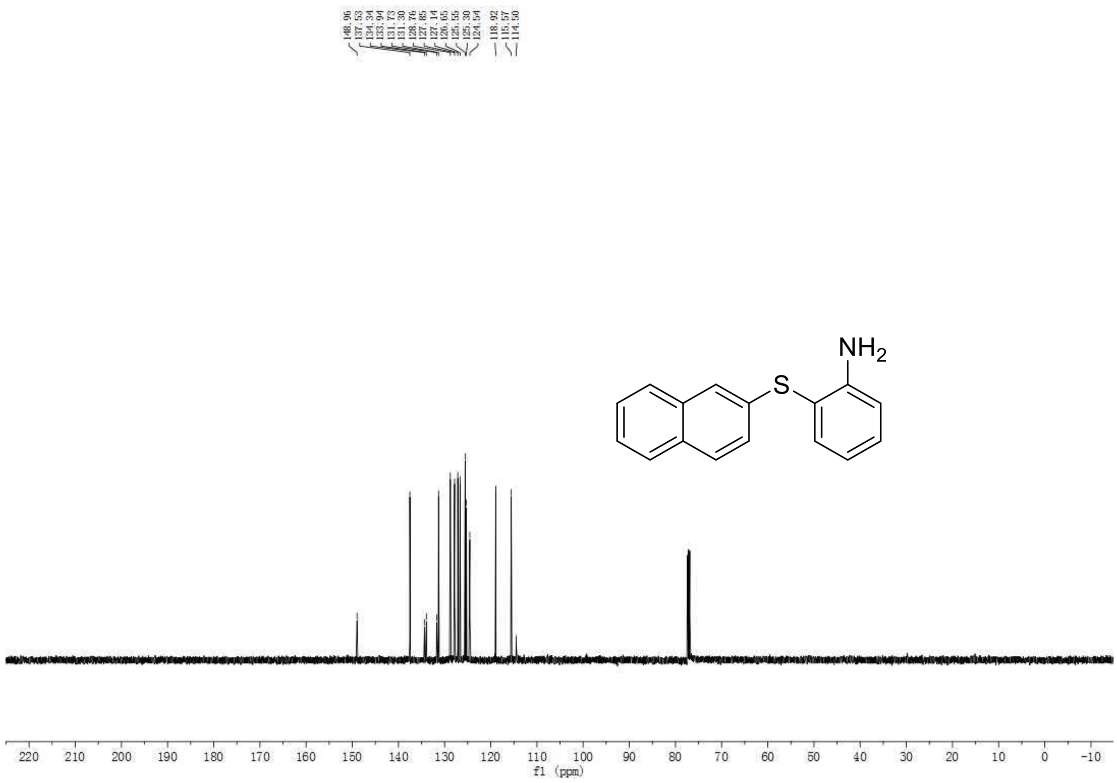
148.96
137.53
134.34
133.94
131.73
131.30
128.76
127.85
127.14
126.65
125.55
125.30
124.54
118.92
115.57
114.50
NH2
S
220
210
200
190
180
170
160
150
140
130
120
110
100
90
80
70
60
50
40
30
20
10
0
-10
f1 (ppm)

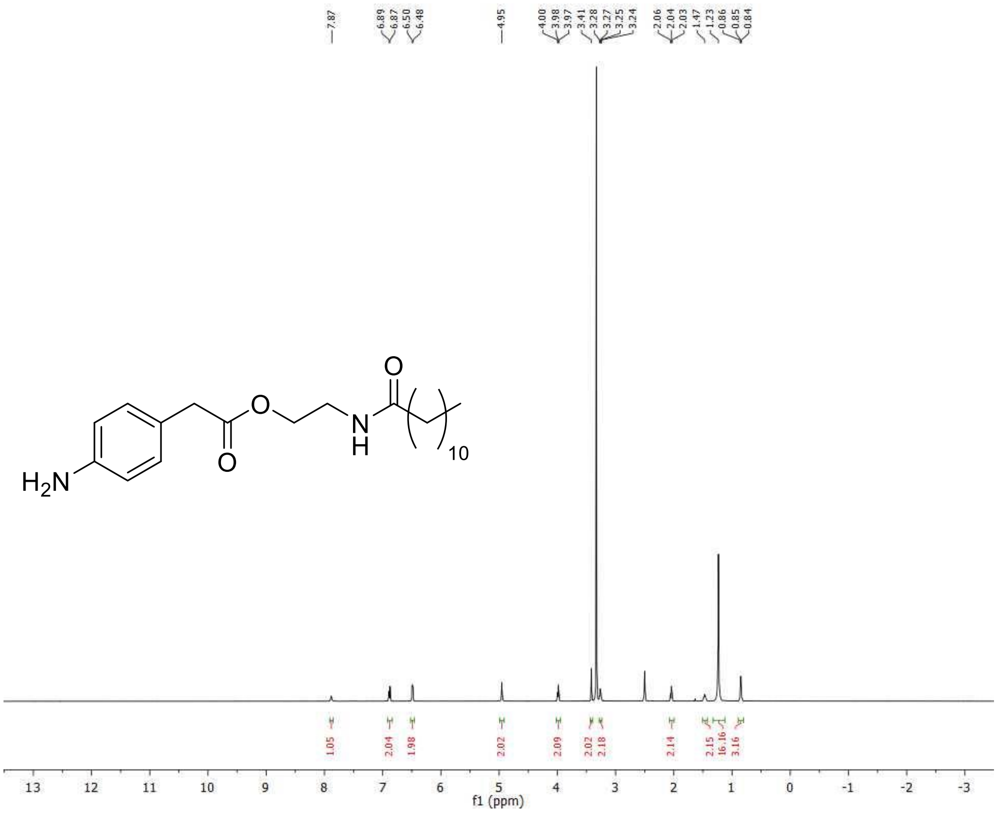
7.87
6.89
6.87
6.50
6.48
4.95
4.00
3.98
3.97
3.41
3.28
3.27
3.25
3.24
2.06
2.04
2.03
1.47
1.23
0.86
0.85
0.84
O
O
O
N
H
10
H_2N
1.05
2.04
1.98
2.02
2.09
2.02
2.18
2.14
2.15
16.16
3.16
13
12
11
10
9
8
7
6
5
4
3
2
1
0
-1
-2
-3
f1 (ppm)

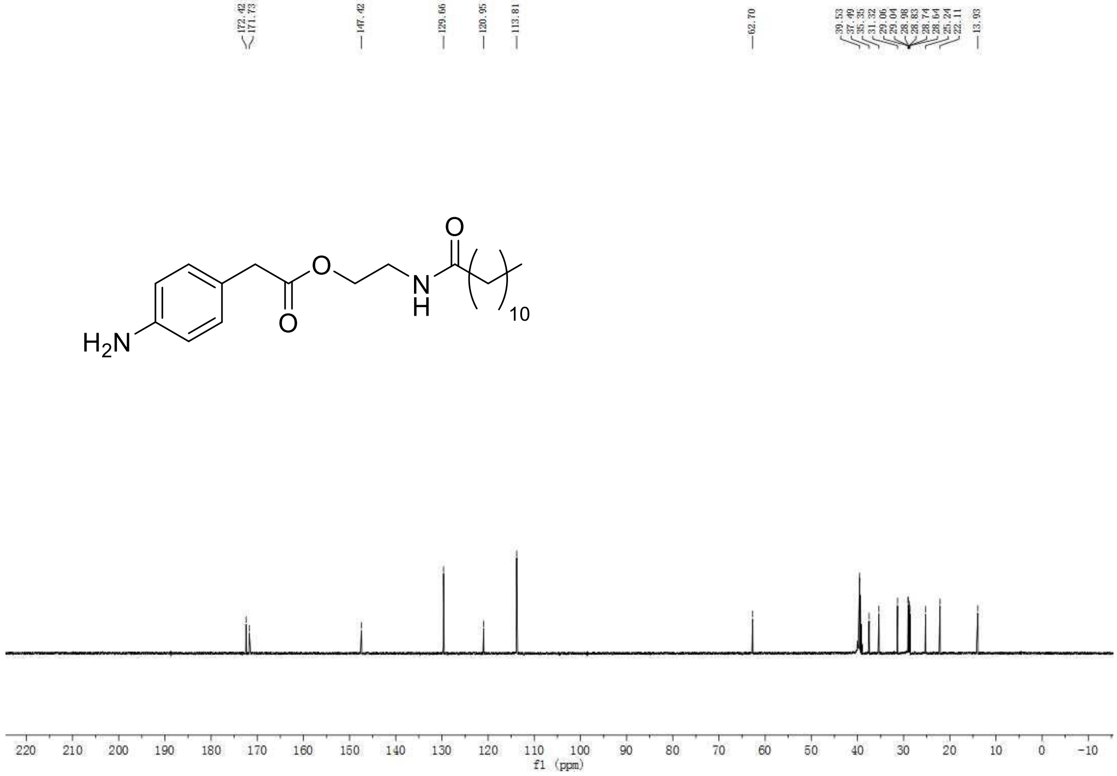
172.42
171.73
147.42
129.66
120.95
113.81
62.70
39.53
37.40
35.35
31.32
29.06
29.04
28.98
28.83
28.74
28.64
25.24
22.11
13.93
O
O
O
N
H
10
H_2N
220
210
200
190
180
170
160
150
140
130
120
110
100
90
80
70
60
50
40
30
20
10
0
-10
f1 (ppm)

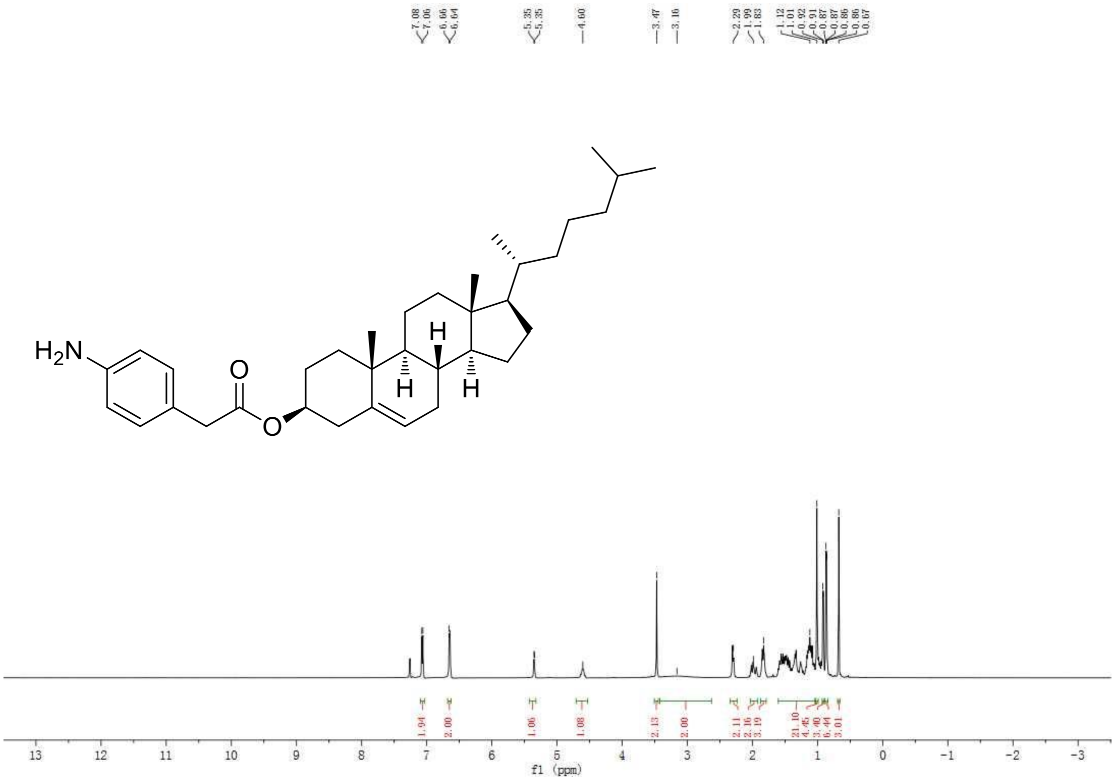
7.08
7.06
6.66
6.64
5.35
5.35
4.60
3.47
3.16
2.29
1.99
1.83
1.12
1.01
0.92
0.91
0.87
0.87
0.86
0.86
0.67
H2N
O
O
H
H
H
1.94
2.00
1.06
1.08
2.13
2.00
2.11
2.16
3.19
21.10
4.45
3.40
6.44
3.01
13
12
11
10
9
8
7
6
5
4
3
2
1
0
-1
-2
-3
f1 (ppm)

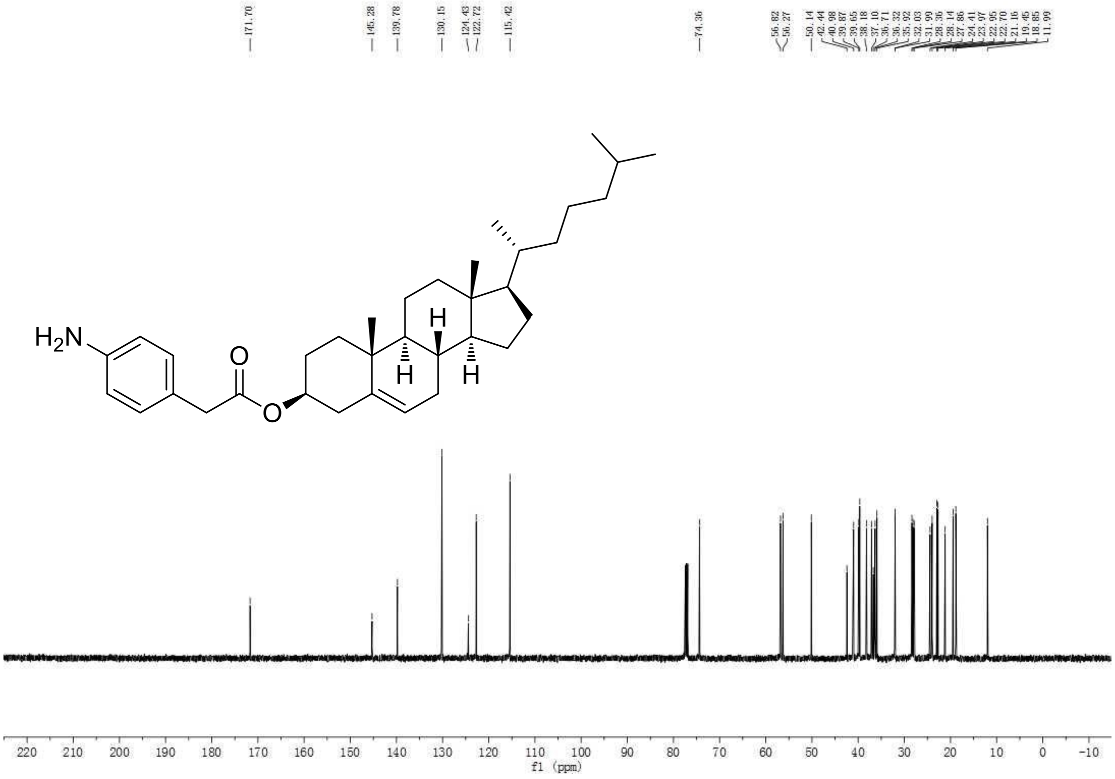
171.70
145.28
139.78
130.15
124.43
122.72
115.42
74.36
56.82
56.27
50.14
42.44
40.98
39.87
39.65
38.18
37.10
36.71
36.32
35.92
32.03
31.99
28.36
28.14
27.86
24.41
23.97
22.95
22.70
21.16
19.45
18.85
11.99
H2N
O
O
H
H
H
220
210
200
190
180
170
160
150
140
130
120
110
100
90
80
70
60
50
40
30
20
10
0
-10
f1 (ppm)

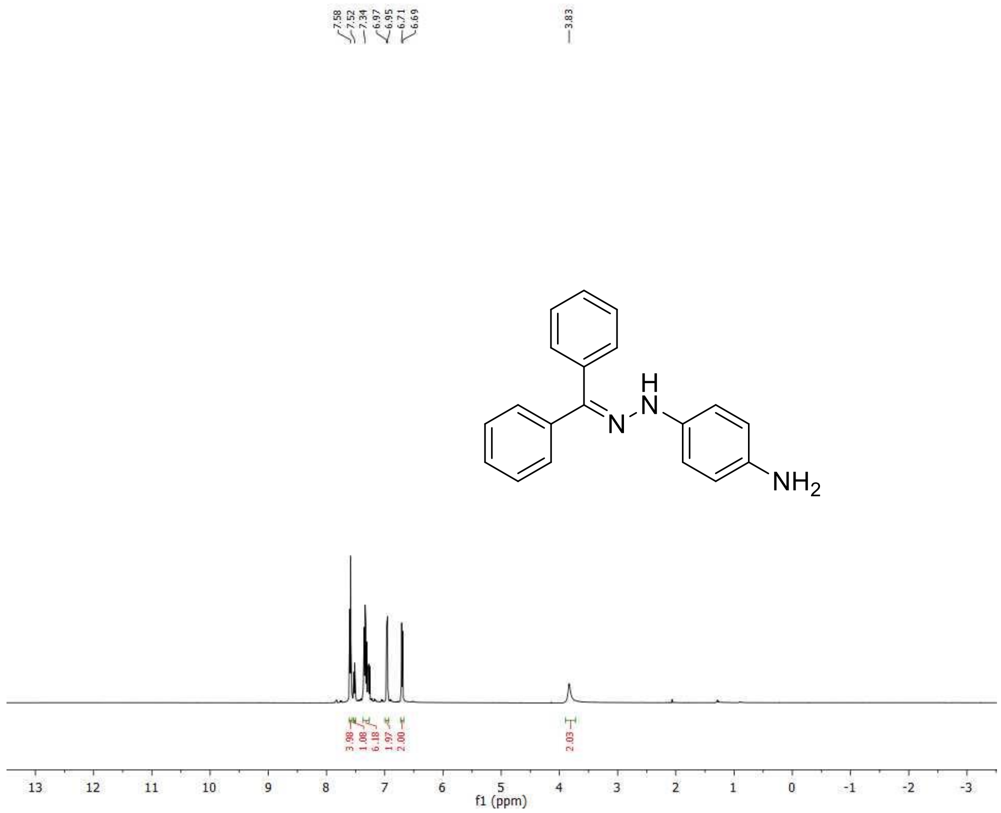
7.58
7.52
7.34
6.97
6.95
6.71
6.69
3.83
H
N
N
NH2
3.98
1.08
6.18
1.97
2.00
2.03
13
12
11
10
9
8
7
6
5
4
3
2
1
0
-1
-2
-3
f1 (ppm)

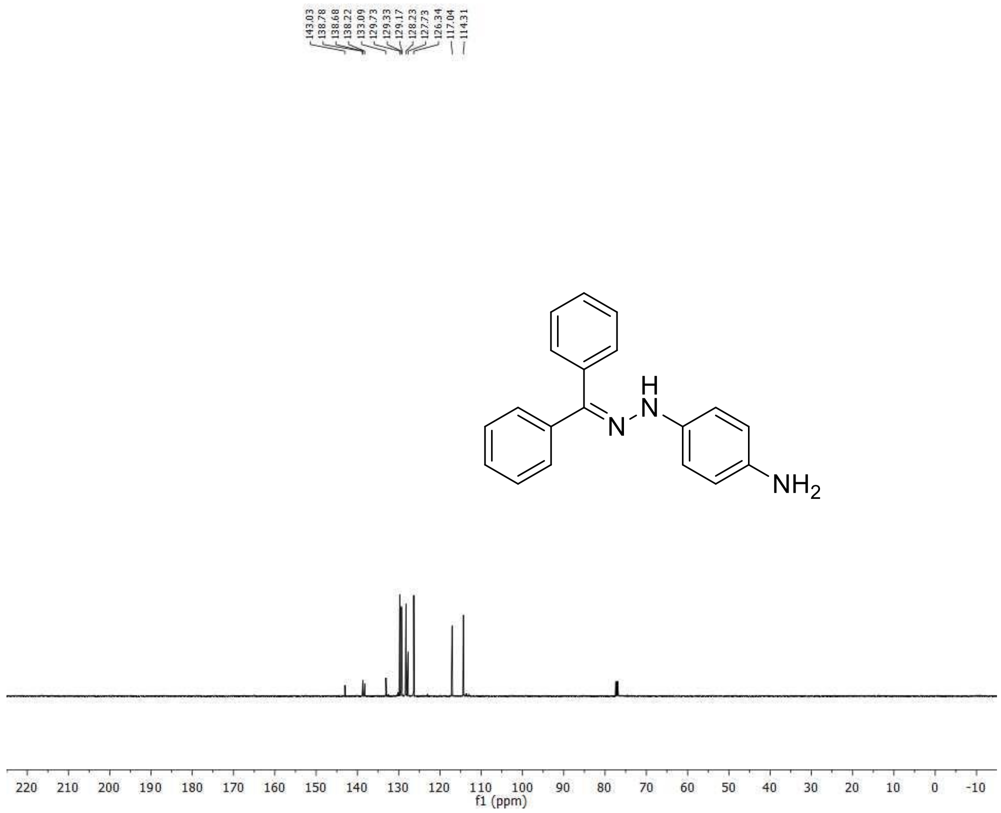
143.03
138.78
138.68
138.22
133.09
129.73
129.33
129.17
128.23
127.73
126.34
117.04
114.31
H
N
N
NH2
220
210
200
190
180
170
160
150
140
130
120
110
100
90
80
70
60
50
40
30
20
10
0
-10
f1 (ppm)

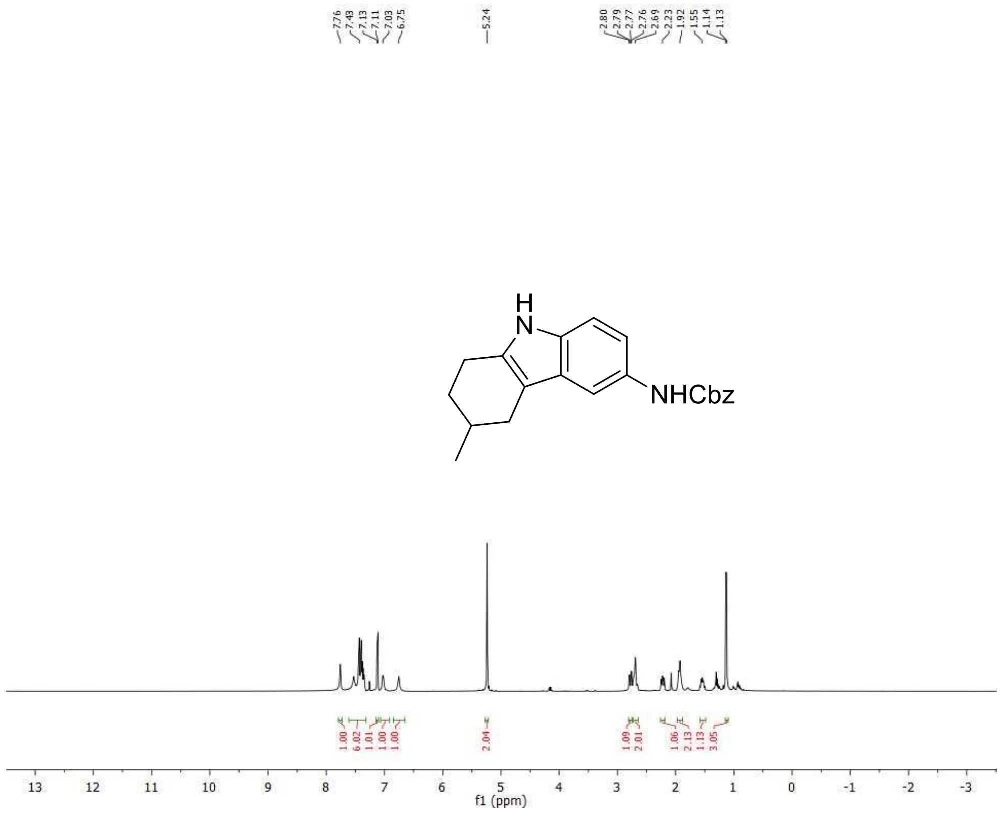

7.76
7.43
7.13
7.11
7.03
6.75
5.24
2.80
2.79
2.77
2.76
2.69
2.23
1.92
1.55
1.14
1.13
H
N
NHCbz
1.00
6.02
1.01
1.00
1.00
2.04
1.09
2.01
1.06
2.13
1.13
3.05
13 12 11 10 9 8 7 6 5 4 3 2 1 0 -1 -2 -3
f1 (ppm)

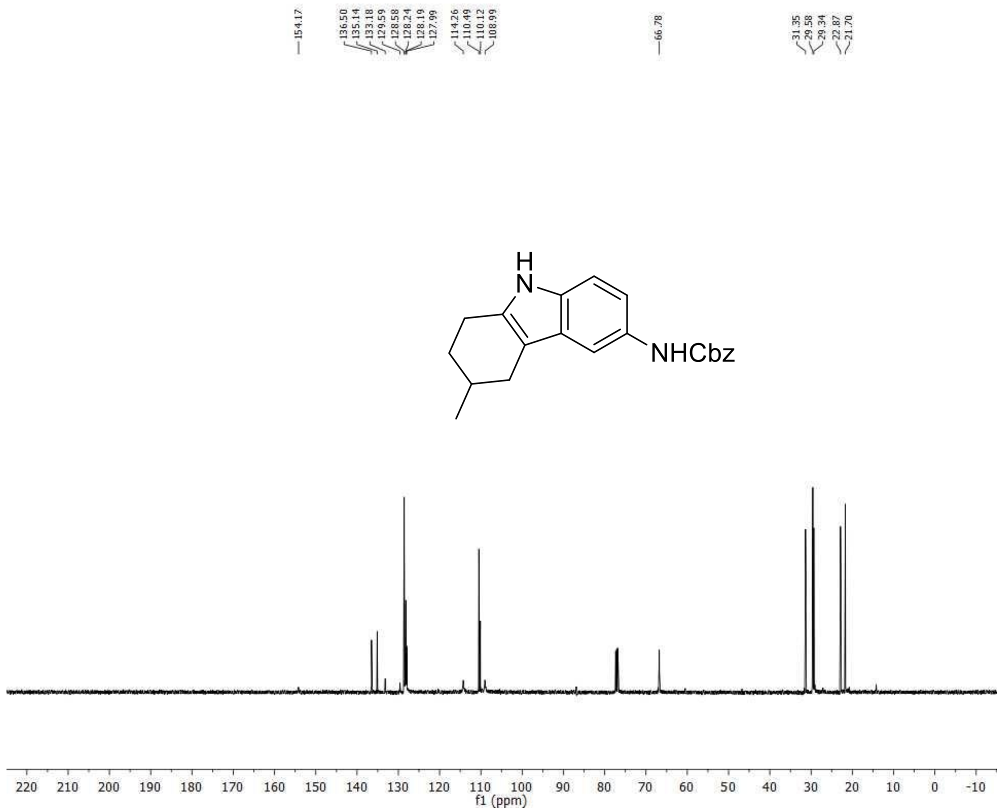

154.17
136.50
135.14
133.18
129.59
128.58
128.24
128.19
127.99
114.26
110.49
110.12
108.99
66.78
31.35
29.58
29.34
22.87
21.70
H
N
NHCbz
220 210 200 190 180 170 160 150 140 130 120 110 100 90 80 70 60 50 40 30 20 10 0 -10
f1 (ppm)

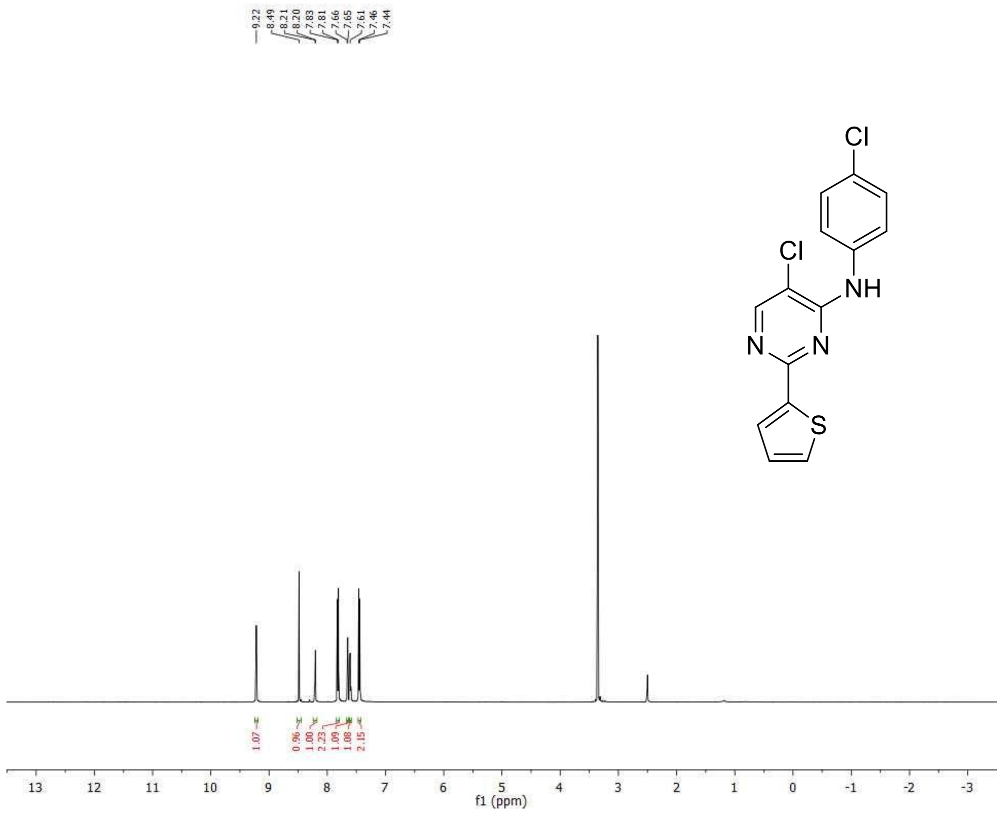
9.22
8.49
8.21
8.20
7.83
7.81
7.66
7.65
7.61
7.46
7.44
Cl
Cl
NH
N
N
S
1.07
0.96
1.00
2.23
1.09
1.08
2.15
13
12
11
10
9
8
7
6
5
4
3
2
1
0
-1
-2
-3
f1 (ppm)

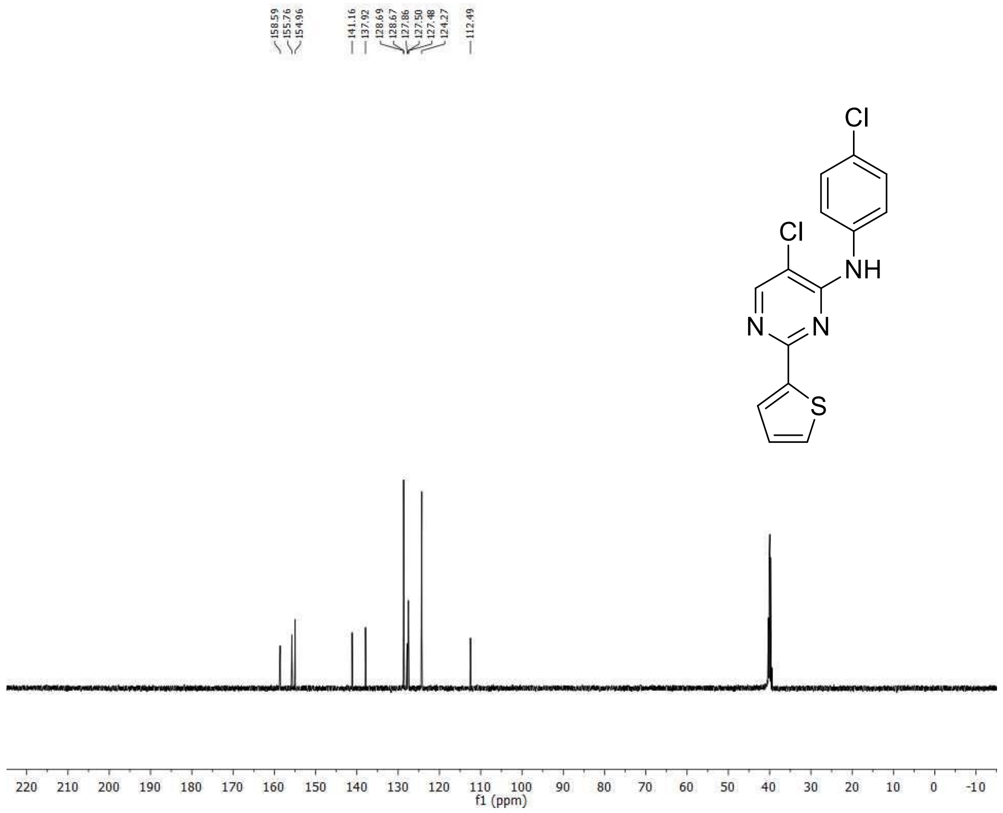
158.59
155.76
154.96
141.16
137.92
128.69
128.67
127.86
127.50
127.48
124.27
112.49
Cl
Cl
NH
N
N
S
220
210
200
190
180
170
160
150
140
130
120
110
100
90
80
70
60
50
40
30
20
10
0
-10
f1 (ppm)

II. Fe-catalyzed reductive couplings of terminal aryl alkenes and alkyl halides

Reproduced with permission from

Pang, H.; Wang, Y.; Gallou, F.; Lipshutz, B. H. Fe-catalyzed reductive couplings of terminal (hetero)aryl alkenes and alkyl halides under aqueous micellar conditions. *J. Am. Chem. Soc.* **2019**, *141*, 17117.

Copyright 2019 American Chemical Society.

General Comments on Hydrocarbonation

The formation of C–C bonds is one of the fundamental transformations in organic synthesis. Over the past few decades, diverse strategies based on catalysis by transition metal reagents have been proposed by chemists to construct these C–C bonds including Suzuki-Miyaura couplings, Heck-Mizoroki couplings, Negishi couplings, etc. As carbon-carbon bond formation plays a crucial role today in organic synthesis, Heck, Negishi and Suzuki shared the 2010 Nobel Prize in Chemistry in recognition of their contributions to coupling reactions. Nevertheless, with the increasing demand for structural diversity in compounds, a host of different approaches have been urgently developed to address the many modern challenges being faced by organic synthesis. In recent years, hydrocarbonation of alkenes and alkynes using halides as precursors to the corresponding coupling products has provided a novel strategy to construct the C-C bonds. In general, such approaches fall into two major categories: 1) hydroarylation of an alkene or alkyne using an aryl halide to form a new Csp^2-Csp^3 or Csp^2-Csp^2 bond; 2) hydroalkylation of an alkene or alkyne using an alkyl halide to form a new Csp^3-Csp^3 or Csp^3-Csp^2 bond. Moreover, due to the different transition metal catalysts used and diverse reaction conditions, different mechanisms have been proposed to explain each reaction process within this series of reactions based on various experimental results.

Hydroarylation

In 2015, Weaver and co-workers reported a hydroarylation of an olefin in the presence of a 2-bromoazole via photoinduced electron transfer catalyzed by *fac*-Ir(ppy)$_3$ (Scheme 1).[1] Subsequently, the authors screened both bromides and alkenes to examine both the scope and mechanism of this new coupling reaction. In terms of aryl bromide, they found that the bromine on the 4 or 5 position of 2-bromothiazole was not active in the hydroarylation, which indicated an element of chemoselectivity. In addition to 2-bromobenzo*[d]*thiazole, the reaction could also afford good yields when 2-bromo-1H-benzo[d]imidazole, 5-bromopyrimidine-2-carbonitrile and 4-bromobenzaldehyde were used as starting materials. As for the olefin, both terminal alkenes and substituted alkenes, (including even cholesterol) could be used as substrates in this process. Moreover, functional groups such as fluoro-, chloro-, bromo-, ester, hydroxy-, aldehyde and nitrile could be tolerated during the reaction. Nonetheless, most of the attention was focused on heteroaromatic bromides during their studies. For aromatic bromide, the authors provided only two cases with both containing electron-withdrawing groups attached. Hence, it remains unclear without further study whether this chemistry can be widely applied.

Scheme 1: Weaver's hydroarylation of olefin with 2-bromoazole

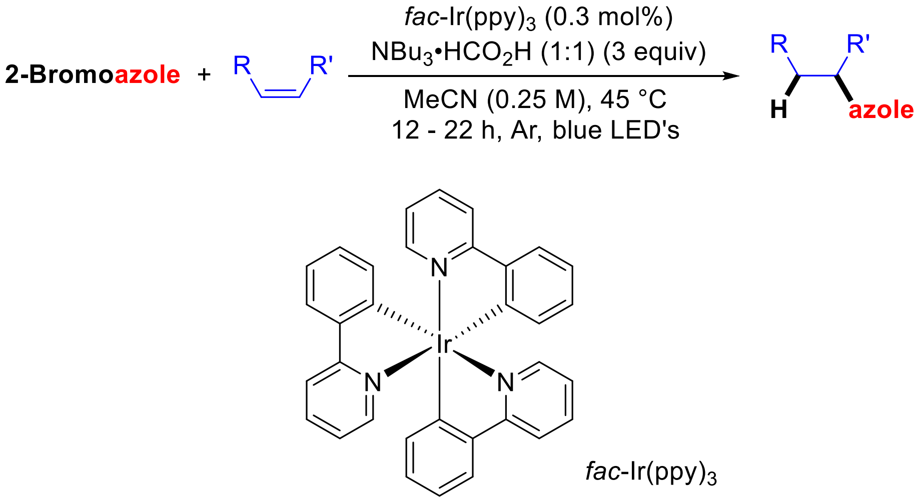

In 2016, Shenvi's group at Scripps developed a branch-selective (Markovnikov) olefin hydroarylation using a combination of cobalt metal hydrides (MH) hydrogen atom transfer (HAT) and nickel in the catalytic cycles (Scheme 2).[2] During optimization of the reaction conditions, the authors filtered the nickel source, cobalt source, hydrogen source and additive. Moreover, the necessity of both cobalt and nickel was shown during optimization.

In terms of the substrates, they found that such HAT hydroarylation was limited to terminal alkenes, since more substituted alkenes were unreactive in the presence of the cobalt catalyst under anaerobic conditions. Nevertheless, the authors also provided a broad scope of olefins with diverse functional groups, such as cyano-, organoboronate (Bpin), organohalides (sp^3-Cl and sp^3-Br), sulfide and alcohol. As for the scope of the iodoarene, when the ring contained electron-withdrawing groups, these educts generally showed much more activity towards hydroarylation compared with the rings bearing electron-donating substituents. In addition, ester, fluoro-, and trifluoromethyl- could also be tolerated. In terms of the heterocycle, substrates with furan, thiophene, pyridine, indole, and pyrazole were examined. In a follow up report from Shenvi's group in 2018, they described a detailed exploration of the mechanism of this reaction.[3] During this study, they excluded the cage escape as well as a radical chain mechanism using a graphical rate law analysis and radical clock cyclization experiments. They then provided evidence for the formation of an organocobalt species using ^{1}H NMR. Furthermore, they determined the role of 1-fluoro-2,4,6-trimethylpyridinium tetrafluoroborate (NFPTB) through subsequent stoichiometric experiments and crystal analysis of cobalt intermediates via X-ray analyses. Based on such evidence, they proposed a reasonable mechanism for hydroarylation, as shown in Scheme 2. Subsequently, in addition to the branch-selective hydroarylation of terminal alkenes, further studies on hydroarylation of mono-, di-, tri-, and tetra-substituted alkenes together with aryl halides catalyzed by the combination of iron and nickel were reported by the same group (Scheme 3).[4] Compared with the previous report in 2016, this work did a deeper exploration on the diversity of substrates, especially on the diversity of alkenes. In addition, as the highlight of this report, the authors could easily construct quaternary carbon centers by hydroarylation of multi-substituted alkenes using the same approach. Moreover, the authors also emphasized that compared with the Friedel−Crafts reaction which requires an electron-rich aromatic ring as substrate, this new route offers better yields for both electron-rich and electron-deficient aromatic rings during the formation of a quaternary carbon center. Therefore, the substrate scope regarding aryl halides was broader. In terms of functional groups, substrates with carbamates, strained cyclobutanes, esters, amides, thioethers, boronates, nitriles, silyl ethers, phthalimides and carbocycles were tolerated and retained high branch selectivity. In addition, unsaturated heterocycles, such as: oxetanes, tetrahydrofurans, pyrans, thianes, pyrrolidines, and piperidines all productively coupled. At the end of the paper, the authors also provided a plausible mechanism for such a process, as shown in Scheme 3.

Scheme 2: Shenvi's branch-selective (Markovnikov) olefin hydroarylation

Reaction:

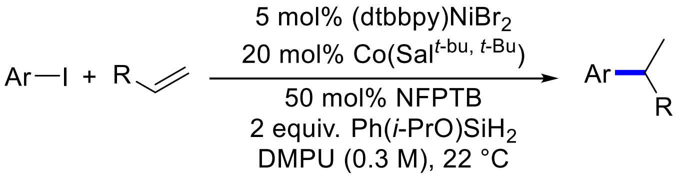
Ar—I + R
5 mol% (dtbbpy)NiBr$_2$
20 mol% Co(Sal$^{t\text{-bu},\ t\text{-Bu}}$)
50 mol% NFPTB
2 equiv. Ph(i-PrO)SiH$_2$
DMPU (0.3 M), 22 °C
Ar
R

Mechanism:

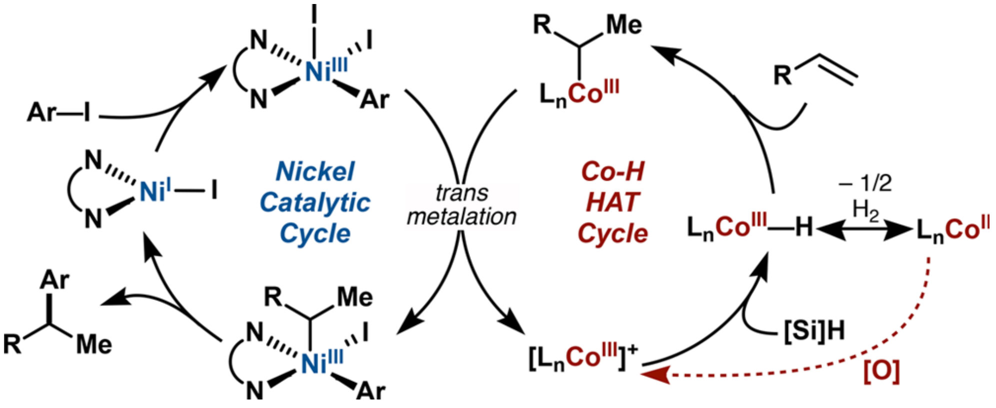
Ar—I
N
N
Ni^{III}
I
I
Ar
Ni^{I}—I
Nickel Catalytic Cycle
Ar
R
Me
R
Me
Ni^{III}
I
Ar
trans metalation
R
Me
L$_n$Co^{III}
R
Co-H HAT Cycle
L$_n$Co^{III}—H
− 1/2 H$_2$
L$_n$Co^{II}
[Si]H
[L$_n$Co^{III}]$^+$
[O]

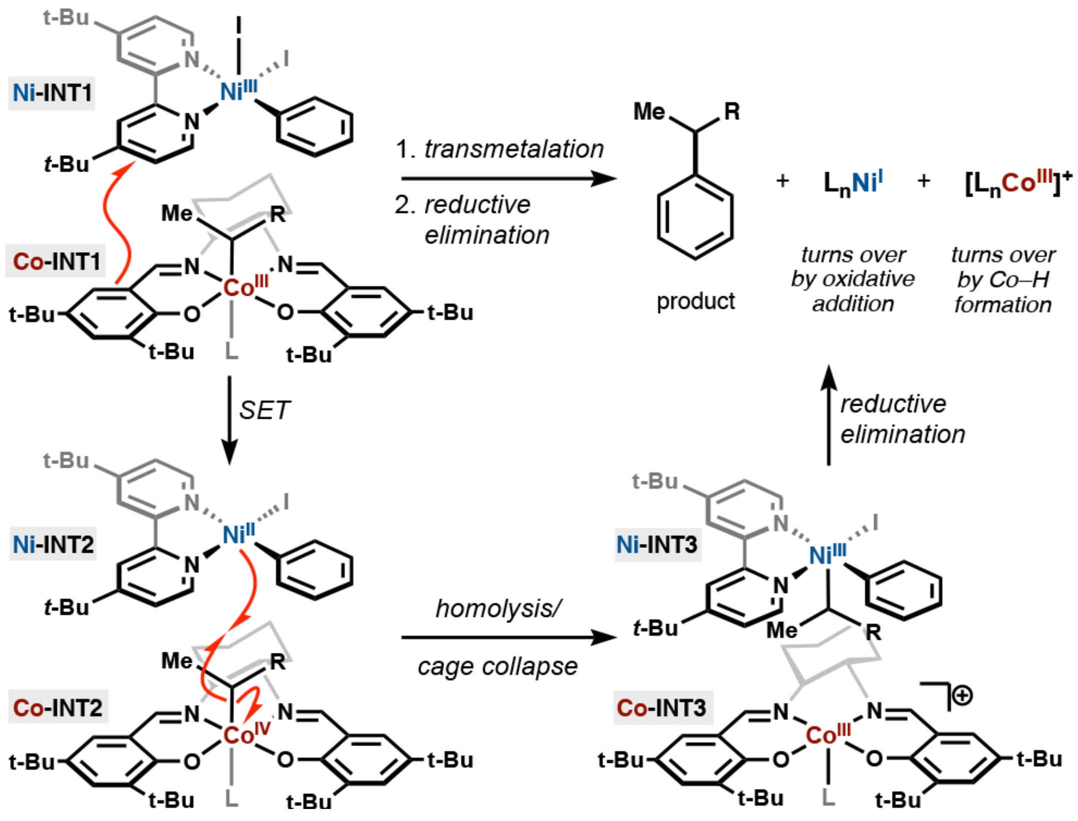
Ni-INT1
Co-INT1
1. transmetalation
2. reductive elimination
product
+ L_nNi^I + $[L_nCo^{III}]^+$
turns over by oxidative addition
turns over by Co–H formation
SET
reductive elimination
Ni-INT2
Co-INT2
homolysis/ cage collapse
Ni-INT3
Co-INT3
t-Bu
Me
R
L

Reproduced with permission from ref 3. Copyright 2018 American Chemical Society.

Scheme 3: Shenvi's olefin hydroarylation with iron−nickel dual-catalysis

Reaction:

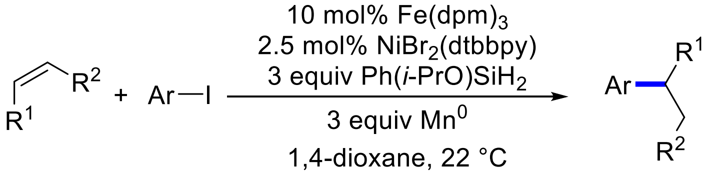
10 mol% $Fe(dpm)_3$
2.5 mol% $NiBr_2(dtbbpy)$
3 equiv $Ph(i\text{-}PrO)SiH_2$
3 equiv Mn^0
1,4-dioxane, 22 °C
R^1
R^2
+ Ar—I
Ar

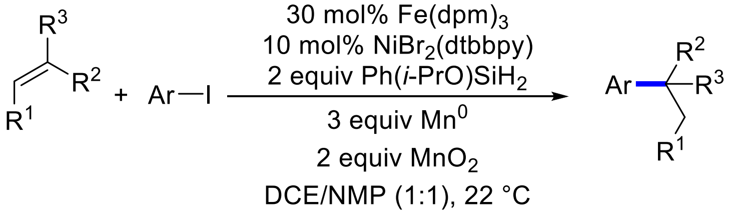
30 mol% $Fe(dpm)_3$
10 mol% $NiBr_2(dtbbpy)$
2 equiv $Ph(i\text{-}PrO)SiH_2$
3 equiv Mn^0
2 equiv MnO_2
DCE/NMP (1:1), 22 °C
R^1
R^2
R^3
+ Ar—I
Ar

Mechanism:

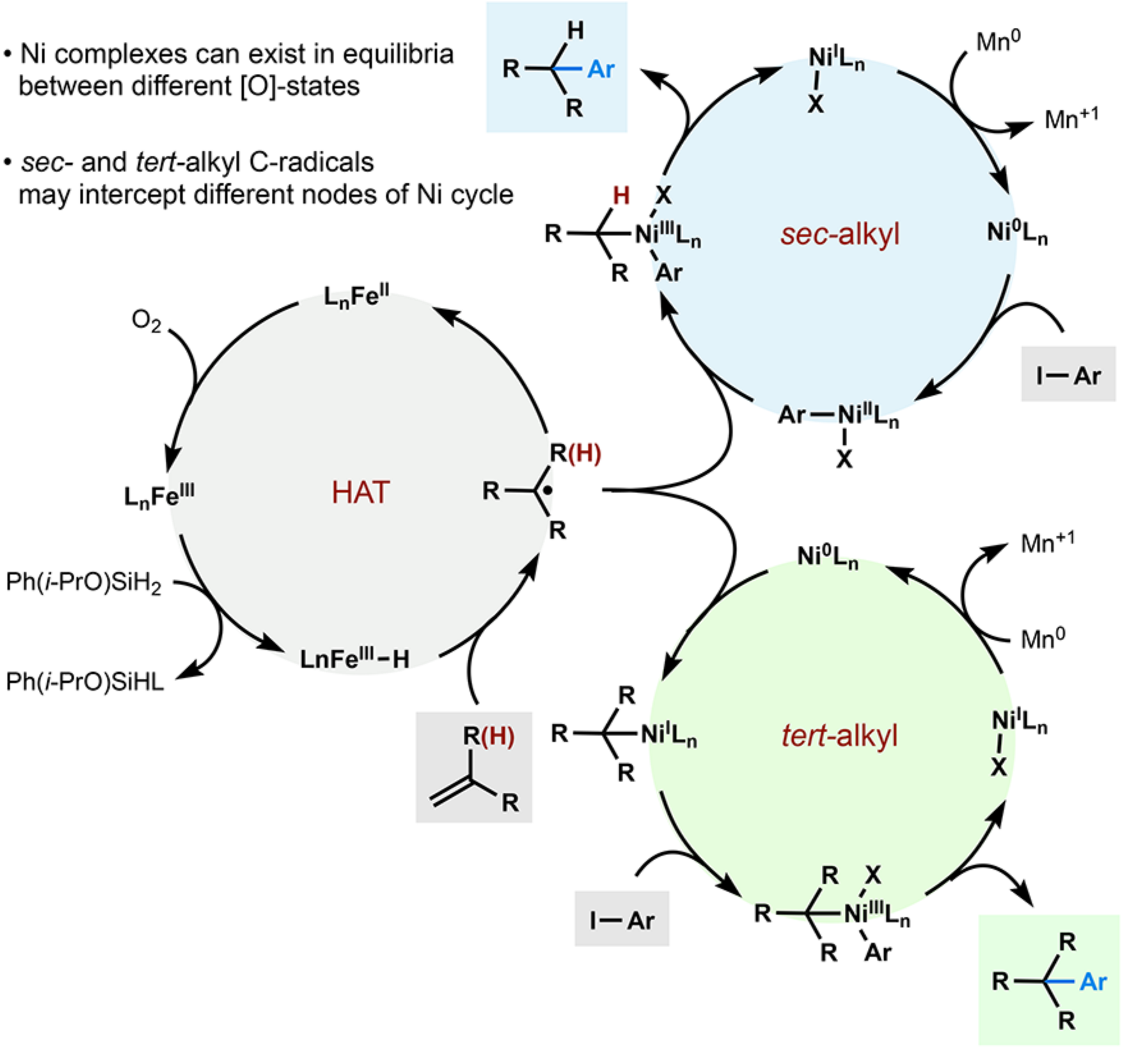
• Ni complexes can exist in equilibria between different [O]-states
• sec- and tert-alkyl C-radicals may intercept different nodes of Ni cycle
HAT
sec-alkyl
tert-alkyl
LnFeII
O2
LnFeIII
Ph(i-PrO)SiH2
Ph(i-PrO)SiHL
LnFeIII-H
R(H)
R
R
R(H)
R
NiILn
X
Mn0
Mn+1
Ni0Ln
I—Ar
Ar—NiIILn
X
H
X
R
NiIIILn
R
Ar
H
R
Ar
R
Ni0Ln
Mn+1
Mn0
NiILn
X
R
R
NiILn
R
I—Ar
R
X
R
NiIIILn
R
Ar
R
R
Ar
R

Reproduced with permission from ref 4. Copyright 2018 American Chemical Society.

Buchwald developed a novel asymmetric branch-selective hydroarylation of vinylarenes using a synergistic combination of CuH and Pd catalysis in 2016, as shown in Scheme 4.[5] According to their mechanism, the authors proposed the active CuH catalyst was formed through the use of Cu salt with chiral ligand and silane. After enantioselective hydrocupration of the olefin, the newly obtained Cu intermediate would form a chiral Pd alkyl complex via transmetalation of the Pd complex derived from the oxidative addition of aryl bromide. The hydroarylation product was obtained after reductive elimination.

Compared with Shenvi's work, this technology achieved asymmetric hydroarylation of vinylarenes using a chiral CuH reagent. Subsequently, the authors showed that a range of functional groups, including ether, ester, thioether, amine, carbamate, aryl chloride and amide were all tolerated in this protocol. As for heterocycles, products containing pyridine, quinoline, pyrimidine, pyridazine, isoquinoline, indole and azaindole are all amenable. Interestingly, in 2017, Buchwald's group reported another strategy with almost the same reaction conditions as in the former paper but replaced the vinylarenes with terminal monosubstituted olefins (Scheme 4).[6] This methodology has an essentially identical mechanism, but the products were linear-selective (anti-Markovnikov) instead of branch-selective (Markovnikov). Moreover, the authors also provided evidence that the branch-selective product would prefer to form with vinylarenes as starting materials even under the updated conditions.

Scheme 4: Buchwald's branch-selective and linear-selective hydroarylation

Reactions:

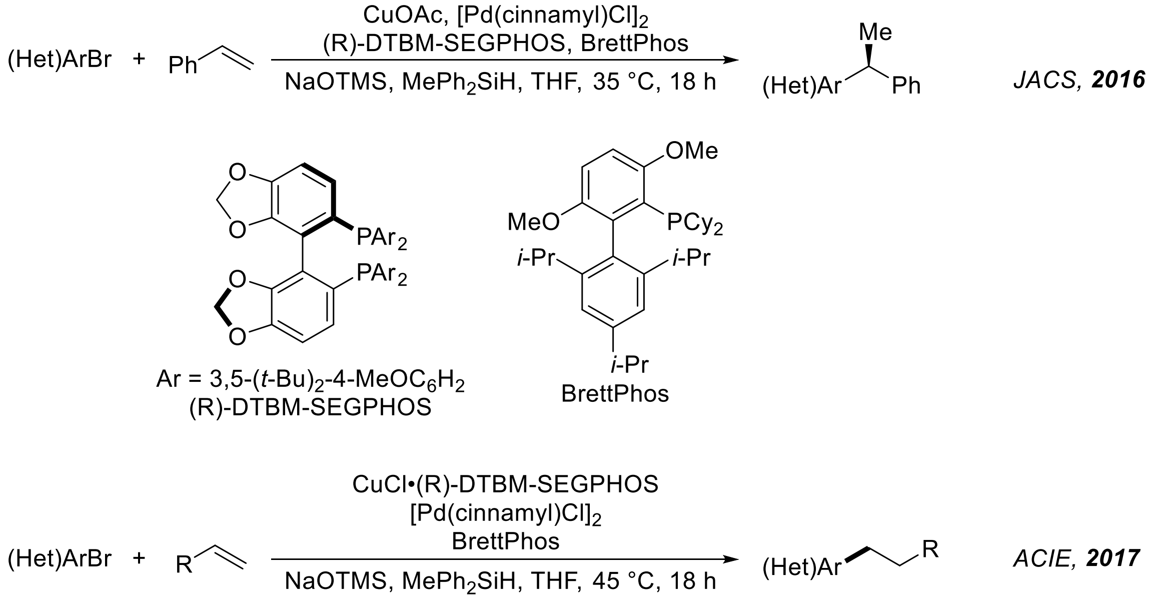
(Het)ArBr + Ph
CuOAc, [Pd(cinnamyl)Cl]$_2$
(R)-DTBM-SEGPHOS, BrettPhos
NaOTMS, MePh$_2$SiH, THF, 35 °C, 18 h
Me
(Het)Ar
Ph
JACS, ***2016***
O
PAr$_2$
Ar = 3,5-(t-Bu)$_2$-4-MeOC$_6$H$_2$
(R)-DTBM-SEGPHOS
OMe
MeO
PCy$_2$
i-Pr
BrettPhos
(Het)ArBr + R
CuCl•(R)-DTBM-SEGPHOS
[Pd(cinnamyl)Cl]$_2$
BrettPhos
NaOTMS, MePh$_2$SiH, THF, 45 °C, 18 h
(Het)Ar
R
ACIE, ***2017***

Mechanism:

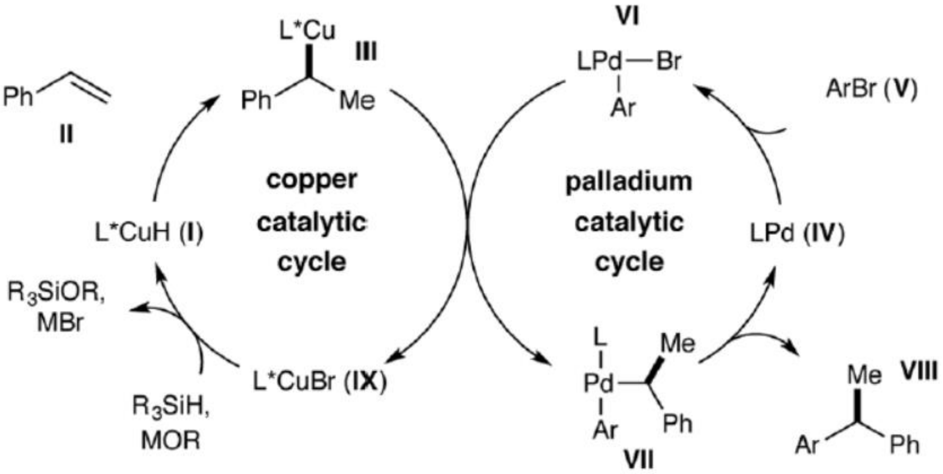

L*Cu
III
Ph
Me
Ph
II
VI
LPd—Br
Ar
ArBr (V)
copper
catalytic
cycle
palladium
catalytic
cycle
L*CuH (I)
LPd (IV)
R3SiOR,
MBr
L*CuBr (IX)
R3SiH,
MOR
L
Pd
Ar
Me
Ph
VII
Me
VIII
Ar
Ph

Reproduced with permission from ref 5. Copyright 2016 American Chemical Society.

From 2017 to 2018, Jui and co-workers published three reports in *JACS* and *Chemical Science* successively on hydropyridylation of alkenes or alkynes (Scheme 5).[7-9] This series of reactions were all catalyzed by an iridium derivative via a photoinduced electron transfer process. The interesting aspect about those reactions is that they all used the Hantzsch ester (HEH) as the hydrogen source during the reaction. A proposed mechanism was also suggested by the authors, as shown in Scheme 5. However, since such a strategy was only successful on bromopyridines or iodopyridines, applications of this technology are therefore, limited.

Scheme 5: Jui's hydropyridylation of alkenes and alkynes

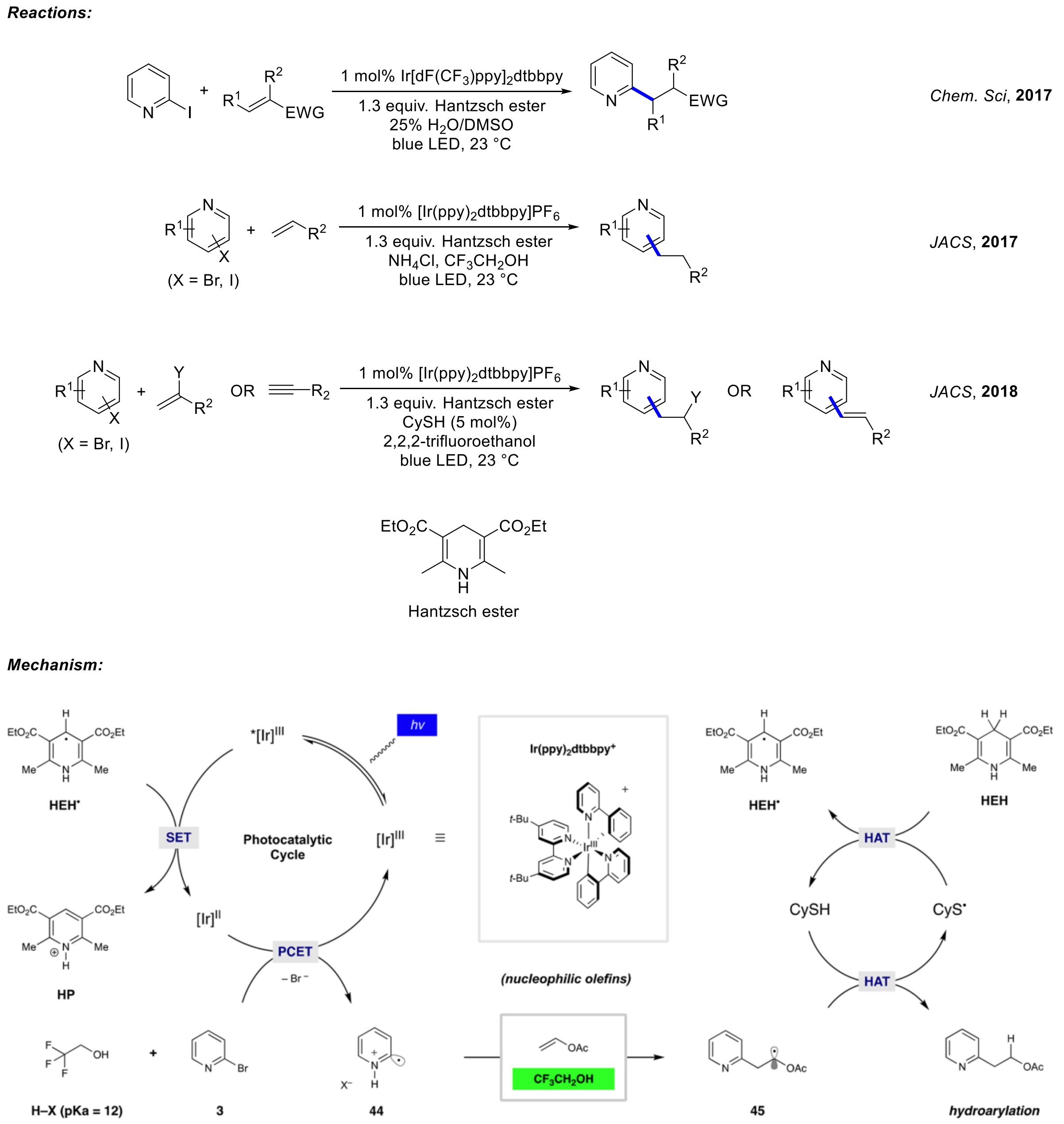
Reactions:
1 mol% Ir[dF(CF3)ppy]2dtbbpy
1.3 equiv. Hantzsch ester
25% H2O/DMSO
blue LED, 23 °C
EWG
Chem. Sci, 2017
1 mol% [Ir(ppy)2dtbbpy]PF6
1.3 equiv. Hantzsch ester
NH4Cl, CF3CH2OH
blue LED, 23 °C
(X = Br, I)
JACS, 2017
OR
1 mol% [Ir(ppy)2dtbbpy]PF6
1.3 equiv. Hantzsch ester
CySH (5 mol%)
2,2,2-trifluoroethanol
blue LED, 23 °C
(X = Br, I)
JACS, 2018
Hantzsch ester
Mechanism:
HEH•
*[Ir]III
hv
SET
Photocatalytic Cycle
[Ir]III
≡
Ir(ppy)2dtbbpy+
HEH•
HEH
HP
[Ir]II
PCET
– Br⁻
(nucleophilic olefins)
HAT
CySH
CyS•
HAT
CF3CH2OH
H–X (pKa = 12)
3
44
45
hydroarylation

Reproduced with permission from ref 9. Copyright 2018 American Chemical Society.

In 2018, Li *et al*. developed another hydroarylation of styrenes using aryl iodides in water catalyzed by copper (Scheme 6).[10] This report uniquely described the intermolecular hydroarylations of olefins with aryl halides in water. In terms of the substrate scope, although the authors did not examine that many cases, some general functional groups such as chloro-, fluoro-, methoxy- and trifluoromethyl- could be tolerated during this process. Further experimental results showed that for the alkenes with terminal substitution, such as trans-β-methylstyrene, yields of the hydroarylation were lower. Li and co-workers also proposed a plausible mechanism, as shown in Scheme 6.

Scheme 6: Li’s hydropyridylation of styrenes with aryl iodides in water

Reaction:

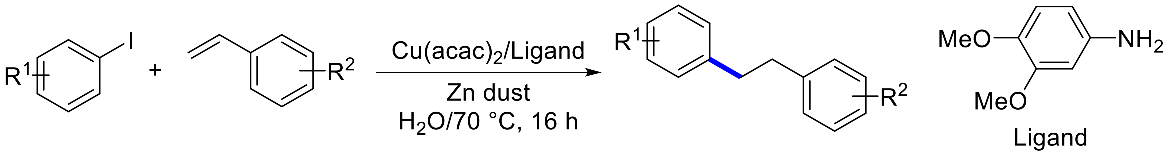
R1
I
+
R2
Cu(acac)2/Ligand
Zn dust
H2O/70 °C, 16 h
R1
R2
MeO
NH2
MeO
Ligand

Mechanism:

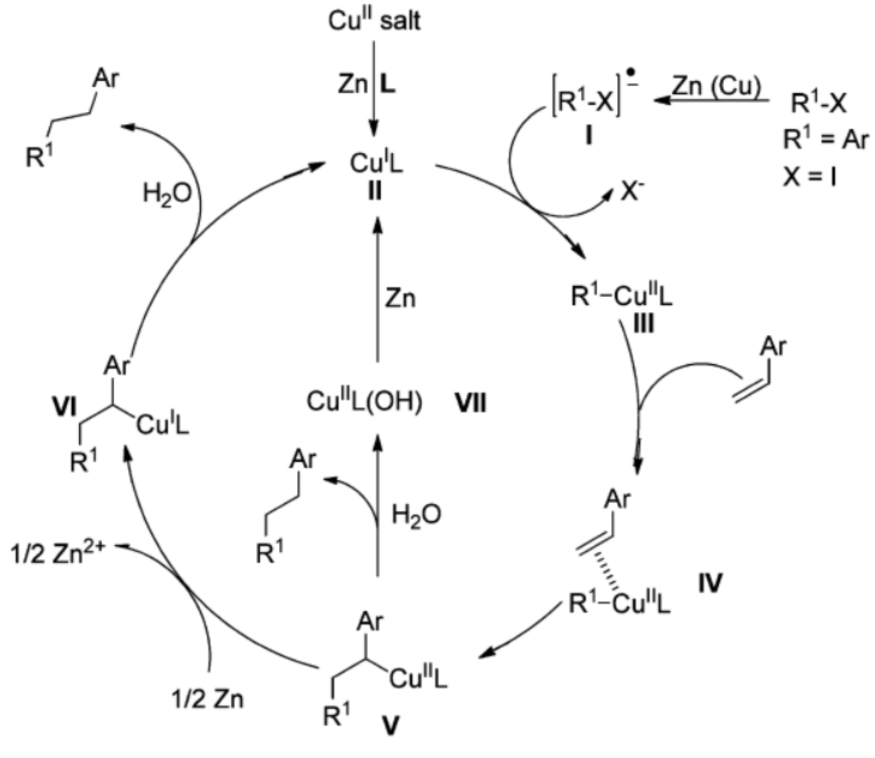
Cu^II salt
Zn L
Cu^IL
II
[R1-X]•−
I
Zn (Cu)
R1-X
R1 = Ar
X = I
X−
R1–Cu^IIL
III
Ar
Ar
R1–Cu^IIL
IV
Ar
Cu^IIL
R1
V
1/2 Zn
1/2 Zn2+
Ar
Cu^IL
R1
VI
H2O
Ar
R1
Zn
Cu^IIL(OH)
VII
H2O
Ar
R1

Reproduced with permission from ref 10. Copyright 2018 American Chemical Society.

Most of the hydroarylations mentioned above were obtained by free radical reactions involving single electron transfer. However, clearly, this is not the only possible path. By changing the classic Heck reaction conditions, Engle and collaborators avoided β-H elimination during the reaction and thus, realized hydroarylation of alkenes (Scheme 7).[11] In this strategy, $Pd_2(dba)_3$ combined with a common ligand, triphenylphosphine, was used as catalyst. In addition to K_3PO_4 as base, tetramethylammonium formate, 30% w/w in aqueous solution ($TMA{\cdot}HCO_2$) served as a superior reductant during the process. The authors provided a broad substrate scope along with excellent functional group tolerance and inclusion of heterocycles, and also determined the source of hydrogen using deuterium. At the end of their report, a plausible mechanism was proposed, as shown in Scheme 7. Their mechanistic picture features the same oxidative addition and migratory insertion as in the Heck reaction. However, after insertion, ion exchange takes place instead of β-H elimination, followed by decarboxylation and reductive elimination to afford the hydroarylation product.

Scheme 7: Engle's hydroarylation of alkenes via reductive Heck coupling

Reaction:

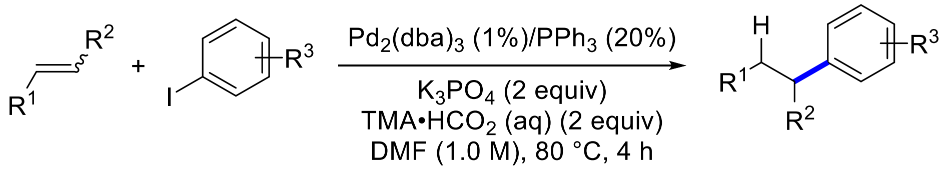

Mechanism:

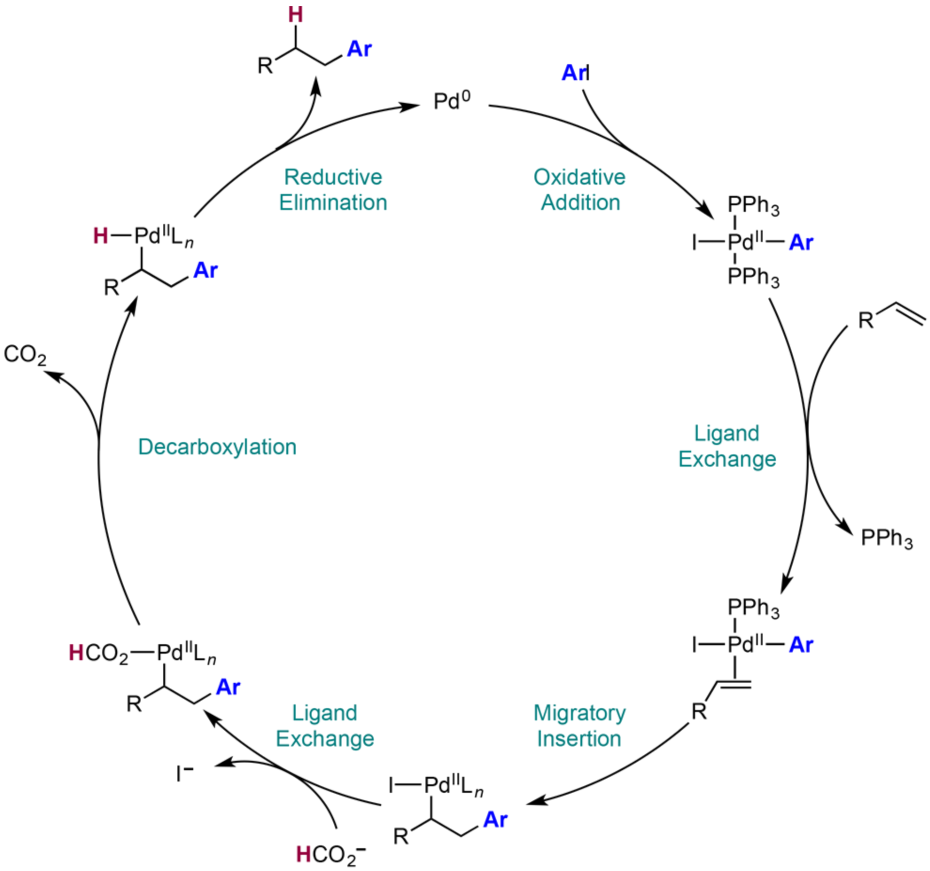
Pd⁰
ArI
Oxidative Addition
PPh3
I—PdII—Ar
PPh3
R
Ligand Exchange
PPh3
PPh3
I—PdII—Ar
R
Migratory Insertion
I—PdIILn
R
Ar
HCO2⁻
Ligand Exchange
I⁻
HCO2—PdIILn
R
Ar
Decarboxylation
CO2
H—PdIILn
R
Ar
Reductive Elimination
H
R
Ar

Reproduced with permission from ref 11. Copyright 2018 American Chemical Society.

In 2019, Lalic and co-workers developed a novel nickel-catalyzed hydroarylation of alkenes using aryl halides as coupling partners (Scheme 8).[12] In this protocol, polymethylhydrosiloxane (PMHS) was used as the hydride source. Insofar as scope is concerned, heterocycles such as benzofuran, indole, pyrrole, benzopyrazole, pyrrolopyridine, quinoline, pyrimidine, and benzopyrazole were all tolerated. Moreover, the authors proposed a mechanism at the end of the paper, shown in Scheme 8. Relatively inexpensive $NiCl_2$(DME) as catalyst reduced the cost of the reaction. In addition, room temperature conditions also reduced the energy required by this hydroarylation process. However, from the environmental perspective, the solvent in this strategy is benzene, which may limit applications to manufacturing.

Scheme 8: Lalic' nickel-catalyzed hydroarylation of alkenes

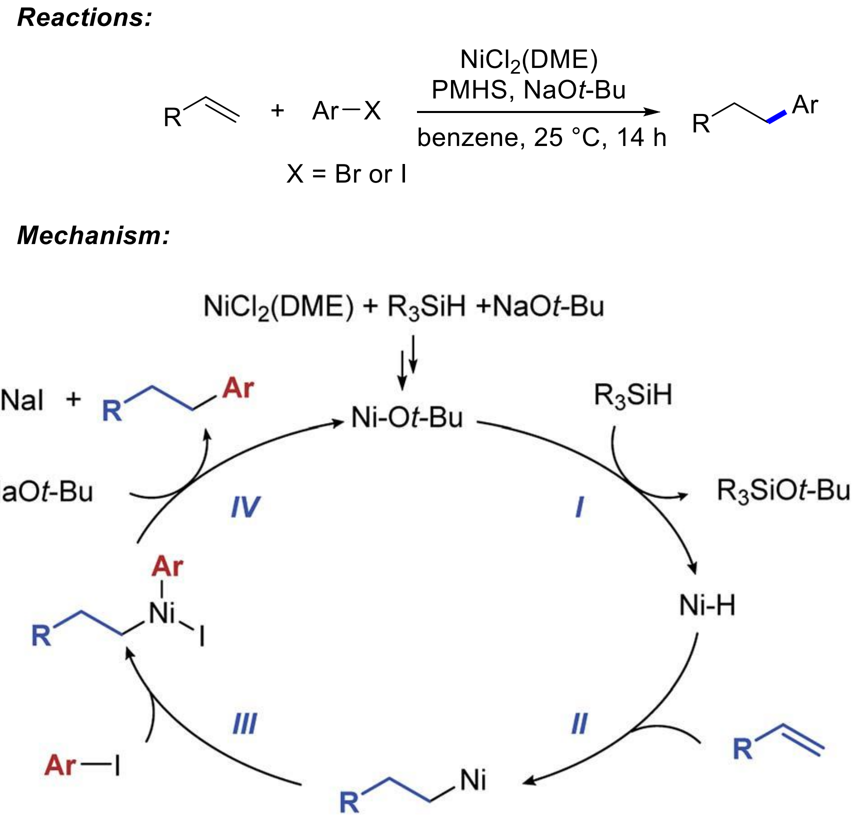
Reactions:
R
+
Ar—X
X = Br or I
NiCl2(DME)
PMHS, NaOt-Bu
benzene, 25 °C, 14 h
R
Ar
Mechanism:
NiCl2(DME) + R3SiH +NaOt-Bu
Ni-Ot-Bu
R3SiH
R3SiOt-Bu
I
Ni-H
II
R
R
Ni
III
Ar—I
Ar
R
Ni
I
IV
NaOt-Bu
NaI + R
Ar

Reproduced with permission from ref 12. Copyright 2019 Royal Society of Chemistry.

In addition to hydroarylation of alkenes, hydroarylation of alkynes has been developed as well. In 2018, Lalic's group reported on a reductive coupling between aryl halides and terminal alkynes to form the anti-Markovnikov product.[13] The sequence is catalyzed by a combination of palladium and copper catalysts with Me_2*i*-PrSiH as reductant. This technique has a broad substrate scope, as well as great functional group tolerance. The mechanism proposed by the authors involves an initial Sonogashira coupling catalyzed by Pd, followed by semi-reduction promoted by the Cu catalyst to generate diastereoselective alkenes (Scheme 9). Moreover, the authors continued to explore a way to achieve isomerization of the *Z*-alkene to convert it to the corresponding *E*-alkene products. Interestingly, this process allows for selective synthesis of either *Z* or *E* diastereoisomers of aryl alkenes from the same set of starting materials using the same catalysts. The selectivity is controlled solely by changes in the stoichiometry of the alcohol additive in the reaction. It was discovered that a larger excess of methanol as additive (from 1.5 to 5 equivalents) can achieve isomerization of *Z*-alkenes. Further studies on the mechanism via control experiments and deuterium tracking experiments indicated that the excess MeOH hinders copper-catalyzed semi-reduction, but promotes both the palladium-catalyzed semi-reduction and isomerization of an *Z*-alkene. This is the explanation behind methanol’s impact on the final diastereoselectivity observed in the product.

Scheme 9: Lalic’s hydroarylation of alkyne catalyzed by Pd/Cu

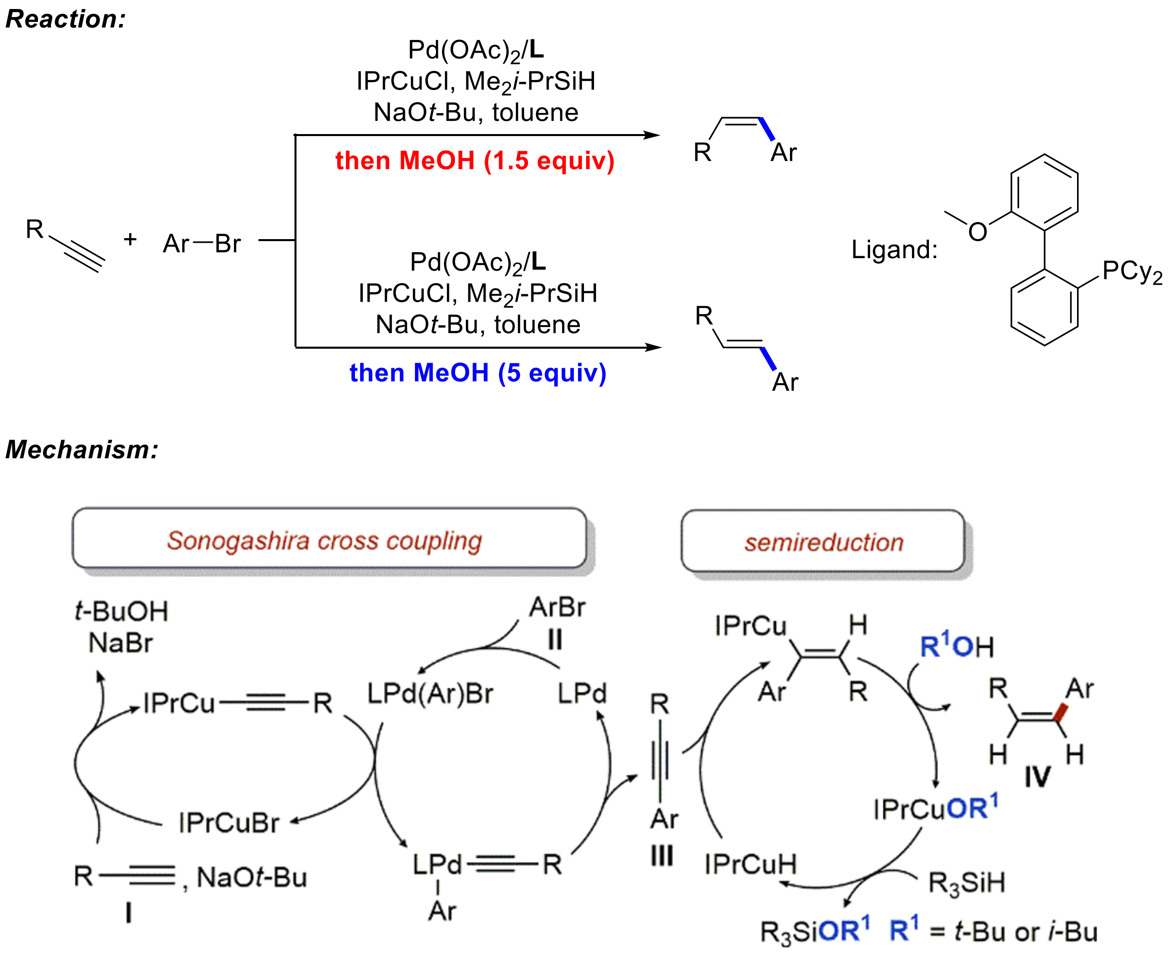
Reaction:
Pd(OAc)2/L
IPrCuCl, Me2i-PrSiH
NaOt-Bu, toluene
then MeOH (1.5 equiv)
then MeOH (5 equiv)
R
Ar—Br
Ar
Ligand:
O
PCy2
Mechanism:
Sonogashira cross coupling
semireduction
t-BuOH
NaBr
IPrCu—R
IPrCuBr
R—, NaOt-Bu
I
ArBr
II
LPd(Ar)Br
LPd
LPd—R
Ar
III
IPrCu
H
R1OH
IV
IPrCuOR1
IPrCuH
R3SiH
R3SiOR1
R1 = t-Bu or i-Bu

Reproduced with permission from ref 13. Copyright 2018 American Chemical Society.

Also in 2018, Sakai and co-workers developed another approach to hydroarylation of alkynes using a Hr or Zr together with Pd as a bimetallic catalyst to generate *E*-alkenes.[14] Although this protocol did not provide a broad substrate scope and excellent functional group compatibility as did the procedure by Lilic, it provided hydroarylation on both terminal as well as internal alkynes, which undoubtedly broadens the scope of this strategy. A different mechanism was also proposed for this reductive coupling, which proceeds via a coupling between an alkenyl metallocene intermediate and aryl halide, as shown in Scheme 10. In addition, it was proven via NMR spectral data that an anion exchange takes place with hafnocene diiodide (Cp_2HfI_2) to regenerate hafnocene difluoride (Cp_2HfF_2) as catalyst, using NaF en route to the product.

Scheme 10: Sakai's hydroarylation of alkyne using Hf or Zr with Pd

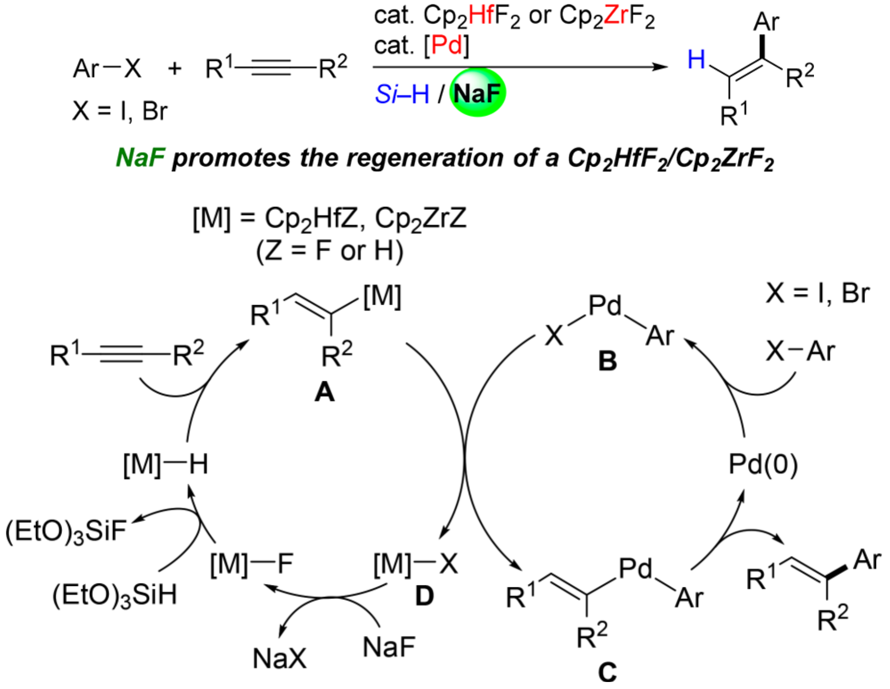
Ar—X + R1—≡—R2
X = I, Br
cat. Cp2HfF2 or Cp2ZrF2
cat. [Pd]
Si–H / NaF
H
Ar
R2
R1
NaF promotes the regeneration of a Cp2HfF2/Cp2ZrF2
[M] = Cp2HfZ, Cp2ZrZ
(Z = F or H)
R1—≡—R2
R1
[M]
R2
A
[M]—H
(EtO)3SiF
(EtO)3SiH
[M]—F
[M]—X
D
NaX
NaF
X
Pd
Ar
B
X = I, Br
X−Ar
Pd(0)
R1
Pd
Ar
R2
C
R1
Ar
R2

Reproduced with permission from ref 14. Copyright 2018 American Chemical Society.

Hydroalkylation

Compared with sp^2 halides, sp^3 halides are relatively unreactive; hence, it is more challenging to activate an sp^3 halide. This may explain why hydro*alkylation* of alkenes has had fewer recorded achievements than does hydro*arylation*. In 2018, Balsells and co-workers developed a novel hydroalkyation of Michael acceptors with unactivated alkyl bromides under visible-light photoredox catalysis (Scheme 11).[15] As for substrate scope, the authors examined bromides and Michael acceptors separately. Ester, amide, trifluoromethyl-, ether, Boc-protected amine and phosphonates were all tolerated under their conditions. Furthermore, deuterium studies showed that hydrogen added to form the product was mainly from MeOH, rather than tris(trimethylsilyl)silane, the latter being used mainly as a radical initiator. In addition, a plausible mechanism was proposed by the authors, as shown in Scheme 11.

Scheme 11: Balsells' photoredox-catalyzed hydroalkylation of Michael acceptors

Reaction:

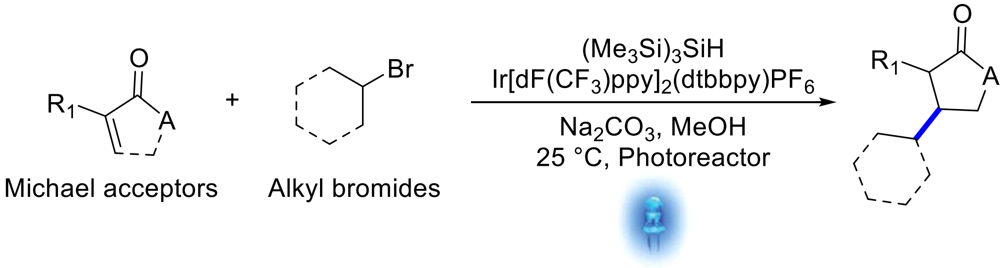

Mechanism:

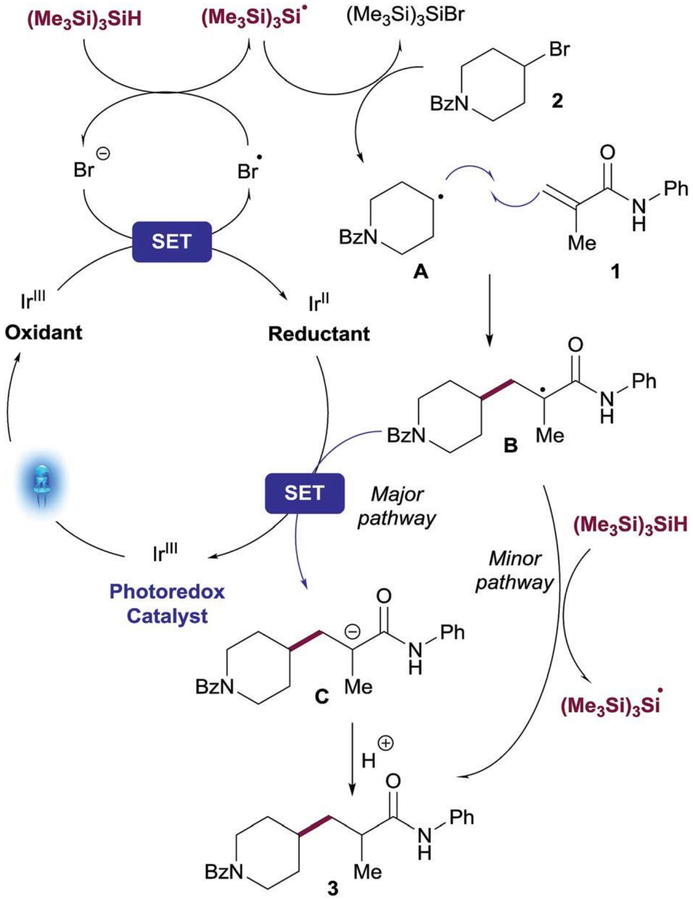

(Me3Si)3SiH
(Me3Si)3Si•
(Me3Si)3SiBr
Br
BzN
2
Br⊖
Br•
SET
IrIII
Oxidant
IrII
Reductant
O
N
H
Ph
Me
A
1
B
SET
Major pathway
Minor pathway
(Me3Si)3SiH
(Me3Si)3Si•
IrIII
Photoredox Catalyst
C
H⊕
3

Reproduced with permission from ref 15. Copyright 2018 Royal Society of Chemistry.

Lin's group at Cornell University in 2018 reported a hydroalkylation of electron-deficient alkenes using secondary and tertiary alkyl chlorides, catalyzed by Ti^{III} (Scheme 12).[16] In this strategy, the chlorine atom on the halide was abstracted by Ti to form a free radical, a process that is reversible. However, in this protocol, Ti^{IV} shows great affinity towards highly electronegative atoms, which makes chlorine atom abstraction thermodynamically favorable. In addition, the comparison of the bonding dissociation energy (BDE) of C–Cl and Ti–Cl supports this tendency (BDE of *t*-Bu−Cl is ca. 85 kcal/mol and BDE of Ti^{IV}−Cl in $TiCl_4$ is 96 kcal/mol). Based on this assumption, the authors designed a Ti-catalyzed hydroalkylation reaction, and optimized the conditions needed (Scheme 12). Subsequently, a broad substrate scope was provided with various functional groups being tolerated, such as trifluoromethyl-, tertiary amine, aryl bromide, aryl boronate, primary alkyl chloride, etc. In the end, based on the results from radical trapping tests and density functional theory (DFT) computations, a plausible mechanism for such a sequence was proposed, as shown in Scheme 12.

Scheme 12: Lin's hydroalkylation of electron-deficient alkene catalyzed by Ti^{III}

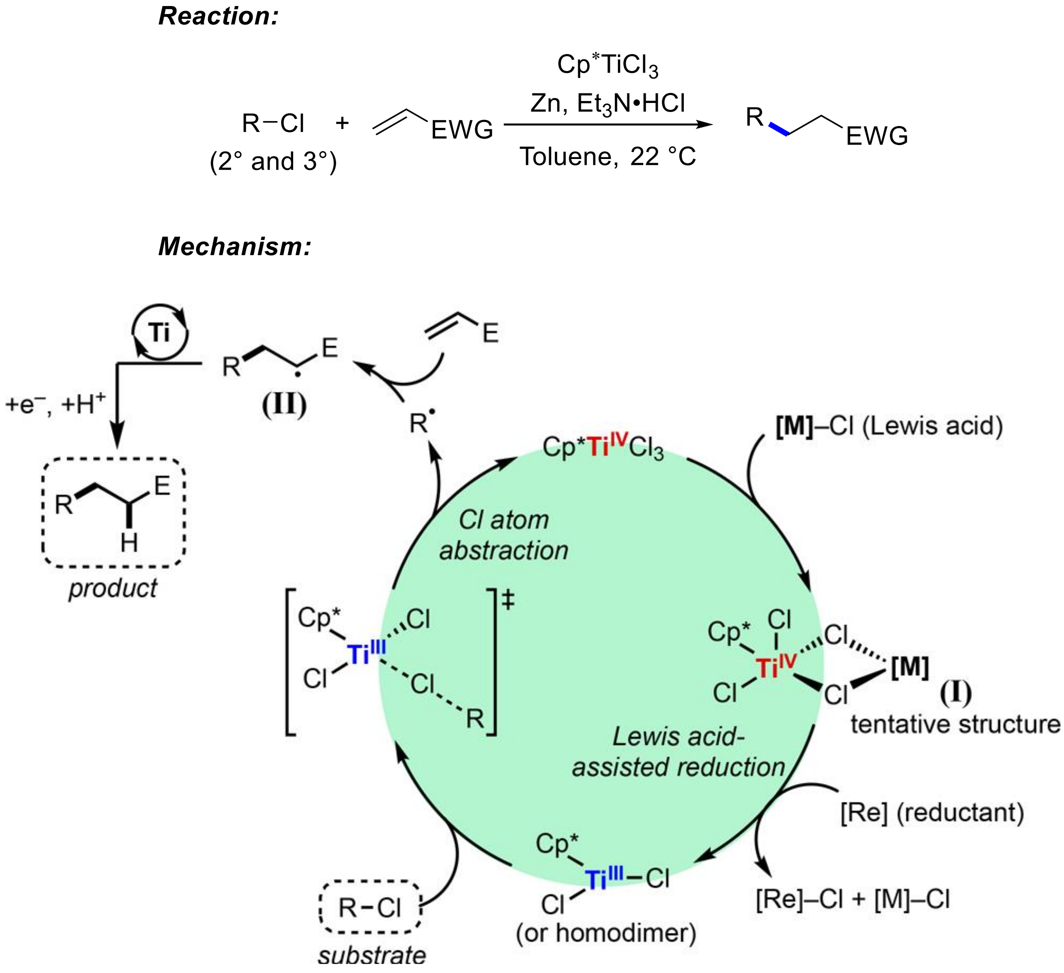
Reaction:
R−Cl
(2° and 3°)
+
EWG
Cp*TiCl3
Zn, Et3N•HCl
Toluene, 22 °C
R
EWG
Mechanism:
Ti
+e⁻, +H⁺
R
E
(II)
E
R•
R
E
H
product
Cp*TiIVCl3
[M]–Cl (Lewis acid)
Cl atom abstraction
Cp*
Cl
Cl
TiIII
Cl
R
‡
Cp*
Cl
TiIV
Cl
Cl
Cl
[M]
(I)
tentative structure
Lewis acid-assisted reduction
[Re] (reductant)
[Re]–Cl + [M]–Cl
Cp*
TiIII–Cl
Cl
(or homodimer)
R−Cl
substrate

Reproduced with permission from ref 16. Copyright 2018 American Chemical Society.

Also in 2018, Fu's group from CalTech reported a protocol for enantioselective hydroalkylation of terminal alkenes, starting from racemic alkyl bromides, to form Csp^3-Csp^3 bonds. These couplings took place in the presence of a hydrosilane through the action of a nonracemically ligated nickel catalyst (Scheme 13).[17] The scope of such a strategy is fairly broad, with a diverse array of functional groups being tolerated, including primary alkyl chlorides and bromides, acetal, amide, ester, carbamate, boronate ester, ether, alcohol, aldehyde, aryl iodide, ketone, secondary amine, thioether, etc., providing the enantio-convergent hydroalkylation products in good ee's and yields. Subsequently, the authors started to investigate the mechanism of this process. First, they excluded the possibility that the olefin undergoes a nickel-catalyzed hydrosilylation and that the resulting alkylsilane serves as a nucleophile in a conventional electrophile–nucleophile (Hiyama-type) cross-coupling, based on control experiments. Then, a metal-hydride hydrogen atom transfer (MHAT) mechanism was proposed, as shown in Scheme 13. In the end, to further demonstrate this mechanism, the authors individually synthesized and crystallographicaly characterized the intermediate. Furthermore, the intermediate was also used to catalyze a hydroalkylation, and compared favorably with the reaction catalyzed by the original catalyst in both yield and enantiomeric excess, thereby proving that the intermediate could be generated in situ under their standard conditions.

Scheme 13: Fu's enantioconvergent hydroalkylation of olefins

Reaction:

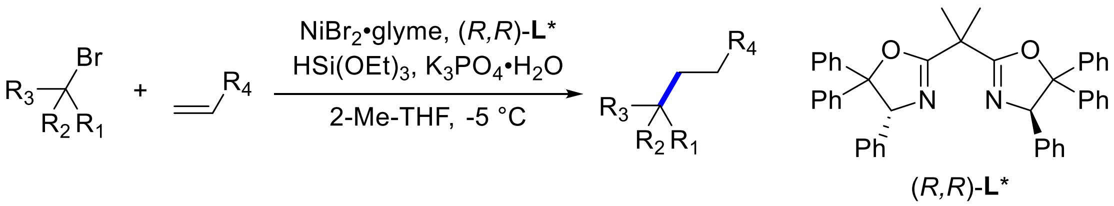

Mechanism:

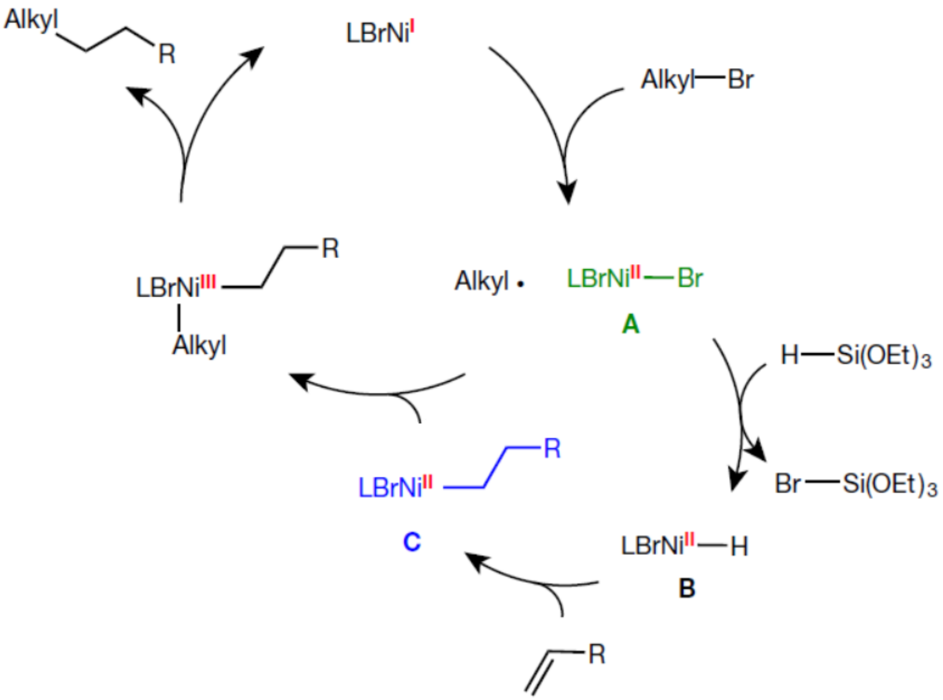

Reproduced with permission from ref 17. Copyright 2017 Springer Nature.

In 2019, Shenvi's group reported another Markovnikov-selective hydroalkylation of olefins using alkyl iodides and benzyl bromides (Scheme 14).[18] In this methodology, the combination of Mn-mediated metal-hydride hydrogen atom transfer (MHAT) catalysis and Ni catalysis enabled the synthesis of quaternary carbons under mild conditions. Also, the author provided a broad substrate scope with robust functional group compatibility. In addition, according to the plausible mechanism provided, which was similar to that put forth in their previous work on olefin hydroarylation with iron−nickel dual-catalysis,[4] use of multi-substituted olefins as starting materials is more likely to stabilize a tertiary radical intermediate, so as to facilitate the subsequent oxidative addition and reductive elimination step to yield the desired branch-selective products.

Scheme 14: Shenvi's hydroalkylation of olefins catalyzed by the combination of Ni and Mn

Reaction:

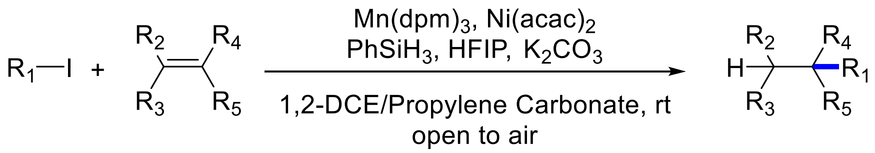
R1—I +
R2
R4
R3
R5
Mn(dpm)3, Ni(acac)2
PhSiH3, HFIP, K2CO3
1,2-DCE/Propylene Carbonate, rt
open to air
H
R1

Mechanism:

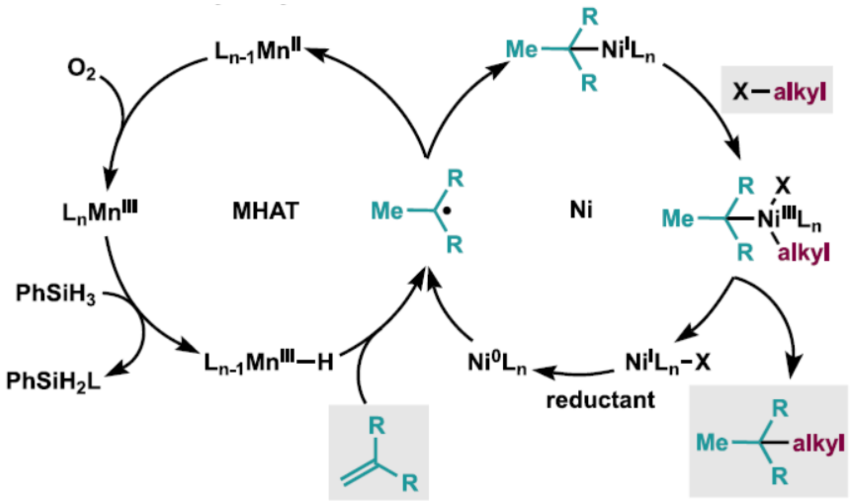
O2
Ln-1MnII
LnMnIII
MHAT
PhSiH3
PhSiH2L
Ln-1MnIII—H
Me
R
Ni
NiILn
X—alkyl
NiIIILn
X
alkyl
Ni0Ln
NiILn–X
reductant

Reproduced with permission from ref 18. Copyright 2019 American Chemical Society.

As with hydroarylations of alkynes, there have also been contributions devoted to hydroalkylations of alkynes. In 2015, Hu and co-workers reported a protocol to form *Z*-alkenes via reductive coupling of terminal arylalkynes with alkyl halides.[19] In this study, $FeBr_2$ serves as the catalyst combined with Zn as reductant. The reactions proceed smoothly between room temperature and 60 °C leading to great yields and geometric selectivity. A broad substrate scope including primary, secondary, and tertiary alkyl halides, as well as good functional group compatibilities were provided by the authors. Moreover, several bioactive molecules were synthesized via this technique to show the potential value in medical industry. Compared with the classic Wittig reaction, this strategy has better geometric selectivity as well as yields in syntheses of those targets. Additionally, the authors proposed a plausible mechanism as shown in Scheme 15 based on the results from deuterium tracking, radical clock, and trapping of radical experiments.

Scheme 15: Hu's hydroalkylation of arylalkyne using $FeBr_2$/Zn

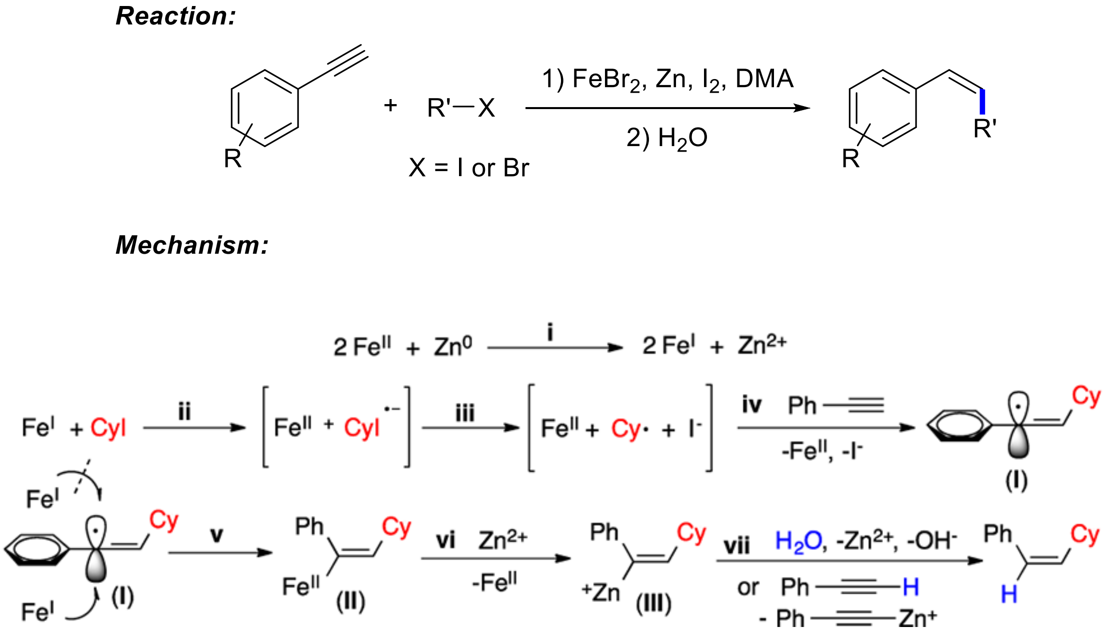
Reaction:
R
+ R'—X
X = I or Br
1) FeBr2, Zn, I2, DMA
2) H2O
R
R'
Mechanism:
2 FeII + Zn0
i
2 FeI + Zn2+
FeI + CyI
ii
FeII + CyI•−
iii
FeII + Cy• + I−
iv Ph
-FeII, -I−
Cy
(I)
FeI
Cy
FeI
(I)
v
Ph
Cy
FeII
(II)
vi Zn2+
-FeII
Ph
Cy
+Zn
(III)
vii H2O, -Zn2+, -OH−
or Ph—H
- Ph—Zn+
Ph
Cy
H

Reproduced with permission from ref 19. Copyright 2015 American Chemical Society.

Also in 2015, Lalic's group developed a copper-catalyzed hydroalkylation of terminal alkynes using alkyl triflates as reaction partners and $(Me_2HSi)_2O$ as hydrogen source.[20] This protocol proceeds under mild conditions (45 °C), smoothly leading to anti-Markovnikov selective *E*-alkenes. A substrate scope including both alkyl- and aryl- alkynes as well as primary triflates was provided. A plausible mechanism involves hydrocupration of the alkyne by a NHC-copper hydride complex, followed by alkylation with an alkyl triflate to generate the product as shown in Scheme 16(a). In 2019, the same group reported another strategy for hydroalkylation of terminal alkynes using alkyl iodides to form *E*-alkenes.[21] IPrCuCl combined with (t*t*-Bu-tpy)NiI is used as a bimetallic catalyst. Various functional groups including ethers, fluoro- bromo-, chloro-, anilines, nitrile, TBS or TIPS protected alcohol and Boc protected amine, as well as heterocycles, such as pyridines, thiazoles, furans, pyrimidine, pyridazine, tetrazole and benzo[*d*]oxazole are tolerated. Considering their previous work on copper-catalyzed hydroalkylation of terminal alkynes, the authors proposed a mechanism as shown in Scheme 16 (b).

Scheme 16: Lalic's hydrolkylation of alkynes

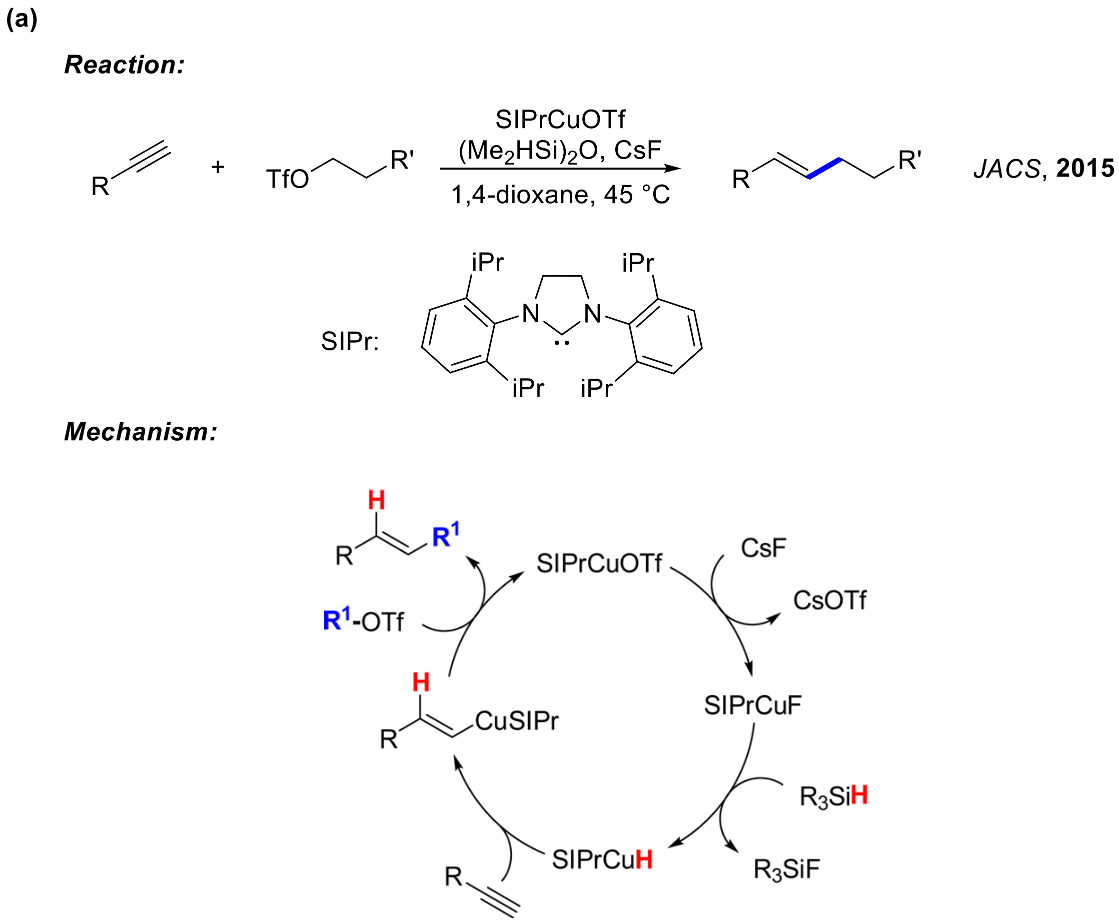
(a)
Reaction:
R
+
TfO
R'
SIPrCuOTf
(Me2HSi)2O, CsF
1,4-dioxane, 45 °C
R
R'
JACS, 2015
SIPr:
iPr
iPr
N
N
iPr
iPr
Mechanism:
H
R
R1
R1-OTf
SIPrCuOTf
CsF
CsOTf
SIPrCuF
H
R
CuSIPr
R3SiH
R3SiF
SIPrCuH
R

Reproduced with permission from ref 20. Copyright 2015 American Chemical Society.

(b)

Reaction:

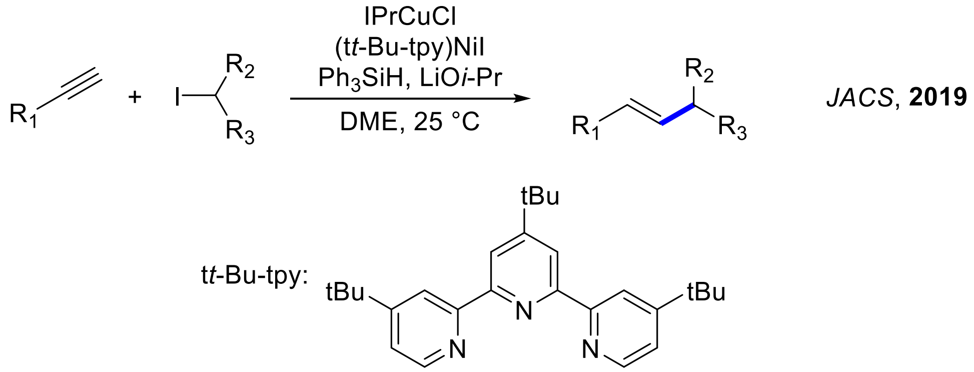
IPrCuCl
(tt-Bu-tpy)NiI
Ph3SiH, LiOi-Pr
DME, 25 °C
R1
R2
R3
JACS, 2019
tt-Bu-tpy:
tBu
N

Mechanism:

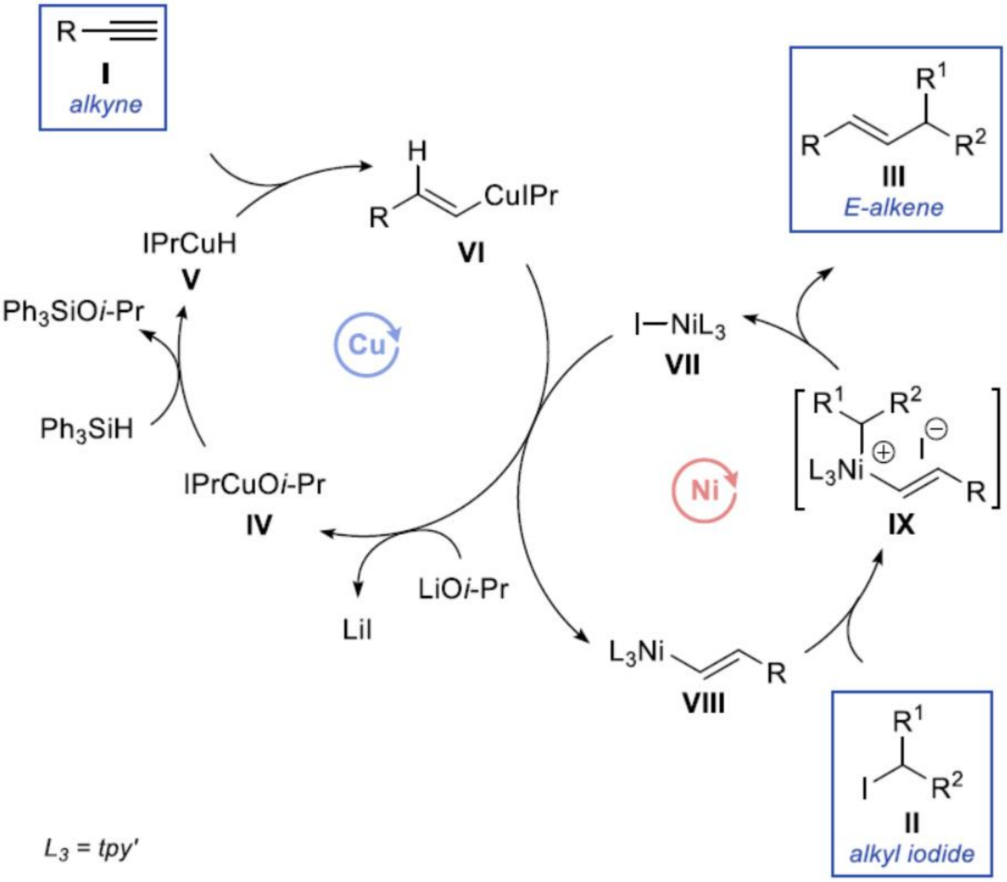
R
I
alkyne
H
CuIPr
VI
IPrCuH
V
Ph3SiOi-Pr
Ph3SiH
IPrCuOi-Pr
IV
Cu
LiOi-Pr
LiI
R1
R2
III
E-alkene
I—NiL3
VII
L3Ni
IX
Ni
VIII
II
alkyl iodide
L3 = tpy'

Reproduced with permission from ref 21. Copyright 2019 American Chemical Society.

Whether involving alkenes or alkynes, the authors usually chose either hydroarylation or hydroalkylation in their studies, as alkyl and aryl halides have different activities. Therefore, different transition metals were selected as catalysts and along with different reaction conditions were selected. However, in 2016, Fu's group from the University of Science and Technology of China developed a novel protocol for the formation of either Csp^2-Csp^3 bonds or Csp^3-Csp^3 bonds through nickel-catalyzed reductive coupling of aryl or alkyl halides with alkenes, which was named reductive olefin hydrocarbonation (Scheme 17).[22] To the best of my knowledge, this is the only report so far where both aryl and alkyl halides can be used to complete such reactions. After optimizations of the reaction conditions, a broad substrate scope with robust functional group compatibility was provided. Moreover, to further demonstrate the wide functional group tolerance in these hydrocarbonations of olefins, more complex biologically interesting molecules such as a cholesterol derivative, hecogenin derivative, calcierol and cinchonidine derivatives were modified using halides or olefins via this technology. Although the authors did not provide a mechanistic rationale at the end of their report, a radical trapping test using TEMPO was offered, indicating involvement of a radical-based mechanism. After a comparison of reaction conditions with those from G. C. Fu's enantioconvergent hydroalkylation of olefins,[17] it can be inferred that they probably have similar or even identical mechanisms.

Scheme 17: Fu's nickel-catalyzed reductive olefin hydrocarbonation

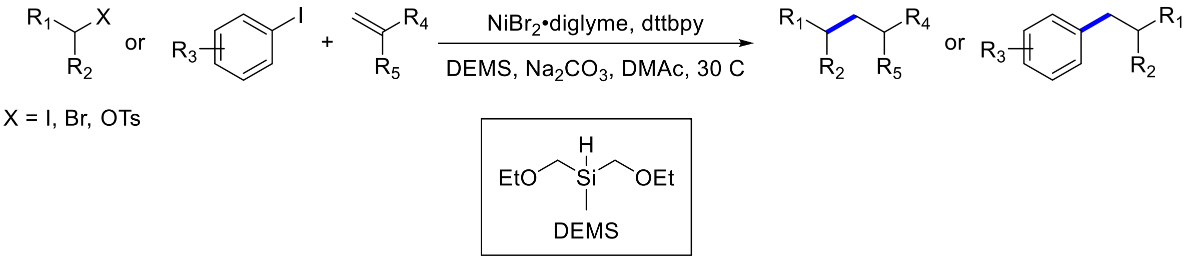

In summary, many contributions have been made with the aim of developing reductive coupling reactions over these past few decades. Whether involving hydrocarbonations (hydroarylations or hydroalkylaions) of alkenes or alkynes, these reactions have provided reliable tools for formation of C-C bonds. Compared with classical transition-metal coupling reactions such as Heck or olefin cross metathesis reactions, these approaches usually use inexpensive and abundant first-row transition metals as catalysts (e.g., Fe, Ni, Mn, Co and Cu). Moreover, for reductive coupling, no hydrogen gas or borohydride was required. Instead, liquid silanes or zinc dust commonly serve as reductants. This not only significantly expands the compatibility of hydrocarbonations, but also enhances both their chemoselectivity and chemofidelity. Especially for alkynes as substrates, these reductive coupling reactions typically lead to single isomer geometrical selectivity (*Z* or *E*) without over reduction. In addition, the reaction conditions for those reductive couplings are usually mild, many of which can proceed smoothly between room temperature and 45 °C. Furthermore, both hydroalkylations and hydroarylations have broad substrate scope with excellent functional group tolerance and apply to various heterocycles. These advantages will no doubt lead to further applications in medical or manufacturing industry, and in natural product total syntheses in the future. In terms of mechanisms, they are mainly divided into three types: 1) based on the formation of radical intermediates induced by metal catalysts, followed by quenching leading to a hydroalkylation or hydroarylation; 2) involvement of metal-catalyzed hydrogen atom transfer en route to products; 3) a classic cross-coupling reaction (Heck, Sonogashia, etc) followed by reduction or semi-reduction to achieve the reductive coupling process. These explorations of the mechanisms will undoubtedly lay a foundation for the design and development of such hydrocarbonations in the future.

References

1. Arora, A.; Teegardin, K. A.; Weaver, J. D. Reductive Alkylation of 2-Bromoazoles via Photoinduced Electron Transfer: A Versatile Strategy to Csp(2)-Csp(3) Coupled Products. *Org. Lett.* **2015**, *17*, 3722.

2. Green, S. A.; Matos, J. L. M.; Yagi, A.; Shenvi, R. A. Branch-Selective Hydroarylation: Iodoarene–Olefin Cross-Coupling. *J. Am. Chem. Soc.* **2016**, *138*, 12779.

3. Shevick, S. L.; Obradors, C.; Shenvi, R. A. Mechanistic Interrogation of Co/Ni-Dual Catalyzed Hydroarylation. *J. Am. Chem. Soc.* **2018**, *140*, 12056.

4. Green, S. A.; Vasquez-Cespedes, S.; Shenvi, R. A. Iron-Nickel Dual-Catalysis: A New Engine for Olefin Functionalization and the Formation of Quaternary Centers. *J. Am. Chem. Soc.* **2018**, *140,* 11317.

5. Friis, S. D.; Pirnot, M. T.; Buchwald, S. L. Asymmetric Hydroarylation of Vinylarenes Using a Synergistic Combination of CuH and Pd Catalysis. *J. Am. Chem. Soc.* **2016**, *138*, 8372.

6. Friis, S. D.; Pirnot, M. T.; Dupuis, L. N.; Buchwald, S. L. A Dual Palladium and Copper Hydride Catalyzed Approach for Alkyl-Aryl Cross-Coupling of Aryl Halides and Olefins. *Angew. Chem., Int. Ed. Engl.* **2017**, *56,* 7242.

7. Aycock, R. A.; Wang, H.; Jui, N. T. A mild catalytic system for radical conjugate addition of nitrogen heterocycles. *Chem Sci* **2017**, *8,* 3121.

8. Boyington, A. J.; Riu, M.-L. Y.; Jui, N. T. Anti-Markovnikov Hydroarylation of Unactivated Olefins via Pyridyl Radical Intermediates. *J. Am. Chem. Soc.* **2017**, *139*, 6582.

9. Seath, C. P.; Vogt, D. B.; Xu, Z.; Boyington, A. J.; Jui, N. T. Radical Hydroarylation of Functionalized Olefins and Mechanistic Investigation of Photocatalytic Pyridyl Radical Reactions. *J. Am. Chem. Soc.* **2018**, *140*, 15525.

10. Zhou, F.; Hu, X.; Zhang, W.; Li, C. J. Copper-Catalyzed Radical Reductive Arylation of Styrenes with Aryl Iodides Mediated by Zinc in Water. *J. Org. Chem.* **2018**, *83*, 7416.

11. Gurak, J. A.; Engle, K. M. Practical Intermolecular Hydroarylation of Terminal Alkenes via Reductive Heck Coupling. *ACS Catal* **2018**, *8*, 8987.

12. Nguyen, J.; Chong, A.; Lalic, G. Nickel-catalyzed anti-Markovnikov hydroarylation of alkenes. *Chem Sci* **2019**, *10*, 3231.

13. Armstrong, M. K.; Goodstein, M. B.; Lalic, G. Diastereodivergent Reductive Cross Coupling of Alkynes through Tandem Catalysis: Z- and E-Selective Hydroarylation of Terminal Alkynes. *J. Am. Chem. Soc.* **2018**, *140*, 10233.

14. Takahashi, K.; Morishita, H.; Ogiwara, Y.; Sakai, N. Group 4 Metallocene Difluoride/Palladium Bimetallic Catalysts for the Reductive Cross-Coupling of Alkynes with Aryl Iodides and Bromides. *J. Org. Chem.* **2018**, *83*, 13734.

15. ElMarrouni, A.; Ritts, C. B.; Balsells, J. Silyl-mediated photoredox-catalyzed Giese reaction: addition of non-activated alkyl bromides. *Chem Sci* **2018**, *9*, 6639.

16. Wu, X.; Hao, W.; Ye, K. Y.; Jiang, B.; Pombar, G.; Song, Z.; Lin, S. Ti-Catalyzed Radical Alkylation of Secondary and Tertiary Alkyl Chlorides Using Michael Acceptors. *J. Am. Chem. Soc.* **2018**, *140*, 14836.

17. Wang, Z.; Yin, H.; Fu, G. C. Catalytic enantioconvergent coupling of secondary and tertiary electrophiles with olefins. *Nature* **2018**, *563*, 379.

18. Green, S. A.; Huffman, T. R.; McCourt, R. O.; van der Puyl, V.; Shenvi, R. A. Hydroalkylation of Olefins To Form Quaternary Carbons. *J. Am. Chem. Soc.* **2019**, *141*, 7709.

19. Cheung, C. W.; Zhurkin, F. E.; Hu, X. Z-Selective Olefin Synthesis via Iron-Catalyzed Reductive Coupling of Alkyl Halides with Terminal Arylalkynes. *J. Am. Chem. Soc.* **2015**, *137*, 4932.

20. Uehling, M. R.; Suess, A. M.; Lalic, G. Copper-catalyzed hydroalkylation of terminal alkynes. *J. Am. Chem. Soc.* **2015**, *137*, 1424.

21. Hazra, A.; Chen, J.; Lalic, G. Stereospecific Synthesis of E-Alkenes through Anti-Markovnikov Hydroalkylation of Terminal Alkynes. *J. Am. Chem. Soc.* **2019**, *141*, 12464.

22. Lu, X.; Xiao, B.; Zhang, Z.; Gong, T.; Su, W.; Yi, J.; Fu, Y.; Liu, L. Practical carbon-carbon bond formation from olefins through nickel-catalyzed reductive olefin hydrocarbonation. *Nat Commun* **2016**, *7*, 11129.

Results and Discussion

Optimization of reaction conditions for hydroalkylation

Our group is dedicated to green chemistry, making organic reactions more environmentally friendly by replacing typical organic solvents with aqueous micellar media. We have developed many techniques and novel catalysts for transition metal-catalyzed coupling reactions, such as Suzuki-Miyaura, Negishi, etc., in aqueous solutions.[1] However, these protocols were mostly based on these classic reactions. Fewer contributions have been made to develop new strategies in water. Hence, hydroalkylation in water, which is unprecedented, has the potential to shift literature cases from classical reactions in organic solvents to the water phase. As shown in the Introduction, Hu and co-workers reported a strategy of hydroalkylation of terminal alkynes using alkyl iodides in DMF followed by quenching with water.[2] This process employed inexpensive and nontoxic iron(II) bromide as catalyst with zinc powder as reductive reagent. To the best of our knowledge, there has been no research focused on iron-catalyzed hydroalkylation of olefins, let alone in water. Hence, it is desirable to develop an alternative technology for reductive couplings of alkenes with alkyl halides. Inspired by Hu's work, an iron salt was selected as catalyst precursor, along with zinc dust as the reducing agent as part of our initial reaction conditions.

A model reaction in 2 wt % TPGS-750-M/H_2O between 4-*tert*-butylstyrene and (3-bromopropoxy)benzene was carried out with different transition metal catalysts in the presence of 1,10-phenanthroline as a ligand (Table 1). Except for 1,10-phenanthroline, some typical P-donor ligands for palladium, such as SPhos and 1,1′-bis(di-*t*-butylphosphino)ferrocene (dtbpf) were also screened in this reaction. The GC yield showed that iron salts worked far better than other metal-based catalysts (e,g., Ni(II), Pd(II), Cu(II), and Co(II)). Further optimizations focused on different iron salts, including Fe(II) and Fe(III) derivatives combined with various anions. Among several iron species evaluated, we were pleased to find that $Fe(acac)_3$ and $(NH_4)_2Fe(SO_4)_2{\cdot}6H_2O$ gave the best results. Additionally, the possibility that this process was catalyzed by trace amounts of other transition metal ions in the iron salt was excluded.

Table 1: Screening of the catalytic metal source

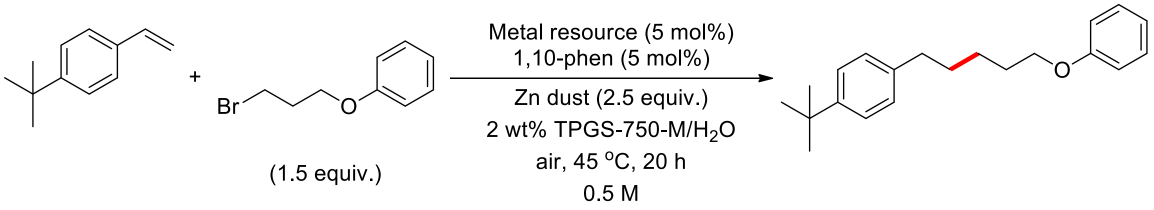

Entry	Metal Source	GC Yield (%)	Entry	Metal Source	GC Yield (%)
1	$FeCl_2$	<1	9	$K_3Fe(CN)_4$	<1
2	$FeCl_3$	4	10	Phthalocyanine Iron	<1
3	$FeCl_3{\cdot}6H_2O$	4	11	$Ni(acac)_2$	<1
4	**$Fe(acac)_3$**	**39**	12	$Pd(OAc)_2$	<1
5	$FeBr_2$	<1	13	$Cu(OAc)_2$	<1
6	FeF_3	18	14	$Co(acac)_2$	<1
7	**$(NH_4)_2Fe(SO_4)_2{\cdot}6H_2O$**	**38**	15[a]	$Pd(OAc)_2$	<1
8	$Fe(NO_3)_3{\cdot}9H_2O$	<1	16	$Pd(dtbpf)Cl_2$	<1

[a]SPhos were used as ligand.

Furthermore, additional optimization focused on the ligand (Table 2). Without any ligand, the hydroalkylation only led to 7% GC-yield (entry 1). Moreover, besides 1,10-phenanthroline, other common P-donor monodentate ligands (entries 2 and 3) and *N*-donor bidentate or tridentate ligands (entries 4 to 7) were tested using 4-*t*-butylstyrene and (3-bromopropoxy)benzene as reaction partners. However, none showed better activity than 1,10-phenanthroline. Further optimization focused on several derivatives of 1,10-

phenanthroline. Eventually, the initial yield using the parent system (39%) was increased to 55% (entry 12) with analog 3,4,7,8-tetramethyl-1,10-phenanthroline. In addition, it was also discovered that attempts to raise the ligand/iron salt ratio from 1/1 to 2/1 did not lead to a better yield, which dropped to 27%.

Table 2: Ligand screening

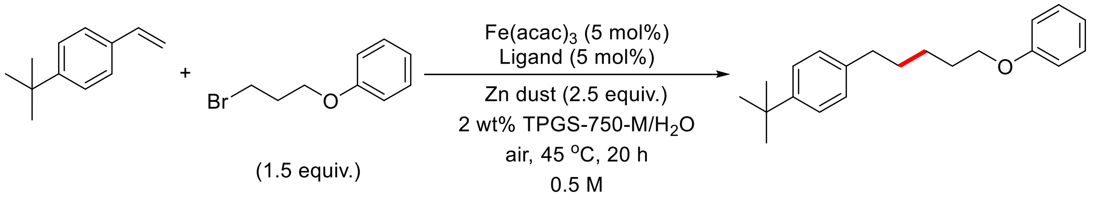

+
Br
O
(1.5 equiv.)
Fe(acac)$_3$ (5 mol%)
Ligand (5 mol%)
Zn dust (2.5 equiv.)
2 wt% TPGS-750-M/H$_2$O
air, 45 °C, 20 h
0.5 M
O

Entry	Ligand	GC Yield (%)
1	-	7
2	PPh_3	18
3	SPhos	20
4	2,2'-bipy	22
5	TMEDA	<1
6	DMEDA	<1
7	Tripyridine	14
8	**L1** (1,10-phen)	39
9	**L2**	47
10	**L3**	<1
11	**L4**	28
12	**L5**	**55**
13	**L5** (10 mol%)	27

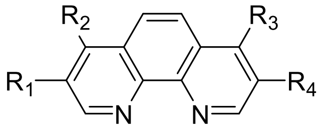

R_2
R_3
R_1
R_4
N
N

L1: R_1, R_2, R_3, R_4 = H
L2: R_1, R_4 = H, R_2, R_3 = Ph
L3: R_1, R_4 = H, R_2, R_3 = Cl
L4: R_1, R_4 = H, R_2, R_3 = NMe_2
L5: R_1, R_2, R_3, R_4 = Me

Additional optimization was aimed at the equivalents of catalyst, coupling partner alkyl bromide and zinc dust (Table 3). The best ligand/iron salt ratio was determined to be 1:1. Hence, the lowest catalyst loading possible was studied, and the result indicated that the yield dropped to 24% when the iron loading was reduced from 3 mol % to 2 mol % (from entry 1 to 4). However, when the catalyst loading was 2 mol %, an increase in the coupling partner bromide to three equivalents led to an improvement in yield, from 24% to 59% (entry 5). Continued increase in zinc dust to six equivalents afforded an even better yield (70%; entry 7). Further increases in equivalents of bromide and/or zinc, however, did not lead to any improvement (entries 8 and 9).

Table 3: Variation in reaction conditions (relative amounts of reactants and reagents)

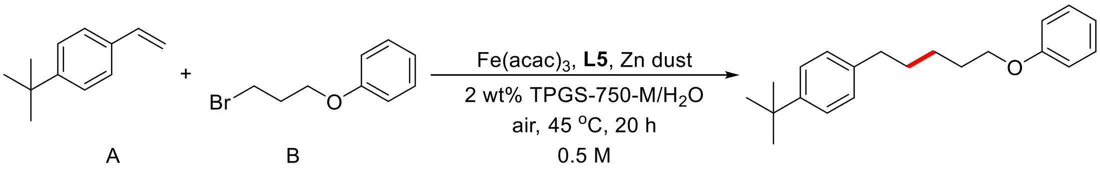

Entry	Fe(acac)$_3$/**L5** (mol%)	B (equiv.)	Zn dust (equiv.)	GC Yield (%)
1	5 / 5	1.5	2.5	55
2	3 / 3	1.5	2.5	54
3	2 / 2	1.5	2.5	24
4	1 / 1	1.5	2.5	23
5	2 / 2	3	2.5	59
6	2 / 2	3	4.5	62
7	**2 / 2**	**3**	**6**	**70**
8	3 / 3	3	8	35
9	2 / 2	3	8	69

Surfactants are molecules with a hydrophobic hydrocarbon chain which, when part of a micellar arrays, solubilizes lipophilic compounds, while polar hydrophilic chain attracts water.[3] Usually, the surfactants we used in an aqueous micellar system have a large polar head and a relatively smaller hydrocarbon chain forming a cone shape, which forms micelles in water with hydrophobic part inside and hydrophilic part outside. Such micelle cannot only help organic substrates dispersed in the aqueous medium, but also provide a small reactor with high concentrations of reagents for reaction within the inner micellar core. Therefore, reactions in aqueous micelles usually lead to better yields than those run in pure water. To prove the influence of TPGS-750-M in these reactions, a control experiment was run in pure water (Table 4, entry 2), and the results indicated that this reaction worked better in the aqueous TPGS-750-M solution. Moreover, different surfactants have different sizes and shapes of the micelles they form, which can lead to different synthetic outcomes. The size of the micelle can often affect the yield of a reaction in water by varying the nanoenvironment available.[4] Hence, except for TPGS-750-M, other surfactants such as Nok[5] and Brij-30 were tested in this process (entries 5 and 6). However, none led to better outcomes than TPGS-750-M. Furthermore, the concentrations of aqueous TPGS-750-M as well as the concentrations of the reaction were also important parameters which may also affect the yield. So, different concentrations of aqueous TPGS-750-M solutions as reaction media were tested, as well as different concentrations of reaction (higher or lower) were studied, but none provided better results.

Table 4: Variation in reaction conditions (surfactant and concentration)

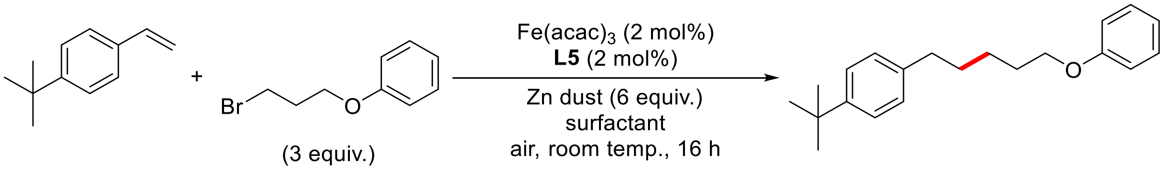

Entry	Surfactant	Conc. of reaction	GC Yield (%)
1	**TPGS-750-M (2 wt%)**	**0.5 M**	**72**
2	pure water	0.5 M	64
3	TPGS-750-M (1 wt%)	0.5 M	69
4	TPGS-750-M (4 wt%)	0.5 M	61
5	Nok (2 wt%)	0.5 M	70
6	Brij-30 (2 wt%)	0.5 M	69
7	TPGS-750-M (2 wt%)	0.25 M	48
8	TPGS-750-M (2 wt%)	1 M	70

Other reaction conditions such as temperature, atmosphere and time were also considered in the course of optimization studies (Table 5). Attempts at raising the reaction temperature from room temperature (25 °C) to 45 °C did not lead to obvious improvements for the hydroalkylation process. In addition, compared with the reaction run in air, no significant influence was observed when the reaction was conducted under argon, indicating that inert atmosphere conditions are not required. Moreover, shortening the reaction time from 20 hours to 16 hours did not afford a lower GC yield. However, an attempt at further reduction in the reaction time led to worse results.

Table 5: Variation in atmosphere, time and temperature

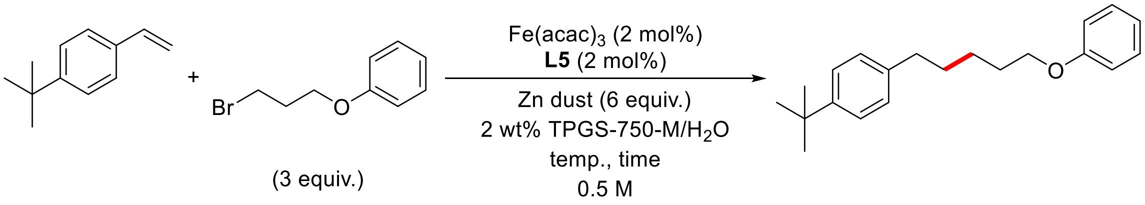

Entry	Temp. (°C)	Atmosphere	Time (h)	GC Yield (%)
1	45	air	20	70
2	35	air	20	70
3	25 (r.t.)	air	20	69
4	25 (r.t.)	Ar	20	61
5	25 (r.t.)	air	8	59
6	**25 (r.t.)**	**air**	**16**	**72**

Based on our previous work, salt additives can alter the pH of the reaction medium, as well as the size of the nanomicelles.[7] In the following optimizations, an acidic salt (NH_4Cl), neutral salt (NaCl) and basic salt (NaOAc) were tested as additives in these couplings. The GC yields showed that NaCl is the best additive for the coupling using $Fe(acac)_3$ as catalyst, but NaOAc as additive can lead to a better yield if $Fe(acac)_3$ was replaced by $Fe(NH_4)_2(SO_4)_2•6H_2O$. During the process of expansion of substrate scope, we discovered that compared to $Fe(acac)_3$, $Fe(NH_4)_2(SO_4)_2•6H_2O$ generally affords the best outcome in these hydroalkylations. Thus, for most substrates, $Fe(NH_4)_2(SO_4)_2•6H_2O$ works better, but for some substrates, $Fe(acac)_3$ leads to a better yield. Hence, finally, two optimized reaction procedures using both salts as the potential catalyst were kept. In addition, the co-solvent not only helps the reagents gain entry into the micelles, but also changes the diameter of the micelle[6] (Table 6). After screening several co-solvents, it was discovered that using $Fe(NH_4)_2(SO_4)_2•6H_2O$ as catalyst, as well as $Na(OAc)_2$ as the additive, the GC yield could be further increased to 81% (75%, isolated) by adding small percentages of acetonitrile as co-solvent (e.g., 10%; Table 6, entry 14). Additional attempts at increasing or decreasing the volume of co-solvent did not lead to better yields. More detailed studies on co-solvent use will be discussed in the following section.

Table 6: Variation in reaction conditions (salt additive and co-solvent)

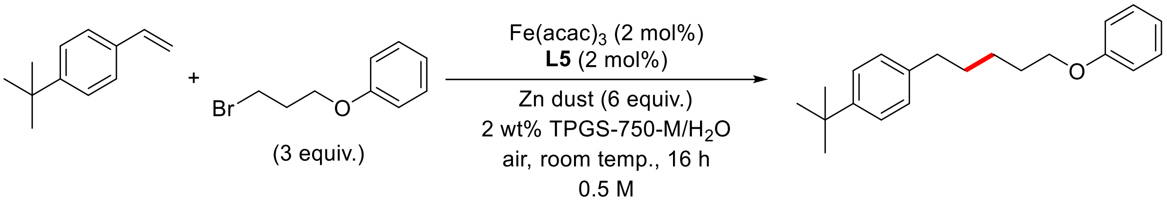

+
Br
O
(3 equiv.)
Fe(acac)3 (2 mol%)
L5 (2 mol%)
Zn dust (6 equiv.)
2 wt% TPGS-750-M/H2O
air, room temp., 16 h
0.5 M
O

Entry	Salt additive (equiv.)	Co-solvent (v/v%)	GC Yield (%)
1	-	-	72
2	NaCl (3)	-	76
3	NaCl (6)	-	74
4	NH_4Cl (0.5)	-	60
5	NH_4Cl (1)	-	42
6	NaOAc (0.5)	-	68
7[a]	NaOAc (0.5)	-	78 (73[b])
8[a]	NaOAc (1)	-	77
9[a]	NaOAc (2)	-	72
10[a]	NaOAc (0.5)	THF (10)	72
11[a]	NaOAc (0.5)	THF (20)	53
12[a]	NaOAc (0.5)	THF (50)	8
13[a]	NaOAc (0.5)	Acetone (10)	68
14[a]	**NaOAc (0.5)**	**MeCN (10)**	**81 (75[b])**
15[a]	NaOAc (0.5)	MeCN (2.5)	33
16[a]	NaOAc (0.5)	MeCN (5)	57
17[a]	NaOAc (0.5)	MeOH (10)	75
18[a]	NaOAc (0.5)	MeCN (20)	64

[a] $(NH_4)_2Fe(SO_4)_2{\bullet}6H_2O$ was used instead of $Fe(acac)_3$. [b] Isolated Yield.

Further studies were made as to various grades of Zn, as well as some substitutes for zinc. According to feedback from Novartis, based on earlier studies at scale of Negishi couplings, such protocols involving zinc metal can form aggregates, resulting in breaking of the stirring shaft during the process, thereby hindering application of this technology in industry. Hence, in order to avoid this issue, tetrakis(dimethylamino)ethylene, as the substitute for Zn powder, was tested in the reaction. Unfortunately, there was no product detected using tetrakis(dimethylamino)-ethylene as reductant. Further optimization regarding the grades of zinc indicated that compared with zinc nanopowder (<50 nm) and zinc powder (~ 100 mesh), zinc dust (<10 μm; Table 7) afforded the best yields. As these three zinc reagents were all taken from the glovebox, it can be excluded that the reaction results were influenced due to different degrees of oxidation by air of each zinc source. Given that zinc dust works better than the zinc powder with larger particle sizes, and zinc nanopowder with its smaller particle size, we speculated that: a) zinc with larger particle size lowers the reaction rate with alkyl bromides leading to lower yields; b) zinc with smaller particle sizes increases the reaction rate with alkyl bromides, so that more zinc bromide intermediate is quenched by water before it reacts with an alkene. This also led to the final, optimized procedure resulting from balancing the requirements of the main reaction with other side reactions.

Table 7: Grade of Zinc and zinc equivalent

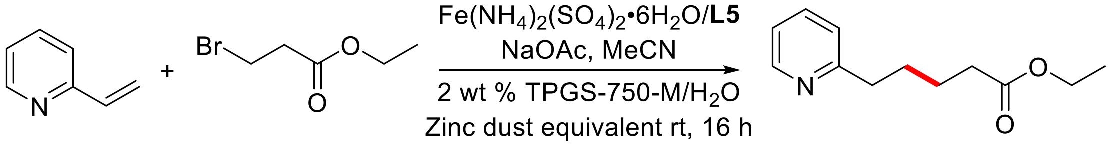

Entry[a]	Zn (equivalent)	Yield (%)
1	**Zn dust (<10 μm)**	**70**
2	Zn nanopowder (< 50 nm)	50
3	Zn powder (~ 100 mesh)	39
4	In powder (~ 60 mesh)	0
5	tetrakis(dimethylamino)ethylene	0

[a] Reaction conditions: olefin (0.2 mmol, 1 equiv), aliphatic bromide (0.6 mmol), $Fe(NH_4)_2(SO_4)_2•6H_2O$ (2 mol %), **L5** (2 mol %), Zn or equivalent (6 equiv), AcONa (0.1 mmol), MeCN (0.04 mL) and 2 wt % TPGS-750-M/H_2O (0.4 mL).

Scope of the hydroalkylation

In order to initially assess the scope of this reaction, several substituted styrenes were examined under optimized conditions (Table 8, top). Most reactions took place quite smoothly affording good yields of coupled products.[8] The reaction is amenable to the presence of either electron-donating or -withdrawing substituents. Various functional groups are tolerated, including alkyl (e.g., *t*-Bu, as in **1** and **5**), trifluoromethyl- (**3**), nitrile- (**4**), chloro- (**7**), ketone (**10**) and amide (**21**) on the aromatic ring. Remarkably, *p*-bromostyrene readily participates without competition from the *p*-bromo residue, suggesting that zinc, as expected, inserts selectively into Csp^3- over Csp^2-bromine bonds giving **2** and **21** in good yield. Moreover, various heteroaromatic rings bearing a vinyl group can also serve as precursor to the ethylene unit between electrophile and in situ-generated nucleophile. As shown in Table 8, bottom, thiazole (**12**, **15**), furan (**8**, **13**, **18**), thiophene and indazole (**14**), piperidine (**16**), morpholine (**19**), indole (**17**, **20**), isoxazole (**18, 21**), pyrimidine (**16**, **19**) and piperazine (**21**) led to good yields of the anticipated products.[9] Many of these have extensive applications to agricultural chemicals and pharmaceuticals.[10]

Table 8: Scope of olefins

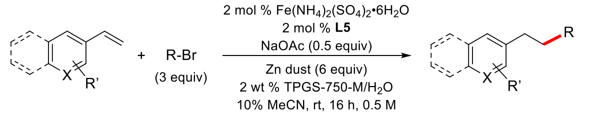
X
R'
+
R-Br
(3 equiv)
2 mol % Fe(NH4)2(SO4)2•6H2O
2 mol % L5
NaOAc (0.5 equiv)
Zn dust (6 equiv)
2 wt % TPGS-750-M/H2O
10% MeCN, rt, 16 h, 0.5 M
R
X
R'

Styrenes:

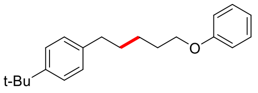

1^{c} 75%

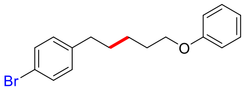

2^{d} 72%

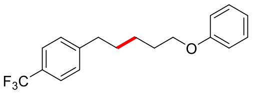

3 71%

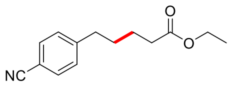

4 80%

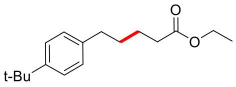

5 67%

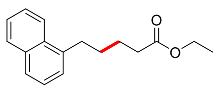

6 45%

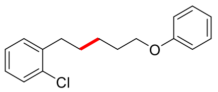

7 73%

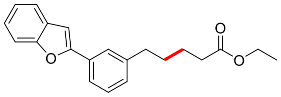

8 47%

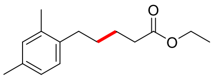

9 61%

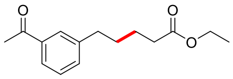

10 56%

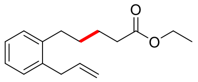

11 62%

Heterocyclic olefins (except pyridines):

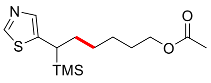

12 93%

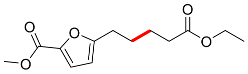

13 72%

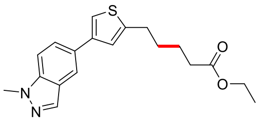

14^{e} 57%

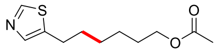

15 51%

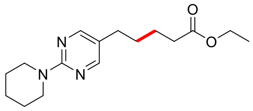

16^{f} 58%

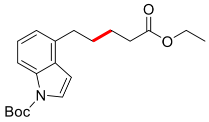

17^{g} 56%

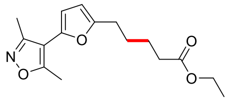

18 42%

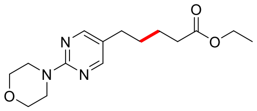

19^{f} 56%

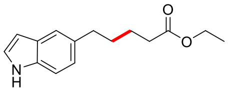

20^{h} 73%

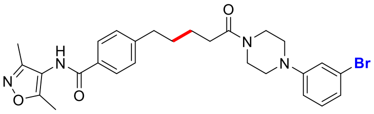
N
O
H
N
O
O
N
N
Br

21^{i} 52%

^{a}Reaction conditions: olefin (0.2 mmol), aliphatic bromide (0.6 mmol), $Fe(NH_4)_2(SO_4)_2•6H_2O$ (0.004 mmol), **L5** (0.004 mmol), Zn dust (1.2 mmol), AcONa (0.1 mmol), MeCN (0.04 mL) and 2 wt % TPGS-750-M/H_2O (0.4 mL). ^{b}Isolated yield. ^{c}Olefin (0.2 mmol), aliphatic bromide (0.6 mmol), $Fe(acac)_3$ (0.004 mmol), **L5** (0.004 mmol), Zn dust (1.2 mmol), NaCl (1.2 mmol) and 2 wt % TPGS-750-M/H_2O (0.4 mL). ^{d}$Fe(NH_4)_2(SO_4)_2•6H_2O$ (0.02 mmol), **L5** (0.02 mmol). ^{e}Olefin (0.1 mmol), aliphatic bromide (1.2 mmol), $Fe(acac)_3$ (0.016 mmol), **L5** (0.016 mmol), Zn dust (2.4 mmol), NaCl (2.4 mmol) and 2 wt % TPGS-750-

M/H_2O (0.8 mL) at 45 °C. [f]Olefin (0.1 mmol), aliphatic bromide (0.8 mmol), Fe(acac)$_3$ (0.008 mmol), **L5** (0.008 mmol), Zn dust (2.4 mmol), NaCl (2.4 mmol) and 2 wt % TPGS-750-M/H_2O (0.8 mL) at 45 °C. [g]Olefin (0.1 mmol), aliphatic bromide (1.2 mmol), Fe(acac)$_3$ (0.008 mmol), **L5** (0.008 mmol), Zn dust (2.4 mmol), NaCl (2.4 mmol) and 2 wt % TPGS-750-M/H_2O (0.8 mL), rt. [h]Olefin (0.1 mmol), aliphatic bromide (0.8 mmol), Fe(acac)$_3$ (0.008 mmol), **L5** (0.008 mmol), Zn dust (2.4 mmol), NaCl (2.4 mmol) and 2 wt % TPGS-750-M/H_2O (0.8 mL), rt. [i]$Fe(NH_4)_2(SO_4)_2 \cdot 6H_2O$ (0.02 mmol), **L5** (0.02 mmol), at 45 °C.

This iron-mediated coupling reaction proceeded smoothly with an array of structurally diverse alkyl halide precursors (Table 9, entries **22** – **50**). Vinylpyridines, given the importance of this ring in numerous pharmaceuticals,[11] was used as alkene source for optimization. Additional substituents present within the halide or on the aromatic/heteroaromatic ring could also be accommodated, reflecting the fundamental compatibility of such reagents with most functional groups, including ether (**22**) ester (**24**, **26**, **28**, **29**), trifluoromethyl- (**27**, **35**), fluoro- (**30, 40**), amide (**27**, **37**), TBS protected alcohol (**32**), alkyne (**33**), Boc protected amine (**34**, **47**) trifluoromethoxy- (**41**) and acetal (**46**). Importantly, not only primary alkyl bromide but also secondary alkyl bromides (**42 - 48**) and even tertiary alkyl bromides (**49**, **50**) were converted to desired products. Of particular note is that in neither case involving *sec*-butyl bromide nor a tertiary bromide (i.e., **44**, **46**, **48**, **49** and **50**, respectively) were any of the products resulting from rearrangement to a more stable intermediate carbanion detected. Moreover, in the case of product **11** and **25**, an isolated olefin did not compete with the alkene present in conjugation with the ring. Placement of the 1-alkenyl array at the 2-, 3- or 4-position on the pyridyl ring appeared to have no impact on the quality of subsequent C-C bond formation.

Table 9: Scope of alkyl bromide

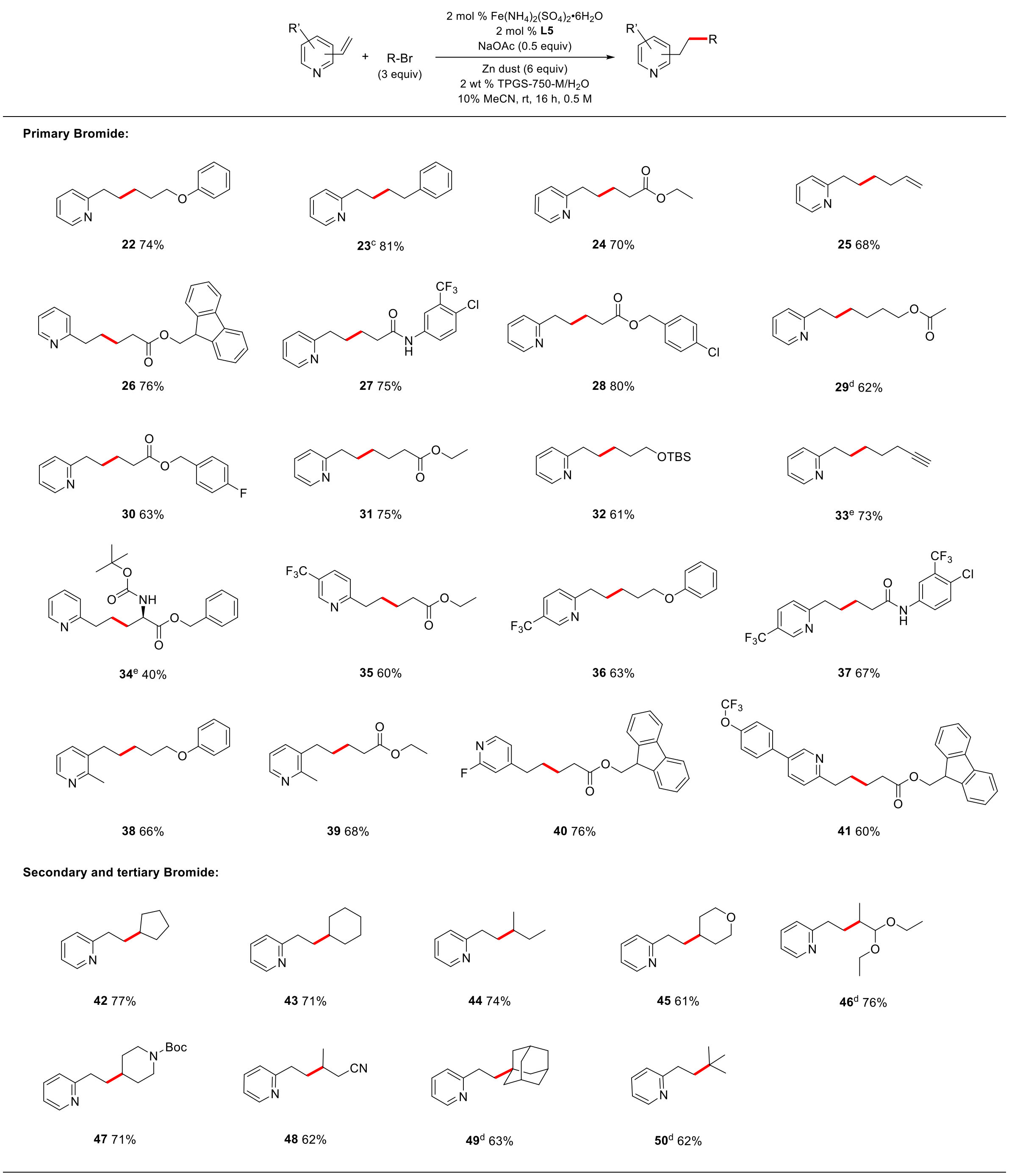
R'
N
+
R-Br
(3 equiv)
2 mol % Fe(NH4)2(SO4)2•6H2O
2 mol % L5
NaOAc (0.5 equiv)
Zn dust (6 equiv)
2 wt % TPGS-750-M/H2O
10% MeCN, rt, 16 h, 0.5 M
R'
R
N
Primary Bromide:
22 74%
23c 81%
24 70%
25 68%
26 76%
27 75%
28 80%
29d 62%
30 63%
31 75%
32 61%
33e 73%
34e 40%
35 60%
36 63%
37 67%
38 66%
39 68%
40 76%
41 60%
Secondary and tertiary Bromide:
42 77%
43 71%
44 74%
45 61%
46d 76%
47 71%
48 62%
49d 63%
50d 62%
OTBS
CF3
Cl
F
F3C
NH
Boc
CN

[a]Reaction conditions: olefin (0.2 mmol), aliphatic bromide (0.6 mmol), $Fe(NH_4)_2(SO_4)_2$•$6H_2O$ (0.004 mmol), **L5** (0.004 mmol), Zn dust (1.2 mmol), AcONa (0.1 mmol), MeCN (0.04 mL) and 2 wt % TPGS-750-M/H_2O (0.4 mL); [b]Isolated yield; [c]Olefin (0.2 mmol), aliphatic bromide (0.6 mmol), $Fe(acac)_3$ (0.004 mmol), **L5** (0.004 mmol), Zn dust (1.2 mmol), NaCl (1.2 mmol) and 2 wt % TPGS-750-M/H_2O (0.4 mL); [d]45 °C; [e]Iodide was used instead of bromide.

Although the broad substrate scope includes various functional groups as well as heterocycles, this protocol also has its limitations (Scheme 1). Firstly, due to excess zinc dust in the pot, some functional groups which can be easily reduced, like nitro, are not compatible in this technique. Moreover, as the target reaction is ongoing, several side reactions occur which affect the total yield. For instance, reduction of the C–C double bonds, as well as polymerization can be detected on the (hetero)aryl alkene. Attempts at hydroalkylation of 3-vinylquinoline with ethyl 3-bromopropanoate did not lead to the targeted product. According to TLC, no olefin remained; however, formation of several products by TLC indicated that polymerization had occurred on 3-vinylquinoline during the reaction. In addition, the GC-MS of many hydroalkylations of 2-vinylpyridines indicated that 2-ethylpyridine is one of the byproducts after the reaction. On the other hand, deuterium trapping of 4-chlorobenzyl 3-bromopropanoate showed that debromination of an alkyl bromide occurs as the background reaction during hydroalkylation under standard conditions. Hence, during optimization of this reaction, both an increase in the number of alkyl bromide equivalents and the addition of excess zinc served to balance the main reaction and minimize various side reactions associated with these reductive couplings in water, leading to higher yields. Nevertheless, excess alkyl bromide led to another problem: although no effect on the liquid alkyl bromides with relatively simple structure, some alkyl bromides with complicated structures as fluffy solids are difficult to disperse in the reaction medium. The volume of these bromides is even larger than the volume of TPGS-750-M/H_2O leading to a pasty mixture that hinders stirring, as well as the subsequent reductive coupling with the aryl alkenes. As shown in Scheme 1, 3-bromopropyl 2-(1-(4-chlorobenzoyl)-5-methoxy-2-methyl-1H-indol-3-yl)acetate was utilized as starting material in efforts to couple it with 2-vinylpyridine. The result from GC-MS indicated that over 90% of the starting bromide remained, with ~8% debromination by-product formed, but no coupling product was detected. Therefore, for these more complex alkyl bromines, coupling is difficult under standard conditions for both the reductive coupling as main desired reaction, or even debromination as a background reaction.

Scheme 1: Limitation of the Fe-catalyzed hydroalkylation

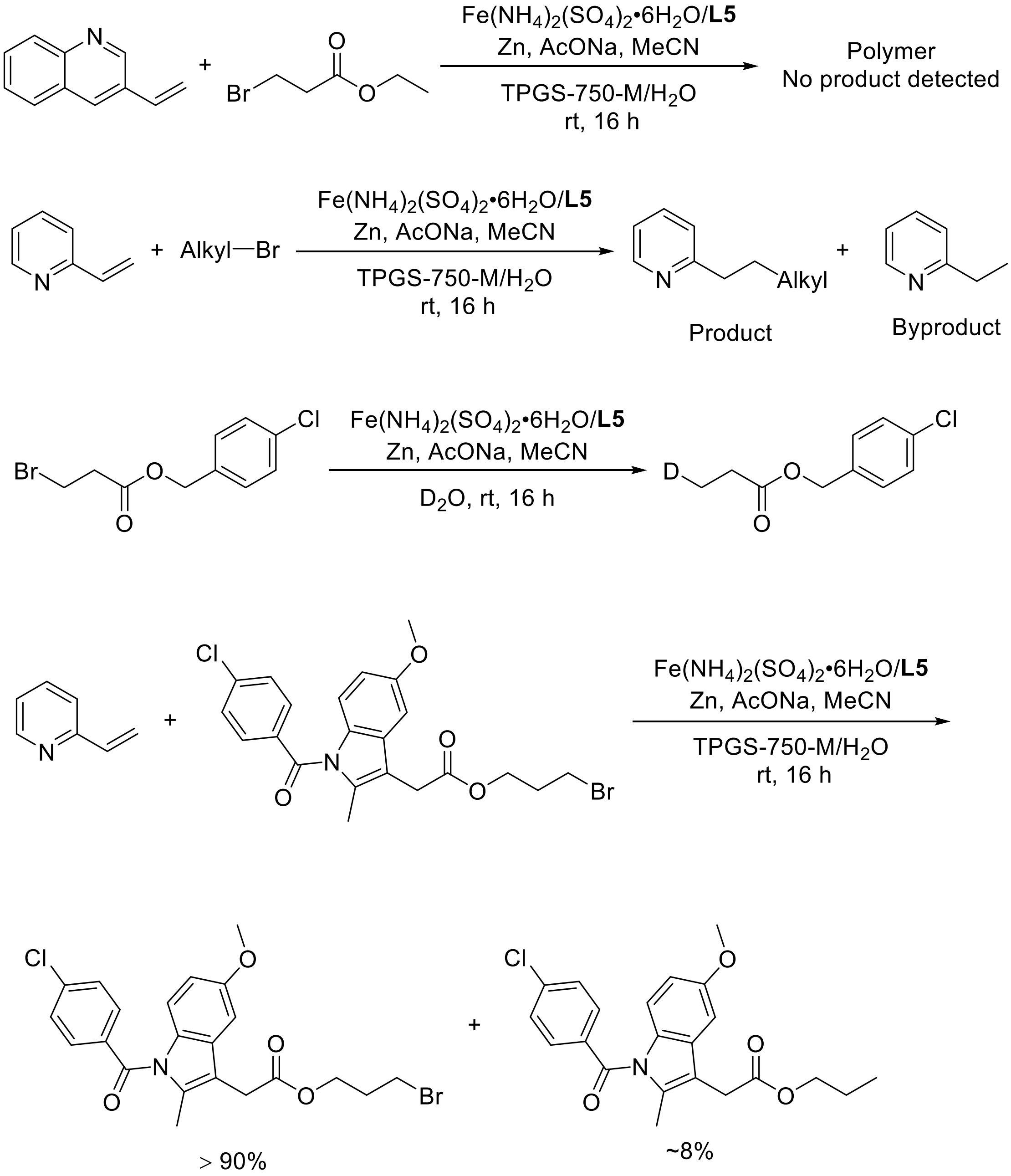
Fe(NH4)2(SO4)2•6H2O/L5
Zn, AcONa, MeCN
TPGS-750-M/H2O
rt, 16 h
Polymer
No product detected
Alkyl—Br
Product
Byproduct
D2O, rt, 16 h
> 90%
~8%

Further research on reaction medium

The impact of the reaction medium was also investigated. Results of reactions run as a function of the ratio of the aqueous reaction medium to added co-solvent, in addition to the acetonitrile (10% v/v) already in the pot (e.g., THF)[6] are shown in Table 10. As the amount of aqueous surfactant solution was reduced and replaced by THF, the yields dropped precipitously. Under otherwise identical conditions, use of pure THF as the reaction medium leads to no cross-coupling product, another observation underscoring the benefits ascribed to the hydrophobic effect in water. Use of 25% PEG-200, another co-solvent found previously to occasionally enhance such reactions,[15] likewise, led to a somewhat reduced 78% yield of coupling product. Furthermore, the background reaction run in water only, for the more water-miscible educts, gave yields that tended to be within 10-12% of those obtained when TPGS-750-M was present. With highly lipophilic substrates (i.e., reactions run "on water"), however, more significant variations in yields were noted clearly indicative of the importance of the amphiphile in enhancing the extent of the desired coupling.[12] In the absence of acetonitrile as co-solvent, yields were found to decrease as well (Table 11).

Table 10: Impact of the proportion of water in the reaction medium

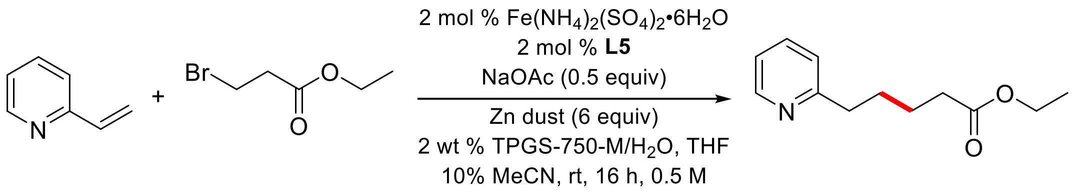

N
Br
O
O
+
2 mol % $Fe(NH_4)_2(SO_4)_2•6H_2O$
2 mol % **L5**
NaOAc (0.5 equiv)
Zn dust (6 equiv)
2 wt % TPGS-750-M/H_2O, THF
10% MeCN, rt, 16 h, 0.5 M
N
O
O

Entry	2 wt % TPGS-750-M/H_2O : THF	Yield (%)
1	100 : 0	83
2	75 : 25	71
3	50 : 50	53
4	25 : 75	14
5	0 : 100	0

Yeild from GC-MS

Table 11: Comparisons between reactions run in pure water vs. 2 wt % TPGS-750-M in H_2O

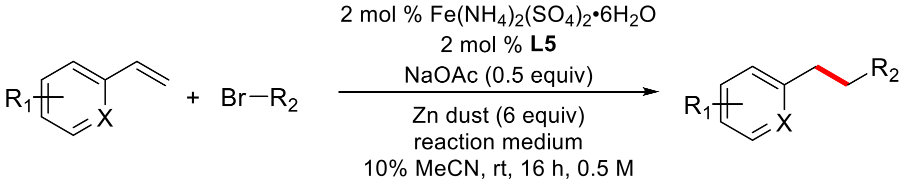

R1
X
+ Br—R2
2 mol % Fe(NH4)2(SO4)2•6H2O
2 mol % L5
NaOAc (0.5 equiv)
Zn dust (6 equiv)
reaction medium
10% MeCN, rt, 16 h, 0.5 M
R1
X
R2

Entry	Product	Yield in 2 wt% TPGS-750-M/H_2O (%)	Yield in pure water (%)
1	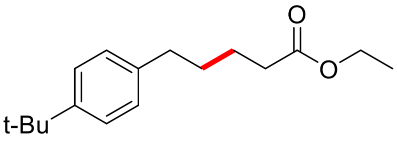	75 (65)[a]	64
2	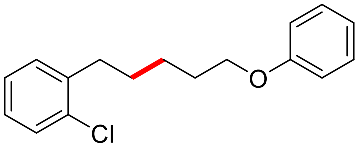	72	59 (23)[a]
3	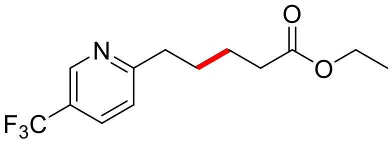	60	58
4	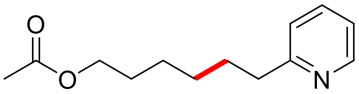	62[b]	57[b]
5	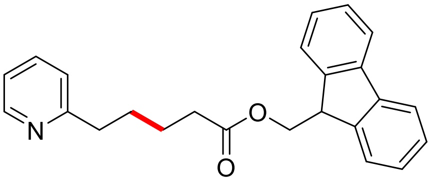	76 (25)[a]	61
6	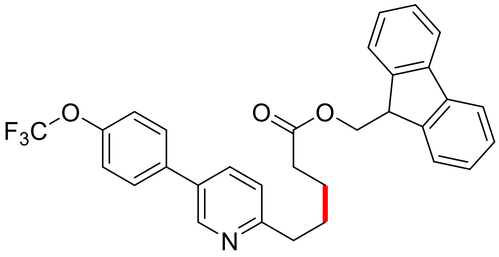	60	37 (20)[a]

[a] No MeCN as cosolvent in parenthesis; [b] 45 °C

Hydroalkylation of alkenes using alkyl iodides and alkyl chlorides

Switching the nature of the alkyl halide coupling from a bromide to chloride led to none of the observed reductive coupling product, presumably reflecting a more challenging insertion into the C-Cl bond (Scheme 2). Perhaps not surprisingly, as noted in previous work,[13] iodides were even more amenable to these couplings, and in both cases examined, afforded higher yields than those using the corresponding bromides. Furthermore, as shown in Scheme 2, in addition to the increased yields, the amount of Zn could be lowered to 4.5 equivalents. A brief study aimed at optimizing the surfactant also revealed that while each of the three studied gave reasonable results, the most enabling medium is that due to nanoreactors derived from TPGS-750-M.

Scheme 2: Reactions of other alkyl halides

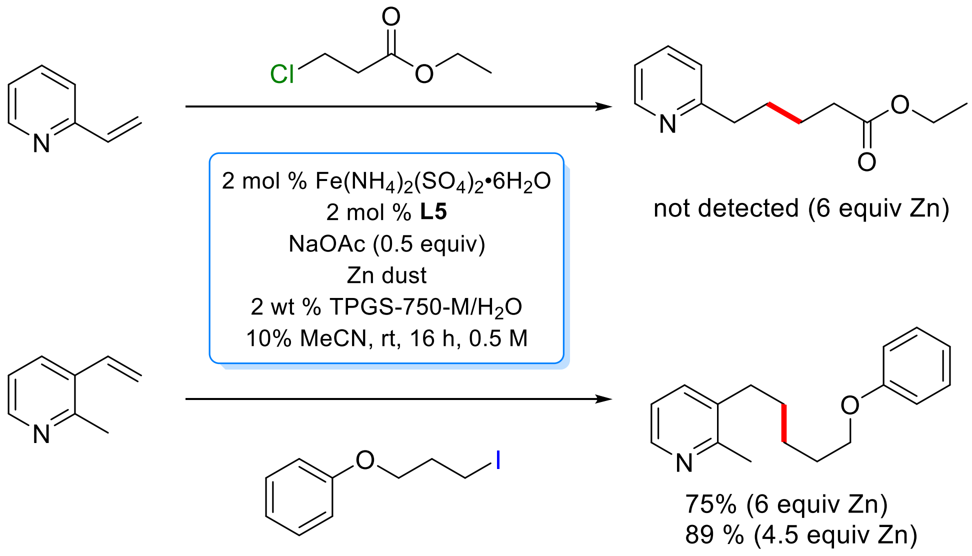
Cl
O
O
N
2 mol % $Fe(NH_4)_2(SO_4)_2•6H_2O$
2 mol % **L5**
NaOAc (0.5 equiv)
Zn dust
2 wt % TPGS-750-M/H_2O
10% MeCN, rt, 16 h, 0.5 M
not detected (6 equiv Zn)
I
75% (6 equiv Zn)
89 % (4.5 equiv Zn)

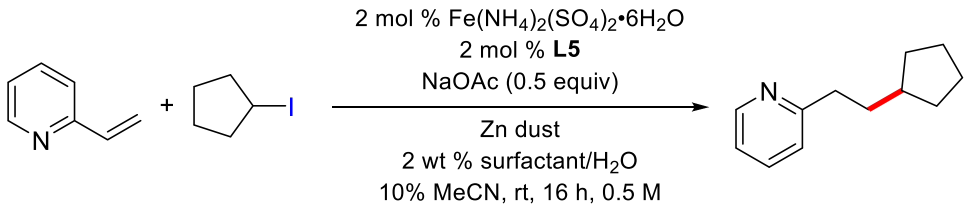

Entry[a]	Surfactant	Zinc dust equiv	Yield (%)
1	TPGS-750-M	6	85
2	PTS-600	6	79
3	Brij 30	6	77
4	**TPGS-750-M**	**4.5**	**91**
5	TPGS-750-M	3	78

[a] Reaction conditions: olefin (0.2 mmol), aliphatic bromide (0.6 mmol), $Fe(NH_4)_2(SO_4)_2•6H_2O$ (0.004 mmol), **L5** (0.004 mmol), Zn dust, AcONa (0.1 mmol), MeCN (0.04 mL) and 2 wt % surfactant/H_2O (0.4 mL).

In an effort to extend this coupling to butadienic arrays, the simple case of 1-phenylbutadiene was investigated under these standard aqueous reductive coupling conditions as shown in Scheme 3. Unfortunately, the coupling was neither efficient nor regio- or stereoselective, giving a mixture of four products. Although the product was a mixture of 4 compounds, some valuable information from the result could also be obtained: 1) There was no hydroalkylation happened on the position 2 of (*E*)-buta-1,3-dien-1-yl, which indicated that such reaction was regioselective for terminal alkene in a conjugated system; 2) The major products from the intermediate **51** were quenched at the benzylic position to afford **56** and **57**, rather than arrival at the more conjugated structure, **55** and **58** (**56** + **57**, 26% versus **55** + **58**, 12%), which on the other hand, proved that the reaction mechanism of this strategy is a free radical process, as the free radical on the benzyl position can be stabilized by benzene ring; 3) In the mixture, more *Z* isomers were found than *E* isomers in the final mixture (**56** + **58**, 30% versus **55** + **57**, 8%), which were indicative presumably of kinetical process.

Scheme 3: Study on hydroalkylation of 1-phenylbutadiene

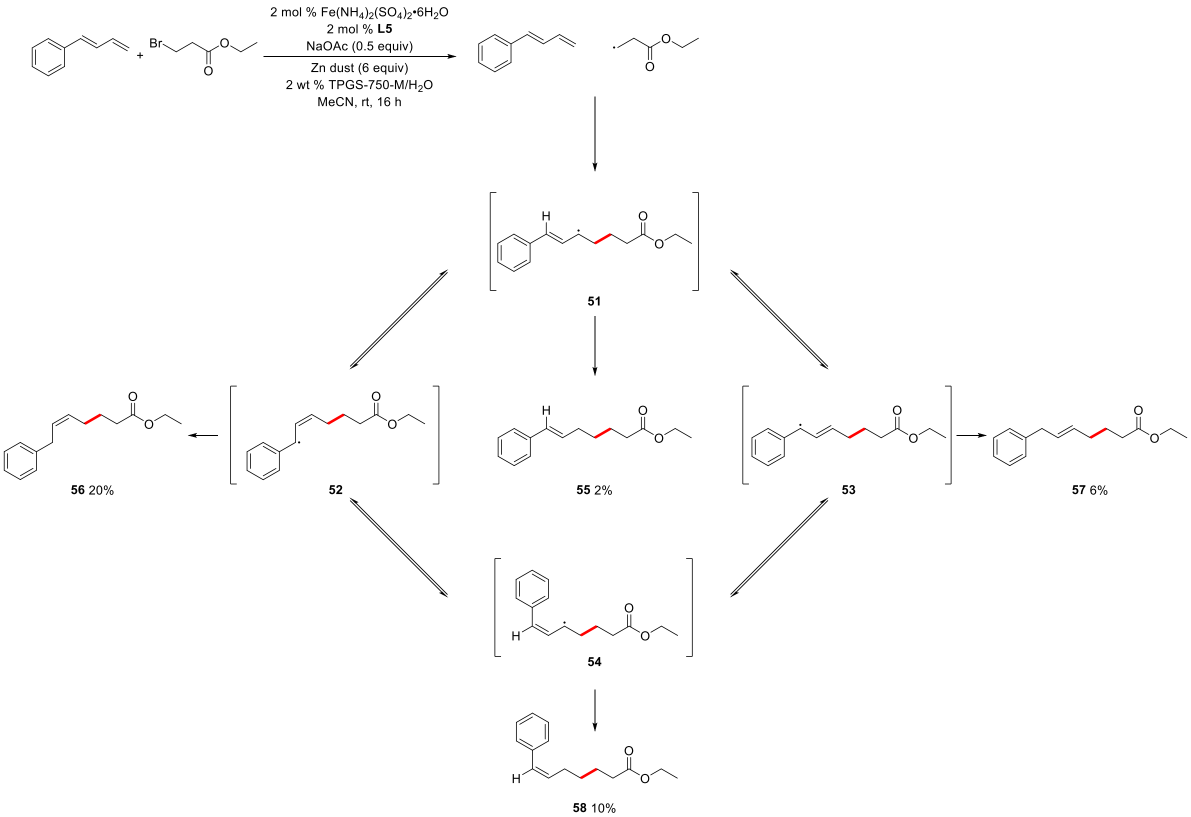
2 mol % Fe(NH4)2(SO4)2•6H2O
2 mol % L5
NaOAc (0.5 equiv)
Zn dust (6 equiv)
2 wt % TPGS-750-M/H2O
MeCN, rt, 16 h
51
52
53
54
55 2%
56 20%
57 6%
58 10%

Recycling and E Factors

One of the hallmarks of this green technology is the ease of handling and recyclability of the aqueous reaction mixture,[14] which dramatically reduces waste water streams. 2-Vinylpyridine and (2-bromoethyl)benzene were chosen as the starting materials. However, the presence of excess zinc dust can form agglomeration of Zn during the reaction, which sticks to the stir bar leading to hinder the following recycle reactions. In order to solve this issue, a filtration was needed to get rid of the agglomeration of zinc. The filtrate was used as the reaction medium with fresh catalyst and reagents for the following recycle. This stands in contrast to the typical “in-flask” extraction, leaving the reaction mixture for recycling in the same reaction vessel. Nonetheless, use of the aqueous filtrate led to essentially the same isolated yield as initially obtained (82%, then 80%). The associated E Factor, as originally introduced by Sheldon and co-workers as a measure of greenness,[15] was a very respectable 4.7 based on the amount of a single (recyclable) organic solvent invested for extraction purposes (Scheme 4).

Scheme 4: Recycling study and determination of E Factors

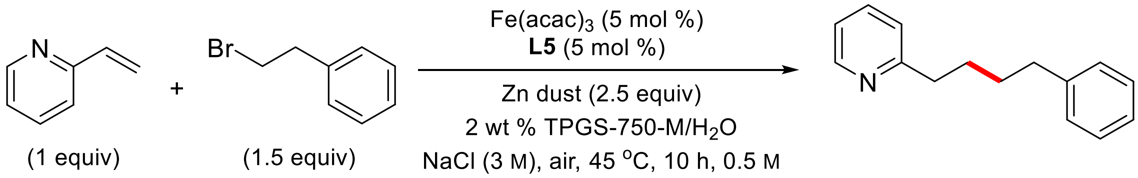

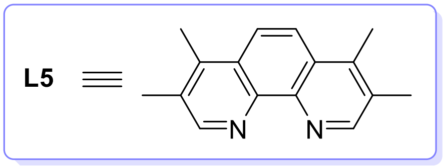

Entry	Isolated Yield (%)	E Factor (solvent)
initial reaction	82%	4.7
1st recycle	80%	4.8

Potential manufacturing applications

The potential application of this protocol to industry needs was mainly explored in terms of two aspects: (1) a scaled up reaction, and (2) synthesis of medicinal precursor. 2-Vinylpyridine and ethyl 3-bromopropanoate were selected as substrates partners. The prognosis for scale up was established by the successful coupling leading to over a gram of the desired product with a relatively good yield (Scheme 5, top). The successful application of this technology to prepare **59**, a precursor to a specific antitumor agent as illustrated in Scheme 5 (bottom), suggests that this approach to a net alkyl-alkyl coupling may find use in the fine chemical industry.

Scheme 5: Gram scale iron-catalyzed coupling reaction and synthesis of precursor of SphK inhibitor

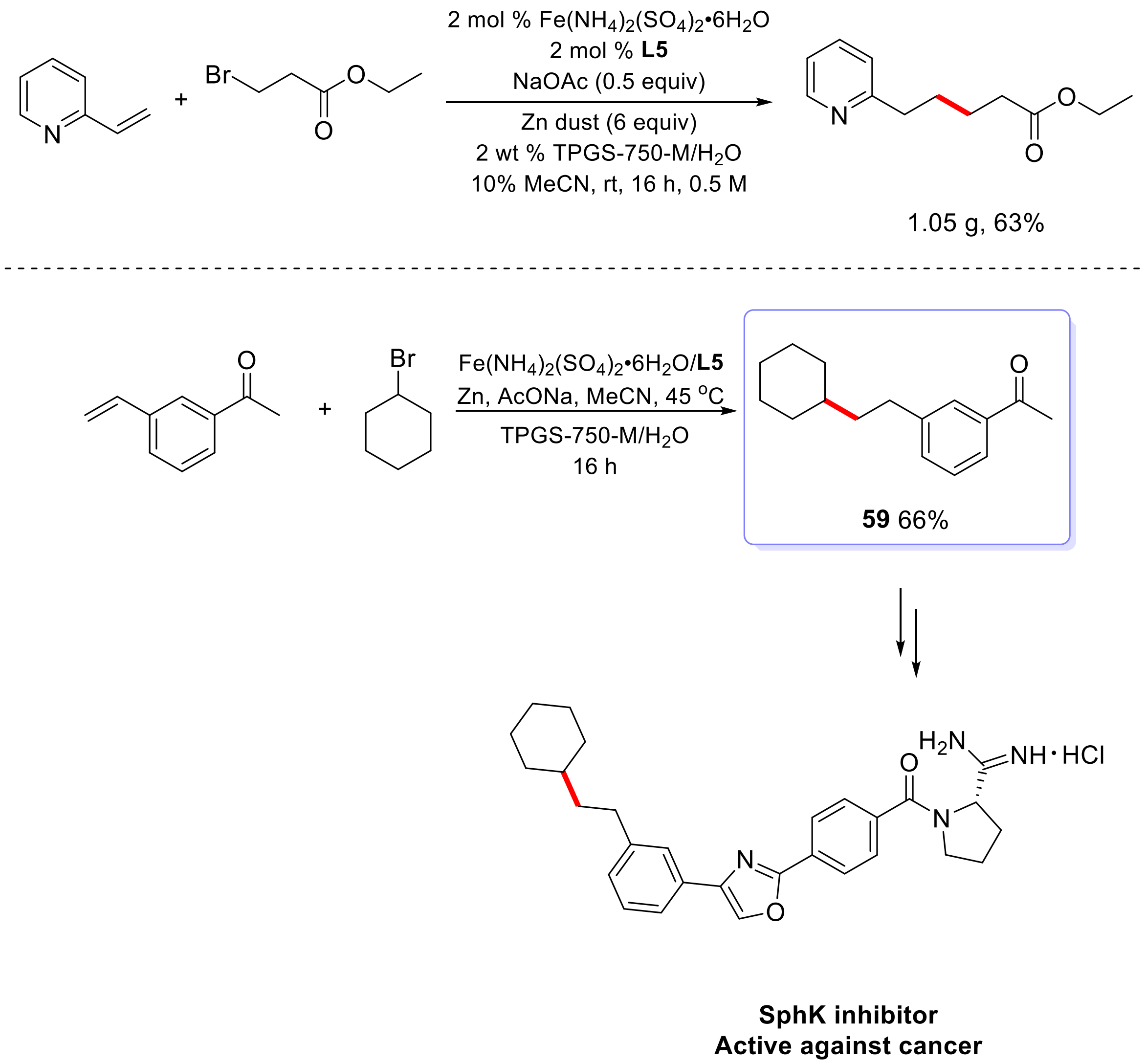
2 mol % Fe(NH4)2(SO4)2•6H2O
2 mol % L5
NaOAc (0.5 equiv)
Zn dust (6 equiv)
2 wt % TPGS-750-M/H2O
10% MeCN, rt, 16 h, 0.5 M
1.05 g, 63%
Fe(NH4)2(SO4)2•6H2O/L5
Zn, AcONa, MeCN, 45 °C
TPGS-750-M/H2O
16 h
59 66%
SphK inhibitor
Active against cancer

Mechanistic Studies

To begin to investigate the mechanism of this reductive cross-coupling reaction, several reactions were conducted in attempts to determine the nature of both the intermediates involved as well as the key bond forming step within the catalytic cycle(s). Firstly, control reactions using the combinations of a 4-*t*-butylstyrene/1° bromide and 2-vinylpyridine with either a 1° or 2° bromide under standard conditions in which either the iron salts, or zinc, were left out of the reaction medium led to no product formation (Scheme 6 (a)). These results indicated that both iron salt and zinc dust are necessary in the coupling process. An early observation indicating that a carbanionic process may be occurring was made when D_2O was used as the medium, since 94% incorporation of deuterium was found at the benzylic site (Scheme 6 (b)). This result indicated that water is not only functioning as the reaction medium, but also as the hydrogen source for this process. In addition, simple exchange from H_2O to D_2O provides a facile entry to deuterium incorporation, yet another outgrowth of this technology in water and may be quite useful en route to deuterium-labeled APIs. Nonetheless, this single observation fails to address the nature of the species undergoing the C-C bond-forming step.

Scheme 6: Control reactions and deuterium trapping test

(a) Control reactions

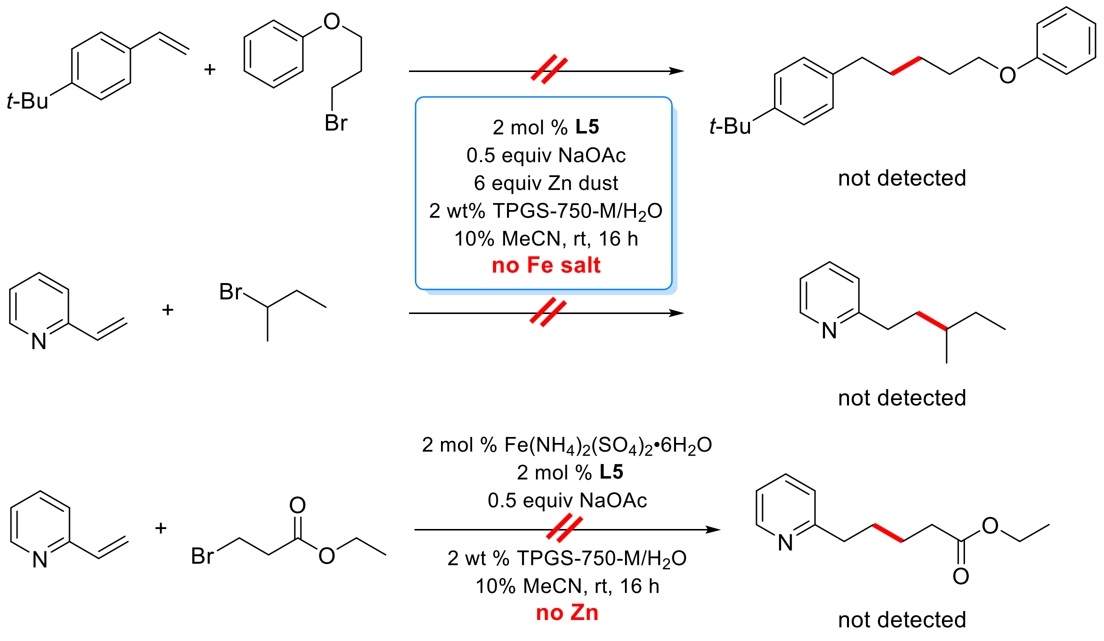

t-Bu
+
O
Br
2 mol % L5
0.5 equiv NaOAc
6 equiv Zn dust
2 wt% TPGS-750-M/H2O
10% MeCN, rt, 16 h
no Fe salt
t-Bu
O
not detected
N
+
Br
N
not detected
N
+
Br
O
O
2 mol % Fe(NH4)2(SO4)2•6H2O
2 mol % L5
0.5 equiv NaOAc
2 wt % TPGS-750-M/H2O
10% MeCN, rt, 16 h
no Zn
N
O
O
not detected

(b) Deuterium trapping experiment

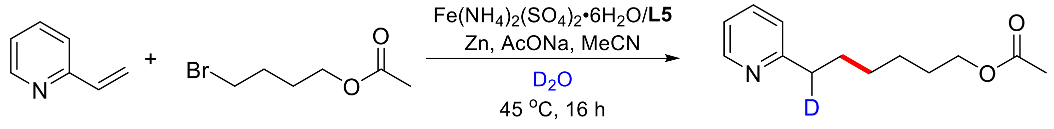

N
+
Br
O
O
Fe(NH4)2(SO4)2•6H2O/L5
Zn, AcONa, MeCN
D2O
45 °C, 16 h
N
D
O
O

60 60%, 94% D

Additional insight into this sequence was eventually achieved by a series of experiments in which substrates were specifically designed to test for radical involvement in both generation of the species undergoing C-C bond formation, as well as in the coupling itself. Initially, typical radical scavengers, such as BHT, TEMPO, and galvinoxyl free radical have been utilized for quenching radical intermediates to examine whether the yield of hydroalkylation would be impacted. However, no significant influence on the final yields was detected regardless of whether primary alkyl or tertiary alkyl bromides were used as coupling partners, as shown in Scheme 7 (a). These results seemed to provide evidence for no radical involvement in the hydroalkylation process. Nevertheless, given that the reaction was run under reductive conditions in the presence of a large excess of zinc dust, the radical scavengers, such as TEMPO or galvinoxyl free radical, might be reduced by excess zinc dust prior to radical-type trapping. To verify whether the radical scavengers remain intact during the reaction, a series of control reactions was conducted, as shown in Scheme 7 (b). TEMPO, as well as galvinoxyl free radical, were examined under the standard reaction conditions leading to complete consumption of active radical trapping reagents. In further studies, only one equivalent of zinc dust associated with one equivalent of TEMPO or galvinoxyl free radical was used in the hydroalkylation process. The results indicated that the zinc dust had been consumed by these scavengers (TEMPO and galvinoxyl free radical) prior to the hydroalkylation process. Hence, even without detection of any radical trapping products, these experiments do not provide sufficient evidence to exclude involvement of radical processes.

Scheme 7: Radical trapping tests via radical scavengers:

(a)

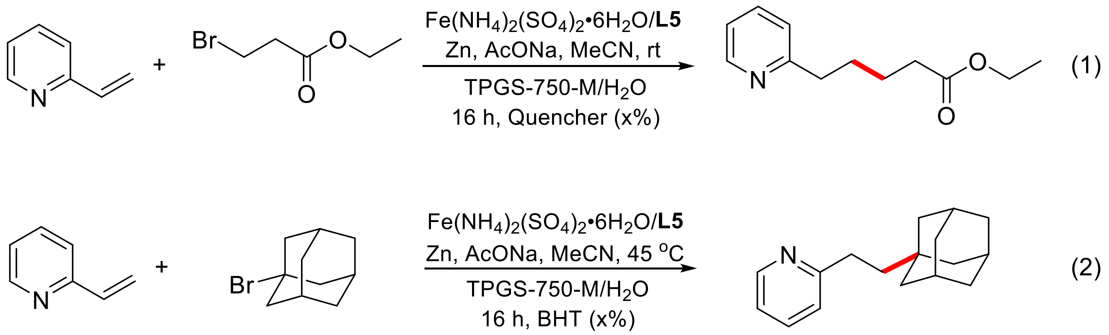
N
Br
O
O
+
Fe(NH4)2(SO4)2•6H2O/L5
Zn, AcONa, MeCN, rt
TPGS-750-M/H2O
16 h, Quencher (x%)
(1)
Fe(NH4)2(SO4)2•6H2O/L5
Zn, AcONa, MeCN, 45 °C
TPGS-750-M/H2O
16 h, BHT (x%)
(2)

Entry[a]	Reaction	Quencher	x	Isolated yield (%)
1	1	none	0	70
2	1	TEMPO	5	71
3	1	galvinoxyl	5	63
4	1	BHT	5	72
5	1	TEMPO	100	57
6	1	galvinoxyl	100	58
7	1	BHT	100	70
8	2	BHT	0	63
9	2	BHT	100	53

[a] Reaction conditions: olefin (0.2 mmol), aliphatic bromide (0.6 mmol), $Fe(NH_4)_2(SO_4)_2•6H_2O$ (0.004 mmol), **L5** (0.004 mmol), Zn dust (1.2 mmol), AcONa (0.1 mmol), MeCN (0.04 mL), quencher (0.01mmol or 0.2 mmol) and 2 wt % TPGS-750-M/H_2O (0.4 mL).

(b)

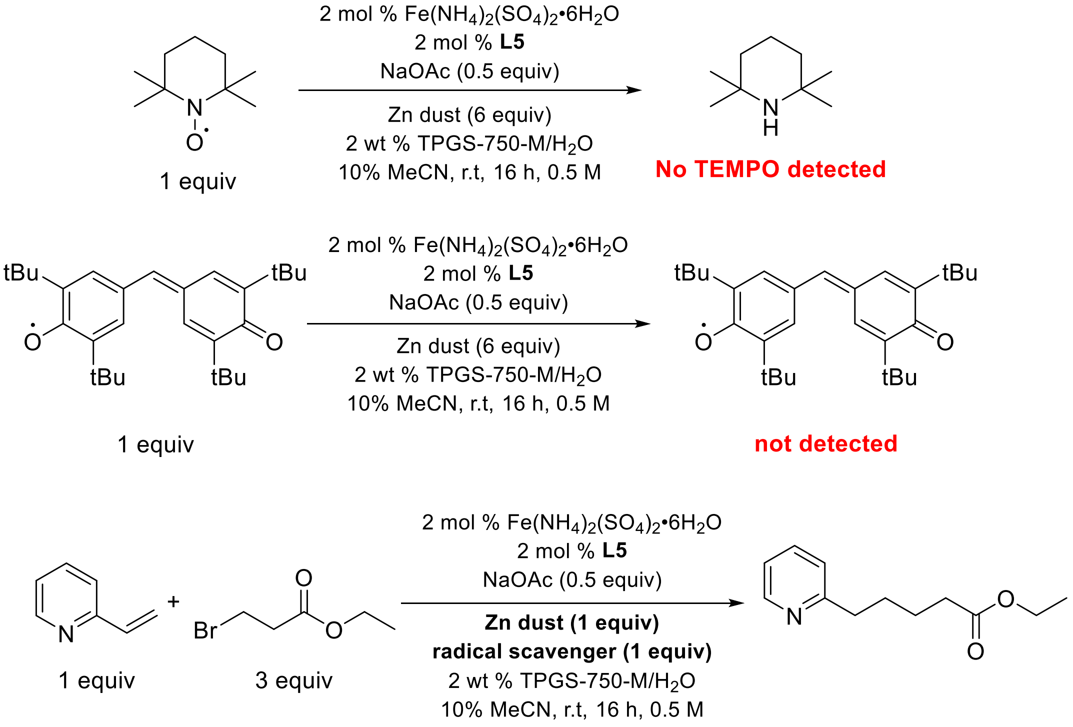
2 mol % Fe(NH4)2(SO4)2•6H2O
2 mol % L5
NaOAc (0.5 equiv)
Zn dust (6 equiv)
2 wt % TPGS-750-M/H2O
10% MeCN, r.t, 16 h, 0.5 M
1 equiv
No TEMPO detected
tBu
O
1 equiv
not detected
N
Br
O
1 equiv
3 equiv
Zn dust (1 equiv)
radical scavenger (1 equiv)

Entry	Radical scavenger	Yield (%)
1	-	28
2	TEMPO	ND
3	galvinoxyl	ND

Other than radical trapping experiments, a radical clock test is another typical tool to provide evidence for radical involvement (Scheme 8). Initially, 6-bromohex-1-ene was chosen as starting material to couple with 2-vinylpyridine, which afforded a 1:1 mix of linear and *cyclized* products **61** and **62**, respectively. Tellingly, the formation of cyclized product clearly indicated that the alkyl bromide formed an alkyl radical in the pot initially. Nonetheless, while this radical could then add directly to the coupling partner to arrive at a stabilized benzylic radical, the presence of excess Zn in the medium could also easily reduce such a radical to the corresponding organozinc halide. This would give rise to an anionic intermediate eventually adding to the alkenylpyridine to arrive at the same benzylic carbanion prior to proton/deuterium quenching.

Additional evidence implicating an initially produced radical that then undergoes C-C bond formation comes from two experiments involving cyclopropane-containing educts. Attempts to add an alkyl bromide to 2-vinylcyclopropyl)benzene failed completely under standard conditions, indicative of the requirement for a truly aromatic/heteroaromatic substrate as coupling partner. On the other hand, the 1-cyclopropyl-substituted styrene **63** (Scheme 8, bottom) reacted to afford, albeit in low yield, a mix of *E*- and *Z*-isomeric olefinic products **64** and **65**, a likely outgrowth reflecting initial radical addition to this styrene derivative. Since α-substituted systems are relatively unreactive towards these couplings, the low yield obtained was not unexpected. Nonetheless, neither linear nor cyclopropane-containing product was observed. Although there is some suggestion in the literature[16] that a cyclopropylmethyl anion can undergo ring opening-ring closing, the likelihood that the derived benzylic cyclopropyl anion is the intermediate involved in this ring-opening process is quite low.

Scheme 8: Radical clock test

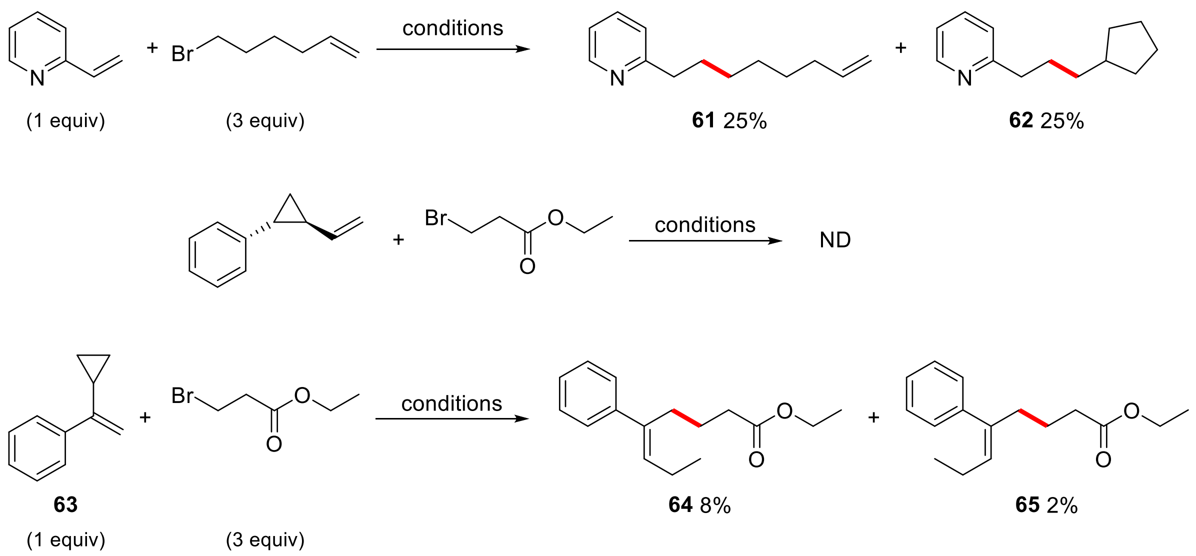

conditions: 2 mol % $Fe(NH_4)_2(SO_4)_2{\cdot}6H_2O$, 2 mol % **L5**, 0.5 equiv NaOAc, 6 equiv Zn dust
2 wt % TPGS-750-M/H_2O, 10% MeCN, rt, 16 h. 0.5 M

To further test for involvement of organozinc intermediates, although the control experiments indicated that such species are not participating in the key bond-forming step, our otherwise standard conditions (both with, and without iron present) were augmented with catalytic copper, along with a 2-cyclohexenone as partner rather than, e.g., 2-vinylpyridine (Scheme 9). Since conjugate additions of alkyl radicals to enones are well known,[17] a 1,4-adduct should be expected even in the absence of any copper(I) in the pot. Leaving iron out of this same mixture, however, where only an organozinc reagent can be formed only to undergo transmetalation to copper to afford the same 1,4-adduct, might result in quite differing levels of conversion relative to that resulting via a radical process. As shown in Scheme 9, since some conjugate addition occurred without iron present, clearly a purely carbanionic intermediate (RZnX) must form and could then, as a background reaction, participate in transmetalation/conjugate addition, as seen previously.[18] Instead, the presence of iron leads to a substantially higher yielding coupling than did the one in its absence, which indicated that even under reductive conditions, most alkyl radicals survive rather than be reduced by the excess zinc dust prior to the formation of the C-C bonds. Further studies focused on determining whether the iron salts play a key role in the formation of alkyl radicals from alkyl bromides. The related experiment involving an acrylate coupling partner, *in the absence of Cu*, also led to both linear and *cyclized* conjugate adducts. However, there is almost no conjugate adducts detected in the absence of iron salt. This case indicated that the radical intermediates form at the initial stage of exposure of the bromide to the iron salts/Zn combination, followed by radical trapping by the unsaturated ester.

Scheme 9: Further tests for involvement of radical intermediates

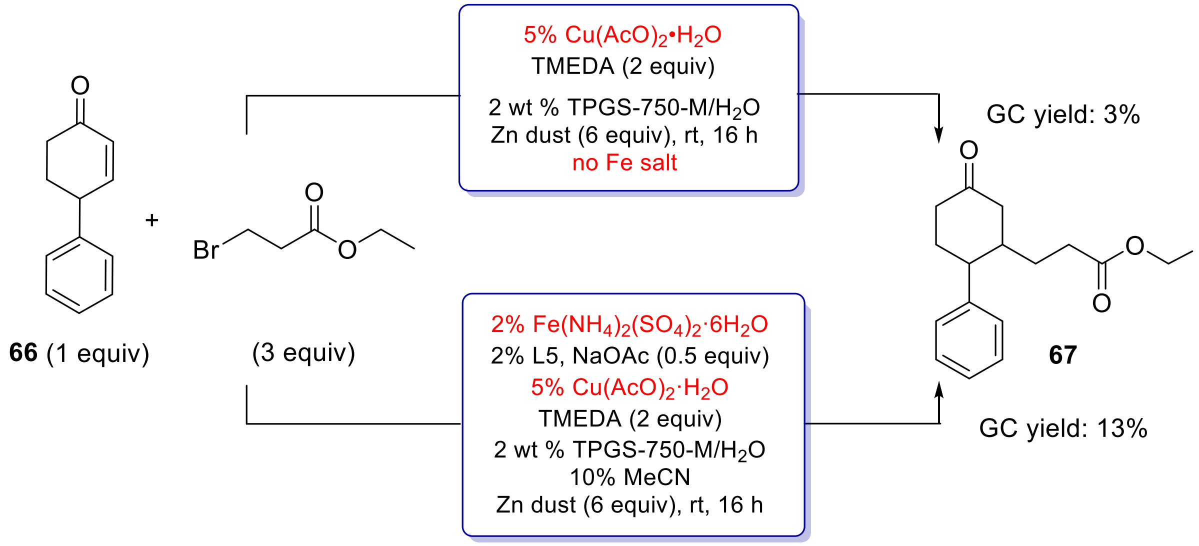

5% $Cu(AcO)_2$•H_2O
TMEDA (2 equiv)
2 wt % TPGS-750-M/H_2O
Zn dust (6 equiv), rt, 16 h
no Fe salt
GC yield: 3%
O
O
Br
O
O
O
O
+
66 (1 equiv)
(3 equiv)
67
2% $Fe(NH_4)_2(SO_4)_2 \cdot 6H_2O$
2% L5, NaOAc (0.5 equiv)
5% $Cu(AcO)_2 \cdot H_2O$
TMEDA (2 equiv)
2 wt % TPGS-750-M/H_2O
10% MeCN
Zn dust (6 equiv), rt, 16 h
GC yield: 13%

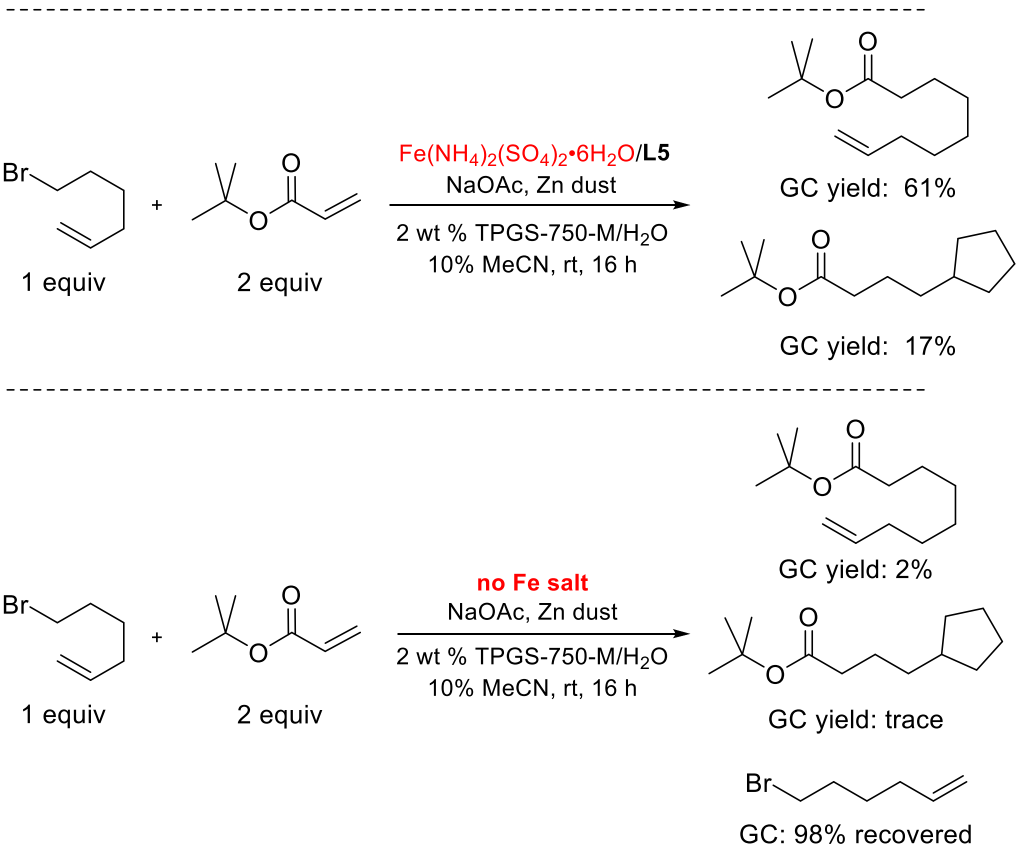
Br
+
O
O
1 equiv
2 equiv
Fe(NH4)2(SO4)2•6H2O/L5
NaOAc, Zn dust
2 wt % TPGS-750-M/H2O
10% MeCN, rt, 16 h
GC yield: 61%
GC yield: 17%
no Fe salt
GC yield: 2%
GC yield: trace
GC: 98% recovered

On the basis of these results, a plausible mechanistic sequence is illustrated in Scheme 10 (pink arrows). The active Fe catalyst is first formed via reduction of either an Fe(III) (**68**) or Fe(II) (**69**) salt by Zn, thereby enabling relatively rapid electron transfer into the C-Br bond. The resulting radical (**70**, or perhaps organoiron intermediate), from loss of bromide ion, adds to the styrene (or equivalent) thereby arriving at a stable benzylic radical (or corresponding organoiron species), which is then reduced by Zn to the benzylic anion **74**. Quenching by water (or D_2O) affords the observed product **75**.

The alternative mechanism that invokes Zn reduction of the initial radical-like species **71** would lead at this point to intermediate organozinc halide **76**, which could add directly to a styrene coupling partner (or the equivalent), giving the same benzylic carbanionic species (**74**) as arrived at in the prior mechanistic scheme. However, since two control reactions (see Scheme 10) both confirm that this sequence, in the absence of iron, does not afford any of the expected adduct, this suggests that even if **74** is generated in situ, it does not go forward to produce any of the observed product **75**.

Scheme 10: Proposed mechanism

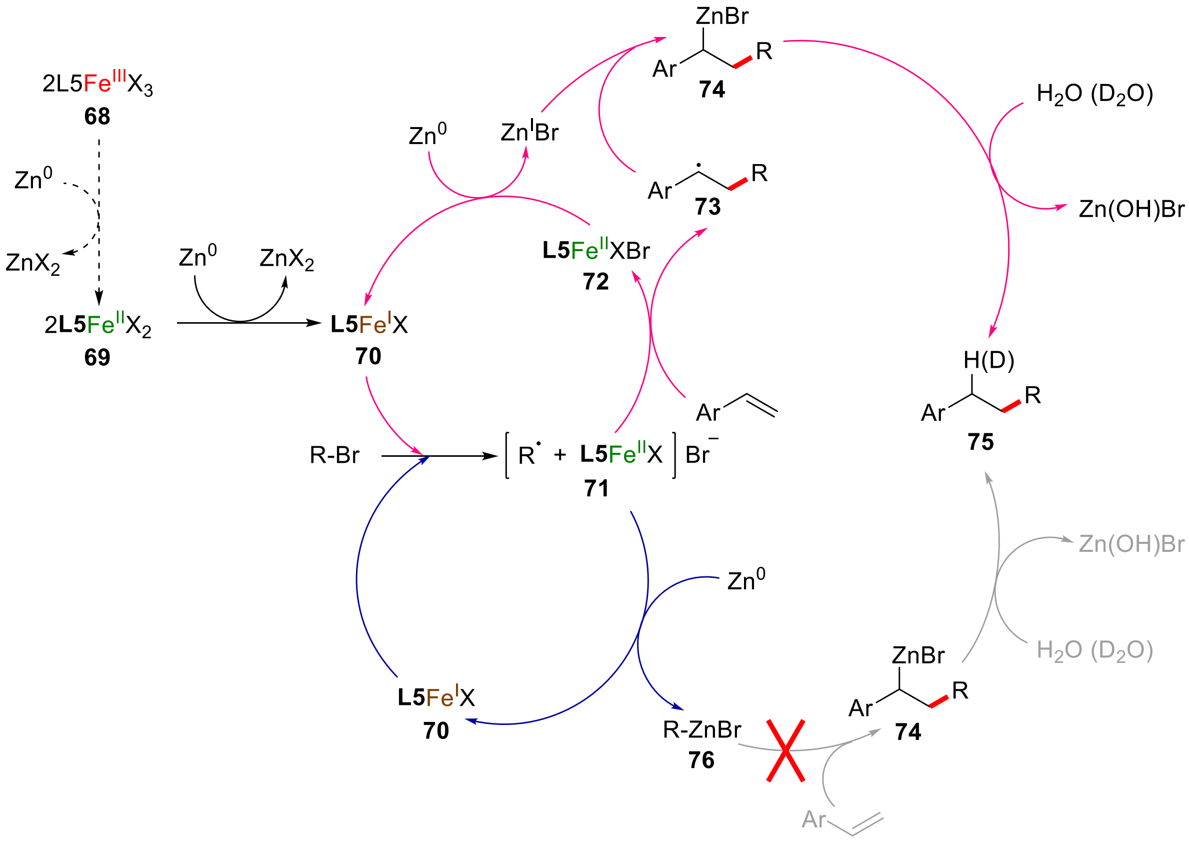

2L5Fe^{III}X$_3$
68
Zn^0
ZnX$_2$
2L5Fe^{II}X$_2$
69
Zn^0
ZnX$_2$
L5Fe^{I}X
70
Zn^0
Zn^{I}Br
ZnBr
Ar
R
74
Ar
R
73
L5Fe^{II}XBr
72
H$_2$O (D$_2$O)
Zn(OH)Br
H(D)
Ar
R
75
R-Br
R$^•$ + L5Fe^{II}X
Br$^-$
71
Ar
Zn(OH)Br
H$_2$O (D$_2$O)
Zn^0
L5Fe^{I}X
70
R-ZnBr
76
ZnBr
Ar
R
74
Ar

Conclusions

In summary, a new reductive coupling reaction between in situ-generated, functionalized, and catalytically active organoiron reaction partners and conjugated alkenyl-substituted aromatic/heteroaromatics has been uncovered. The process takes place under very mild, green conditions in aqueous micellar media, leading to facile product isolation as well as recycling of the aqueous reaction mixture. Preliminary mechanistic studies suggest that a sequence of steps involves two distinct types of intermediates. Initially, a radical process ensues leading to C-C bond formation between the reaction partners, followed by generation of a likely carbanionic, benzylic zinc halide which is ultimately protonated by the surrounding water.

References

1. (a) Handa, S.; Wang, Y.; Gallou, F.; Lipshutz, B. H. Sustainable Fe–ppm Pd nanoparticle catalysis of Suzuki-Miyaura cross-couplings in water. *Science* **2015**, *349*, 1087. (b) Handa, S.; Slack, E. D.; Lipshutz, B. H. Nanonickel-Catalyzed Suzuki–Miyaura Cross-Couplings in Water. *Angew. Chem., Int. Ed.* **2015**, *54*, 11994. (c) Krasovskiy, A.; Duplais, C.; Lipshutz, B. H. Stereoselective Negishi-like Couplings Between Alkenyl and Alkyl Halides in Water at Room Temperature. *Org. Lett.* **2010**, *12*, 4742. (d) Duplais, C.; Krasovskiy, A.; Lipshutz, B. H. Organozinc Chemistry Enabled by Micellar Catalysis. Palladium-Catalyzed Cross-Couplings between Alkyl and Aryl Bromides in Water at Room Temperature. *Organometallics* **2011**, *30*, 6090.

2. Cheung, C. W.; Zhurkin, F. E.; Hu, X. Z-Selective Olefin Synthesis via Iron-Catalyzed Reductive Coupling of Alkyl Halides with Terminal Arylalkynes. *J. Am. Chem. Soc.* **2015**, *137*, 4932.

3. Pileni, M.-P. The role of soft colloidal templates in controlling the size and shape of inorganic nanocrystals. *Nat. Mater.* **2003**, *2*, 145.

4. Lipshutz, B. H.; Ghorai, S.; Abela, A. R.; Moser, R.; Nishikata, T.; Duplais, C.; Krasovskiy, A.; Gaston, R. D.; Gadwood, R. C. TPGS-750-M: A Second-Generation Amphiphile for Metal-Catalyzed Cross-Couplings in Water at Room Temperature. *J. Org. Chem.* **2011**, *76*, 4379.

5. Klumphu, P.; Lipshutz, B. H. "Nok": a phytosterol-based amphiphile enabling transition metal-catalyzed couplings in water at room temperature. *J. Org. Chem.* **2014**, *79*, 888.

6. Gabriel, C. M.; Lee, N. R.; Bigorne, F.; Klumphu, P.; Parmentier, M.; Gallou, F.; Lipshutz, B. H. Effects of Co-solvents on Reactions Run under Micellar Catalysis Conditions. *Org. Lett.* **2017**, *19*, 194.

7. Lipshutz, B. H.; Ghorai, S.; Leong, W. W. Y.; Taft, B. R.; Krogstad, D. V. Manipulating Micellar Environments for Enhancing Transition Metal-Catalyzed Cross-Couplings in Water at Room Temperature. *J. Org. Chem.* **2011**, *76*, 5061.

8. (a) Matyjaszewski, K.; Xia, J. Atom Transfer Radical Polymerization. *Chem. Rev.* **2001**, *101*, 2921. (b) Pintauer, T.; Matyjaszewski, K. Atom transfer radical addition and polymerization reactions catalyzed by ppm amounts of copper complexes. *Chem. Soc. Rev.* **2008**, *37*, 1087.

9. The remaining mass consisted of mainly polymerized olefin, along with small amounts of recovered bromide.

10. (a) Kim, E.; Kang, W. Simultaneous determination of N1-acetyl sulfisoxazole and its metabolites, and relative bioavailability compare to sulfisoxazole in rats. *J. Pharm. Biomed. Anal.* **2016**, *129*, 117. (b) Vohra, M.; Sandbhor, M.; Wozniak, A. Efficient synthesis of deuterium labeled hydroxyzine and aripiprazole. *J. Labelled Compd. Radiopharm.* **2015**, *58*, 304. (c) Mans, D. J.; Callahan, R. J.; Dunn, J. D.; Gryniewicz-Ruzicka, C. M. Rapid-screening detection of acetildenafils, sildenafils and avanafil by ion mobility spectrometry. *J. Pharm. Biomed. Anal.* **2013**, *75*, 153. (d) Díaz, N.; Sordo, T. L.; Suárez, D.; Méndez, R.; Villacorta, J. M.; Simón, L.; Rico, M.; Jiménez, M. Á. Assessing the Protonation State of Drug Molecules: The Case of Aztreonam. *J. Med. Chem.* **2006**, *49*, 3235. (e) Li, H.; Xiao, H.; Lin, L.; Jou, D.; Kumari, V.; Lin, J.; Li, C. Drug Design Targeting Protein–Protein Interactions (PPIs) Using Multiple Ligand Simultaneous Docking (MLSD) and Drug Repositioning: Discovery of Raloxifene and Bazedoxifene as Novel Inhibitors of IL-6/GP130 Interface. *J. Med. Chem.* **2014**, *57*, 632.

11. (a) Raju, M. N.; Kumar, N. U.; Reddy, B. S.; Anitha, N.; Srinivas, G.; Bhattacharya, A.; Mukkanti, K.; Kolla, N.; Bandichhor, R. An efficient synthesis of dexlansoprazole employing asymmetric oxidation strategy. *Tetrahedron Lett.* **2011**, *52*, 5464. (b) Huang, Q.; Johnson, T. W.; Bailey, S.; Brooun, A.; Bunker, K. D.; Burke, B. J.; Collins, M. R.; Cook, A. S.; Cui, J. J.; Dack, K. N.; Deal, J. G.; Deng, Y.-L.; Dinh, D.; Engstrom, L. D.; He, M.; Hoffman, J.; Hoffman, R. L.; Johnson, P. S.; Kania, R. S.; Lam, H.; Lam, J. L.; Le, P. T.; Li, Q.; Lingardo, L.; Liu, W.; Lu, M. W.; McTigue, M.; Palmer, C. L.; Richardson, P. F.; Sach, N. W.; Shen, H.; Smeal, T.; Smith, G. L.; Stewart, A. E.; Timofeevski, S.; Tsaparikos, K.; Wang, H.; Zhu, H.; Zhu, J.; Zou, H. Y.; Edwards, M. P. Design of Potent and Selective Inhibitors to Overcome Clinical Anaplastic Lymphoma Kinase Mutations Resistant to Crizotinib. *J. Med. Chem.* **2014**, *57*, 1170. (c) Chen, B.-C.; Bednarz, M. S.; Zhang, H.; Guo, P.; Jemal, M.; Robl, J. A.; Biller, S. A.; Sundeen, J. E.; Balasubramanian, B.; Barrish, J. C. Synthesis of d3-cerivastatin for use as internal standard in a LC/MS/MS method developed for quantitation of the drug in human serum. *J. Labelled Compd. Radiopharm.* **2006**, *49*, 311. (d) Harikrishnan, A.; Sanjeevi, J.; Ramaraj Ramanathan, C. The cooperative effect of Lewis pairs in the Friedel–Crafts hydroxyalkylation reaction: a simple and effective route for the synthesis of (±)-carbinoxamine. *Org. Biomol. Chem.* **2015**, *13*, 3633.

12. (a) Lipshutz, B. H.; Aguinaldo, G. T.; Ghorai, S.; Voigtritter, K. Olefin Cross-Metathesis Reactions at Room Temperature Using the Nonionic Amphiphile “PTS”: Just Add Water. *Org. Lett.* **2008**, *10*, 1325. (b) Blackmond, D. G.; Armstrong, A.; Coombe, V.; Wells, A. Water in Organocatalytic Processes: Debunking the Myths. *Angew. Chem., Int. Ed.* **2007**, *46*, 3798.

13. (a) Duplais, C.; Krasovskiy, A.; Lipshutz, B. H. Organozinc Chemistry Enabled by Micellar Catalysis. Palladium-Catalyzed Cross-Couplings between Alkyl and Aryl Bromides in Water at Room Temperature. *Organometallics* **2011**, *30*, 6090. (b) Krasovskiy, A.; Duplais, C.; Lipshutz, B. H. Zn-Mediated, Pd-Catalyzed Cross-

Couplings in Water at Room Temperature Without Prior Formation of Organozinc Reagents. *J. Am. Chem. Soc.* **2009**, *131*, 15592.

14. Lipshutz, B. H.; Isley, N. A.; Fennewald, J. C.; Slack, E. D. On the Way Towards Greener Transition-Metal-Catalyzed Processes as Quantified by E Factors. *Angew. Chem., Int. Ed.* **2013**, *52*, 10911.

15. (a) Sheldon, R. A.; Arends, I. W. C. E.; Hanefeld, U. Introduction: Green Chemistry and Catalysis. *Green Chemistry and Catalysis*, Wiley-VCH, Weinheim, **2007**. 1; (b) Sheldon, R. A. The E Factor: fifteen years on. *Green Chem*. **2007**, *9*, 1273.

16. Maercker, A.; Güthlein, P.; Wittmany, H., Einflüsse von α- und β-Alkylgruppen auf die Umlagerung von 3-Butenyl-Grignardverbindungen: Ein stabiles, primäres Cyclopropylmethyl-Anion. *Angew. Chem.* **1973,** *85*, 823.

17. Ryu, I.; Uehara, S.; Hirao, H.; Fukuyama, T., Tin-Free Giese Reaction and the Related Radical Carbonylation Using Alkyl Iodides and Cyanoborohydrides. *Org. Lett.* **2008,** *10*, 1005.

18. Lipshutz, B. H.; Huang, S.; Leong, W. W. Y.; Zhong, G.; Isley, N. A., C–C Bond Formation via Copper-Catalyzed Conjugate Addition Reactions to Enones in Water at Room Temperature. *J. Am. Chem. Soc.* **2012,** *134* (49), 19985-19988.

Appendix

General Remarks

All manipulations were carried out under air unless otherwise noted. TLC plates (UV 254 indicator, glass backed, thickness 200 mm and silica gel (standard grade, 230 – 400 mesh) were purchased from Merck. Ethyl acetate and hexanes were purchased from Fisher Scientific. THF was taken from Innovative Technologies Solvent Purification System (SPS) and used immediately. Ligands were either purchased from Sigma-Aldrich or gifted by Johnson Matthey. Pure NMR solvents were purchased from Cambridge Isotopes Laboratories. The coupling reactions were performed in 4 mL close cap microwave vials either under argon atmosphere or air conditions. Microwave reaction vials were either made in the UCSB glass shop or purchased from VWR international. Reaction vials were also recycled and re-used. Aqueous solution of TPGS-750-M was well purged with argon before use. HPLC grade water was used to prepare surfactant solutions. TPGS-750-M was synthesized according to the published procedure[1] and is also commercially available from Sigma-Aldrich (catalog number 733857). Unless otherwise mentioned, all NMR spectra were recorded at 23 °C on Varian Unity INOVA (400, 500 and 600 MHz) spectrometers. Reported chemical shifts are referenced to residual solvent peaks.[2] IR spectra were acquired on a FTIR Perkin Elmer Spectrum Two: UATR Two spectrometer using 1 cm^{-1} resolution. High resolution mass analyses were obtained using a 5975C Mass Selective Detector, coupled with a 7890A Gas Chromatograph (Agilent Technologies). As capillary column a HP-5MS cross-linked 5% phenylmethyl- polysiloxanediphenyl column (30 m × 0.250 mm, 0.25 micron, Agilent Technologies) was employed. Helium was used as carrier gas at a constant flow of 1 mL/min.

Optimized General Procedure for Coupling Reactions

Procedure. In a flame dried 4 mL microwave reaction vial, Fe(acac)$_3$ (1.4 mg, 0.004 mmol), 3,4,7,8-tetramethyl-1,10-phenanthroline (1 mg, 0.004 mmol) and NaCl (70.2 mg, 1.2 mmol) were mixed together. Then, 0.4 mL of an aqueous solution 2 wt % TPGS-750-M was added to the vial followed by sequential addition of olefin (0.2 mmol, 1.0 equiv) and Zn dust (<10 μm, ≥98% from Sigma-Aldrich) (1.2 mmol, 6 equiv). After 5 min of stirring, the aliphatic bromide (0.6 mmol, 3 equiv) was added and the reaction vial was closed with a rubber septum under air. The reaction mixture was stirred at 25 °C for 16 h.

For screening experiments, EtOAc (1.0 mL) was added to the reaction mixture, and the mixture was stirred for 5 min at rt. Stirring was then stopped and the organic layer was removed with a pipette. It was then passed through a very small silica plug. GC yields were determined by GC-MS using naphthalene as internal standard. After the reaction, Zn complex would form agglomeration attach the vial and stir bar, which usually occurs in the Zn reaction. Additional research was needed to approve that problem.

For isolation of product, after 16 h of reaction, the mixture was extracted with EtOAc (0.2 mL × 3) with the help of centrifuge to effect phase separation. The combined organic extracts were dried over anhydrous Na_2SO_4. Volatiles were removed under reduced pressure to obtain crude product which were further purified by flash chromatography over silica gel using EtOAc/hexanes as eluent.

Altered Reaction conditions. In a flame dried 4 mL microwave reaction vial, $(NH_4)_2Fe(SO_4)_2\cdot 6H_2O$ (1.6 mg, 0.004 mmol), 3,4,7,8-tetramethyl-1,10-phenanthroline (1 mg, 0.004 mmol) and NaOAc (8.2 mg, 0.1 mmol) were mixed together. Then, 0.4 mL of an aqueous solution of 2 wt % TPGS-750-M/H_2O and 0.04 mL MeCN were added to the vial followed by sequential addition of olefin (0.2 mmol, 1.0 equiv) and Zn dust (<10 μm, ≥98%

from Sigma-Aldrich) (1.2 mmol, 6 equiv). After 5 min of stirring, the aliphatic bromide (0.6 mmol, 3 equiv) was added and the reaction vial was closed with a rubber septum under air. The reaction mixture was stirred at 25 °C for 16 h.

For screening experiments, the same procedure as above was followed.

For isolation of the product after 16 h of stirring, the mixture was extracted with EtOAc (0.2 mL × 3) with the help of centrifuge to phase separation. The combined organic extracts were dried over anhydrous Na_2SO_4. Volatiles were removed under reduced pressure to obtain crude product which were further purified by flash chromatography over silica gel using EtOAc/hexanes as eluent.

Preparation of substrates

Olefin: 1-(*t*-butyl)-4-vinylbenzene, 1-bromo-4-vinylbenzene, 1-(trifluoromethyl)-4-vinylbenzene, 1-chloro-2-vinylbenzene, 1-vinylnaphthalene and 2-vinylpyridine are commercially available. Bromides: (3-bromopropoxy)benzene, 4-bromobutyl acetate, 4-bromobut-1-ene, bromocyclohexane and ethyl 3-bromopropanoate are commercially available.

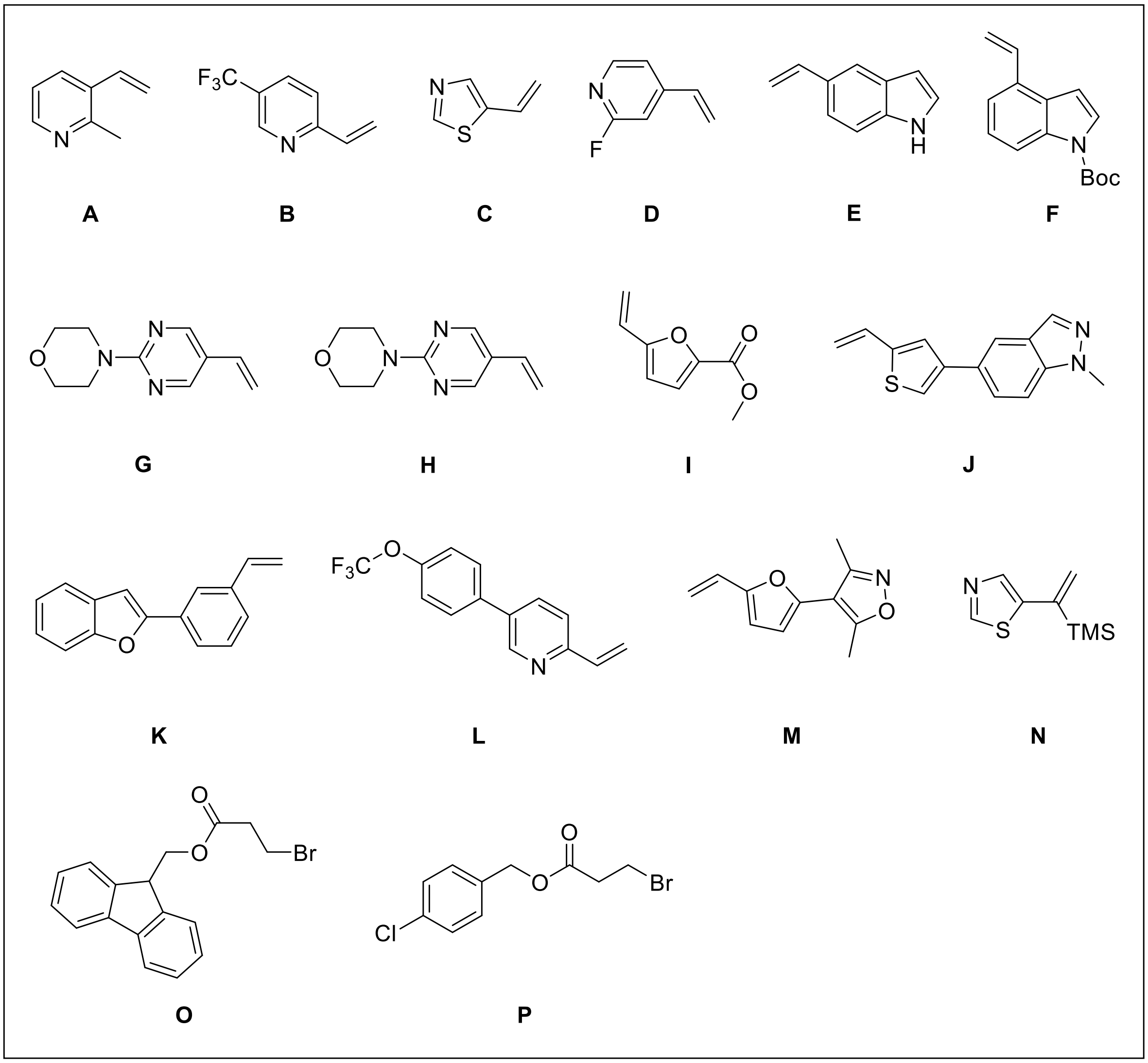

Substrates **A** – **I** were synthesized using the general procedure 1 (below) by Suzuki-Miyaura reactions with the corresponding bromides. Substrates **J** – **M** were synthesised using the general procedure 2. Substrate **N** was synthesised by procedure 3. Substrates **O** and **P** were synthesised by general procedure 4.

General procedure 1

In an oven-dried 10 mL round bottom flask containing a PTFE-coated magnetic stir bar, the corresponding bromide (2 mmol, 1 equiv), vinylboronic acid pinacol ester (2.2 mmol, 1.1 equiv), Pd(dtbpf)Cl_2 (39.1 mg, 0.06 mmol, 0.03 equiv), Et_3N (607 mg, 6 mmol, 3 equiv)

and 4 mL 2 wt % TPGS-750-M/H_2O were added. The mixture was stirred under 45 °C until TLC showed completion. The reaction medium was extracted with EtOAc. The organic layer was separated and dried over anhydrous Na_2SO_4. Volatiles were removed under reduced pressure to obtain crude product which was purified by flash chromatography on silica gel with a gradient eluent using hexanes and EtOAc.[3]

General procedure 2

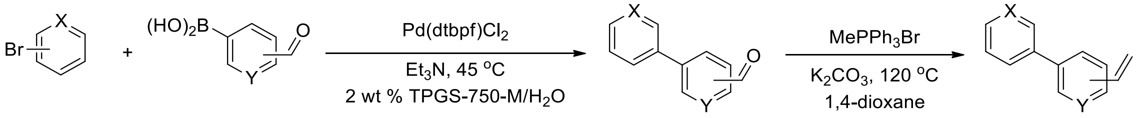

In an oven-dried 10 mL round bottom flask containing a PTFE-coated magnetic stir bar, corresponding bromide (2 mmol, 1 equiv), boronic acid (2.2 mmol, 1.1 equiv), Pd(dtbpf)Cl_2 (39.1 mg, 0.06 mmol, 0.03 equiv), Et_3N (607 mg, 6 mmol, 3 equiv) and 2 wt % TPGS-750-M/H_2O were added. The mixture was stirred under 45 °C until TLC showed completion. The reaction medium was extracted with EtOAc. The organic layer was separated and dried over anhydrous Na_2SO_4. Volatiles were removed under reduced pressure to obtain crude product which was purified by flash chromatography on silica gel with a gradient eluent using hexanes and EtOAc.[3]

In an oven-dried 25 mL round bottom flask containing a PTFE-coated magnetic stir bar, the carbonyl compound (2 mmol, 1 equiv), Ph_3PMeBr (857.3 mg, 2.4 mmol, 1.2 equiv), K_2CO_3 (415 mg, 3 mmol, 1.5 equiv) and 5 mL dioxane were added. The mixture was refluxed at 120 °C overnight. After completion, the reaction mixture was diluted by EtOAc and then the solution was washed with water three times and then with brine. The organic layer was dried over anhydrous Na_2SO_4. Volatiles were removed under reduced pressure to obtain crude product which was purified by flash chromatography on silica gel with a gradient eluent using hexanes and EtOAc.[4]

General procedure 3

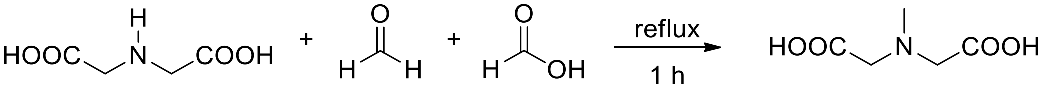

In a 3-neck 50 mL round bottom flask equipped with a PTFE-coated magnetic stir bar, iminodiacetic acid (6.7 g, 50 mmol, 1 equiv) and formic acid (4.6 mg, 100 mmol, 2 equiv) were added. A water-cooled Friedrichs condenser vented to the atmosphere was placed on the flask and the mixture was stirred at 90 °C for 30 min. Formalin (37 wt % in H_2O, 75 mmol, 1.5 equiv) was added drop by drop by syringe over 10 min. Following the addition the mixture was maintained at reflux for an additional 1 h. The solution was cooled to rt and was then transferred to an Erlenmeyer flask. The round bottom flask was washed with water (4 × 1.7 mL). 50 mL EtOH was added to the aqueous phase drop by drop. The aqueous phase was left undisturbed overnight, during which time the product crystallized as large colorless needle-like crystals. The crystals were collected via filtration, washed with EtOH to afford *N*-methyliminodiacetic acid (6.88 g, 93%).[5]

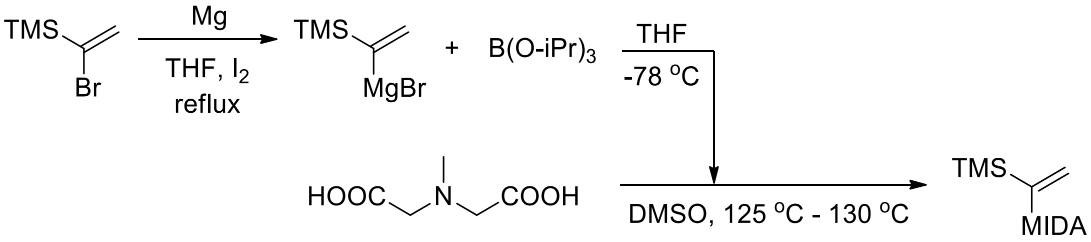

In a 3-neck 50 mL round bottom flask attached with a water-cooled Friedrichs condenser equipped with a PTFE-coated magnetic stir bar, Mg (124.8 mg, 5.2 mmol, 1.04 equiv) and I_2 (0.5 mg) were added. The flask was sealed with a rubber septum and was assembled and kept under argon. To this flask was added (1-bromovinyl)trimethylsilane (895.5 mg, 5 mmol, 1 equiv) and 4 mL anhydrous THF. The mixture was refluxed until no more Mg was left in the mixture. To a second round-bottom flask under argon equipped with a Teflon stir bar and septum, $B(O\text{-}i\text{-}Pr)_3$ (987.4 mg, 5.25 mmol, 1.05 equiv) and 4 mL anhydrous THF were added and the solution was cooled to -78 °C. The Grignard reagent was transferred drop by drop to the B(O-*i*-Pr)$_3$ solution at -78 °C via syringe over 20 min. The mixture was stirred at -78 °C for another 20 min. after which the cooling bath was removed and the solution was allowed to warm to room temperature. This solution was stirred at rt for 2 h.

A dry 3-necked flask, with a stir bar, an addition funnel with a pressure equalizing side arm, along with a jacketed-condenser attached to a 100-mL round bottom flask was assembled and kept under argon as it cooled to rt. Next, *N*-methyliminodiacetic acid (1.47 g, 10 mmol, 2 equiv) was added into the 3-necked flask followed by DMSO (6.5 mL) via syringe. The solution was heated to 130 °C with an oil bath and stirred. Once the reaction medium became homogeneous upon heating, the complex in THF in a second round-bottom flask was added via syringe to the addition funnel. The solution was slowly added to the DMSO solution (over 1 h). While the THF was added to the DMSO solution, it was rapidly distilled off during this addition process into a 100 mL round bottom flask. After the addition was complete, the solution was heated for an additional 30 min at ca. 120 °C.

Next, the oil bath was set to 80 °C and the DMSO was slowly distilled off into the round bottom flask under reduced pressure (slowly reducing pressure from 400 torr to ~1 torr) over the course of ~20 min. Once nearly all the DMSO was distilled, the oil bath temperature was increased to 100 °C, driving off the remaining DMSO, affording a brown clump, which was purified by flash chromatography on silica gel with a gradient eluent using hexanes and EtOAc, with KMnO$_4$ as stain for monitoring the product by TLC to afford 839 mg (66%) 1-trimethylsilanevinylboronic acid MIDA ester as white solid.[6]

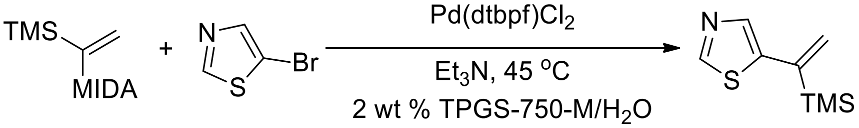

In an oven-dried 10 mL round bottom flask containing a PTFE-coated magnetic stir bar, 5-bromothiazole (162 mg, 1 mmol), 1-trimethylsilanevinylboronic acid MIDA ester (280.5 mg, 1.1 mmol), Pd(dtbpf)Cl_2 (19.6 mg, 0.03 mmol), Et_3N (304 mg, 3 mmol) and 2 mL 2 wt % TPGS-750-M/H_2O were added. The mixture was stirred under 45 °C until the TLC showed completion. The reaction medium was extracted with EtOAc. The organic layer was separated and dried over anhydrous Na_2SO_4. Volatiles were removed under reduced pressure to obtain crude product which was purified by flash chromatography on silica gel with a gradient eluent using hexanes and EtOAc.[3]

General procedure 4

3-Bromopropionic acid (3.6 mmol. 1.8 equiv) and the corresponding benzyl alcohol (3 mmol, 1.5 equiv) were dissolved in 10 mL dry toluene. A catalytic amount of toluenesulfonic acid monohydrate (0.04 mmol, 0.02 equiv) was added. A Dean-Stark trap and condenser were added and the mixture was then heated to 140 ºC overnight, the toluene/water azeotrope mixture was removed 3 times. The toluene was removed by evaporation and the mixture was re-dissolved in EtOAc. The solution was washed with saturated $NaHCO_3$ solution, brine, and then dried over anhydrous Na_2SO_4. Volatiles were removed under reduced pressure to obtain crude product which was purified by flash chromatography on silica gel with a gradient eluent using hexanes and EtOAc.[7]

Selectivity on 1-phenylbutadiene

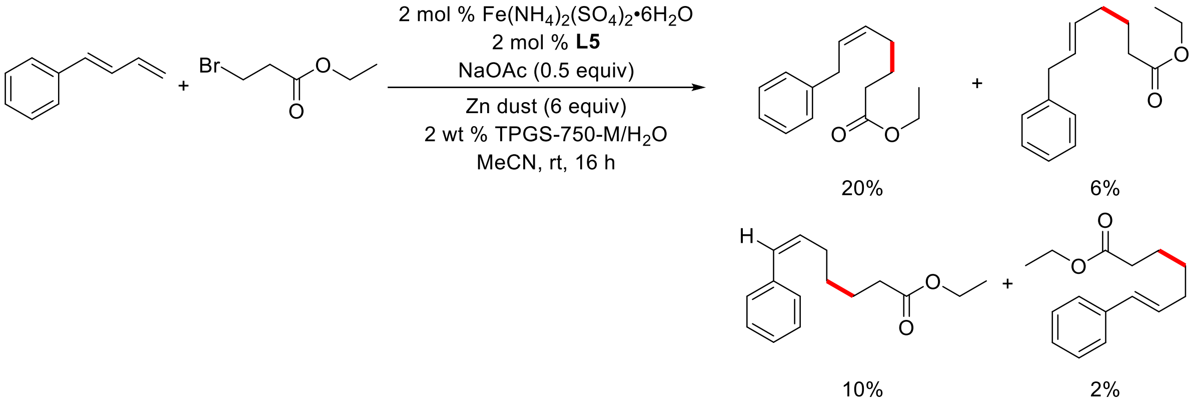

Br
O
O
+
2 mol % Fe(NH4)2(SO4)2•6H2O
2 mol % L5
NaOAc (0.5 equiv)
Zn dust (6 equiv)
2 wt % TPGS-750-M/H2O
MeCN, rt, 16 h
20%
6%
H
10%
2%

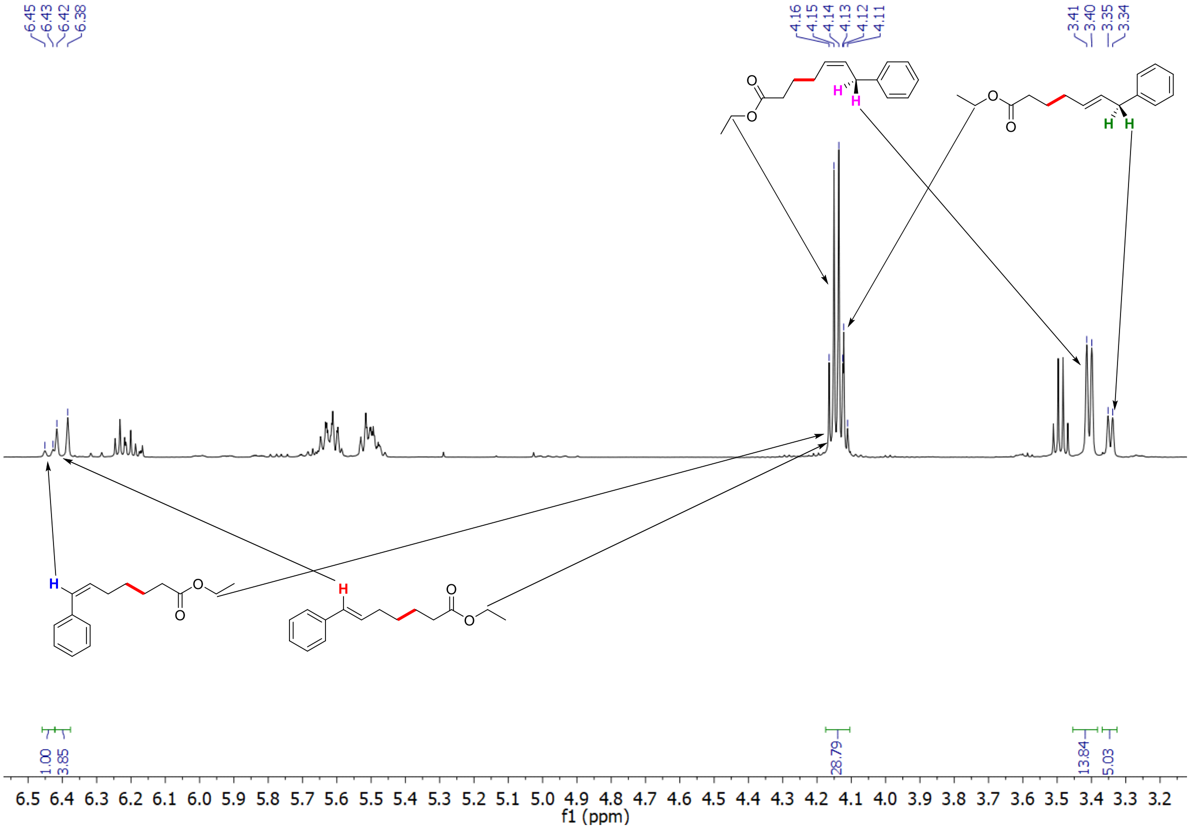

1-Phenylbutadiene (52 mg, 0.4 mmol), ethyl 3-bromopropanoate (217.2 mg, 1.2 mmol), $Fe(NH_4)_2(SO_4)_2 \cdot 6H_2O$ (3.2 mg, 0.008 mmol), 3,4,7,8-tetramethyl-1,10-phenanthroline (2 mg, 0.008 mmol), Zn dust (156 mg, 2.4 mmol) and NaOAc (16.4 mg, 0.2 mmol) in 0.8 mL 2 wt % TPGS-750-M/H_2O with MeCN (0.08 mL) as co-solvent were reacted at rt for 16 h.

The reaction was monitored by the TLC stained with Seebach's magic TLC stain. After the reaction complete the produced mixture was detected by GC-MS and purified by flash chromatography on silica gel yielding 35.3 mg (38%) of mixture (hexane/EtOAc : 90/10).

E Factor and Recycle Studies

Initial reaction. In a flame dried 4 mL microwave reaction vial, Fe(acac)$_3$ (0.025 mmol, 5 mol %), 3,4,7,8-tetramethyl-1,10-phenanthroline (0.025 mmol, 5 mol %), NaCl (70.2 mg, 1.2 mmol) were mixed together. Then, 1.0 mL aqueous solution 2 wt % TPGS-750-M was added to the vial followed by sequential addition of 2-vinylpyridine (0.5 mmol, 1.0 equiv) and (2-bromoethyl)benzene (0.75 mmol, 1.5 equiv). After 5 min of stirring, Zn dust (1.25 mmol, 2.5 equiv) was added and the reaction vial was closed with a rubber septum under air. The reaction mixture was stirred at 45 °C for 10 h. The resulting mixture was extracted with EtOAc (0.15 mL × 3). The organic layer was then separated (with the aid of centrifuge, if needed) and dried over anhydrous Na_2SO_4, after which the volatiles were removed under reduced pressure and purified by flash chromatography over silica gel with EtOAc/hexanes to obtain 2-(4-phenylbutyl)pyridine. (86.8 mg, 0.41 mmol, 82%).

1st Recycle. In order to remove the Zn, the reaction residue was filtered using a fritted glass filter into a new 4 mL microwave reaction vial. The vial was charged with fresh Fe(acac)$_3$ (0.025 mmol, 5 mol %), 3,4,7,8-tetramethyl-1,10-phenanthroline (0.025 mmol, 5 mol %), 2-vinylpyridine (0.5 mmol, 1.0 equiv) and 0.5 mL of an aqueous solution of 2 wt % TPGS-750-M/H_2O and the vial was again covered. After 5 min of stirring, Zn dust (1.25 mmol, 2.5 equiv) and (2-bromoethyl)benzene (0.75 mmol, 1.5 equiv) were added and the reaction vial was closed with a rubber septum under air. The reaction mixture was stirred at 45 °C for 10 h. The resulting mixture was then extracted with EtOAc (0.15 mL × 3). The organic layer was separated (with the aid of centrifuge, if needed) and dried over anhydrous Na_2SO_4, after which the volatiles were removed under reduced pressure and purified by flash chromatography over silica gel with EtOAc/hexanes to obtain 2-(4-phenylbutyl)pyridine. (84.6 mg, 0.4 mmol, 80%).

Reaction at the gram scale

In a flame dried 100 mL round bottom flask, $(NH_4)_2Fe(SO_4)_2 \cdot 6H_2O$ (62.7 mg, 0.16 mmol, 2 mol %), 3,4,7,8-tetramethyl-1,10-phenanthroline (37.8 mg, 0.16 mmol, 2 mol %) and NaOAc (0.328 g, 4 mmol) were mixed together. Then, 16 mL of an aqueous solution of 2 wt % TPGS-750-M and 2.1 mL MeCN were added to the vial followed by sequential addition of 2-vinylpyridine (0.84 g, 8 mmol, 1.0 equiv.) and Zn dust (3.12 g, 48 mmol, 6 equiv). After 5 min of stirring, the ethyl 3-bromopropanoate (4.34 mg, 24 mmol, 3 equiv.) was added and the round bottom flask was closed with a rubber septum under air. The reaction mixture was stirred at 25 °C for 16 h after which the mixture was filtered by a fritted glass filter under vacuum. The complex cake was washed by EtOAc. While washing, the cake needed to be stirred in the EtOAc using a spatula. The aqueous medium was further extracted with EtOAc (10 mL × 5). The combined organic extracts were dried over anhydrous Na_2SO_4. Volatiles were removed under reduced pressure to obtain crude product which were further purified by flash chromatography over silica gel using EtOAc/hexanes as eluent yielding 1.05 g (63%) ethyl 5-(pyridin-2-yl)pentanoate.

Synthesis of the precursor to a SphK inhibitor

1-(3-Vinylphenyl)ethanone (58.5 mg, 0.4 mmol), bromocyclohexane (195.7 mg, 1.2 mmol), $Fe(NH_4)_2(SO_4)_2 \cdot 6H_2O$ (3.2 mg, 0.008 mmol), 3,4,7,8-tetramethyl-1,10-phenanthroline (2 mg, 0.008 mmol), Zn dust (156 mg, 2.4 mmol) and NaOAc (16.4 mg, 0.2

mmol), in 0.8 mL 2 wt % TPGS-750-M/H_2O with MeCN (0.08 mL) as co-solvent were reacted at 45 °C for 16 h yielding 60.7 mg (66%) of 1-(3-(2-cyclohexylethyl)-phenyl)ethanone as a slight yellow oil (hexane/EtOAc : 90/10).

^{1}H NMR (500 MHz, $CDCl_3$) δ 7.81 – 7.72 (m, 2H), 7.39 – 7.33 (m, 2H), 2.69 – 2.63 (m, 2H), 2.59 (s, 3H), 1.78 – 1.62 (m, 5H), 1.55 – 1.48 (m, 2H), 1.27 – 1.14 (m, 4H), 1.00 – 0.89 (m, 2H).

^{13}C NMR (126 MHz, $CDCl_3$) δ 198.49, 143.86, 137.31, 133.31, 128.54, 128.13, 125.91, 39.40, 37.45, 33.38, 33.25, 26.77, 26.75, 26.41.

HRMS(EI): Calcd. for $C_{16}H_{22}O$ $[M]^+$ 230.1671. Found: 230.1668.

Mechanistic studies

a) Control experiments

1-(*t*-Butyl)-4-vinylbenzene (32 mg, 0.2 mmol), (3-bromopropoxy)benzene (129.1 mg, 0.6 mmol), 3,4,7,8-tetramethyl-1,10-phenanthroline (1 mg, 0.004 mmol), Zn dust (78 mg, 1.2 mmol), NaOAc (8.2 mg, 0.1 mmol) in 0.4 mL 2 wt % TPGS-750-M/H2O with MeCN (0.04 mL) as co-solvent were reacted at rt for 16 h. After 16 h, EtOAc was added and the mixture stirred for 2 min at rt. Stirring was then stopped and the organic layer was decanted via pipette. The organic layer was passed through a very small silica plug. Yields were determined by GC using naphthalene as internal standard.

2-Vinylpyridine (21 mg, 0.2 mmol), 2-bromobutane (82.2 mg, 0.6 mmol), 3,4,7,8-tetramethyl-1,10-phenanthroline (1 mg, 0.004 mmol), Zn dust (78 mg, 1.2 mmol) and NaOAc (8.2 mg, 0.1 mmol), in 0.4 mL 2 wt % TPGS-750-M/H_2O with MeCN (0.04 mL) as co-solvent were reacted at rt for 16 h. Stirring was then stopped and the organic layer was decanted via pipette. The organic layer was passed through a very small silica plug. Yields were determined by GC using naphthalene as internal standard.

2-Vinylpyridine (21 mg, 0.2 mmol), ethyl 3-bromopropanoate (108.6 mg, 0.6 mmol), $Fe(NH_4)_2(SO_4)_2·6H_2O$ (1.6 mg, 0.004 mmol), 3,4,7,8-tetramethyl-1,10-phenanthroline (1 mg, 0.004 mmol) and NaOAc (8.2 mg, 0.1 mmol), in 0.4 mL 2 wt % TPGS-750-M/H_2O with MeCN (0.04 mL) as co-solvent were reacted at rt for 16 h. Stirring was then stopped and the organic layer was decanted via pipette. The organic layer was passed through a very small silica plug. Yields were determined by GC using naphthalene as internal standard.

b) H/D transfer experiment

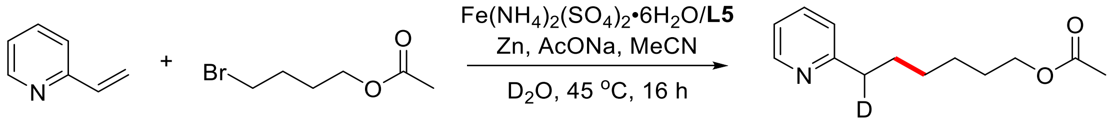

56 60%

To investigate the proposed mechanism of this reaction, an experiment was run using proton NMR to monitor product(s) formation. In the first H/D experiment, 2-vinylpyridine (21 mg, 0.2 mmol), 4-bromobutyl acetate (117 mg, 0.6 mmol), $Fe(NH_4)_2(SO_4)_2·6H_2O$ (1.6 mg 0.004 mmol), 3,4,7,8-tetramethyl-1,10-phenanthroline (1 mg, 0.004 mmol), NaOAc (8.2 mg, 0.1 mmol), MeCN (0.04 mL) and Zn dust (78 mg, 1.2 mmol) were placed in the 0.4 mL of D_2O and the reaction conducted at 45 °C for 16 h yielding 26.8 mg (60%) of 6-(pyridin-2-yl)hexyl-6-d acetate as a faint yellow oil (hexane/EtOAc : 80/20).

^{1}H NMR (500 MHz, $CDCl_3$) δ 8.50 (d, J = 4.2 Hz, 1H), 7.56 (td, J = 7.7, 1.8 Hz, 1H), 7.14 – 7.04 (m, 2H), 4.02 (t, J = 6.7 Hz, 2H), 2.75 (t, J = 7.8 Hz, 1H), 2.01 (s, 3H), 1.75 – 1.68 (m, 2H), 1.60 (p, J = 6.9 Hz, 2H), 1.37 (p, J = 3.6 Hz, 4H).

^{13}C NMR (126 MHz, $CDCl_3$) δ 171.25, 162.29, 149.27, 136.32, 122.75, 120.99, 64.60, 37.99 (m), 29.71, 29.00, 28.58, 25.86, 21.05.

^{2}H NMR (61 MHz, $CHCl_3$) δ 2.76.

HRMS(ESI): Calcd. for $C_{13}H_{19}DNO_2$ $[M+H]^+$ 223.1557. Found: 223.1552.

The product was analyzed by ^{1}H NMR and compared with the ^{1}H NMR of the product from 2 wt % TPGS-750-M/H_2O. This experiment indicated that the proton/deuteron in the product comes from the medium, in this case, D_2O.

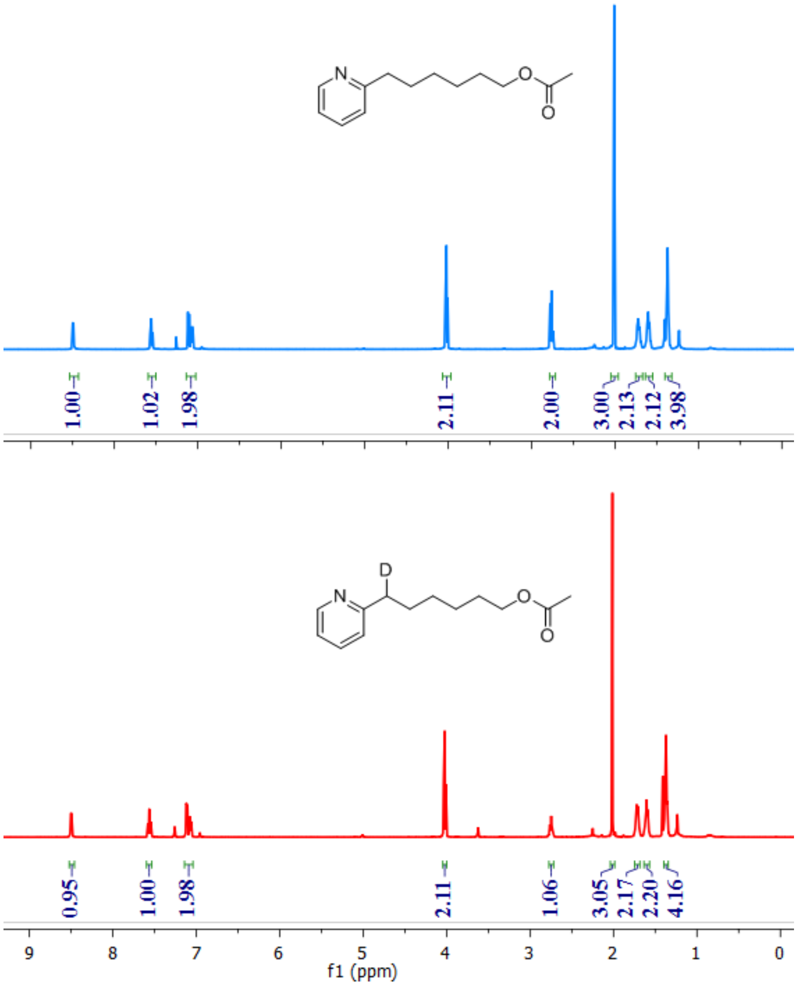

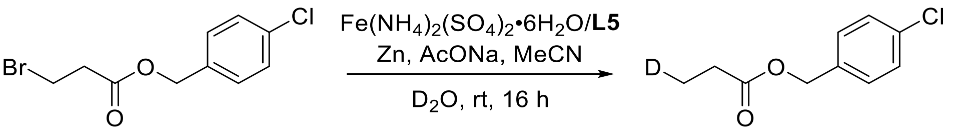
Br
O
O
Cl
Fe(NH4)2(SO4)2•6H2O/L5
Zn, AcONa, MeCN
D2O, rt, 16 h
D
O
O
Cl

In addition, the main by-product from debromination was analyzed by a similar experiment. Hence, 4-chlorobenzyl 3-bromopropanoate (166.5 mg, 0.6 mmol), $Fe(NH_4)_2(SO_4)_2 \cdot 6H_2O$ (1.6 mg 0.004 mmol), 3,4,7,8-tetramethyl-1,10-phenanthroline (1 mg, 0.004 mmol), NaOAc (8.2 mg, 0.1 mmol), MeCN (0.04 mL) and Zn dust (78 mg, 1.2 mmol) were placed in reaction vessel containing 0.4 mL D_2O and the reaction was run for 16 h. The product was analyzed by ^{1}H NMR and compared with the ^{1}H NMR derived from 4-chlorobenzyl 3-bromopropanoate. The experiment indicated the proton of the by-product also comes from D_2O.

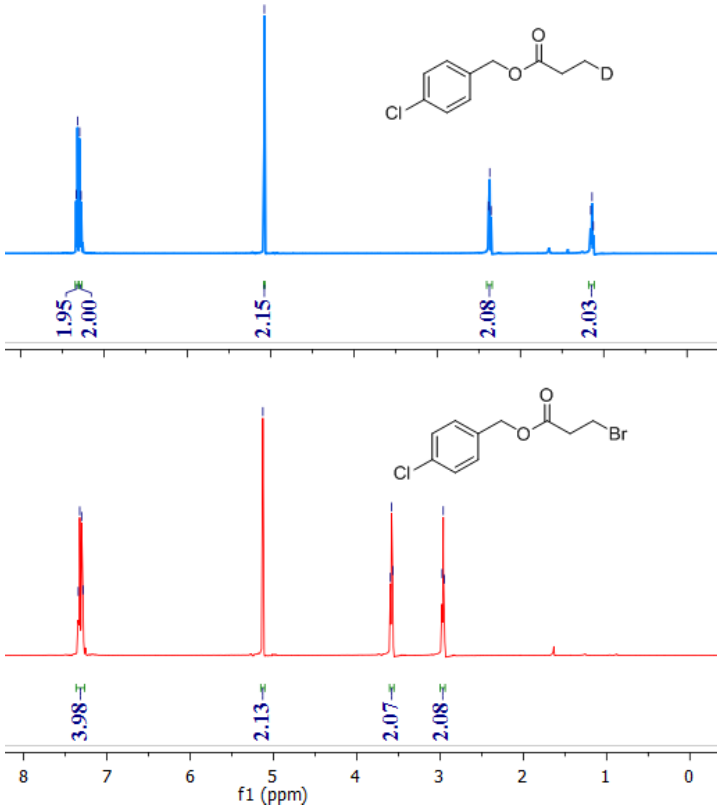

c) Radical clock experiments

Substrate synthesis

(1-Cyclopropylvinyl)benzene

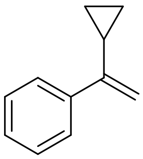

In a 250 mL round bottom flask methyltriphenylphosphonium bromide (7.2 g, 20 mmol) was dissolved in anhydrous THF (60 mL) and the mixture was cooled to -78 °C under an argon atmosphere. *n*-BuLi (8.0 mL, 2.5 M, 20 mmol) was added dropwise within 45 min, after which the cooling bath was removed. To this mixture cyclopropyl phenyl ketone (1.46 g, 10.0 mmol) dissolved in anhydrous THF (6 mL) was added dropwise and the reaction was left to stir for 1 h. The reaction was monitored by TLC. Brine (30 mL) was added and the phases were separated. The aqueous phase was extracted with pentane (3 × 20 mL), and the combined organic phases were dried over anhydrous MgSO$_4$, filtered and the crude mixture was further purified by flash chromatography over silica gel using pure pentane as eluent yielding 1.43 g (99%) (1-cyclopropylvinyl)benzene as a colorless oil.

Spectral data matched that reported in the literature.[8]

^{1}H NMR (500 MHz, CDCl$_3$) δ 7.66 – 7.53 (m, 2H), 7.40 – 7.31 (m, 2H), 7.31 – 7.26 (m, 1H), 5.29 (s, 1H), 4.95 (s, 1H), 1.67 (dddd, *J* = 13.6, 8.2, 5.4, 1.1 Hz, 1H), 0.87 – 0.79 (m, 2H), 0.64 – 0.55 (m, 2H).

^{13}C NMR (126 MHz, CDCl$_3$) δ 149.52, 141.79, 128.28, 127.58, 126.26, 109.14, 15.78, 6.82.

GC-MS, *m/z*: 144 [M$^+$].

Radical clock reaction

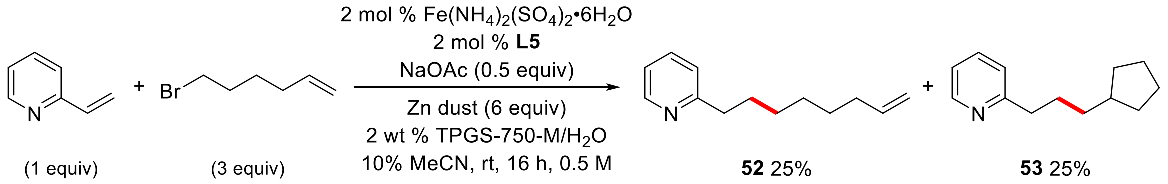

2-Vinylpyridine (42 mg, 0.4 mmol), 6-bromohex-1-ene (195.7 mg, 1.2 mmol), Fe(NH$_4$)$_2$(SO$_4$)$_2$·6H$_2$O (3.2 mg, 0.008 mmol), 3,4,7,8-tetramethyl-1,10-phenanthroline (2 mg, 0.008 mmol), Zn dust (156 mg, 2.4 mmol) and NaOAc (16.4 mg, 0.2 mmol) were added to 0.8 mL 2 wt % TPGS-750-M/H$_2$O with MeCN (0.08 mL) as co-solvent, and the mixture was vigorously stirred at room temperature for 16 h yielding 37.8 mg (50%) of a mixture containing 2-(oct-7-en-1-yl)pyridine (25%) and 2-(3-cyclopentylpropyl)pyridine (25%) as a faint yellow oil (hexane/EtOAc : 85/15).

^{1}H NMR (500 MHz, $CDCl_3$) δ 8.57 – 8.43 (m, 2H), 7.57 – 7.50 (m, 2H), 7.09 (d, *J* = 7.7 Hz, 2H), 7.07 – 7.01 (m, 2H), 5.76 (ddt, *J* = 16.9, 10.2, 6.7 Hz, 1H), 4.98 – 4.92 (m, 1H), 4.89 (d, *J* = 10.2 Hz, 1H), 2.74 (t, *J* = 7.8 Hz, 4H), 2.00 (q, *J* = 6.8, 6.4 Hz, 2H), 1.80 – 1.62 (m, 7H), 1.57 – 1.43 (m, 3H), 1.39 – 1.27 (m, 9H), 1.12 – 0.97 (m, 2H).

^{13}C NMR (126 MHz, $CDCl_3$) δ 162.60, 162.51, 149.23, 139.13, 136.23, 122.71, 120.88, 120.86, 114.23, 40.12, 38.79, 38.48, 36.01, 33.81, 32.74, 29.91, 29.28, 29.21, 29.01, 28.86, 25.23.

HRMS(EI): Calcd. for $C_{13}H_{19}N$ $[M]^+$ 189.1517. Found: 189.1513.

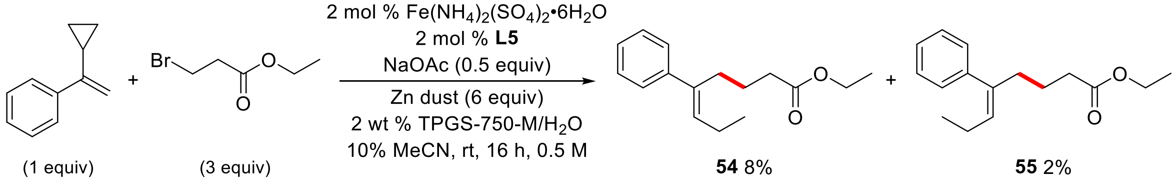

Cyclopropylvinyl)benzene (576.8 mg, 4 mmol), ethyl 3-bromopropanoate (2.17 g, 12 mmol), $Fe(NH_4)_2(SO_4)_2{\cdot}6H_2O$ (32 mg, 0.08 mmol), 3,4,7,8-tetramethyl-1,10-phenanthroline (20 mg, 0.08 mmol), Zn dust (1.56 g, 24 mmol) and NaOAc (164 mg, 2 mmol), in 8 mL 2 wt % TPGS-750-M/H_2O with MeCN (0.8 mL) as co-solvent were reacted at rt for 16 h yielding 98.5 mg (10%) of a mixture with ethyl (*E*)-5-phenyloct-5-enoate (8%) and ethyl (*Z*)-5-phenyloct-5-enoate (2%) as a colorless oil (hexane/Et_2O: 90/10).

^{1}H NMR (500 MHz, $CDCl_3$) δ (*E*) 7.36 – 7.28 (m, 4H), 7.25 – 7.20 (m, 1H), 5.70 (t, *J* = 7.2 Hz, 1H), 4.12 (q, *J* = 7.1 Hz, 2H), 2.58 – 2.53 (m, 2H), 2.28 (t, *J* = 7.4 Hz, 2H), 2.21 (p, *J* = 7.5 Hz, 2H), 1.72 – 1.64 (m, 2H), 1.25 (t, *J* = 7.1 Hz, 3H), 1.07 (t, *J* = 7.5 Hz, 3H). (*Z*) 7.36 – 7.28 (m, 2H), 7.25 – 7.20 (m, 1H), 7.16 – 7.12 (m, 2H), 5.46 (t, *J* = 7.3 Hz, 1H), 4.11

(q, *J* = 7.1 Hz, 2H), 2.37 (t, *J* = 7.4 Hz, 2H), 2.31 – 2.26 (m, 2H), 1.95 (p, *J* = 7.4 Hz, 2H), 1.72 – 1.64 (m, 2H), 1.24 (t, *J* = 7.1 Hz, 3H), 0.93 (t, *J* = 7.5 Hz, 3H).

^{13}C NMR (126 MHz, $CDCl_3$) δ (*E*) 173.65, 142.96, 138.52, 131.75, 128.34, 126.69, 126.41, 60.34, 33.87, 28.91, 23.90, 21.98, 14.52, 14.36. (*Z*) 173.78, 140.98, 139.29, 130.07, 128.50, 128.15, 126.59, 60.28, 38.53, 33.72, 23.50, 22.36, 14.78, 14.36.

HRMS(ESI): Calcd. for $C_{16}H_{22}O_2Na$ $[M+Na]^+$ 269.1518. Found: 269.1522.

d) Radical intermediate trapping test

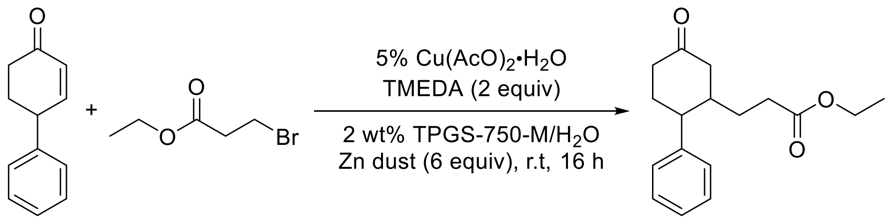

5% Cu(AcO)₂•H₂O
TMEDA (2 equiv)
2 wt% TPGS-750-M/H₂O
Zn dust (6 equiv), r.t, 16 h
Br

GC-MS yield: 3%

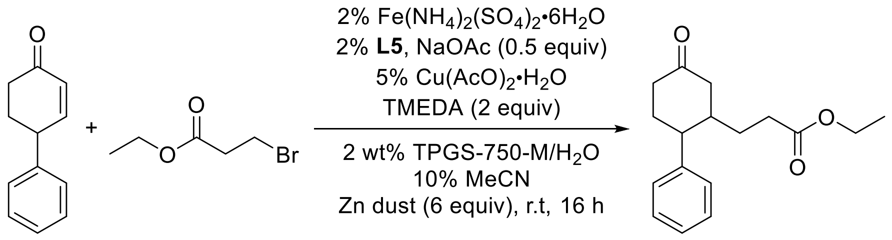

2% Fe(NH₄)₂(SO₄)₂•6H₂O
2% L5, NaOAc (0.5 equiv)
5% Cu(AcO)₂•H₂O
TMEDA (2 equiv)
2 wt% TPGS-750-M/H₂O
10% MeCN
Zn dust (6 equiv), r.t, 16 h
Br

GC-MS yield: 13%

No iron salts. Following the procedure reported in the literature,[9] to 4 mL microwave vial (oven-dried and under Ar) containing a Teflon® stir bar was charged with zinc powder (78 mg, 1.2 mmol), $Cu(OAc)_2 \cdot H_2O$ (2.0 mg, 0.01 mmol, 5 mol %), 4-phenyl-2-cyclohexenone (34.4 mg, 0.2 mmol), and *N,N,N',N'*-tetramethylethylene-diamine (TMEDA, 46.5 mg, 0.4 mmol). The vial was capped with a rubber septum and placed under an argon atmosphere, and 0.4 mL of a 2 wt % TPGS-750-M/H_2O was added *via* syringe followed by the addition of ethyl 3-bromopropanoate (108.6 mg, 0.6 mmol). The resulting mixture was stirred vigorously at rt. After 16 h, EtOAc was added and the mixture was stirred for 2 min at rt. Stirring was then stopped and the organic layer was decanted *via* pipette. The organic layer was passed through a very small silica plug. Yields were determined by GC using naphthalene as internal standard.

With iron salts. To a flame dried 4 mL microwave reaction vial, $(NH_4)_2Fe(SO_4)_2 \cdot 6H_2O$ (1.6 mg, 0.004 mmol), 3,4,7,8-tetramethyl-1,10-phenanthroline (1 mg, 0.004 mmol) and NaOAc (8.2 mg, 0.1 mmol) were mixed together. Then, 0.4 mL of an aqueous solution of 2 wt % TPGS-750-M/H_2O and 0.04 mL MeCN were added to the vial followed by sequential addition of 4-phenyl-2-cyclohexenone (34.4 mg, 0.2 mmol) and Zn dust (<10 µm, ≥98% from Sigma-Aldrich; 78 mg, 1.2 mmol, 6 equiv). After 5 min of stirring, $Cu(OAc)_2 \cdot H_2O$ (2.0 mg, 0.01 mmol, 5 mol %) and TMEDA (46.5 mg, 0.4 mmol) were added to the mixture. The vial was capped with a rubber septum and placed under an argon atmosphere. Ethyl 3-bromopropanoate (108.6 mg, 0.6 mmol, 3 equiv) was added via syringe. The reaction mixture was stirred at rt. After 16 h, EtOAc was added and the mixture was stirred for 2 min at rt. Stirring was then stopped and the organic layer was decanted *via* pipette. The organic layer was passed through a very small silica plug. Yields were determined by GC using naphthalene as internal standard.

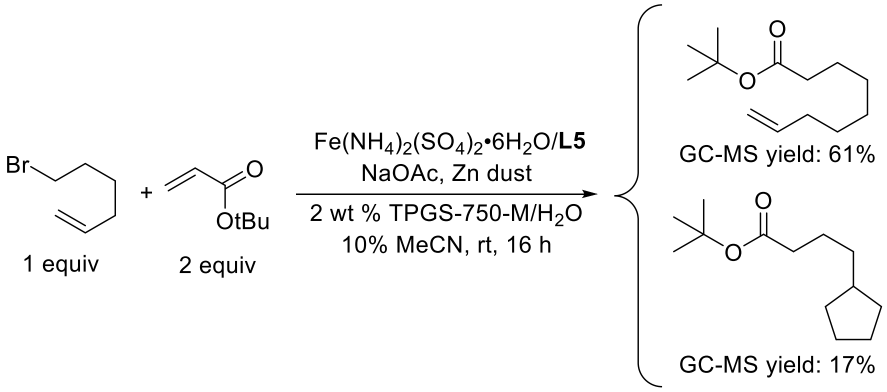
Br
+
O
OtBu
1 equiv
2 equiv
Fe(NH4)2(SO4)2•6H2O/L5
NaOAc, Zn dust
2 wt % TPGS-750-M/H2O
10% MeCN, rt, 16 h
O
O
GC-MS yield: 61%
O
O
GC-MS yield: 17%

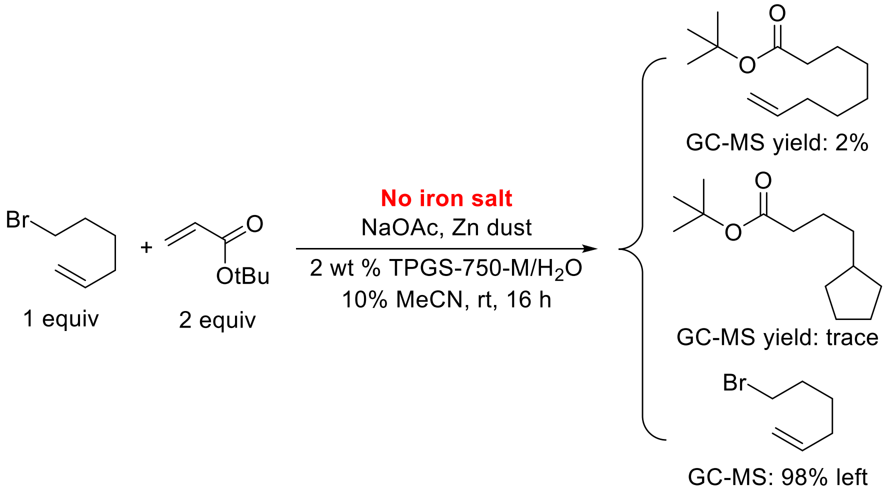
Br
+
O
OtBu
1 equiv
2 equiv
No iron salt
NaOAc, Zn dust
2 wt % TPGS-750-M/H2O
10% MeCN, rt, 16 h
O
O
GC-MS yield: 2%
O
O
GC-MS yield: trace
Br
GC-MS: 98% left

With iron salts. To a flame dried 4 mL microwave reaction vial, 6-bromohex-1-ene (195.7 mg, 1.2 mmol), *t*-butyl acrylate (307.7 mg, 2.4 mmol), $Fe(NH_4)_2(SO_4)_2 \cdot 6H_2O$ (3.2 mg, 0.008 mmol), 3,4,7,8-tetramethyl-1,10-phenanthroline (2 mg, 0.008 mmol), Zn dust (156 mg, 2.4 mmol) and NaOAc (16.4 mg, 0.2 mmol) were added to 0.8 mL 2 wt % TPGS-750-M/H_2O with MeCN (0.08 mL) as co-solvent, and the mixture was vigorously stirred at rt. After 16 h, EtOAc was added and the mixture stirred for 2 min at rt. Stirring was then stopped and the organic layer was decanted *via* pipette. The organic layer was passed through a very small silica plug. Yields were determined by GC using naphthalene as internal standard.

No iron salts. To a flame dried 4 mL microwave reaction vial, 6-bromohex-1-ene (195.7 mg, 1.2 mmol), *t*-butyl acrylate (307.7 mg, 2.4 mmol), Zn dust (156 mg, 2.4 mmol) and

NaOAc (16.4 mg, 0.2 mmol) were added to 0.8 mL 2 wt % TPGS-750-M/H_2O with MeCN (0.08 mL) as co-solvent, and the mixture was vigorously stirred at rt. After 16 h, EtOAc was added and the mixture stirred for 2 min at rt. Stirring was then stopped and the organic layer was decanted *via* pipette. The organic layer was passed through a very small silica plug. Yields were determined by GC using naphthalene as internal standard.

e) Radical scavenger test

2-Vinylpyridine (21 mg, 0.2 mmol), ethyl 3-bromopropanoate (108.6 mg, 0.6 mmol), $Fe(NH_4)_2(SO_4)_2 \cdot 6H_2O$ (1.6 mg, 0.004 mmol), 3,4,7,8-tetramethyl-1,10-phenanthroline (1 mg, 0.004 mmol), Zn dust (78 mg, 1.2 mmol), radical scavenger (0.01 mmol or 0.2 mmol) and NaOAc (8.2 mg, 0.1 mmol), were added to 0.4 mL 2 wt % TPGS-750-M/H_2O with MeCN (0.04 mL) as co-solvent were reacted at rt for 16 h.

2-Vinylpyridine (21 mg, 0.2 mmol), 1-bromoadamantane (129.1 mg, 0.6 mmol), $Fe(NH_4)_2(SO_4)_2 \cdot 6H_2O$ (1.6 mg, 0.004 mmol), 3,4,7,8-tetramethyl-1,10-phenanthroline (1 mg, 0.004 mmol), Zn dust (78 mg, 1.2 mmol), radical scavenger (0.01 mmol or 0.2 mmol) and NaOAc (8.2 mg, 0.1 mmol) were added to 0.4 mL 2 wt % TPGS-750-M/H_2O with MeCN (0.04 mL) as co-solvent were reacted at 45 °C for 16 h.

Analytical data

1-(*t*-Butyl)-4-(5-phenoxypentyl)benzene (1)

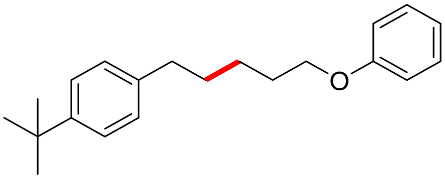

1-(*t*-Butyl)-4-vinylbenzene (32 mg, 0.2 mmol), (3-bromopropoxy)benzene (129.1 mg, 0.6 mmol), $Fe(acac)_3$ (1.4 mg, 0.004 mmol), 3,4,7,8-tetramethyl-1,10-phenanthroline (1 mg, 0.004 mmol), Zn dust (78 mg, 1.2 mmol) and NaCl (70.2 mg, 1.2 mmol), in 0.4 mL 2 wt %

TPGS-750-M/H_2O were reacted at room temperature for 16 hours yielding 44.2 mg (75%) of 1-(*t*-butyl)-4-(5-phenoxypentyl)benzene as a colorless oil (hexane/EtOAc : 95/5).

^{1}H NMR (500 MHz, $CDCl_3$) δ 7.34-7.26 (m, 4H), 7.13 (d, *J* = 8.1 Hz, 2H), 6.94 (t, *J* = 7.3 Hz, 1H), 6.90 (d, *J* = 8.3 Hz, 2H), 3.97 (t, *J* = 6.5 Hz, 2H), 2.63 (t, 2H), 1.90-1.78 (m, 2H), 1.76-1.66 (m, 2H), 1.58-1.49 (m, 3H), 1.32 (s, 9H).

^{13}C NMR (126 MHz, $CDCl_3$) δ 159.2, 148.6, 139.6, 129.5, 128.2, 125.3, 120.6, 114.6, 77.4, 77.2, 76.9, 67.9, 35.5, 34.5, 31.6, 31.4, 29.3, 26.0.

HRMS(EI): Calcd. for $C_{21}H_{28}O$ $[M]^+$ 296.2140. Found: 296.2141.

1-Bromo-4-(5-phenoxypentyl)benzene (2)

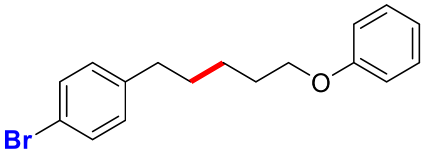

1-Bromo-4-vinylbenzene (36.6 mg, 0.2 mmol), (3-bromopropoxy)benzene (129.1 mg, 0.6 mmol), $Fe(NH_4)_2(SO_4)_2 \cdot 6H_2O$ (8 mg, 0.02 mmol), 3,4,7,8-tetramethyl-1,10-phenanthroline (5 mg, 0.02 mmol), Zn dust (78 mg, 1.2 mmol) and NaOAc (8.2 mg, 0.1 mmol), in 0.4 mL 2 wt % TPGS-750-M/H_2O with MeCN (0.04 mL) as co-solvent were reacted at room temperature for 16 hours yielding 45.5 mg (72%) of 1-bromo-4-(5-phenoxypentyl)benzene as a colorless oil (hexane/EtOAc : 95/5).

^{1}H NMR (500 MHz, $CDCl_3$) δ 7.39 (d, *J* = 6.9 Hz, 2H), 7.31-7.24 (m, 2H), 7.06 (d, *J* = 7.1 Hz, 2H), 6.93 (t, *J* = 7.3 Hz, 1H), 6.89 (d, *J* = 7.7 Hz, 2H), 3.95 (t, *J* = 6.4 Hz, 2H), 2.60 (t, *J* = 7.6 Hz, 2H), 1.91-1.73 (m, 2H), 1.71-1.63 (m, 2H), 1.54-1.45 (m, 2H).

^{13}C NMR (126 MHz, $CDCl_3$) δ 159.2, 141.6, 131.5, 130.3, 129.6, 120.7, 119.5, 114.6, 67.8, 35.4, 31.2, 29.3, 25.8.

HRMS(EI): Calcd. for $C_{17}H_{19}BrO$ $[M]^+$ 318.0619. Found: 318.0611.

1-(5-Phenoxypentyl)-4-(trifluoromethyl)benzene (3)

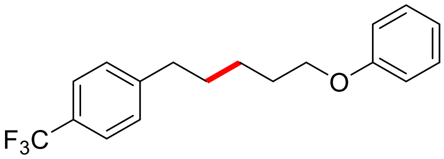

1-(Trifluoromethyl)-4-vinylbenzene (34.4 mg, 0.2 mmol), (3-bromopropoxy)benzene (129.1 mg, 0.6 mmol), $Fe(NH_4)_2(SO_4)_2 \cdot 6H_2O$ (1.6 mg, 0.004 mmol), 3,4,7,8-tetramethyl-1,10-phenanthroline (1 mg, 0.004 mmol), Zn dust (78 mg, 1.2 mmol) and NaOAc (8.2 mg, 0.1 mmol), in 0.4 mL 2 wt % TPGS-750-M/H_2O with MeCN (0.04 mL) as co-solvent were reacted at room temperature for 16 hours yielding 43.5 mg (71%) of 1-(5-phenoxypentyl)-4-(trifluoromethyl)benzene as a slight yellow oil (hexane/EtOAc : 90/10).

^1H NMR (500 MHz, $CDCl_3$) δ 7.53 (d, *J* = 8.0 Hz, 2H), 7.34-7.25 (m, 3H), 6.98-6.86 (m, 4H), 3.96 (t, *J* = 6.4 Hz, 2H), 2.70 (t, *J* = 7.7 Hz, 2H), 1.87-1.77 (m, 2H), 1.76-1.67 (m, 2H), 1.55-1.49 (m, 2H).

^{13}C NMR (126 MHz, $CDCl_3$) δ 159.1, 146.7, 129.6, 128.8, 128.6 (q, $^1J_{(C\text{-}F)}$ = 67 Hz), 125.4 (q, $^1J_{(C\text{-}F)}$ = 3.8 Hz), 124.5 (q, $^1J_{(C\text{-}F)}$ = 272 Hz), 120.7, 114.6, 67.7, 35.8, 31.1, 29.3, 25.9.

^{19}F NMR (376 MHz, $CDCl_3$) δ -62.28.

HRMS(EI): Calcd. for $C_{18}H_{19}F_3O$ $[M]^+$ 308.1388. Found: 308.1385.

Ethyl 5-(4-cyanophenyl)pentanoate (4)

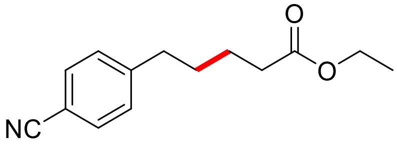

4-Vinylbenzonitrile (25.8 mg, 0.2 mmol), ethyl 3-bromopropanoate (108.6 mg, 0.6 mmol), $Fe(NH_4)_2(SO_4)_2{\cdot}6H_2O$ (1.6 mg, 0.004 mmol), 3,4,7,8-tetramethyl-1,10-phenanthroline (1 mg, 0.004 mmol), Zn dust (78 mg, 1.2 mmol) and NaOAc (8.2 mg, 0.1 mmol), in 0.4 mL 2 wt % TPGS-750-M/H_2O with MeCN (0.04 mL) as co-solvent were reacted at room temperature for 16 hours yielding 36.9 mg (80%) of ethyl 5-(4-cyanophenyl)pentanoate as a slight yellow oil (hexane/EtOAc : 90/10).

^{1}H NMR (500 MHz, $CDCl_3$) δ 7.56 (d, *J* = 8.2 Hz, 2H), 7.27 (d, *J* = 7.9 Hz, 2H), 4.11 (q, *J* = 7.1 Hz, 2H), 2.74-2.62 (m, 2H), 2.38-2.26 (m, 2H), 1.72-1.58 (m, 4H), 1.24 (t, *J* = 7.1 Hz, 3H).

^{13}C NMR (126 MHz, $CDCl_3$) δ 173.5, 147.9, 132.3, 129.3, 119.2, 109.9, 60.5, 35.9, 34.1, 30.4, 24.6, 14.4.

HRMS(EI): Calcd. for $C_{14}H_{17}NO_2$ $[M]^+$ 231.1259. Found: 231.1260.

Ethyl 5-(4-(*t*-butyl)phenyl)pentanoate (5)

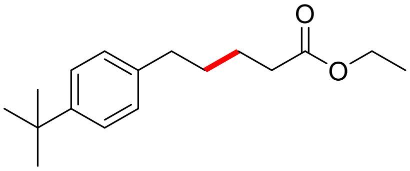

1-(*t*-Butyl)-4-vinylbenzene (32 mg, 0.2 mmol), ethyl 3-bromopropanoate (108.6 mg, 0.6 mmol), $Fe(NH_4)_2(SO_4)_2{\cdot}6H_2O$ (1.6 mg, 0.004 mmol), 3,4,7,8-tetramethyl-1,10-phenanthroline (1 mg, 0.004 mmol), Zn dust (78 mg, 1.2 mmol) and NaOAc (8.2 mg, 0.1 mmol), in 0.4 mL 2 wt % TPGS-750-M/H_2O with MeCN (0.04 mL) as co-solvent were reacted at room temperature for 16 hours yielding 35.1 mg (67%) of ethyl 5-(4-(*tert*-butyl)phenyl)pentanoate as a slight yellow oil (hexane/EtOAc : 90/10).

^{1}H NMR (500 MHz, $CDCl_3$) δ 7.30 (d, *J* = 8.2 Hz, 2H), 7.11 (d, *J* = 8.1 Hz, 2H), 4.12 (q, *J* = 7.1 Hz, 2H), 2.60 (t, *J* = 7.2 Hz, 2H), 2.33 (t, *J* = 7.0 Hz, 2H), 1.74-1.62 (m, 4H), 1.31 (s, 9H), 1.25 (t, *J* = 7.1 Hz, 3H).

^{13}C NMR (126 MHz, $CDCl_3$) δ 173.8, 148.7, 139.2, 128.2, 125.3, 77.4, 77.2, 76.9, 60.4, 35.2, 34.5, 34.4, 31.6, 31.0, 24.8, 14.4.

HRMS(ESI): Calcd. for $C_{17}H_{26}O_2Na$ $[M+Na]^+$ 285.1830. Found: 285.1838.

Ethyl 5-(naphthalen-1-yl)pentanoate (6)

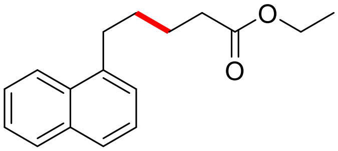

1-Vinylnaphthalene (30.8 mg, 0.2 mmol), ethyl 3-bromopropanoate (108.6 mg, 0.6 mmol), $Fe(NH_4)_2(SO_4)_2\cdot 6H_2O$ (1.6 mg, 0.004 mmol), 3,4,7,8-tetramethyl-1,10-phenanthroline (1 mg, 0.004 mmol), Zn dust (78 mg, 1.2 mmol) and NaOAc (8.2 mg, 0.1 mmol), in 0.4 mL 2 wt % TPGS-750-M/H_2O with MeCN (0.04 mL) as co-solvent were reacted at room temperature for 16 hours yielding 22.9 mg (45%) of ethyl 5-(naphthalen-1-yl)pentanoate as a colorless oil (hexane/EtOAc : 90/10).

^{1}H NMR (500 MHz, $CDCl_3$) δ 7.82-7.74 (m, 3H), 7.63-7.59 (m, 1H), 7.48-7.39 (m, 2H), 7.34-7.30 (m, 1H), 4.13 (q, *J* = 7.1 Hz, 2H), 2.80 (t, *J* = 7.2 Hz, 2H), 2.35 (t, *J* = 7.1 Hz, 2H), 1.80-1.67 (m, 4H), 1.25 (t, *J* = 7.1 Hz, 3H).

^{13}C NMR (126 MHz, $CDCl_3$) δ 173.8, 139.8, 133.8, 132.1, 128.0, 127.7, 127.5, 127.4, 126.5, 126.0, 125.2, 60.4, 35.9, 34.4, 30.9, 24.8, 14.4.

HRMS(ESI): Calcd. for $C_{17}H_{20}O_2Na$ $[M+Na]^+$ 279.1361. Found: 279.1364.

1-Chloro-2-(5-phenoxypentyl)benzene (7)

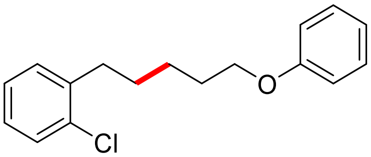

2-Chlorostyrene (27.6 mg, 0.2 mmol), (3-bromopropoxy)benzene (129.1 mg, 0.6 mmol), $Fe(NH_4)_2(SO_4)_2 \cdot 6H_2O$ (1.6 mg, 0.004 mmol), 3,4,7,8-tetramethyl-1,10-phenanthroline (1 mg, 0.004 mmol), Zn dust (78 mg, 1.2 mmol) and NaOAc (8.2 mg, 0.1 mmol), in 0.4 mL 2 wt % TPGS-750-M/H_2O with MeCN (0.04 mL) as co-solvent were reacted at room temperature for 16 hours yielding 40.1 mg (73%) of 1-chloro-2-(5-phenoxypentyl)benzene as a colorless oil (hexane/EtOAc : 90/10).

^{1}H NMR (500 MHz, $CDCl_3$) δ 7.45-7.09 (m, 6H), 7.02-6.87 (m, 3H), 3.98 (t, *J* = 6.5 Hz, 2H), 2.83-2.73 (m, 2H), 1.91-1.81 (m, 2H), 1.76-1.66 (m, 2H), 1.62-1.51 (m, 2H).

^{13}C NMR (126 MHz, $CDCl_3$) δ 159.2, 140.2, 134.0, 130.5, 129.6, 129.6, 127.3, 126.8, 120.6, 114.6, 67.9, 33.7, 29.7, 29.3, 26.0.

HRMS(EI): Calcd. for $C_{17}H_{19}ClO$ $[M]^+$ 274.1125. Found: 274.1123.

Ethyl 5-(3-(benzofuran-2-yl)phenyl)pentanoate (8)

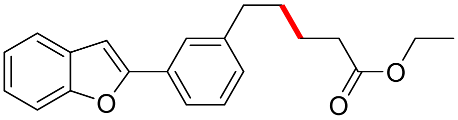

2-(3-Vinylphenyl)benzofuran (44.0 mg, 0.2 mmol), ethyl 3-bromopropanoate (108.6 mg, 0.6 mmol), $Fe(NH_4)_2(SO_4)_2 \cdot 6H_2O$ (1.6 mg, 0.004 mmol), 3,4,7,8-tetramethyl-1,10-phenanthroline (1 mg, 0.004 mmol), Zn dust (78 mg, 1.2 mmol) and NaOAc (8.2 mg, 0.1 mmol), in 0.4 mL 2 wt % TPGS-750-M/H_2O with MeCN (0.04 mL) as co-solvent were reacted at room temperature for 16 hours yielding 30.1 mg (47%) of ethyl 5-(3-(benzofuran-2-yl)phenyl)pentanoate as a colorless oil (hexane/EtOAc : 90/10).

^{1}H NMR (500 MHz, CDCl$_3$) δ 7.73-7.66 (m, 2H), 7.58 (d, *J* = 7.6 Hz, 1H), 7.53 (d, *J* = 8.0 Hz, 1H), 7.36 (t, *J* = 7.9 Hz, 1H), 7.30-7.26 (m, 1H), 7.23 (t, *J* = 7.4 Hz, 1H), 7.17 (d, *J* = 7.4 Hz, 1H), 7.02 (s, 1H), 4.13 (q, *J* = 7.1 Hz, 2H), 2.75-2.65 (m, 2H), 2.40-2.31 (m, 2H), 1.80-1.62 (m, 4H), 1.25 (t, *J* = 7.1 Hz, 3H).

^{13}C NMR (126 MHz, CDCl$_3$) δ 173.8, 156.2, 155.0, 142.9, 130.6, 129.4, 128.9, 128.9, 125.0, 124.3, 123.0, 122.7, 121.0, 111.3, 101.4, 60.4, 35.8, 34.4, 31.0, 24.8, 14.4.

HRMS(ESI): Calcd. for $C_{21}H_{22}O_3Na$ [M+Na]$^+$ 345.1467. Found: 345.1471.

Ethyl 5-(2,4-dimethylphenyl)pentanoate (9)

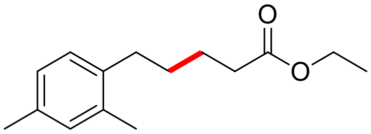

2,4-dimethyl-1-vinylbenzene (26.4 mg, 0.2 mmol), ethyl 3-bromopropanoate (108.6 mg, 0.6 mmol), $Fe(NH_4)_2(SO_4)_2{\cdot}6H_2O$ (1.6 mg, 0.004 mmol), 3,4,7,8-tetramethyl-1,10-phenanthroline (1 mg, 0.004 mmol), Zn dust (78 mg, 1.2 mmol) and NaOAc (8.2 mg, 0.1 mmol), in 0.4 mL 2 wt % TPGS-750-M/H_2O with MeCN (0.04 mL) as co-solvent were reacted at room temperature for 16 hours yielding 28.5 mg (61%) of ethyl 5-(2,4-dimethylphenyl)pentanoate as a yellow oil (hexane/EtOAc : 90/10).

^{1}H NMR (500 MHz, CDCl$_3$) δ 7.04 (dd, *J* = 7.6, 1.8 Hz, 1H), 7.00 – 6.93 (m, 2H), 4.15 (qd, *J* = 7.1, 2.1 Hz, 2H), 2.60 (t, *J* = 8.7 Hz, 2H), 2.36 (td, *J* = 7.5, 2.0 Hz, 2H), 2.31 (s, 3H), 2.29 (s, 3H), 1.74 (p, *J* = 7.4 Hz, 2H), 1.61 (p, *J* = 7.0, 6.5 Hz, 2H), 1.28 (td, *J* = 7.1, 2.1 Hz, 3H).

^{13}C NMR (126 MHz, CDCl$_3$) δ 173.73, 137.38, 135.69, 135.38, 131.07, 128.84, 126.63, 60.31, 34.37, 32.64, 30.01, 25.08, 20.98, 19.29, 14.36.

HRMS(ESI): Calcd. for $C_{15}H_{22}O_2Na$ [M+Na]$^+$ 257.1518. Found: 257.1509.

Ethyl 5-(3-acetylphenyl)pentanoate (10)

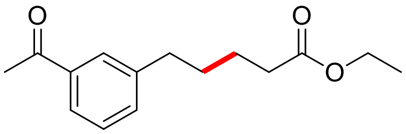

1-(3-Vinylphenyl)ethanone (29.3 mg, 0.2 mmol), ethyl 3-bromopropanoate (108.6 mg, 0.6 mmol), $Fe(NH_4)_2(SO_4)_2 \cdot 6H_2O$ (1.6 mg, 0.004 mmol), 3,4,7,8-tetramethyl-1,10-phenanthroline (1 mg, 0.004 mmol), Zn dust (78 mg, 1.2 mmol) and NaOAc (8.2 mg, 0.1 mmol), in 0.4 mL 2 wt % TPGS-750-M/H_2O with MeCN (0.04 mL) as co-solvent were reacted at room temperature for 16 hours yielding 27.8 mg (56%) of ethyl 5-(3-acetylphenyl)pentanoate as a colorless oil (hexane/EtOAc : 80/20).

^1H NMR (500 MHz, $CDCl_3$) δ 7.80 – 7.73 (m, 2H), 7.41 – 7.33 (m, 2H), 4.11 (q, *J* = 7.1 Hz, 2H), 2.68 (t, *J* = 6.9 Hz, 2H), 2.59 (s, 3H), 2.32 (t, *J* = 6.8 Hz, 2H), 1.67 (p, *J* = 3.7 Hz, 4H), 1.24 (t, *J* = 7.1 Hz, 3H).

^{13}C NMR (126 MHz, $CDCl_3$) δ 198.43, 173.60, 142.79, 137.38, 133.33, 128.65, 128.17, 126.17, 60.37, 35.54, 34.22, 30.87, 26.79, 24.63, 14.35.

HRMS(ESI): Calcd. for $C_{15}H_{20}O_3Na$ $[M+Na]^+$ 271.1310. Found: 271.1322.

Ethyl 5-(2-allylphenyl)pentanoate (11)

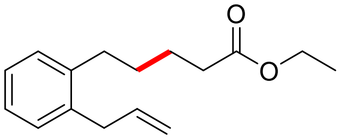

1-Allyl-2-vinylbenzene (28.8 mg, 0.2 mmol), ethyl 3-bromopropanoate (108.6 mg, 0.6 mmol), $Fe(NH_4)_2(SO_4)_2 \cdot 6H_2O$ (1.6 mg, 0.004 mmol), 3,4,7,8-tetramethyl-1,10-phenanthroline (1 mg, 0.004 mmol), Zn dust (78 mg, 1.2 mmol) and NaOAc (8.2 mg, 0.1

mmol) in 0.4 mL 2 wt % TPGS-750-M/H_2O with MeCN (0.04 mL) as co-solvent were reacted at room temperature for 16 hours yielding 30.5 mg (62%) of ethyl 5-(2-allylphenyl)pentanoate as a faint yellow oil (hexane/EtOAc : 90/10).

^{1}H NMR (500 MHz, $CDCl_3$) δ 7.16 (s, 4H), 5.97 (ddt, *J* = 16.5, 10.1, 6.3 Hz, 1H), 5.07 (dq, *J* = 10.1, 1.5 Hz, 1H), 5.01 (dq, *J* = 17.1, 1.7 Hz, 1H), 4.14 (q, *J* = 7.1 Hz, 2H), 3.40 (dt, *J* = 6.3, 1.6 Hz, 2H), 2.69 – 2.59 (m, 2H), 2.34 (t, *J* = 7.4 Hz, 2H), 1.73 (dt, *J* = 14.6, 7.1 Hz, 2H), 1.62 (p, *J* = 7.4 Hz, 2H), 1.26 (t, *J* = 7.1 Hz, 3H).

^{13}C NMR (126 MHz, $CDCl_3$) δ 173.72, 140.37, 137.62, 137.44, 129.75, 129.29, 126.49, 126.22, 115.76, 60.36, 37.16, 34.37, 32.52, 30.56, 25.15, 14.39.

HRMS(ESI): Calcd. for $C_{16}H_{22}O_2Na$ $[M+Na]^+$ 269.1518. Found: 269.1509.

6-(Thiazol-5-yl)-6-(trimethylsilyl)hexyl acetate (12)

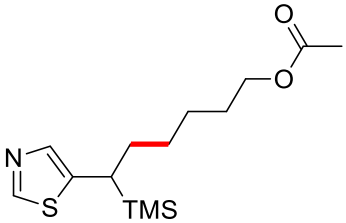

5-(1-(Trimethylsilyl)vinyl)thiazole (36.7 mg, 0.2 mmol), 4-bromobutyl acetate (117 mg, 0.6 mmol), $Fe(NH_4)_2(SO_4)_2{\cdot}6H_2O$ (1.6 mg, 0.004 mmol), 3,4,7,8-tetramethyl-1,10-phenanthroline (1 mg, 0.004 mmol), Zn dust (78 mg, 1.2 mmol) and NaOAc (8.2 mg, 0.1 mmol), in 0.4 mL 2 wt % TPGS-750-M/H_2O with MeCN (0.04 mL) as co-solvent were reacted at room temperature for 16 hours yielding 55.5 mg (93%) of 6-(thiazol-5-yl)-6-(trimethylsilyl)hexyl acetate as a faint yellow oil (hexane/EtOAc : 80/20).

^{1}H NMR (500 MHz, $CDCl_3$) δ 8.56 (s, 1 H), 7.42 (s, 1 H), 3.99 (t, *J* = 7 Hz, 2 H), 2.32 (dd, *J* = 12 Hz, *J* = 3 Hz, 1 H), 2.01 (s, 3 H), 1.74 (m, 1 H), 1.55 (m, 3 H), 1.35 (m, 2 H), 1.23 (m, 2 H), -0.02 (s, 9 H);

^{13}C NMR (126 MHz, CDCl$_3$) δ 171.25, 149.90, 142.18, 138.99, 64.56, 31.69, 28.97, 28.87, 28.52, 25.76, 21.09, -3.02.

HRMS(ESI): Calcd. for $C_{14}H_{26}NO_2SSi$ [M+H]$^+$ 300.1454. Found: 300.1460.

Methyl 5-(5-ethoxy-5-oxopentyl)furan-2-carboxylate (13)

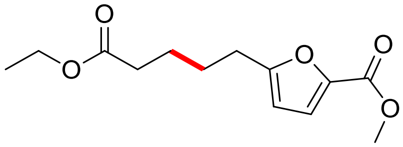

Methyl 5-vinylfuran-2-carboxylate (30.4 mg, 0.2 mmol), ethyl 3-bromopropanoate (108.6 mg, 0.6 mmol), Fe(acac)$_3$ (1.4 mg, 0.004 mmol), 3,4,7,8-tetramethyl-1,10-phenanthroline (1 mg, 0.004 mmol), Zn dust (78 mg, 1.2 mmol) and NaCl (70.2 mg, 1.2 mmol), in 0.4 mL 2 wt % TPGS-750-M/H$_2$O were reacted at room temperature for 16 hours yielding 36.7 mg (72%) of methyl 5-(5-ethoxy-5-oxopentyl)furan-2-carboxylate as a faint yellow oil (hexane/EtOAc : 90/10).

^{1}H NMR (500 MHz, CDCl$_3$) δ 7.05 (m, 1H), 6.11 (m, 1H), 4.08 (q, J = 7.1 Hz, 2H), 3.83 (s, 3H), 2.68 (t, J = 7.0 Hz, 2H), 2.29 (t, J = 7.0 Hz, 2H), 1.73 – 1.60 (m, 4H), 1.21 (t, J = 7.1 Hz, 3H).

^{13}C NMR (126 MHz, CDCl$_3$) δ 173.35, 160.80, 159.25, 143.04, 119.27, 107.84, 60.35, 51.74, 33.95, 28.05, 27.22, 24.43, 14.28.

HRMS(ESI): Calcd. for $C_{13}H_{18}O_5Na$ [M+Na]$^+$ 277.1052. Found: 277.1052.

Ethyl 5-(4-(1-methyl-1H-indazol-5-yl)thiophen-2-yl)pentanoate (14)

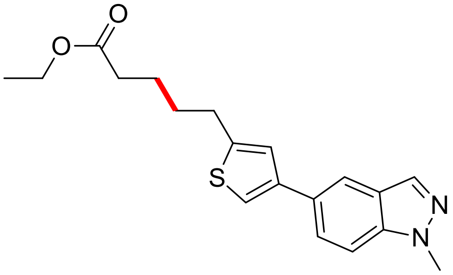

1-Methyl-5-(5-vinylthiophen-3-yl)-1H-indazole (24.0 mg, 0.1 mmol), ethyl 3-bromopropanoate (217.1 mg, 1.2 mmol), Fe(acac)$_3$ (2.8 mg, 0.008 mmol), 3,4,7,8-tetramethyl-1,10-phenanthroline (2 mg, 0.008 mmol), Zn dust (156 mg, 2.4 mmol), 0.1 mL THF and NaCl (140.4 mg, 2.4 mmol), in 0.8 mL 2 wt % TPGS-750-M/H_2O were reacted at 45 °C for 16 hours yielding 19.6 mg (57%) of ethyl 5-(4-(1-methyl-1H-indazol-5-yl)thiophen-2-yl)pentanoate as a white solid (hexane/EtOAc : 80/20).

^{1}H NMR (500 MHz, $CDCl_3$) δ 7.98 (s, 1H), 7.88 (s, 1H), 7.63 (dd, *J* = 8.7, 1.5 Hz, 1H), 7.39 (d, *J* = 8.7 Hz, 1H), 7.21 (d, *J* = 1.4 Hz, 1H), 7.13 (s, 1H), 4.13 (q, *J* = 7.1 Hz, 2H), 4.08 (s, 3H), 2.88 (t, *J* = 6.8 Hz, 2H), 2.36 (t, *J* = 6.9 Hz, 2H), 1.82 – 1.72 (m, 4H), 1.26 (t, *J* = 7.1 Hz, 3H).

^{13}C NMR (126 MHz, $CDCl_3$) δ 173.61, 146.00, 142.15, 139.34, 133.12, 129.25, 125.86, 124.62, 124.00, 118.16, 117.29, 109.25, 60.42, 35.72, 34.19, 31.18, 30.05, 24.56, 14.39.

HRMS(ESI): Calcd. for $C_{19}H_{22}N_2O_2SNa$ $[M+Na]^+$ 365.1300. Found: 365.1313.

6-(Thiazol-5-yl)hexyl acetate (15)

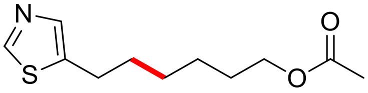

5-Vinylthiazole (22.3 mg, 0.2 mmol), 4-bromobutyl acetate (117 mg, 0.6 mmol), $Fe(NH_4)_2(SO_4)_2\cdot 6H_2O$ (1.6 mg, 0.004 mmol), 3,4,7,8-tetramethyl-1,10-phenanthroline (1 mg, 0.004 mmol), Zn dust (78 mg, 1.2 mmol) and NaOAc (8.2 mg, 0.1 mmol), in 0.4 mL 2 wt %

TPGS-750-M/H_2O with MeCN (0.04 mL) as co-solvent were reacted at room temperature for 16 hours yielding 23.1 mg (51%) of 6-(thiazol-5-yl)hexyl acetate as a faint yellow liquid (hexane/EtOAc : 80/20).

^{1}H NMR (500 MHz, $CDCl_3$) 8.64 (s, 1H), 7.58 (s, 1H), 4.04 (t, *J* = 6.7 Hz, 2H), 2.85 (t, *J* = 7.6 Hz, 2H), 2.04 (s, 3H), 1.69 (p, *J* = 7.4 Hz, 2H), 1.61 (p, *J* = 6.8 Hz, 2H), 1.38 (m, 4H).

^{13}C NMR (126 MHz, $CDCl_3$) δ 171.16, 151.32, 140.26, 139.33, 64.40, 31.49, 28.58, 28.47, 26.61, 25.60, 20.99.

HRMS(ESI): Calcd. for $C_{11}H_{17}NO_2SNa$ $[M+Na]^+$ 250.0878. Found: 250.0867.

Ethyl 5-(2-(piperidin-1-yl)pyrimidin-5-yl)pentanoate (16)

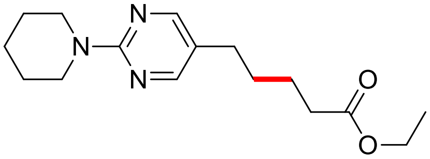

2-(Piperidin-1-yl)-5-vinylpyrimidine (18.9 mg, 0.1 mmol), ethyl 3-bromopropanoate (144.8 mg, 0.8 mmol), Fe(acac)$_3$ (2.8 mg, 0.008 mmol), 3,4,7,8-tetramethyl-1,10-phenanthroline (2 mg, 0.008 mmol), Zn dust (104 mg, 1.6 mmol) and NaCl (140.4 mg, 2.4 mmol), in 0.8 mL 2 wt % TPGS-750-M/H_2O were reacted at 45 °C for 16 hours yielding 16.9 mg (58%) of ethyl 5-(2-(piperidin-1-yl)pyrimidin-5-yl)pentanoate as a faint yellow oil (hexane/EtOAc : 90/10).

^{1}H NMR (500 MHz, $CDCl_3$) δ 8.10 (s, 2H), 4.09 (q, *J* = 7.1 Hz, 2H), 3.74 – 3.68 (m, 4H), 2.39 (t, *J* = 7.4 Hz, 2H), 2.28 (t, *J* = 7.3 Hz, 2H), 1.56 (m, 10H), 1.21 (t, *J* = 7.1 Hz, 3H).

^{13}C NMR (126 MHz, $CDCl_3$) δ 173.49, 161.02, 157.50, 121.75, 60.34, 45.02, 34.15, 30.81, 29.25, 25.80, 24.98, 24.37, 14.34.

HRMS(ESI): Calcd. for $C_{16}H_{25}N_3O_2Na$ $[M+Na]^+$ 314.1844. Found: 314.1842.

t-Butyl 4-(5-ethoxy-5-oxopentyl)-1H-indole-1-carboxylate (17)

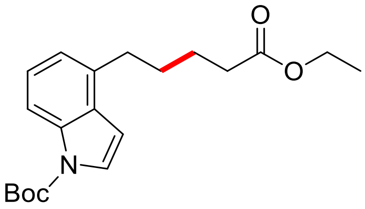

t-Butyl 4-vinyl-1H-indole-1-carboxylate (24.3 mg, 0.1 mmol), ethyl 3-bromopropanoate (217.2 mg, 1.2 mmol), Fe(acac)$_3$ (2.8 mg, 0.008 mmol), 3,4,7,8-tetramethyl-1,10-phenanthroline (2 mg, 0.008 mmol), Zn dust (156 mg, 2.4 mmol) and NaCl (140.4 mg, 2.4 mmol), in 0.8 mL 2 wt % TPGS-750-M/H$_2$O were reacted at room temperature for 16 hours yielding 19.3 mg (56%) of *tert*-butyl 4-(5-ethoxy-5-oxopentyl)-1H-indole-1-carboxylate as a colorless oil (hexane/EtOAc : 90/10).

^{1}H NMR (500 MHz, CDCl$_3$) δ 8.00 (d, *J* = 7.9 Hz, 1H), 7.59 (d, *J* = 3.6 Hz, 1H), 7.26 – 7.21 (m, 1H), 7.04 (d, *J* = 7.3 Hz, 1H), 6.61 (d, *J* = 3.8 Hz, 1H), 4.12 (q, *J* = 7.1 Hz, 2H), 2.88 (t, *J* = 7.1 Hz, 2H), 2.33 (t, *J* = 7.0 Hz, 2H), 1.72 (m, 4H), 1.67 (s, 9H), 1.24 (t, *J* = 7.1 Hz, 3H).

^{13}C NMR (126 MHz, CDCl$_3$) δ 173.74, 149.94, 135.29, 134.67, 129.79, 125.53, 124.39, 122.32, 113.10, 105.56, 83.68, 60.35, 34.34, 32.82, 30.37, 28.33, 24.95, 14.37.

HRMS(ESI): Calcd. for $C_{20}H_{27}NO_4Na$ $[M+Na]^+$ 368.1838. Found: 368.1829.

Ethyl 5-(5-(3,5-dimethylisoxazol-4-yl)furan-2-yl)pentanoate (18)

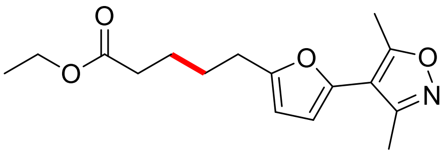

3,5-Dimethyl-4-(5-vinylfuran-2-yl)isoxazole (37.8 mg, 0.2 mmol), ethyl 3-bromopropanoate (108.6 mg, 0.6 mmol), Fe(NH$_4$)$_2$(SO$_4$)$_2$·6H$_2$O (1.6 mg, 0.004 mmol), 3,4,7,8-tetramethyl-1,10-phenanthroline (1 mg, 0.004 mmol), Zn dust (78 mg, 1.2 mmol) and NaOAc (8.2 mg, 0.1 mmol), in 0.4 mL 2 wt % TPGS-750-M/H_2O with MeCN (0.04 mL) as co-solvent were reacted at room temperature for 16 hours yielding 24.4 mg (42%) of ethyl 5-(5-(3,5-dimethylisoxazol-4-yl)furan-2-yl)pentanoate as a faint yellow oil (hexane/EtOAc : 80/20).

^{1}H NMR (500 MHz, $CDCl_3$) δ 6.22 (d, *J* = 3.2 Hz, 1H), 6.07 (d, *J* = 4.0 Hz, 1H), 4.11 (q, *J* = 7.1 Hz, 2H), 2.68 (t, *J* = 6.4 Hz, 2H), 2.54 (s, 3H), 2.37 (s, 3H), 2.33 (t, *J* = 6.9 Hz, 2H), 1.70 (m, 4H), 1.24 (t, *J* = 7.1 Hz, 3H).

^{13}C NMR (126 MHz, $CDCl_3$) δ 173.55, 164.90, 157.74, 155.36, 143.87, 108.58, 107.38, 106.58, 60.40, 34.13, 27.78, 27.59, 24.54, 14.36, 12.49, 11.67.

HRMS(ESI): Calcd. for $C_{16}H_{21}NO_4Na$ $[M+Na]^+$ 314.1368. Found: 314.1365.

Ethyl 5-(2-morpholinopyrimidin-5-yl)pentanoate (19)

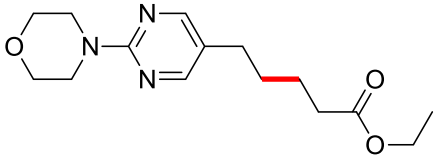

4-(5-Vinylpyrimidin-2-yl)morpholine (19.1 mg, 0.1 mmol), ethyl 3-bromopropanoate (144.8 mg, 0.8 mmol), $Fe(acac)_3$ (2.8 mg, 0.008 mmol), 3,4,7,8-tetramethyl-1,10-phenanthroline (2 mg, 0.008 mmol), Zn dust (104 mg, 1.6 mmol) and NaCl (140.4 mg, 2.4 mmol), in 0.8 mL 2 wt % TPGS-750-M/H_2O were reacted at 45 °C for 16 hours yielding 16.4 mg (56%) of ethyl 5-(2-morpholinopyrimidin-5-yl)pentanoate as a colorless oil (hexane/EtOAc : 80/20).

^{1}H NMR (500 MHz, $CDCl_3$) δ 8.14 (s, 2H), 4.09 (q, *J* = 7.1 Hz, 2H), 3.73 (s, 8H), 2.42 (t, *J* = 7.4 Hz, 2H), 2.29 (t, *J* = 7.3 Hz, 2H), 1.62 (q, *J* = 7.9, 7.1 Hz, 2H), 1.56 (q, *J* = 7.3 Hz, 2H), 1.22 (t, *J* = 7.1 Hz, 3H).

^{13}C NMR (126 MHz, $CDCl_3$) δ 173.44, 161.04, 157.52, 123.13, 66.91, 60.36, 44.51, 34.10, 30.73, 29.26, 24.35, 14.34.

HRMS(ESI): Calcd. for $C_{15}H_{23}N_3O_3Na$ $[M+Na]^+$ 316.1637. Found: 316.1633.

Ethyl 5-(1H-indol-5-yl)pentanoate (20)

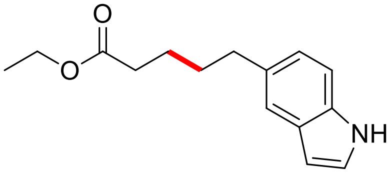

5-Vinyl-1H-indole (14.3 mg, 0.1 mmol), ethyl 3-bromopropanoate (144.8 mg, 0.8 mmol), $Fe(acac)_3$ (2.8 mg, 0.008 mmol), 3,4,7,8-tetramethyl-1,10-phenanthroline (2 mg, 0.008 mmol), Zn dust (156 mg, 2.4 mmol) and NaCl (140.4 mg, 2.4 mmol), in 0.8 mL 2 wt % TPGS-750-M/H_2O were reacted at room temperature for 16 hours yielding 17.9 mg (73%) of ethyl 5-(1H-indol-5-yl)pentanoate as a colorless oil (hexane/EtOAc : 90/10).

^1H NMR (500 MHz, $CDCl_3$) δ 8.14 (s, 1H), 7.45 (s, 1H), 7.30 (d, *J* = 8.3 Hz, 1H), 7.19 – 7.15 (m, 1H), 7.04 (dd, *J* = 8.3, 1.5 Hz, 1H), 6.50 (m, 1H), 4.14 (q, *J* = 7.1 Hz, 2H), 2.74 (t, *J* = 6.9 Hz, 2H), 2.35 (t, *J* = 7.1 Hz, 2H), 1.72 (m, 4H), 1.26 (t, *J* = 7.1 Hz, 3H).

^{13}C NMR (126 MHz, $CDCl_3$) δ 173.98, 134.49, 133.62, 128.17, 124.41, 123.05, 119.91, 110.88, 102.29, 60.33, 35.76, 34.45, 31.80, 24.80, 14.37.

HRMS(ESI): Calcd. for $C_{15}H_{19}NO_2Na$ $[M+Na]^+$ 268.1313. Found: 268.1325.

4-(5-(4-(3-Bromophenyl)piperazin-1-yl)-5-oxopentyl)-N-(3,5-dimethylisoxazol-4-yl)benzamide (21)

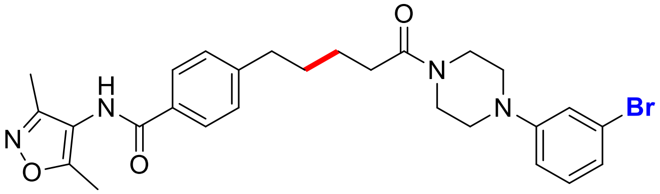

N-(3,5-dimethylisoxazol-4-yl)-4-vinylbenzamide (48.4 mg, 0.2 mmol), 3-bromo-1-(4-(3-bromophenyl)piperazin-1-yl)propan-1-one (225.7 mg, 0.6 mmol), $Fe(NH_4)_2(SO_4)_2{\cdot}6H_2O$ (8 mg, 0.02 mmol), 3,4,7,8-tetramethyl-1,10-phenanthroline (5 mg, 0.02 mmol), Zn dust (78 mg, 1.2 mmol) and NaOAc (8.2 mg, 0.1 mmol), in 0.4 mL 2 wt % TPGS-750-M/H_2O with MeCN (0.04 mL) as co-solvent were reacted at 45 °C for 16 hours yielding 56.2 mg (52%) of 4-(5-(4-(3-bromophenyl)piperazin-1-yl)-5-oxopentyl)-N-(3,5-dimethylisoxazol-4-yl)benzamide as a white solid (hexane/EtOAc : 25/75); mp 164 – 166 °C.

^{1}H NMR (400 MHz, $CDCl_3$) δ 9.17 (s, 1H), 7.84 (d, *J* = 7.7 Hz, 2H), 7.23 (d, *J* = 7.6 Hz, 2H), 7.10 (t, *J* = 7.9 Hz, 1H), 6.98 (d, *J* = 8.4 Hz, 2H), 6.79 (d, *J* = 7.8 Hz, 1H), 3.78 – 3.64 (m, 2H), 3.62 – 3.49 (m, 2H), 3.21 – 2.99 (m, 4H), 2.67 (t, *J* = 7.5 Hz, 2H), 2.36 (t, *J* = 7.5 Hz, 2H), 2.17 (s, 3H), 1.90 (s, 3H), 1.75 – 1.54 (m, 4H).

^{13}C NMR (126 MHz, $CDCl_3$) δ 171.60, 164.81, 162.03, 156.79, 152.10, 147.38, 130.54, 130.39, 128.79, 128.07, 123.32, 123.11, 119.26, 114.96, 103.75, 49.18, 48.88, 45.35, 41.40, 35.69, 33.00, 30.73, 24.73, 10.76, 7.46.

HRMS(ESI): Calcd. for $C_{27}H_{31}BrN_4O_3Na$ $[M+Na]^+$ 561.1477. Found: 561.1473.

2-(5-Phenoxypentyl)pyridine (22)

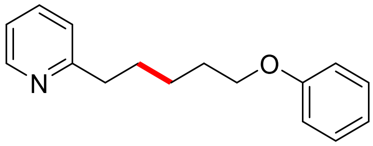

2-Vinylpyridine (21 mg, 0.2 mmol), (3-bromopropoxy)benzene (129.1 mg, 0.6 mmol), $Fe(NH_4)_2(SO_4)_2{\cdot}6H_2O$ (1.6 mg, 0.004 mmol), 3,4,7,8-tetramethyl-1,10-phenanthroline (1 mg, 0.004 mmol), Zn dust (78 mg, 1.2 mmol) and NaOAc (8.2 mg, 0.1 mmol), in 0.4 mL 2 wt % TPGS-750-M/H_2O with MeCN (0.04 mL) as co-solvent were reacted at room temperature for 16 hours yielding 35.5 mg (74%) of 2-(5-phenoxypentyl)pyridine as a slight yellow oil (hexane/EtOAc : 80/20).

^1H NMR (500 MHz, $CDCl_3$) δ 8.52 (d, *J* = 4.2 Hz, 1H), 7.61-7.55 (m, 1H), 7.30-7.23 (m, 2H), 7.17-7.06 (m, 2H), 6.95-6.85 (m, 3H), 3.95 (t, *J* = 6.5 Hz, 2H), 2.83 (t, *J* = 8.0 Hz, 2H), 1.88-1.77 (m, 4H), 1.59-1.50 (m, 2H).

^{13}C NMR (126 MHz, $CDCl_3$) δ 162.2, 159.2, 149.3, 136.5, 129.5, 122.9, 121.1, 120.6, 114.6, 67.8, 38.4, 29.7, 29.3, 26.0.

HRMS(EI): Calcd. for $C_{16}H_{19}NO$ $[M]^+$ 241.1467. Found: 241.1461.

2-(4-Phenylbutyl)pyridine (23)

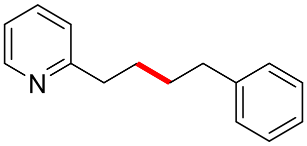

2-Vinylpyridine (21 mg, 0.2 mmol), (2-bromoethyl)benzene (111 mg, 0.6 mmol), $Fe(acac)_3$ (1.4 mg, 0.004 mmol), 3,4,7,8-tetramethyl-1,10-phenanthroline (1 mg, 0.004 mmol), Zn dust (78 mg, 1.2 mmol) and NaCl (70.2 mg, 1.2 mmol), in 0.4 mL 2 wt % TPGS-750-M/H_2O were reacted at room temperature for 16 hours yielding 34.1 mg (81%) of 2-(4-phenylbutyl)pyridine as a slight yellow oil (hexane/EtOAc : 80/20).

^1H NMR (500 MHz, $CDCl_3$) δ 8.60-8.47 (m, 1H), 7.63-7.54 (m, 1H), 7.31-7.23 (m, 2H), 7.22-7.05 (m, 5H), 2.82 (t, *J* = 7.5 Hz, 2H), 2.65 (t, *J* = 7.5 Hz, 2H), 1.85-1.75 (m, 2H), 1.74-1.65 (m, 2H).

^{13}C NMR (126 MHz, $CDCl_3$) δ 162.2, 149.2, 142.6, 136.5, 128.5, 128.4, 125.8, 122.9, 121.1, 38.3, 35.9, 31.3, 29.6.

HRMS(EI): Calcd. for $C_{15}H_{17}N$ $[M]^+$ 211.1361. Found: 211.1351.

Ethyl 5-(pyridin-2-yl)pentanoate (24)

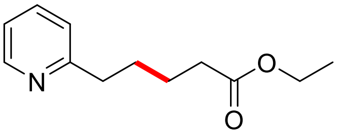

2-Vinylpyridine (21 mg, 0.2 mmol), ethyl 3-bromopropanoate (108.6 mg, 0.6 mmol), $Fe(NH_4)_2(SO_4)_2{\cdot}6H_2O$ (1.6 mg, 0.004 mmol), 3,4,7,8-tetramethyl-1,10-phenanthroline (1 mg, 0.004 mmol), Zn dust (78 mg, 1.2 mmol) and NaOAc (8.2 mg, 0.1 mmol), in 0.4 mL 2 wt % TPGS-750-M/H_2O with MeCN (0.04 mL) as co-solvent were reacted at room temperature for 16 hours yielding 29.1 mg (70%) of ethyl 5-(pyridin-2-yl)pentanoate as a slight yellow oil (hexane/EtOAc : 70/30).

^1H NMR (500 MHz, $CDCl_3$) δ 8.51 (d, *J* = 4.8 Hz, 1H), 7.61-7.55 (m, 1H), 7.13 (d, *J* = 7.8 Hz, 1H), 7.11-7.06 (m, 1H), 4.10 (q, *J* = 7.1 Hz, 2H), 2.80 (t, *J* = 7.6 Hz, 2H), 2.32 (t, *J* = 7.4 Hz, 2H), 1.82-1.72 (m, 2H), 1.72-1.63 (m, 2H), 1.23 (t, *J* = 7.1 Hz, 3H).

^{13}C NMR (126 MHz, $CDCl_3$) δ 173.7, 161.8, 149.2, 136.6, 122.9, 121.2, 60.4, 38.0, 34.3, 29.3, 24.8, 14.4.

HRMS(ESI): Calcd. for $C_{12}H_{18}NO_2$ $[M+H]^+$ 208.1338. Found: 208.1344.

2-(Hex-5-en-1-yl)pyridine (25)

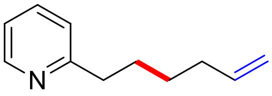

2-Vinylpyridine (21 mg, 0.2 mmol), 4-bromo-1-butene (81 mg, 0.6 mmol), $Fe(NH_4)_2(SO_4)_2{\cdot}6H_2O$ (1.6 mg, 0.004 mmol), 3,4,7,8-tetramethyl-1,10-phenanthroline (1 mg, 0.004 mmol), Zn dust (78 mg, 1.2 mmol) and NaOAc (8.2 mg, 0.1 mmol), in 0.4 mL 2 wt %

TPGS-750-M/H_2O with MeCN (0.04 mL) as co-solvent were reacted at room temperature for 16 hours yielding 21.8 mg (68%) of 2-(hex-5-en-1-yl)pyridine as a slight yellow oil (hexane/EtOAc : 80/20).

^{1}H NMR (500 MHz, $CDCl_3$) δ 8.57-8.47 (m, 1H), 7.63-7.52 (m, 1H), 7.14 (d, *J* = 7.8 Hz, 1H), 7.11-7.05 (m, 1H), 5.87-5.73 (m, 1H), 5.03-4.96 (m, 1H), 4.95-4.89 (m, 1H), 2.79 (t, *J* = 8.0 Hz, 2H), 2.14-2.02 (m, 2H), 1.80-1.69 (m, 2H), 1.52-1.39 (m, 2H).

^{13}C NMR (126 MHz, $CDCl_3$) δ 162.4, 149.2, 138.9, 136.5, 122.9, 121.1, 114.6, 38.3, 33.8, 29.5, 28.8.

HRMS(EI): Calcd. for $C_{11}H_{15}N$ $[M]^+$ 161.1205. Found: 161.1198.

(9H-Fluoren-9-yl)methyl 5-(pyridin-2-yl)pentanoate (26)

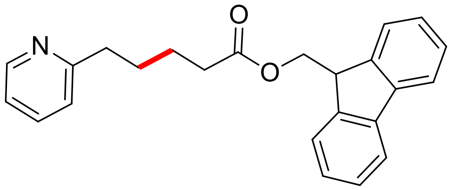

2-Vinylpyridine (21 mg, 0.2 mmol), (9H-fluoren-9-yl)methyl 3-bromopropanoate (198.7 mg, 0.6 mmol), $Fe(NH_4)_2(SO_4)_2\cdot 6H_2O$ (1.6 mg, 0.004 mmol), 3,4,7,8-tetramethyl-1,10-phenanthroline (1 mg, 0.004 mmol), Zn dust (78 mg, 1.2 mmol) and NaOAc (8.2 mg, 0.1 mmol), in 0.4 mL 2 wt % TPGS-750-M/H_2O with MeCN (0.04 mL) as co-solvent were reacted at room temperature for 16 hours yielding 54.3 mg (76%) of (9H-fluoren-9-yl)methyl 5-(pyridin-2-yl)pentanoate as a faint viscous yellow oil (hexane/EtOAc : 80/20).

^{1}H NMR (500 MHz, $CDCl_3$) δ 8.54 (d, *J* = 4 Hz, 1 H), 7.76 (d, *J* = 7.5 Hz, 2 H), 7.57 (m, 3 H), 7.39 (m, 2 H), 7.30 (m, 2 H), 7.12 (m, 2 H), 4.38 (d, *J* = 7 Hz, 2 H), 4.19 (t, *J* = 7 Hz, 1 H), 2.81 (t, *J* = 7 Hz, 2 H), 2.43 (t, *J* = 7 Hz, 2 H), 1.72 (m, 4 H);

^{13}C NMR (126 MHz, $CDCl_3$) δ 173.50, 161.73, 149.30, 143.90, 141.36, 136.38, 127.81, 127.14, 125.07, 122.82, 121.11, 120.07, 66.23, 46.93, 37.97, 34.24, 29.20, 24.65.

HRMS(ESI): Calcd. for $C_{24}H_{24}NO_2$ $[M+H]^+$ 358.1807. Found: 358.1801; $C_{24}H_{23}NO_2Na$ $[M+Na]^+$ 380.1627. Found: 380.1621.

N-(4-Chloro-3-(trifluoromethyl)phenyl)-5-(pyridin-2-yl)pentanamide (27)

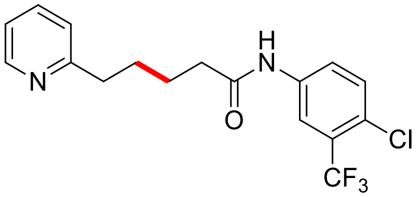

2-Vinylpyridine (21 mg, 0.2 mmol), 3-bromo-*N*-(4-chloro-3-(trifluoromethyl)-phenyl)propanamide (198.3 mg, 0.6 mmol), $Fe(NH_4)_2(SO_4)_2·6H_2O$ (1.6 mg, 0.004 mmol), 3,4,7,8-tetramethyl-1,10-phenanthroline (1 mg, 0.004 mmol), Zn dust (78 mg, 1.2 mmol) and NaOAc (8.2 mg, 0.1 mmol), in 0.4 mL 2 wt % TPGS-750-M/H_2O with MeCN (0.04 mL) as co-solvent were reacted at room temperature for 16 hours yielding 53.6 mg (75%) of *N*-(4-chloro-3-(trifluoromethyl)phenyl)-5-(pyridin-2-yl)pentanamide as a faint yellow oil (hexane/EtOAc : 80/20).

^{1}H NMR (500 MHz, $CDCl_3$) δ 8.64 (s, 1 H), 8.48 (d, J = 5 Hz, 1 H), 7.87 (m, 1 H), 7.76 (m, 1 H), 7.61 (m, 1 H), 7.40 (d, J = 9 Hz, 1 H), 7.17 (d, J = 8 Hz, 1 H), 7.13 (m, 1 H), 2.84 (t, J = 7 Hz, 2 H), 2.41 (t, J = 7 Hz, 2 H), 1.79 (m, 4 H);

^{13}C NMR (126 MHz, $CDCl_3$) δ 172.0, 161.6, 149.0, 137.4, 136.9, 132.0, 128.9 (q, $^1J_{(C-F)}$ = 297 Hz), 128.8 (q, $^1J_{(C-F)}$ = 32 Hz), 124.0, 123.8 (q, $^1J_{(C-F)}$ = 272 Hz), 123.4, 121.5, 119.0 (q, $^1J_{(C-F)}$ = 5.6 Hz), 37.4, 37.1, 28.8, 24.8;

^{19}F NMR (376 MHz, $CDCl_3$) δ -62.83

HRMS(ESI): Calcd. for $C_{17}H_{17}ClF_3N_2O$ $[M+H]^+$ 357.0981. Found: 357.0977.

4-Chlorobenzyl 5-(pyridin-2-yl)pentanoate (28)

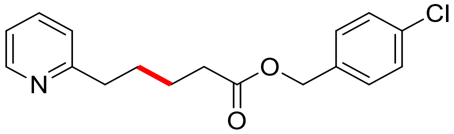

2-Vinylpyridine (21 mg, 0.2 mmol), 4-chlorobenzyl 3-bromopropanoate (166.5 mg, 0.6 mmol), $Fe(NH_4)_2(SO_4)_2{\cdot}6H_2O$ (1.6 mg, 0.004 mmol), 3,4,7,8-tetramethyl-1,10-phenanthroline (1 mg, 0.004 mmol), Zn dust (78 mg, 1.2 mmol) and NaOAc (8.2 mg, 0.1 mmol), in 0.4 mL 2 wt % TPGS-750-M/H_2O with MeCN (0.04 mL) as co-solvent were reacted at room temperature for 16 hours yielding 48.6 mg (80%) of 4-chlorobenzyl 5-(pyridin-2-yl)pentanoate as a faint yellow oil (hexane/EtOAc : 80/20).

^{1}H NMR (500 MHz, $CDCl_3$) δ 8.50 (d, *J* = 4 Hz, 1 H), 7.55 (m, 1 H), 7.29 (m, 2 H), 7.26 (m, 2H), 7.08 (m, 2 H), 5.04 (s, 2 H), 2.77 (t, *J* = 7.5 Hz, 2 H), 2.38 (t, *J* = 7.5 Hz, 2 H), 1.71 (m, 4 H);

^{13}C NMR (126 MHz, $CDCl_3$) δ 173.3, 161.7, 149.3, 136.4, 134.7, 134.1, 129.7, 128.8, 122.8, 121.1, 65.4, 38.0, 34.2, 29.2, 24.7.

HRMS(ESI): Calcd. for $C_{17}H_{18}ClNO_2Na$ $[M+Na]^+$ 326.0924. Found: 326.0916.

6-(Pyridin-2-yl)hexyl acetate (29)

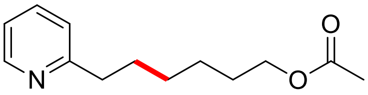

2-Vinylpyridine (21 mg, 0.2 mmol), 4-bromobutyl acetate (117 mg, 0.6 mmol), $Fe(NH_4)_2(SO_4)_2{\cdot}6H_2O$ (1.6 mg, 0.004 mmol), 3,4,7,8-tetramethyl-1,10-phenanthroline (1 mg, 0.004 mmol), Zn dust (78 mg, 1.2 mmol) and NaOAc (8.2 mg, 0.1 mmol), in 0.4 mL 2 wt % TPGS-750-M/H_2O with MeCN (0.04 mL) as co-solvent were reacted at 45 °C for 16 hours yielding 27.4 mg (62%) of 6-(pyridin-2-yl)hexyl acetate as a faint yellow oil (hexane/EtOAc : 80/20).

^{1}H NMR (500 MHz, $CDCl_3$) δ 8.50 (d, *J* = 4 Hz, 1 H), 7.56 (m, 1 H), 7.12 (d, *J* = 8 Hz, 1 H), 7.07 (m, 1 H), 4.02 (t, *J* = 4 Hz, 2 H), 2.76 (t, *J* = 4 Hz, 2 H), 2.01 (s, 3 H), 1.72 (m, 2 H), 1.60 (m, 2 H), 1.37 (m, 4 H);

^{13}C NMR (126 MHz, $CDCl_3$) δ 171.29, 162.32, 149.28, 136.36, 122.78, 121.01, 64.63, 38.37, 29.81, 29.05, 28.60, 25.88, 21.09.

HRMS(ESI): Calcd. for $C_{13}H_{19}NO_2Na$ $[M+Na]^+$ 244.1313. Found: 244.1315.

4-Fluorobenzyl 5-(pyridin-2-yl)pentanoate (30)

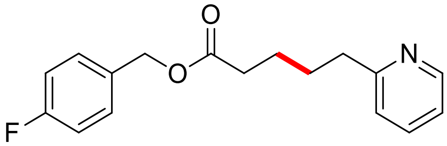

2-Vinylpyridine (21 mg, 0.2 mmol), 4-fluorobenzyl 3-bromopropanoate (156.7 mg, 0.6 mmol), $Fe(NH_4)_2(SO_4)_2·6H_2O$ (1.6 mg, 0.004 mmol), 3,4,7,8-tetramethyl-1,10-phenanthroline (1 mg, 0.004 mmol), Zn dust (78 mg, 1.2 mmol) and NaOAc (8.2 mg, 0.1 mmol), in 0.4 mL 2 wt % TPGS-750-M/H_2O with MeCN (0.04 mL) as co-solvent were reacted at room temperature for 16 hours yielding 36.2 mg (63%) of 4-fluorobenzyl 5-(pyridin-2-yl)pentanoate as a faint yellow oil (hexane/EtOAc : 80/20).

^{1}H NMR (500 MHz, $CDCl_3$) δ 8.51 (s, 1H), 7.56 (td, *J* = 7.7, 1.7 Hz, 1H), 7.31 (dd, *J* = 8.5, 5.4 Hz, 2H), 7.12 – 7.06 (m, 2H), 7.02 (t, *J* = 8.7 Hz, 2H), 5.05 (s, 2H), 2.78 (t, *J* = 7.4 Hz, 2H), 2.38 (t, *J* = 7.3 Hz, 2H), 1.74 (ddt, *J* = 24.0, 15.5, 7.2 Hz, 4H).

^{13}C NMR (126 MHz, $CDCl_3$) δ 173.43, 163.69, 161.79 (d, $^1J_{(C\text{-}F)}$ = 8.8 Hz), 149.37, 136.41, 132.06 (d, $^1J_{(C\text{-}F)}$ = 8.8 Hz), 130.33 (d, $^1J_{(C\text{-}F)}$ = 8.8 Hz), 122.83, 121.14, 115.64 (d, $^1J_{(C\text{-}F)}$ = 21.4 Hz), 65.50, 38.03, 34.22, 29.27, 24.72.

^{19}F NMR (376 MHz, $CDCl_3$) δ -113,81.

HRMS(ESI): Calcd. for $C_{17}H_{19}FNO_2$ $[M+H]^+$ 288.1400. Found: 288.1407.

Ethyl 6-(pyridin-2-yl)hexanoate (31)

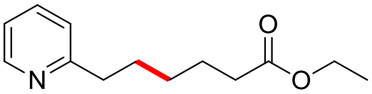

2-Vinylpyridine (21 mg, 0.2 mmol), ethyl 4-bromobutanoate (117 mg, 0.6 mmol), $Fe(NH_4)_2(SO_4)_2{\cdot}6H_2O$ (1.6 mg, 0.004 mmol), 3,4,7,8-tetramethyl-1,10-phenanthroline (1 mg, 0.004 mmol), Zn dust (78 mg, 1.2 mmol) and NaOAc (8.2 mg, 0.1 mmol), in 0.4 mL 2 wt % TPGS-750-M/H_2O with MeCN (0.04 mL) as co-solvent were reacted at room temperature for 16 hours yielding 33.2 mg (75%) of ethyl 6-(pyridin-2-yl)hexanoate as a colorless oil (hexane/EtOAc : 80/20).

^{1}H NMR (500 MHz, $CDCl_3$) δ 8.49 (d, *J* = 4.8 Hz, 1H), 7.55 (td, *J* = 7.7, 1.7 Hz, 1H), 7.10 (d, *J* = 7.8 Hz, 1H), 7.08 – 7.03 (m, 1H), 4.08 (q, *J* = 7.1 Hz, 2H), 2.78 – 2.72 (m, 2H), 2.27 (t, *J* = 7.5 Hz, 2H), 1.72 (p, *J* = 7.7 Hz, 2H), 1.64 (p, *J* = 7.6 Hz, 2H), 1.40 – 1.33 (m, 2H), 1.21 (t, *J* = 7.1 Hz, 3H).

^{13}C NMR (126 MHz, $CDCl_3$) δ 173.80, 162.22, 149.30, 136.32, 122.77, 121.00, 60.25, 38.26, 34.35, 29.57, 28.92, 24.91, 14.33.

HRMS(ESI): Calcd. for $C_{13}H_{19}NO_2$ $[M+H]^+$ 222.1494. Found: 222.1499.

2-(5-((*t*-Butyldimethylsilyl)oxy)pentyl)pyridine (32)

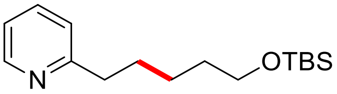

2-Vinylpyridine (21 mg, 0.2 mmol), (3-bromopropoxy)(*t*-butyl)dimethylsilane (152 mg, 0.6 mmol), $Fe(NH_4)_2(SO_4)_2{\cdot}6H_2O$ (1.6 mg, 0.004 mmol), 3,4,7,8-tetramethyl-1,10-

phenanthroline (1 mg, 0.004 mmol), Zn dust (78 mg, 1.2 mmol) and NaOAc (8.2 mg, 0.1 mmol), in 0.4 mL 2 wt % TPGS-750-M/H_2O with MeCN (0.04 mL) as co-solvent were reacted at room temperature for 16 hours yielding 34.1 mg (61%) of 2-(5-((*t*-butyldimethylsilyl)oxy)pentyl)pyridine as a colorless oil (hexane/EtOAc : 80/20).

^{1}H NMR (500 MHz, $CDCl_3$) δ 8.49 (d, *J* = 4.7 Hz, 1H), 7.53 (t, *J* = 7.6 Hz, 1H), 7.10 (d, *J* = 7.8 Hz, 1H), 7.08 – 7.02 (m, 1H), 3.57 (t, *J* = 6.5 Hz, 2H), 2.78 – 2.73 (m, 2H), 1.72 (p, *J* = 7.7 Hz, 2H), 1.53 (p, *J* = 6.7 Hz, 2H), 1.40 – 1.33 (m, 2H), 0.85 (s, 9H), 0.00 (s, 6H).

^{13}C NMR (126 MHz, $CDCl_3$) δ 162.43, 149.30, 136.25, 122.76, 120.92, 63.20, 38.52, 32.82, 29.78, 26.06, 25.71, 18.43, -5.18.

HRMS(ESI): Calcd. for $C_{16}H_{30}ONSi$ $[M+H]^+$ 280.2097. Found: 280.2084.

2-(Hept-6-yn-1-yl)pyridine (33)

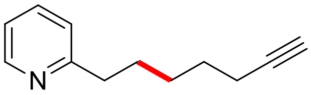

2-Vinylpyridine (21 mg, 0.2 mmol), 5-iodopent-1-yne (116.4 mg, 0.6 mmol), $Fe(NH_4)_2(SO_4)_2{\cdot}6H_2O$ (1.6 mg, 0.004 mmol), 3,4,7,8-tetramethyl-1,10-phenanthroline (1 mg, 0.004 mmol), Zn dust (78 mg, 1.2 mmol) and NaOAc (8.2 mg, 0.1 mmol), in 0.4 mL 2 wt % TPGS-750-M/H_2O with MeCN (0.04 mL) as co-solvent were reacted at room temperature for 16 hours yielding 25.3 mg (73%) of 2-(hept-6-yn-1-yl)pyridine as a faint yellow oil (hexane/EtOAc : 80/20).

^{1}H NMR (500 MHz, $CDCl_3$) δ 8.50 (d, *J* = 4.2 Hz, 1H), 7.56 (t, *J* = 7.6 Hz, 1H), 7.11 (d, *J* = 7.7 Hz, 1H), 7.10 – 7.04 (m, 1H), 2.81 – 2.74 (m, 2H), 2.17 (td, *J* = 6.7, 2.2 Hz, 2H), 1.91 (s, 1H), 1.73 (p, *J* = 7.5 Hz, 2H), 1.56 (p, *J* = 7.1 Hz, 2H), 1.46 (p, *J* = 7.5, 6.9 Hz, 2H).

^{13}C NMR (126 MHz, $CDCl_3$) δ 162.27, 149.34, 136.32, 122.78, 121.01, 84.65, 68.30, 38.36, 29.43, 28.58, 28.43, 18.43.

HRMS(EI): Calcd. for $C_{12}H_{14}N$ $[M-H]^+$ 172.1126. Found: 172.1126.

(*R*)-Benzyl 2-((*t*-butoxycarbonyl)amino)-5-(pyridin-2-yl)pentanoate (34)

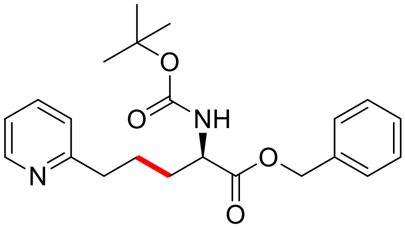

2-Vinylpyridine (21 mg, 0.2 mmol), (S)-benzyl 2-((*t*-butoxycarbonyl)amino)-3-iodopropanoate (243 mg, 0.6 mmol), $Fe(NH_4)_2(SO_4)_2·6H_2O$ (1.6 mg, 0.004 mmol), 3,4,7,8-tetramethyl-1,10-phenanthroline (1 mg, 0.004 mmol), Zn dust (78 mg, 1.2 mmol) and NaOAc (8.2 mg, 0.1 mmol), in 0.8 mL 2 wt % TPGS-750-M/H_2O with MeCN (0.08 mL) as co-solvent were reacted at room temperature for 16 hours yielding 61.5 mg (80%) of (*R*)-benzyl 2-((*t*-butoxycarbonyl)amino)-5-(pyridin-2-yl)pentanoate as a yellow oil (hexane/EtOAc : 50/50).

^{1}H NMR (500 MHz, $CDCl_3$) δ 8.56 – 8.41 (m, 1H), 7.55 (t, *J* = 7.5 Hz, 1H), 7.44 – 7.27 (m, 6H), 7.11 – 7.04 (m, 2H), 5.18 – 5.08 (m, 2H), 4.42 – 4.29 (m, 1H), 2.87 – 2.67 (m, 2H), 1.90 – 1.66 (m, 4H), 1.42 (s, 9H).

^{13}C NMR (126 MHz, $CDCl_3$) δ 172.72, 161.34, 155.51, 149.31, 136.44, 135.55, 128.65, 128.43, 128.32, 122.90, 121.21, 79.89, 67.04, 53.55, 37.60, 32.16, 28.42, 25.42.

HRMS(ESI): Calcd. for $C_{22}H_{29}O_4N_2$ $[M+H]^+$ 385.2127. Found: 385.2139.

Ethyl 5-(5-(trifluoromethyl)pyridin-2-yl)pentanoate (35)

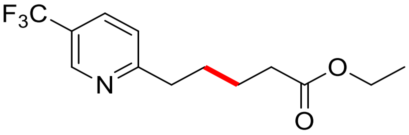

5-(Trifluoromethyl)-2-vinylpyridine (34.6 mg, 0.2 mmol), ethyl 3-bromopropanoate (108.6 mg, 0.6 mmol), $Fe(NH_4)_2(SO_4)_2{\cdot}6H_2O$ (1.6 mg, 0.004 mmol), 3,4,7,8-tetramethyl-1,10-phenanthroline (1 mg, 0.004 mmol), Zn dust (78 mg, 1.2 mmol) and NaOAc (8.2 mg, 0.1 mmol), in 0.4 mL 2 wt % TPGS-750-M/H_2O with MeCN (0.04 mL) as co-solvent were reacted at room temperature for 16 hours yielding 33.1 mg (60%) of ethyl 5-(5-(trifluoromethyl)pyridin-2-yl)pentanoate as a faint yellow oil (hexane/EtOAc : 80/20).

^{1}H NMR (500 MHz, $CDCl_3$) δ 8.77 (s, 1 H), 7.82 (m, 1 H), 7.27 (d, *J* = 10 Hz, 1 H), 4.11 (q, *J* = 5 Hz, 2 H), 2.87 (t, *J* = 8 Hz, 2 H), 2.33 (t, *J* = 8 Hz, 2 H), 1.79 (m, 2 H), 1.68 (m, 2 H), 1.23 (t, *J* = 7 Hz, 3 H);

^{13}C NMR (126 MHz, $CDCl_3$) δ 173.55, 165.98, 146.3 (q, $^1J_{(C\text{-}F)}$ = 2.5 Hz), 133.51 (q, $^1J_{(C\text{-}F)}$ = 3.8 Hz), 124.94 (q, $^1J_{(C\text{-}F)}$ = 270 Hz), 124.5 (q, $^1J_{(C\text{-}F)}$ = 33.8 Hz), 122.58, 60.41, 38.05, 34.18, 28.99, 24.65, 14.35;

^{19}F NMR (376 MHz, $CDCl_3$) δ -62.32.

HRMS(ESI): Calcd. for $C_{13}H_{16}F_3NO_2Na$ $[M+Na]^+$ 298.1031. Found: 298.1030.

2-(5-Phenoxypentyl)-5-(trifluoromethyl)pyridine (36)

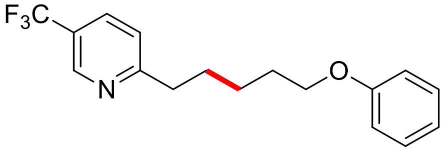

5-(Trifluoromethyl)-2-vinylpyridine (34.6 mg, 0.2 mmol), (3-bromopropoxy)benzene (129.1 mg, 0.6 mmol), $Fe(NH_4)_2(SO_4)_2{\cdot}6H_2O$ (1.6 mg, 0.004 mmol), 3,4,7,8-tetramethyl-1,10-phenanthroline (1 mg, 0.004 mmol), Zn dust (78 mg, 1.2 mmol) and NaOAc (8.2 mg, 0.1 mmol), in 0.4 mL 2 wt % TPGS-750-M/H_2O with MeCN (0.04 mL) as co-solvent were reacted at room temperature for 16 hours yielding 40.0 mg (63%) of 2-(5-phenoxypentyl)-5-(trifluoromethyl)pyridine as a faint yellow oil (hexane/EtOAc : 80/20).

^{1}H NMR (500 MHz, $CDCl_3$) δ 8.80 (s, 1 H), 7.83 (d, *J* = 8 Hz, 1 H), 7.28 (m, 3 H), 6.93 (t, *J* = 7.5 Hz, 1 H), 6.89 (d, *J* = 8.5 Hz, 2 H), 3.96 (t, *J* = 6 Hz, 2 H), 2.90 (t, *J* = 7.5 Hz, 2 H), 1.84 (m, 4 H), 1.56 (m, 2 H);

^{13}C NMR (126 MHz, $CDCl_3$) δ 166.3, 159.1, 146.3 (q, $^1J_{(C\text{-}F)}$ = 4 Hz), 133.5 (q, $^1J_{(C\text{-}F)}$ = 3.4 Hz), 129.5, 125.0 (q, $^1J_{(C\text{-}F)}$ = 270 Hz), 124.1 (q, $^1J_{(C\text{-}F)}$ = 32.6 Hz), 122.6, 120.7, 114.6, 67.7, 38.4, 29.4, 29.2, 25.9;

^{19}F NMR (376 MHz, $CDCl_3$) δ -62.25.

HRMS(EI): Calcd. for $C_{17}H_{18}F_3NO$ $[M]^+$ 309.1341. Found: 309.1342.

N-(4-Chloro-3-(trifluoromethyl)phenyl)-5-(5-(trifluoromethyl)pyridin-2-yl)pentanamide (37)

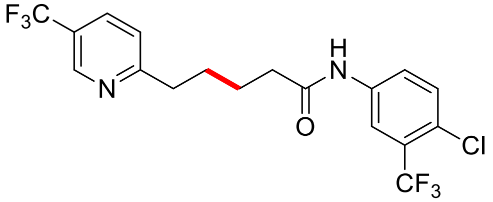

5-(Trifluoromethyl)-2-vinylpyridine (34.6 mg, 0.2 mmol), 3-bromo-*N*-(4-chloro-3-(trifluoromethyl)phenyl)propanamide (198.3 mg, 0.6 mmol), $Fe(NH_4)_2(SO_4)_2\cdot 6H_2O$ (1.6 mg, 0.004 mmol), 3,4,7,8-tetramethyl-1,10-phenanthroline (1 mg, 0.004 mmol), Zn dust (78 mg, 1.2 mmol) and NaOAc (8.2 mg, 0.1 mmol), in 0.4 mL 2 wt % TPGS-750-M/H_2O with MeCN (0.04 mL) as co-solvent were reacted at room temperature for 16 hours yielding 56.9 mg (67%) of *N*-(4-chloro-3-(trifluoromethyl)phenyl)-5-(5-(trifluoromethyl)pyridin-2-yl)pentanamide as a faint yellow oil (hexane/EtOAc : 70/30).

^{1}H NMR (500 MHz, $CDCl_3$) δ 8.75 (s, 1 H), 8.06 (br, 1 H), 7.83 (m, 2 H), 7.73 (d, *J* = 8.5 Hz, 1H) , 7.40 (d, *J* = 8.5 Hz, 1 H), 7.28 (d, *J* = 8.5 Hz, 1 H), 2.90 (t, *J* = 8 Hz, 2H), 2.42 (t, *J* = 7 Hz, 2H), 1.79 (m, 4H);

^{13}C NMR (126 MHz, CDCl$_3$) δ 171.6, 165.7, 146.2 (q, $^1J_{(C\text{-}F)}$ = 4.2 Hz), 137.0, 133.8 (q, $^1J_{(C\text{-}F)}$ = 3.4 Hz), 132.1, 128.9 (q, $^1J_{(C\text{-}F)}$ = 32 Hz), 126.9 (q, $^1J_{(C\text{-}F)}$ = 252 Hz), 124.7 (q, $^1J_{(C\text{-}F)}$ = 32.9 Hz), 124.2 (q, $^1J_{(C\text{-}F)}$ = 186 Hz), 123.9, 123.7 (q, $^1J_{(C\text{-}F)}$ = 272 Hz), 122.9, 118.9 (q, $^1J_{(C\text{-}F)}$ = 5.4 Hz), 37.7, 37.2, 28.7, 24.8;

^{19}F NMR (376 MHz, CDCl$_3$) δ -62.10, -62.66.

HRMS(ESI): Calcd. for $C_{18}H_{15}ClF_6N_2ONa$ $[M+Na]^+$ 447.0675. Found: 447.0681.

2-Methyl-3-(5-phenoxypentyl)pyridine (38)

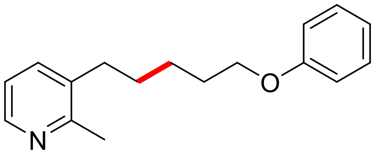

2-Methyl-3-vinylpyridine (23.8 mg, 0.2 mmol), (3-bromopropoxy)benzene (129.1 mg, 0.6 mmol), $Fe(NH_4)_2(SO_4)_2\cdot 6H_2O$ (1.6 mg, 0.004 mmol), 3,4,7,8-tetramethyl-1,10-phenanthroline (1 mg, 0.004 mmol), Zn dust (78 mg, 1.2 mmol) and NaOAc (8.2 mg, 0.1 mmol), in 0.4 mL 2 wt % TPGS-750-M/H_2O with MeCN (0.04 mL) as co-solvent were reacted at room temperature for 16 hours yielding 33.8 mg (66%) of 2-methyl-3-(5-phenoxypentyl)pyridine as a light yellow oil (hexane/EtOAc : 80/20).

^{1}H NMR (500 MHz, CDCl$_3$) δ 8.40-8.31 (m, 1H), 7.45 (d, J = 7.4 Hz, 1H), 7.33-7.22 (m, 2H), 7.15-7.05 (m, 1H), 6.94 (t, J = 7.4 Hz, 1H), 6.89 (d, J = 7.9 Hz, 2H), 3.97 (t, J = 6.4 Hz, 2H), 2.64 (t, J = 7.8 Hz, 2H), 2.57 (s, 3H), 1.89-1.80 (m, 2H), 1.71-1.62 (m, 2H), 1.62-1.52 (m, 2H).

^{13}C NMR (126 MHz, CDCl$_3$) δ 159.1, 156.4, 146.1, 137.0, 136.1, 129.6, 121.6, 120.7, 114.6, 67.7, 32.7, 29.6, 29.3, 26.2, 22.0.

HRMS(EI): Calcd. for $C_{17}H_{21}NO$ $[M]^+$ 255.1623. Found: 255.1626.

Ethyl 5-(2-methylpyridin-3-yl)pentanoate (39)

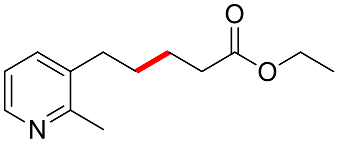

2-Methyl-3-vinylpyridine (23.8 mg, 0.2 mmol), ethyl 3-bromopropanoate (108.6 mg, 0.6 mmol), $Fe(NH_4)_2(SO_4)_2\cdot6H_2O$ (1.6 mg, 0.004 mmol), 3,4,7,8-tetramethyl-1,10-phenanthroline (1 mg, 0.004 mmol), Zn dust (78 mg, 1.2 mmol) and NaOAc (8.2 mg, 0.1 mmol), in 0.4 mL 2 wt % TPGS-750-M/H_2O with MeCN (0.04 mL) as co-solvent were reacted at room temperature for 16 hours yielding 29.9 mg (68%) of ethyl 5-(2-methylpyridin-3-yl)pentanoate as a faint yellow liquid (hexane/ EtOAc : 80/20).

^{1}H NMR (500 MHz, $CDCl_3$) δ 8.32 (d, *J* = 4.7 Hz, 1H), 7.38 (d, *J* = 8 Hz, 1H), 7.04 (m, 1H), 4.12 (q, *J* = 7.1 Hz, 2H), 2.61 (t, *J* = 7.8 Hz, 2H), 2.52 (s, 3H), 2.34 (t, *J* = 7.3 Hz, 2H), 1.70 (p, *J* = 7.3 Hz, 2H), 1.61 (p, *J* = 7.5, 7.0 Hz, 2H), 1.24 (t, *J* = 7.1 Hz, 3H).

^{13}C NMR (126 MHz, $CDCl_3$) δ 173.42, 156.51, 146.60, 136.20, 135.21, 121.23, 60.30, 34.09, 32.38, 29.16, 24.76, 22.14, 14.24.

HRMS(ESI): Calcd. for $C_{13}H_{20}NO_2$ $[M+H]^+$ 222.1494. Found: 222.1487.

(9H-Fluoren-9-yl)methyl 5-(2-fluoropyridin-4-yl)pentanoate (40)

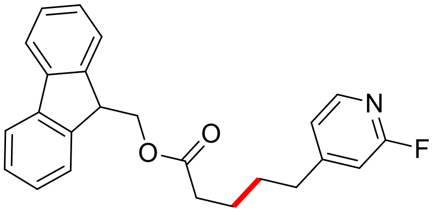

2-Fluoro-4-vinylpyridine (24.6 mg, 0.2 mmol), (9H-fluoren-9-yl)methyl 3-bromopropanoate (198.7 mg, 0.6 mmol), $Fe(NH_4)_2(SO_4)_2\cdot6H_2O$ (1.6 mg, 0.004 mmol), 3,4,7,8-tetramethyl-1,10-phenanthroline (1 mg, 0.004 mmol), Zn dust (78 mg, 1.2 mmol) and NaOAc (8.2 mg, 0.1 mmol), in 0.4 mL 2 wt % TPGS-750-M/H_2O with MeCN (0.04 mL) as co-solvent were reacted at room temperature for 16 hours yielding 57.7 mg (76%) of (9H-fluoren-9-yl)methyl 5-(2-fluoropyridin-4-yl)pentanoate as a colorless oil (hexane/EtOAc : 80/20).

^{1}H NMR (500 MHz, $CDCl_3$) δ 8.10 (d, *J* = 5.1 Hz, 1H), 7.76 (d, *J* = 7.6 Hz, 2H), 7.58 (d, *J* = 7.5 Hz, 2H), 7.40 (t, *J* = 7.4 Hz, 2H), 7.31 (td, *J* = 7.5, 1.1 Hz, 2H), 6.97 (d, *J* = 5.1 Hz, 1H), 6.72 (s, 1H), 4.44 (d, *J* = 6.8 Hz, 2H), 4.20 (t, *J* = 6.8 Hz, 1H), 2.62 (t, *J* = 7.0 Hz, 2H), 2.39 (t, *J* = 6.9 Hz, 2H), 1.63 (m, 4H).

^{13}C NMR (126 MHz, $CDCl_3$) δ 173.11, 165.07 (d, $^1J_{(C\text{-}F)}$ = 239.4 Hz), 157.01 (d, $^1J_{(C\text{-}F)}$ = 7.6 Hz), 147.41 (d, $^1J_{(C\text{-}F)}$ = 16.4 Hz), 143.75, 141.34, 127.80, 127.08, 124.89, 121.60 (d, $^1J_{(C\text{-}F)}$ = 3.8 Hz), 120.04, 109.20 (d, $^1J_{(C\text{-}F)}$ = 36.5), 66.07, 46.89, 34.73 (d, $^1J_{(C\text{-}F)}$ = 2.5 Hz), 33.90, 29.28, 24.32.

^{19}F NMR (376 MHz, $CDCl_3$) δ -69.07.

HRMS(ESI): Calcd. for $C_{24}H_{22}FNO_2Na$ $[M+Na]^+$ 398.1532. Found: 398.1544.

(9H-Fluoren-9-yl)methyl 5-(5-(4-(trifluoromethoxy)phenyl)pyridin-2-yl)pentanoate (41)

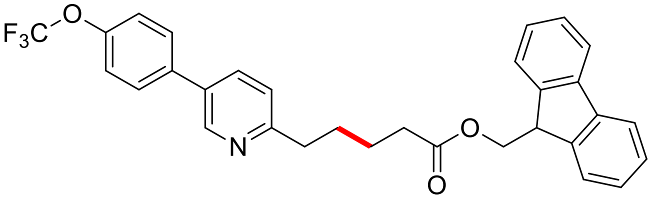

5-(4-(Trifluoromethoxy)phenyl)-2-vinylpyridine (53.1 mg, 0.2 mmol), (9H-fluoren-9-yl)methyl 3-bromopropanoate (198.7 mg, 0.6 mmol), $Fe(NH_4)_2(SO_4)_2 \cdot 6H_2O$ (1.6 mg, 0.004 mmol), 3,4,7,8-tetramethyl-1,10-phenanthroline (1 mg, 0.004 mmol), Zn dust (78 mg, 1.2 mmol) and NaOAc (8.2 mg, 0.1 mmol), in 0.4 mL 2 wt % TPGS-750-M/H_2O with MeCN (0.04 mL) as co-solvent were reacted at room temperature for 16 hours yielding 62.3 mg

(60%) of (9H-fluoren-9-yl)methyl 5-(5-(4-(trifluoromethoxy)phenyl)pyridin-2-yl)pentanoate as a colorless oil (hexane/EtOAc : 80/20).

^{1}H NMR (500 MHz, $CDCl_3$) δ 8.74 (s, 1 H), 7.75 (m, 3 H), 7.58 (m, 4 H), 7.40 (t, *J* = 7.4 Hz, 2 H), 7.31 (m, 4 H), 7.23 (d, *J* = 8 Hz, 1 H), 4.40 (d, *J* = 7 Hz, 2 H), 4.20 (t, *J* = 7 Hz, 1 H), 2.87 (t, *J* = 7.5 Hz, 2 H), 2.46 (t, *J* = 7.3 Hz, 2 H), 1.82 (m, 4 H).

^{13}C NMR (126 MHz, CDC_3) δ 173.51, 161.11, 149.15 (q, $^1J_{(C-F)}$ = 1.7 Hz), 147.60, 143.92, 141.41, 136.71, 134.85, 132.88, 128.47, 127.86, 127.17, 125.62 (q, $^1J_{(C-F)}$ = 413 Hz), 125.10, 122.85, 121.59, 120.11, 119.57, 66.28, 46.97, 37.63, 34.26, 29.20, 24.68.

^{19}F NMR (376 MHz, CDCl3) δ -57.84.

HRMS(ESI): Calcd. for $C_{31}H_{27}F_3NO_3$ $[M+H]^+$ 518.1943. Found: 518.1954.

2-(2-Cyclopentylethyl)pyridine (42)

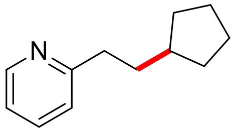

2-Vinylpyridine (21 mg, 0.2 mmol), bromocyclopentane (89.4 mg, 0.6 mmol), $Fe(NH_4)_2(SO_4)_2\cdot 6H_2O$ (1.6 mg, 0.004 mmol), 3,4,7,8-tetramethyl-1,10-phenanthroline (1 mg, 0.004 mmol), Zn dust (78 mg, 1.2 mmol) and NaOAc (8.2 mg, 0.1 mmol), in 0.4 mL 2 wt % TPGS-750-M/H_2O with MeCN (0.04 mL) as co-solvent were reacted at room temperature for 16 hours yielding 27.1 mg (77%) of 2-(2-cyclopentylethyl)pyridine as a faint yellow oil (hexane/EtOAc : 80/20).

^{1}H NMR (500 MHz, $CDCl_3$) δ 8.53 – 8.46 (m, 1H), 7.54 (t, *J* = 8.4 Hz, 1H), 7.11 (d, *J* = 7.8 Hz, 1H), 7.09 – 7.02 (m, 1H), 2.81 – 2.74 (m, 2H), 1.81 – 1.68 (m, 5H), 1.64 – 1.54 (m, 2H), 1.54 – 1.43 (m, 2H), 1.13 (m, 2H).

^{13}C NMR (126 MHz, $CDCl_3$) δ 162.78, 149.27, 136.27, 122.70, 120.87, 40.04, 37.81, 36.47, 32.73, 25.32.

HRMS(ESI): Calcd. For $C_{12}H_{18}N$ $[M+H]^+$ 176.1439. Found: 176.1435.

2-(2-Cyclohexylethyl)pyridine (43)

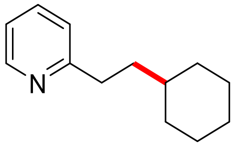

2-Vinylpyridine (21 mg, 0.2 mmol), bromocyclohexane (98 mg, 0.6 mmol), $Fe(NH_4)_2(SO_4)_2\cdot 6H_2O$ (1.6 mg, 0.004 mmol), 3,4,7,8-tetramethyl-1,10-phenanthroline (1 mg, 0.004 mmol), Zn dust (78 mg, 1.2 mmol) and NaOAc (8.2 mg, 0.1 mmol), in 0.4 mL 2 wt % TPGS-750-M/H_2O with MeCN (0.04 mL) as co-solvent were reacted at room temperature for 16 hours yielding 27.0 mg (71%) of 2-(2-cyclohexylethyl)pyridine as a slight yellow oil (hexane/EtOAc : 80/20).

^{1}H NMR (500 MHz, $CDCl_3$) δ 8.58-8.47 (m, 1H), 7.57 (t, *J* = 7.6 Hz, 1H), 7.13 (d, *J* = 7.7 Hz, 1H), 7.10-7.04 (m, 1H), 2.78 (t, *J* = 8.0 Hz, 2H), 1.82-1.53 (m, 7H), 1.34-1.07 (m, 4H), 1.01-0.86 (m, 2H).

^{13}C NMR (126 MHz, $CDCl_3$) δ 163.0, 149.2, 136.4, 122.8, 120.9, 37.8, 37.7, 36.0, 33.4, 26.8, 26.5.

HRMS(EI): Calcd. for $C_{13}H_{19}N$ $[M]^+$ 189.1517. Found: 189.1508.

2-(3-Methylpentyl)pyridine (44)

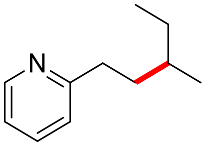

2-Vinylpyridine (21 mg, 0.2 mmol), 2-bromobutane (82.2 mg, 0.6 mmol), $Fe(NH_4)_2(SO_4)_2 \cdot 6H_2O$ (1.6 mg, 0.004 mmol), 3,4,7,8-tetramethyl-1,10-phenanthroline (1 mg, 0.004 mmol), Zn dust (78 mg, 1.2 mmol) and NaOAc (8.2 mg, 0.1 mmol), in 0.4 mL 2 wt % TPGS-750-M/H_2O with MeCN (0.04 mL) as co-solvent were reacted at room temperature for 16 hours yielding 24.3 mg (74%) of 2-(3-methylpentyl)pyridine as a faint yellow oil (hexane/EtOAc : 80/20).

^{1}H NMR (500 MHz, $CDCl_3$) δ 8.51 (d, *J* = 4.7 Hz, 1H), 7.56 (td, *J* = 7.7, 1.8 Hz, 1H), 7.13 (d, *J* = 7.8 Hz, 1H), 7.11 – 7.04 (m, 1H), 2.81 (ddd, *J* = 13.6, 10.8, 5.6 Hz, 1H), 2.73 (ddd, *J* = 13.6, 10.6, 5.9 Hz, 1H), 1.74 (ddt, *J* = 13.3, 10.8, 5.5 Hz, 1H), 1.52 (dddd, *J* = 13.2, 10.7, 7.4, 5.7 Hz, 1H), 1.43 – 1.38 (m, 2H), 1.19 (dt, *J* = 14.9, 7.5 Hz, 1H), 0.93 (d, *J* = 6.3 Hz, 3H), 0.87 (t, *J* = 7.2 Hz, 3H).

^{13}C NMR (126 MHz, $CDCl_3$) δ 162.98, 149.32, 136.33, 122.72, 120.90, 36.95, 36.28, 34.46, 29.49, 19.20, 11.46.

HRMS(EI): Calcd. For $C_{11}H_{17}N$ $[M]^+$ 163.1361. Found: 163.1360.

2-(2-(Tetrahydro-2H-pyran-4-yl)ethyl)pyridine (45)

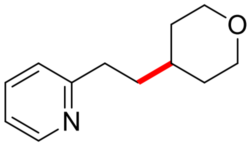

2-Vinylpyridine (21 mg, 0.2 mmol), 4-bromotetrahydropyran (99 mg, 0.6 mmol), $Fe(NH_4)_2(SO_4)_2 \cdot 6H_2O$ (1.6 mg, 0.004 mmol), 3,4,7,8-tetramethyl-1,10-phenanthroline (1 mg, 0.004 mmol), Zn dust (78 mg, 1.2 mmol) and NaOAc (8.2 mg, 0.1 mmol), in 0.4 mL 2 wt % TPGS-750-M/H_2O with MeCN (0.04 mL) as co-solvent were reacted at room temperature for 16 hours yielding 23.4 mg (61%) of 2-(2-(tetrahydro-2H-pyran-4-yl)ethyl)pyridine as a colorless oil (hexane/EtOAc : 50/50).

^{1}H NMR (500 MHz, CDCl$_3$) δ 8.55 – 8.44 (m, 1H), 7.55 (td, *J* = 7.7, 1.7 Hz, 1H), 7.21 – 7.03 (m, 2H), 3.92 (dd, *J* = 10.8, 3.2 Hz, 2H), 3.33 (td, *J* = 11.9, 1.8 Hz, 2H), 2.81 – 2.74 (m, 2H), 1.69 – 1.60 (m, 4H), 1.50 (dtt, *J* = 14.1, 6.9, 3.2 Hz, 1H), 1.30 (qd, *J* = 12.2, 4.4 Hz, 2H).

^{13}C NMR (126 MHz, CDCl$_3$) δ 162.27, 149.31, 136.38, 122.69, 121.03, 68.12, 37.02, 35.35, 34.86, 33.11.

HRMS(EI): Calcd. For $C_{12}H_{17}NO$ $[M]^+$ 191.1310. Found: 191.1310.

(±)-2-(4,4-Diethoxy-3-methylbutyl)pyridine (46)

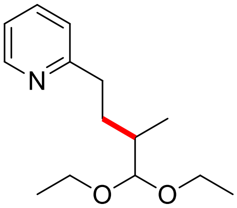

2-Vinylpyridine (21 mg, 0.2 mmol), 2-bromo-1,1-diethoxypropane (126.7 mg, 0.6 mmol), $Fe(NH_4)_2(SO_4)_2 \cdot 6H_2O$ (1.6 mg, 0.004 mmol), 3,4,7,8-tetramethyl-1,10-phenanthroline (1 mg, 0.004 mmol), Zn dust (78 mg, 1.2 mmol) and NaOAc (8.2 mg, 0.1 mmol), in 0.4 mL 2 wt % TPGS-750-M/H_2O with MeCN (0.04 mL) as co-solvent were reacted at 45 °C for 16 hours yielding 36.2 mg (76%) of (±)-2-(4,4-diethoxy-3-methylbutyl)pyridine as a colorless oil (hexane/EtOAc : 80/20).

^{1}H NMR (500 MHz, CDCl$_3$) δ 8.45 (d, *J* = 4.0 Hz, 1H), 7.51 (td, *J* = 7.6, 1.6 Hz, 1H), 7.10 (d, *J* = 7.8 Hz, 1H), 7.01 (dd, *J* = 7.3, 5.0 Hz, 1H), 4.16 (d, *J* = 6.1 Hz, 1H), 3.66 – 3.52 (m, 2H), 3.48 – 3.35 (m, 2H), 2.84 (ddd, *J* = 13.7, 10.7, 5.4 Hz, 1H), 2.69 (ddd, *J* = 13.7, 10.4, 6.3 Hz, 1H), 1.97 – 1.87 (m, 1H), 1.79 – 1.69 (m, 1H), 1.56 – 1.43 (m, 1H), 1.13 (td, *J* = 7.0, 1.6 Hz, 6H), 0.94 (d, *J* = 6.8 Hz, 3H).

^{13}C NMR (126 MHz, $CDCl_3$) δ 162.52, 149.18, 136.22, 122.65, 120.87, 106.85, 62.28, 62.26, 36.32, 35.98, 32.10, 15.35, 14.47.

HRMS(ESI): Calcd. For $C_{14}H_{23}NO_2Na$ $[M+Na]^+$ 260.1627. Found: 260.1626.

t-Butyl 4-(2-(pyridin-2-yl)ethyl)piperidine-1-carboxylate (47)

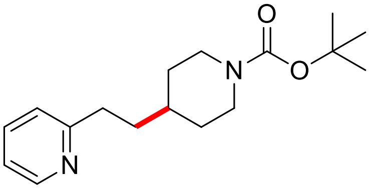

2-Vinylpyridine (21 mg, 0.2 mmol), 1-*N*-Boc-4-bromopiperidine (158.5 mg, 0.6 mmol), $Fe(NH_4)_2(SO_4)_2\cdot 6H_2O$ (1.6 mg, 0.004 mmol), 3,4,7,8-tetramethyl-1,10-phenanthroline (1 mg, 0.004 mmol), Zn dust (78 mg, 1.2 mmol) and NaOAc (8.2 mg, 0.1 mmol), in 0.4 mL 2 wt % TPGS-750-M/H_2O with MeCN (0.04 mL) as co-solvent were reacted at room temperature for 16 hours yielding 41 mg (71%) of *tert*-butyl 4-(2-(pyridin-2-yl)ethyl)piperidine-1-carboxylate as a yellow oil (hexane/EtOAc : 70/30).

^1H NMR (500 MHz, $CDCl_3$) δ 8.42 (d, *J* = 3.0 Hz, 1H), 7.48 (td, *J* = 7.6, 1.9 Hz, 1H), 7.04 (d, *J* = 7.8 Hz, 1H), 6.99 (dd, *J* = 6.9, 4.3 Hz, 1H), 3.99 (br, 2H), 2.75 – 2.68 (m, 2H), 2.58 (br, 2H), 1.68 – 1.54 (m, 4H), 1.36 (s, 10H), 1.10 – 1.00 (m, 2H).

^{13}C NMR (126 MHz, $CDCl_3$) δ 162.07, 154.78, 149.16, 136.24, 122.56, 120.90, 79.05, 43.95 (br), 36.46, 35.72, 35.44, 32.02 (br), 28.42.

HRMS(ESI): Calcd. For $C_{17}H_{27}N_2O_2$ $[M+H]^+$ 291.2072. Found: 291.2068.

3-Methyl-5-(pyridin-2-yl)pentanenitrile (48)

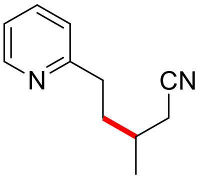

2-Vinylpyridine (21 mg, 0.2 mmol), 3-bromobutanenitrile (88.8 mg, 0.6 mmol), $Fe(NH_4)_2(SO_4)_2 \cdot 6H_2O$ (1.6 mg, 0.004 mmol), 3,4,7,8-tetramethyl-1,10-phenanthroline (1 mg, 0.004 mmol), Zn dust (78 mg, 1.2 mmol) and NaOAc (8.2 mg, 0.1 mmol), in 0.4 mL 2 wt % TPGS-750-M/H_2O with MeCN (0.04 mL) as co-solvent were reacted at room temperature for 16 hours yielding 21.5 mg (62%) of 3-methyl-5-(pyridin-2-yl)pentanenitrile as a yellow oil (hexane/EtOAc : 70/30).

^{1}H NMR (500 MHz, $CDCl_3$) δ 8.47 (d, *J* = 4.3 Hz, 1H), 7.63 – 7.46 (m, 1H), 7.19 – 6.97 (m, 2H), 2.86 – 2.68 (m, 2H), 2.30 (qd, *J* = 16.7, 5.9 Hz, 2H), 1.93 – 1.78 (m, 2H), 1.75 – 1.64 (m, 1H), 1.09 (d, *J* = 6.5 Hz, 3H).

^{13}C NMR (126 MHz, $CDCl_3$) δ 161.08, 149.29, 136.55, 122.74, 121.29, 118.74, 35.76, 35.51, 30.11, 24.44, 19.34.

HRMS(ESI): Calcd. For $C_{11}H_{14}N_2Na$ $[M+Na]^+$ 197.1051. Found: 197.1055.

2-(2-(Adamantan-1-yl)ethyl)pyridine (49)

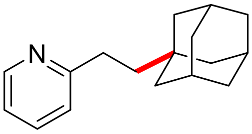

2-Vinylpyridine (21 mg, 0.2 mmol), 1-bromoadamantane (129.1 mg, 0.6 mmol), $Fe(NH_4)_2(SO_4)_2 \cdot 6H_2O$ (1.6 mg, 0.004 mmol), 3,4,7,8-tetramethyl-1,10-phenanthroline (1 mg, 0.004 mmol), Zn dust (78 mg, 1.2 mmol) and NaOAc (8.2 mg, 0.1 mmol), in 0.4 mL 2 wt % TPGS-750-M/H_2O with MeCN (0.04 mL) as co-solvent were reacted at 45 °C for 16 hours yielding 30.4 mg (63%) of 2-(2-(adamantan-1-yl)ethyl)pyridine as a colorless oil (hexane/EtOAc : 80/20).

^{1}H NMR (500 MHz, CDCl$_3$) δ 8.51 (d, *J* = 5.7 Hz, 1H), 7.57 (td, *J* = 7.7, 1.8 Hz, 1H), 7.14 (d, *J* = 7.8 Hz, 1H), 7.11 – 7.04 (m, 1H), 2.78 – 2.69 (m, 2H), 1.97 (s, 3H), 1.72 (d, *J* = 12.0 Hz, 3H), 1.65 (d, *J* = 11.2 Hz, 3H), 1.56 (d, *J* = 2.4 Hz, 6H), 1.51 – 1.45 (m, 2H).

^{13}C NMR (126 MHz, CDCl$_3$) δ 163.62, 149.31, 136.39, 122.78, 120.85, 44.93, 42.55, 37.38, 32.60, 32.00, 28.92.

HRMS(ESI): Calcd. For $C_{17}H_{24}N$ $[M+H]^+$ 242.1909. Found: 242.1900.

2-(3,3-Dimethylbutyl)pyridine (50)

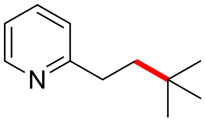

2-Vinylpyridine (21 mg, 0.2 mmol), 2-bromo-2-methylpropane (82.2 mg, 0.6 mmol), $Fe(NH_4)_2(SO_4)_2\cdot 6H_2O$ (1.6 mg, 0.004 mmol), 3,4,7,8-tetramethyl-1,10-phenanthroline (1 mg, 0.004 mmol), Zn dust (78 mg, 1.2 mmol) and NaOAc (8.2 mg, 0.1 mmol), in 0.4 mL 2 wt % TPGS-750-M/H_2O with MeCN (0.04 mL) as co-solvent were reacted at 45 °C for 16 hours yielding 20.2 mg (62%) of 2-(3,3-dimethylbutyl)pyridine as a colorless oil (hexane/EtOAc : 80/20).

Spectral data matched that in the reported literature.[10] ^{1}H NMR (500 MHz, CDCl$_3$) δ 8.51 (d, *J* = 4.8 Hz, 1H), 7.57 (td, *J* = 7.6, 1.4 Hz, 1H), 7.14 (d, *J* = 7.8 Hz, 1H), 7.07 (dd, *J* = 7.3, 5.0 Hz, 1H), 2.79 – 2.72 (m, 2H), 1.64 – 1.58 (m, 2H), 0.97 (s, 9H).

^{13}C NMR (126 MHz, CDCl$_3$) δ 163.32, 149.33, 136.41, 122.72, 120.90, 44.46, 34.07, 30.47, 29.48.

References

1. Lipshutz, B. H.; Ghorai, S.; Abela, A. R.; Moser, R.; Nishikata, T.; Duplais, C.; Krasovskiy, A.; Gaston, R. D.; Gadwood, R. C. TPGS-750-M: A Second-Generation Amphiphile for Metal-Catalyzed Cross-Couplings in Water at Room Temperature. *J. Org. Chem.* **2011**, *76*, 4379.

2. Gottlieb, H. E.; Kotlyar, V.; Nudelman, A. NMR Chemical Shifts of Common Laboratory Solvents as Trace Impurities. *J. Org. Chem.* **1997**, *62*, 7512.

3. Lipshutz, B. H.; Petersen, T. B.; Abela, A. R. Room-Temperature Suzuki−Miyaura Couplings in Water Facilitated by Nonionic Amphiphiles. *Org. Lett.* **2008**, *10*, 1333.

4. Zhang, J.-z.; Tang, Y. Iron-Catalyzed Regioselective Oxo- and Hydroxy-Phthalimidation of Styrenes: Access to α-Hydroxyphthalimide Ketones. *Adv. Synth. Catal.* **2016**, *358*, 752.

5. Dick, G. R.; Knapp, D. M.; Gillis, E. P.; Burke, M. D. General Method for Synthesis of 2-Heterocyclic N-Methyliminodiacetic Acid Boronates. *Org. Lett.* **2010**, *12*, 2314.

6. Isley, N. A.; Wang, Y.; Gallou, F.; Handa, S.; Aue, D. H.; Lipshutz, B. H. A Micellar Catalysis Strategy for Suzuki–Miyaura Cross-Couplings of 2-Pyridyl MIDA Boronates: No Copper, in Water, Very Mild Conditions. *ACS Catal.* **2017**, *7*, 8331.

7. Strauch, R. C.; Mastarone, D. J.; Sukerkar, P. A.; Song, Y.; Ipsaro, J. J.; Meade, T. J. Reporter Protein-Targeted Probes for Magnetic Resonance Imaging. *J. Am. Chem. Soc.* **2011**, *133*, 16346.

8. Kristensen, S. K.; Laursen, S. L. R.; Taarning, E.; Skrydstrup, T. Ex Situ Formation of Methanethiol: Application in the Gold(I)-Promoted Anti-Markovnikov Hydrothiolation of Olefins. *Angew. Chem., Int. Ed.* **2018**, *57*, 13887.

9. Lipshutz, B. H.; Huang, S.; Leong, W. W. Y.; Zhong, G.; Isley, N. A. C–C Bond Formation via Copper-Catalyzed Conjugate Addition Reactions to Enones in Water at Room Temperature. *J. Am. Chem. Soc.* **2012**, *134*, 19985.

10. Lewis, J. C.; Bergman, R. G.; Ellman, J. A. Rh(I)-Catalyzed Alkylation of Quinolines and Pyridines via C−H Bond Activation. *J. Am. Chem. Soc.* **2007**, *129*, 5332.

NMR spectra

^1H NMR (500 MHz, $CDCl_3$), ^{13}C NMR (126 MHz, $CDCl_3$)

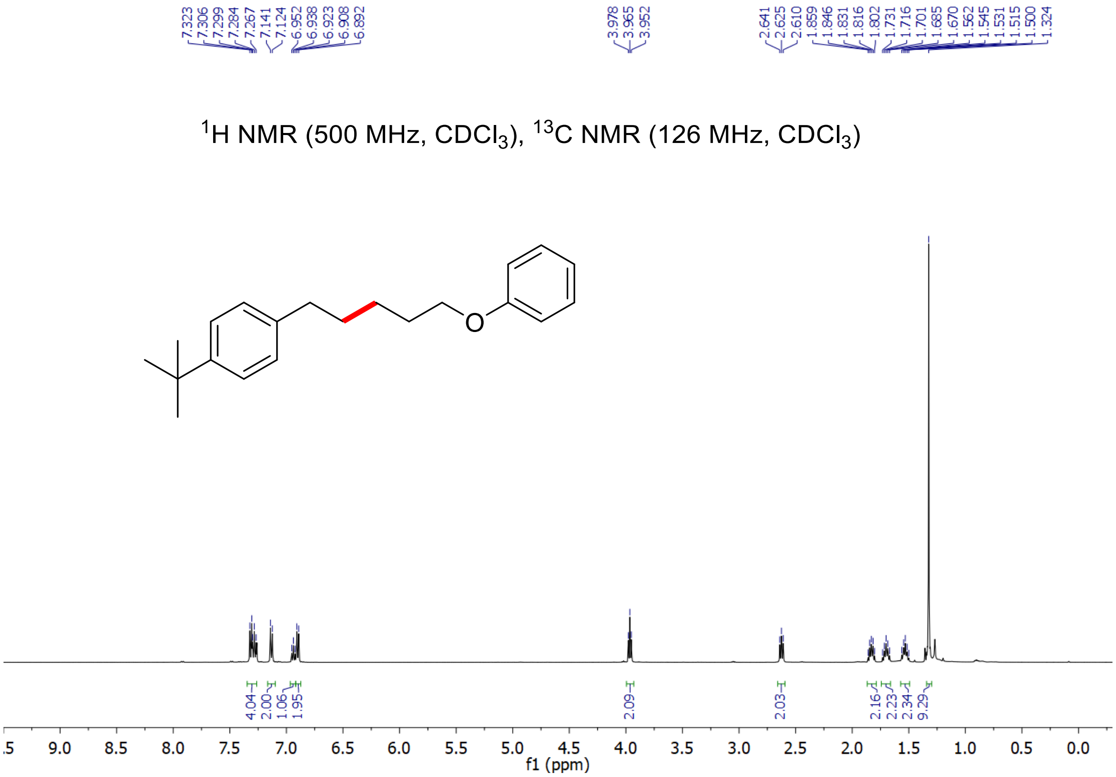

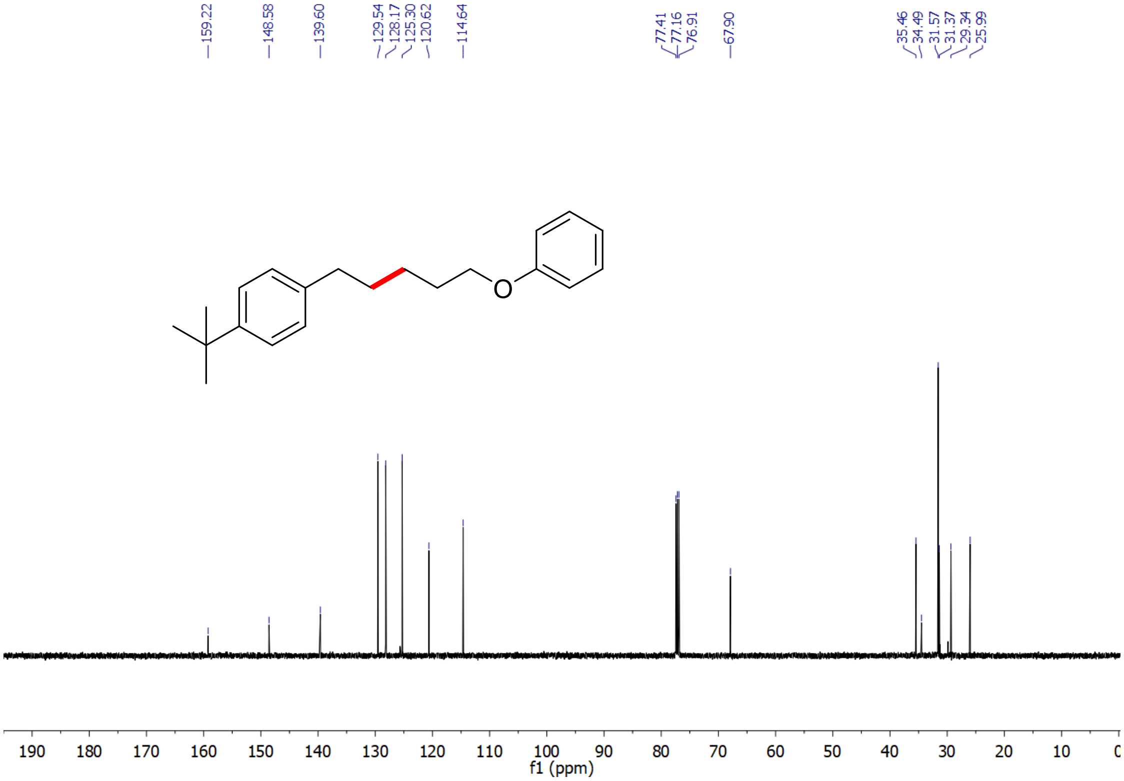

^{1}H NMR (500 MHz, CDCl$_3$), ^{13}C NMR (126 MHz, CDCl$_3$)

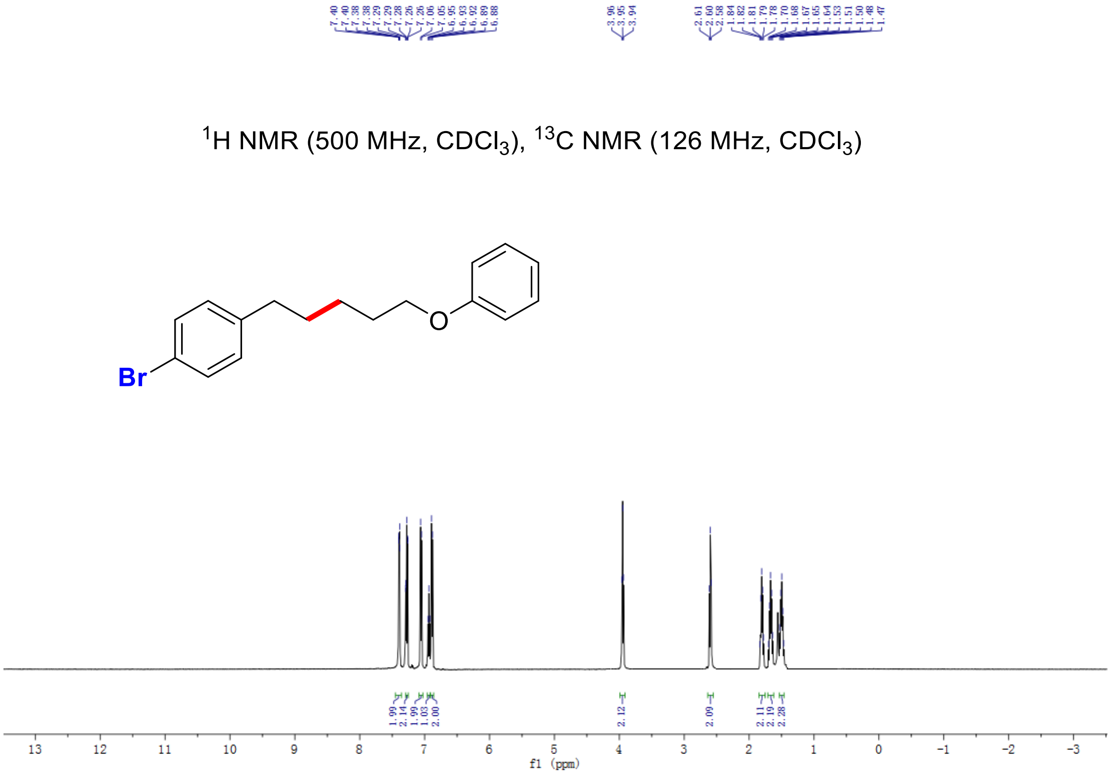

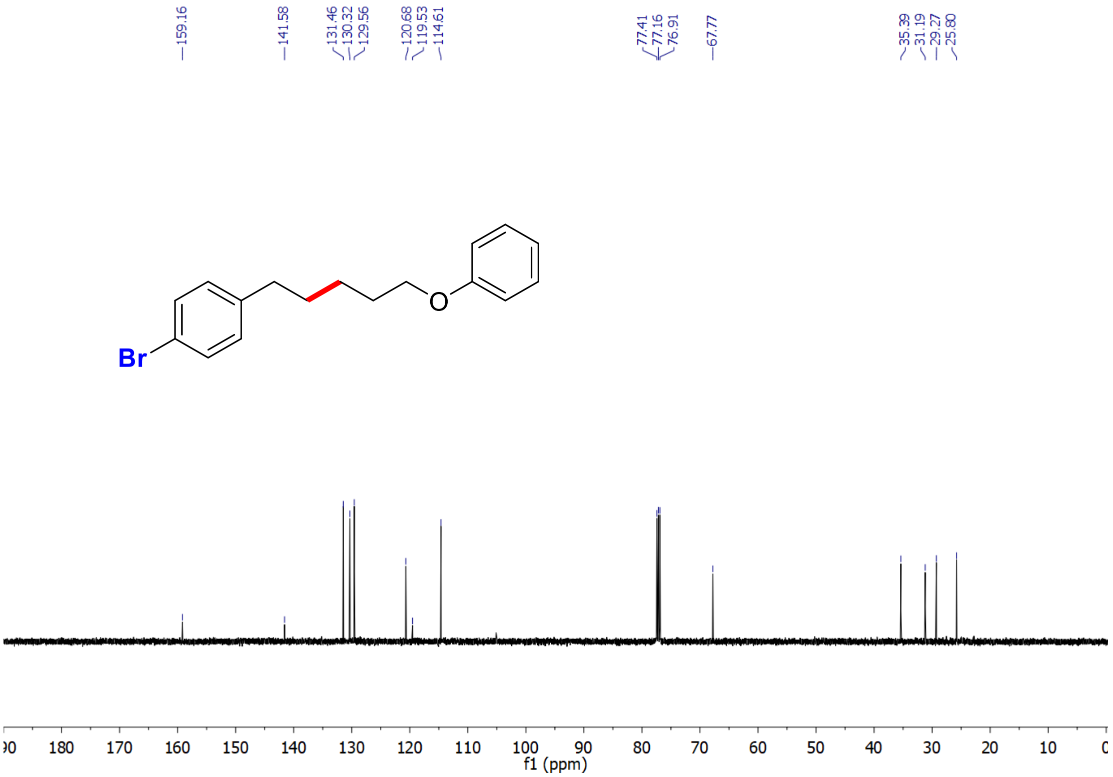

^{1}H NMR (500 MHz, CDCl$_3$), ^{13}C NMR (126 MHz, CDCl$_3$), ^{19}F NMR (376 MHz, CDCl$_3$)

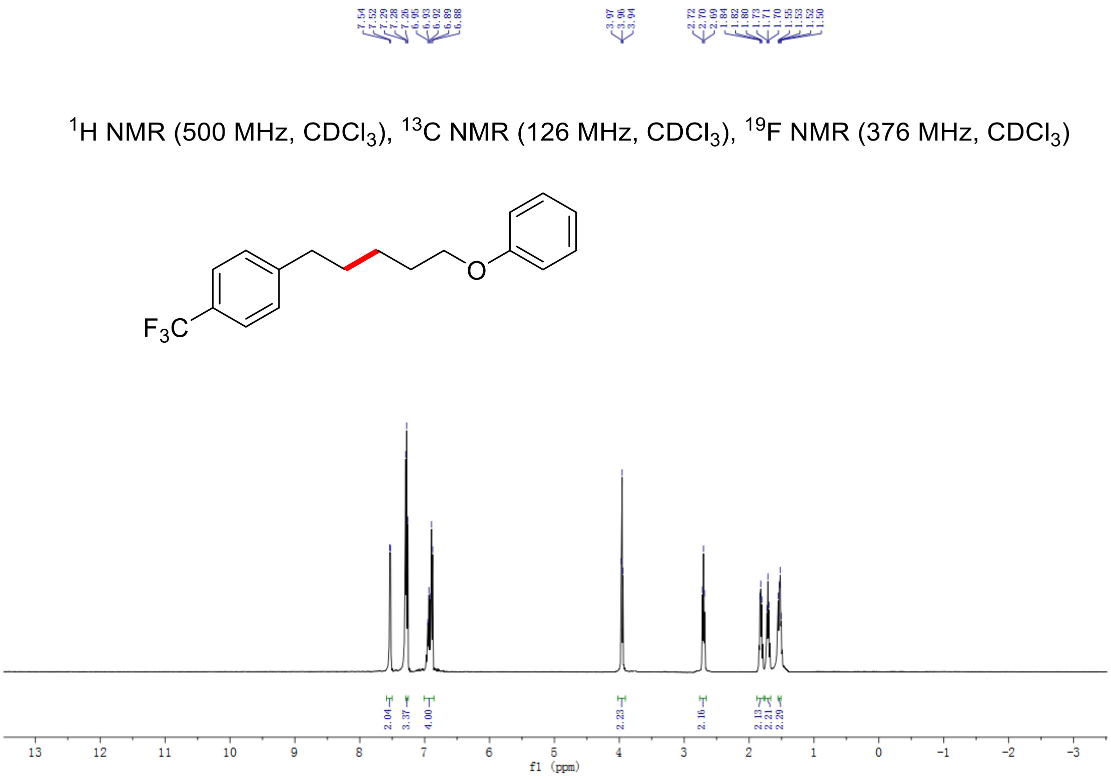

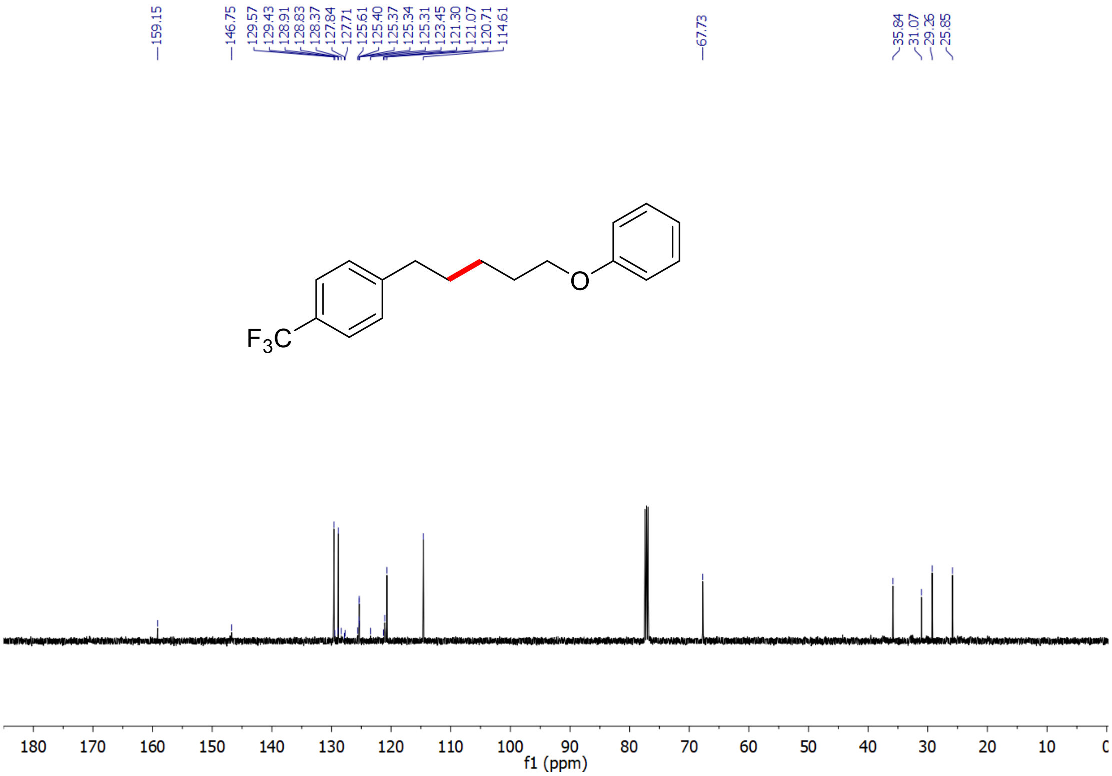

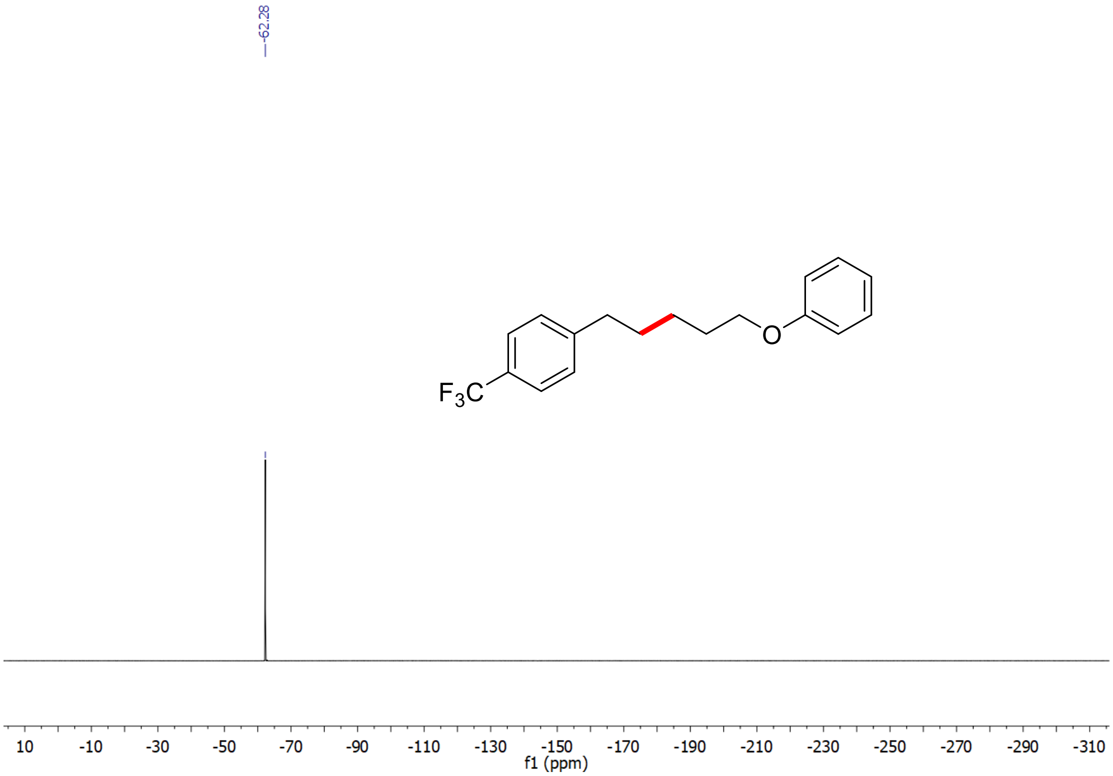

-62.28
F3C
O
10
-10
-30
-50
-70
-90
-110
-130
-150
-170
-190
-210
-230
-250
-270
-290
-310
f1 (ppm)

^{1}H NMR (500 MHz, CDCl$_3$), ^{13}C NMR (126 MHz, CDCl$_3$)

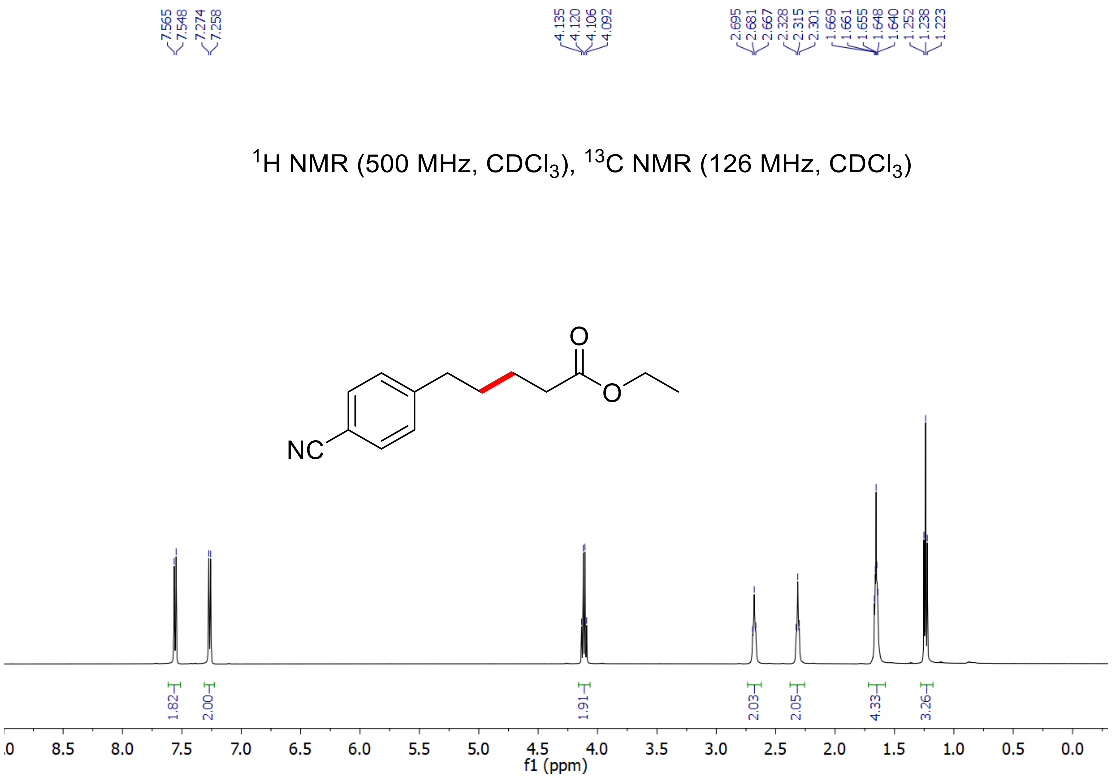

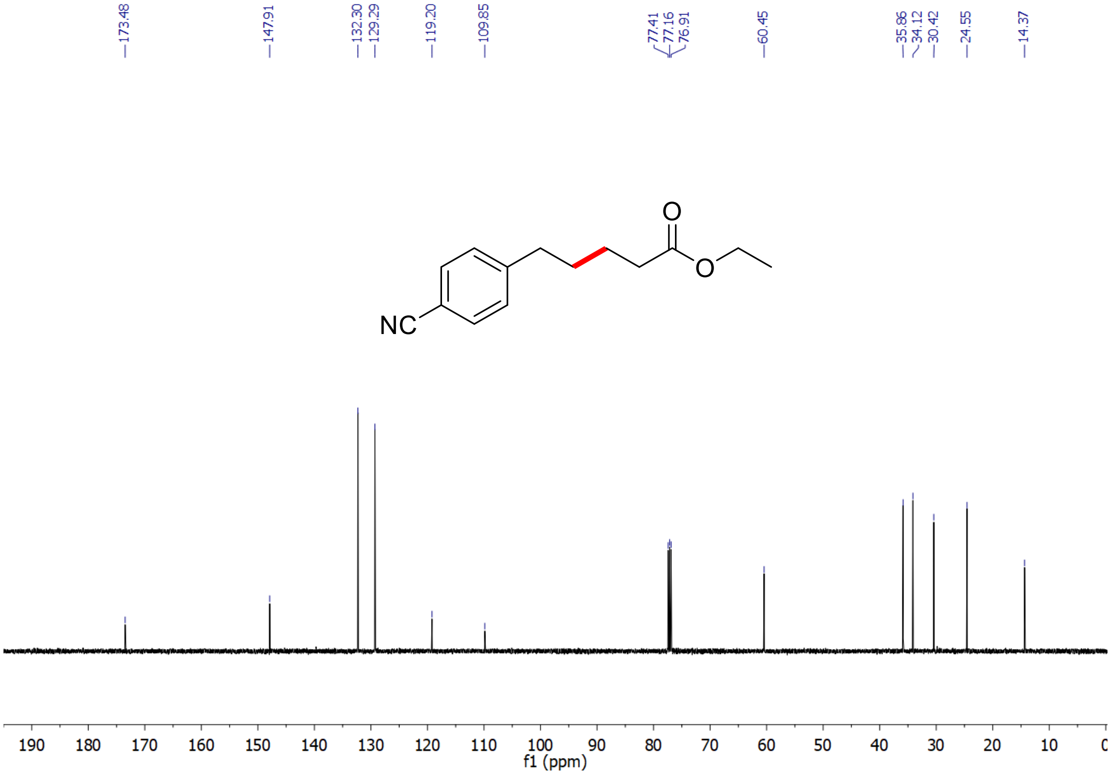

^1H NMR (500 MHz, $CDCl_3$), ^{13}C NMR (126 MHz, $CDCl_3$)

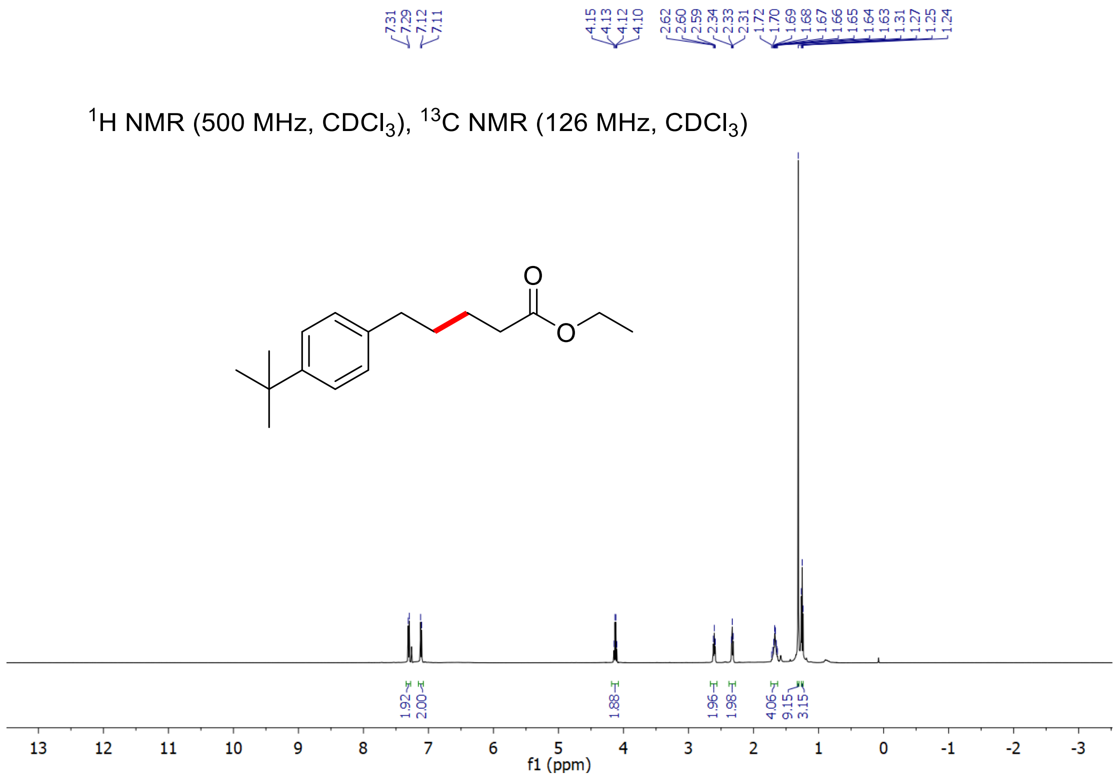

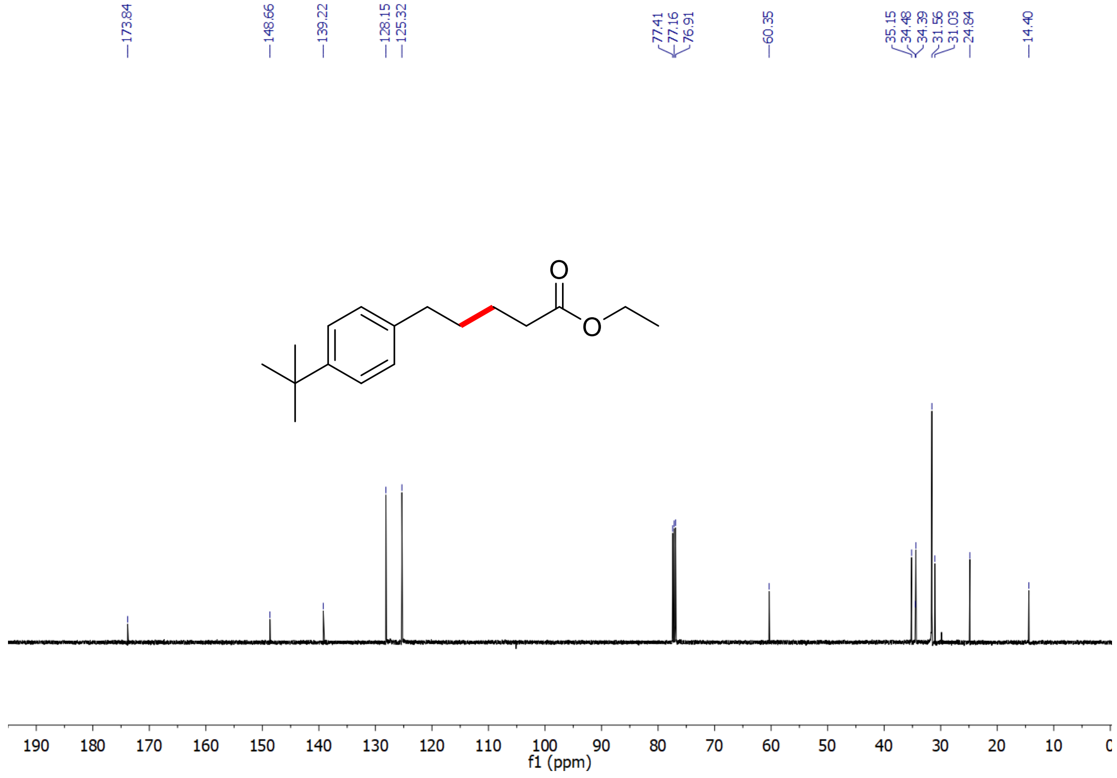

^{1}H NMR (500 MHz, $CDCl_3$), ^{13}C NMR (126 MHz, $CDCl_3$)

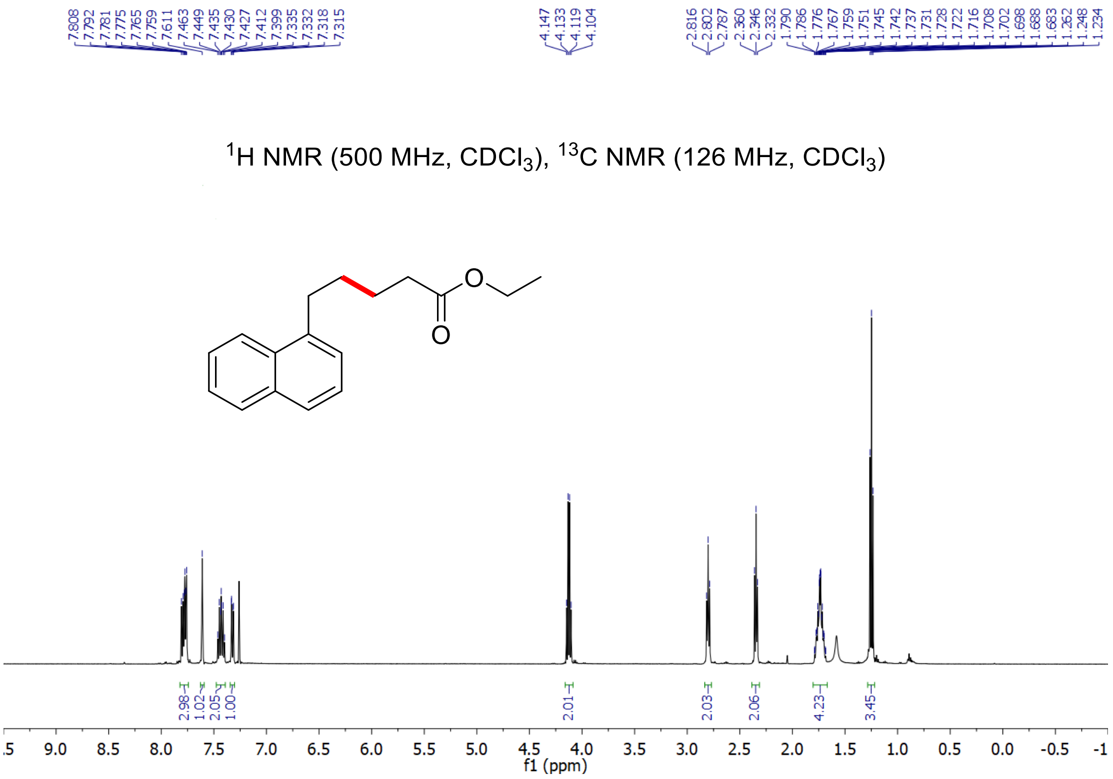

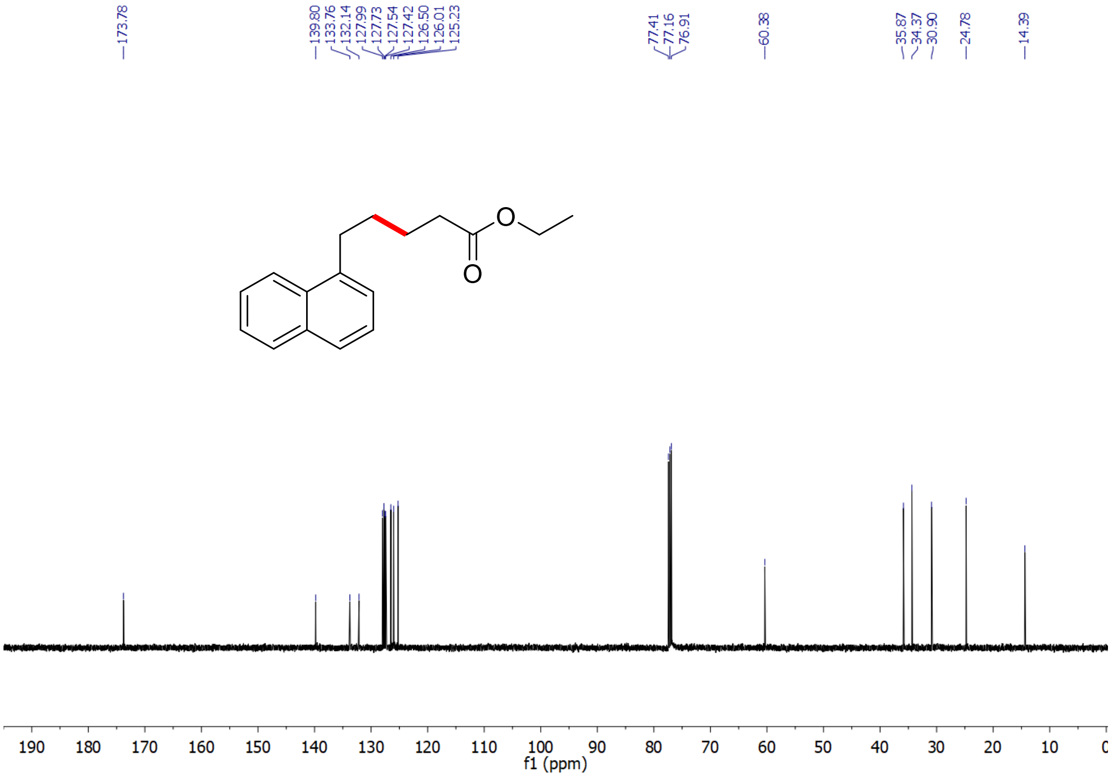

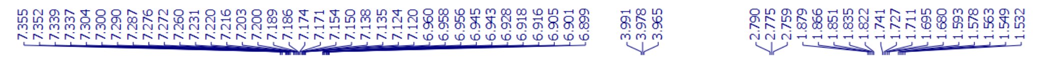

^{1}H NMR (500 MHz, CDCl$_3$), ^{13}C NMR (126 MHz, CDCl$_3$)

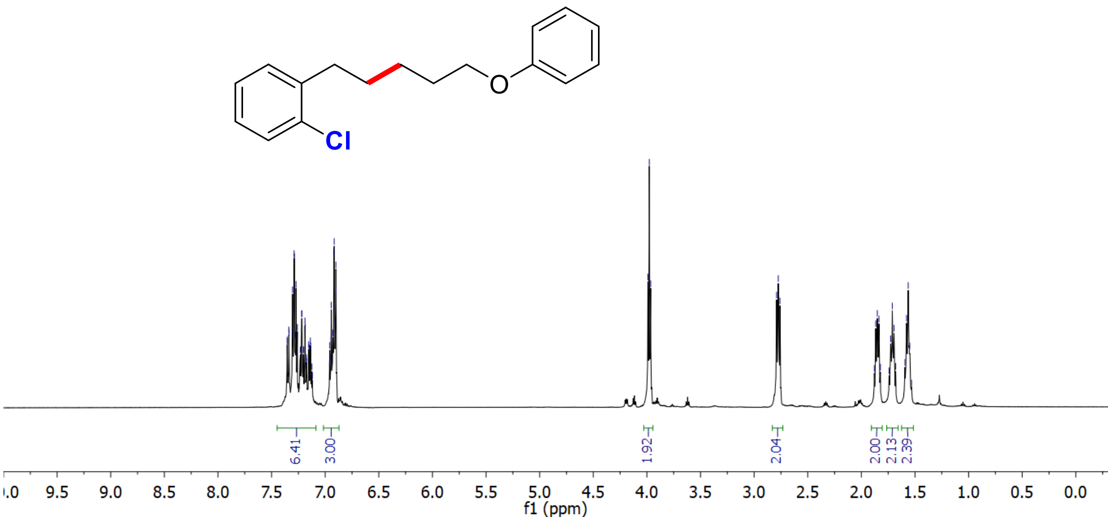

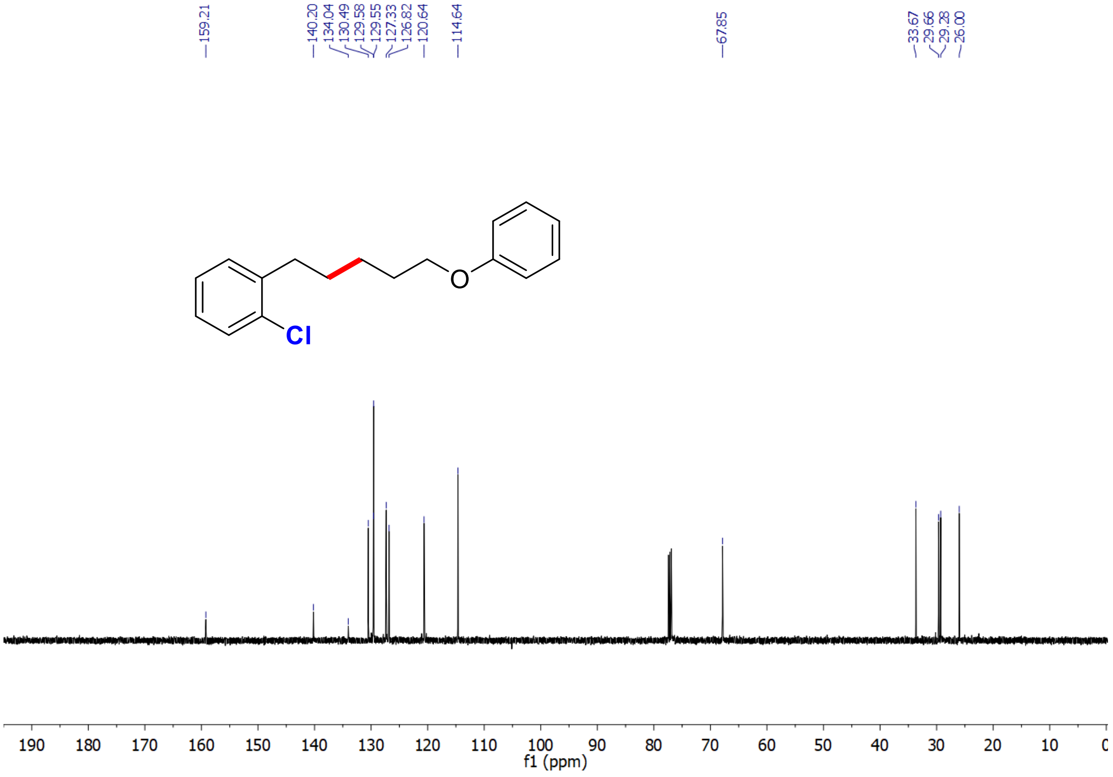

^{1}H NMR (500 MHz, CDCl$_3$), ^{13}C NMR (126 MHz, CDCl$_3$)

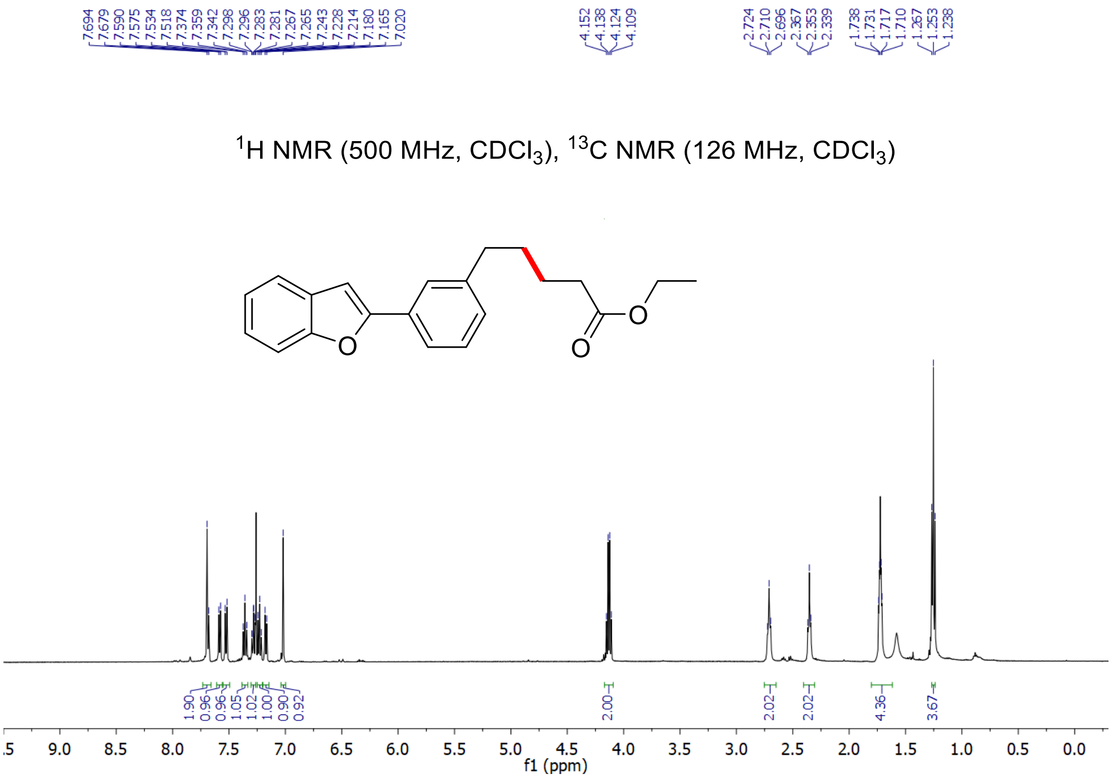

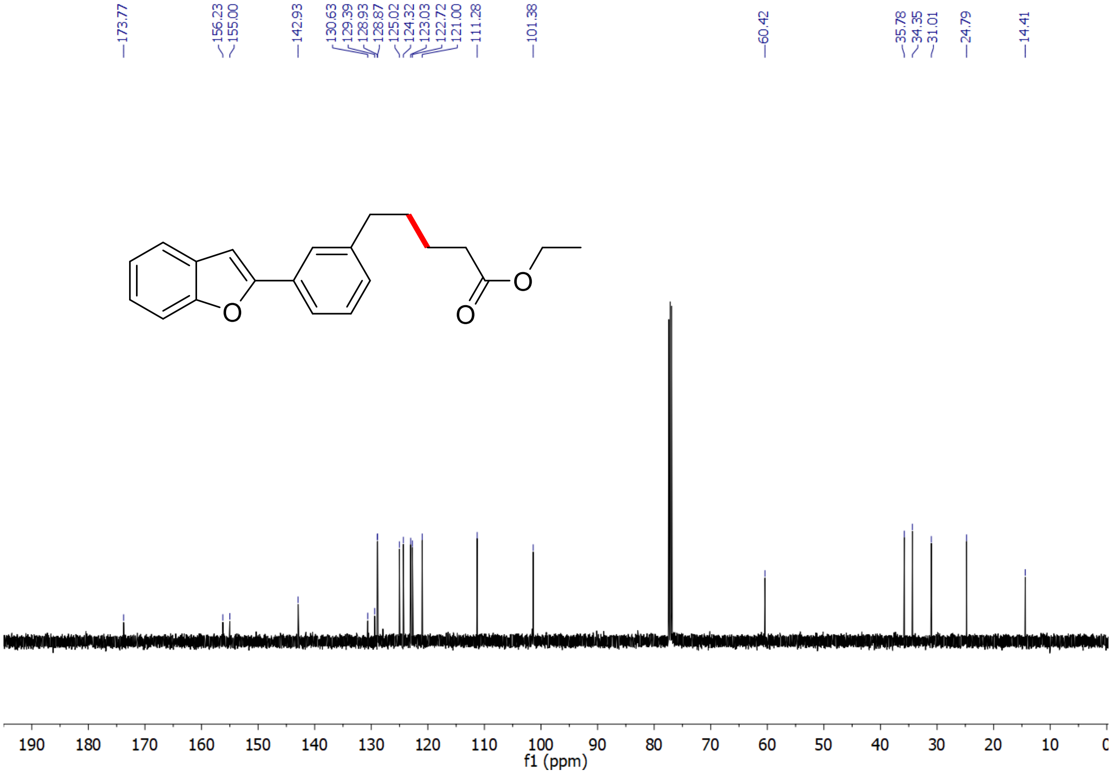

^{1}H NMR (500 MHz, $CDCl_3$), ^{13}C NMR (126 MHz, $CDCl_3$)

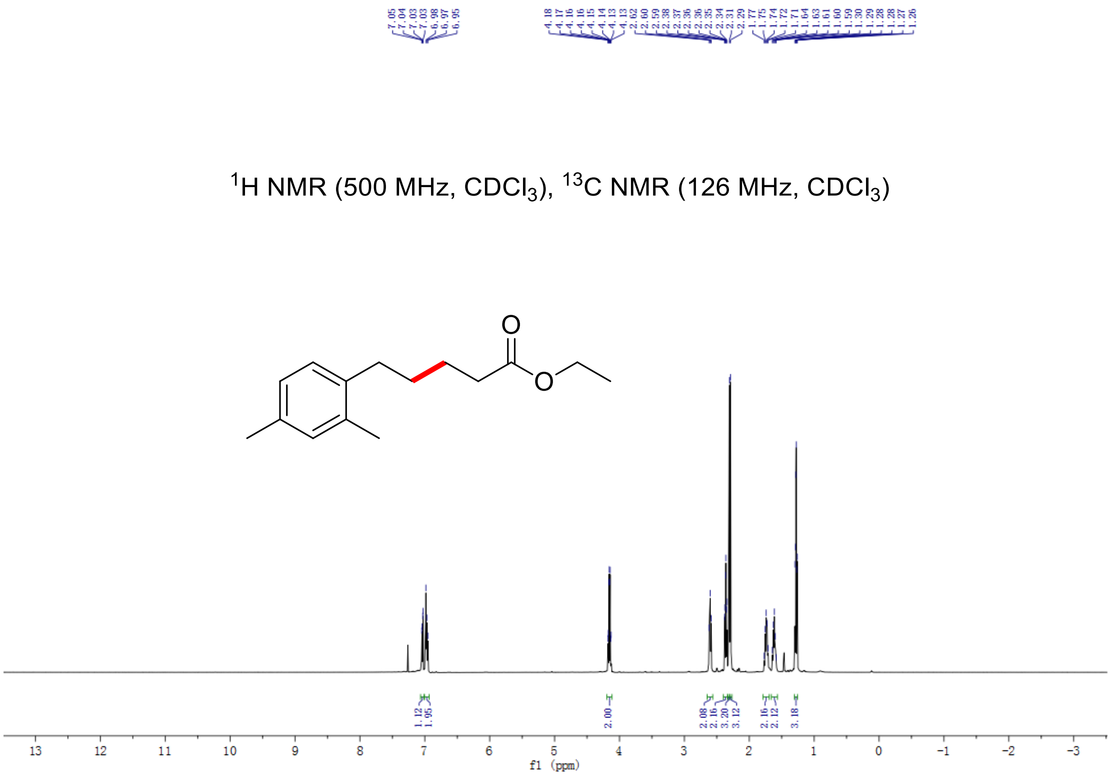

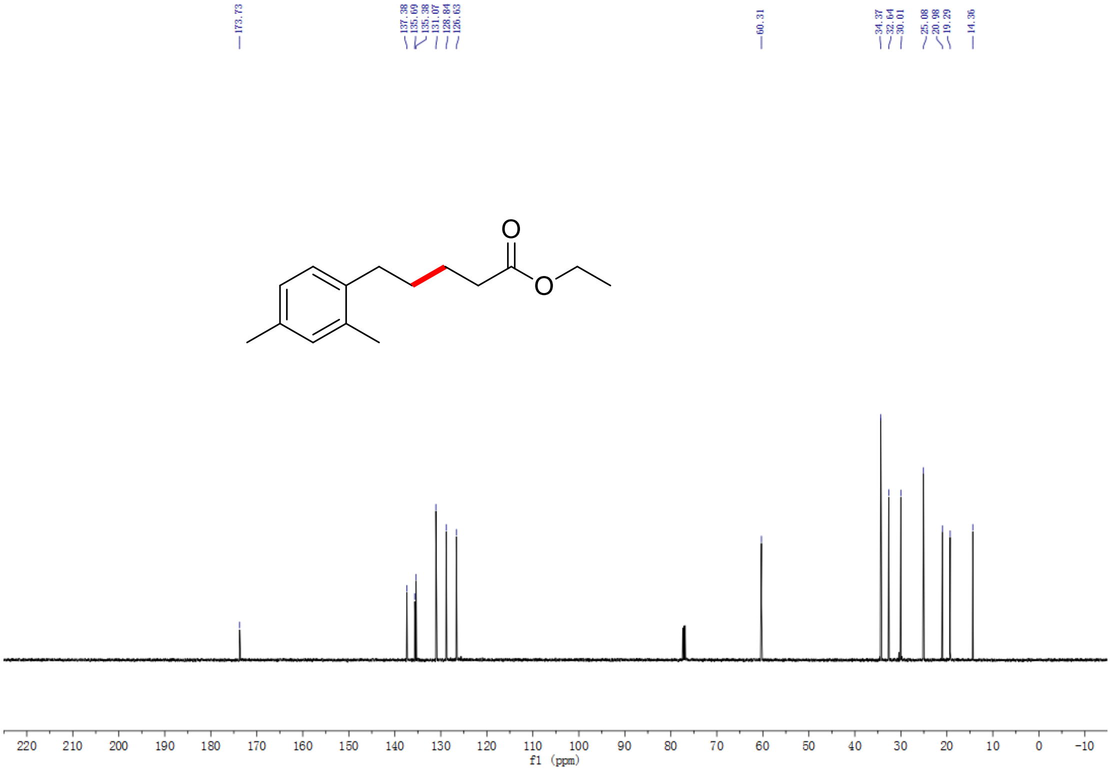

^1H NMR (500 MHz, $CDCl_3$), ^{13}C NMR (126 MHz, $CDCl_3$)

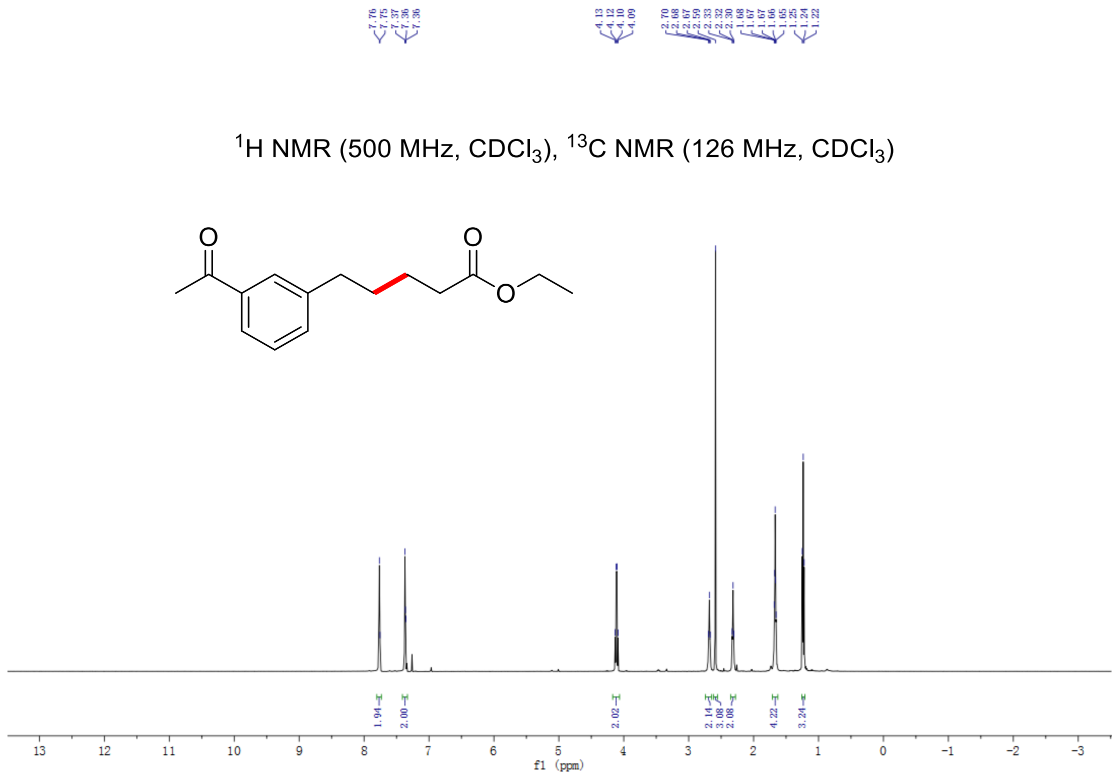

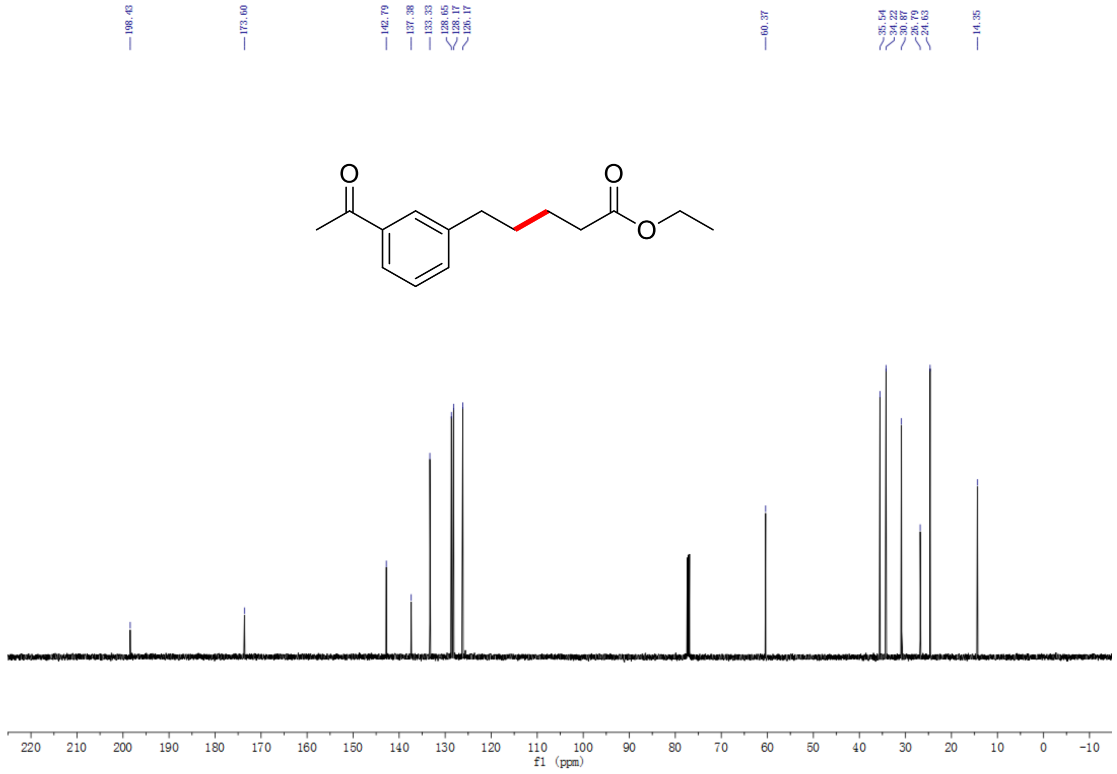

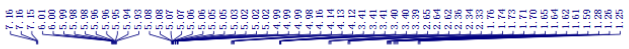

^{1}H NMR (500 MHz, CDCl$_3$), ^{13}C NMR (126 MHz, CDCl$_3$)

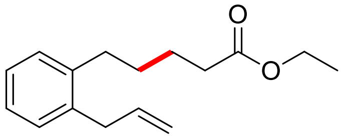

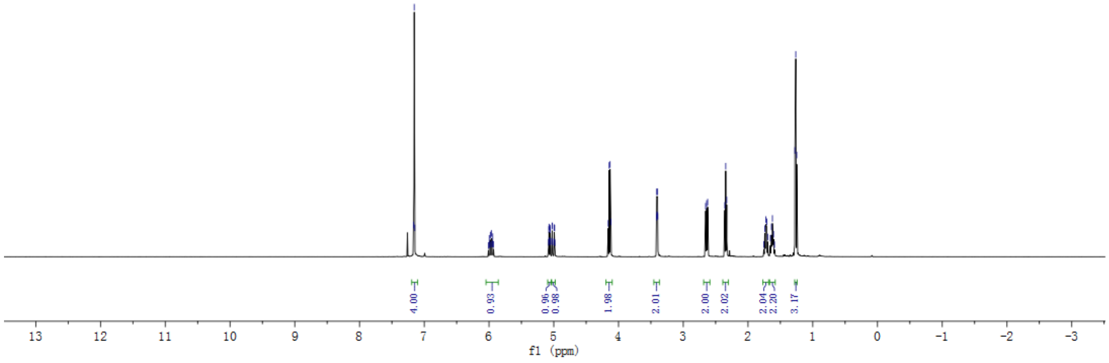

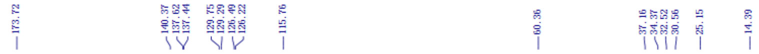

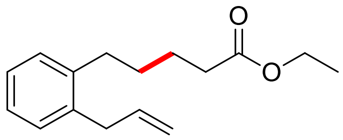

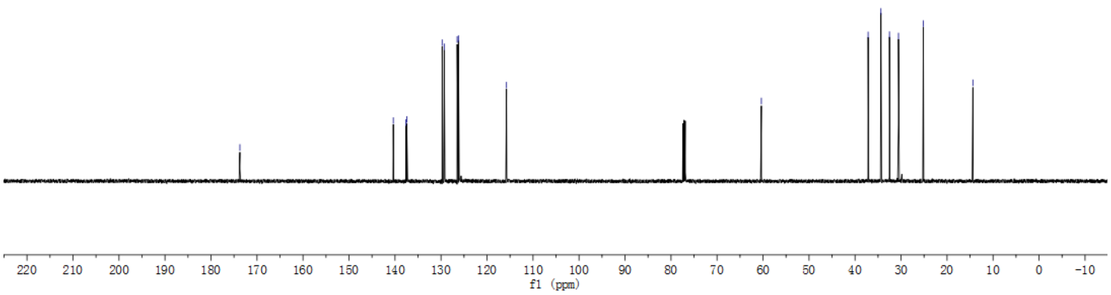

^1H NMR (500 MHz, $CDCl_3$), ^{13}C NMR (126 MHz, $CDCl_3$)

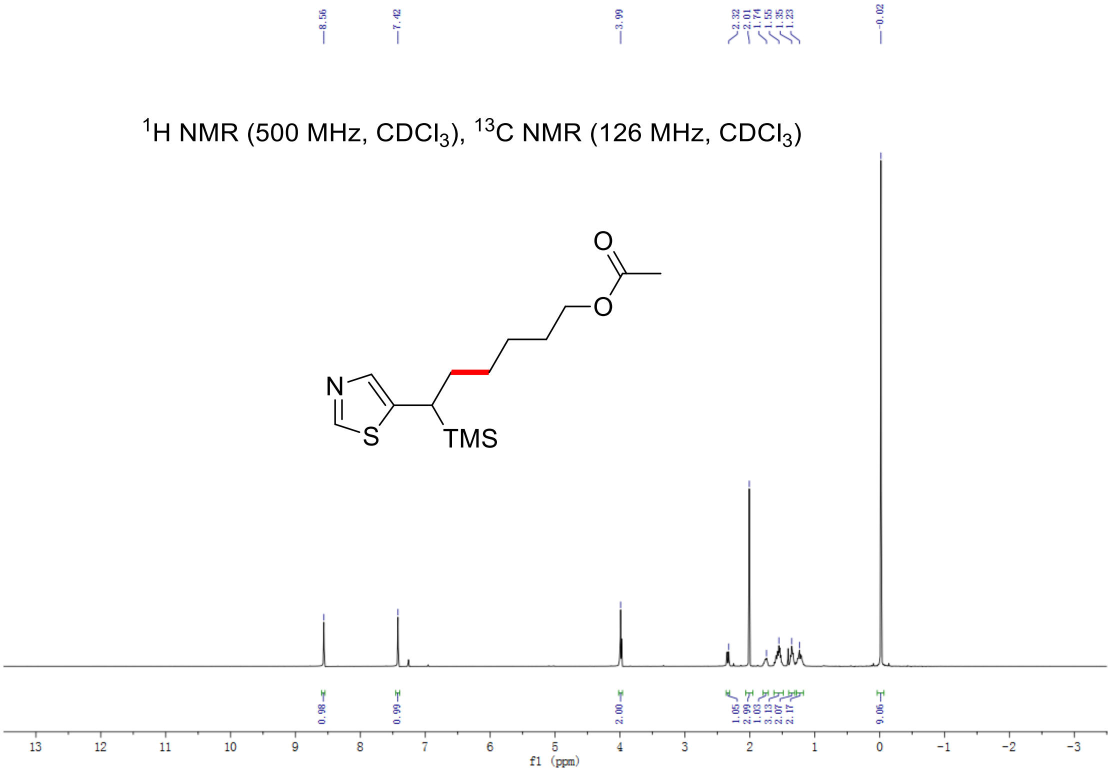

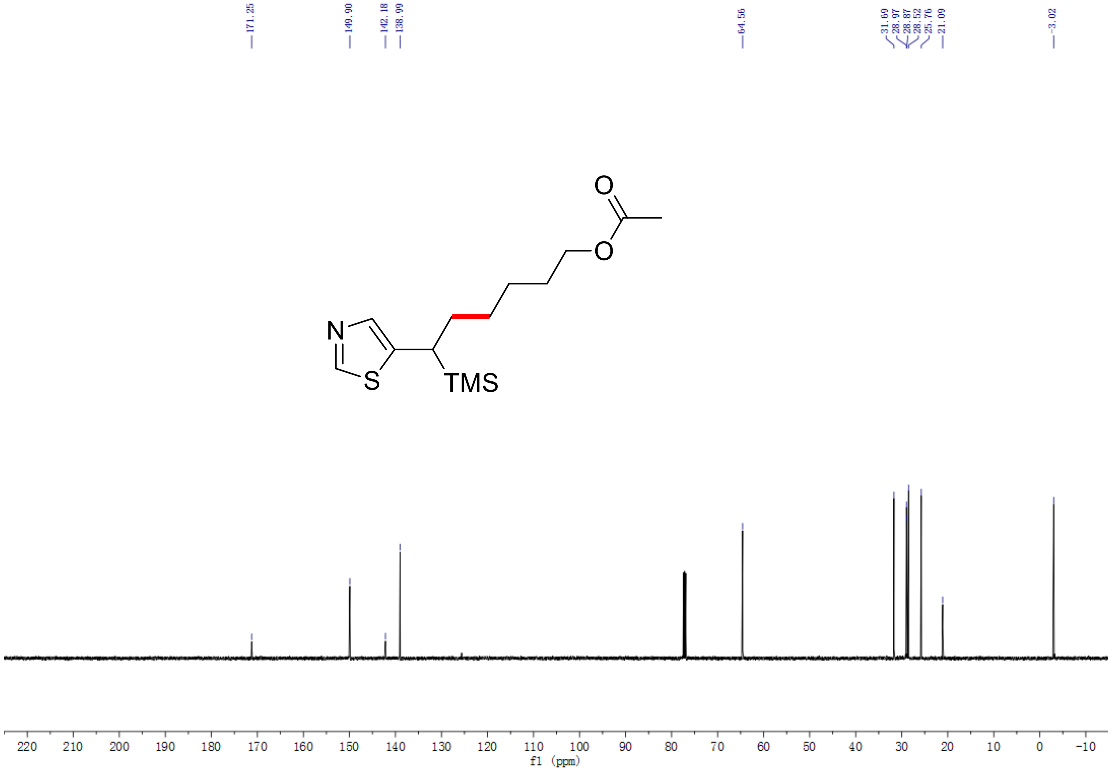

^{1}H NMR (500 MHz, CDCl$_3$), ^{13}C NMR (126 MHz, CDCl$_3$)

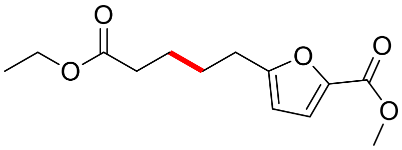

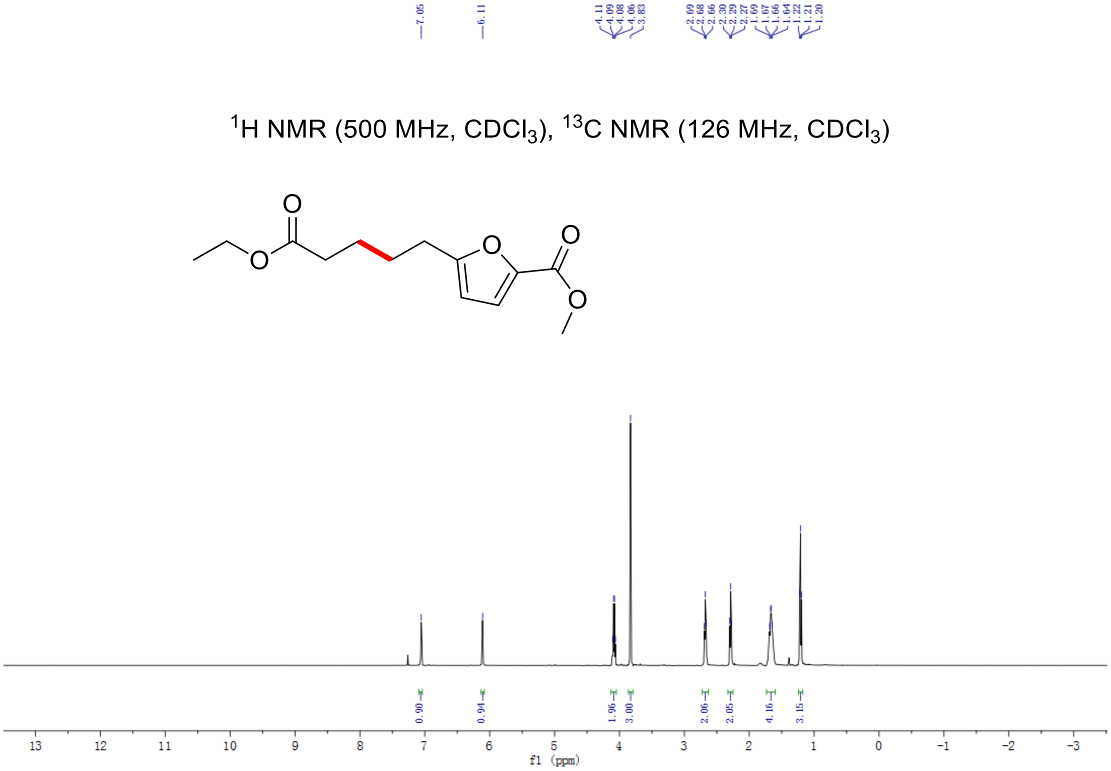

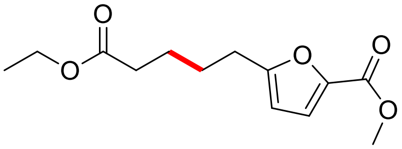

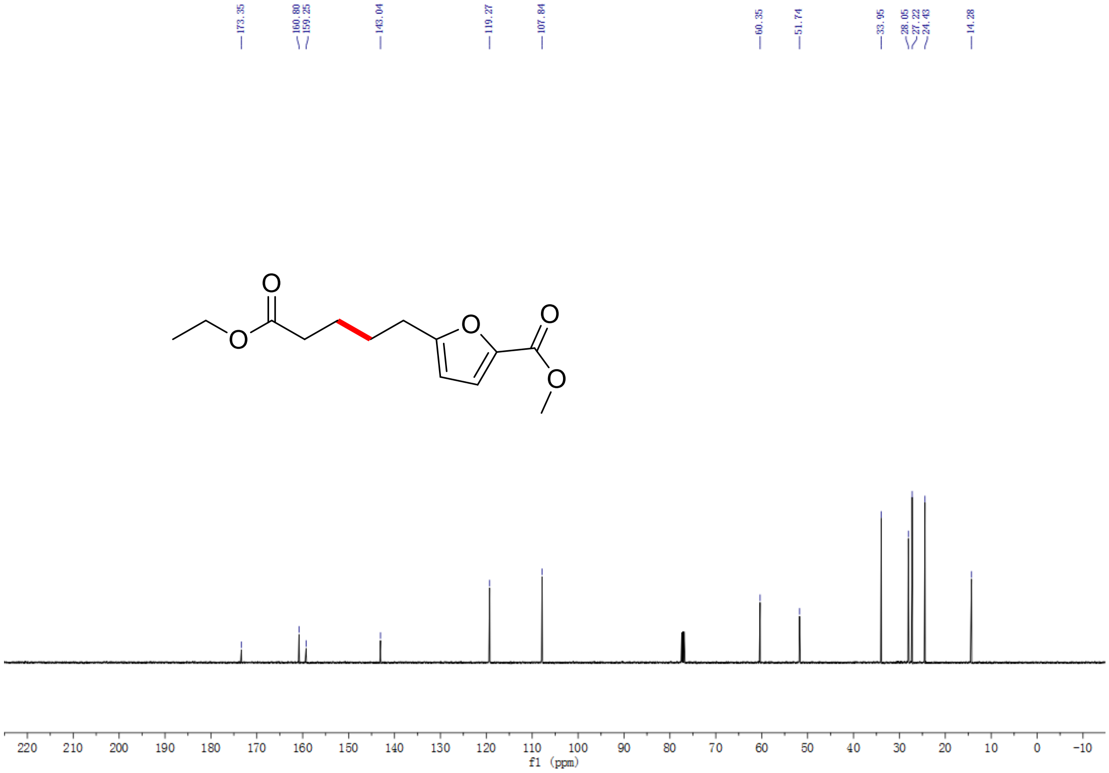

^{1}H NMR (500 MHz, $CDCl_3$), ^{13}C NMR (126 MHz, $CDCl_3$)

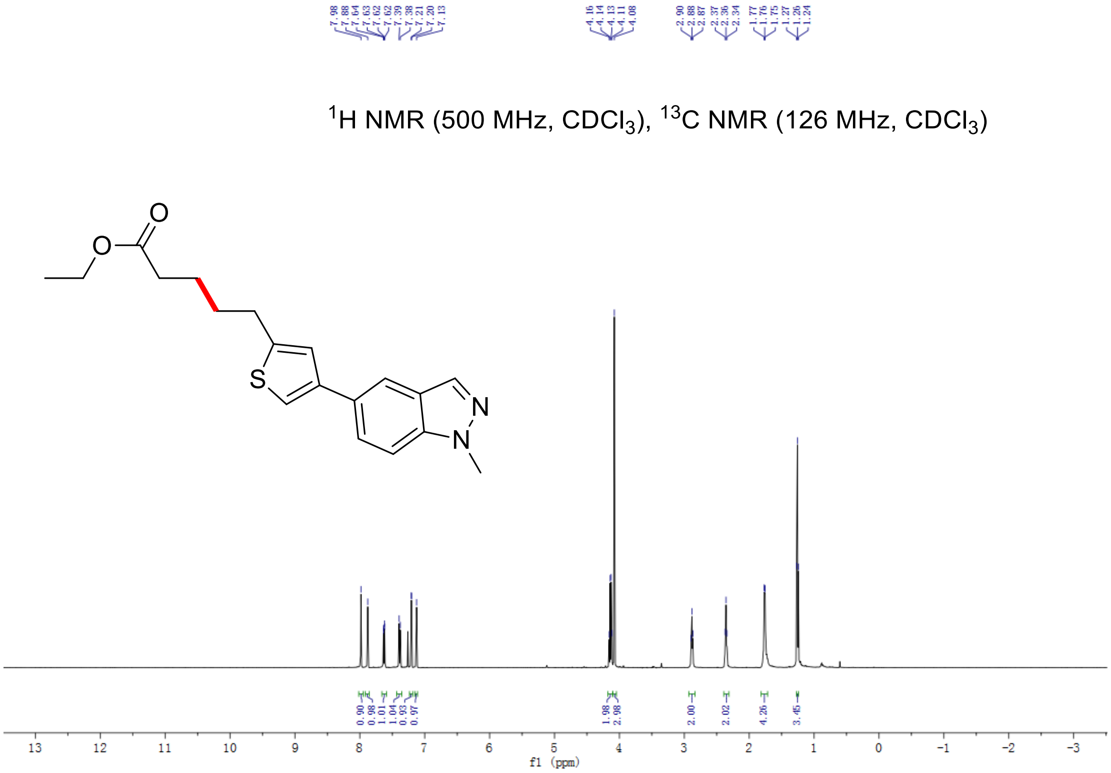

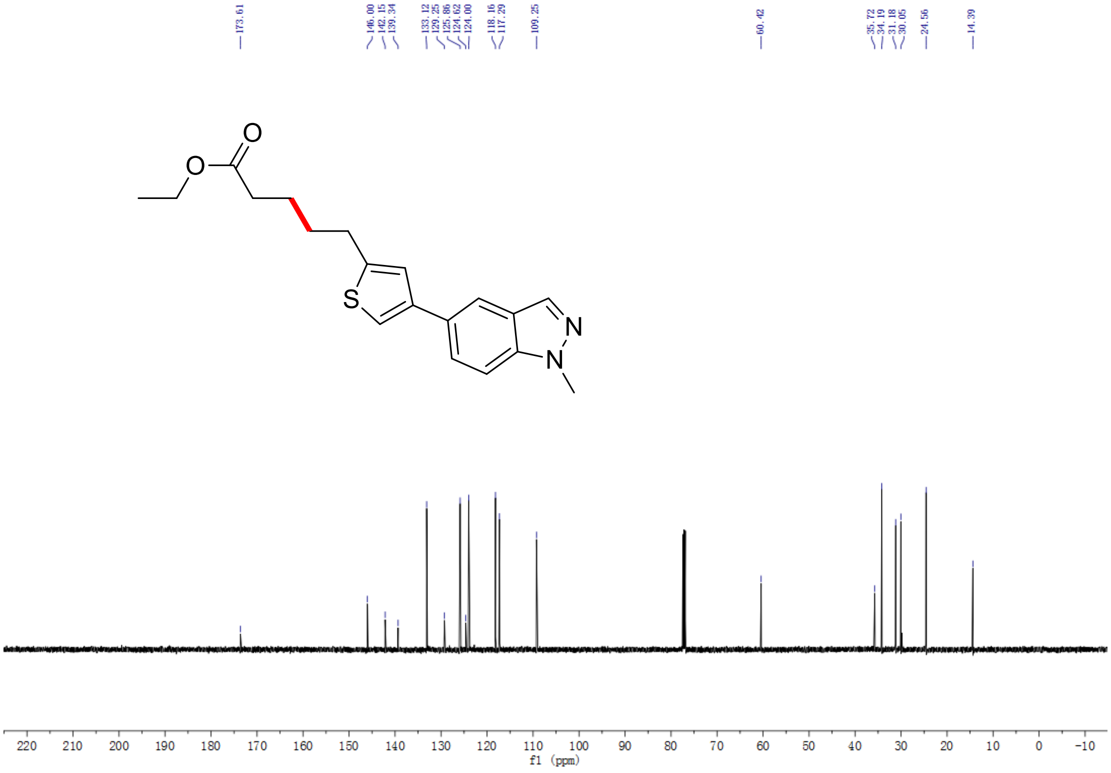

^{1}H NMR (500 MHz, CDCl$_3$), ^{13}C NMR (126 MHz, CDCl$_3$)

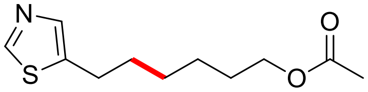

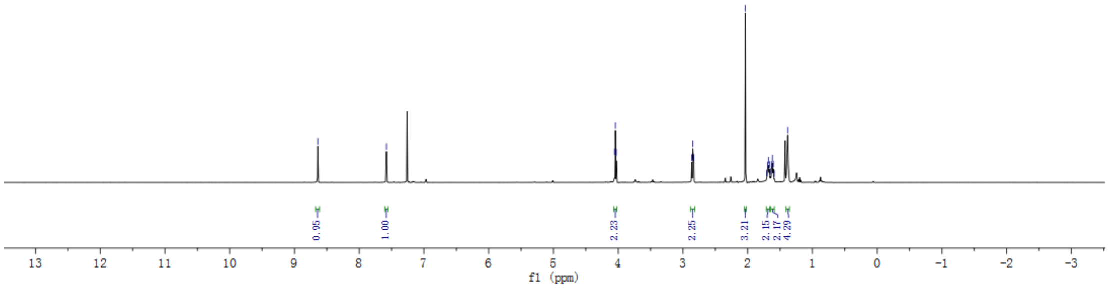

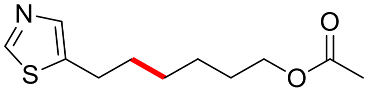

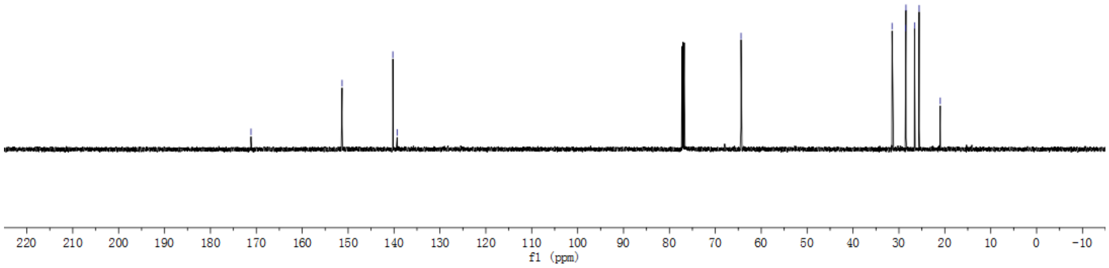

^{1}H NMR (500 MHz, CDCl$_3$), ^{13}C NMR (126 MHz, CDCl$_3$)

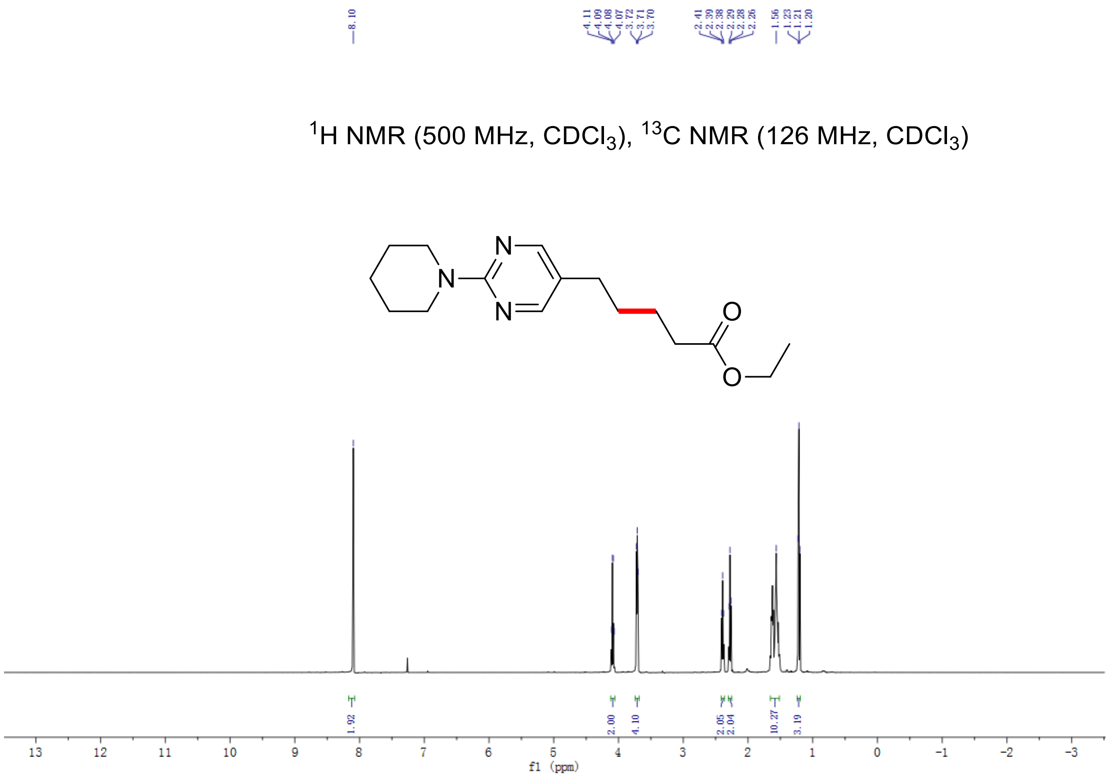

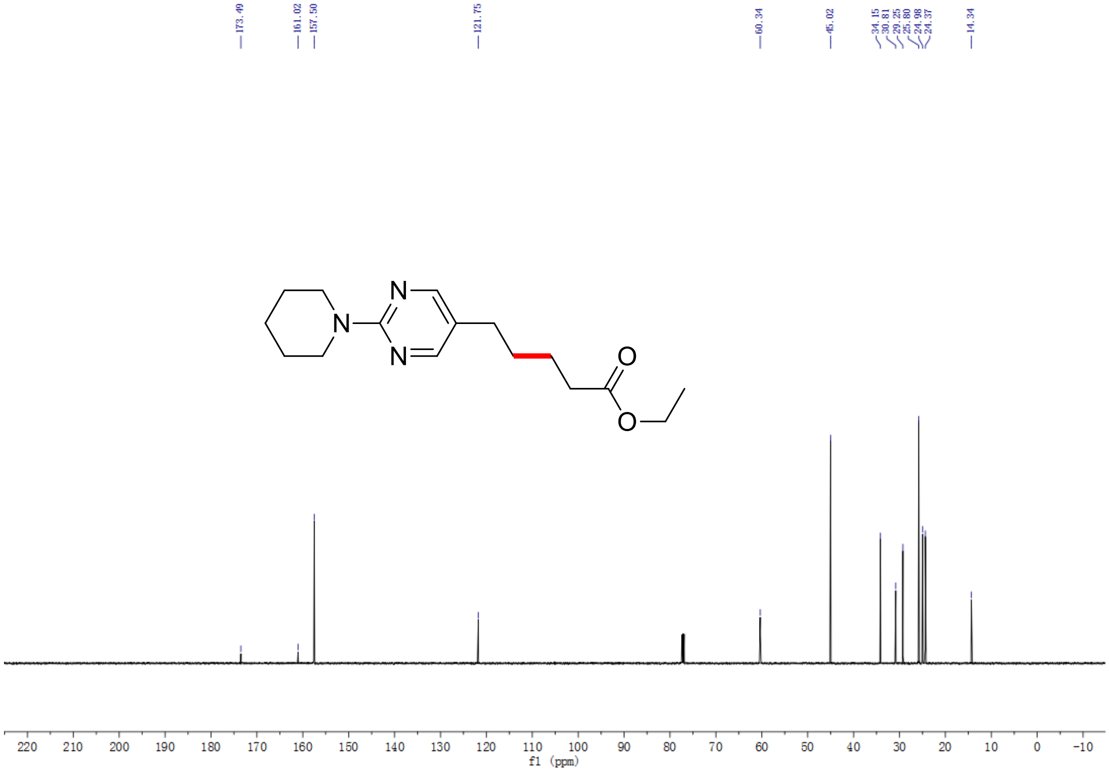

^{1}H NMR (500 MHz, CDCl$_3$), ^{13}C NMR (126 MHz, CDCl$_3$)

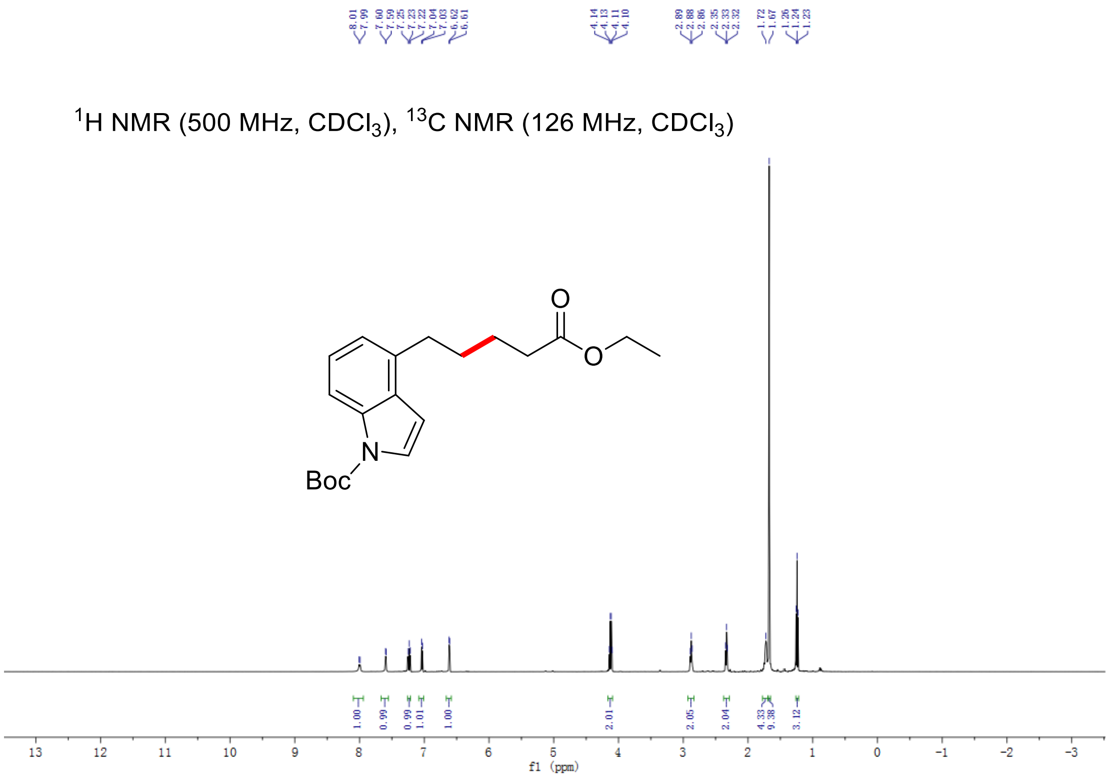

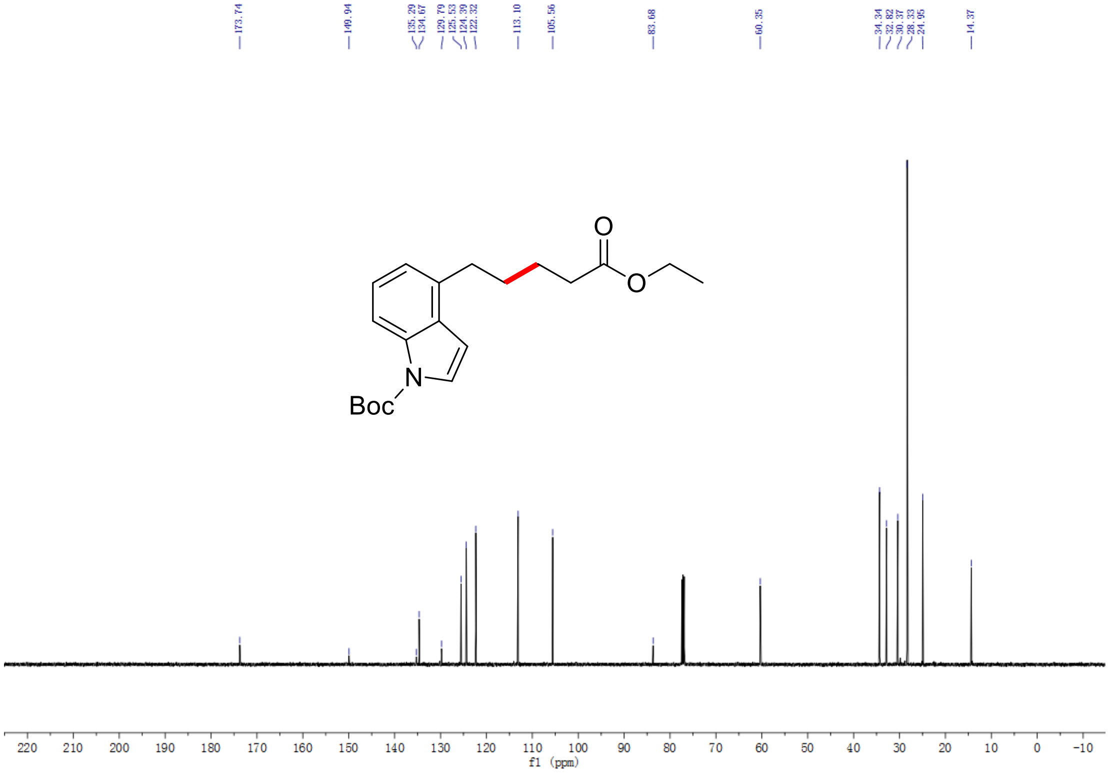

^{1}H NMR (500 MHz, CDCl$_3$), ^{13}C NMR (126 MHz, CDCl$_3$)

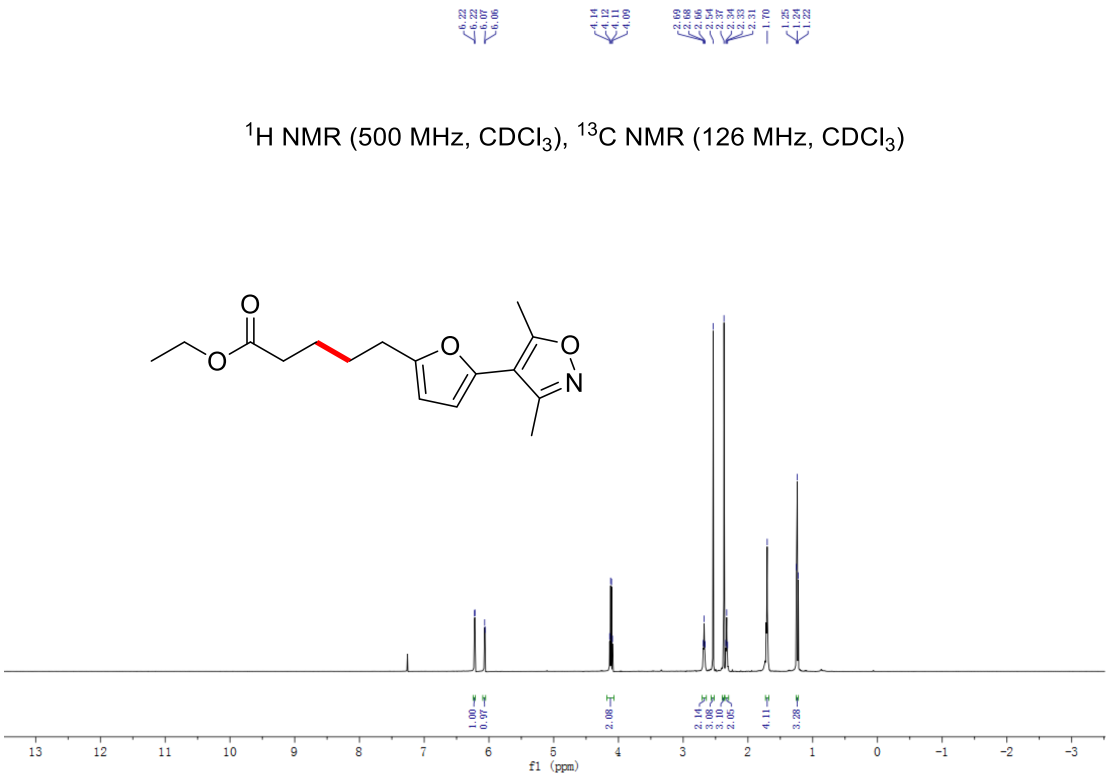

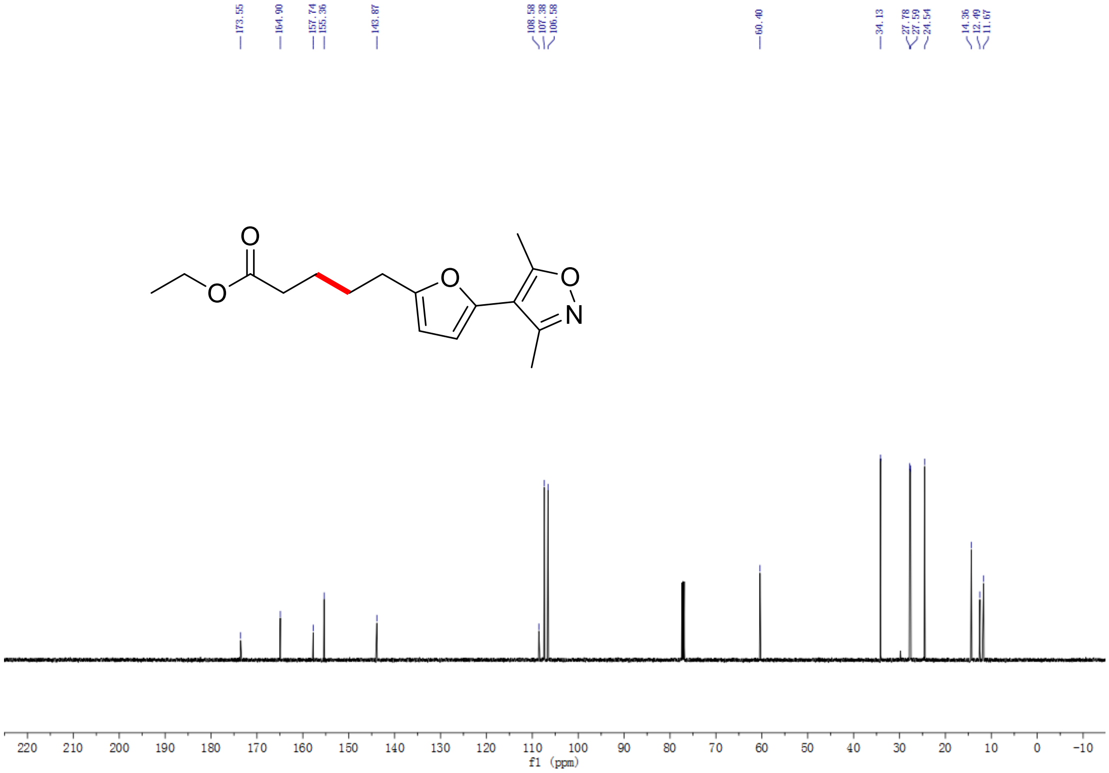

^{1}H NMR (500 MHz, CDCl$_3$), ^{13}C NMR (126 MHz, CDCl$_3$)

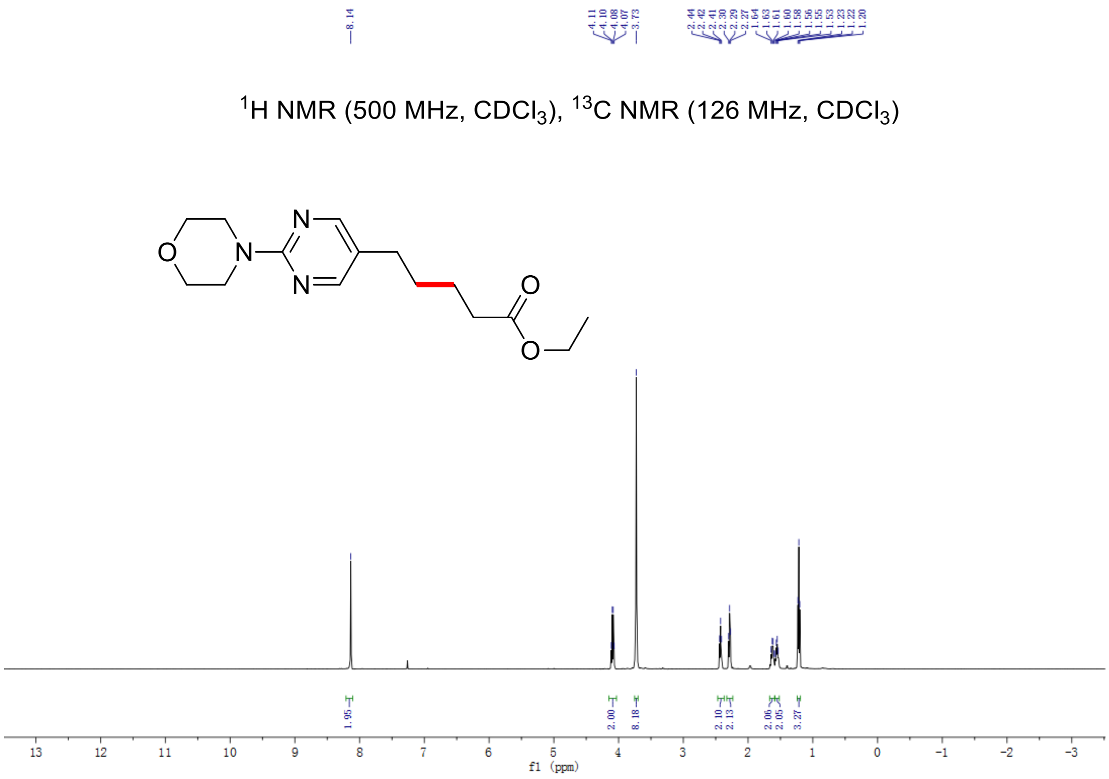

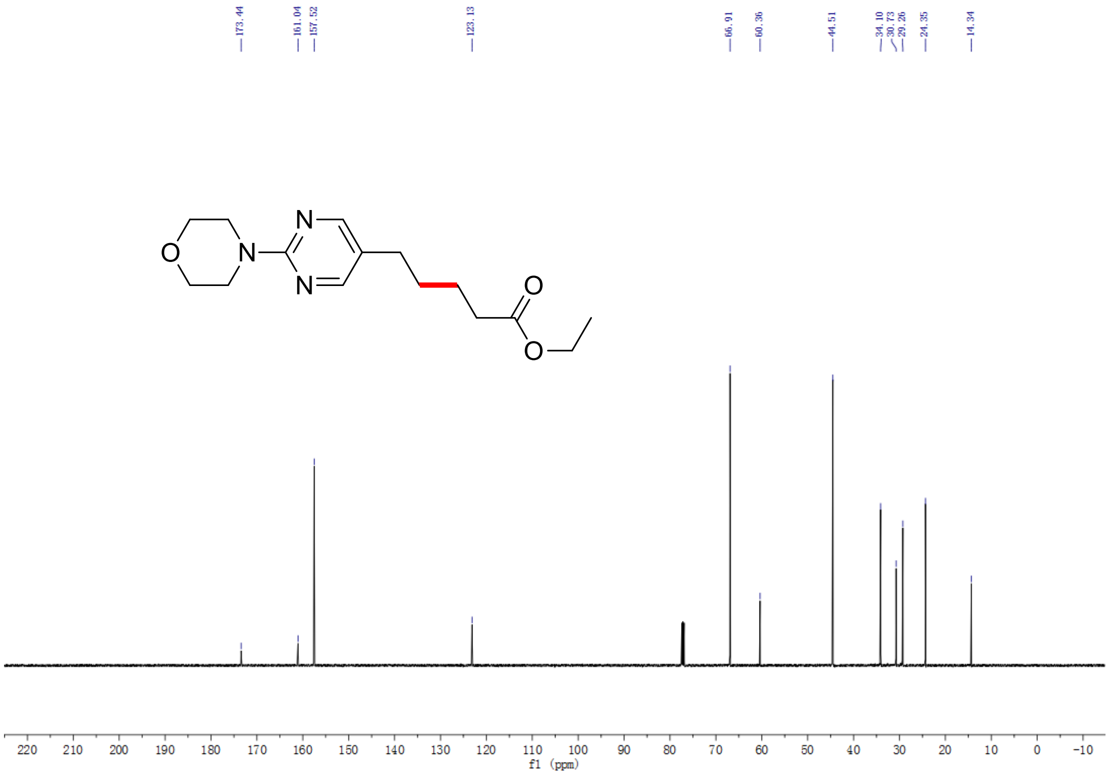

^{1}H NMR (500 MHz, CDCl$_3$), ^{13}C NMR (126 MHz, CDCl$_3$)

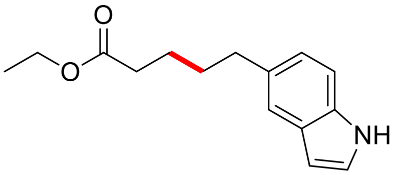

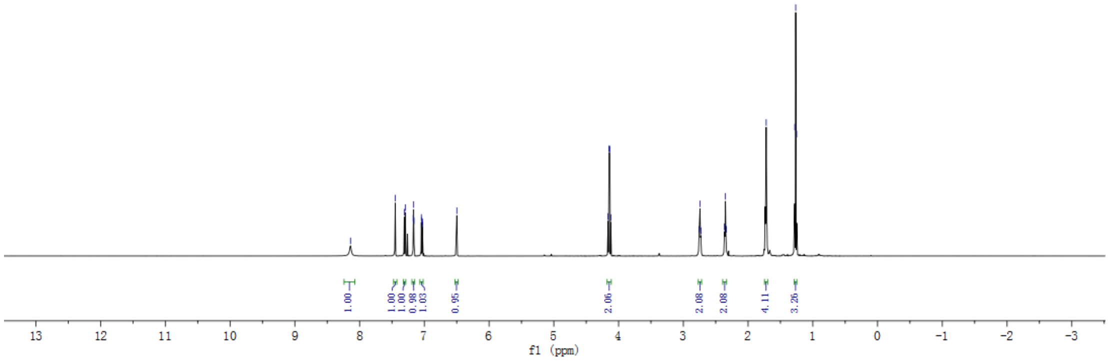

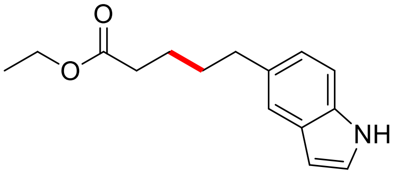

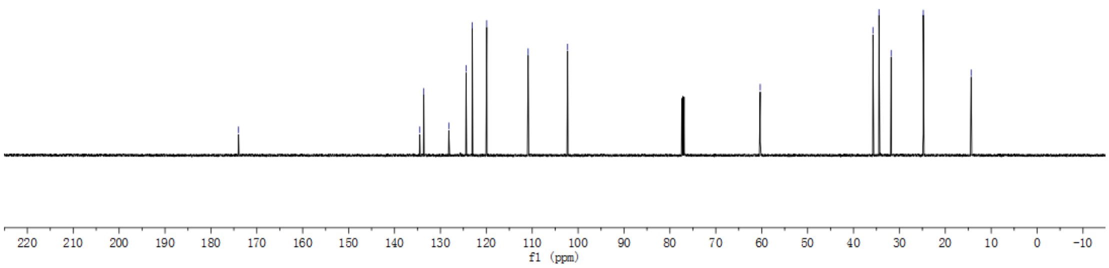

^{1}H NMR (400 MHz, CDCl$_3$), ^{13}C NMR (126 MHz, CDCl$_3$)

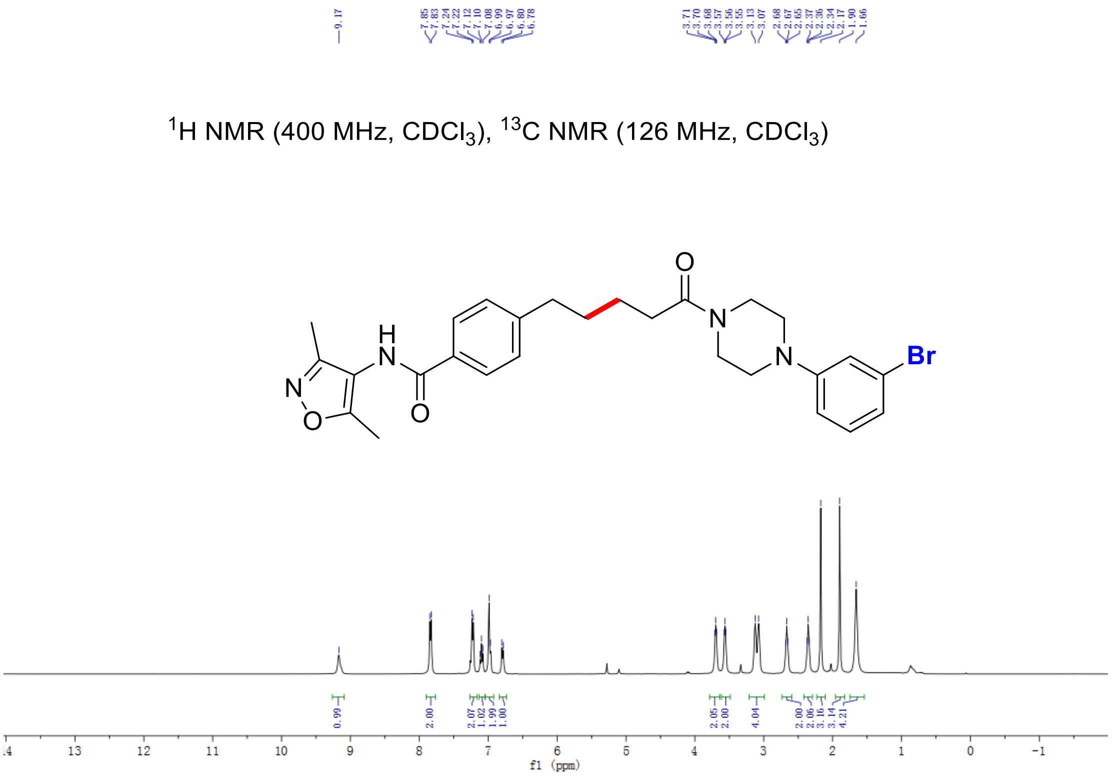

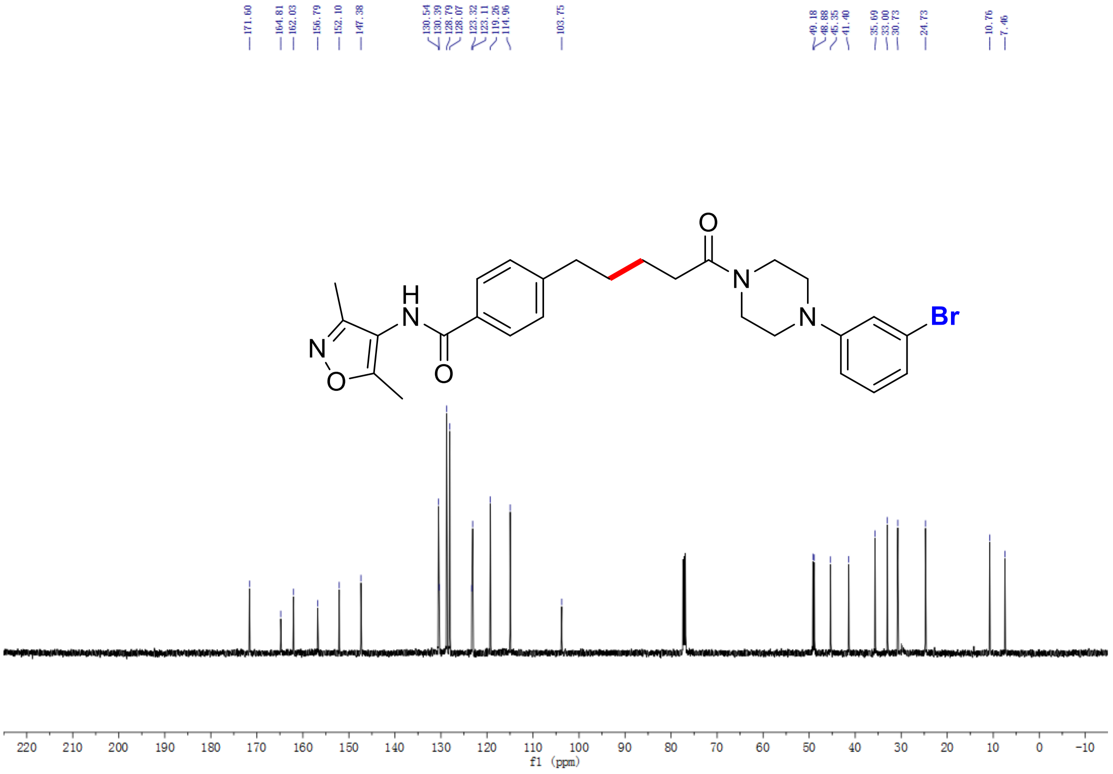

^{1}H NMR (500 MHz, CDCl$_3$), ^{13}C NMR (126 MHz, CDCl$_3$)

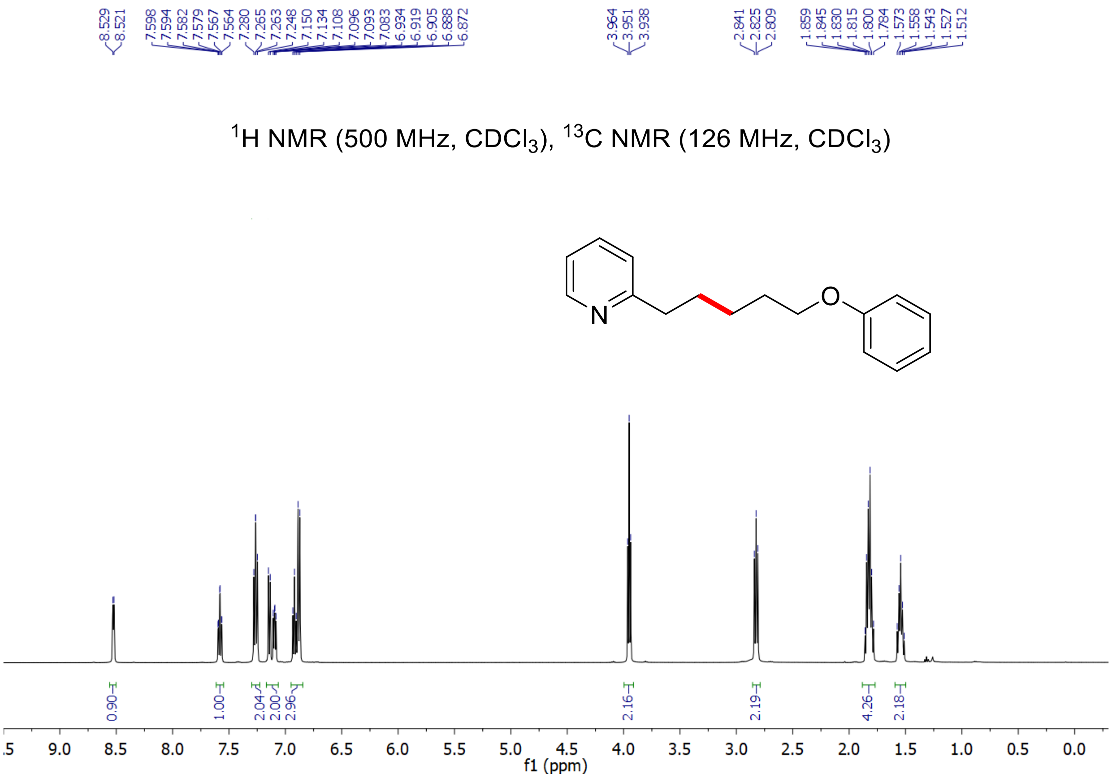

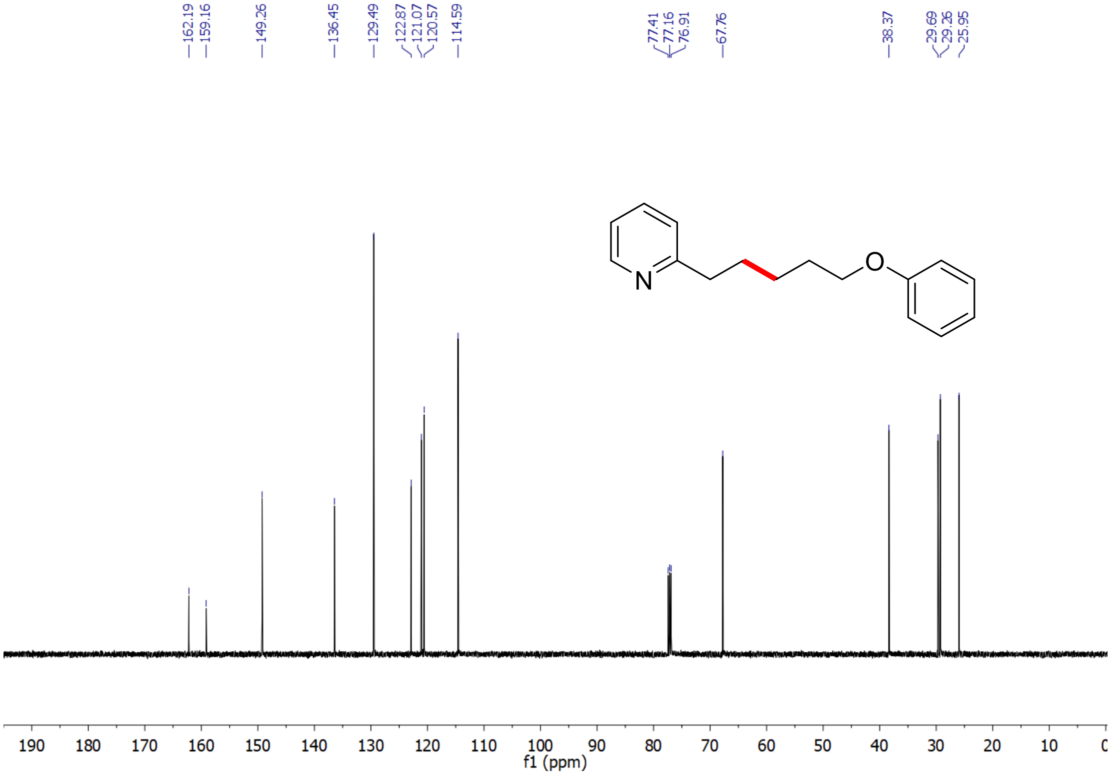

^{1}H NMR (500 MHz, $CDCl_3$), ^{13}C NMR (126 MHz, $CDCl_3$)

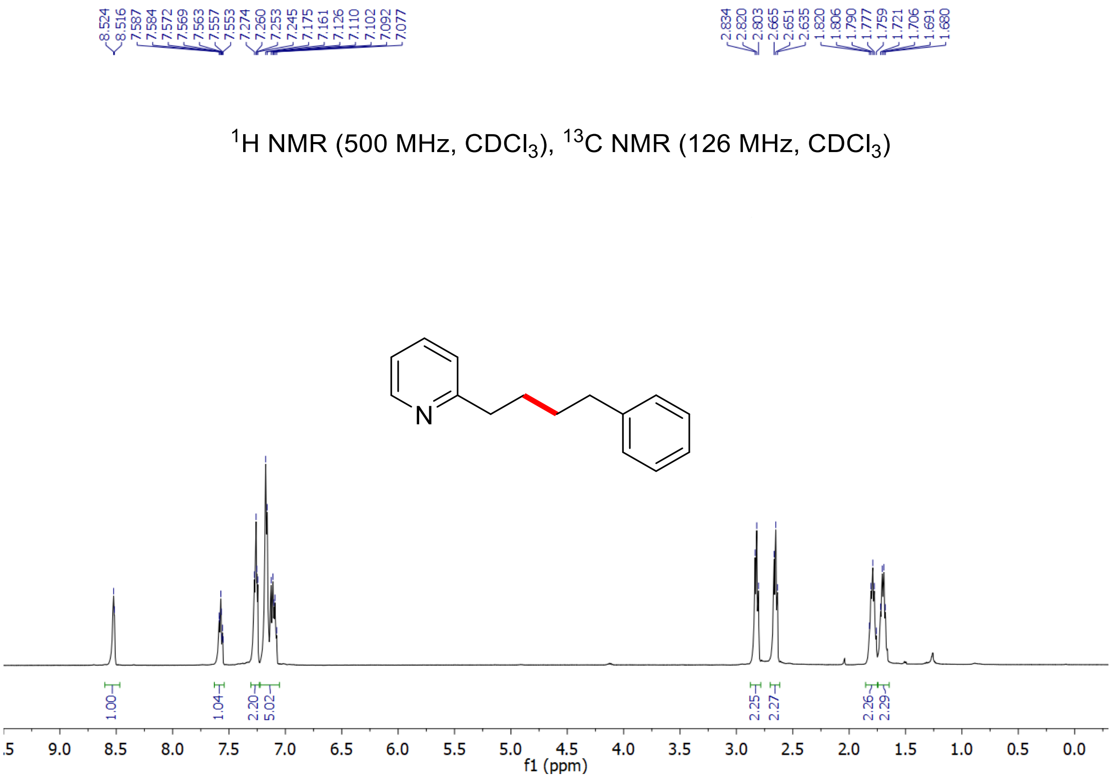

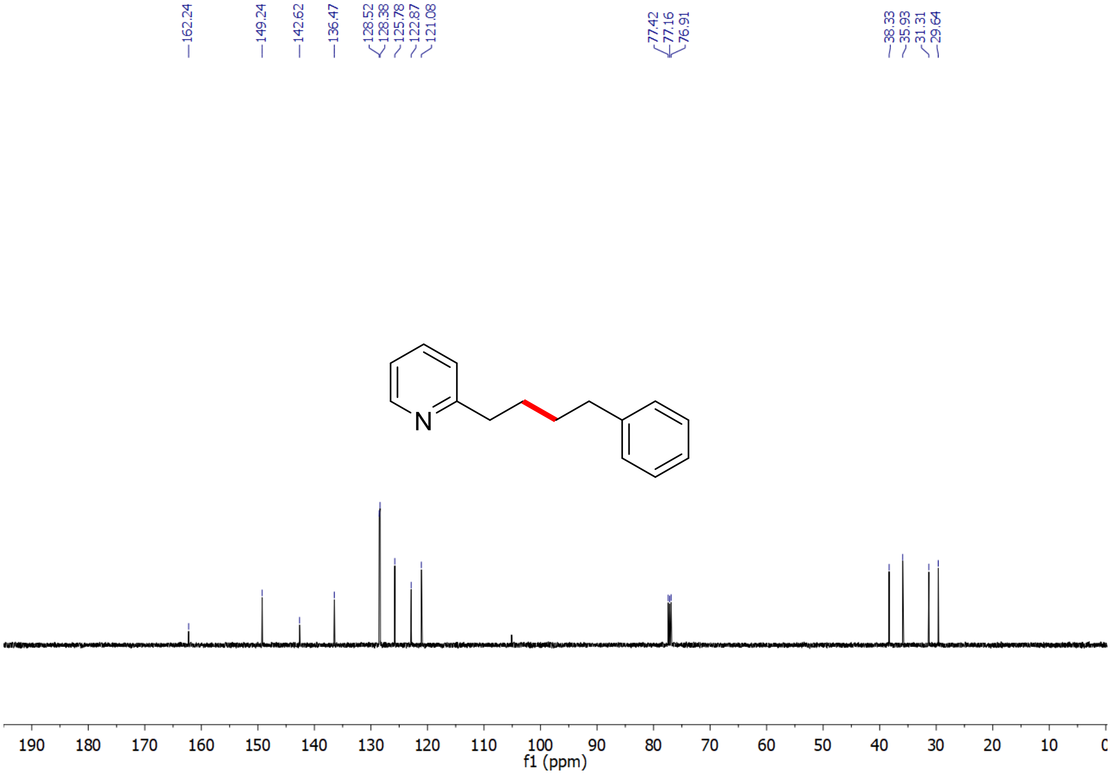

^1H NMR (500 MHz, $CDCl_3$), ^{13}C NMR (126 MHz, $CDCl_3$)

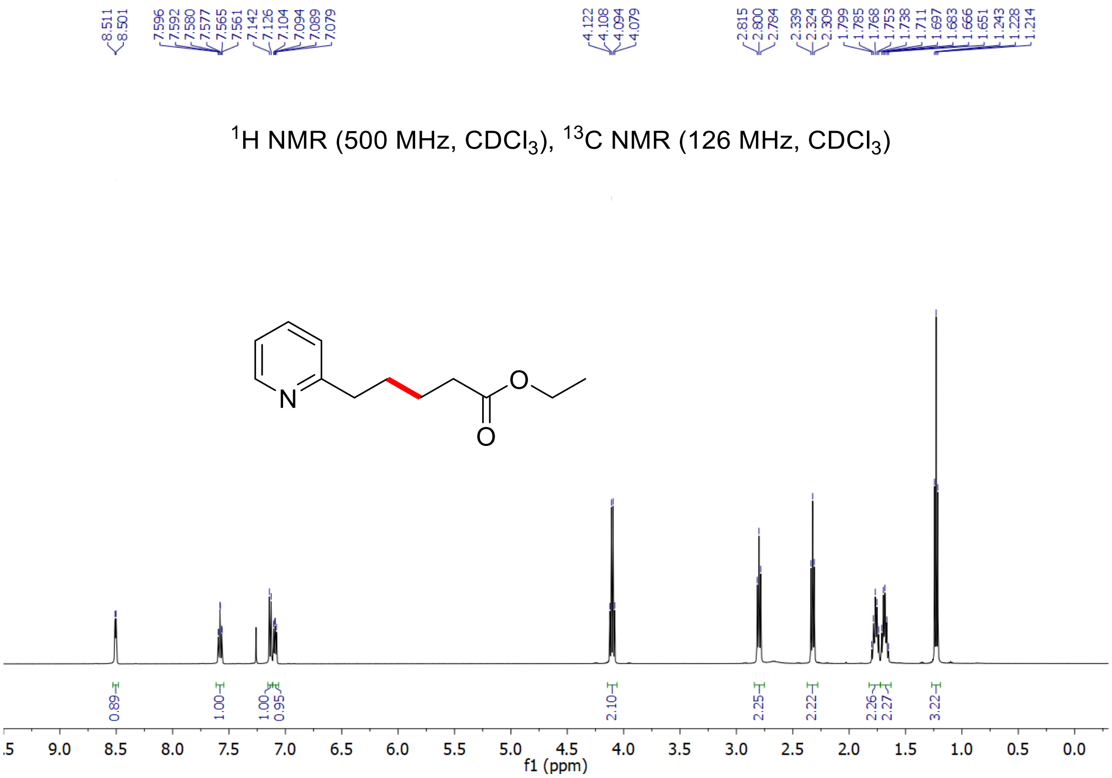

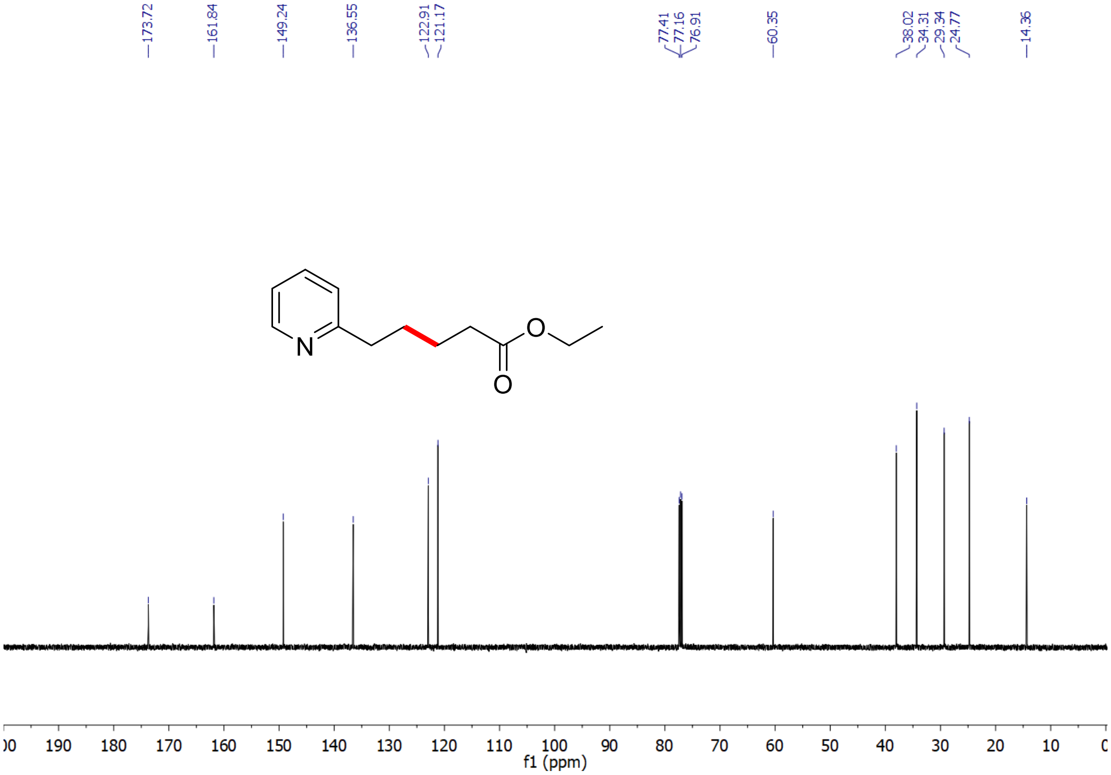

^{1}H NMR (500 MHz, CDCl$_3$), ^{13}C NMR (126 MHz, CDCl$_3$)

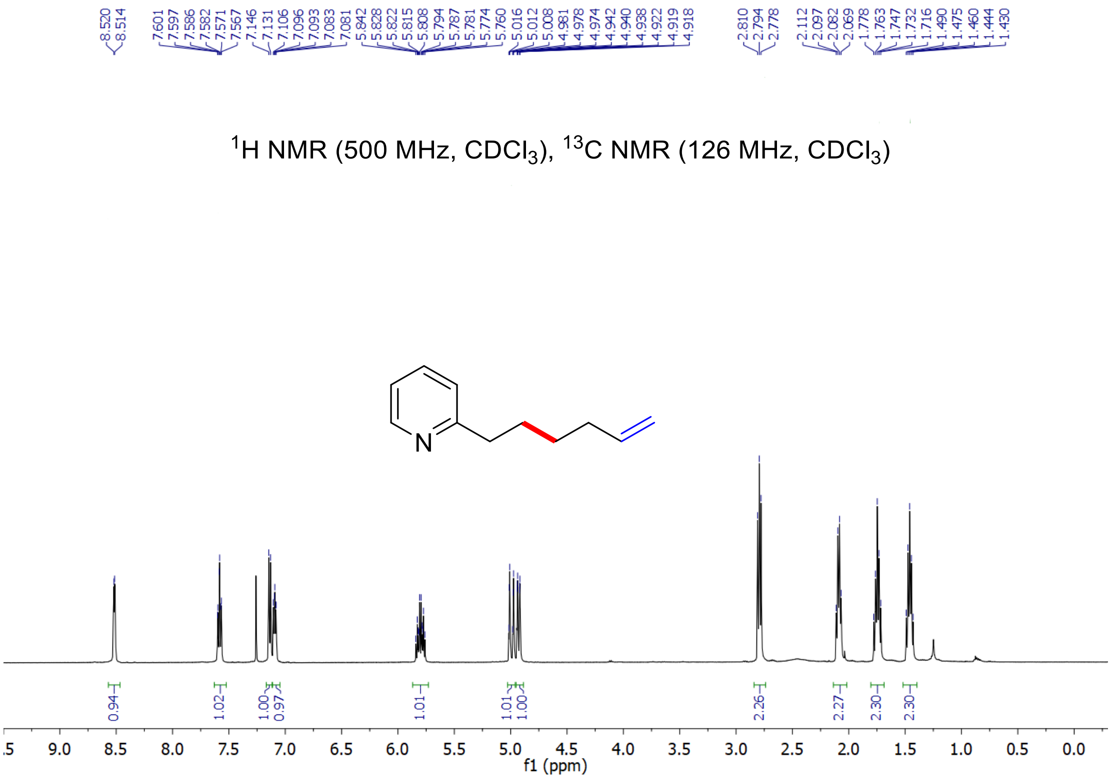

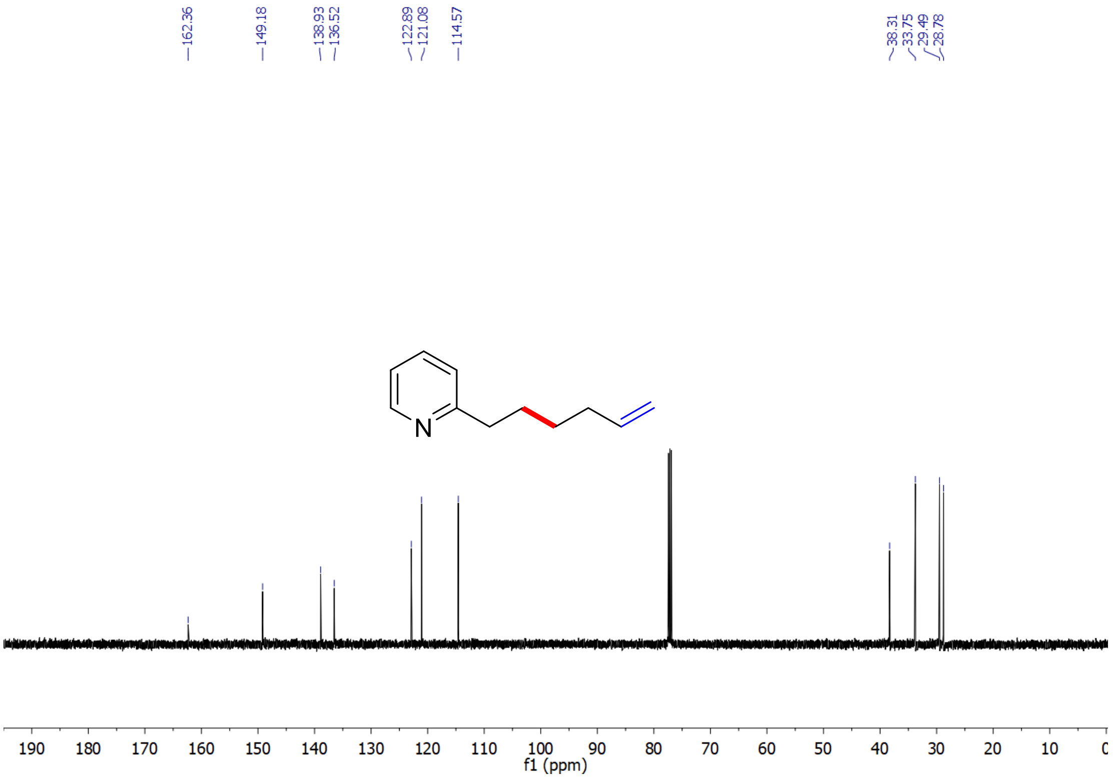

^{1}H NMR (500 MHz, CDCl$_3$), ^{13}C NMR (126 MHz, CDCl$_3$)

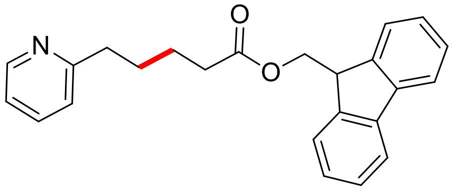

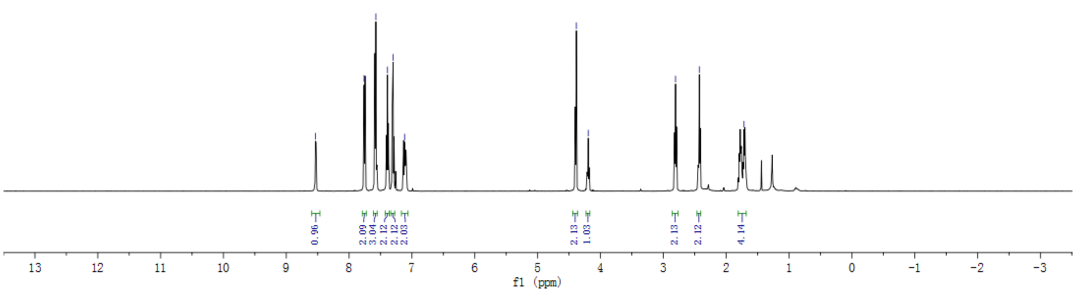

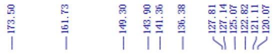

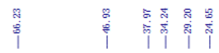

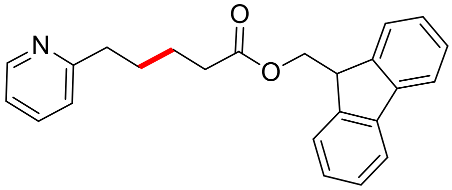

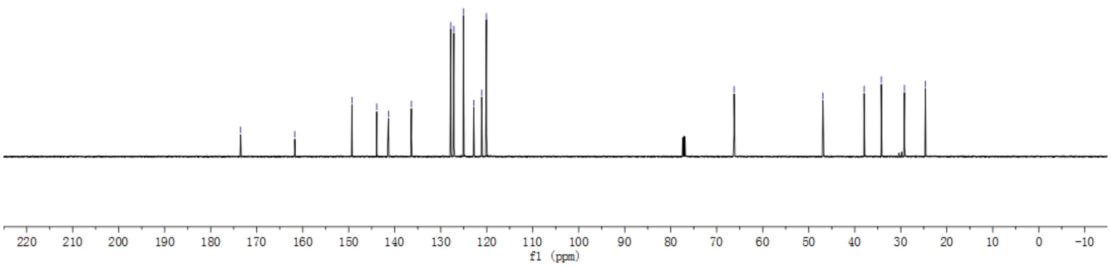

^{1}H NMR (500 MHz, CDCl$_3$), ^{13}C NMR (126 MHz, CDCl$_3$), ^{19}F NMR (376 MHz, CDCl$_3$)

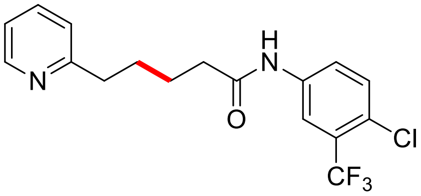

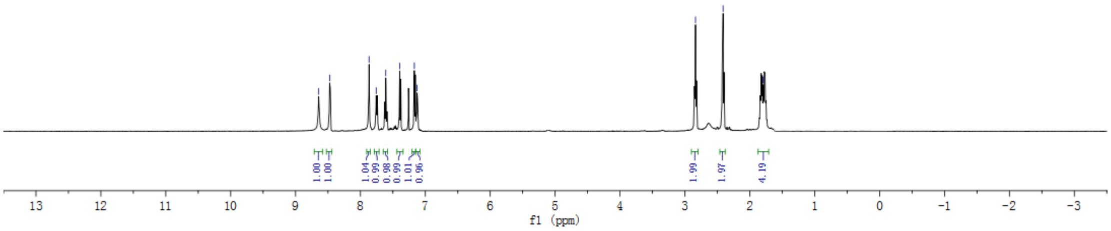

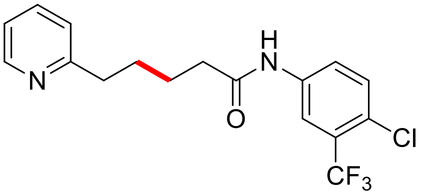

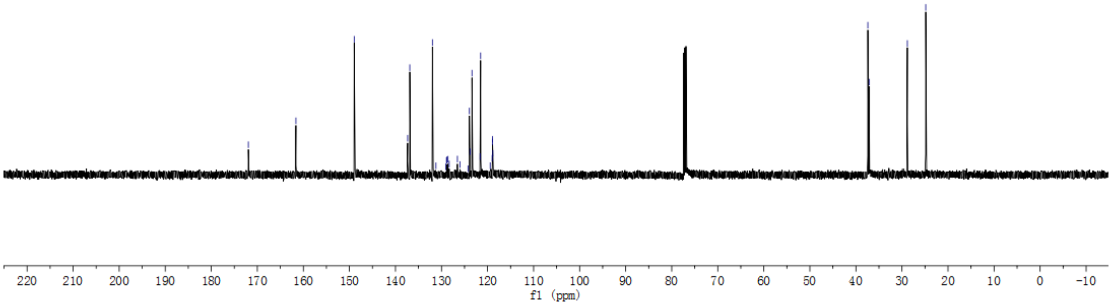

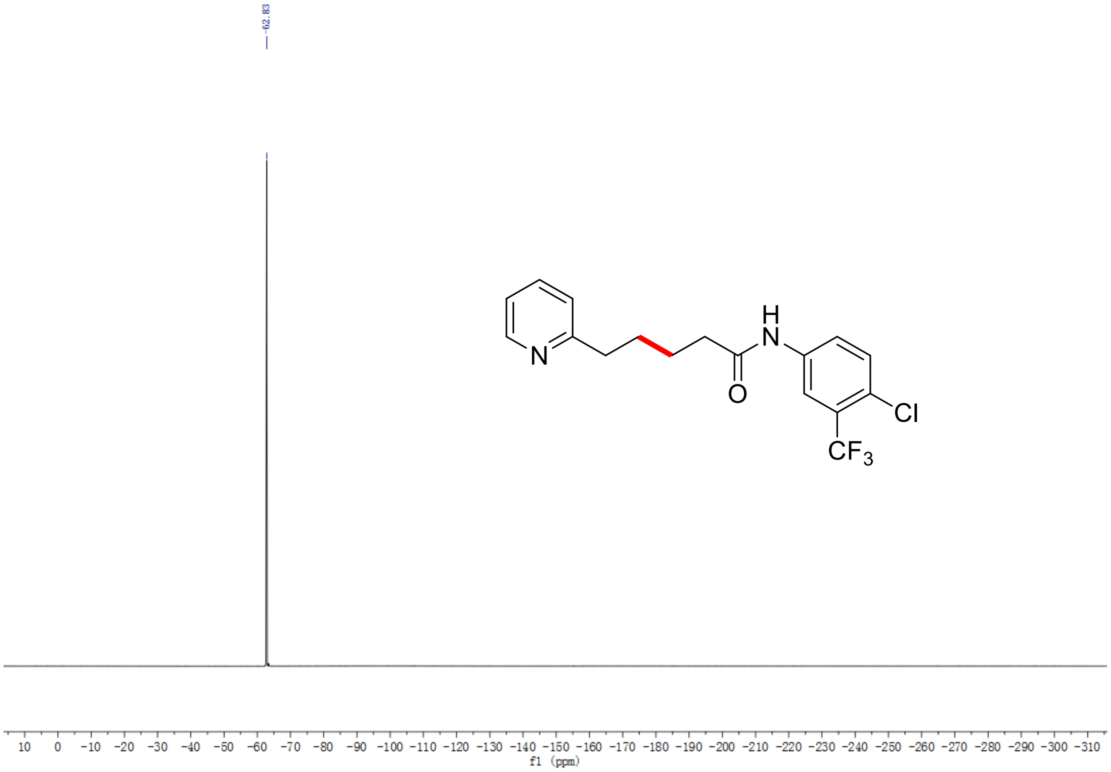
-62.83
H
N
N
O
Cl
CF3
10 0 -10 -20 -30 -40 -50 -60 -70 -80 -90 -100 -110 -120 -130 -140 -150 -160 -170 -180 -190 -200 -210 -220 -230 -240 -250 -260 -270 -280 -290 -300 -310
f1 (ppm)

^{1}H NMR (500 MHz, CDCl$_3$), ^{13}C NMR (126 MHz, CDCl$_3$)

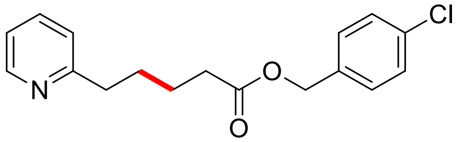

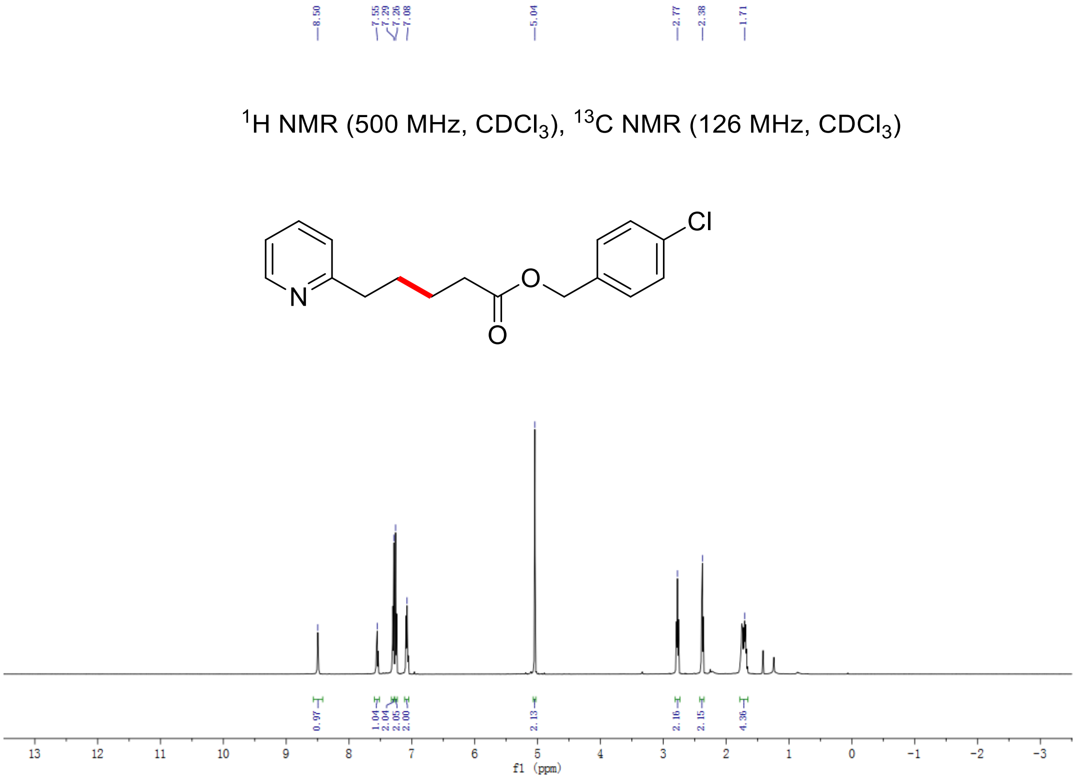

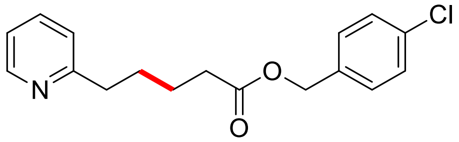

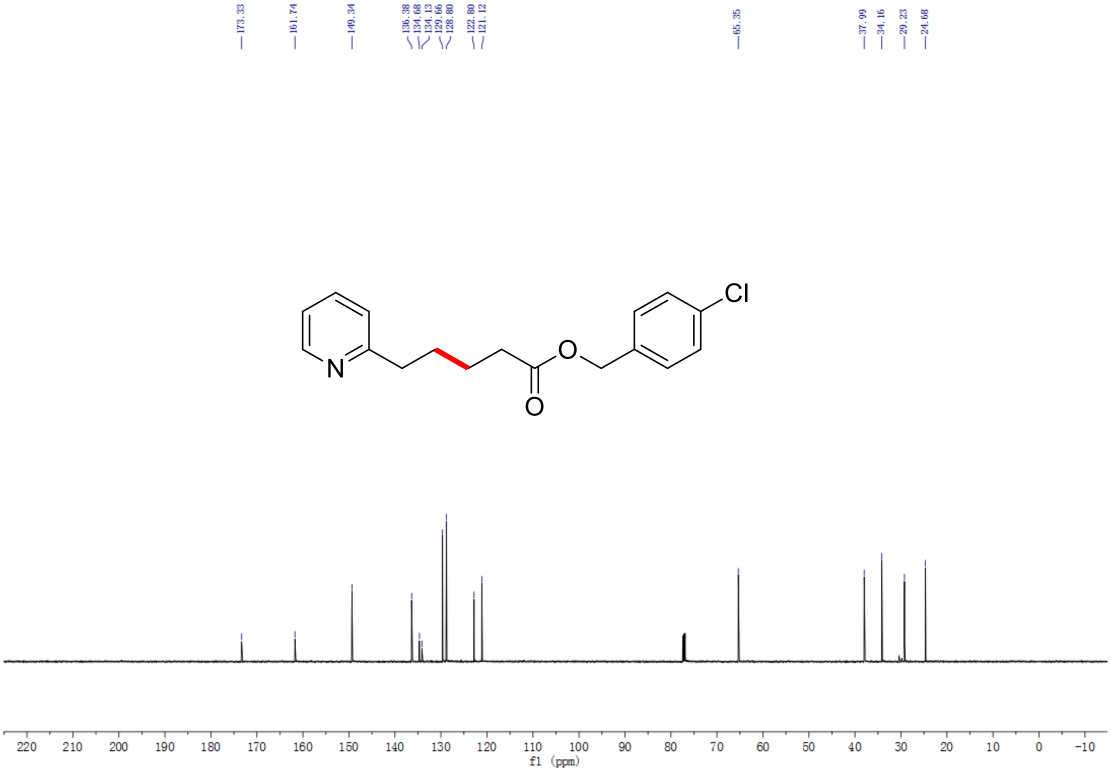

^{1}H NMR (500 MHz, $CDCl_3$), ^{13}C NMR (126 MHz, $CDCl_3$)

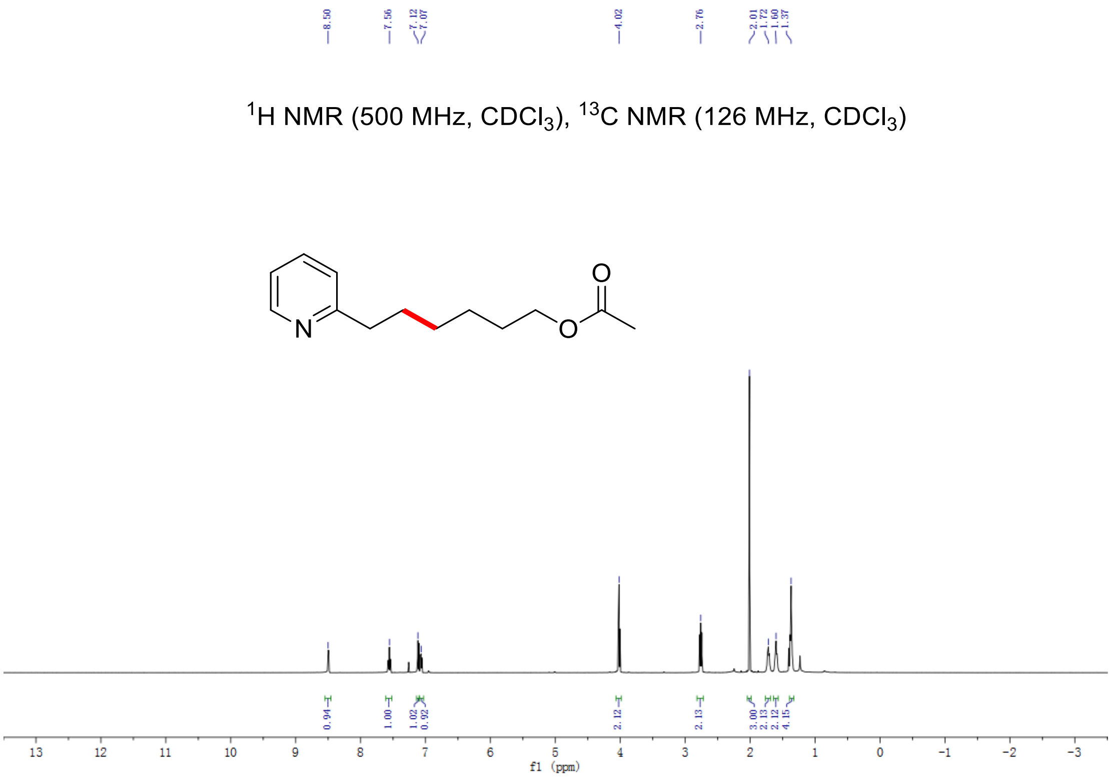

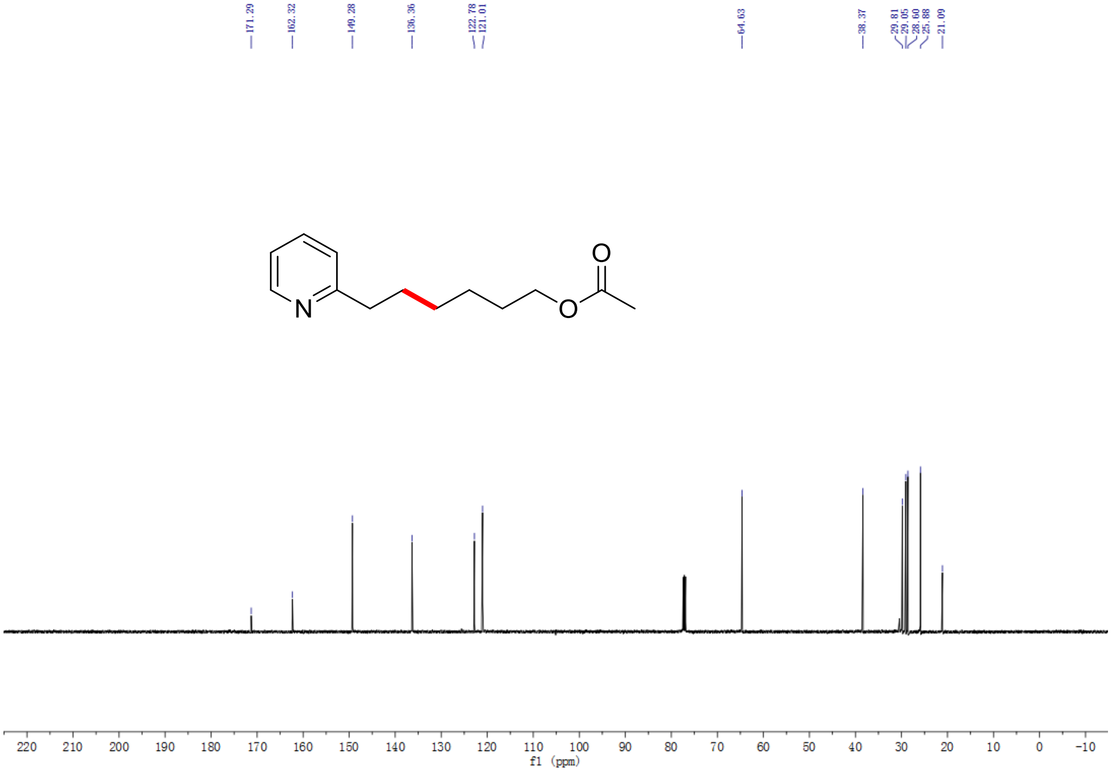

^{1}H NMR (500 MHz, CDCl$_3$), ^{13}C NMR (126 MHz, CDCl$_3$), ^{19}F NMR (376 MHz, CDCl$_3$)

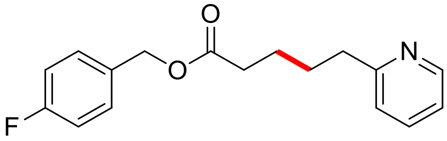

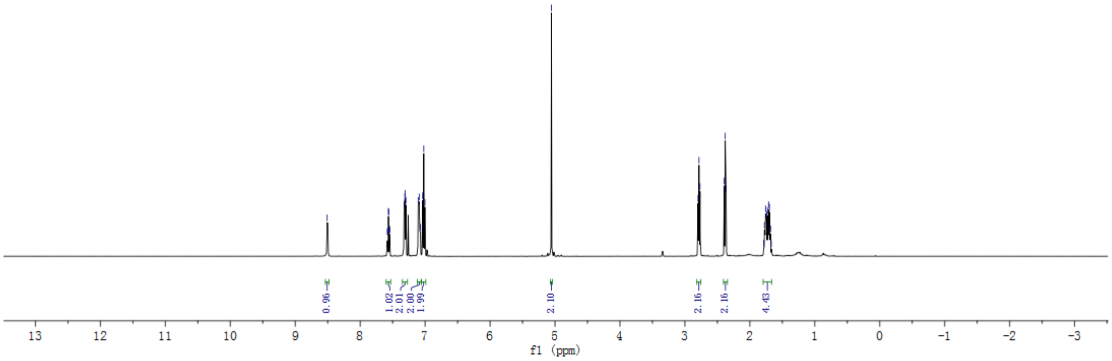

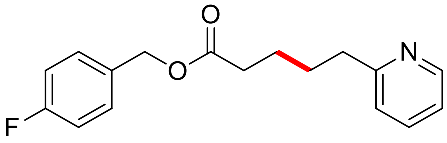

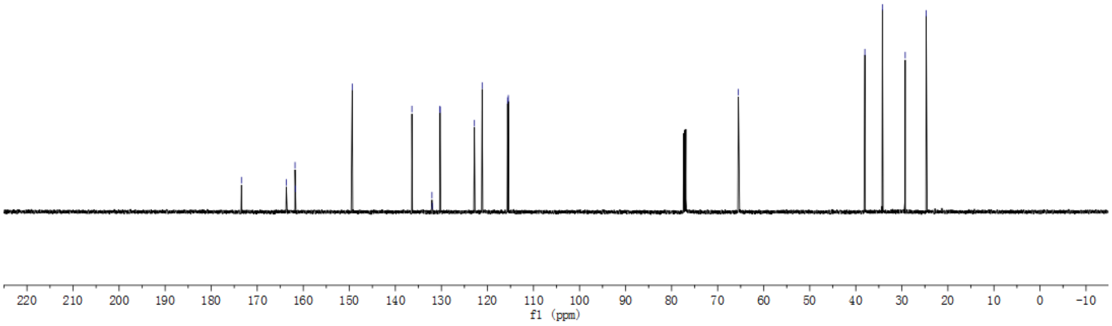

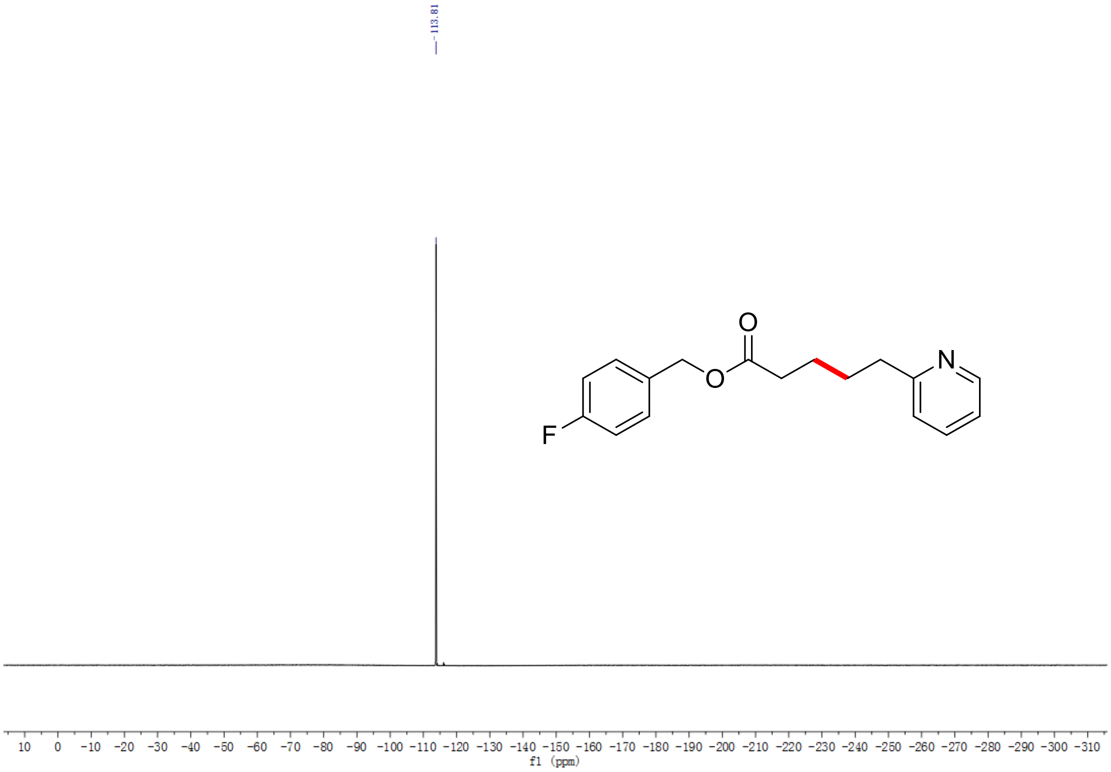

-113.81
O
O
N
F
10
0
-10
-20
-30
-40
-50
-60
-70
-80
-90
-100
-110
-120
-130
-140
-150
-160
-170
-180
-190
-200
-210
-220
-230
-240
-250
-260
-270
-280
-290
-300
-310
f1 (ppm)

^{1}H NMR (500 MHz, CDCl$_3$), ^{13}C NMR (126 MHz, CDCl$_3$)

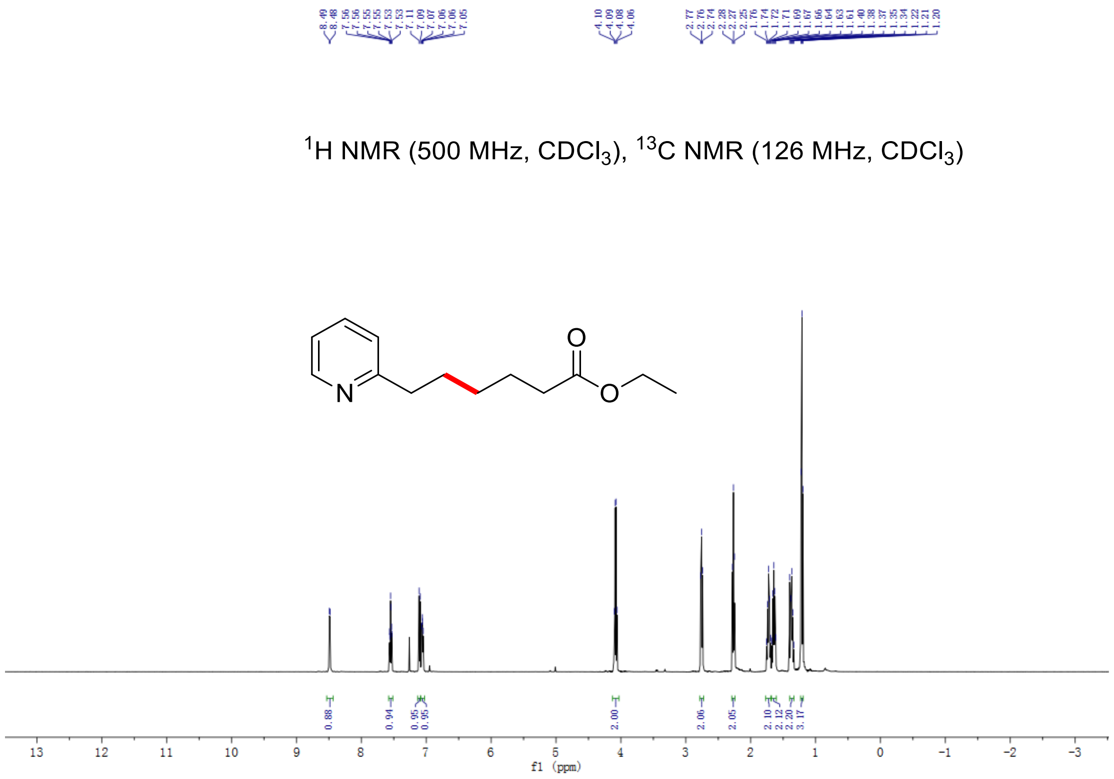

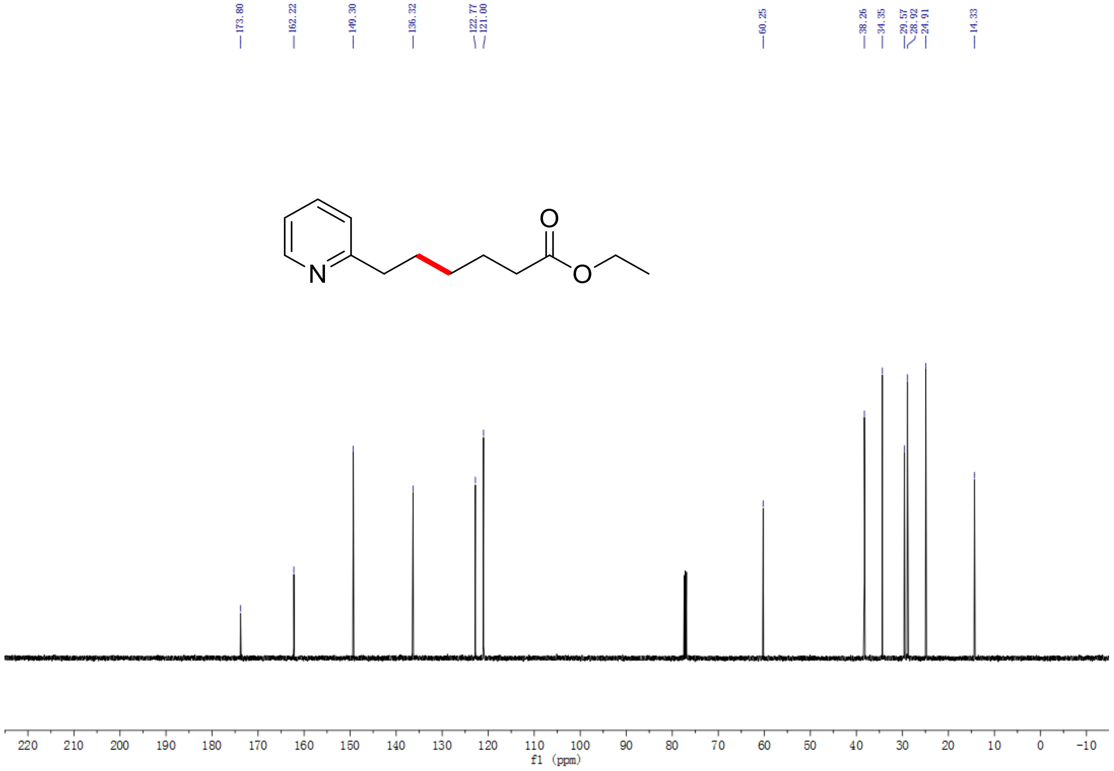

^{1}H NMR (500 MHz, CDCl$_3$), ^{13}C NMR (126 MHz, CDCl$_3$)

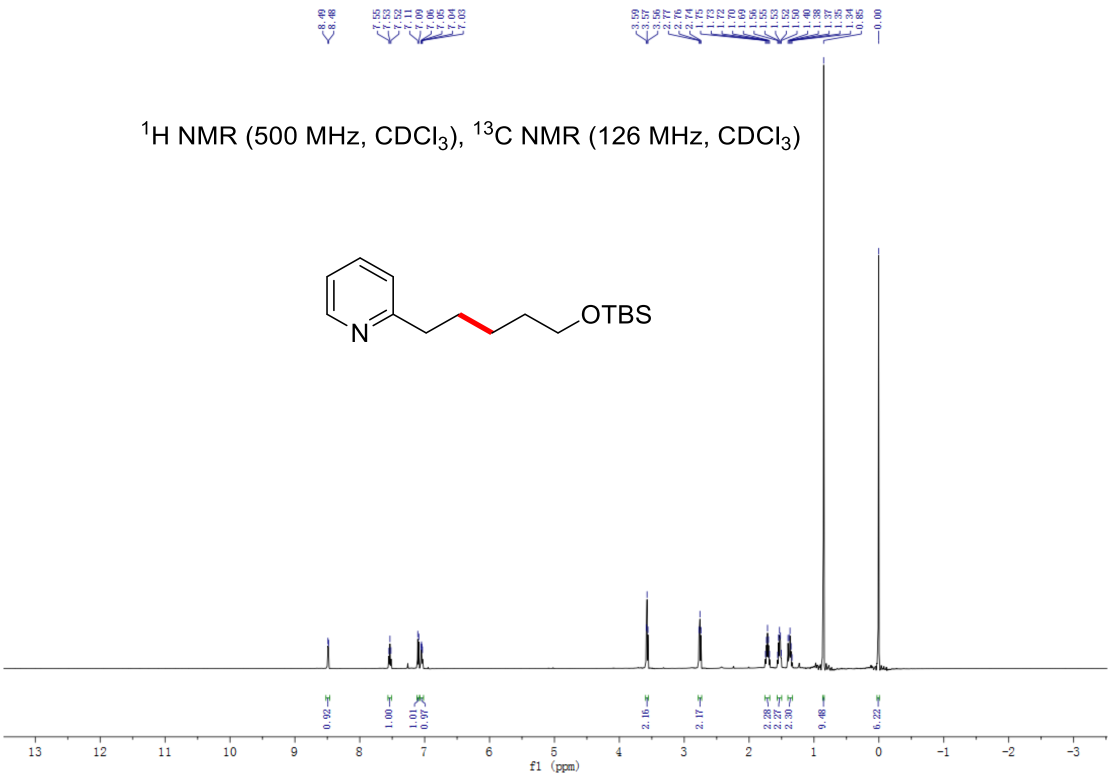

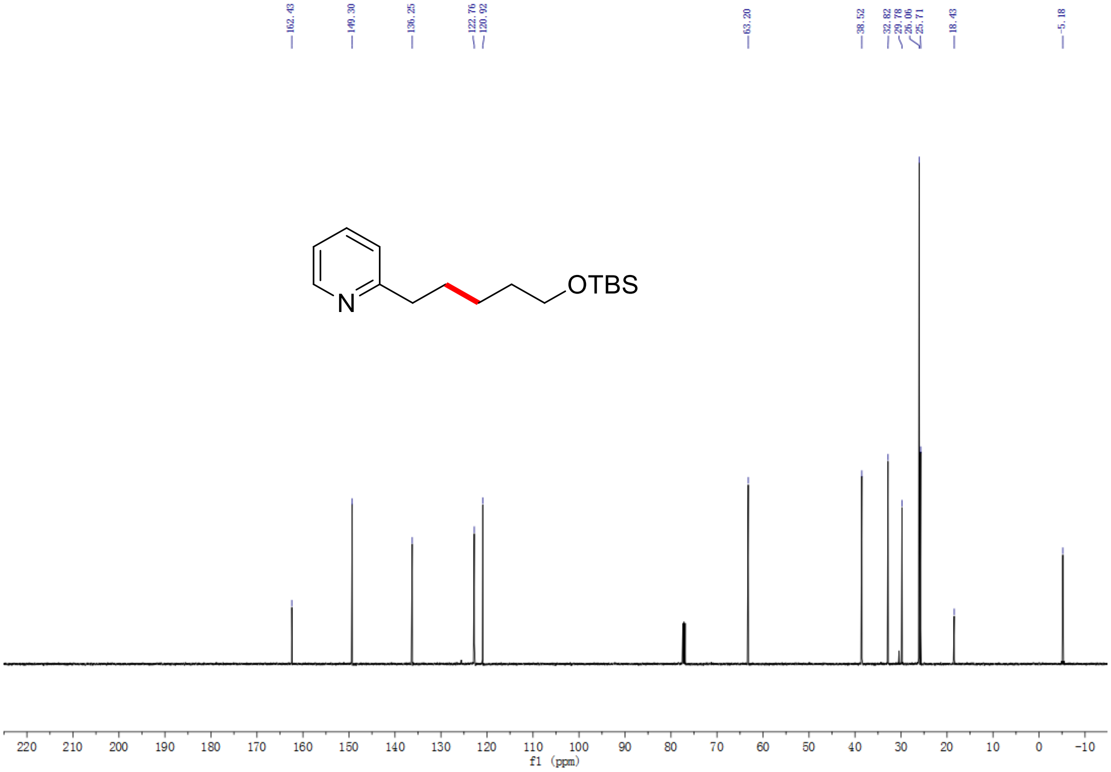

^{1}H NMR (500 MHz, CDCl$_3$), ^{13}C NMR (126 MHz, CDCl$_3$)

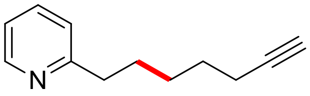

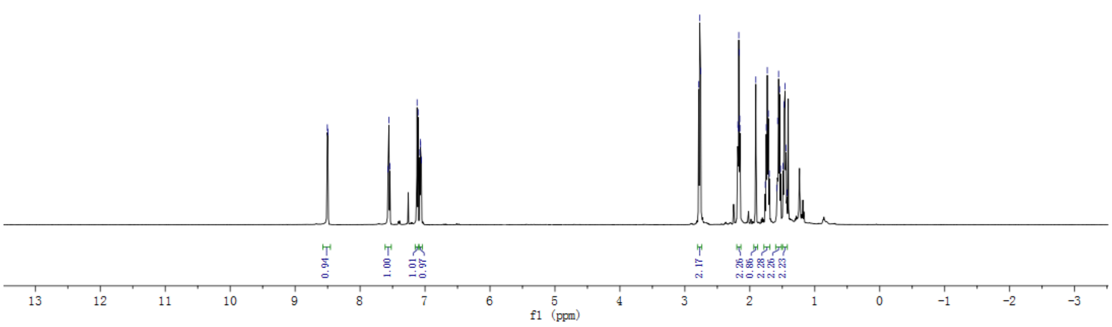

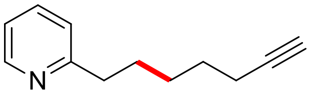

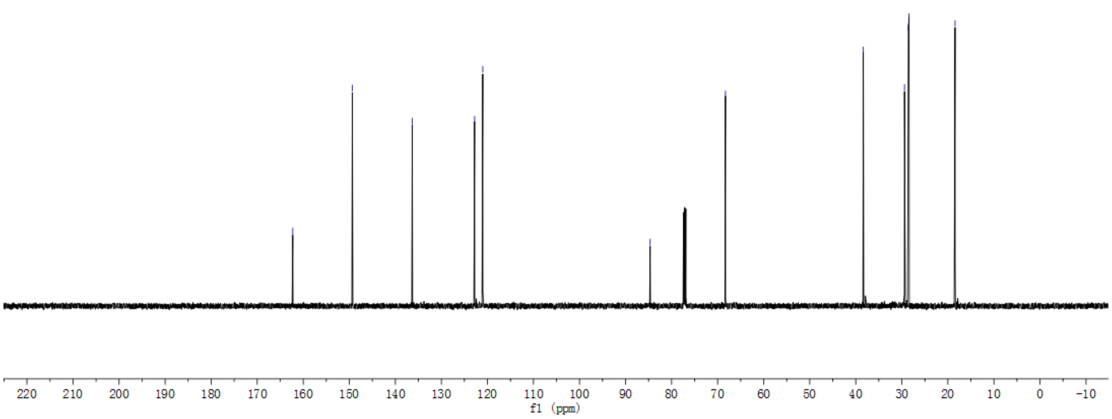

^{1}H NMR (500 MHz, $CDCl_3$), ^{13}C NMR (126 MHz, $CDCl_3$)

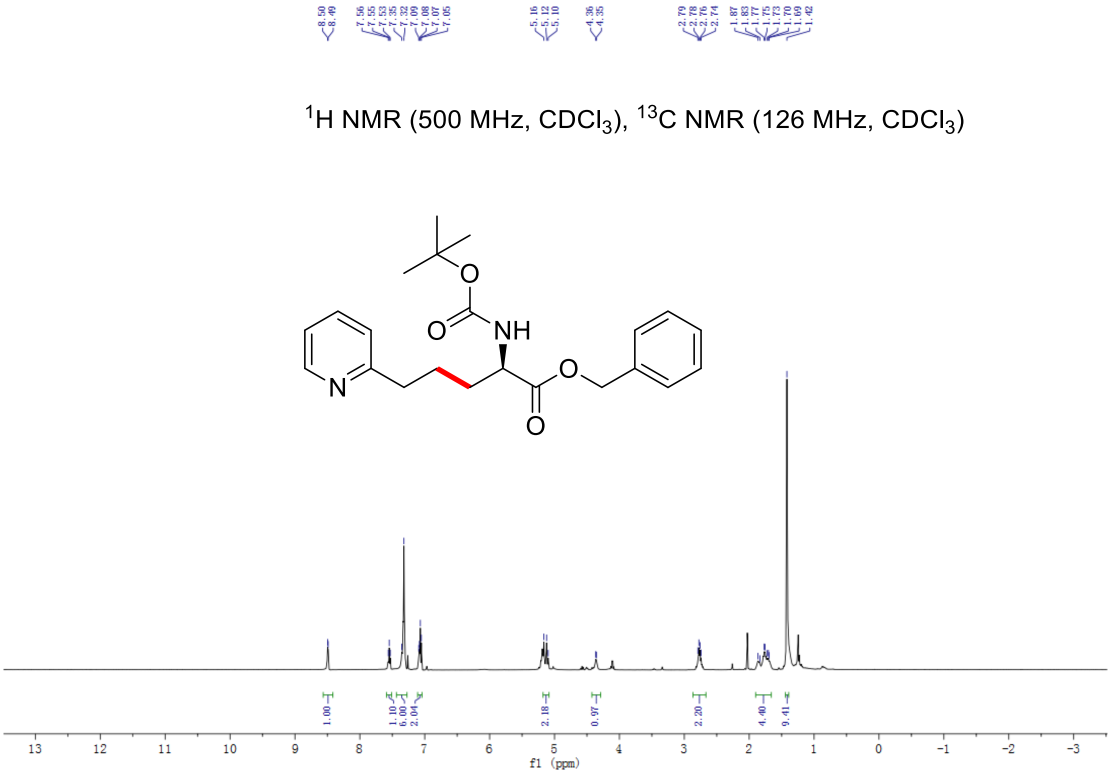

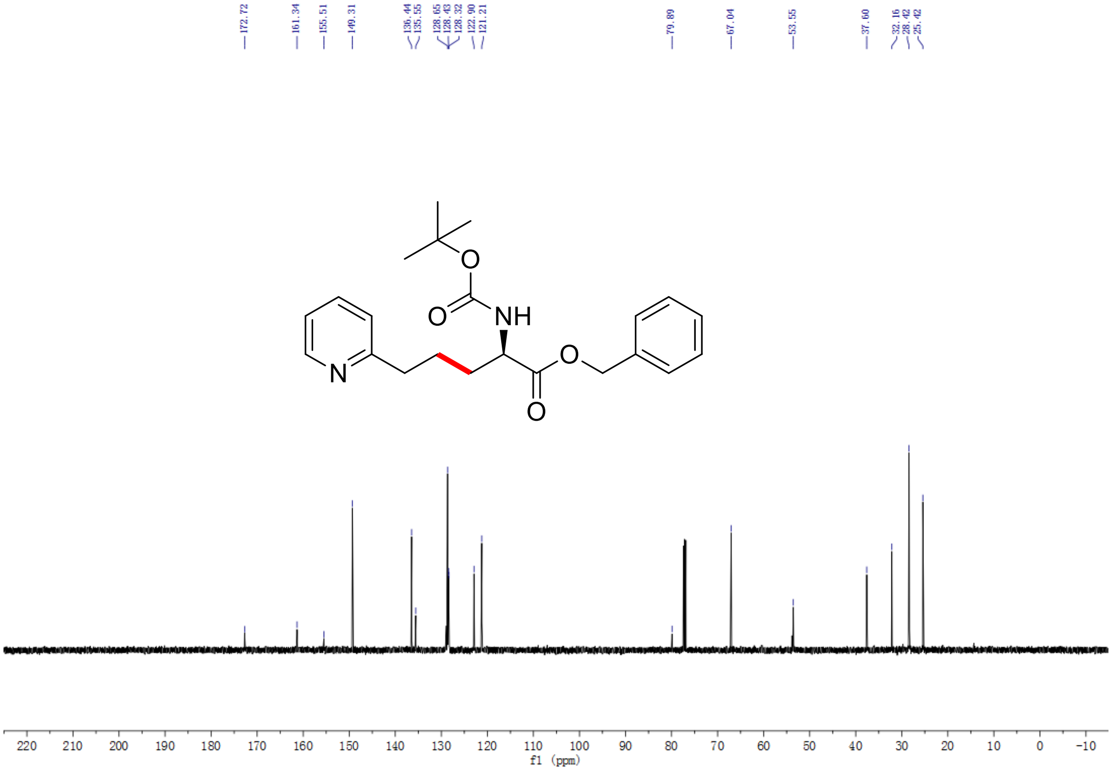

^{1}H NMR (500 MHz, CDCl$_3$), ^{13}C NMR (126 MHz, CDCl$_3$), ^{19}F NMR (376 MHz, CDCl$_3$)

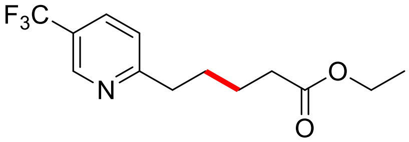

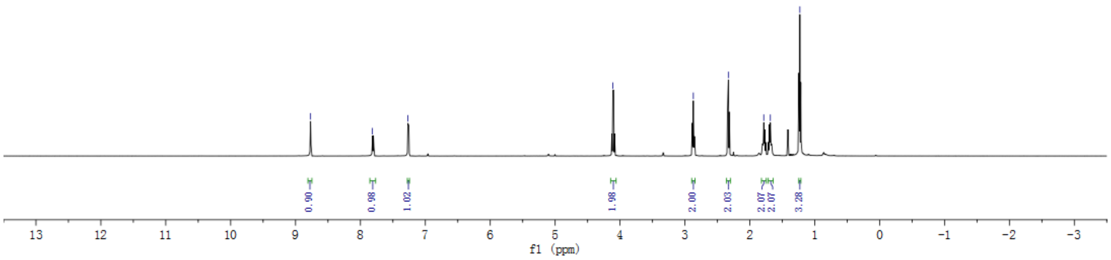

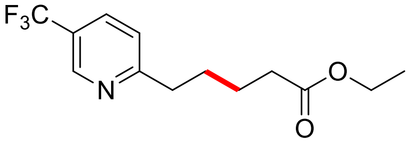

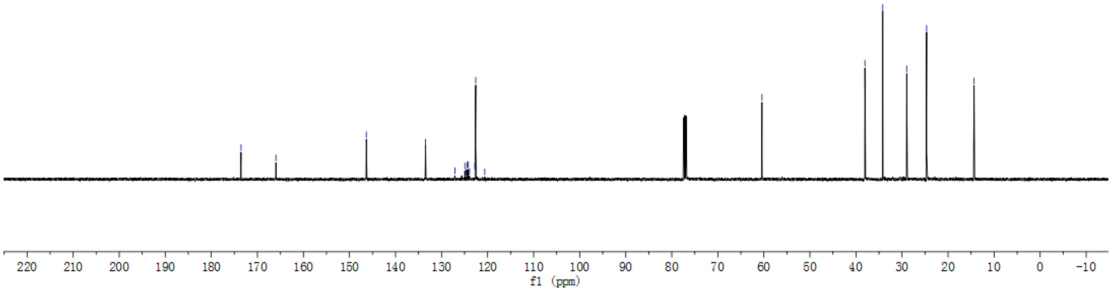

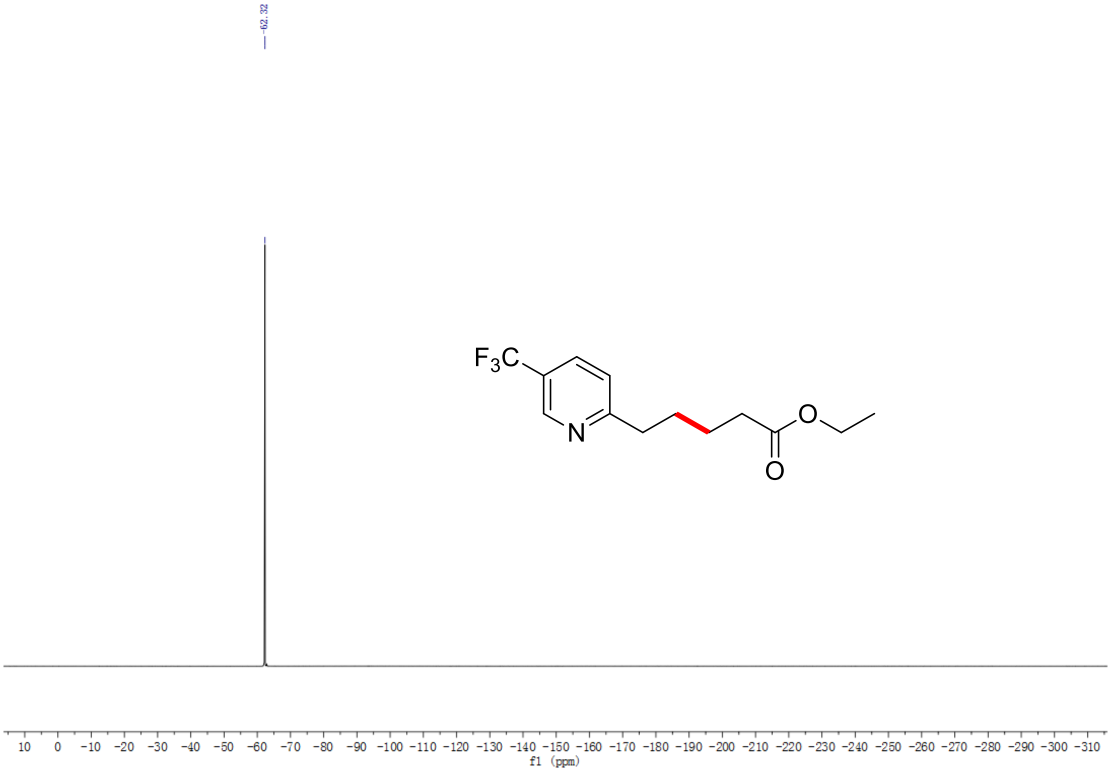
-62.32
F3C
N
O
O
10 0 −10 −20 −30 −40 −50 −60 −70 −80 −90 −100 −110 −120 −130 −140 −150 −160 −170 −180 −190 −200 −210 −220 −230 −240 −250 −260 −270 −280 −290 −300 −310
f1 (ppm)

^1H NMR (500 MHz, $CDCl_3$), ^{13}C NMR (126 MHz, $CDCl_3$), ^{19}F NMR (376 MHz, $CDCl_3$)

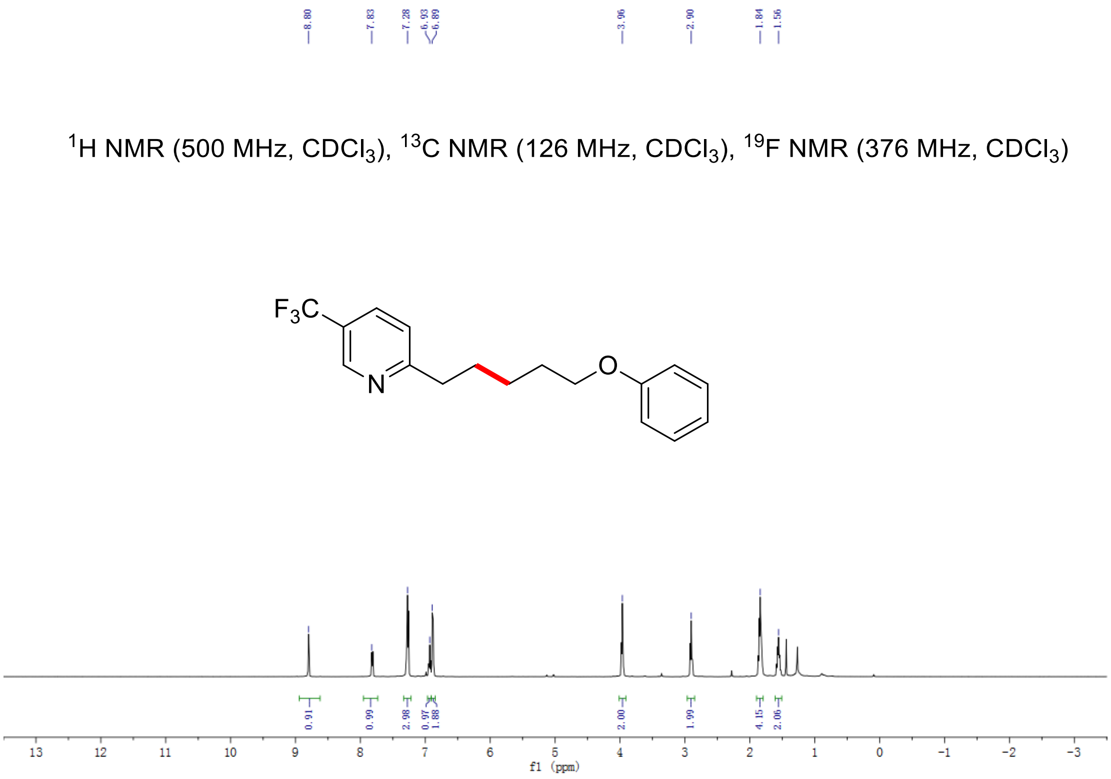

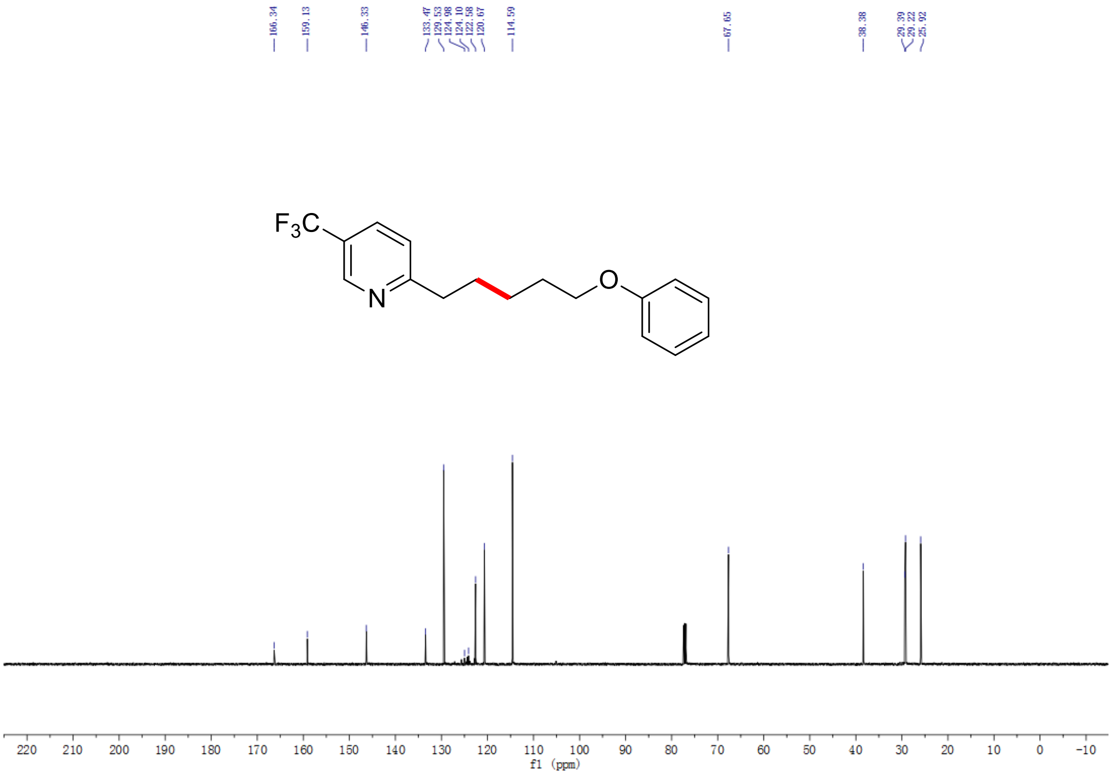

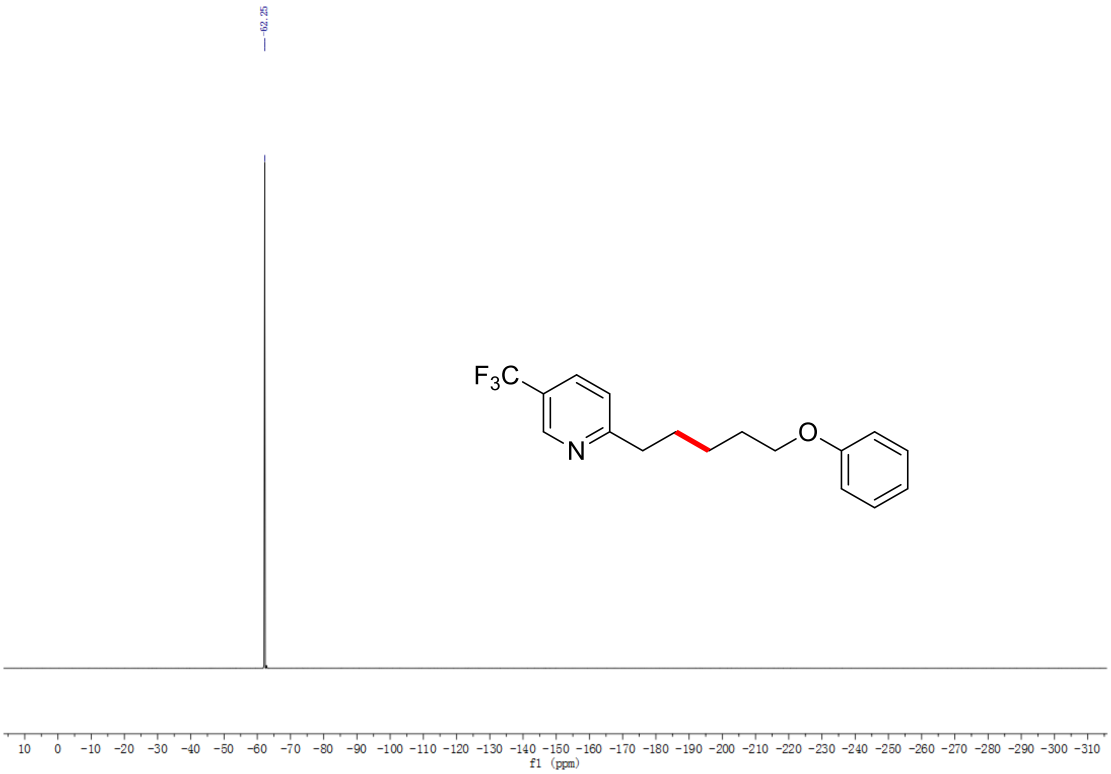

-62.25
F3C
N
O
10 0 −10 −20 −30 −40 −50 −60 −70 −80 −90 −100 −110 −120 −130 −140 −150 −160 −170 −180 −190 −200 −210 −220 −230 −240 −250 −260 −270 −280 −290 −300 −310
f1 (ppm)

^{1}H NMR (500 MHz, CDCl$_3$), ^{13}C NMR (126 MHz, CDCl$_3$), ^{19}F NMR (376 MHz, CDCl$_3$)

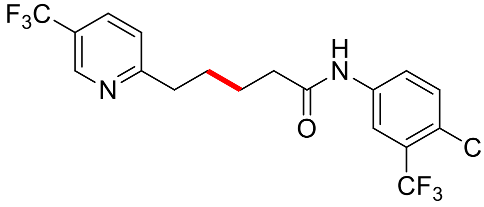
F3C
N
H
N
O
Cl
CF3

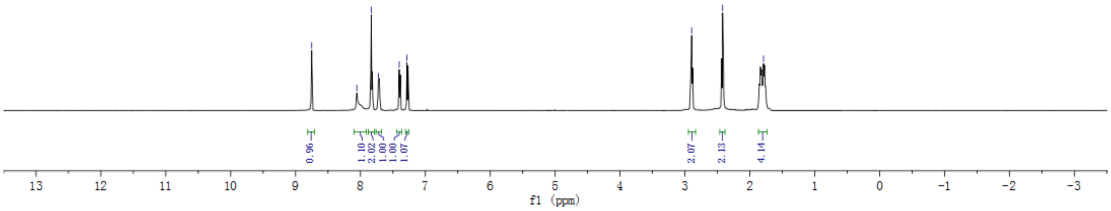

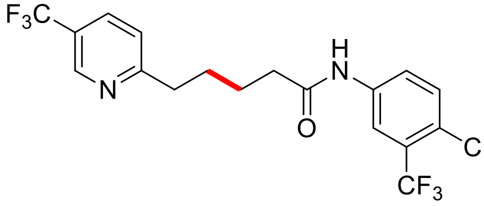
F3C
N
H
N
O
Cl
CF3

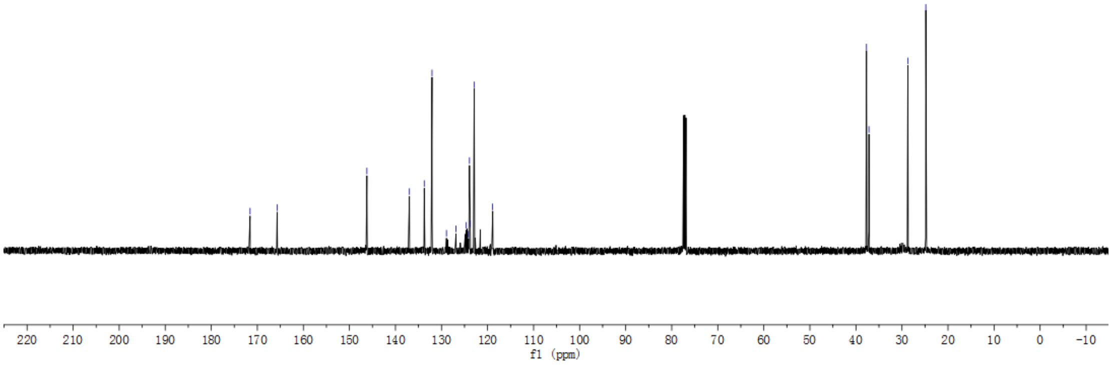

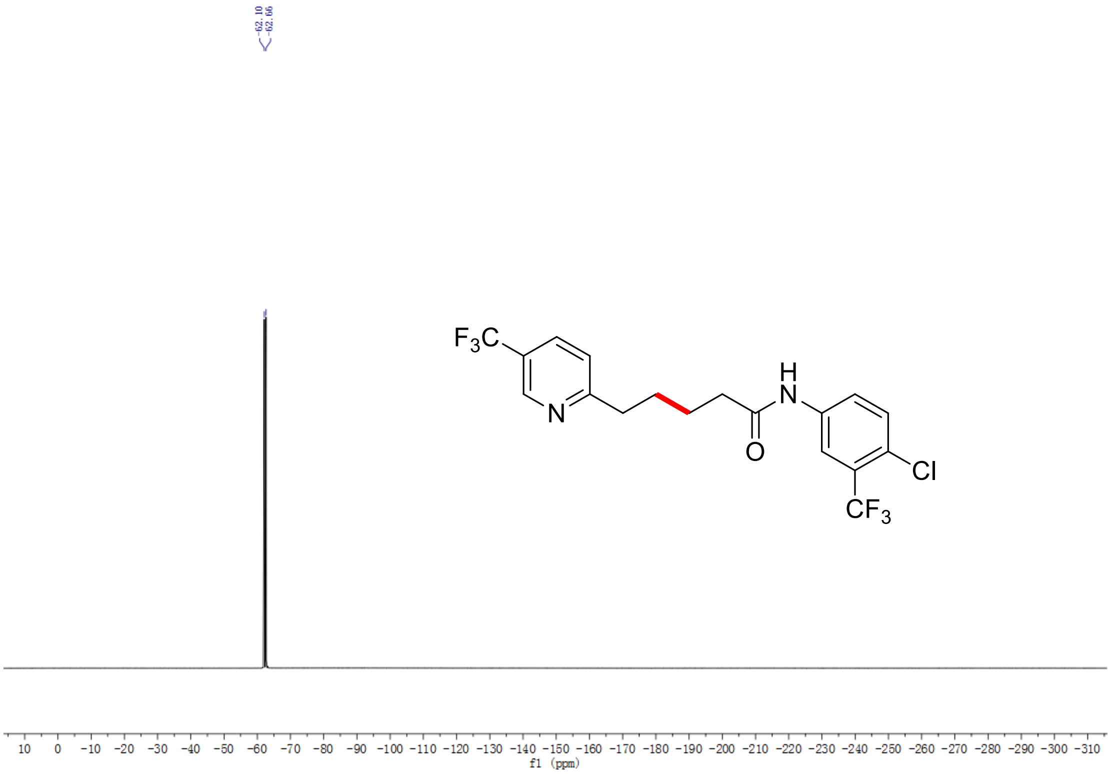
-62.10
-62.66
F3C
N
H
N
O
Cl
CF3
10 0 −10 −20 −30 −40 −50 −60 −70 −80 −90 −100 −110 −120 −130 −140 −150 −160 −170 −180 −190 −200 −210 −220 −230 −240 −250 −260 −270 −280 −290 −300 −310
f1 (ppm)

^{1}H NMR (500 MHz, CDCl$_3$), ^{13}C NMR (126 MHz, CDCl$_3$)

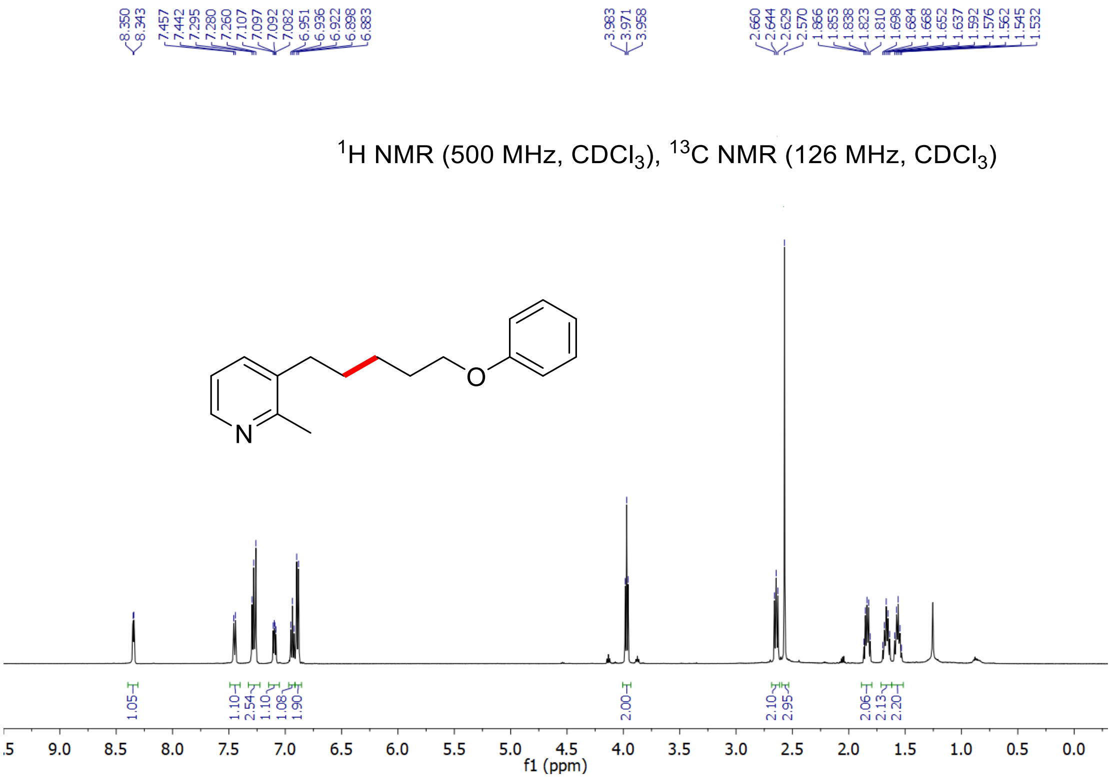

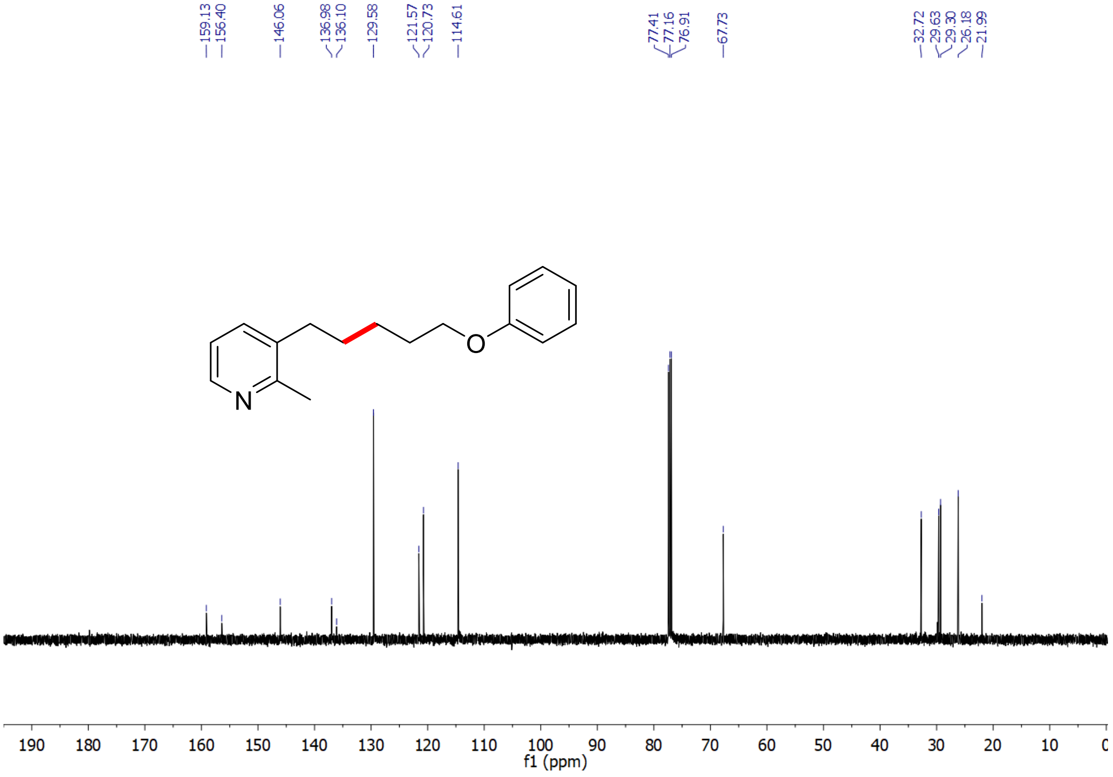

^{1}H NMR (500 MHz, CDCl$_3$), ^{13}C NMR (126 MHz, CDCl$_3$)

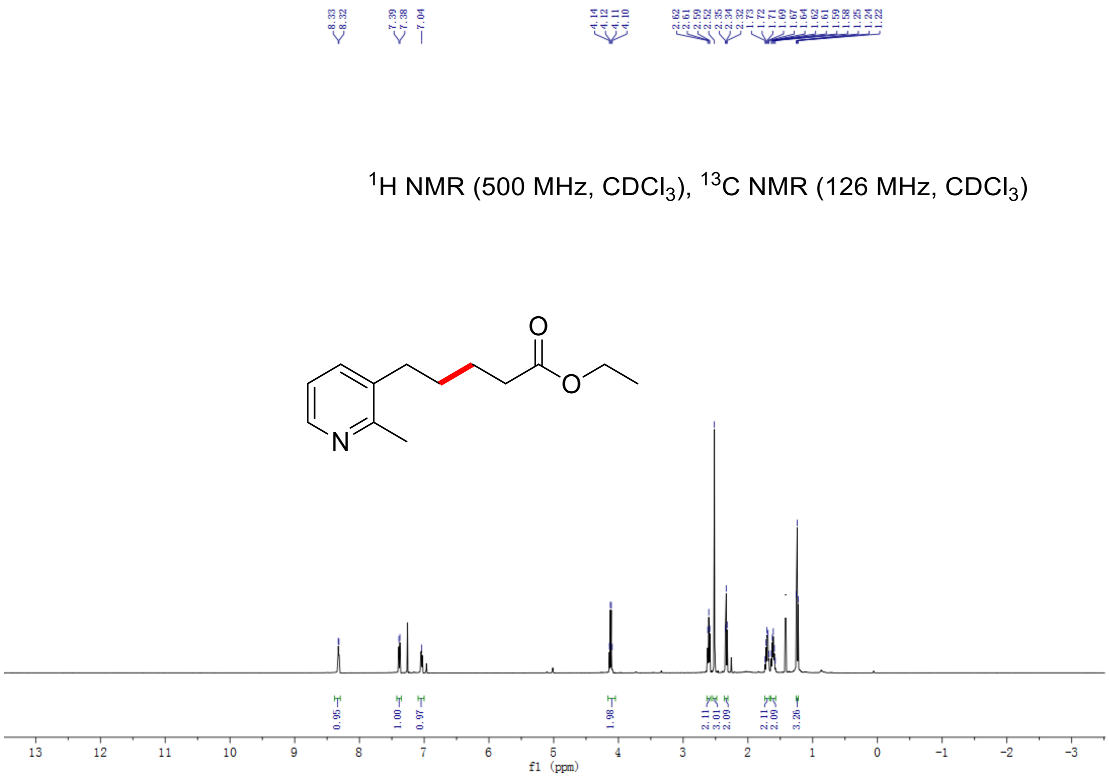

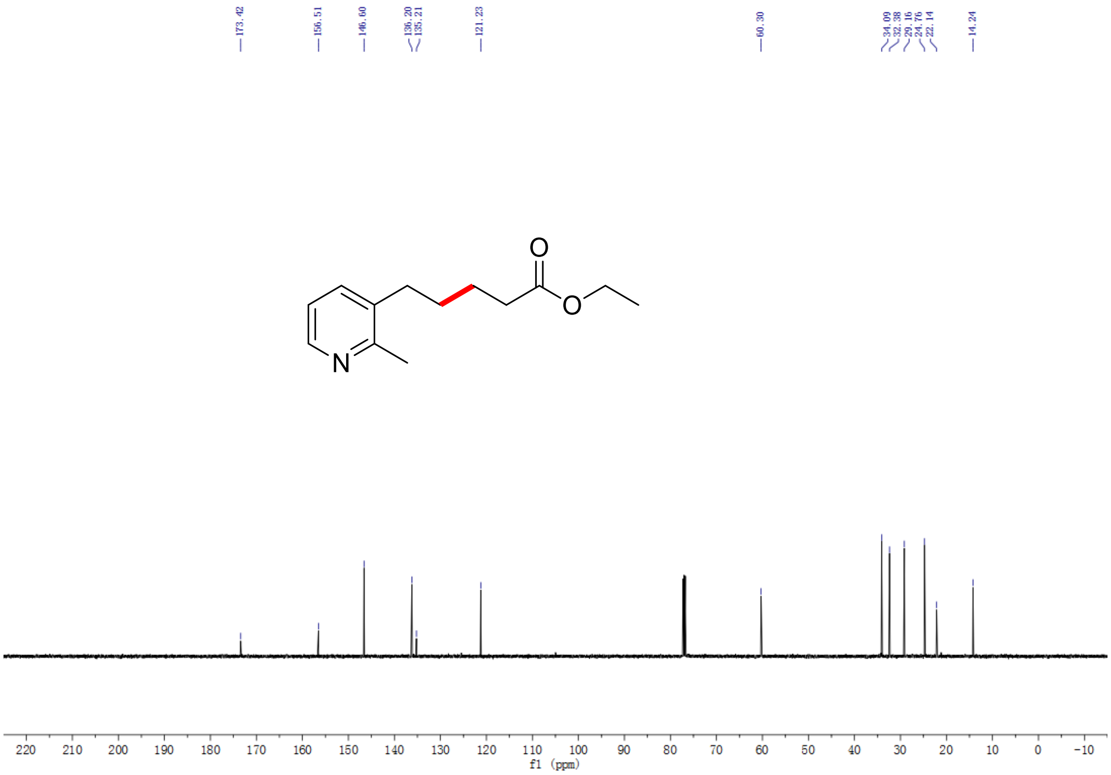

^{1}H NMR (500 MHz, CDCl$_3$), ^{13}C NMR (126 MHz, CDCl$_3$), ^{19}F NMR (376 MHz, CDCl$_3$)

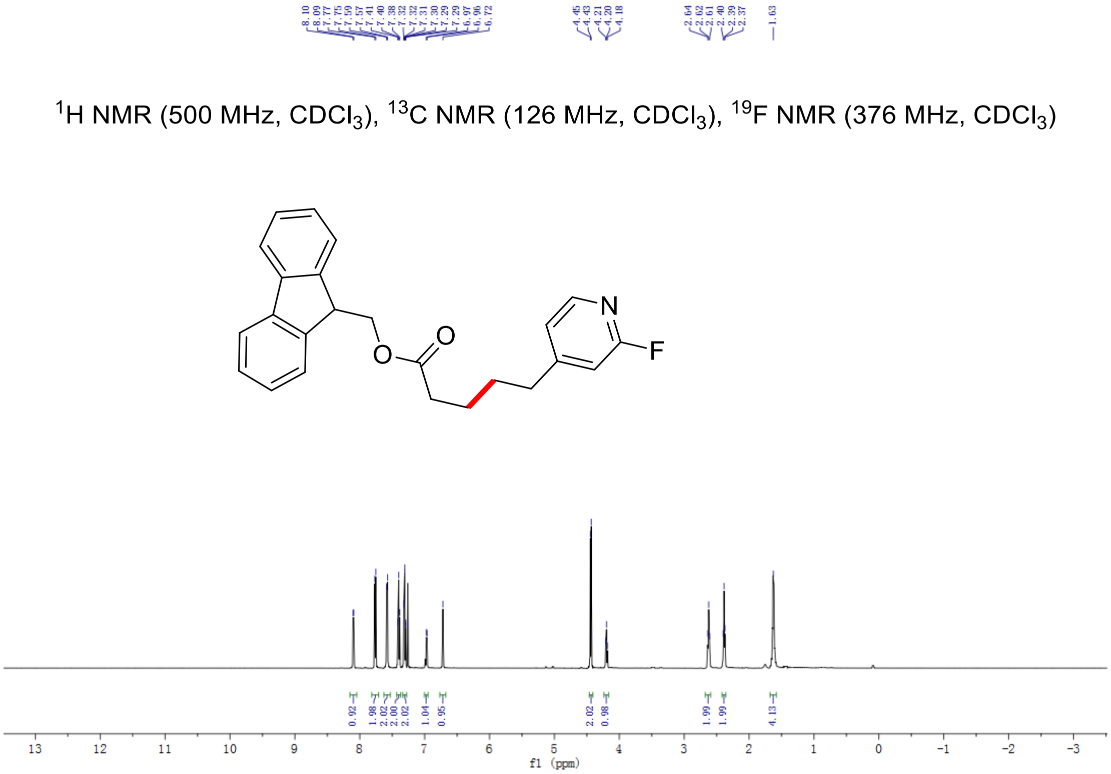

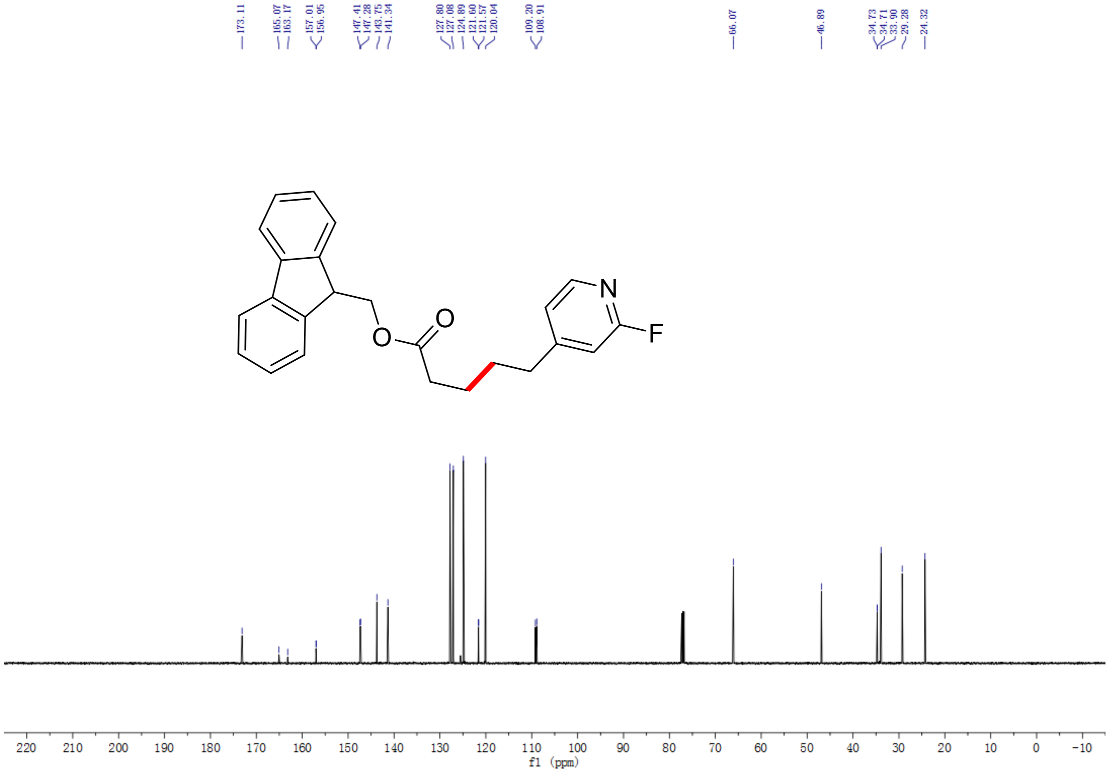

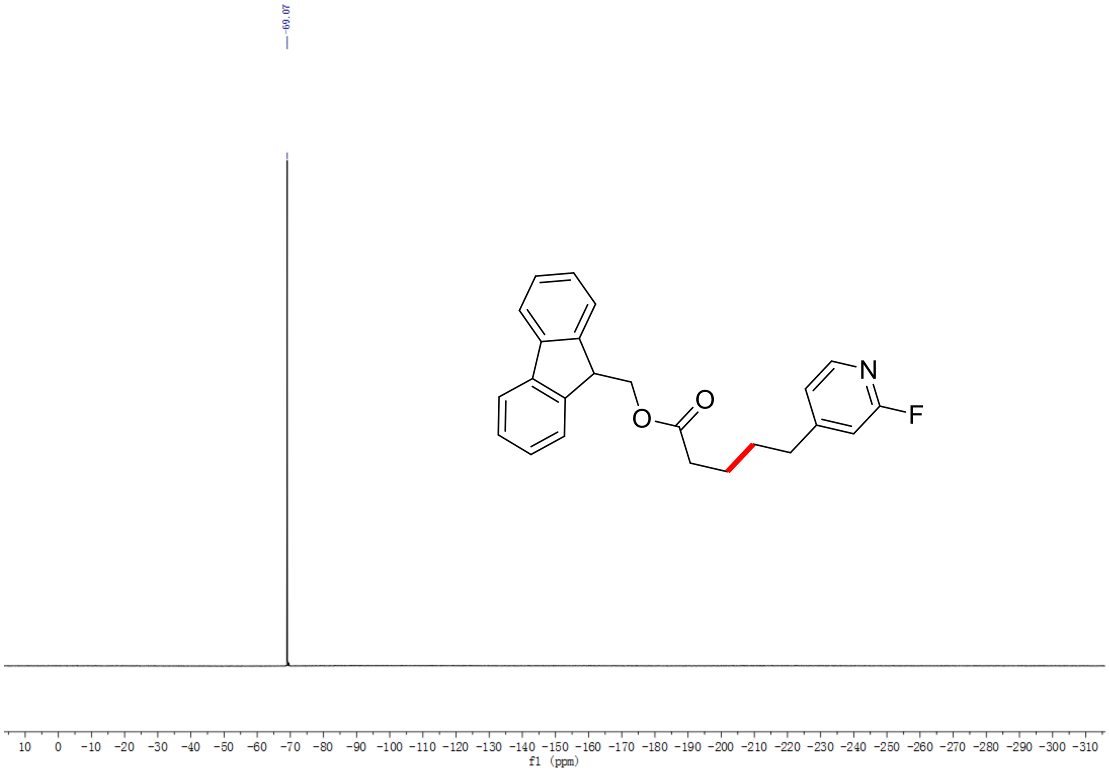
-69.07
O
O
N
F
10 0 -10 -20 -30 -40 -50 -60 -70 -80 -90 -100 -110 -120 -130 -140 -150 -160 -170 -180 -190 -200 -210 -220 -230 -240 -250 -260 -270 -280 -290 -300 -310
f1 (ppm)

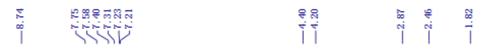

^{1}H NMR (500 MHz, CDCl$_3$), ^{13}C NMR (126 MHz, CDCl$_3$), ^{19}F NMR (376 MHz, CDCl$_3$)

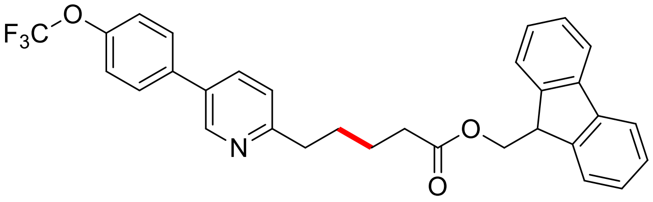

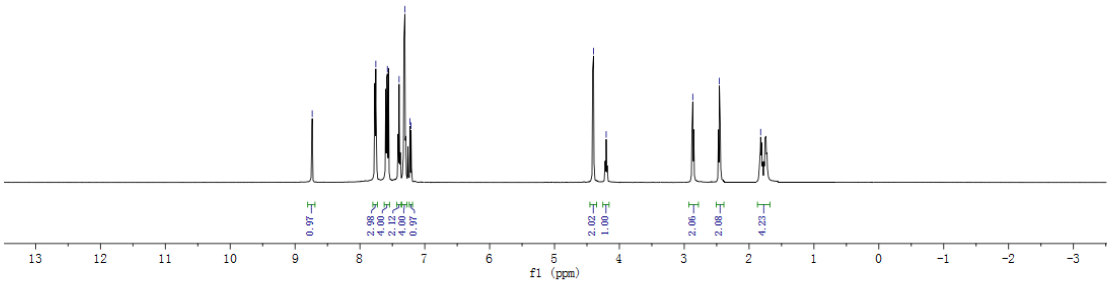

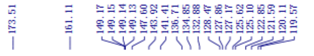

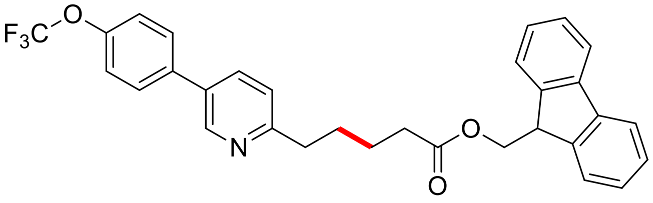

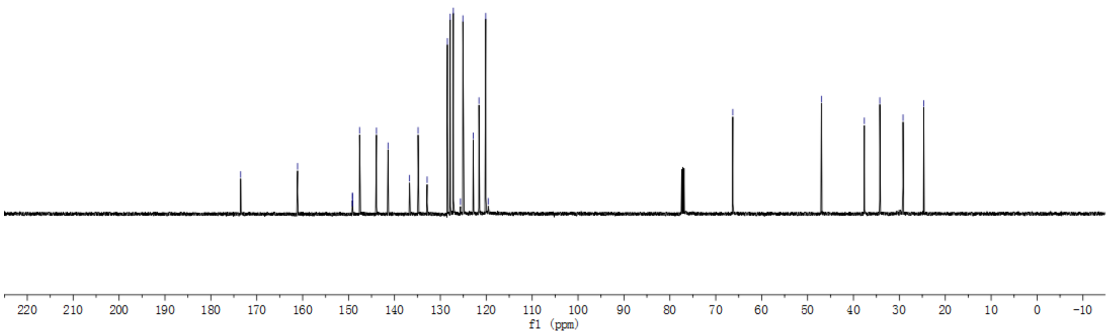

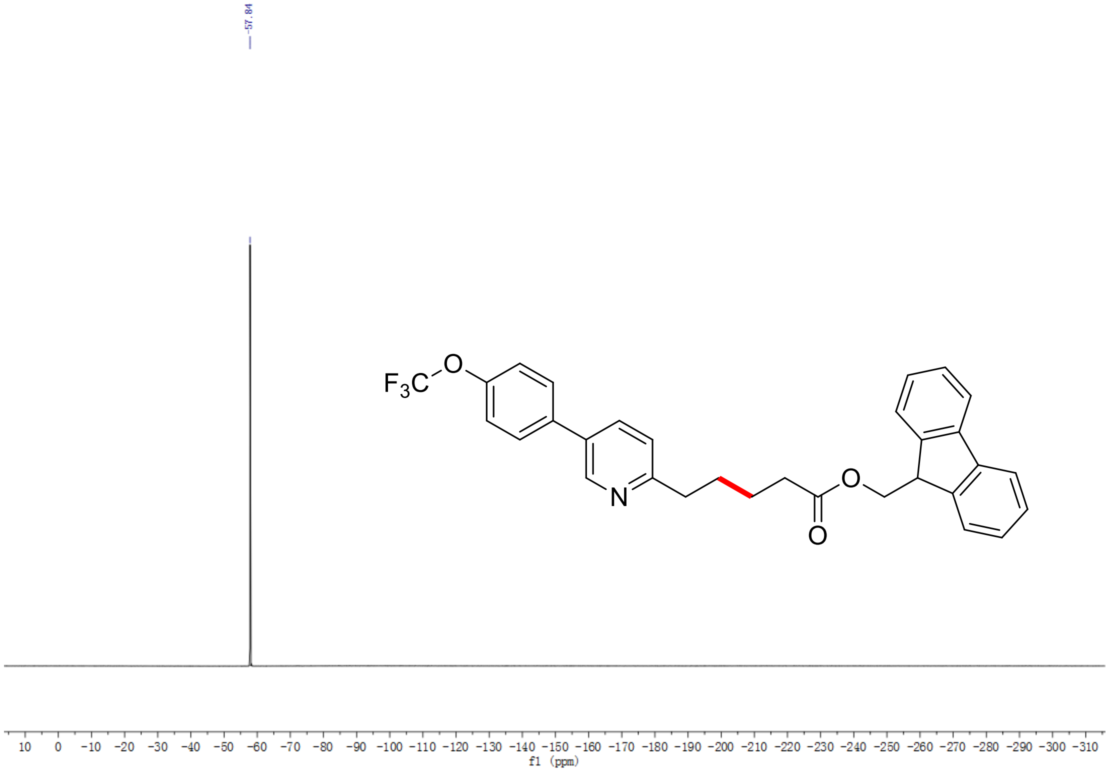
-57.84
F3C
O
N
O
O
10 0 -10 -20 -30 -40 -50 -60 -70 -80 -90 -100 -110 -120 -130 -140 -150 -160 -170 -180 -190 -200 -210 -220 -230 -240 -250 -260 -270 -280 -290 -300 -310
f1 (ppm)

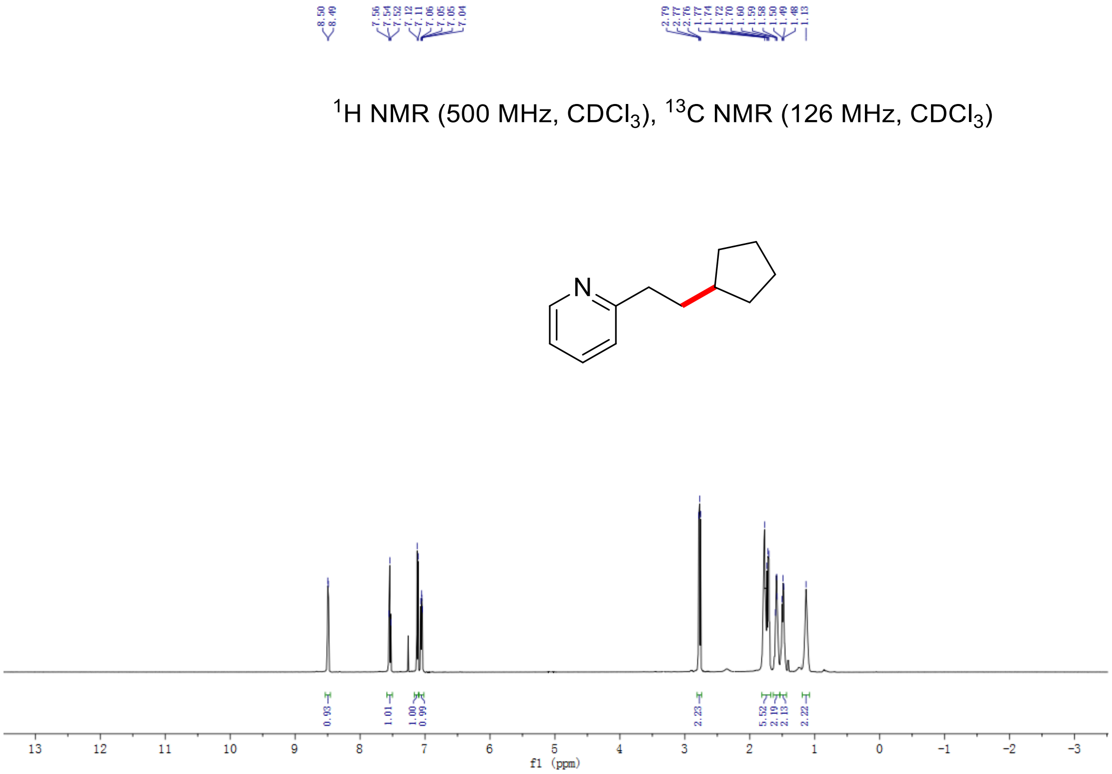

^{1}H NMR (500 MHz, CDCl$_3$), ^{13}C NMR (126 MHz, CDCl$_3$)

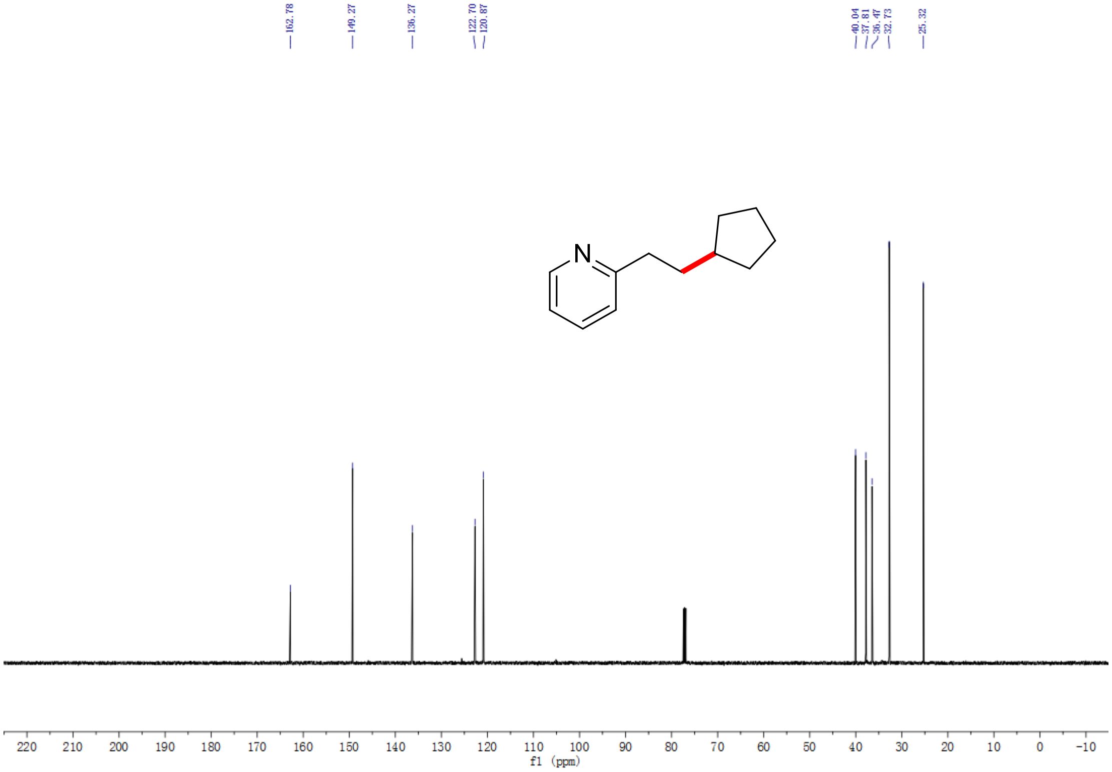

^{1}H NMR (500 MHz, $CDCl_3$), ^{13}C NMR (126 MHz, $CDCl_3$)

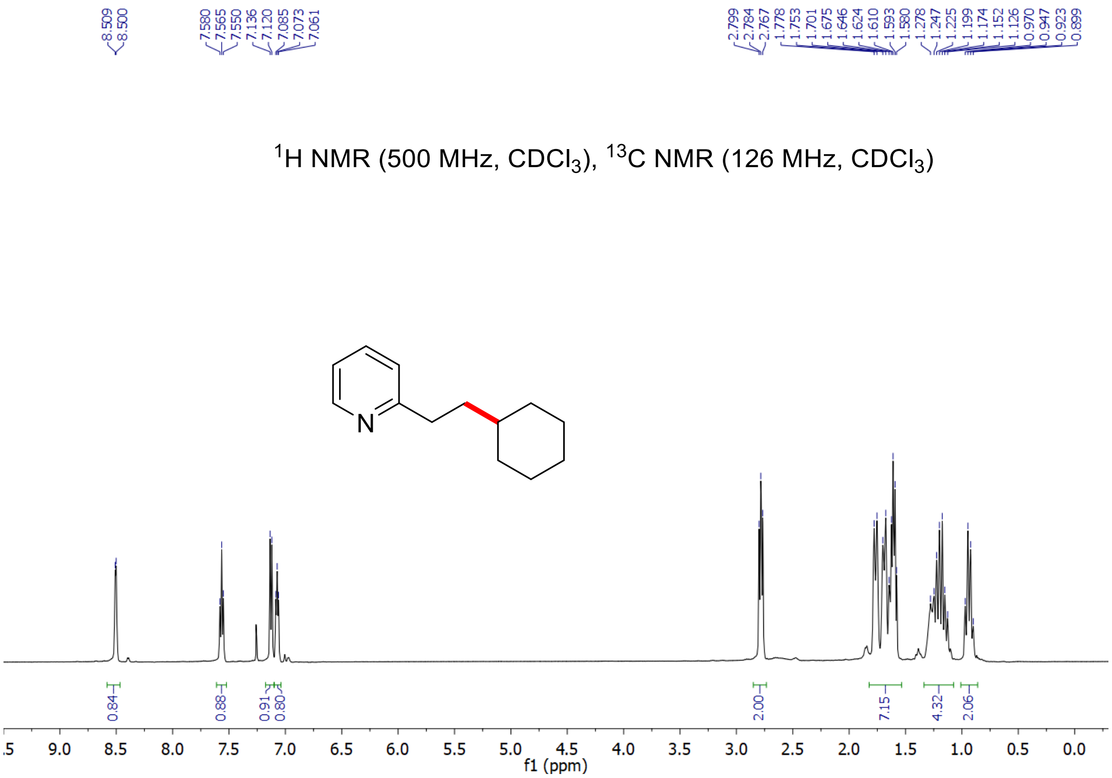

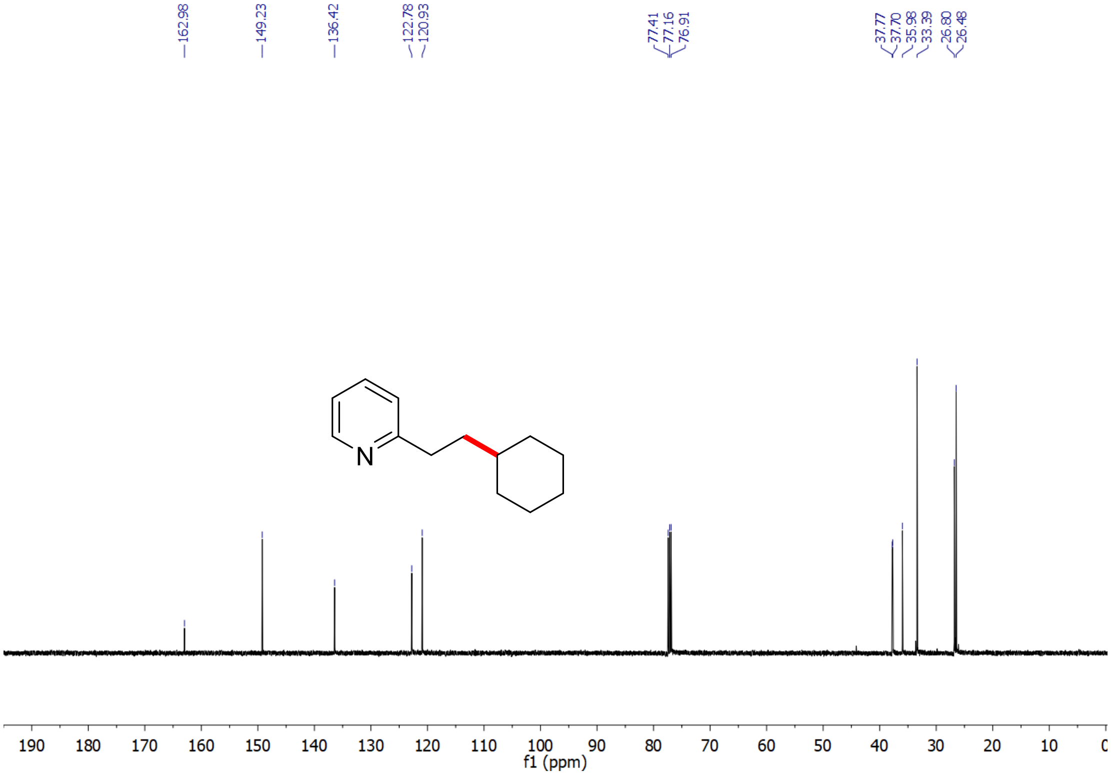

^{1}H NMR (500 MHz, CDCl$_3$), ^{13}C NMR (126 MHz, CDCl$_3$)

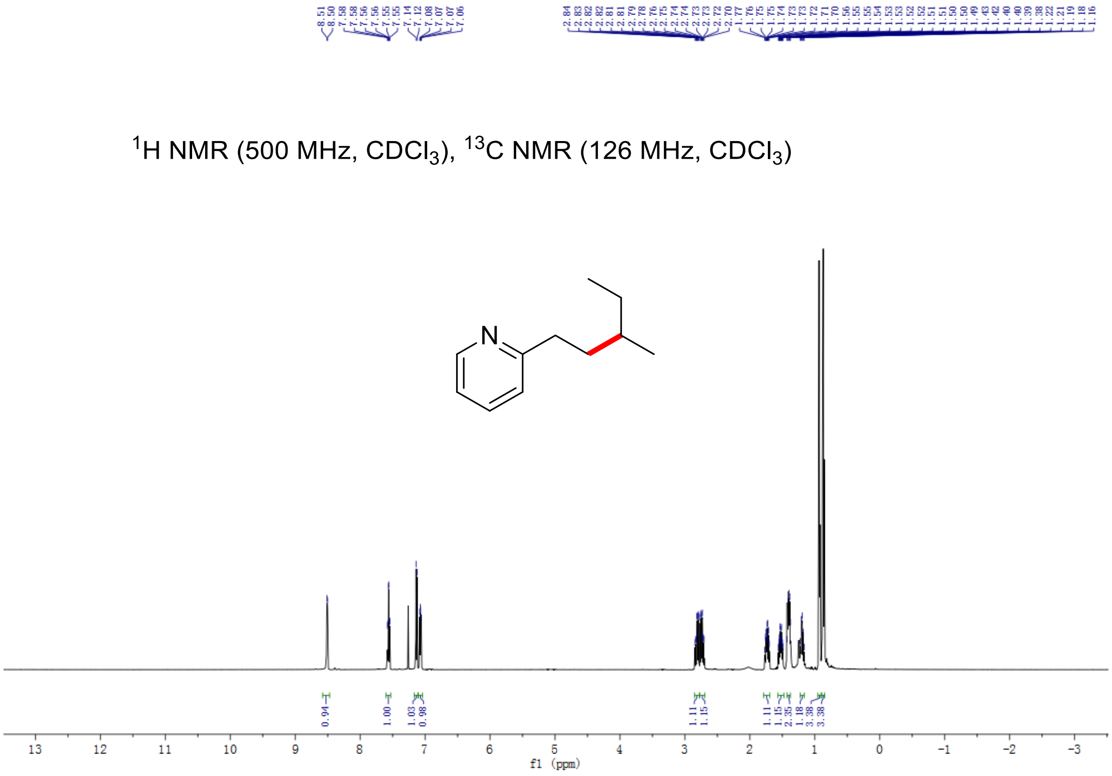

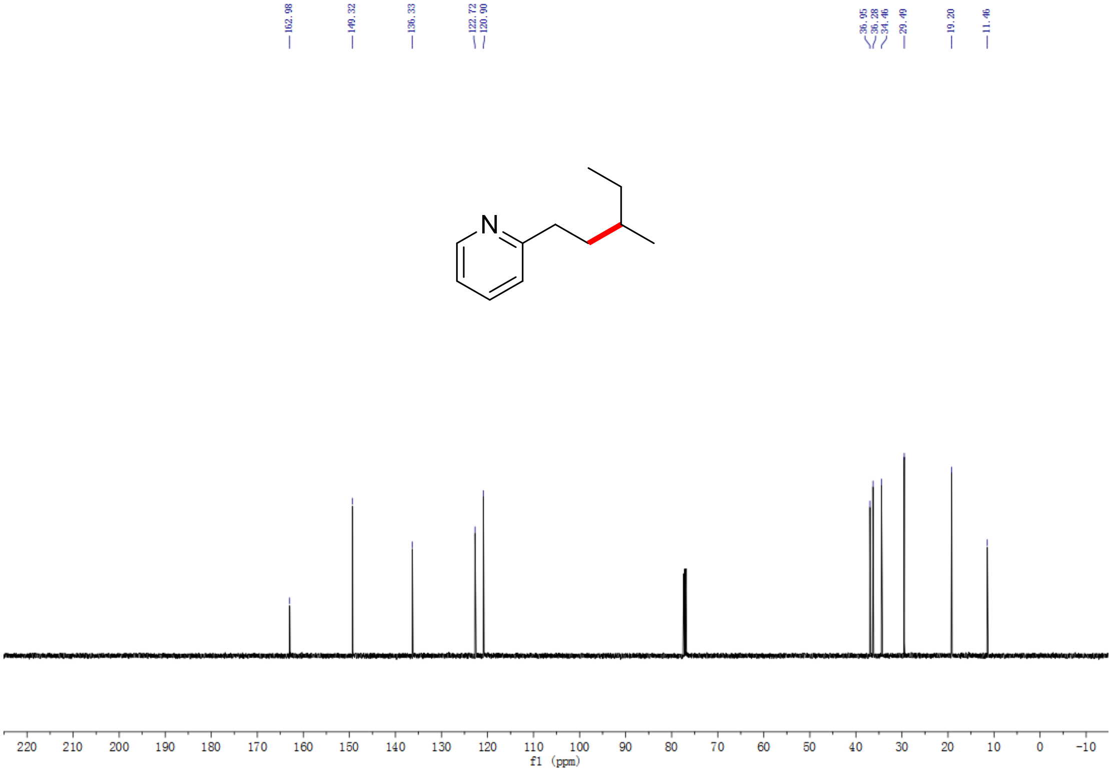

^{1}H NMR (500 MHz, $CDCl_3$), ^{13}C NMR (126 MHz, $CDCl_3$)

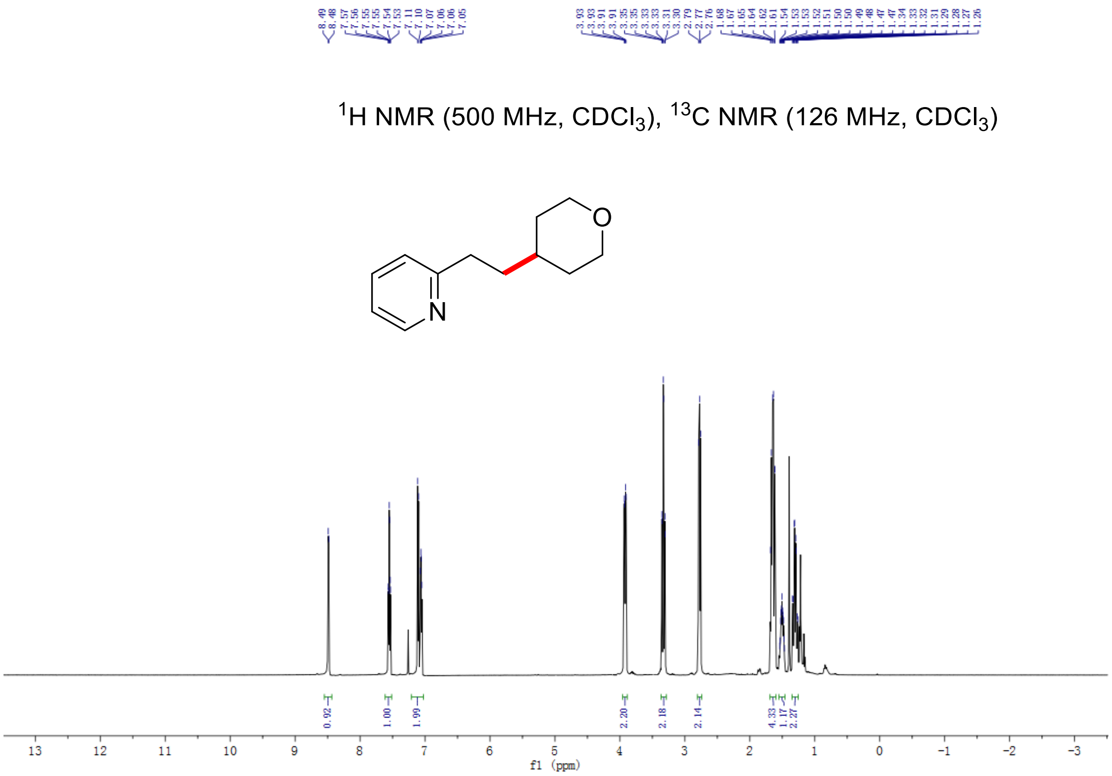

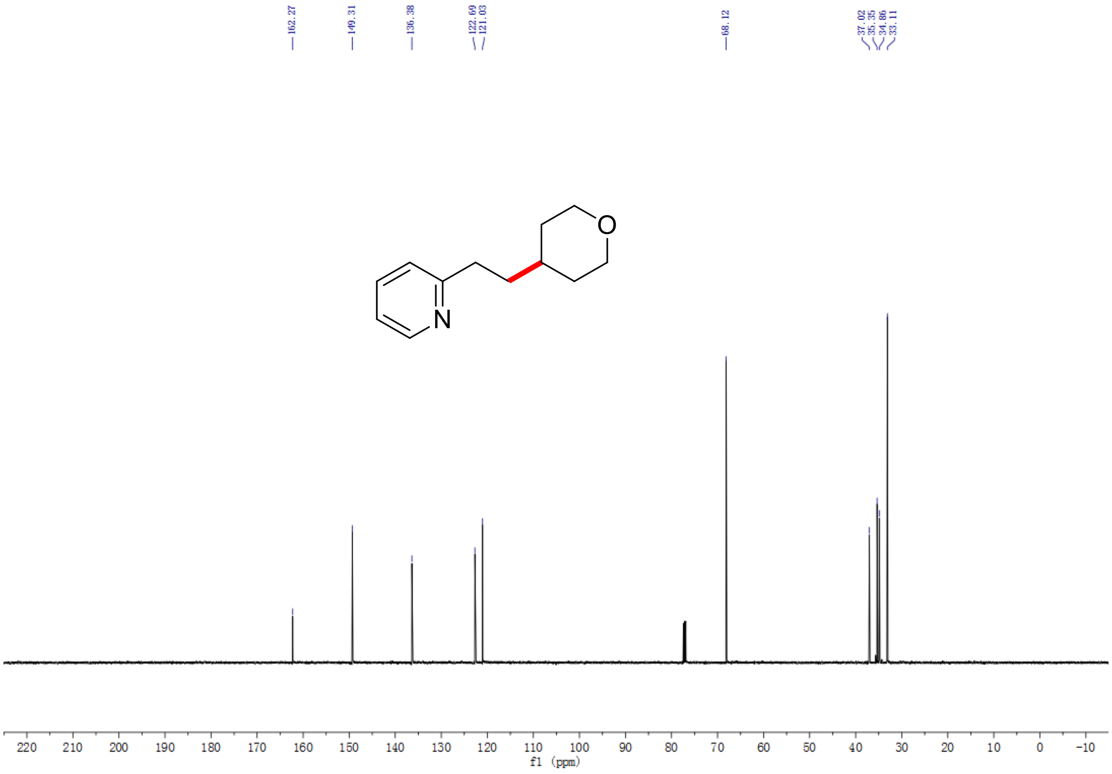

^{1}H NMR (500 MHz, $CDCl_3$), ^{13}C NMR (126 MHz, $CDCl_3$)

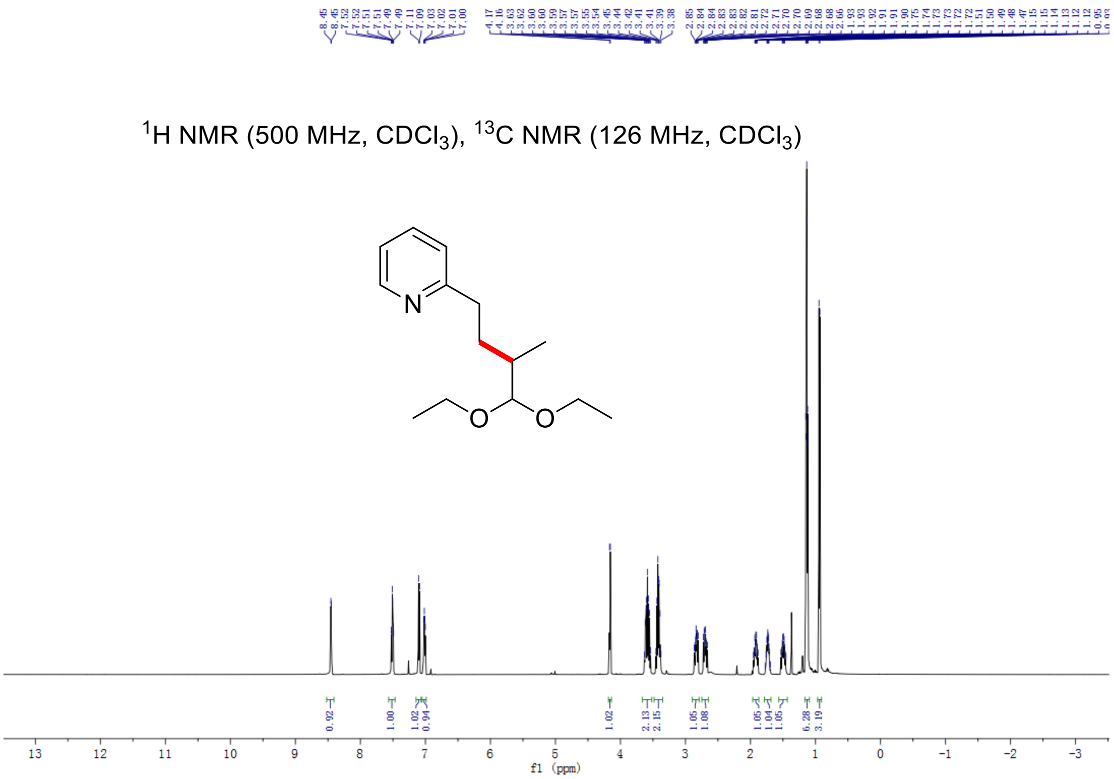

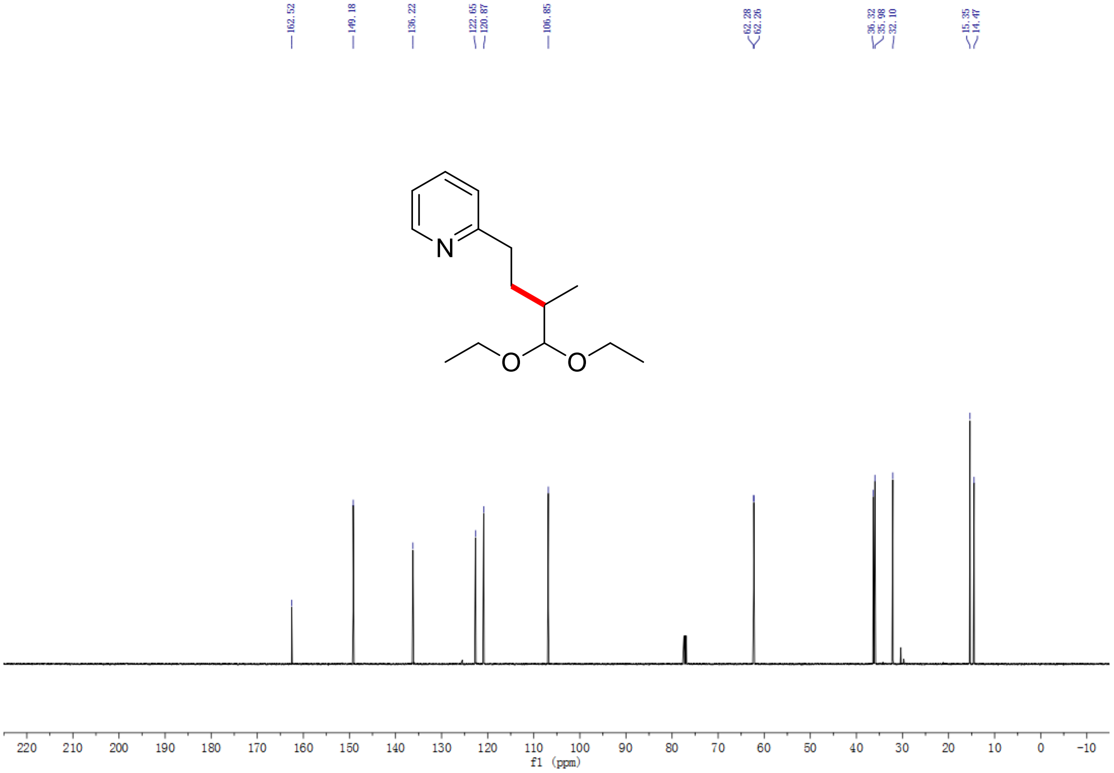

^{1}H NMR (500 MHz, CDCl$_3$), ^{13}C NMR (126 MHz, CDCl$_3$)

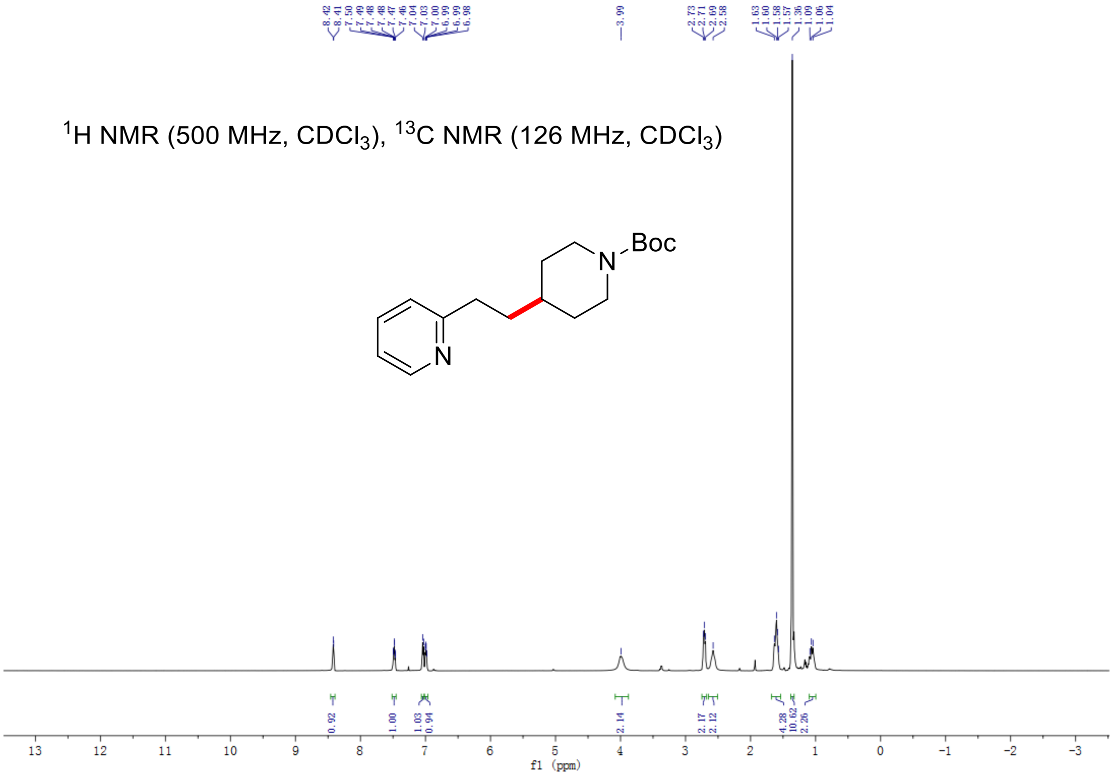

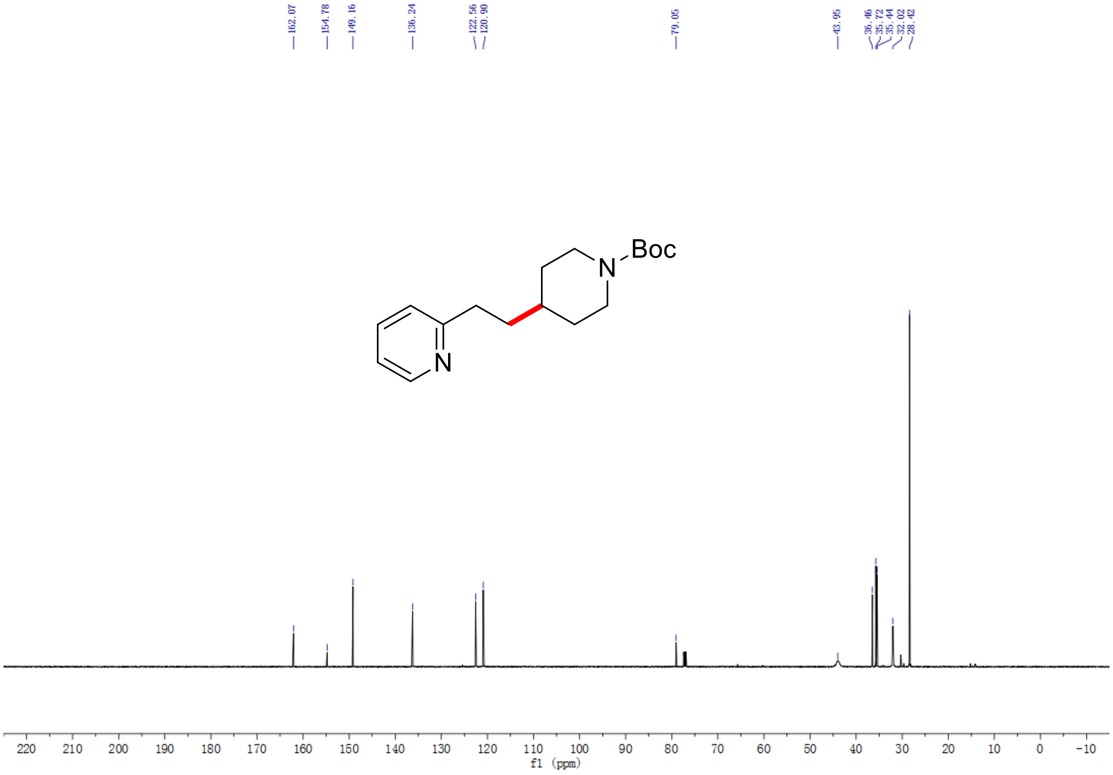

^{1}H NMR (500 MHz, $CDCl_3$), ^{13}C NMR (126 MHz, $CDCl_3$)

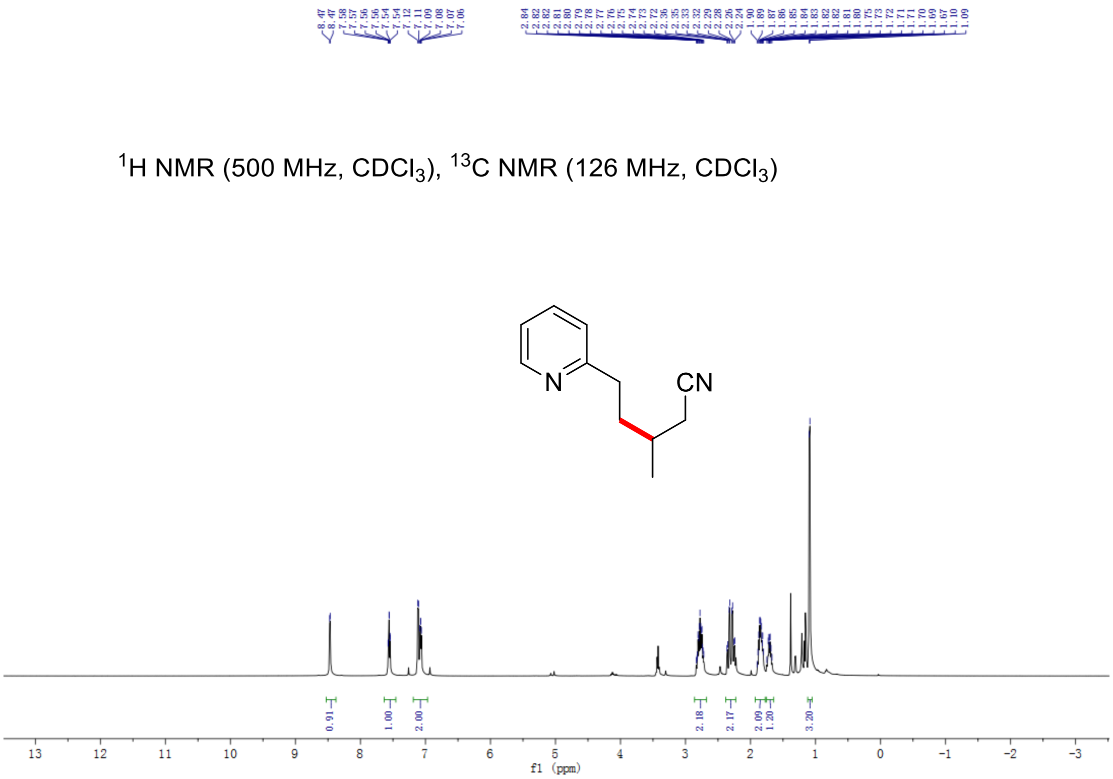

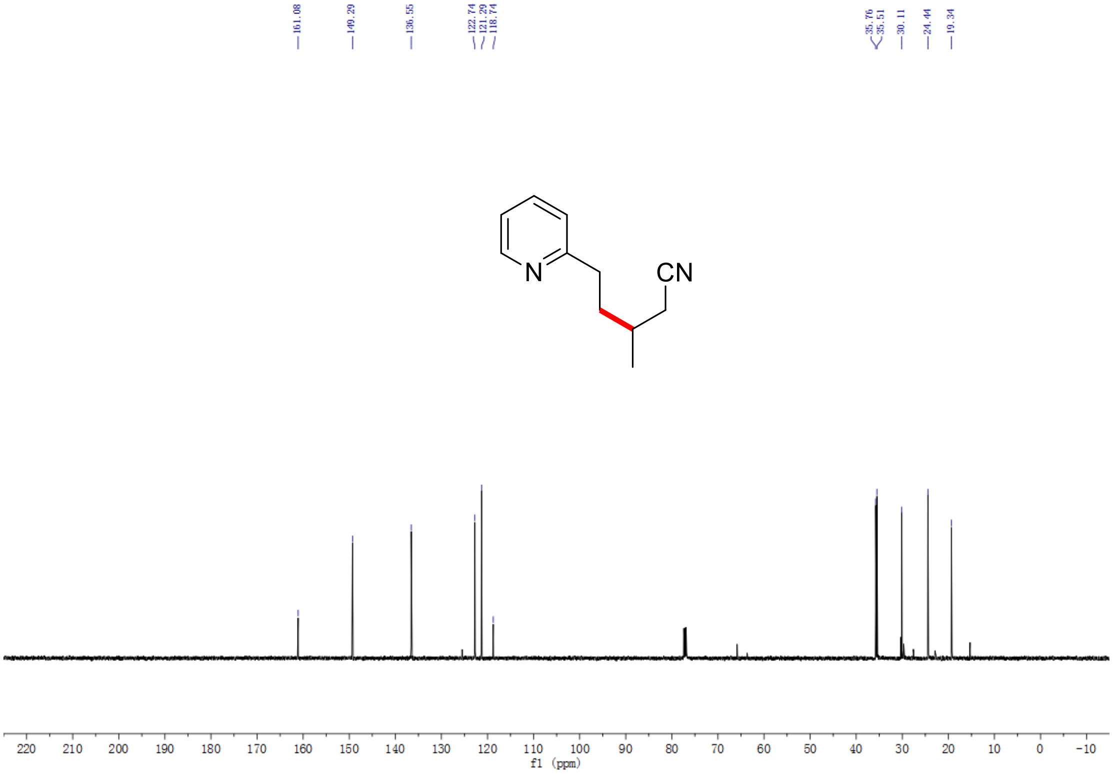

^{1}H NMR (500 MHz, $CDCl_3$), ^{13}C NMR (126 MHz, $CDCl_3$)

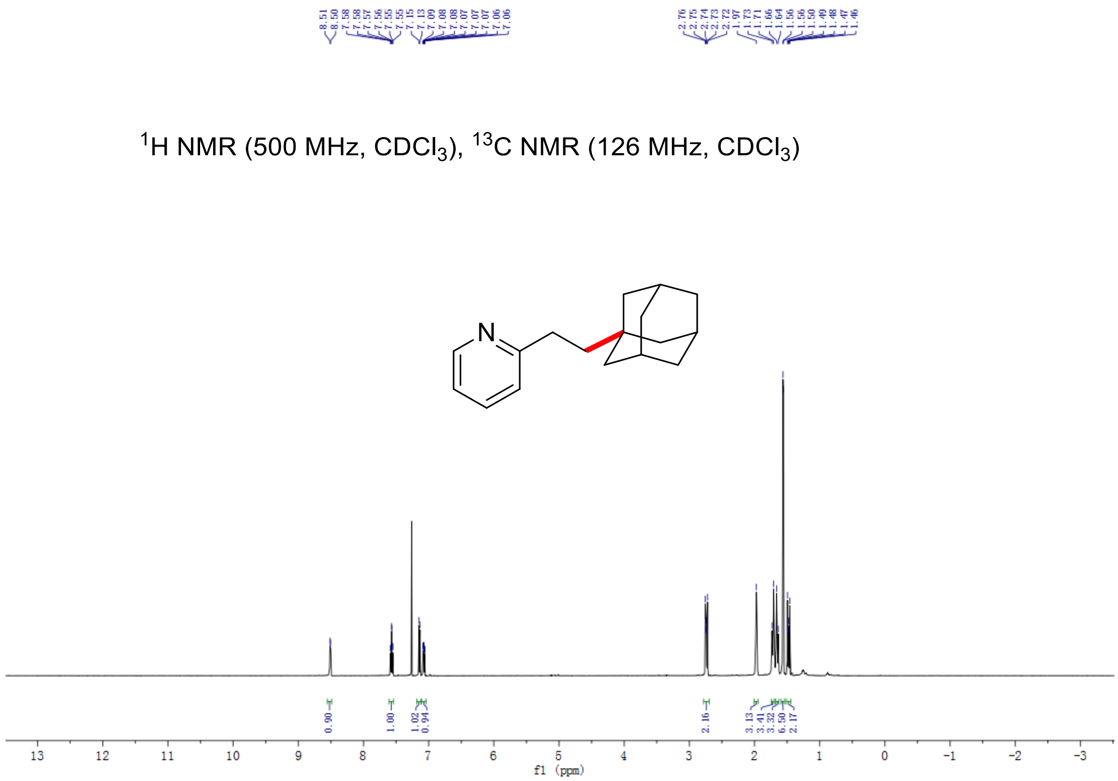

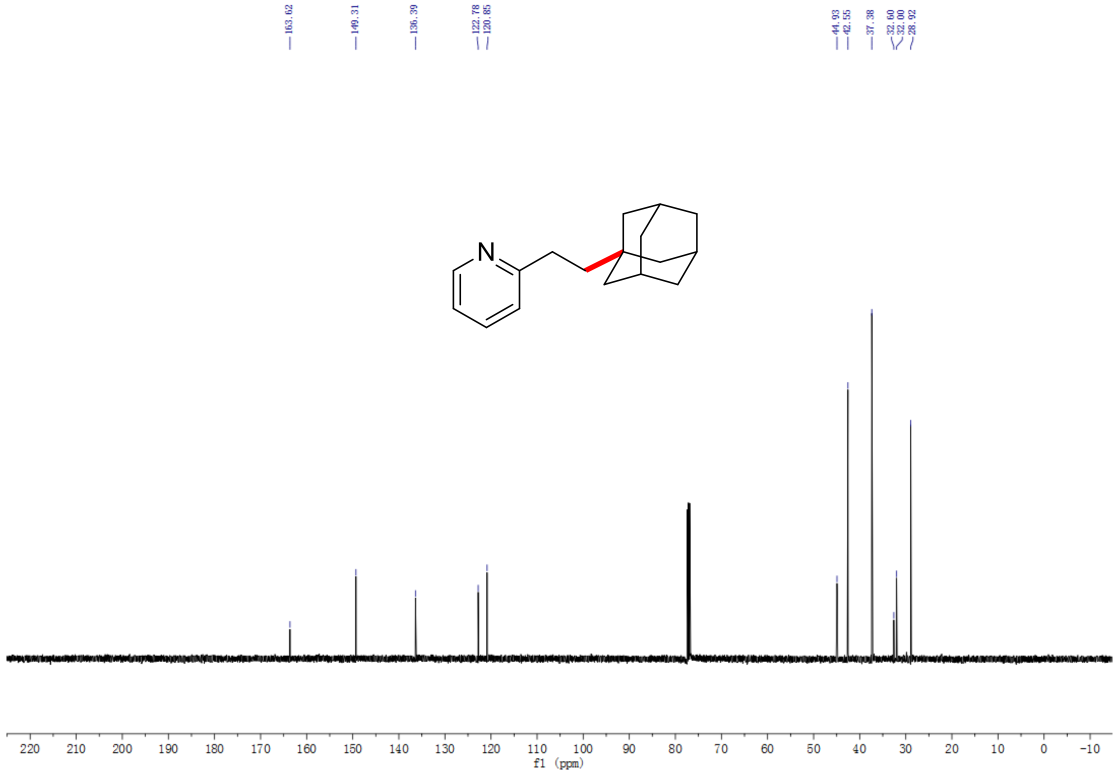

^{1}H NMR (500 MHz, CDCl$_3$), ^{13}C NMR (126 MHz, CDCl$_3$)

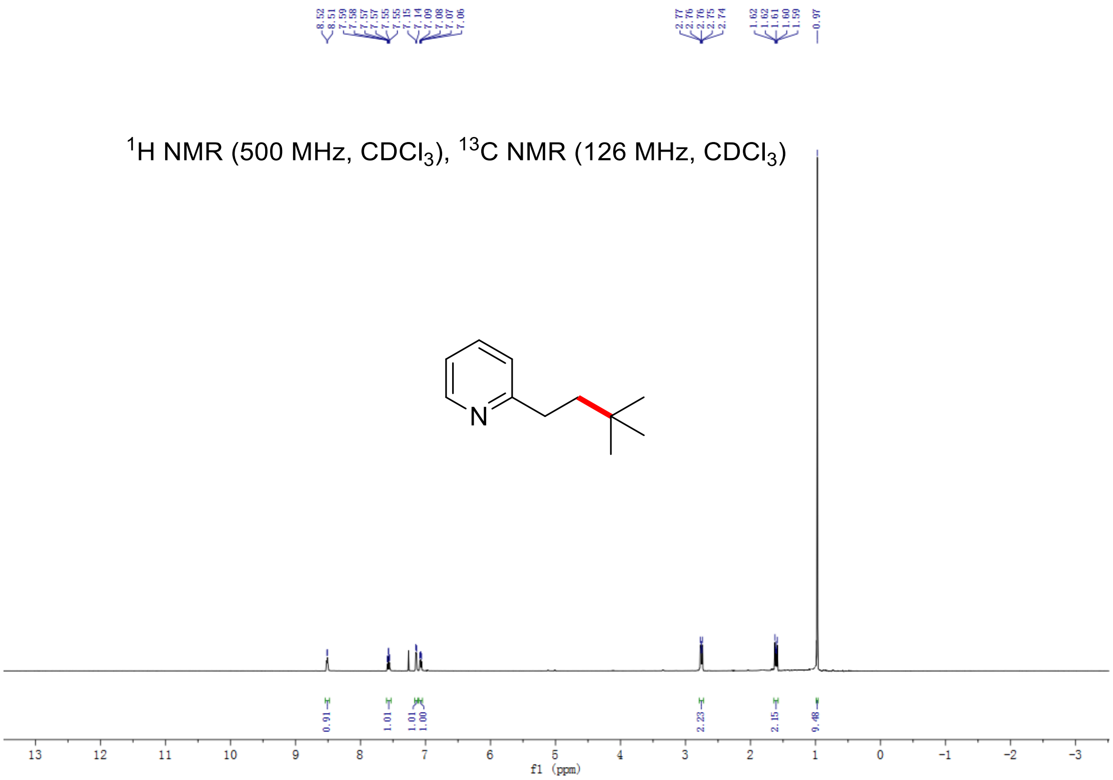

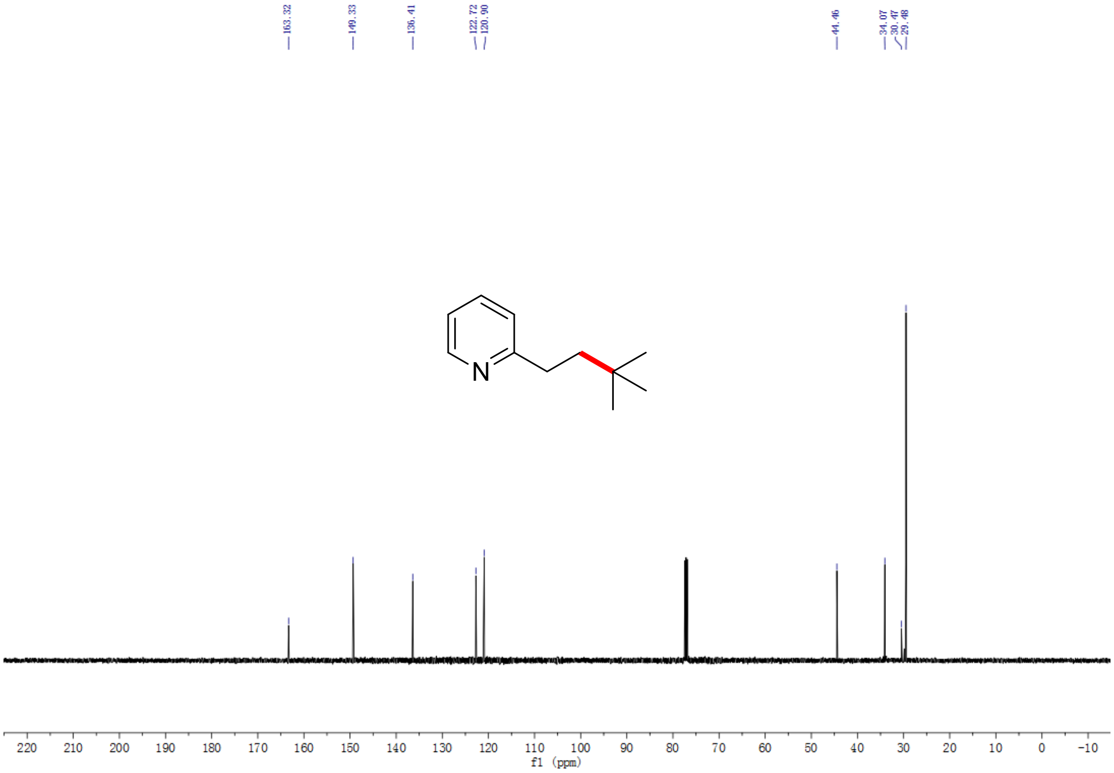

^{1}H NMR (500 MHz, CDCl$_3$), ^{13}C NMR (126 MHz, CDCl$_3$)

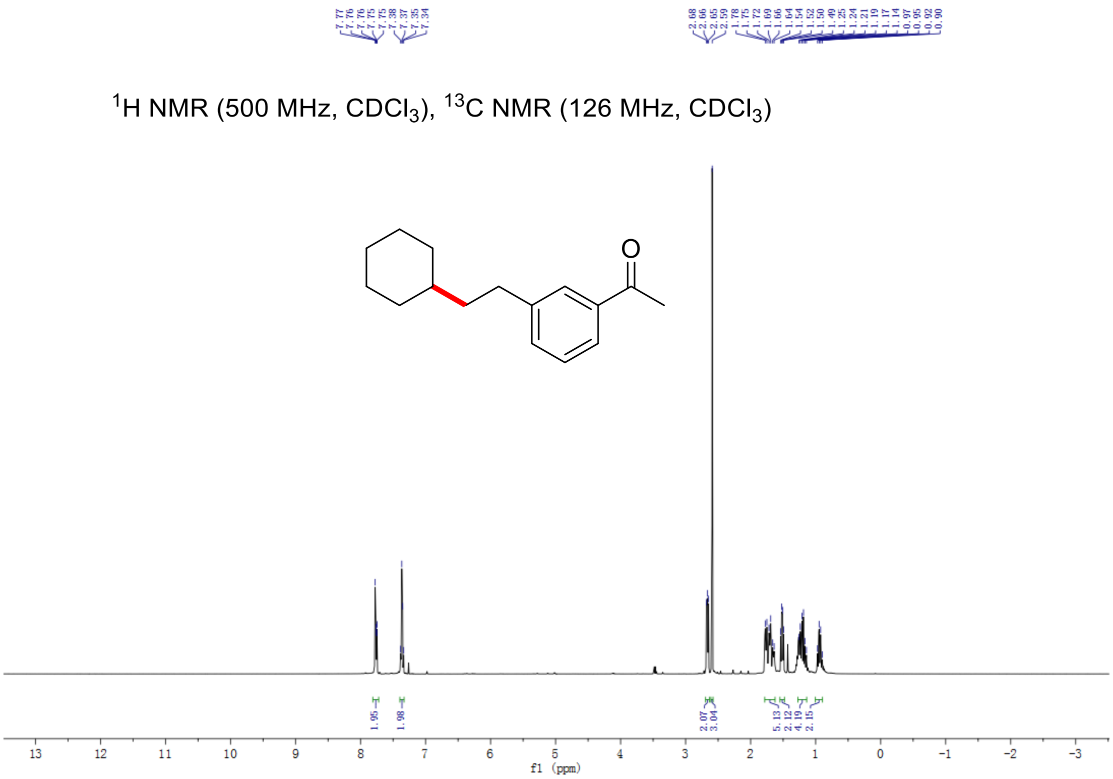

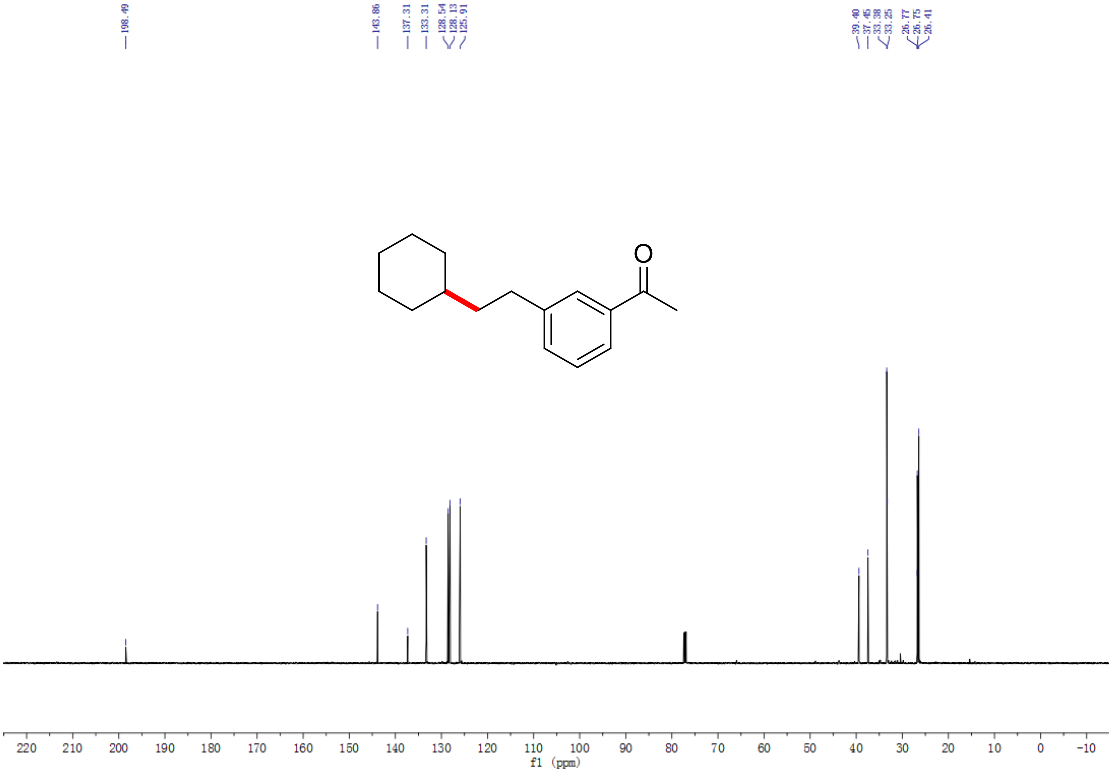

^{1}H NMR (500 MHz, CDCl$_3$), ^{13}C NMR (126 MHz, CDCl$_3$)

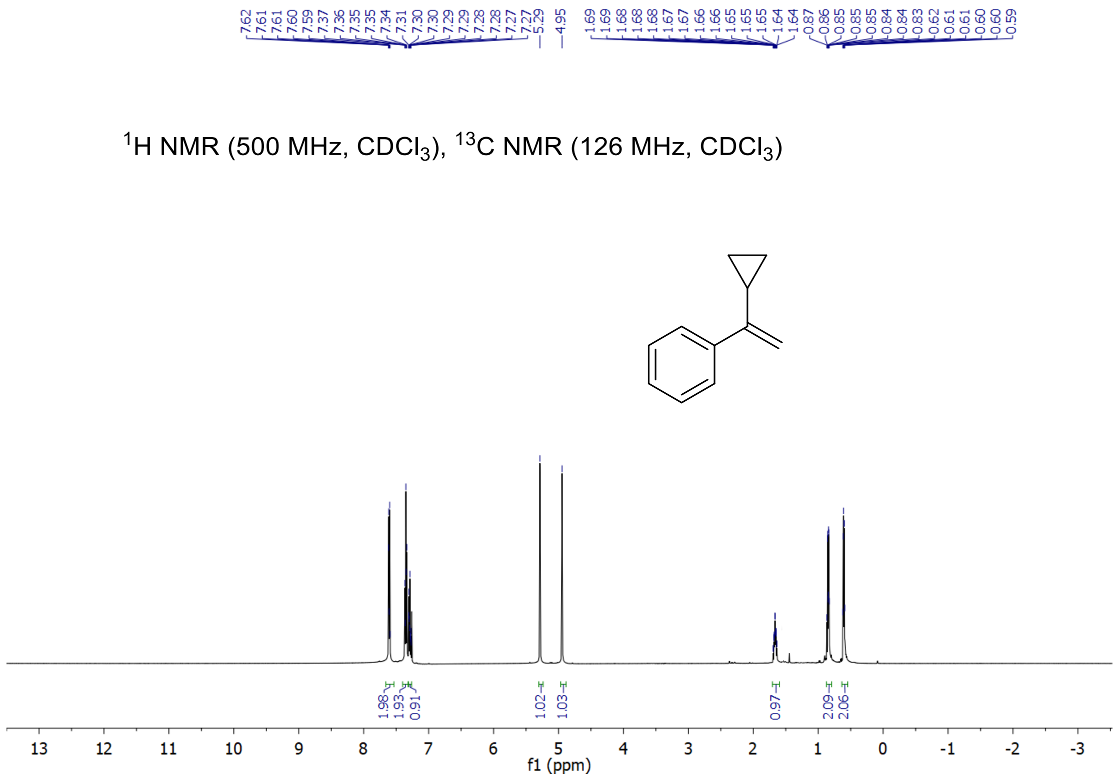

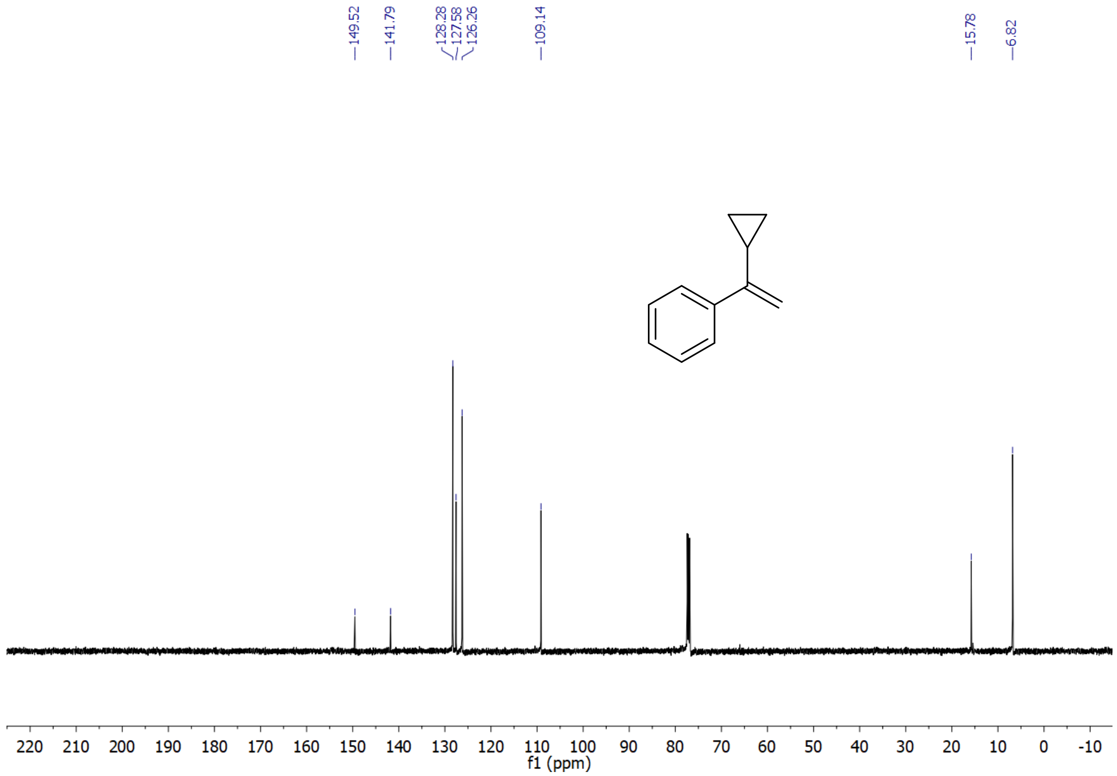

^{1}H NMR (500 MHz, $CDCl_3$), ^{13}C NMR (126 MHz, $CDCl_3$)

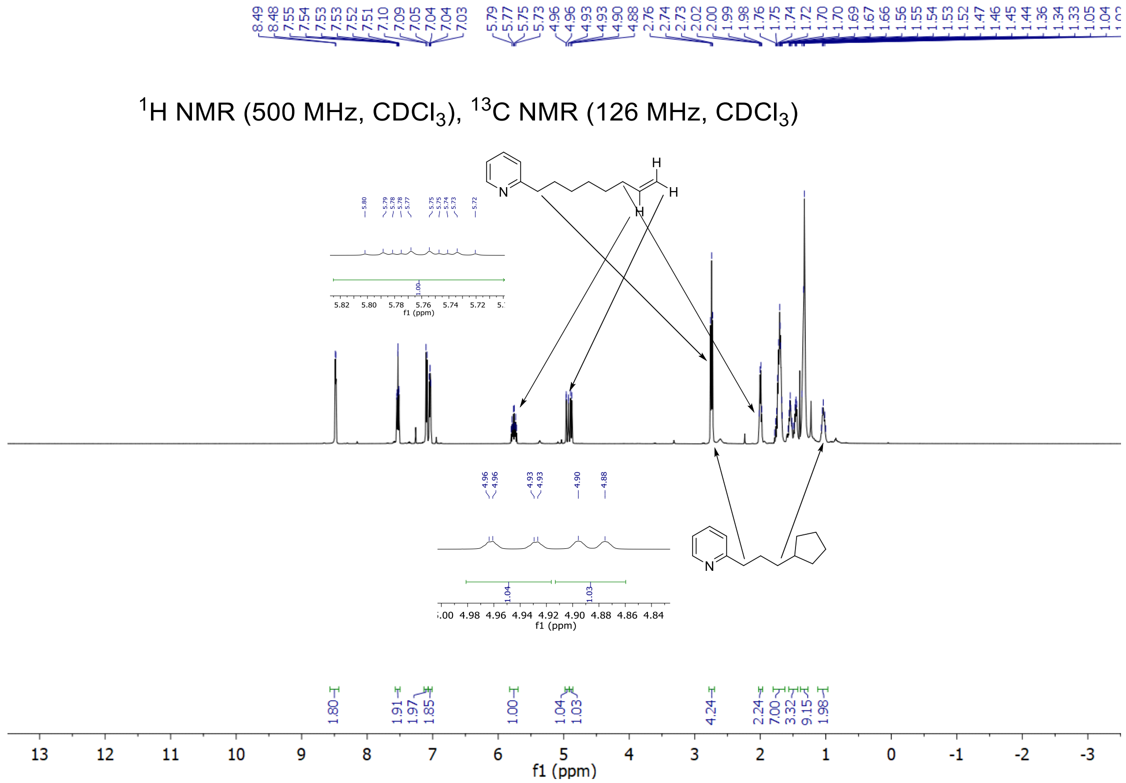

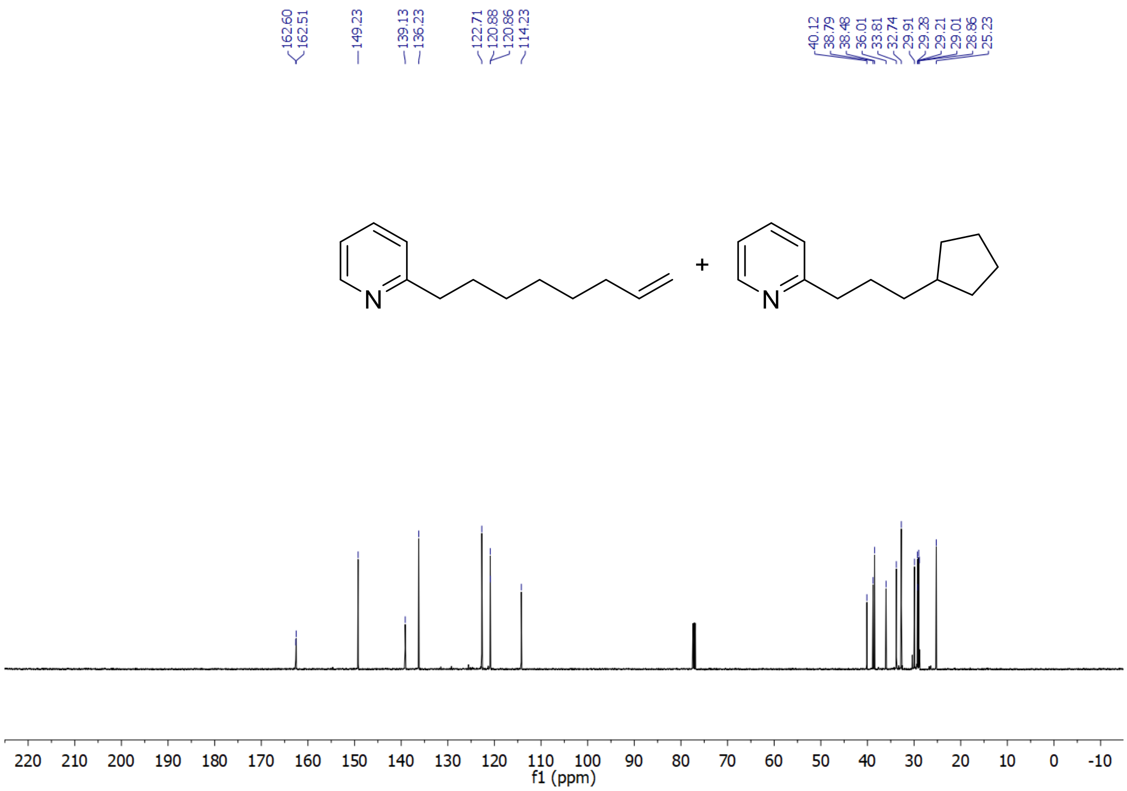

^{1}H NMR (500 MHz, CDCl$_3$), ^{13}C NMR (126 MHz, CDCl$_3$)

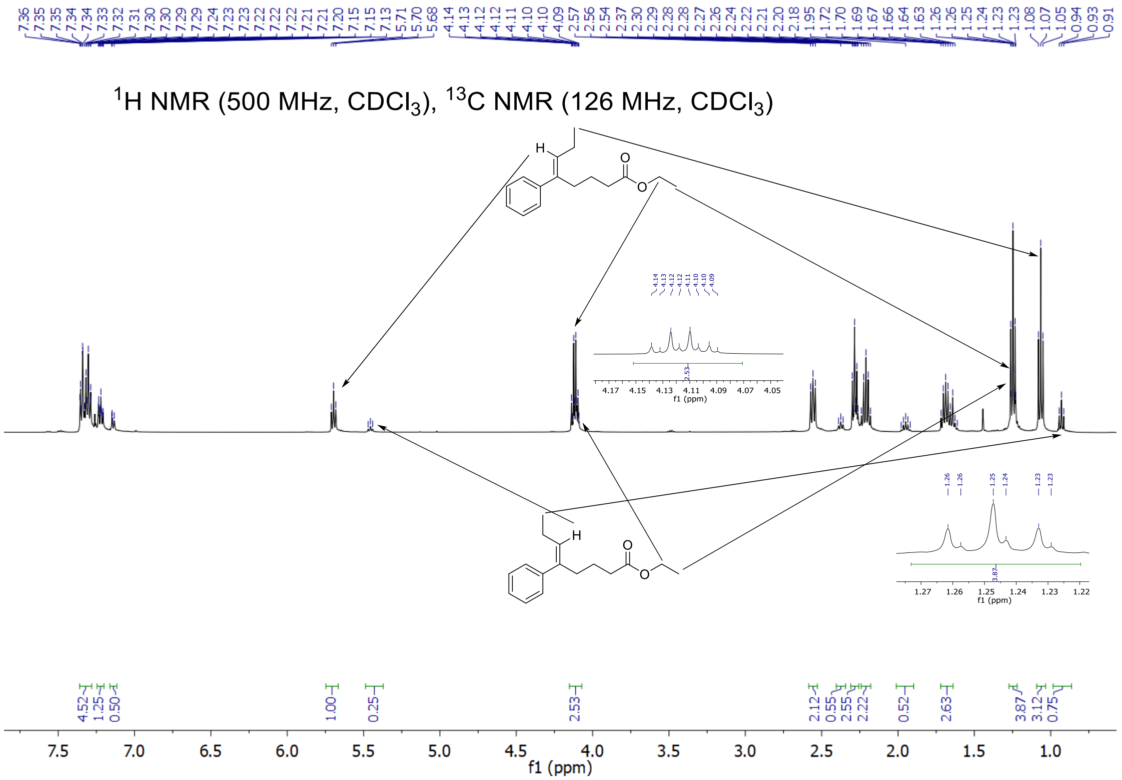

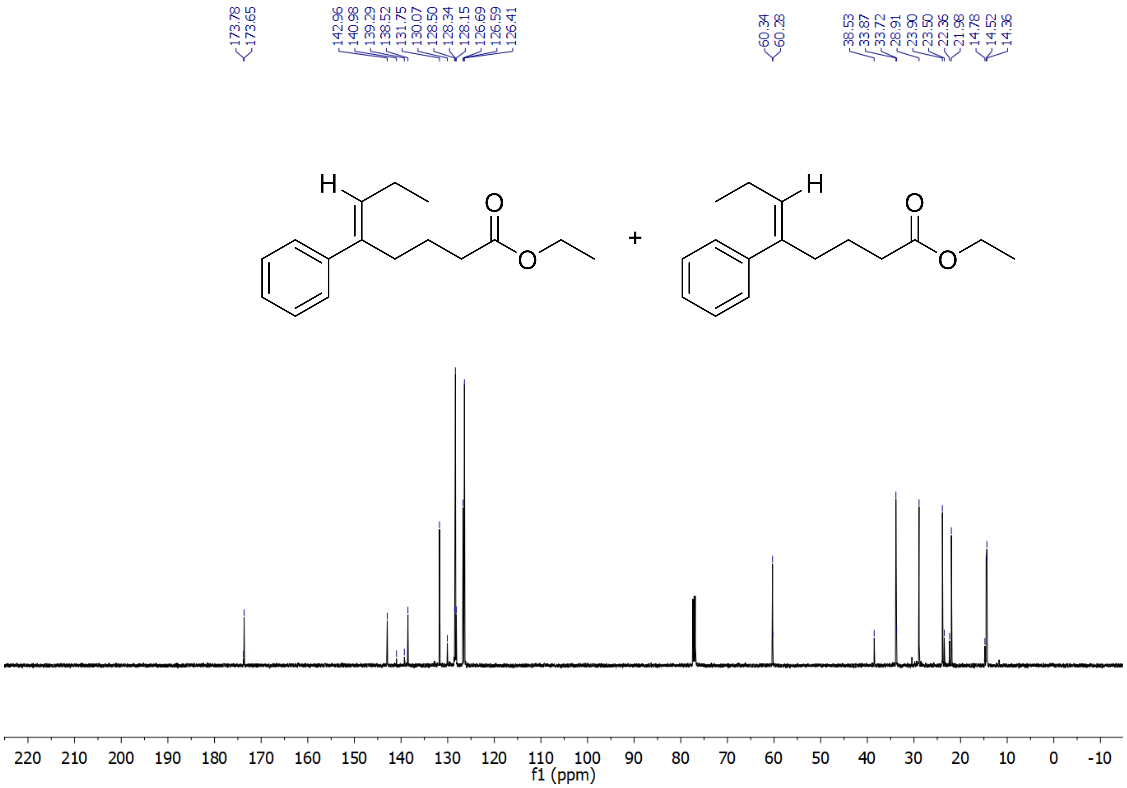

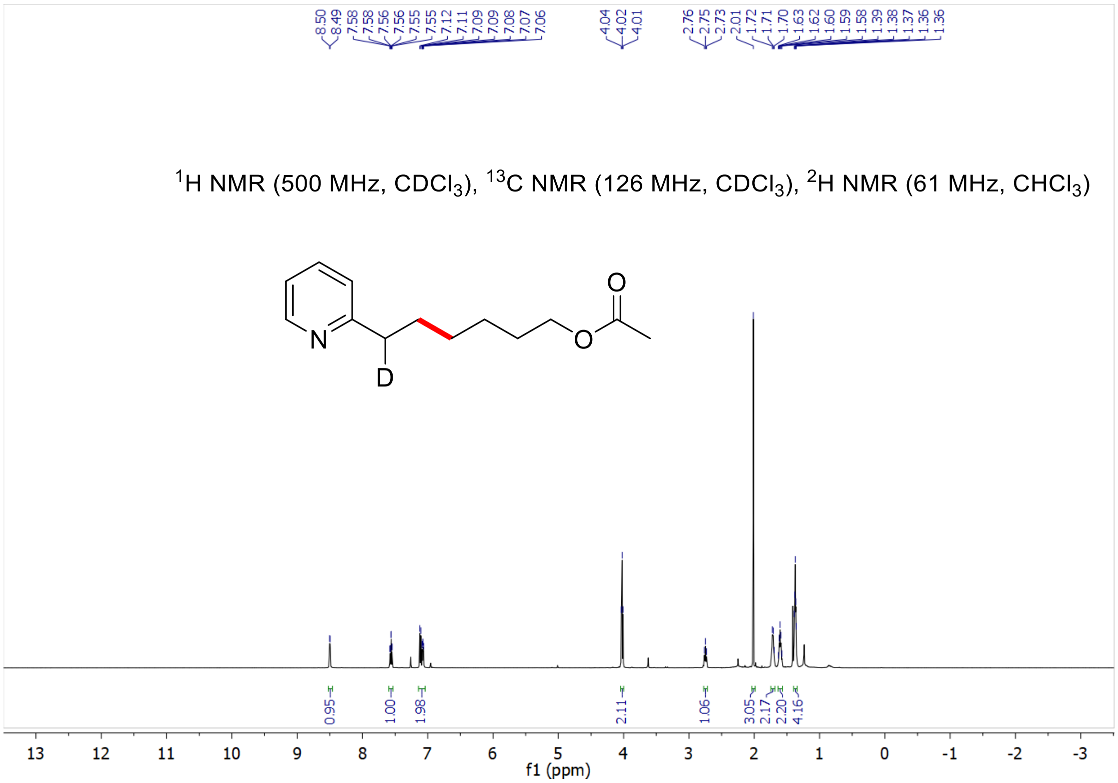
^{1}H NMR (500 MHz, CDCl$_3$), ^{13}C NMR (126 MHz, CDCl$_3$), ^{2}H NMR (61 MHz, CHCl$_3$)

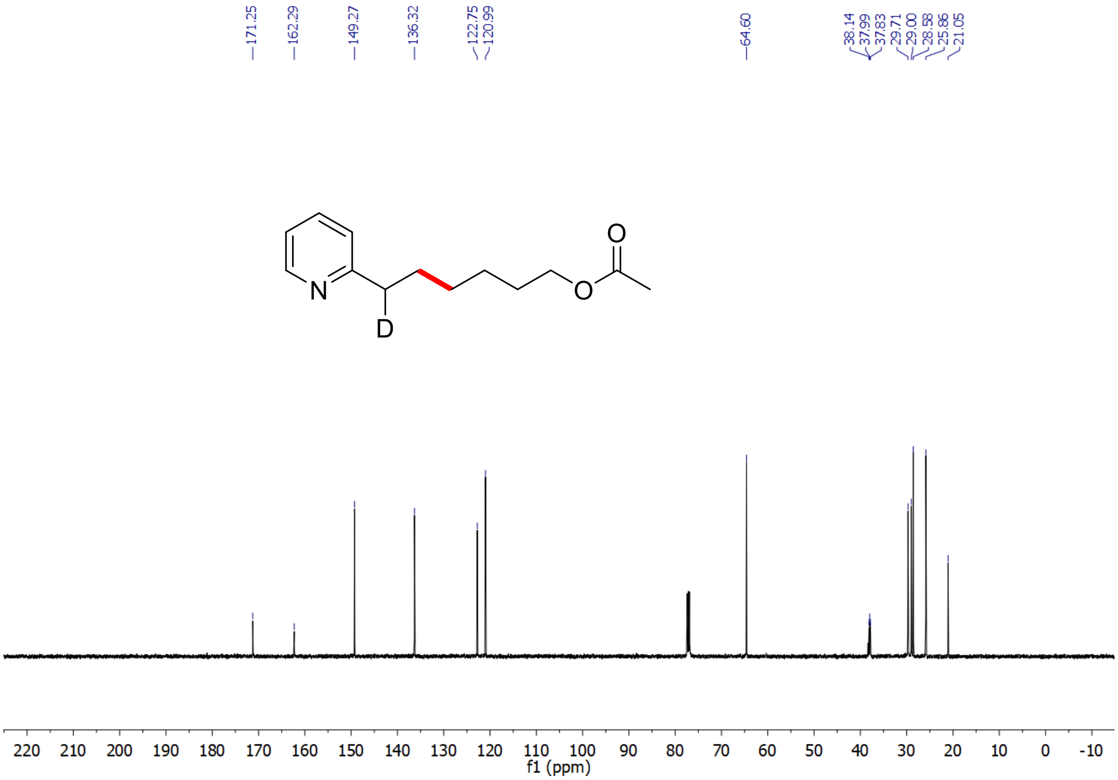

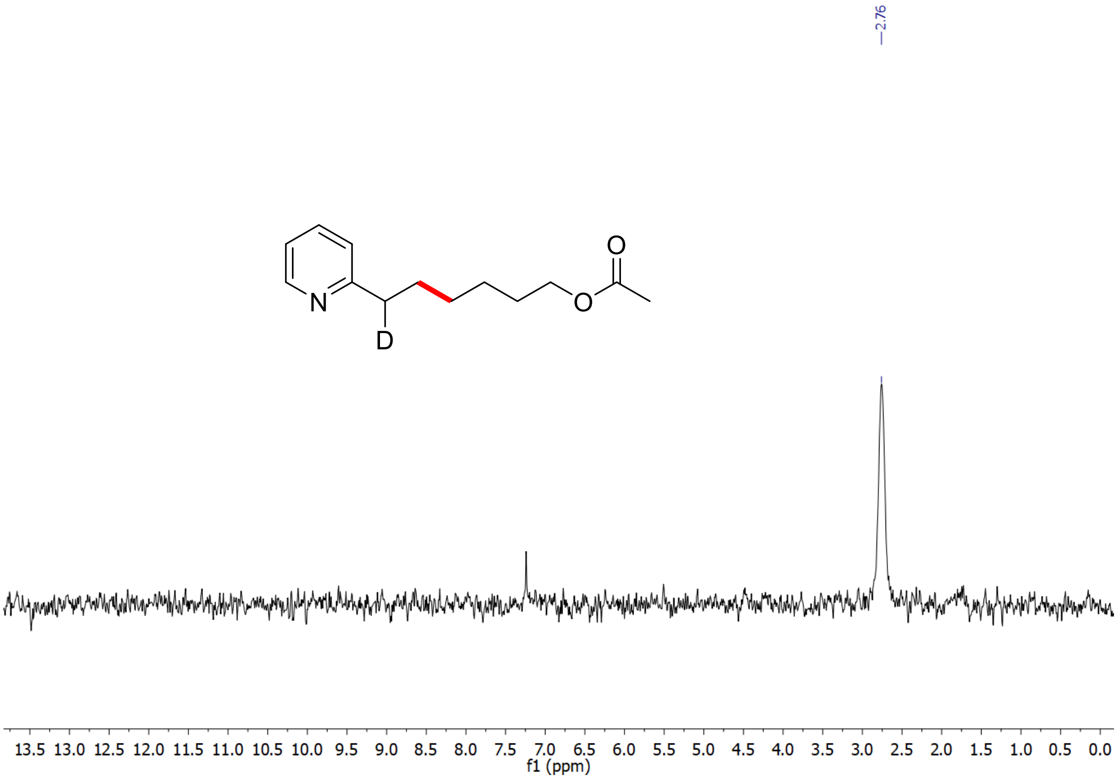
2.76
O
N
O
D
13.5 13.0 12.5 12.0 11.5 11.0 10.5 10.0 9.5 9.0 8.5 8.0 7.5 7.0 6.5 6.0 5.5 5.0 4.5 4.0 3.5 3.0 2.5 2.0 1.5 1.0 0.5 0.0
f1 (ppm)

III. Water-sculpting of a pre-catalyst into an active catalyst for Heck couplings

General Introduction on Heck-Mizoroki coupling reactions

In recent decades, the formation of the C-C bond has been broadly studied in organic synthesis, especially involving transition-metal-catalyzed cross coupling reactions. As more and more types of cross-coupling reactions were developed, palladium has been discovered as the key element for those reactions including Heck, Suzuki, Negishi, Stille, Sonogarshira, Hiyama reactions, et al. Among these reactions, Heck-Mizoroki (HM) reaction, as one of the earliest metal coupling reactions, has been powerful studied. It not only provides a reliable and efficient tool for complex molecule constructions derived from stryrenes in the medicinal chemistry toolbox significantly, but also inspired the following transition metal catalyzed cross-coupling reactions. Because of the profound significance and influence of Heck-Mizoroki reactions for the synthesis of a large variety of agrochemicals, pharmaceuticals, polymers and fine chemical products, Richard F. Heck shared the Nobel Prize in Chemistry for 'palladium-catalyzed cross-couplings in organic synthesis' with Akira Suzuki and Ei-ichi Negishi in 2010.

The Heck-Mizoroki reaction was first reported by T. Mizoroki[1] in 1971 and R. F. Heck[2] in 1972 independently as shown in Scheme 1. In Mizoroki's investigation, iodo benzene was used as starting material coupled with olefins including ethylene, styrene, and methyl acrylate, in which $PdCl_2$ was used as catalyst without any ligand. They noticed that the $PdCl_2$ could be reduced during the reaction. In Heck's research, the authors not only expended the substrate scope to include styrene with diverse functional groups, but also proposed a prototype of the cross-coupling mechanism. Subsequently, based on this version, Heck's group reported an enhanced protocol in 1974.[3] In this strategy, PPh_3 as ligand combined with $Pd(OAc)_2$ as catalyst, which was the first time that a phosphine ligand was introduced into the Heck-Mizoroki reaction. In terms of substrate scope, not only iodobenzenes but also bromobenzenes could be used as coupling partners. Moreover, given the former studies of this group on the mechanism of arylation and carbomethoxylation of olefins with organopalladium compounds,[4] a detailed, plausible mechanism for the Heck-Mizoroki reaction was proposed. After being augmented by later studies,[5] a detailed mechanism was presented, as shown in Scheme 2. The first step is an oxidative addition, in which the Pd(0) complex has inserted into an aryl halide bond. And then an intermediate is formed by generating a π complex via association with the olefin, followed by migratory insertion. After Pd hydride elimination, the coupling product forms after dissociation of the Pd(II) complex generated, and the Pd(0) is regenerated via subsequent reductive elimination of Pd(II) by base to further catalyze the cycle.

Scheme 1: Heck-Mizoroki reaction was discovered

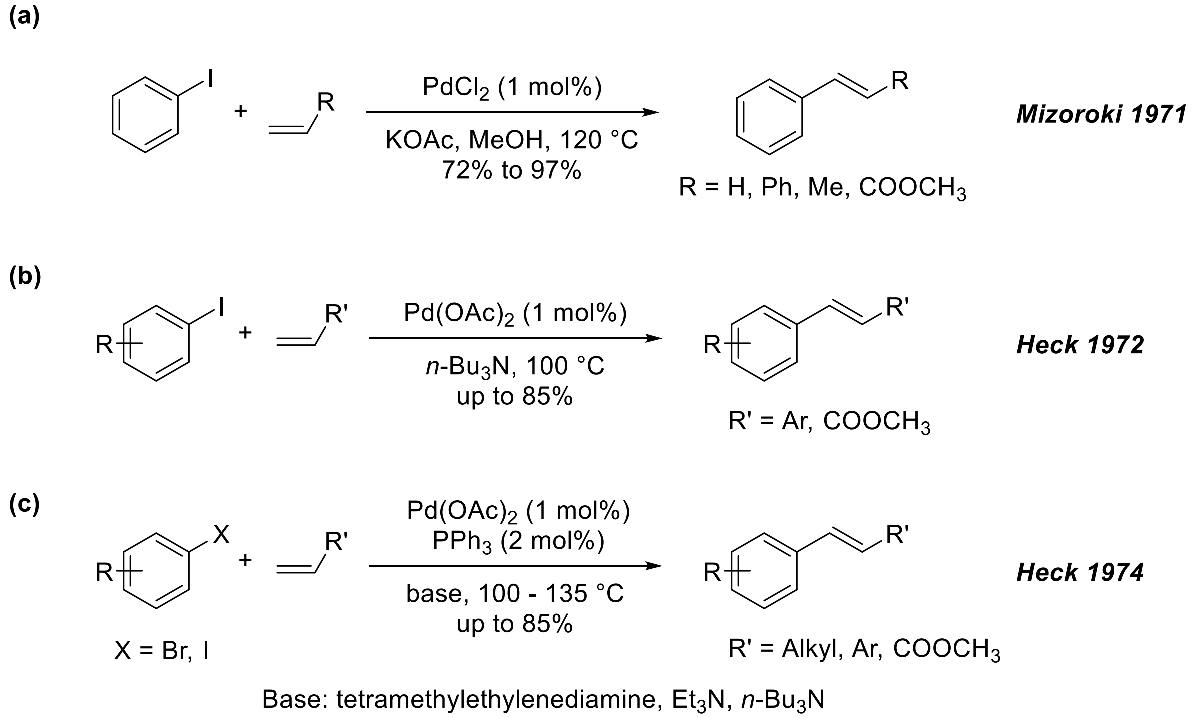
(a)
I
+
R
PdCl$_2$ (1 mol%)
KOAc, MeOH, 120 °C
72% to 97%
R
R = H, Ph, Me, COOCH$_3$
Mizoroki 1971
(b)
R
I
+
R'
Pd(OAc)$_2$ (1 mol%)
n-Bu$_3$N, 100 °C
up to 85%
R
R'
R' = Ar, COOCH$_3$
Heck 1972
(c)
R
X
+
R'
Pd(OAc)$_2$ (1 mol%)
PPh$_3$ (2 mol%)
base, 100 - 135 °C
up to 85%
R
R'
X = Br, I
R' = Alkyl, Ar, COOCH$_3$
Heck 1974
Base: tetramethylethylenediamine, Et$_3$N, n-Bu$_3$N

Scheme 2: Heck-Mizoroki reaction mechanism

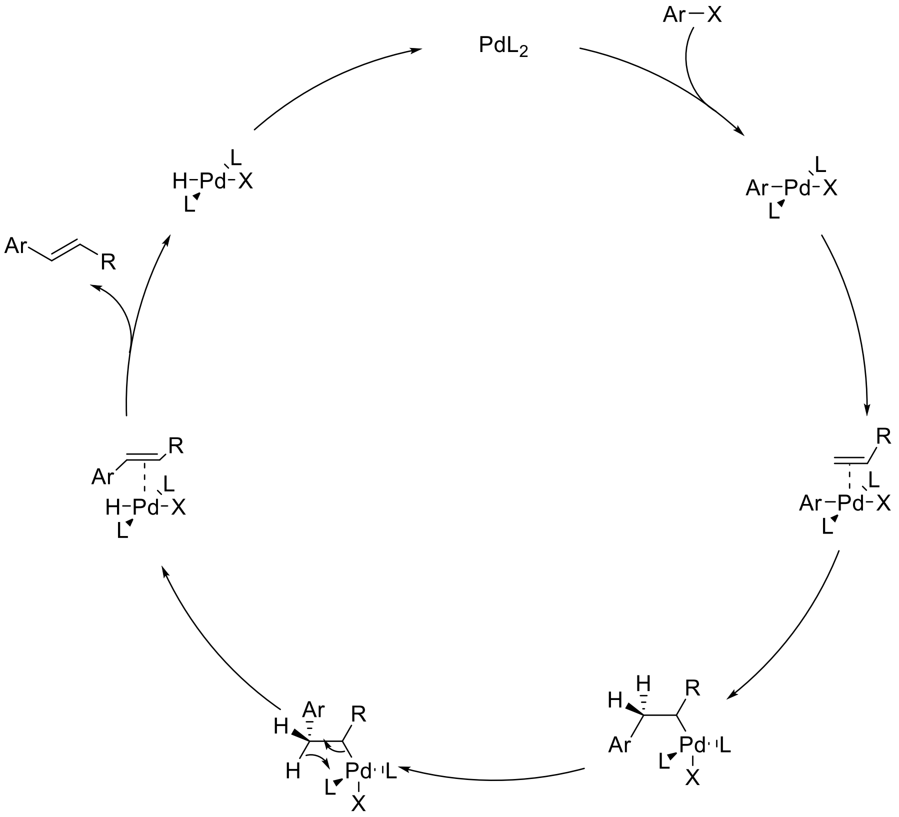

However, along with widespread applications of Heck-Mizoroki coupling reactions to the synthetic processes of a large variety of pharmaceuticals, agrochemicals, polymers, APIs and fine chemicals, potential problems associated with use of homogeneous Pd complexes as catalysts have begun to appear with increasing frequency, since: 1) catalytic Pd utilized in HM couplings dissolved in the reaction medium requires tedious post-reaction processing for re-isolation and recycling, as well as issues concerning the amounts of residual Pd in the products after the reaction, especially for the pharmaceutical products; 2) efforts to reuse or recycle expensive homogeneous Pd for economic and sustainability reasons are difficult, further hindering industrial processes otherwise more broadly applicable to such homogeneous Pd catalysis.

In order to solve these problems, not surprisingly, more and more scientists focused on heterogeneous Pd catalysis. Compared with homogeneous Pd processes, heterogeneous Pd catalysts have the advantages of more facile recyclability, lower toxic residual metals, relatively stable performance, etc. On the other hand, nanoscience and nanotechnology are also gradually being applied to preparing heterogeneous catalysts. The development of uniformly prepared nanoparticles with controlled shapes, sizes, compositions, and structures has further promoted extension and improvements of heterogeneous catalysis. For the purpose of conducting HM coupling reactions under a sustainable, greener, and economical condition, as well as to further extend the potential applications of HM couplings to pharmaceuticals and manufacturing, chemists have more recently designed and developed diverse nanoparticles or nanomaterials for catalyzing HM couplings heterogeneously.

In 2002, Choudary and co-workers designed a new layered double hydroxide (LDH) supported nanopalladium(0) catalyst, as shown in Scheme 3.[6] The nanocatalyst LDH-Pd^0 was prepared by an ion-exchange of $PdCl_4^{2-}$ with LDH (Mg-Al-Cl) in aqueous solution followed by reduction with hydrazine hydrate in ethanol. This ligand-free heterogeneous LDH Pd^0 can be used for catalyzing HM coupling reactions of chloroarenes with olefins at 130 °C, or under microwave heating to obtain good yields. In addition, their nanocatalyst can be recycled five times in the HM coupling of 4-chloroanisole with styrene under microwave and thermal conditions. Furthermore, a mechanism for the heterogeneous HM reaction was proposed in their report. This nanocatalyst could not only be used in HM reactions, but also could be applied to Suzuki-Miyaura, Sonogarshia and Stille couplings with good activity and selectivity.

Scheme 3: Choudary's LDH Pd^0 nanocatalyst for HM couplings

Reaction:

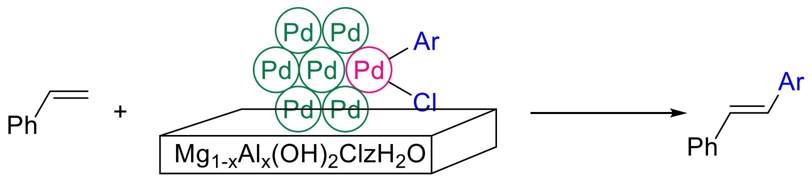

Ph
+
Pd
Ar
Cl
$Mg_{1-x}Al_x(OH)_2ClzH_2O$
Ar
Ph

Mechanism:

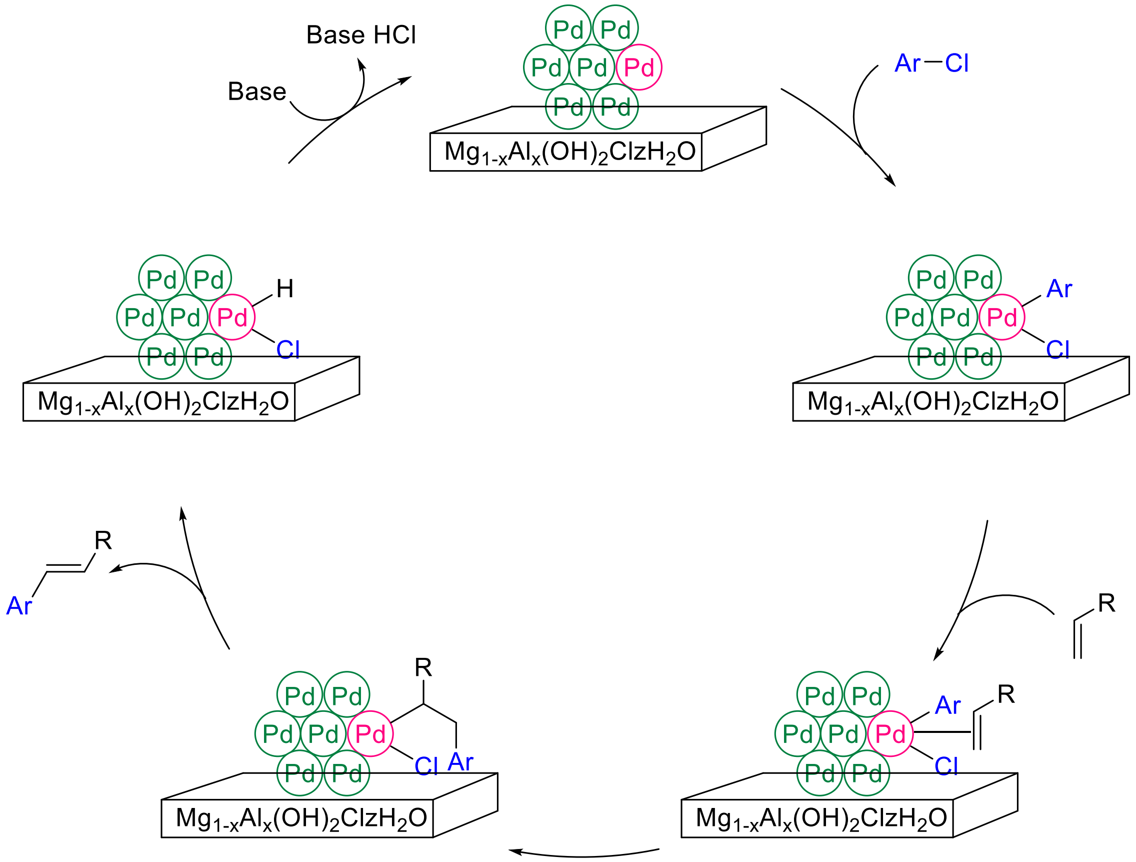

Base HCl
Base
Pd
$Mg_{1-x}Al_x(OH)_2ClzH_2O$
Ar—Cl
Ar
Cl
H
R
Ar

In 2004, Sastry's group developed a new nanomaterial based on incorporation between the Pd NPs and zeolites using amine functionalization.[7] Initially, they synthesized and functionalized the Na-Y zeolite by (3-aminopropyl)trimethoxysilane (APTS) grafting to obtain the white amine-functionalized APTS-Y. Subsequently, the Pd nanoparticles were made by reduction of palladium nitrate using NaBH$_4$ in aqueous solution to afford a Pd colloidal suspension, which was then followed by adding amine-functionalized APTS-Y to form the [Pd]-APTS-Y nanomaterial by immobilization of Pd nanoparticles on the amine-functionalized APTS-Y. XPS and TEM analyses of the [Pd]-APTS-Y nanomaterial were provided in their paper (Scheme 4). The authors also demonstrated that this novel nanomaterial, [Pd]-APTS-Y, showed a relatively high catalytic activity and selectivity for HM couplings of iodobenzene with styrene in *N*,*N*-dimethylacetamide. Additionally, after the initial reaction, the [Pd]-APTS-Y retains its catalytic activity for HM couplings for two recycles. However, no further expansion of substrate scope was provided, so, it is hard to evaluate the compatibilities of functional groups and heterocycles.

Scheme 4: The TEM images and XPS (Pd 3d) of [Pd]-APTS-Y from Sastry's group

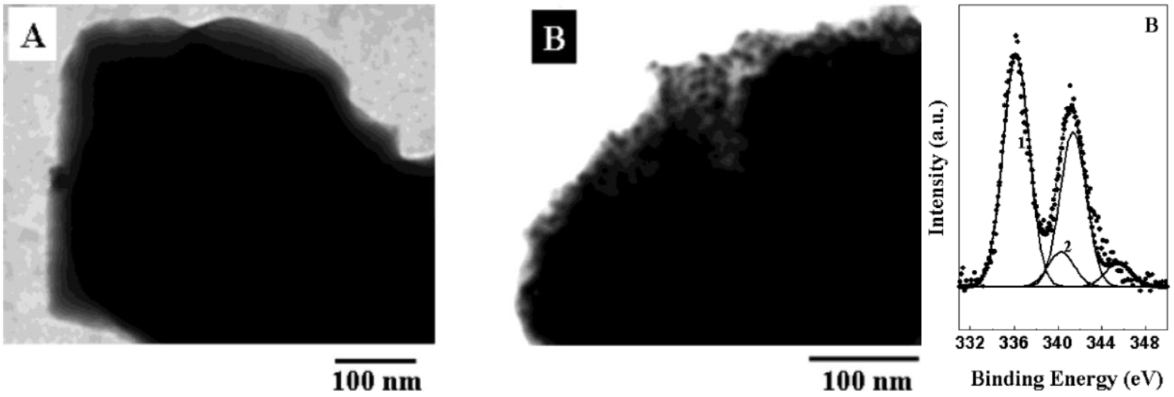

Reproduced with permission from ref 7. Copyright 2004 American Chemical Society.

In 2008, Yokoyama's group developed an imidazolium-styrene copolymer nanocatalyst with supported Pd, as shown in Scheme 5.[8] 1-Vinyl-3-butylimidazolium chloride derived from 1-vinyl-1H-imidazole was copolymerized with styrene triggered by AIBN under an inert atmosphere leading to imidazolium-stryene copolymers (PS-IL[Cl]). This nanocatalyst, Pd/PS-IL[Cl], was ultimately obtained after immobilization of $Pd(OAc)_2$ on the surface of the copolymers. The Pd/PS-IL[Cl] can be applied for catalyzing HM couplings of olefins with iodoarenes leading to good yields in water with triethylamine as a base at 100 °C.

However, it is worth mentioning that the catalytic Pd loading for each reaction is only 0.2 mol %. In addition, this nanocatalyst can be recycled four times with almost the same activity.

Scheme 5: Yokoyama's Pd/PS-IL[Cl] for HM coupling reactions

Preparation:

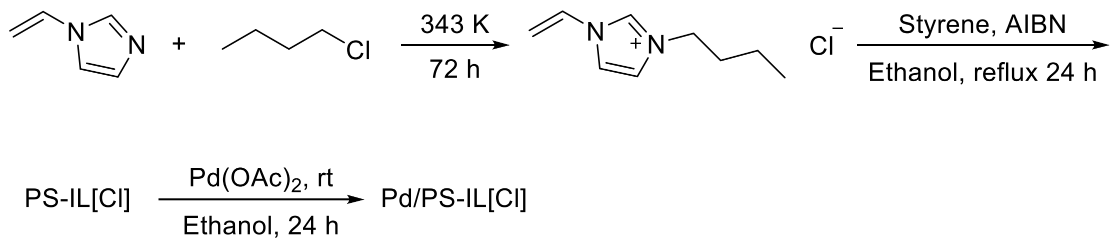

TEM and electron diffraction:

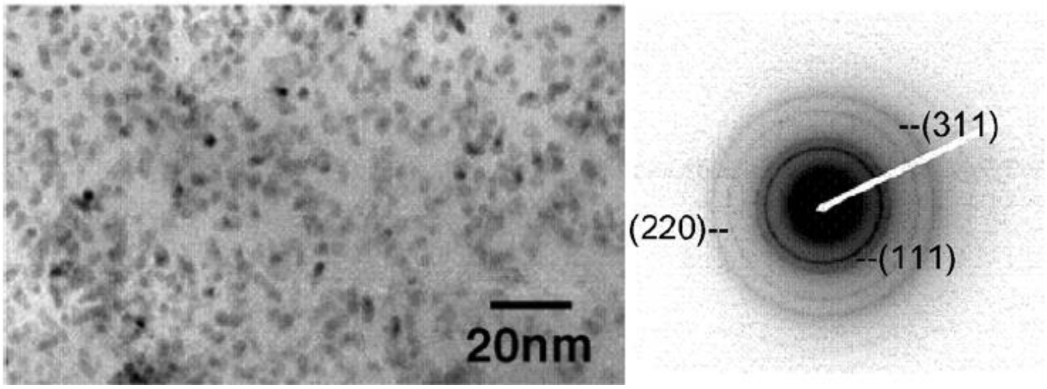

Reproduced with permission from ref 8. Copyright 2008 Elsevier.

Based on the ultrafine three-dimensional networks of the bacteria-cellulose (BC) nanofiber providing extensive specific area and large surface-to-volume ratio of cellulose nanostructures, which can be applied as an ideal support for Pd NPs immobilization, Tang's team developed a Pd bacteria-cellulose-nanofiber-supported (Pd/BC) nanocatalyst in 2012 (Scheme 6).[9] $PdCl_2$ was first added to a suspension of BC nanofiber freshly prepared in water, followed by heating, with stirring. The mixture was then reduced by addition of potassium borohydride to obtain Pd^0 NPs, and the Pd NPs were immobilized on the surface of the BC nanofibers leading to the nanocatalyst, Pd/BC. The Pd/BC nanomaterial can be used for catalyzing HM couplings to afford good yields in DMF at 120 °C with only 0.1 mol % catalytic Pd loading. Such a nanocatalyst can keep its activity after five reaction cycles. In addition, no Pd leaching was detected in the final coupling product. The authors' explanation was that the Pd leaching is protected by the ordered water layers covering the BC fibers via H-bonding.

Scheme 6: Tang's Pd/BC (SEM, TEM and XPS) for HM coupling reactions

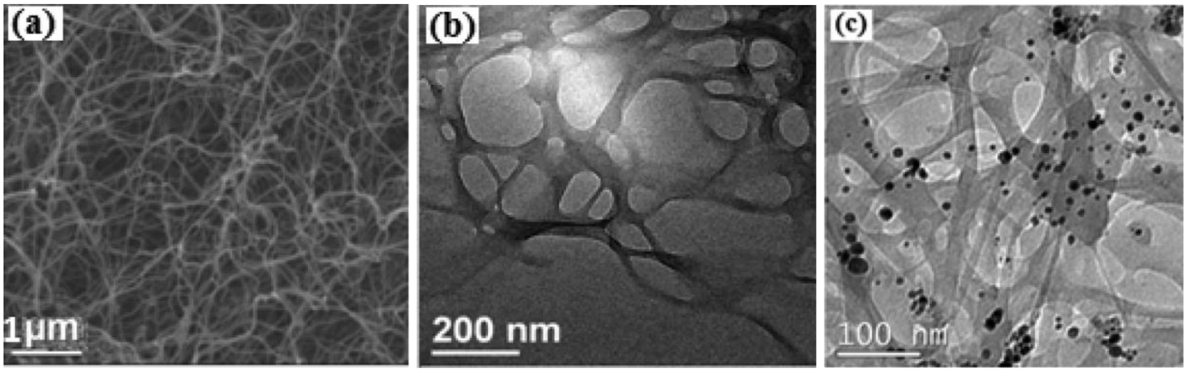

(a) SEM image of the dried BC nanofibers, (b)TEM images ofwet BC nanofibers, (c) the as-prepared Pd/BC catalyst

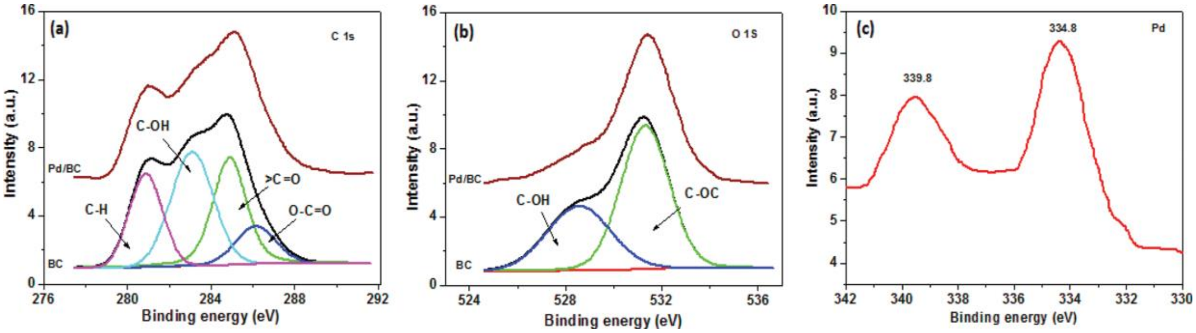

XPS analysis of (a) C 1s, (b) O 1s, and (c) Pd for BC nanofibers and Pd/BC catalyst.
Reproduced with permission from ref 9. Copyright 2012 American Chemical Society.

In the same year, Kamal and co-workers designed a Pd nanomaterial, Pd/CSP, with porous carbon nanostructures as the support for hosting a Pd nanocatalyst (Scheme 7).[10] They prepared this nanocatalyst by immobilization of $PdCl_2$ onto carbon spheres dispersed in EtOH. This nanomaterial can be used for catalyzing HM couplings in water at 90 °C leading to good yields using iodides or bromides as coupling partners. The Pd loading for each reaction is only 0.5 mol % relative to halides. However, the author also proved that such a catalyst cannot work very well at 50 °C. Their protocol has good compatibility with functional groups. Moreover, the catalyst could also retain activity for four catalytic cycles.

Scheme 7: Kamal's Pd/CSP (TEM) for HM coupling reactions

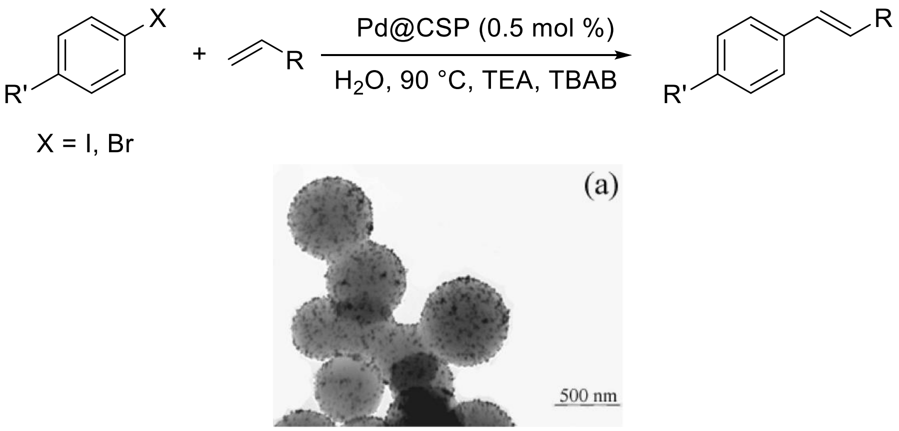

Reproduced with permission from ref 10. Copyright 2012 Royal Society of Chemistry.

In 2013, Yamada et al. reported a silicon-nanowire-array-stabilized Pd nanocatalyst using silicon wafers as support.[11] They prepared the nanoparticle catalyst as shown in Scheme 8. First, they immersed a boron doped p-type Si (100) wafer in a mixture of conc. H_2SO_4 and H_2O_2, following by treating it with HF. They obtained the Ag-coated Si wafer by treating the Si wafer with HF and $AgNO_3$, followed by treating the Ag-coated Si wafer with HF and H_2O_2 to afford Si nanowire array (SiNA) on the supporting material. Finally, the Ag was removed using HNO_3 and the Pd was immobilized on the Si nanowire array by reduction from K_2PdCl_4 to Pd NPs to generate the SiNA-stabilized Pd nanoparticle catalyst. This nanocatalyst can be used for HM reactions at 100 to 140 °C with only 0.3 mol % Pd in each reaction. Remarkably, in addition to HM couplings, this nanomaterial can also be used as catalyst for reductions of alkenes and nitrobenzenes, hydrosilylations of an α,β-unsaturated ketone, as well as C-H bond functionalization reactions of thiophenes and indoles.

Scheme 8: Preparation procedure for Yamada's SiNA-stabilized Pd nanoparticle catalyst for HM coupling reactions

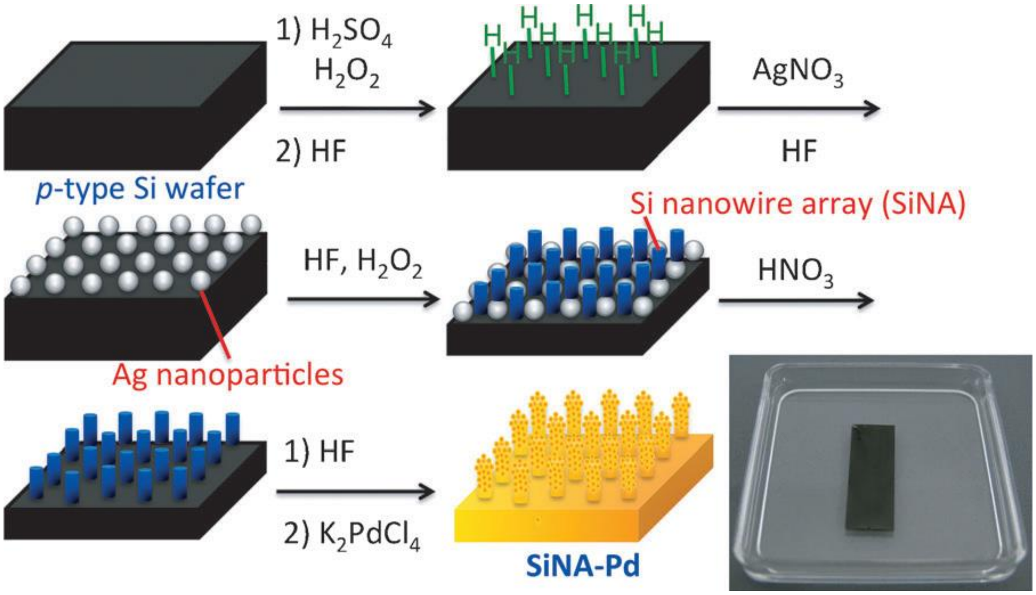

Reproduced with permission from ref 11. Copyright 2014 John Wiley and Sons.

In 2014, Rahmati's group developed a green protocol for preparing Pd NPs supported on a gelatin/pectin mixture as a novel nanocatalyst for HM coupling reactions.[12] Gelatin is a colorless, fragile, water-soluble solid that contains free carboxyl groups, which has the potential for chelating and reducing metals. Moreover, pectin is a flexible, non-toxic, inexpensive, easily available complex containing free hydroxyl groups, which can be used as supporting material for transition metal nanocatalysts. The Pd NPs/gelatin/pectin nanocatalyst was prepared via reduction of $PdCl_2$ to Pd(0) by gelatin in the pectin aqueous solution (Scheme 9). This nanocatalyst could be used for HM coupling for bromoarenes or iodoarenes and *n*-butyl acrylate as coupling partners, with only 0.2 mol % Pd under solvent-free conditions at 140 °C leading to good to excellent yields.

Scheme 9: Preparation procedure for Rahmati's Pd NPs/gelatin/pectin nanoparticle catalyst for HM coupling reactions

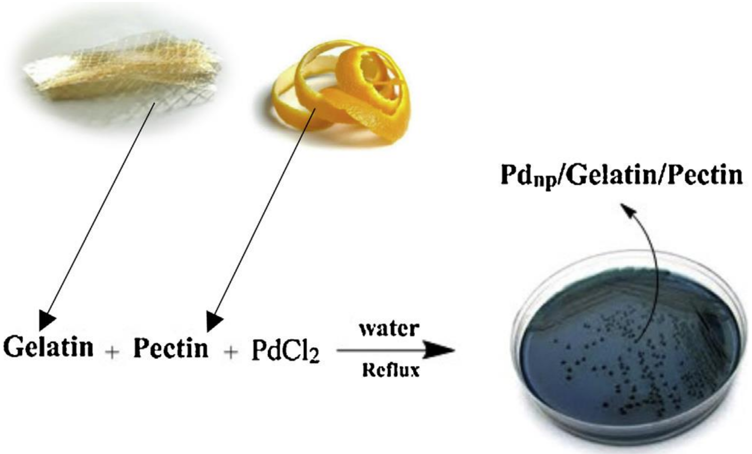

Reproduced with permission from ref 12. Copyright 2015 Elsevier.

In 2015, Li's group reported a novel Pd nanocatalyst, palladium(II) carboxymethylcellulose (CMC-Pd^{II}) derived from addition of aqueous solution of sodium carboxymethylcellulose (CMC-Na) to the $PdCl_2$ aqueous solution.[13] Moreover, the author discovered that the CMC-Pd^0 formed by reduction of the CMC-Pd^{II} precursor in situ during the reaction, as shown in Scheme 10, which showed relatively high catalytic activities for Suzuki-Miyaura and HM reactions. The latter reactions proceeded smoothly in 90% DMF with 0.9 mol % Pd loading at 110 °C, leading to 68-90% yields using bromoarenes or iodoarenes with olefins as coupling partners.

Scheme 10: Li's generation of Pd NPs on a CMC Skeleton for HM coupling reactions

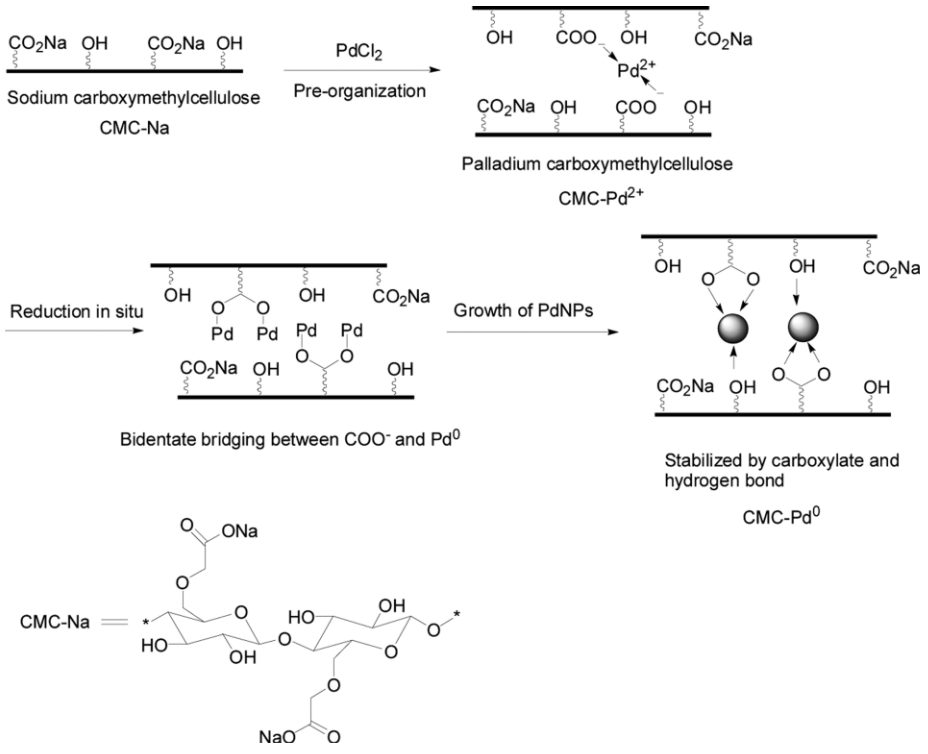
Sodium carboxymethylcellulose
CMC-Na
PdCl2
Pre-organization
Palladium carboxymethylcellulose
CMC-Pd2+
Reduction in situ
Bidentate bridging between COO- and Pd0
Growth of PdNPs
Stabilized by carboxylate and hydrogen bond
CMC-Pd0
CMC-Na

Reproduced with permission from ref 13. Copyright 2015 American Chemical Society.

In 2016, Gruttadauria's group designed a Pd-based nanocatalyst supported on single-walled carbon nanotube polyamidoamine dendrimers hybrids (SWCNTs−PAMAM), and showed its catalytic activity for Suzuki-Miyaura and HM reactions.[14] The support material, SWCNTs-PAMAM, was prepared by addition of a PAMAM methanol solution to pristine SWCNTs in a toluene suspension, followed by addition of AIBN and refluxing, as shown in Scheme 11. The authors then added an aqueous solution of tetrachloropalladate to the SWCNTs-PAMAM aqueous suspension, followed by reduction by $NaBH_4$ to afford the SWCNTs-PAMAM-Pd NPs. This nanocatalyst (0.1 mol % Pd) could be applied to HM coupling reactions using iodoarenes and methyl acrylate as coupling partners in the presence of triethylamine in DMF/H_2O (4:1) solution at 90 °C. Moreover, a plausible reaction mechanism of release and catch was also proposed in the report.

Scheme 11: Gruttadauria's SWCNTs-PAMAM-Pd NPs (preparation, HR-TEM) for HM coupling reactions

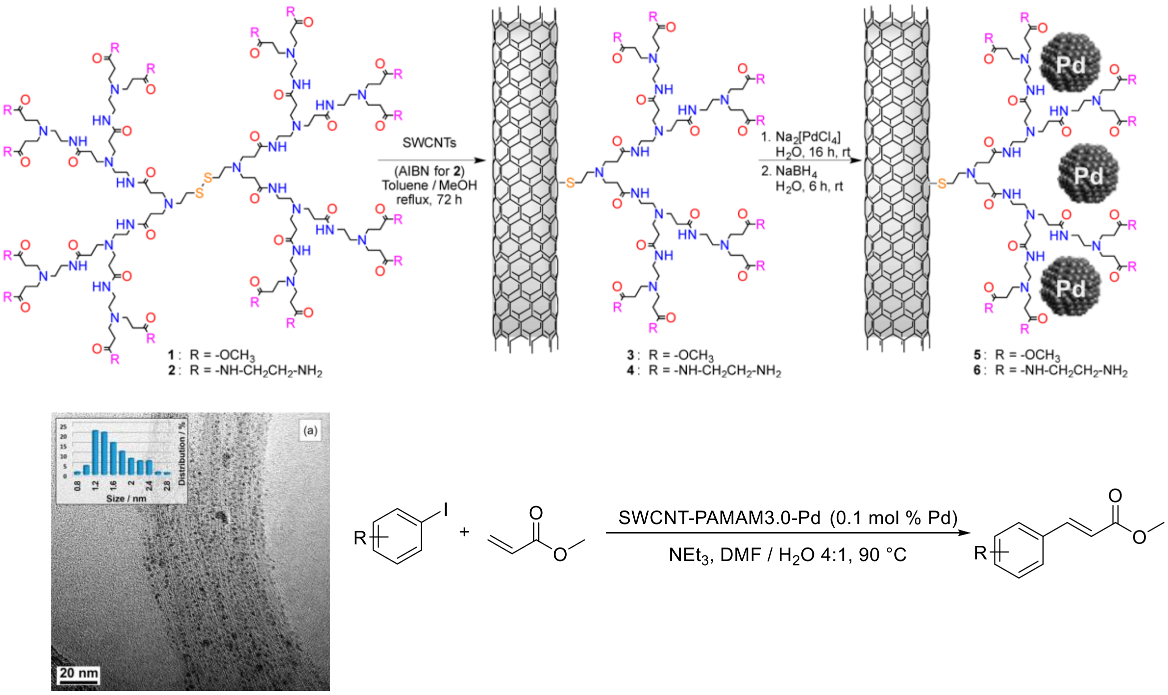
SWCNTs
(AIBN for 2)
Toluene / MeOH
reflux, 72 h
1. Na2[PdCl4]
H2O, 16 h, rt
2. NaBH4
H2O, 6 h, rt
Pd
1: R = -OCH3
2: R = -NH-CH2CH2-NH2
3: R = -OCH3
4: R = -NH-CH2CH2-NH2
5: R = -OCH3
6: R = -NH-CH2CH2-NH2
(a)
Size / nm
Distribution / %
20 nm
SWCNT-PAMAM3.0-Pd (0.1 mol % Pd)
NEt3, DMF / H2O 4:1, 90 °C

Reproduced with permission from ref 14. Copyright 2016 American Chemical Society.

In the same year, Menéndez's group reported a protocol for preparing a novel graphene Pd heterogeneous catalyst, TRGO-NPy-Pd, by decorating the surface of a reduced graphite oxide with a N_2-bidentate ligand to obtain TRGO-NPy, followed by coordination of $Pd(AcO)_2$ to afford the graphite oxide supported Pd nanomaterial (Scheme 12).[15] This material (0.3 mol% Pd based) could be used for catalyzing HM couplings of olefins with aryl bromides in the presence of Na_2CO_3 as base in DMF at 140 °C. In addition, the nanocatalyst retains a high catalytic activity over eight reaction cycles without any leaching of palladium, as detected by the ICP measurements.

Scheme 12: Menéndez’s TRGO-NPy-Pd (preparation, TEM) for HM coupling reactions

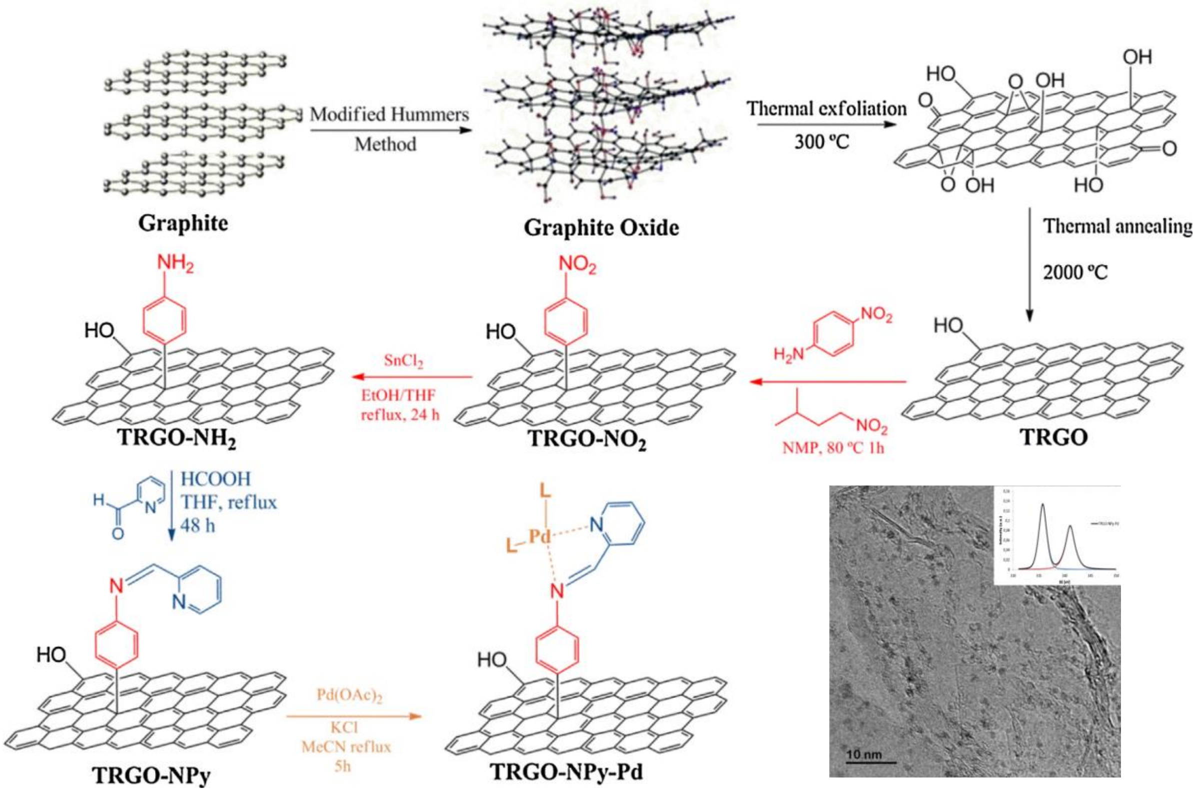
Graphite
Modified Hummers Method
Graphite Oxide
Thermal exfoliation 300 ºC
HO
O
OH
OH
O
O
OH
HO
Thermal annealing 2000 ºC
TRGO
HO
H_2N
NO_2
NMP, 80 ºC 1h
TRGO-NO_2
NO_2
$SnCl_2$
EtOH/THF reflux, 24 h
TRGO-NH_2
NH_2
HCOOH THF, reflux 48 h
H
N
O
N
TRGO-NPy
$Pd(OAc)_2$
KCl
MeCN reflux
5h
L
L
Pd
N
N
TRGO-NPy-Pd
10 nm

Reproduced with permission from ref 15. Copyright 2016 Elsevier.

Nowadays, Pd-catalyzed HM couplings have been widely applied to pharmaceuticals and agrochemicals.[16] Actually, HM reactions are known to be one of the crucial protocols for the synthesis of natural products, medicines, APIs, and fine chemicals. Although compared with heterogeneous Pd catalysts, homogeneous Pd catalysts usually show higher activity and selectivity, however, these catalysts are not appropriate for applications to large-scale industry due to their high cost, separation problems, high Pd residue the products, and difficulty recycling. Hence, various nanomaterials have been designed and developed as support materials for Pd nanocatalysts for achieving greener, economical, sustainable processes, including HM cross couplings. However, even though diverse Pd nanocatalysts have been reported, the requirement for the input of the energy in the form of heating for these protocols remains stubbornly high, which undoubtedly has hindered development of HM couplings in a greener and more sustainable direction. Thus, the development of a new catalyst applicable to HM reactions the functions in aqueous solution under mild conditions, requires a low Pd loading has been the aim of the following research.

References

1. Tsutomu, M.; Kunio, M.; Atsumu, O. Arylation of Olefin with Aryl Iodide Catalyzed by Palladium. *Bull. Chem. Soc. Jpn.* **1971**, *44*, 581.

2. Heck, R. F.; Nolley, J. P. Palladium-catalyzed vinylic hydrogen substitution reactions with aryl, benzyl, and styryl halides. *J. Org. Chem.* **1972**, *37*, 2320.

3. Dieck, H. A.; Heck, R. F. Organophosphinepalladium complexes as catalysts for vinylic hydrogen substitution reactions. *J. Am. Chem. Soc.* **1974**, *96*, 1133.

4. Heck, R. F. Mechanism of arylation and carbomethoxylation of olefins with organopalladium compounds. *J. Am. Chem. Soc.* **1969**, *91*, 6707.

5. Cabri, W.; Candiani, I. Recent Developments and New Perspectives in the Heck Reaction. *Acc. Chem. Res.* **1995**, *28*, 2.

6. Choudary, B. M.; Madhi, S.; Chowdari, N. S.; Kantam, M. L.; Sreedhar, B. Layered Double Hydroxide Supported Nanopalladium Catalyst for Heck-, Suzuki-, Sonogashira-, and Stille-Type Coupling Reactions of Chloroarenes. *J. Am. Chem. Soc.* **2002**, *124*, 14127.

7. Mandal, S.; Roy, D.; Chaudhari, R. V.; Sastry, M. Pt and Pd Nanoparticles Immobilized on Amine-Functionalized Zeolite: Excellent Catalysts for Hydrogenation and Heck Reactions. *Chem. Mater.* **2004**, *16*, 3714.

8. Qiao, K.; Sugimura, R.; Bao, Q.; Tomida, D.; Yokoyama, C. An efficient Heck reaction in water catalyzed by palladium nanoparticles immobilized on imidazolium–styrene copolymers. *Catal. Commun.* **2008**, *9*, 2470.

9. Zhou, P.; Wang, H.; Yang, J.; Tang, J.; Sun, D.; Tang, W. Bacteria Cellulose Nanofibers Supported Palladium(0) Nanocomposite and Its Catalysis Evaluation in Heck Reaction. *Ind. Eng. Chem. Res* **2012**, *51*, 5743.

10. Kamal, A.; Srinivasulu, V.; Seshadri, B. N.; Markandeya, N.; Alarifi, A.; Shankaraiah, N. Water mediated Heck and Ullmann couplings by supported palladium nanoparticles: importance of surface polarity of the carbon spheres. *Green Chem.* **2012**, *14*, 2513.

11. Yamada, Y. M.; Yuyama, Y.; Sato, T.; Fujikawa, S.; Uozumi, Y. A palladium-nanoparticle and silicon-nanowire-array hybrid: a platform for catalytic heterogeneous reactions. *Angew. Chem., Int. Ed. Engl.* **2014**, *53*, 127.

12. Khazaei, A.; Khazaei, M.; Rahmati, S. A green method for the synthesis of gelatin/pectin stabilized palladium nano-particles as efficient heterogeneous catalyst for solvent-free Mizoroki–Heck reaction. *J. Mol. Catal. A: Chem.* **2015**, *398*, 241.

13. Xiao, J.; Lu, Z.; Li, Y. Carboxymethylcellulose-Supported Palladium Nanoparticles Generated in Situ from Palladium(II) Carboxymethylcellulose: An Efficient and Reusable Catalyst for Suzuki–Miyaura and Mizoroki–Heck Reactions. *Ind. Eng. Chem. Res* **2015**, *54*, 790.

14. Giacalone, F.; Campisciano, V.; Calabrese, C.; La Parola, V.; Syrgiannis, Z.; Prato, M.; Gruttadauria, M. Single-Walled Carbon Nanotube-Polyamidoamine Dendrimer Hybrids for Heterogeneous Catalysis. *ACS Nano* **2016**, *10*, 4627.

15. Fernández-García, L.; Blanco, M.; Blanco, C.; Álvarez, P.; Granda, M.; Santamaría, R.; Menéndez, R. Graphene anchored palladium complex as efficient and recyclable catalyst in the Heck cross-coupling reaction. *J. Mol. Catal. A: Chem.* **2016**, *416*, 140.

16. L. Budarin, V.; S. Shuttleworth, P.; H. Clark, J.; Luque, R. Industrial Applications of C-C Coupling Reactions. *Curr. Org. Synth.* **2010**, *7*, 614.

Results and discussion

Transition metal-containing nanoparticles (NPs) offer timely opportunities for development of new heterogeneous catalysts and their applications to a broad range of synthetic processes.[1] Given the endangered status of the platinoids, and Pd in particular,[2] reducing the common use of 1-5 mol % of Pd catalysts by an order of magnitude provides one solution to this problem. While numerous types of Pd NPs have been described over the past two decades,[3] few have found their way into the toolbox of *general* reagents for effecting C-C bond formation, with most of the interest focused on their physical characteristics and properties. Oftentimes, Pd-containing NPs, whether composed of pure atoms or metal on the surface of solid supports (such as Al_2O_3) require exposure to gases at elevated temperatures to arrive at the active form(s), which can be reversible both during and once reactions are completed.[4] Such conditions are associated with distinct changes in NP shape and size under such reaction conditions that can dramatically alter, and thereby, decrease catalyst activity.

Back in 2015,[5] we described new NPs that could be easily fashioned upon simple treatment of inexpensive $FeCl_3$ with MeMgCl in THF solution containing SPhos as ligand, performed at room temperature (Scheme 1). Catalyst loading at the ppm level of Pd, whether found naturally as an “impurity” in this iron salt, or as added $Pd(OAc)_2$ (>320 ppm) to pure $FeCl_3$ was sufficient to mediate Suzuki-Miyaura cross-couplings, reactions that could be run in aqueous micellar media under very mild conditions (20-45 °C). Characterization of these NPs via numerous techniques, including cryo-TEM analysis of their aqueous reaction medium revealed their size and raft-like shape. Switching ligands to XPhos, as well as the Grignard reagent to MeMg*Br*, resulted in NPs that are very effective for catalyzing Sonogashira couplings under similar aqueous conditions (Scheme 1).[6] When our interests turned towards developing related NPs that might provide entry to ppm Pd-catalyzed Heck-Mizoroki (HM) couplings in water, not only was a different ligand required, but a significant change in the mode of preparation of what are, seemingly, the same type of NPs. These changes necessitated a more complete analysis of the initially formed, spherical NPs (in THF). This has led us to discover the remarkable *room temperature* transformation to their active state upon simple exposure to the aqueous conditions under which they would normally be used. In this report, we disclose this unexpected and rare water-mediated conversion,[7] the generality of this catalyst sculpting in water, and the application of these new ppm Pd-containing NPs as a new heterogeneous catalyst for HM reactions that take place in recyclable water under environmentally responsible conditions.[8]

Scheme 1: Reactions catalyzed by ligand-dependent, ppm Pd-containing NPs

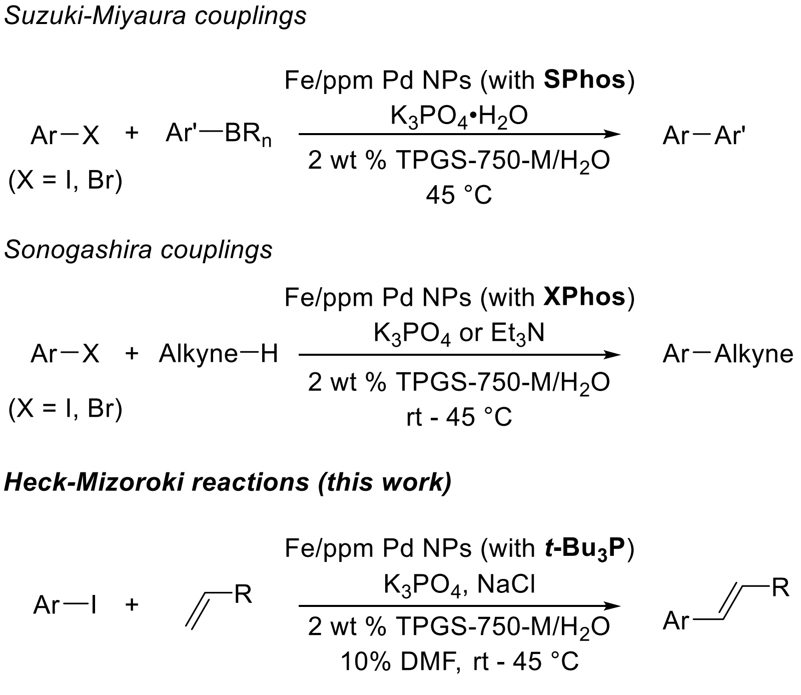
Suzuki-Miyaura couplings
Fe/ppm Pd NPs (with SPhos)
K3PO4•H2O
2 wt % TPGS-750-M/H2O
45 °C
Ar—X + Ar'—BRn
(X = I, Br)
Ar—Ar'
Sonogashira couplings
Fe/ppm Pd NPs (with XPhos)
K3PO4 or Et3N
2 wt % TPGS-750-M/H2O
rt - 45 °C
Ar—X + Alkyne—H
(X = I, Br)
Ar—Alkyne
Heck-Mizoroki reactions (this work)
Fe/ppm Pd NPs (with t-Bu3P)
K3PO4, NaCl
2 wt % TPGS-750-M/H2O
10% DMF, rt - 45 °C
Ar—I +
R
Ar
R

Optimization of Fe/ppm Pd NPs

After an extensive ligand screening indicating that *t*-Bu$_3$P was, by far, the best ligand for the intended Heck-Mizoroki reactions, the corresponding Fe/ppm Pd NPs were formed, and used, following our earlier prescription: in an oven dried 4 mL microwave reaction vial covered with a septum containing a PTFE-coated magnetic stir bar, 0.1 mL THF solution of 0.1 M $FeCl_3$ (0.01 mmol), 0.1 mL THF solution of 0.01 M $Pd(t\text{-}Bu_3P)_2$ (0.001 mmol) and 0.1 mL THF solution of 0.04 M $t\text{-}Bu_3P$ (0.004 mmol) were added under dry argon. While maintaining a dry atmosphere at rt, a 0.1 M solution of MeMgCl in THF was very slowly (1 drop/2 sec) added to the reaction mixture. After complete addition of the Grignard reagent, the mixture was stirred for an additional 10 min at rt. THF was then evaporated under reduced pressure at rt to arrive at the targeted Fe/Pd NPs (Scheme 2, Method A). After evaporation, the NPs need to be stored under argon. 1-iodo-4-methoxybenzene and *t*-butyl acrylate were chosen as partners for this model reaction. 1-Iodo-4-methoxybenzene (46.8 mg, 0.2 mmol, 1 equiv) and NaCl (70.2 mg, 1.2 mmol) were added to the vial with the in situ-prepared Fe/ppm Pd NPs followed by sequential addition of an aqueous solution 5 wt % PTS/H_2O (0.4 mL), *t*-butyl acrylate (51.3 mg, 0.4 mmol, 2 equiv) and triethylamine (60.7 mg, 0.6 mmol, 3 equiv). The reaction vial was closed with a septum under argon and stirred vigorously at rt for 16 h. After 16 h, EtOAc was added and the mixture was gently stirred for 2 min at rt. Stirring was then stopped and the organic layer was decanted via pipette. The organic layer was passed through a very small silica plug. Yields were determined by GCMS using naphthalene as internal standard. NPs with different equivalents of MeMgCl were tested in 2 wt % PTS/H_2O at room temperature, but none led to significant product formation (entries 1 to 5).

During the preparation of the NPs via the original procedures, we discovered that when the dry THF was added to the mixture of $FeCl_3$, $Pd(t\text{-}Bu_3P)_2$ and $t\text{-}Bu_3P$, the complex formed a suspension, which was similar to the phenomena of the addition of Grignard reagent indicating that partial reduction of $FeCl_3$ in THF had occurred. Moreover, given that *t*-Bu_3P and Pd(*t*-Bu_3P)$_2$ are sensitive to air, we inferred that prior to the addition of Grignard reagent, the *t*-Bu_3P and Pd(*t*-Bu_3P)$_2$ had been oxidized by $FeCl_3$ leading to an inactive catalyst for HM couplings. Hence, the question was how to lower the impact of $FeCl_3$ on *t*-Bu_3P and Pd(*t*-Bu_3P)$_2$ so that a more active Pd complex was formed and deposited within the nanocatalyst. At that time, previous failures at developing analogous iridium nanoparticles were inspiring. Attempts to prepare Fe/ppm Ir NPs for α-alkylation, dipyridine was examined as ligand for iridium. Dipyridine can also coordinate with iron ions. Different from the phenomena observed with Fe/ppm Pd-*t*-Bu_3P NPs, during the preparation of Fe/ppm Ir-dipyridine NPs, a red solution formed indicating that the iron ions had been coordinated by dipyridine, thereby the likelihood of forming nanoparticles was slim, regardless of the amount of Grignard reagent that had been added. Consequently, to solve this issue, Grignard reagent was used to reduce the combination of iron chloride and iridium first, to which was then added dipyridine as ligand. Unfortunately, however, a usable catalyst was not obtained. Hence, when the same $FeCl_3$-ligand problem arose, it was decided to change the method of preparation for the NPs.

Therefore, modified sequences for reagent formation, as shown in Scheme 2 (Methods B-D), were investigated to enhance the level of activation of the resulting NPs for these same couplings (entries 6 to 11):

General procedure for preparation of in situ-derived Fe/ppm Pd NPs; procedure B:

In an oven dried 4 mL microwave reaction vial covered with a septum containing a PTFE-coated magnetic stir bar, 0.1 mL THF solution of 0.1 M $FeCl_3$ (0.01 mmol) and 0.1 mL THF solution of 0.04 M *t*-Bu_3P (0.004 mmol) were added under dry argon. While maintaining a dry atmosphere at rt, a 0.1 M solution of MeMgCl in THF was very slowly (1 drop/2 sec) added to the reaction mixture. Then the mixture was stirred for an additional 1 min at rt. After that time, 0.1 mL THF solution of 0.01 M Pd(*t*-Bu_3P_3)$_2$ (0.001 mmol) was added to the reaction mixture. After addition, additional 0.1 M solution of MeMgCl in THF was very slowly (1 drop/2 sec) added to the reaction mixture. After complete addition of the Grignard reagent, the mixture was stirred for an additional 10 min at rt. THF was then evaporated under reduced pressure at rt. After evaporation, the NPs need to be stored under argon.

General procedure for preparation of in situ-derived Fe/ppm Pd NPs; procedure C:

In an oven dried 4 mL microwave reaction vial covered with a septum containing a PTFE-coated magnetic stir bar, 0.1 mL THF solution of 0.1 M $FeCl_3$ (0.01 mmol) and 0.1 mL THF solution of 0.01 M Pd(*t*-Bu_3P)$_2$ (0.001 mmol) were added under dry argon. While maintaining a dry atmosphere at rt, a 0.1 M solution of MeMgCl in THF was very slowly (1 drop/2 sec) added to the reaction mixture. Then the mixture was stirred for an additional 1 min at rt. After that time, 0.1 mL THF solution of 0.04 M *t*-Bu_3P (0.004 mmol) was added to the reaction mixture. After addition, additional 0.1 M solution of MeMgCl in THF was very slowly (1 drop/2 sec) added to the reaction mixture. After complete addition of the Grignard reagent, the mixture was stirred for an additional 10 min at rt. THF was then evaporated under reduced pressure at rt. After evaporation, the NPs need to be stored under argon.

General procedure for preparation of in situ-derived Fe/ppm Pd NPs; procedure D:

In an oven dried 4 mL microwave reaction vial covered with a septum containing a PTFE-coated magnetic stir bar, 0.1 mL THF solution of 0.1 M $FeCl_3$ (0.01 mmol) was added under dry argon. While maintaining a dry atmosphere at rt, a 0.1 M solution of MeMgCl in THF was very slowly (1 drop/2 sec) added to the reaction mixture. Then the mixture was stirred for an additional 1 min at rt. After that time, 0.1 mL THF solution of 0.01 M Pd(*t*-Bu_3P)$_2$ (0.001 mmol) and 0.1 mL THF solution of 0.04 M *t*-Bu_3P (0.004 mmol) were added to the reaction mixture. After addition, additional 0.1 M solution of MeMgCl in THF was very slowly (1 drop/2 sec) added to the reaction mixture. After complete addition of the Grignard reagent, the mixture was stirred for an additional 10 min at rt. THF was then evaporated under reduced pressure at rt. After evaporation, the NPs need to be stored under argon.

From the GC yields obtained, Method D afforded the best coupling yields indicating the success of minimizing the influence of $FeCl_3$ to both to *t*-Bu_3P and Pd(*t*-$Bu_3P)_2$ via pre-reduction by MeMgCl. Further refinements focused on further lowering the Pd loading for each reaction (from 0.5 mol % to 0.25 mol %). The main path for improving the catalytic activity of the nanocatalyst was also by adjusting the equivalents of Grignard reagent. Hence, the optimizations based on equivalents of MeMgCl, both prior to, and after the addition of Pd and ligand were conducted subsequently. The utilization of the nanocatalyst prepared by initial 2 equivalents of MeMgCl followed by 1.5 equivalents (relative to $FeCl_3$), even together with a Pd loading of 0.25 mol % led to 80% GC-yield in the model reaction, which was the best combination for preparation (entry 12 to 14). Refinement of the amount of ligand afforded a further improved yield (90%; entry 16). However, other palladium salts, such as $Pd(OAc)_2$ or $[Pd(allyl)Cl]_2$ could not work as well as Pd(*t*-$Bu_3P)_2$ in the NPs as the Pd source (entry 17 and 18). Finally, various types of phosphoric ligands including Cy-cBRIDP,[9] dppp, *N*-Ph-2-(*t*-Bu)$_2$P-pyrrole), and SPhos were also examined to prepare the nanocatalyst. Nevertheless, no relatively stable alternative of *t*-Bu_3P was found, which clearly showed that the combination of Pd(*t*-$Bu_3P)_2$ and *t*-Bu_3P afforded far better yields in the aqueous PTS medium than did other sources of palladium or ligands (entries 19 to 28).

Scheme 2: Optimization for the preparation of Fe/ppm Pd NPs

Various combinations of reagents to arrive at optimized NPs for Heck-Mizoroki (HM) couplings:

Method A: $FeCl_3$ + Pd complex + Ligand $\xrightarrow[\text{THF}]{\text{MeMgCl}}$ Fe/ppm Pd NPs [original preparation; Ligand = SPhos][5]

Method B: $FeCl_3$ + Ligand $\xrightarrow[\text{THF}]{\text{MeMgCl}}$ Fe NP core with Ligand $\xrightarrow{\text{+ Pd complex}}$ $\xrightarrow[\text{THF}]{\text{+ MeMgCl}}$ Fe/ppm Pd NPs

Method C: $FeCl_3$ + Pd complex $\xrightarrow[\text{THF}]{\text{MeMgCl}}$ Fe NP core with Pd complex $\xrightarrow{\text{+ Ligand}}$ $\xrightarrow[\text{THF}]{\text{+ MeMgCl}}$ Fe/ppm Pd NPs

Method D: $FeCl_3$ $\xrightarrow[\text{THF}]{\text{MeMgCl}}$ Fe NP core $\xrightarrow[\text{+ Ligand}]{\text{+ Pd complex}}$ $\xrightarrow[\text{THF}]{\text{+ MeMgCl}}$ Fe/ppm Pd NPs

Heck reaction test:

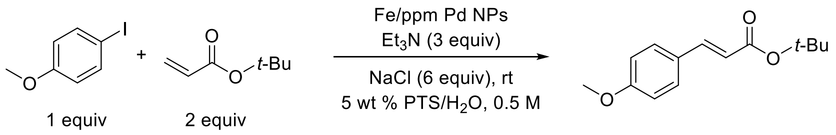
I
+
O
O
t-Bu
1 equiv
2 equiv
Fe/ppm Pd NPs
Et3N (3 equiv)
NaCl (6 equiv), rt
5 wt % PTS/H2O, 0.5 M
O
O
t-Bu
O

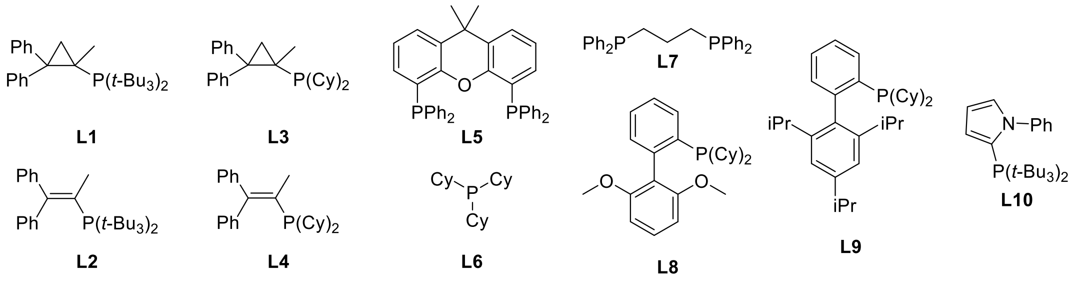
Ph
Ph
P(t-Bu3)2
L1
Ph
Ph
P(Cy)2
L3
O
PPh2
PPh2
L5
Ph2P
PPh2
L7
P(Cy)2
O
O
L8
P(Cy)2
iPr
iPr
iPr
L9
N–Ph
P(t-Bu3)2
L10
Ph
Ph
P(t-Bu3)2
L2
Ph
Ph
P(Cy)2
L4
Cy
P
Cy
Cy
L6

Entry	Method	Pd complex/(mmol)	L/(mmol)	MeMgCl (mmol)	GC Yield (%)
1	A	Pd(*t*-Bu$_3$P)$_2$/0.001	*t*-Bu$_3$P/0.004	0.015	NR
2	A	Pd(*t*-Bu$_3$P)$_2$/0.001	*t*-Bu$_3$P/0.004	0.02	NR
3	A	Pd(*t*-Bu$_3$P)$_2$/0.001	*t*-Bu$_3$P/0.004	0.025	NR
4	A	Pd(*t*-Bu$_3$P)$_2$/0.001	*t*-Bu$_3$P/0.004	0.03	<5
5	A	Pd(*t*-Bu$_3$P)$_2$/0.001	*t*-Bu$_3$P/0.004	0.035	<5
6	B	Pd(*t*-Bu$_3$P)$_2$/0.001	*t*-Bu$_3$P/0.004	0.01 + 0.025	NR
7	C	Pd(*t*-Bu$_3$P)$_2$/0.001	*t*-Bu$_3$P/0.004	0.01 + 0.02	NR
8	C	Pd(*t*-Bu$_3$P)$_2$/0.001	*t*-Bu$_3$P/0.004	0.01 + 0.025	<5
9	C	Pd(*t*-Bu$_3$P)$_2$/0.001	*t*-Bu$_3$P/0.004	0.01 + 0.03	NR
10	C	Pd(*t*-Bu$_3$P)$_2$/0.001	*t*-Bu$_3$P/0.004	0.01 + 0.04	NR
11	D	Pd(*t*-Bu$_3$P)$_2$/0.001	*t*-Bu$_3$P/0.004	0.01 + 0.025	89
12	D	Pd(*t*-Bu$_3$P)$_2$/0.0005	*t*-Bu$_3$P/0.004	0.01 + 0.025	31
13	D	Pd(*t*-Bu$_3$P)$_2$/0.0005	*t*-Bu$_3$P/0.004	0.015 + 0.02	65
14	D	Pd(*t*-Bu$_3$P)$_2$/0.0005	*t*-Bu$_3$P/0.004	0.02 + 0.015	80
15	D	Pd(*t*-Bu$_3$P)$_2$/0.0005	*t*-Bu$_3$P/0.008	0.02 + 0.015	86
16	**D**	**Pd(*t*-Bu$_3$P)$_2$/0.0005**	***t*-Bu$_3$P/0.012**	**0.02 + 0.015**	**90**
17	D	Pd(OAc)$_2$/0.0005	*t*-Bu$_3$P/0.012	0.02 + 0.015	15
18	D	[Pd(allyl)Cl]$_2$/0.0005	*t*-Bu$_3$P/0.012	0.02 + 0.015	17
19	D	Pd(OAc)$_2$/0.0005	**L1**/0.012	0.02 + 0.015	NR
20	D	Pd(OAc)$_2$/0.0005	**L2**/0.012	0.02 + 0.015	NR
21	D	Pd(OAc)$_2$/0.0005	**L3**/0.012	0.02 + 0.015	NR
22	D	Pd(OAc)$_2$/0.0005	**L4**/0.012	0.02 + 0.015	NR
23	D	Pd(OAc)$_2$/0.0005	**L5**/0.012	0.02 + 0.015	NR
24	D	Pd(OAc)$_2$/0.0005	**L6**/0.012	0.02 + 0.015	NR
25	D	Pd(OAc)$_2$/0.0005	**L7**/0.012	0.02 + 0.015	<5
26	D	Pd(OAc)$_2$/0.0005	**L8**/0.012	0.02 + 0.015	NR
27	D	Pd(OAc)$_2$/0.0005	**L9**/0.012	0.02 + 0.015	NR
28	D	Pd(OAc)$_2$/0.0005	**L10**/0.012	0.02 + 0.015	8

Optimization of reaction conditions

From the previous section the best combination for preparing the NPs used for catalyzing HM couplings in aqueous micelles was determined. To arrive at finalized reaction conditions for use of these NPs, an evaluation of the base and surfactant was undertaken (Scheme 3). Switching to K$_3$PO$_4$ from Et$_3$N gave similar results, even though the loading of

Pd was reduced from 2500 to 1000 ppm (i.e., 0.1 mol %; entry 5). Moreover, replacement of 5 wt % PTS/H_2O with 2 wt % TPGS-750-M/H_2O could also further improve the yield slightly (entry 9). Other surfactants[10] as well as different amounts of surfactant in water were screened subsequently as reaction medium, but none of them led to better yields than those based on used of 2 wt % TPGS-750-M (entries 10 to 20).

Scheme 3: Optimization of reaction conditions

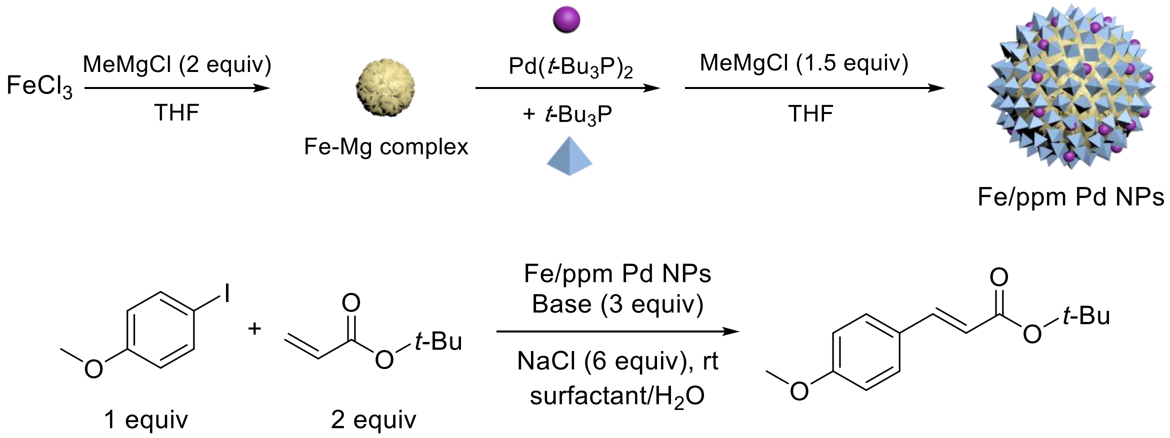
$FeCl_3$
MeMgCl (2 equiv)
THF
Fe-Mg complex
Pd(*t*-$Bu_3P)_2$
+ *t*-Bu_3P
MeMgCl (1.5 equiv)
THF
Fe/ppm Pd NPs
I
O
O
t-Bu
+
1 equiv
2 equiv
Fe/ppm Pd NPs
Base (3 equiv)
NaCl (6 equiv), rt
surfactant/H_2O
O
O
t-Bu
O

Entry	Pd (%)	Fe (%)	L (%)	Base	Surfactant	GC Yield (%)
1	0.25	5	6	NEt_3	5 wt % PTS/H_2O	90
2	0.1	2	2.4	NEt_3	5 wt % PTS/H_2O	<3
3	0.1	2	2.4	$NaHCO_3$	5 wt % PTS/H_2O	<3
4	0.1	2	2.4	Na_2CO_3	5 wt % PTS/H_2O	16
5	0.1	2	2.4	K_3PO_4	5 wt % PTS/H_2O	90
6	0.1	2	2.4	NaOAc	5 wt % PTS/H_2O	<3
7	0.25	5	6	NEt_3	2 wt % TPGS/H_2O	93
8	0.25	5	6	NEt_3	5 wt % TPGS/H_2O	7
9[a]	**0.1**	**2**	**2.4**	**K_3PO_4**	**2 wt % TPGS/H_2O**	**99 (99)**
10	0.1	2	2.4	K_3PO_4	2 wt % Brij 30/H_2O	8
11	0.1	2	2.4	K_3PO_4	2 wt % Brij 35/H_2O	58
12	0.1	2	2.4	K_3PO_4	2 wt % PTS/H_2O	91
13	0.1	2	2.4	K_3PO_4	2 wt % TWEEN 60/H_2O	30
14	0.1	2	2.4	K_3PO_4	2 wt % Tritonr X-100/H_2O	49
15	0.1	2	2.4	K_3PO_4	2 wt % Pluronic/H_2O	36
16	0.1	2	2.4	K_3PO_4	2 wt % Nok/H_2O	98
17	0.1	2	2.4	K_3PO_4	1 wt % TPGS/H_2O	56
18	0.1	2	2.4	K_3PO_4	3 wt % TPGS/H_2O	22
19	0.1	2	2.4	K_3PO_4	4 wt % TPGS/H_2O	61
20	0.1	2	2.4	K_3PO_4	5 wt % TPGS/H_2O	98

[a] isolated yield was in parentheses.

However, when *t*-butyl acrylate was switched to styrene as the coupling partner, no coupling product was detected under optimized conditions. To achieve HM coupling between styrene and 4-iodoanisole, using the optimized conditions, the Pd loading was increased from 0.1 mol % to 0.25 mol %, while the reaction temperature was also increased to 45 °C (Scheme 4). Nonetheless, no coupling occurred under such modified conditions (entry 1). Further efforts paid attention to the potential role of co-solvent. After screening several co-solvents commonly used, we discovered that if needed, DMF was the co-solvent of choice (entry 7). The isolated yield could reach up to 87% after an increase in reaction time.

Scheme 4: Optimization of co-solvent

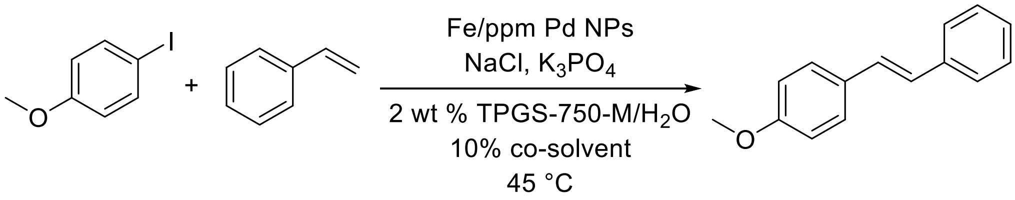

Entry	Cosolvent	Time (h)	GC Yield (%)
1	-	16	n.d.
2	DCM	16	n.d.
3	DMSO	16	13
4	THF	16	<10
5	toluene	16	n.d.
6	MeCN	16	<10
7[a]	**DMF**	**16**	**67 (62)**
8	MeOH	16	<10
9	EtOAc	16	n.d.
10[a]	**DMF**	**40**	**96 (87)**
11[b]	DMF	40	n.d.

[a] isolated yield was in parentheses; [b] Room temperature.

Under otherwise identical conditions, use of pure THF as the reaction medium together with these same NPs (albeit containing 0.25% Pd) led to the expected product in only 9% yield. Running this reaction in micellar media in the presence of the same amounts of Pd(*t*-Bu$_3$P)$_2$ and *t*-Bu$_3$P but *without prior NP formation* gave a significant reduction in yield (19% with FeCl$_3$; 8% in the absence of FeCl$_3$; see Appendix), indicative of the important role played by nanoparticle formation.

Characterization of the NPs

We next turned our attention to investigating the nature of the NPs that catalyze these HM couplings. As previously pursued, a variety of techniques were applied to establishing the makeup of the surface of this catalyst. Most informative, however, was determination of their morphology when present within an aqueous reaction mixture via cryo-TEM analyses. To broaden this study, it was decided to do similar analyses on these NPs as initially prepared (in THF), which had never been performed on previous NPs containing either SPhos or XPhos, prior to their use under aqueous micellar catalysis conditions. We were certainly not anticipating the remarkable changes in NP morphology that would be forthcoming from these cryo-TEM studies.

Examination of these new NPs (following Method D, L = *t*-Bu$_3$P) under typical aqueous reaction conditions (i.e., in 2 wt % TPGS-750-M/H$_2$O) indicated that, as seen previously in both cases of NPs containing SPhos-ligated Pd used for Suzuki-Miyaura couplings,[5] and NPs composed of XPhos-ligated Pd for Sonogashira couplings,[6] nanorods measuring 30 to 100 nm in length were present (Fig. 1C). However, the corresponding analyses of the initially formed NPs prepared in THF revealed a completely different morphology: these (as a dry powder) are spherical, measuring 2-5 nm (Fig. 1A). Exposure of the initial spherical NPs to just water begins the "sculpting" process (Fig. 1A to 1B). Upon addition of an aqueous solution of TPGS-750-M the conversion to nanorods is complete (Fig. 1B to 1C). Hence, the original NPs formed, in fact, are not the actual catalyst being used for these couplings; rather, their exposure to the aqueous surfactant had transformed them entirely into the active form capable of catalyzing HM couplings at the ppm level of Pd. In addition, STEM images of the NPs after the coupling indicated that the nanomaterial had aggregated and lost its morphological character (see Appendix), which accounted for lack of activity after initial use.

Figure 1: High angle annular dark-field scanning transmission electron microscopy (HAADF-STEM) image

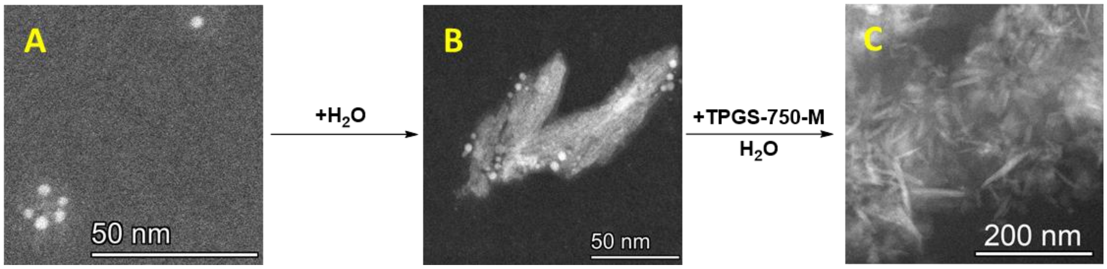

(A) dry Fe/ppm Pd nanoparticles; (B) Fe/ppm Pd nanomaterial in pure degassed water; (C) Fe/ppm Pd nanorods in 2 wt % TPGS-750-M/H_2O.

As revealed by elemental mapping images of dry powder NPs, O, P, Cl, Mg and Fe elements are homogeneously distributed throughout these nanoclusters, although the presence of Pd is too low to be detected (Fig. 2A). The corresponding energy-dispersive X-ray (EDX) spectrum confirmed the existence of O, P, Cl, Mg and Fe (with low atomic percentage of Pd; see Fig. 2B). Elemental mappings showed the distribution of O, Cl, Mg and Fe elements throughout the nanorods. By contrast, while nanorods showed the same Cl, O, and Mg distributed throughout the medium, phosphorus was noticeably absent.

Figure 2: Elemental mapping and EDX

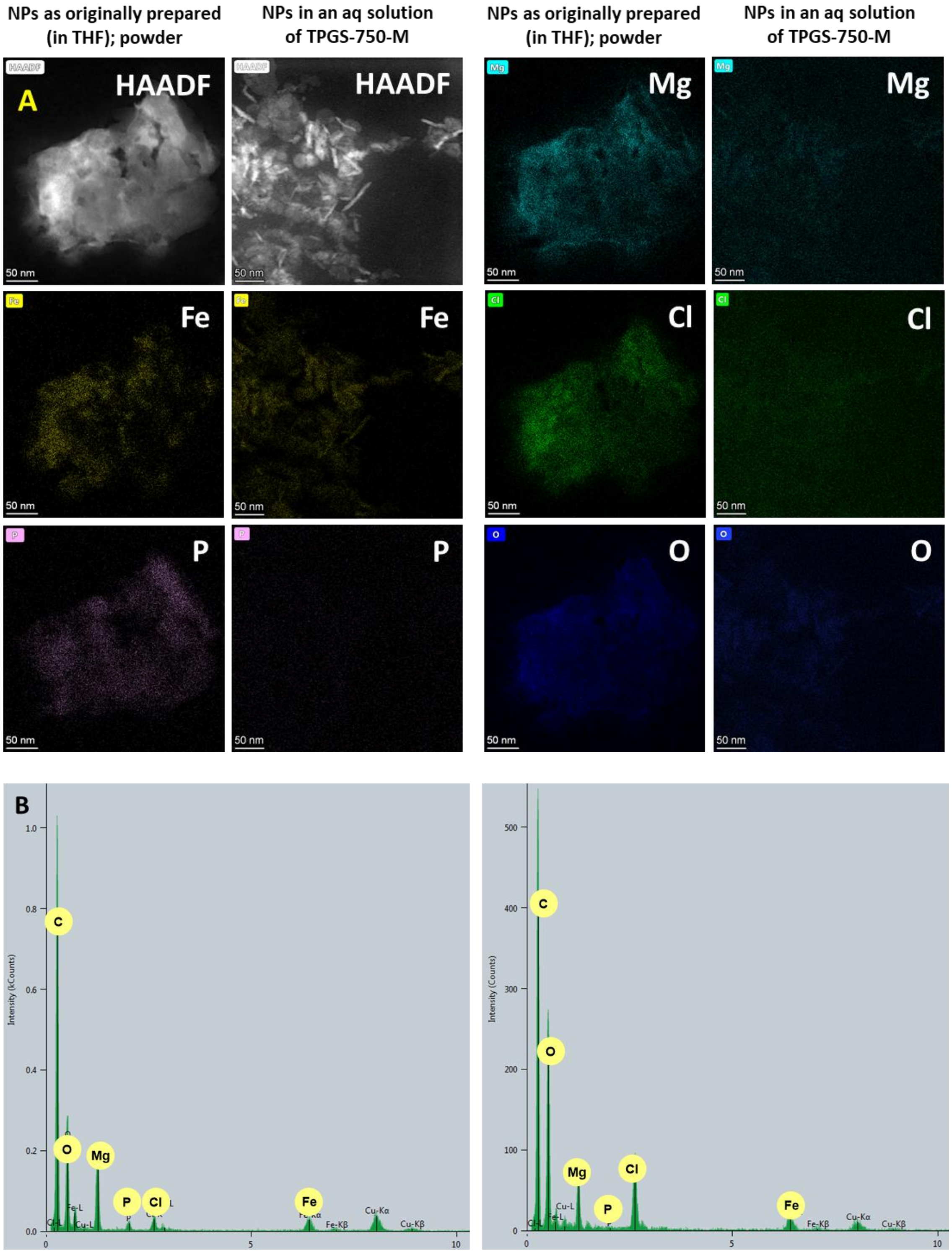

(A) HAADF-STEM elemental mapping of dry Fe/ppm Pd nanoparticles vs. Fe/ppm Pd nanorod in 2 wt % TPGS-750-M/H_2O and (B) EDX of dry Fe/ppm Pd nanoparticles (left) vs. Fe/ppm Pd nanorod in 2 wt % TPGS-750-M/H_2O (right).

To determine if this water-induced change in morphology of *t*-Bu$_3$P-containing NPs is independent of the associated ligand, two additional sets of NPs were made using the same approach (i.e., Scheme 2, Method D) but in these cases, *t*-Bu$_3$P was replaced with SPhos and Cy-cBRIDP. The Fe/ppm Pd NPs for each consisted of very similar looking dry powders. Likewise, their analyses by STEM showed related nanospheres (2 to 5 nm; Fig. 3A and 3D), as seen previously (see Fig. 1A). After stirring each in pure degassed water, both formed nanorods to varying extents (see Fig. 3B and 3E). However, upon addition of 2 wt % TPGS-750-M/H$_2$O, which is the usually added reaction medium, further stirring for one hour led to the complete conversion to nanorods (50 to 130 nm Fig. 3C and 3F). Thus, a change in morphology, independent of the ligand associated with the Pd within, results upon exposure of the NPs to water to varying extents, and with the help of dissolved TPGS-750-M, complete conversion from small spherical NPs to far larger nanorods takes place.

Figure 3: HAADF-STEM image of Fe/ppm Pd NPs with SPhos and Cy-cBRIDP

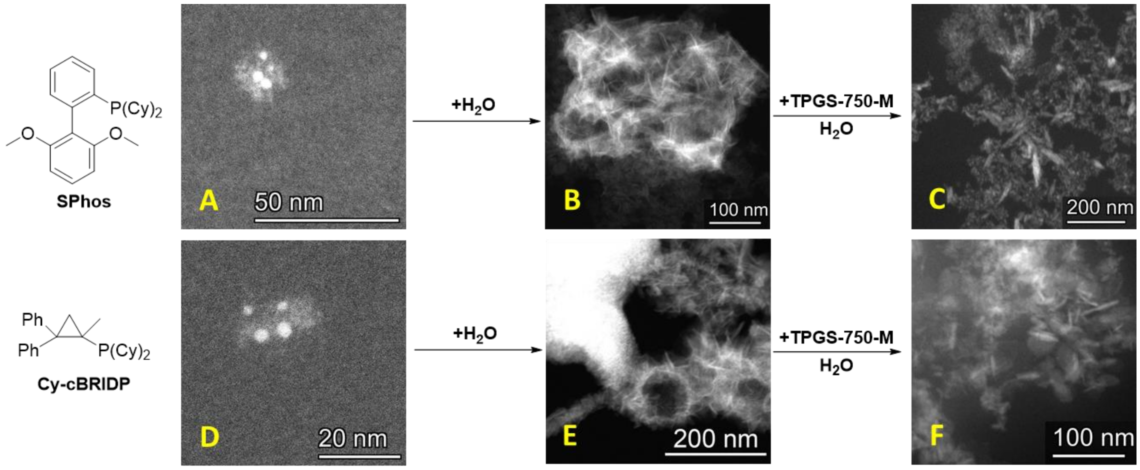

(A) dry Fe/ppm Pd nanoparticles with SPhos as ligand; (B) Fe/ppm Pd nanocatalyst with SPhos as ligand in pure water; (C) Fe/ppm Pd nanocatalyst with SPhos as ligand in aqueous TPGS-750-M; (D) dry Fe/ppm Pd nanoparticles with Cy-cBRIDP as ligand; (E) Fe/ppm Pd nanocatalyst with Cy-cBRIDP as ligand in pure water; (F) Fe/ppm Pd nanocatalyst with Cy-cBRIDP as ligand in aqueous TPGS-750-M.

Figure 4: X-ray photoelectron spectroscopy (XPS) of Fe/ppm Pd NPs

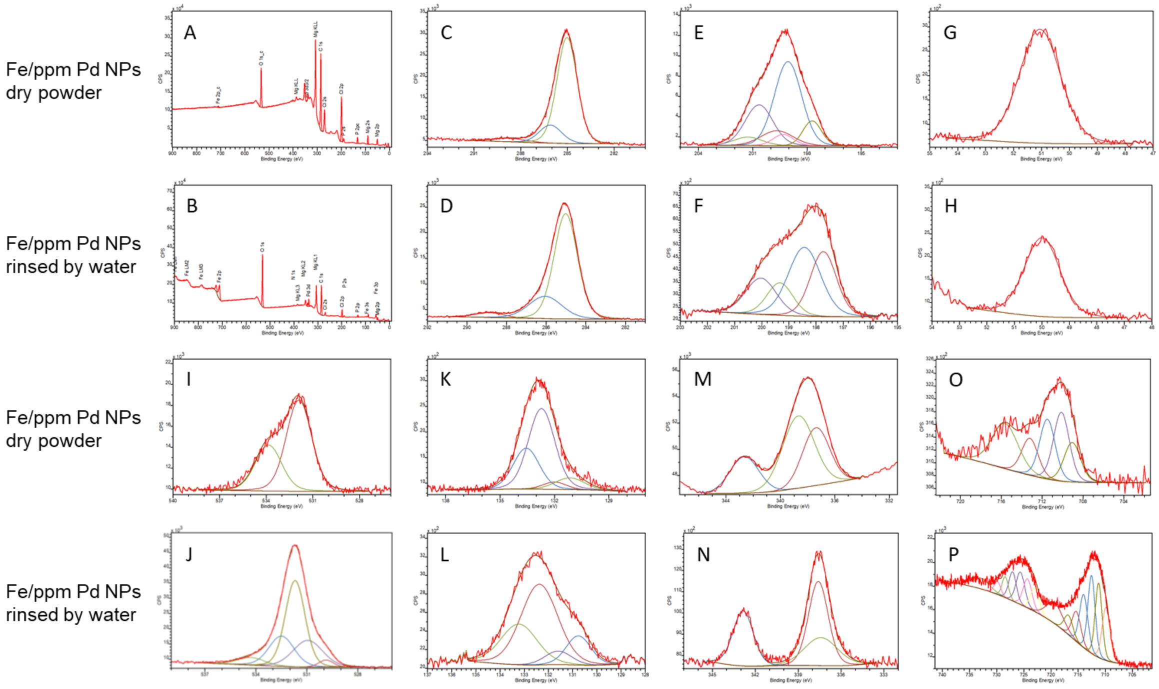

(A) and (B) full scan, (C) and (D) C 1s, (E) and (F) Cl 2p, (G) and (H) Mg 2p, (I) and (J) O 1s, (K) and (L) P 2p, (M) and (N) Pd 3d, (O) and (P) Fe 2p.

Table 1: ICP-MS analyses of dry powder, remaining material, and supernatant

	Dry powder (10 mg)	Leftover (1.2 mg)	Supernatant (1.7 mL)
Mg (mg)	0.983	0.089	0.894
Fe (mg)	0.627	0.587	0.051
Pd (mg)	0.039	0.033	0.0018

X-ray photoelectron spectroscopy (XPS) was also used to analyze both the initially prepared powders, as well as the catalytically active NPs used for Heck-Mizoroki couplings. These full scans reveal the surface of the *pre-nanocatalyst* (i.e., the powder form) consists of oxygen (13.15%), carbon (55.56%), iron (0.21%), chlorine (16.24%), phosphorus (3.23%), magnesium (11.48%) and palladium (0.13%) (Fig. 4). However, after stirring in water for the same one hour period, over 85% of their masses had dissolved in water, with XPS analysis now showing the surface of the newly formed nanorods to contain oxygen (30.58%), carbon (48.65%), iron (5.02%), chlorine (4.60%), phosphorus (2.65%), magnesium (7.63%) and palladium (0.88%) (Fig. 4). Hence, these comparisons between pre-catalyst spheres and water-sculpted nanorods show that the proportions of oxygen, iron, and palladium have *increased*, while the levels of phosphorus, chlorine, and magnesium have *decreased*, which is consistent with observations from elemental mapping. The percentage changes in metal content in the NPs before and after rinsing with water could be determined by ICP-MS (Table 1). Thus, in 10 mg of dry NP powder, there was found to be present 0.983 mg Mg, 0.627 mg Fe, and 0.039 mg Pd. After stirring in pure water for one hour, 90% of the Mg had dissolved. By contrast, over 90% of both Fe and Pd remained on the nanorods. Nonetheless, close to 90% of the mass of the original nanoparticles had been dispersed into the aqueous medium during this one hour process.

High resolution XPS measurements further disclosed the oxidation states and variation of content of different elements in the nanomaterial before and after exposure to water (see Fig. 4). The doublet peaks Cl 2p3/2 (199.05 eV) and Cl 2p1/2 (200.65 eV) in the Cl 2p spectrum for dry powder reveal the existence of Cl – Mg in the material.[11] However, these doublet peaks cannot be found in the Cl 2p spectrum for the nanorod. Instead, as the proportion of iron increases in the nanorod, another doublet peaks Cl 2p3/2 (198.43 eV) and Cl 2p1/2 (200.03 eV) can be detected, which belongs to Cl – Fe.[12] In addition, the peak at 51.06 eV in the Mg 2p spectrum of dry powder further provides the evidence for the existence of Mg – Cl.[13] Nevertheless, the peak at 49.99 eV in the Mg 2p spectrum of nanorod is assigned to Mg – O,[14] which provides a plausible explanation that Cl^- is replaced by O^{2-} or OH^- as the counterion to Mg. As expected, the O – Mg peak at 530.95 eV can also be found in the O 1s spectrum of these nanorods.[14] Moreover, the peak at 529.87 eV is assigned to O – Fe bond,[15] which indicates that Cl – Fe and O – Fe exist in the nanorod simultaneously. Additionally, the peak at 532.50 eV represents the presence of H_2O in the nanorod.[16]

The P 2p spectrum of the dry powder shows the isolated peaks at P 2p1/2 (132.00 eV) and P 2p3/2 (131.16 eV), which are attributed to P(III), while the peaks at 133.56 eV and 132.72 eV are assigned to the P 2p1/2 and P 2p3/2 orbitals of P(V).[17] The spectrum reveals that the proportion of P(V) is much higher than that of P(III) on the surface of the dry powder. However, compared with the dry powder, the proportion of P(III) (P 2p1/2 at 131.60 eV and P 2p3/2 at 130.76 eV) in the P 2p spectrum of nanorod has increased. Nonetheless, there is still a considerable amount of phosphorus which has been oxidized to P(V) (P 2p1/2 at 133.22 eV and P 2p3/2 at 132.38 eV). This result indicates that most of the ligand has been oxidized during preparation of the NPs, which provides an explanation for why excess ligand is needed for nanoparticle activity. Insofar as palladium is concerned, independent of exposure, or not to water, both Pd 3d spectra (Pd 3d5/2 at 337.38 eV and Pd 3d3/2 at 342.64 eV vs. Pd 3d5/2 at 337.59 eV and Pd 3d3/2 at 342.85 eV) indicated that the oxidation state of Pd in the nanomaterial is Pd(II) and not Pd(0).[18] In Fe 2p spectrum for both, no peak is detected at 706 to 708 eV. All peaks are found over 709 eV, which indicates that the valence state of Fe is either (II) or (III), without any Fe(0).[19]

Control experiments, the results from which are shown in Table 2, were conducted to correlate NP catalyst changes and resulting activity with changes in reactions conditions used for these HM couplings. Firstly, and as expected, neither nanomicelles nor nanorods were formed (i.e., the NPs remained as spheres) when an organic solvent such as THF (entry 2) or DMF (entry 3) was used as the reaction medium, ultimately leading to only 9% and 41% yields, respectively. Reaction in pure, degassed water, in which the nanorod structure could form but in the absence of nanomicelles (entry 4), led to a 68% yield of desired coupling product. The reaction containing both nanomicelles and nanorod catalyst in water, but in the absence the majority of ligand (*t*-Bu$_3$P) associated with the surrounding water (entry 5) gave only a 78% yield. Replenishing the aqueous reaction mixture by addition of fresh ligand (entry 6) resulted in the expected yield increase, while reinjecting the initially removed aqueous supernatant (entry 7) to freshly added reaction partners (along with base and NaCl), likewise, returned the isolated yield to similar levels as seem previously (entries 1 and 6) which all contained the same amount of *t*-Bu$_3$P in the pot. These last two entries provide strong evidence that all reaction components, although most notably, the required levels of phosphine, which under the reaction conditions are distributed between the surface of the NPs and, mainly, best accommodated within the nanomicelles in the water, must be present for a highly successful reaction outcome.

Table 2: Control experiments

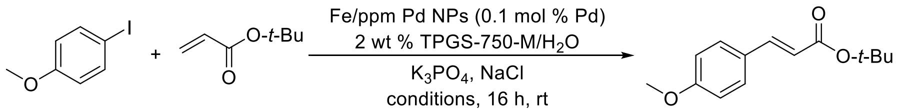

Entry	Condition	Nanorod structure	Aqueous micelles	Excess ligand	Yield
1	2 wt % TPGS-750-M/H_2O as reaction medium	**yes**	**yes**	**yes**	99%
2	THF as reaction medium	**no**	**no**	**yes**	9%
3	DMF as reaction medium	**no**	**no**	**yes**	41%
4	Degassed H_2O as reaction medium	**yes**	**no**	**yes**	68%
5	Fe/ppm Pd NPs stirred in degassed H_2O for 1 h; remove H_2O; add starting materials, K_3PO_4, and NaCl; add fresh 2 wt % TPGS-750-M/H_2O as reaction medium (**no phosphine**)	**yes**	**yes**	**no**	78%
6	Fe/ppm Pd NPs stirred in degassed H_2O for 1 h; remove H_2O; **add *t*-Bu$_3$P**, starting materials, K_3PO_4, and NaCl; add fresh 2 wt % TPGS-750-M/H_2O as reaction medium	**yes**	**yes**	**yes**	95%
7	Fe/ppm Pd NPs stirred in degassed H_2O for 1 h; remove H_2O; add starting materials, K_3PO_4, and NaCl; get the 2 wt % TPGS-750-M/H_2O back as reaction medium	**yes**	**yes**	**yes**	92%

Cryo-TEM analyses provided insight as to the special role played by DMF as "co-solvent", which has been found to facilitate these HM reactions in water. Other potential solvents (DMSO, MeOH, etc.) that could, in principle, function similarly (if for substrate dissolution purposes) were totally ineffective (see Scheme 4). The images in Figure 5 reveal that the size of the typically spherical nanomicelle derived from TPGS-750-M (40-60 nm) is expanded upon addition of DMF to 100 nm. Moreover, it is also clear that the nanorod NPs present in water alone are distinctly separated from these nanomicelles; there is no interaction between them. However, upon addition of DMF, and in addition to nanomicelle swelling, the crucial "nano-to-nano" effect[20] is now operating, leading to substrate delivery (within the micelles) to the observed NP catalyst and the resulting reactivity enhancement manifested by far higher levels of conversion and associated isolated yields.

Figure 5: Cryo-TEM for nanocatalysts in TPGS-750-M aqueous solution

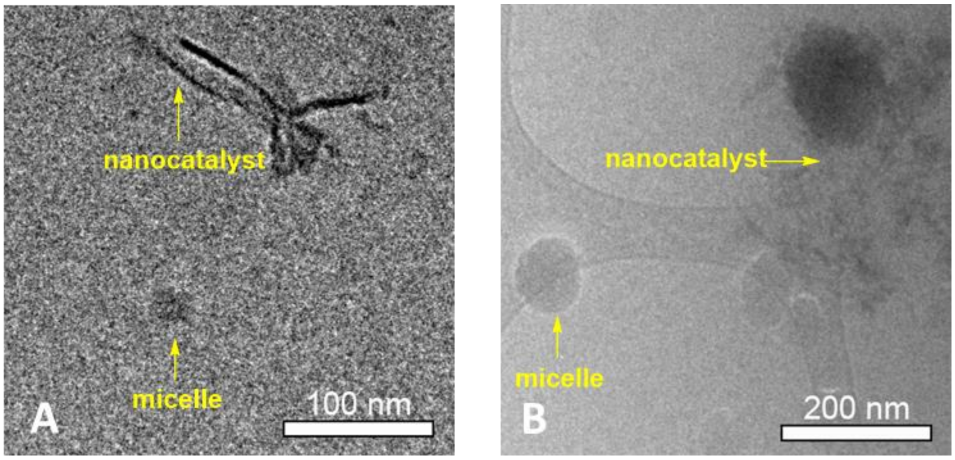

(A): Cryo-TEM analyses of NP catalyst among nanomicelles of TPGS-750-M; (B): Cryo-TEM of NP catalyst in the same micellar media, but after adding DMF as "co-solvent."

Scope of HM coupling reaction

With considerable insight as to the nature of the active catalyst involved (i.e., the optimized preparation of these NPs; the nanomicelles present in the aqueous medium, and the role of added DMF), the scope of this technology was ready for evaluation. Several aryl and heteroaryl iodides, together with various alkenyl partners, were examined. Most reactions took place quite smoothly and afforded excellent yields of coupled products. Numerous functional groups are tolerated, including methoxy- (**1**, **3**, **6**), ester (**1**, **2**, **4**, **5**, **7**, **8**), ketone (**2**), chloride- (**5**), nitrile- (**7**, **9**), trifluoromethyl- (**10**, **11**, **12**, **14**), thio- (**10**), nitro- (**11**, **14**), a Boc-protected amine (**12**), fluoride- (**17**, **24**), isolated olefins (**19**), aldehyde (**20**, **25**), alkyne (**23**) and a TIPS-protected phenol (**24**). Moreover, various heterocyclic rings, such as pyridine (**3**, **15**), pyrazole (**8**), pyrrole (**9**), piperazine (**10**), dihydrobenzofuran (**11**), benzodioxol (**13**), thiophene (**14**), a THP-protected indazole (**15**), morpholine (**16**, **22**), pyrimidine (**16**, **21**, **26**), indole (**17**, **22**), pyrrolindine (**18**), tetrahydrofuran (**20**, **23**) and benzo[d]oxazol (**26**) all led to good yields of the anticipated products. Many of these have extensive applications to targets in the agricultural and pharmaceutical industries.[21]

Table 3: Substrate scope[a, b]

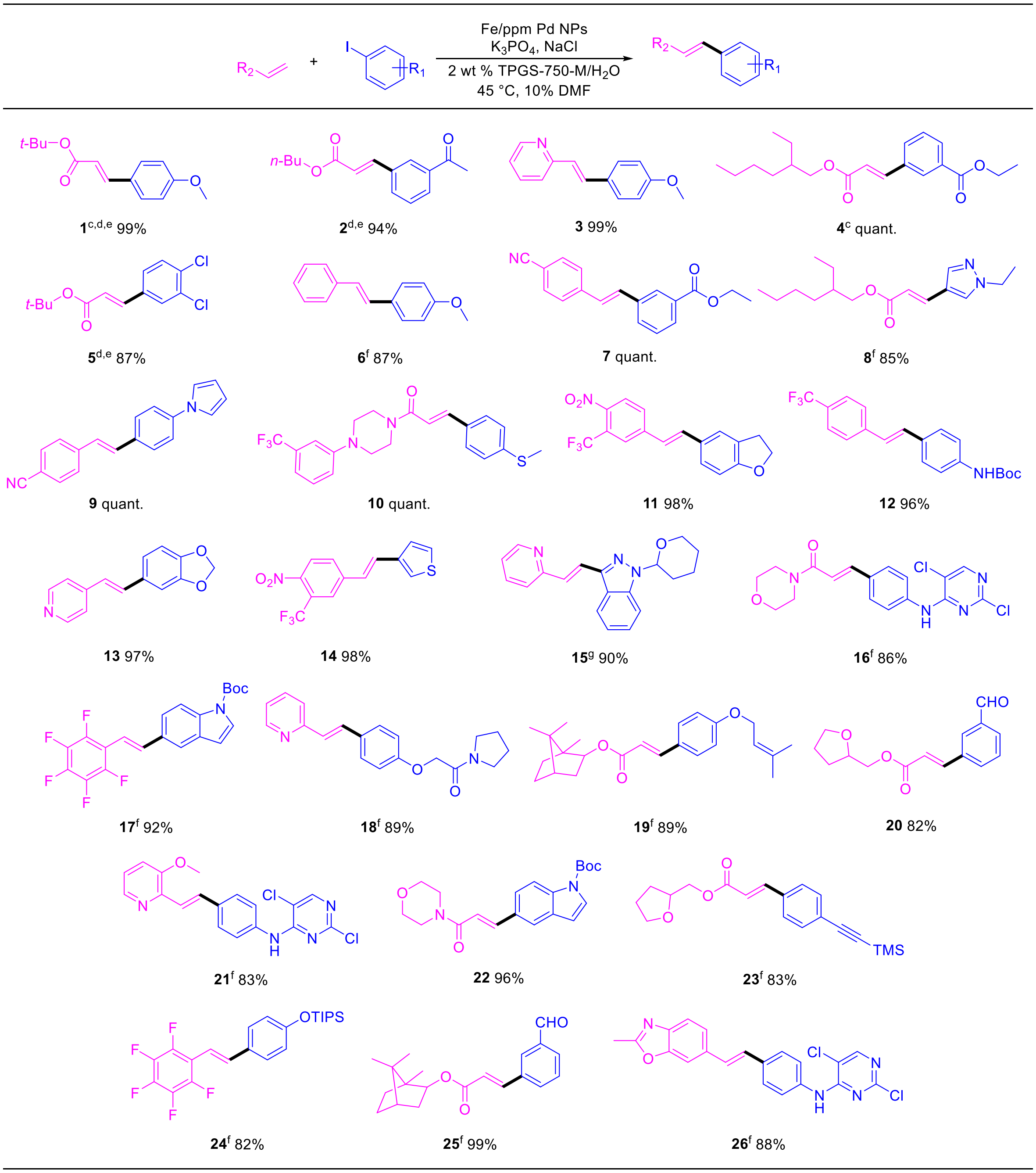
Fe/ppm Pd NPs
K_3PO_4, NaCl
2 wt % TPGS-750-M/H_2O
45 °C, 10% DMF
$\mathbf{1}^{c,d,e}$ 99%
$\mathbf{2}^{d,e}$ 94%
3 99%
$\mathbf{4}^{c}$ quant.
$\mathbf{5}^{d,e}$ 87%
$\mathbf{6}^{f}$ 87%
7 quant.
$\mathbf{8}^{f}$ 85%
9 quant.
10 quant.
11 98%
12 96%
13 97%
14 98%
$\mathbf{15}^{g}$ 90%
$\mathbf{16}^{f}$ 86%
$\mathbf{17}^{f}$ 92%
$\mathbf{18}^{f}$ 89%
$\mathbf{19}^{f}$ 89%
20 82%
$\mathbf{21}^{f}$ 83%
22 96%
$\mathbf{23}^{f}$ 83%
$\mathbf{24}^{f}$ 82%
$\mathbf{25}^{f}$ 99%
$\mathbf{26}^{f}$ 88%

[a] iodide (0.2 mmol), alkene (0.4 mmol), NaCl (1.2 mmol), K_3PO_4 (0.6 mmol) and Fe/ppm Pd (12.5 mg, 0.25% Pd), 2 wt % TPGS-750-M/H_2O (0.4 mL), DMF (0.04 mL), 45 °C, 16 h; [b] isolated yield; [c] Fe/ppm Pd NPs (5 mg, 0.1% Pd); [d] No DMF; [e] at rt; [f] 40 h; [g] 72 h.

Additionally, bromoarenes have been investigated as coupling partners in this protocol. Most, however, did not lead to a good yield under optimized conditions. Only the HM coupling of 4-bromoanisole and *t*-butyl (*E*)-3-(4-methoxyphenyl)acrylate proceeded smoothly at 45 °C with 0.25 mol % Pd loading, leading to a 91% isolated yield. Hence, further utilization of bromoarenes as starting materials was not pursued. A nanomaterial with higher activity was needed for catalyzing HM couplings for bromoarenes and olefins with low Pd loading under these mild conditions.

Comparisons between reported catalysts

A direct comparison with literature precedent on Heck-Mizoroki couplings, in this case leading to *t*-butyl (*E*)-3-(4-methoxyphenyl)acrylate, is illustrated in Table 4. As indicted by these results, this NP technology leads to the cinnamate product in comparable or better yield, can be accomplished using lower catalyst loadings and temperatures, and does so in an aqueous reaction medium that is far more environmentally friendly than is use of organic solvents, especially those that are dipolar aprotic in nature.

Table 4: Comparisons between reported catalysts

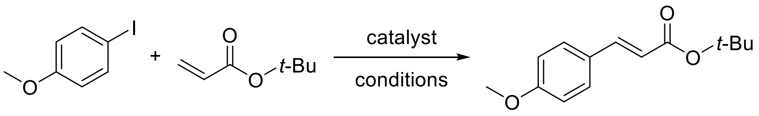

Entry	Catalyst	Pd(%)	Temperature (°C)	Solvent	Yield(%)	Ref
1	**Fe/ppm Pd NPs**	**0.1**	**rt**	**2 wt % TPGS-750-M/H_2O**	**99**	**this work**
2	SiO_2@Fe_3O_4-Pd	1	100	DMF	96	22
3	K-Pd-Me_{10}CB[5]	1	140	DMF	88	23
4	NO_2-NHC-Pd@Fe_3O_4	1	80	EtOH : H_2O (1 : 1)	90	24
5	Pd-pyridinophane unit	5	100	DMF	94	25
6	$Pd(OAc)_2$/DABCO	2	120	DMF	100	26
7	Pd/$CuFe_2O_4$	4	120	DMSO	95	27
8	Pd-Fe_3O_4	1	110	DMF	82	28

Recycle, E Factor, and scale up reaction

As is characteristic of designer surfactant technology in water, recycling of an aqueous reaction mixture is straightforward and routine, thereby decreasing wastewater streams (e.g., Scheme 5). In order to introduce fresh NPs, the typical 'in-flask' extraction of the reaction mixture using methyl *t*-butyl ether (MTBE) was followed by its transfer to a vessel containing pre-measured Fe/ppm Pd NPs and K_3PO_4. The E Factor, [29] introduced by Sheldon and co-workers as a measure of greenness, is even lower when the product of interest is a solid that precipitates out from the reaction and is simply filtered. As a representative example, *t*-butyl 5-iodo-1H-indole-1-carboxylate and 4-nitrostryene as starting materials, product **27** was thus obtained in 97% isolated yield. The crude product was washed with small amounts of DI water and then purified by filtration through a column. The E Factor associated with this process based on solvent usage is only 0.62, while that including water is only 6.3. A gram-scale reaction run as a measure of the potential for industrial application using the same educts (albeit with fewer equivalents of alkene), under otherwise identical conditions, afforded the desired product in 87% isolated yield (Scheme 5, middle).

Scheme 5: Recycle, E Factor, scale up reaction, and residual Pd in products from HM reactions

recycling of the reaction medium

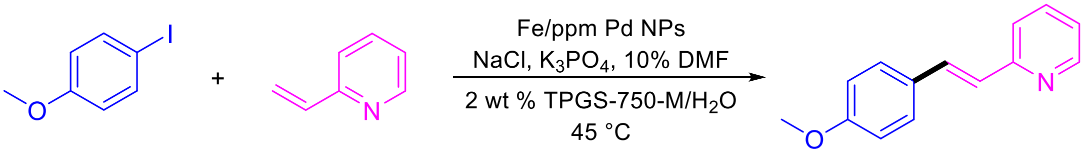

Cycle	0	1	2	3
Yield (%)	93	92	94	90

1-Iodo-4-methoxybenzene (0.2 mmol), 2-vinlypyridine (0.4 mmol), NaCl (1.2 mmol), K_3PO_4 (0.6 mmol) and Fe/ppm Pd (12.5 mg, 0.25 mol % Pd), 2 wt % TPGS-750-M/H_2O (0.4 mL), DMF (0.04 mL), 45 °C, 7 h or 10 h.

E Factor determination (solvent only) and gram-scale reaction

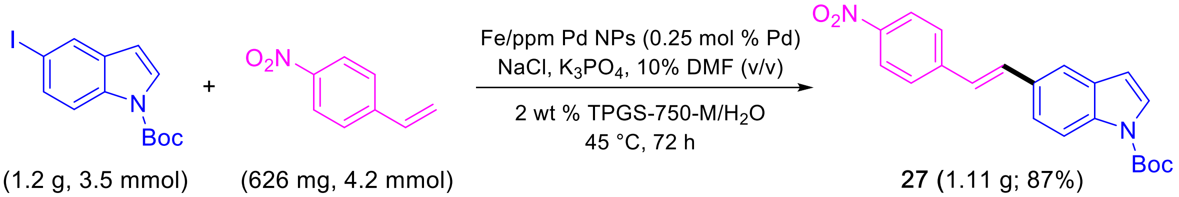

(1.2 g, 3.5 mmol) (626 mg, 4.2 mmol) **27** (1.11 g; 87%)

$$\text{E Factor} = \frac{\text{mass of organic waste}}{\text{mass of product}} = 0.62$$

Residual Pd in products from HM reactions

residual Pd in products from HM couplings[a]

Products	Pd loading for HM reaction	weight of sample used (mg)	palladium [µg/g] average[b]	palladium [µg/g] Stdev
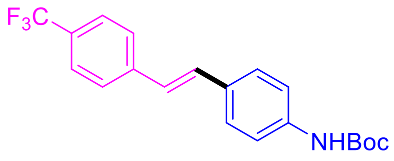	2500 ppm	9.15	ND[c]	ND[c]
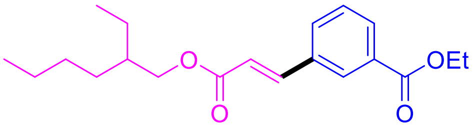	1000 ppm	9.41	ND[c]	ND[c]

[a] ICP-MS data was obtained from the UC Center for Environmental Implications of Nanotechnology at UCLA; [b] Each sample was done in triplicate with background correction; [c] ND = not detected.

Another important outgrowth of these ppm level Pd-catalyzed HM couplings concerns the amounts of residual metal found in the product after filtration or standard extraction/purification. According to FDA-approved levels,[30] residual Pd residue must be below 10 ppm per dose. Exceeding these limits, which is routine when using traditional levels of Pd catalysts (i.e., 1-5 mol %), requires additional time and cost associated with this chemistry. Hence, two products (Scheme 5, bottom) were chosen randomly and analyzed independently by ICP-MS. The results obtained indicated *undetectable levels of Pd in each sample*.

1-Pot sequences

The option for sequential reactions in 1-pot represents one of the hallmarks of this technology, given the variety of reactions that can now be run under aqueous micellar conditions. By "telescoping" such consecutive reactions, there is typically a dramatic decrease in both organic waste created, and the effort normally devoted to purification associated with each step. In the first example shown (Scheme 6), HM coupling using led to product **27**, that without isolation, was followed by nitro group reduction using added Fe/ppm (Ni+Pd) NPs described previously.[31] In this step, it was important to form these *ligandless* NPs in 2 wt % Coolade/H_2O,[32] since the addition of $NaBH_4$ leads to frothing that is eliminated using this designer surfactant. This reagent is then transferred to the reaction vial in which the HM reaction takes place. The resulting aniline **28** was then treated directly, again, within the same reaction vessel, with 2,4,5-trichloropyrimidine leading to an S_NAr reaction, ultimately affording final product **29** in 86% overall isolated yield. As a second, alternative example (Scheme 6, bottom), by taking advantage of inherent differences in activity between an aryl iodide and bromide, an initial HM reaction with **30** led to bromide **31**, which then (and without isolation) participated in a Suzuki-Miyaura cross-coupling to give biaryl product **32** in 82% overall yield.

Scheme 6: 1-Pot sequence

1st Sequence: 3 steps, 1-pot

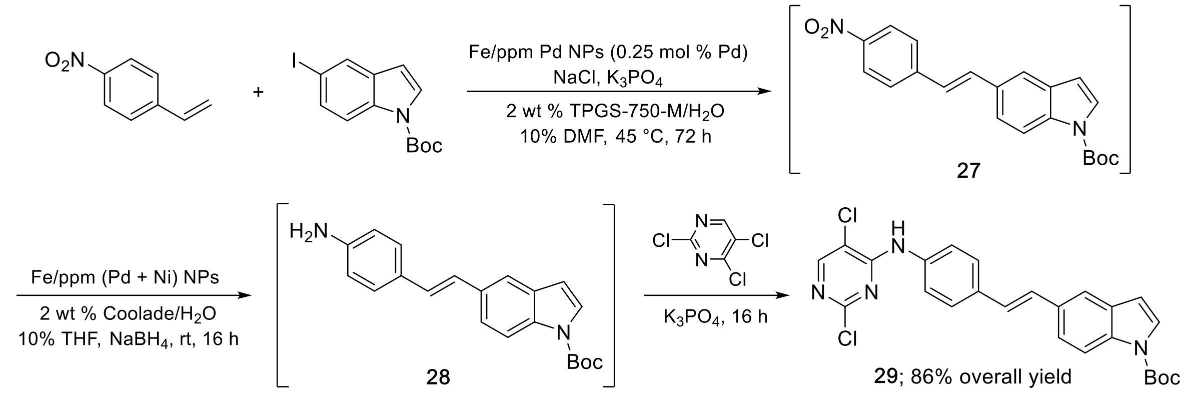
Fe/ppm Pd NPs (0.25 mol % Pd)
NaCl, K_3PO_4
2 wt % TPGS-750-M/H_2O
10% DMF, 45 °C, 72 h
Fe/ppm (Pd + Ni) NPs
2 wt % Coolade/H_2O
10% THF, $NaBH_4$, rt, 16 h
K_3PO_4, 16 h
27
28
29; 86% overall yield

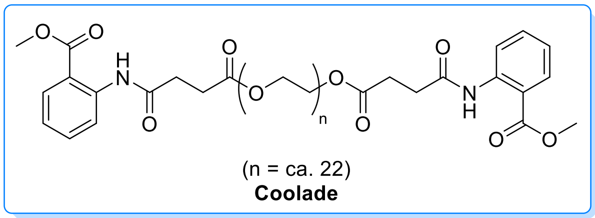

(n = ca. 22)
Coolade

2nd Sequence: Heck-Mizoroki followed by a Suzuki-Miyaura coupling, in 1-pot

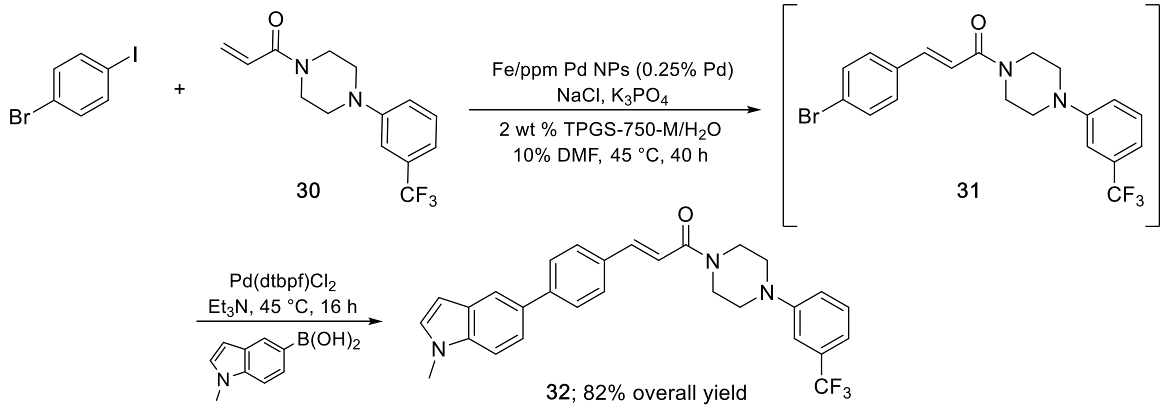
Fe/ppm Pd NPs (0.25% Pd)
NaCl, K_3PO_4
2 wt % TPGS-750-M/H_2O
10% DMF, 45 °C, 40 h
Pd(dtbpf)Cl_2
Et_3N, 45 °C, 16 h
30
31
32; 82% overall yield

Conclusions

In summary, new nanoparticles (NPs) derived from $FeCl_3$ have been discovered that effectively catalyze Heck-Mizoroki couplings with considerable generality, and can be used under uncharacteristically mild and environmentally responsible conditions. Their formation, unlike those previously prepared from similar precursors, requires both a modified protocol as well as a significant change in ligand required for optimal catalyst activity. Notwithstanding their differences that enable HM *heterogeneous* couplings to now occur in water under such mild conditions, these spherical NPs have been found to be, in fact, a pre-catalyst to the species that effect these couplings. Using several methods of analyses, the actual active catalytic species results only upon exposure to (usually surfactant-containing) water, which is responsible for their significant alterations, or sculpting, thereby quickly transforming these small, inactive spherical NPs into far larger, reactive nanorod-shaped materials. Documentation is provided as to the extent of greenness in the form of both E Factor determination, and well as the facility with which an aqueous reaction mixture can be recycled. Notably, in situations where residual levels of metal must meet rigorously prescribed (FDA) standards, ICP-MS analyses reveal that products resulting from these couplings contain undetectable amounts of palladium. The prognosis for applications to industrial targets is further strengthened by (1) a gram-scale experiment that affords the intended product without variation in yield, and (2) opportunities for tandem reactions to be carried out in a 1-pot sequence, thereby eliminating individual step handling, processing, and waste generation.

References

1. (a) Petkar, D. R.; Kadu, B. S.; Chikate, R. C. Highly efficient and chemoselective transfer hydrogenation of nitroarenes at room temperature over magnetically separable Fe–Ni bimetallic nanoparticles. *RSC Adv.* **2014**, *4*, 8004. (b) Chen, H.; Zhou, L.; Wen, M.; Wu, Q.; Wang, C. A branched-dumbbell Pt/NiFe nanostructure and its high catalytic reduction activity for nitro-aromatic compounds. *Mater. Res. Bull.* **2014**, *60*, 322; (c) Chu, C.; Su, Z. Facile Synthesis of AuPt Alloy Nanoparticles in Polyelectrolyte Multilayers with Enhanced Catalytic Activity for Reduction of 4-Nitrophenol. *Langmuir* **2014**, *30*, 15345.

2. (a) Choudary, B. M.; Madhi, S.; Chowdari, N. S.; Kantam, M. L.; Sreedhar, B. Layered Double Hydroxide Supported Nanopalladium Catalyst for Heck-, Suzuki-, Sonogashira-, and Stille-Type Coupling Reactions of Chloroarenes. *J. Am. Chem. Soc.* **2002**, *124*, 14127; (b) 1. Liu, Y.; Bai, X. Argon glow discharge plasma-reduced palladium nanoparticles supported on activated carbon for Suzuki and Heck coupling reactions. *Appl. Organomet. Chem.* **2017**, *31*, e3561; (c) Reetz, M. T.; Westermann, E. Phosphane-Free Palladium-Catalyzed Coupling Reactions: The Decisive Role of Pd Nanoparticles. *Angew. Chem., Int. Ed.* **2000**, *39*, 165.

3. Hong, K.; Sajjadi, M.; Suh, J. M.; Zhang, K.; Nasrollahzadeh, M.; Jang, H. W.; Varma, R. S.; Shokouhimehr, M. Palladium Nanoparticles on Assorted Nanostructured Supports: Applications for Suzuki, Heck, and Sonogashira Cross-Coupling Reactions. *ACS Appl. Nano Mater.* **2020**, *3*, 2070.

4. (a) Nyathi, T. M.; Fischer, N.; York, A. P. E.; Morgan, D. J.; Hutchings, G. J.; Gibson, E. K.; Wells, P. P.; Catlow, C. R. A.; Claeys, M. Impact of Nanoparticle–Support Interactions in Co_3O_4/Al_2O_3 Catalysts for the Preferential Oxidation of Carbon Monoxide. *ACS Catal.* **2019**, *9*, 7166; (b) Camposeco, R.; Castillo, S.; Mejía-Centeno, I. Performance of V_2O_5/NPTiO_2–Al_2O_3-nanoparticle- and V_2O_5/NTiO_2–Al_2O_3-nanotube model catalysts in the SCR–NO with NH_3. *Catal. Commun.* **2015**, *60*, 114; (c) Lira, E.; Merte, L. R.; Behafarid, F.; Ono, L. K.; Zhang, L.; Roldan Cuenya, B. Role and Evolution of Nanoparticle Structure and Chemical State during the Oxidation of NO over Size- and Shape-Controlled Pt/γ-Al_2O_3 Catalysts under Operando Conditions. *ACS Catal.* **2014**, *4*, 1875.

5. Handa, S.; Wang, Y.; Gallou, F.; Lipshutz, B. H. Sustainable Fe–ppm Pd nanoparticle catalysis of Suzuki-Miyaura cross-couplings in water. *Science* **2015**, *349*, 1087.

6. Handa, S.; Jin, B.; Bora, P. P.; Wang, Y.; Zhang, X.; Gallou, F.; Reilly, J.; Lipshutz, B. H. Sonogashira Couplings Catalyzed by Fe Nanoparticles Containing ppm Levels of Reusable Pd, under Mild Aqueous Micellar Conditions. *ACS Catal.* **2019**, *9*, 2423.

7. (a) Zhang, H.; Gilbert, B.; Huang, F.; Banfield, J. F. Water-driven structure transformation in nanoparticles at room temperature. *Nature* **2003**, *424*, 1025; (2)

Wang, P.; Wang, R.-Y.; Jin, J.-Y.; Xu, L.; Shi, Q.-F. The Morphological Change of Silver Nanoparticles in Water. *Chin. Phys. Lett.* **2012**, *29*, 017805.

8. Christoffel, F.; Ward, T. R. Palladium-Catalyzed Heck Cross-Coupling Reactions in Water: A Comprehensive Review. *Catal. Lett.* **2017**, *148*, 489.

9. Suzuki, K.; Hori, Y.; Kobayashi, T. A New Hybrid Phosphine Ligand for Palladium-Catalyzed Amination of Aryl Halides. *Adv. Synth. Catal.* **2008**, *350*, 652.

10. Klumphu, P.; Lipshutz, B. H. "Nok": A Phytosterol-Based Amphiphile Enabling Transition-Metal-Catalyzed Couplings in Water at Room Temperature. *J. Org. Chem.* **2014**, *79*, 888.

11. Karakalos, S.; Siokou, A.; Ladas, S. The interfacial properties of $MgCl_2$ films grown on a flat SiO_2/Si substrate. An XPS and ISS study. *Appl. Surf. Sci.* **2009**, *255*, 8941.

12. Kishi, K.; Ikeda, S. X-ray photoelectron spectroscopic study of the reaction of evaporated metal films with chlorine gas. *J. Phys. Chem.* **1974**, *78*, 107.

13. Sears, J. D.; Munoz, S. B., 3rd; Daifuku, S. L.; Shaps, A. A.; Carpenter, S. H.; Brennessel, W. W.; Neidig, M. L. The Effect of beta-Hydrogen Atoms on Iron Speciation in Cross-Couplings with Simple Iron Salts and Alkyl Grignard Reagents. *Angew. Chem., Int. Ed. Engl.* **2019**, *58*, 2769.

14. Haycock, D. E.; Kasrai, M.; Nicholls, C. J.; Urch, D. S. The electronic structure of magnesium hydroxide (brucite) using X-ray emission, X-ray photoelectron, and auger spectroscopy. *J. Chem. Soc., Dalton Trans.* **1978**, 1791.

15. Brion, D. Etude par spectroscopie de photoelectrons de la degradation superficielle de FeS_2, $CuFeS_2$, ZnS et PbS a l'air et dans l'eau. *Appl. Surf. Sci.* **1980**, *5*, 133.

16. Wagner, C. D.; Zatko, D. A.; Raymond, R. H. Use of the oxygen KLL Auger lines in identification of surface chemical states by electron spectroscopy for chemical analysis. *Anal. Chem.* **1980**, *52*, 1445.

17. (a) Grutsch, P. A.; Zeller, M. V.; Fehlner, T. P. Photoelectron spectroscopy of tin compounds. *Inorg. Chem.* **1973**, *12*, 1431. (b) Clark, D. T.; Adams, D. B.; Briggs, D. X-Ray photoelectron studies of platinum and palladium complexes; observation of the trans-influence and distinction between terminal and bridging chlorine. *J. Chem. Soc. D* **1971**, 602.

18. Blackburn, J. R.; Nordberg, R.; Stevie, F.; Albridge, R. G.; Jones, M. M. Photoelectron spectroscopy of coordination compounds. Triphenylphosphine and its complexes. *Inorg. Chem.* **1970**, *9*, 2374.

19. Grosvenor, A. P.; Kobe, B. A.; Biesinger, M. C.; McIntyre, N. S. Investigation of multiplet splitting of Fe 2p XPS spectra and bonding in iron compounds. *Surf. Interface Anal.* **2004**, *36*, 1564.

20. Lipshutz, B. H. The ‘Nano-to-Nano’ Effect Applied to Organic Synthesis in Water. *Johnson Matthey Technol. Rev.* **2017**, *61*, 196.

21. (a) Chekal, B. P.; Guinness, S. M.; Lillie, B. M.; McLaughlin, R. W.; Palmer, C. W.; Post, R. J.; Sieser, J. E.; Singer, R. A.; Sluggett, G. W.; Vaidyanathan, R.; Withbroe, G. J. Development of an Efficient Pd-Catalyzed Coupling Process for Axitinib. *Org. Process Res. Dev.* **2014**, *18*, 266; (b) King, A. O.; Corley, E. G.; Anderson, R. K.; Larsen, R. D.; Verhoeven, T. R.; Reider, P. J.; Xiang, Y. B.; Belley, M.; Leblanc, Y. An efficient synthesis of LTD4 antagonist L-699,392. *J. Org. Chem.* **1993**, *58*, 3731; (c) Kumar, U. S.; Sankar, V. R.; Rao, M. M.; Jaganathan, T. S.; Buchi Reddy, R. Investigational Study into the Formation of Methoxy Derivative and Other Impurities during the Optimization of Eletriptan Hydrobromide. *Org. Process Res. Dev.* **2012**, *16*, 1917; (d) Guillemont, J.; Pasquier, E.; Palandjian, P.; Vernier, D.; Gaurrand, S.; Lewi, P. J.; Heeres, J.; de Jonge, M. R.; Koymans, L. M. H.; Daeyaert, F. F. D.; Vinkers, M. H.; Arnold, E.; Das, K.; Pauwels, R.; Andries, K.; de Béthune, M.-P.; Bettens, E.; Hertogs, K.; Wigerinck, P.; Timmerman, P.; Janssen, P. A. J. Synthesis of Novel Diarylpyrimidine Analogues and Their Antiviral Activity against Human Immunodeficiency Virus Type 1. *J. Med. Chem.* **2005**, *48*, 2072.

22. Li, P.; Wang, L.; Zhang, L.; Wang, G.-W., Magnetic Nanoparticles-Supported Palladium: A Highly Efficient and Reusable Catalyst for the Suzuki, Sonogashira, and Heck Reactions. *Adv. Synth. Catal.* **2012,** *354*, 1307.

23. Li, H.; Lü, J.; Lin, J.; Huang, Y.; Cao, M.; Cao, R., Crystalline Hybrid Solid Materials of Palladium and Decamethylcucurbit[5]uril as Recoverable Precatalysts for Heck Cross-Coupling Reactions. *Chem. Eur. J.* **2013,** *19*, 15661.

24. Kandathil, V.; Fahlman, B. D.; Sasidhar, B. S.; Patil, S. A.; Patil, S. A., A convenient, efficient and reusable N-heterocyclic carbene-palladium(ii) based catalyst supported on magnetite for Suzuki–Miyaura and Mizoroki–Heck cross-coupling reactions. *New J. Chem.* **2017,** *41*, 9531.

25. Morisaki, Y.; Ishida, T.; Chujo, Y. Synthesis and Characterization of Dithia[3.3](2,6)pyridinophane-Containing Polymers: Application to the Palladium-Catalyzed Heck Reaction. *Org. Lett.* **2006**, *8*, 1029.

26. Li, J.-H.; Wang, D.-P.; Xie, Y.-X. $Pd(OAc)_2$/DABCO as a Highly Active Catalytic System for the Heck Reaction. *Synthesis* **2005**, *2005*, 2193.

27. Lakshminarayana, B.; Mahendar, L.; Ghosal, P.; Sreedhar, B.; Satyanarayana, G.; Subrahmanyam, C., Fabrication of Pd/CuFe2O4 hybrid nanowires: a heterogeneous catalyst for Heck couplings. *New J. Chem.* **2018,** *42*, 1646.

28. Chung, J.; Kim, J.; Jang, Y.; Byun, S.; Hyeon, T.; Kim, B. M. Heck and Sonogashira cross-coupling reactions using recyclable Pd–Fe_3O_4 heterodimeric nanocrystal catalysts. *Tetrahedron Lett.* **2013**, *54*, 5192.

29. (a) Sheldon, R. A.; Arends, I. W. C. E.; Hanefeld, U. Introduction: Green Chemistry and Catalysis. *Green Chemistry and Catalysis*; Wiley-VCH: Weinheim, 2007; p 1. (b) Sheldon, R. A. The E Factor: fifteen years on. *Green Chem*. **2007**, *9*, 1273.

30. F.D.A., Q3D Elemental Impurities Guidance for Industry, https://www.fda.gov/downloads/drugs/guidances/ ucm371025.pdf.

31. Pang, H.; Gallou, F.; Sohn, H.; Camacho-Bunquin, J.; Delferro, M.; Lipshutz, B. H. Synergistic effects in Fe nanoparticles doped with ppm levels of (Pd + Ni). A new catalyst for sustainable nitro group reductions. *Green Chem.* **2018**, *20*, 130.

32. Lee, N. R.; Cortes-Clerget, M.; Wood, A. B.; Lippincott, D. J.; Pang, H.; Moghadam, F. A.; Gallou, F.; Lipshutz, B. H. Coolade. A Low-Foaming Surfactant for Organic Synthesis in Water. *ChemSusChem* **2019**, *12*, 3159.

Appendix

General Remarks

A solution of 2 wt % TPGS-750-M/H_2O solution was prepared by dissolving TPGS-750-M in degassed HPLC grade water and was stored under argon. TPGS-750-M was made as previously described[1] and is available from Sigma-Aldrich (catalog number 733857). A solution of 5 wt % PTS/H_2O solution was prepared by dissolving PTS in degassed HPLC grade water and was stored under argon. A solution of 2 wt % Coolade/H_2O solution was prepared by dissolving Coolade in degassed HPLC grade water and was stored under argon. Coolade was made as previously described.[2] $FeCl_3$ anhydrous, 98% was purchased from Alfa Aesar (stock number 12357-22). Methylmagnesium chloride solution was purchased from Sigma-Aldrich (catalog number 189901). Pd(*t*-$Bu_3P)_2$ was purchased from Sigma-Aldrich (catalog number 676578). *t*-Bu_3P was purchased from Sigma-Aldrich (catalog number 570958). All commercially available reagents were used without further purification. All reactions were carried out in a sample vial (4 mL) equipped with a Teflon-coated magnetic stir bar. Thin layer chromatography (TLC) was done using Silica Gel 60 F254 plates (0.25 mm thick), purchased from Merck. Column chromatography was done in glass columns using Silica gel 60 (EMD, 40-63 μm) or with pre-packed 25-gram KP-Sil Biotage$^{\Theta}$ SNAP Cartridges on the Biotage$^{\Theta}$ Isolera Prime autocolumn. GC-MS data was recorded on an Agilent Technologies 7890A GC system coupled with Agilent Technologies 5975C mass spectrometer using HP-5MS column (30 m × 0.250 mm, 0.25 μ) purchased from Agilent Technologies. ^{1}H and ^{13}C NMR spectra were obtained in $CDCl_3$ or DMSO-d_6 using 400 MHz or 500 MHz Varian NMR spectrometer. Chemical shifts in ^{1}H NMR spectra are reported in parts per million (ppm) on the δ scale from an internal standard of residual

$CDCl_3$ (7.26 ppm) or the central peak of DMSO-d_6 (2.50 ppm). Data are reported as follows: chemical shift, multiplicity (s = singlet, d = doublet, t = triplet, q = quartet, quin = quintet), integration, and coupling constant in Hertz (Hz). Chemical shifts in ^{13}C NMR spectra are reported in ppm on the δ scale from the central peak of residual $CDCl_3$ (77.16 ppm) or the central peak of DMSO-d_6 (39.52 ppm). XPS images were obtained using ThermoFisher Escalab Xi+. ICP-MS images were obtained using NexION 2000, PerkinElmer. STEM images were obtained using ThermoFisher Talos G2 200X TEM/STEM w/ChemiSTEM EDS. Cryo-TEM images were obtained using FEI Tecnai G2 Sphera 200kV EDX.

Final Optimized Preparation of Fe/ppm Pd Nanoparticles

In an oven dried round-bottomed flask, $FeCl_3$ (81.1 mg, 0.5 mmol) was added under an atmosphere of dry argon. The flask was covered with a septum, and 2.5 mL dry THF was added by syringe. The reaction mixture was stirred for 20 min at rt. While maintaining a dry atmosphere at rt, a 1 M solution of MeMgCl in THF was very slowly (1 drop/2 sec) added to the reaction mixture (1 mL, 1 mmol). And then, the mixture was stirred for an additional 1 min at rt. After that time, 2.4 mL THF solution of 0.01 M Pd(*t*-$Bu_3P)_2$ (0.025 mmol) and 0.25 M *t*-Bu_3P (0.6 mmol) were added to the reaction mixture. After addition, an additional 1 M solution of MeMgCl in THF was very slowly (1 drop/2 sec) added to the reaction mixture (0.75 mL, 1.75 mmol). After complete addition of the Grignard reagent, the mixture was stirred for an additional 30 min at rt. (The solution of MeMgCl in THF was titrated by LiCl/I_2, and needs to be added precisely. The NPs are not active if more or less MeMgCl is added during their formation). THF was then evaporated under reduced pressure at rt to provide black nanomaterial as a powder. The Fe nanoparticles obtained were dried under reduced pressure at rt for 3 h yielding 0.63 g Fe/ppm Pd NPs. These nanoparticles need to be stored under argon in a glovebox. The material was used as such for subsequent reactions under micellar conditions.

Comparison between Pd catalyst and Fe/ppm Pd NPs

1-Iodo-4-methoxybenzene (93.6 mg, 0.4 mmol, 1 equiv) K_3PO_4 (254.2 g, 1.2 mmol) and NaCl (140.4 mg, 2.4 mmol) were added to the vial followed by sequential addition of a palladium complex, *t*-Bu_3P (2 mg, 0.0096 mmol) and $FeCl_3$ (1.8 mg, 0.008) in the glovebox. The reaction vial was closed with a septum under an argon atmosphere. An aqueous solution of 2 wt % TPGS-750-M (0.8 mL), *t*-butyl acrylate (102.6 mg, 0.8 mmol, 2 equiv) and DMF (0.08 mL) was added to the vial by syringe insertion and the mixture was stirred vigorously at rt for 16 h. After 16 h, EtOAc was added and the mixture stirred gently for 2 min at rt. Stirring was then stopped and the organic layer was decanted via pipette. The organic layer was passed through a very small silica plug. Yields were determined by GCMS using naphthalene as internal standard.

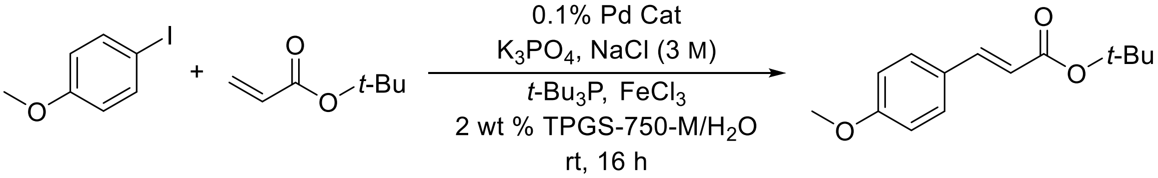

Entry	Pd source	*t*-Bu_3P (%)	$FeCl_3$ (%)	GC Yield (%)
1	Pd(*t*-$Bu_3P)_2$	0	0	3
2	Pd(*t*-$Bu_3P)_2$	2.4	0	8
3	Pd(*t*-$Bu_3P)_2$	2.4	2	19
4	$Pd(OAc)_2$	2.4	0	ND
5	$Pd(OAc)_2$	2.4	2	ND

In an oven dried 4 mL microwave reaction vial covered with a septum containing a PTFE-coated magnetic stir bar, 0.1 mL THF solution of 0.1 M $FeCl_3$ (0.01 mmol) was added under dry argon. While maintaining a dry atmosphere at rt, a 0.1 M solution of MeMgCl in THF was very slowly (1 drop/2 sec) added to the reaction mixture (0.35 mL, 0.035 mmol).

After complete addition of the Grignard reagent, the mixture was stirred for an additional 10 min at rt. THF was then evaporated under reduced pressure at rt. After evaporation, the NPs need to be stored under argon. To this vial, NaCl (70.2 mg, 1.2 mmol), K_3PO_4 (127.2 mg, 0.6 mmol), 1-iodo-4-methoxybenzene (0.2 mmol, 1 equiv), alkene (0.4 mmol, 2 equiv) and Fe/ppm Pd NPs (12.5 mg) were added in the glovebox. The vial was capped with a septum and removed from the glovebox. Through the septum, 0.4 mL aqueous solution of 2 wt % TPGS-750-M was added followed by sequential addition of 0.04 mL DMF via syringe. The mixture was vigorously stirred at 45 °C for 16 h. After 16 h, EtOAc was added and the mixture stirred for 2 min at rt. Stirring was then stopped and the organic layer was decanted via pipette. The organic layer was passed through a very small silica plug. Yields were determined by GCMS using naphthalene as internal standard.

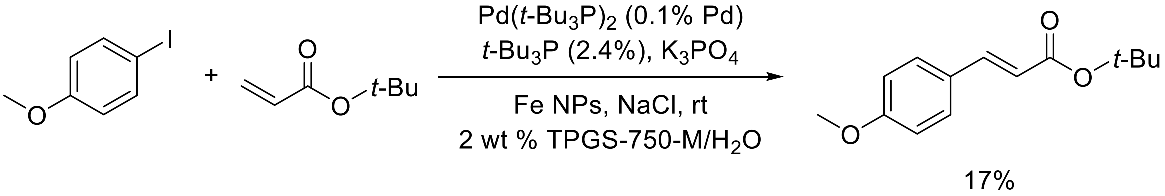

Titration of MeMgCl solution by LiCl-I_2

To an oven dried 25 mL round bottom flask, anhydrous LiCl (424 mg, 10 mmol) was added under an argon atmosphere in the glovebox. The flask was covered with a septum, and 20 mL dry THF was added by syringe and the mixture was stirred for 24 h at rt until the LiCl was completely dissolved, resulting in the formation of a 0.5 M solution of LiCl.

A 10 mL microwave vial equipped with a magnetic stirring bar and a septum was heated with a heat gun under reduced pressure and cooled to rt under an argon atmosphere. In the glovebox, the dry microwave vial was charged with accurately weighed I_2 (127 mg, 0.5 mmol) and capped with a rubber septum. The saturated solution of LiCl in THF (2 mL) was added and stirring was started. After the iodine was completely dissolved, the resulting brown solution was cooled to 0 °C in an ice bath. Another 5 mL round bottom flask equipped with a magnetic stirring bar and a septum was heated with a heat gun under reduced pressure and cooled to rt under an argon atmosphere. To this round bottom flask, methyl magnesium chloride solution from Sigma-Aldrich (catalog No. 189901; 1 mL) and dry THF (2 mL) were added by syringe and stirred. The methyl magnesium chloride solution was added dropwise via a 1.00 mL syringe (0.01 mL graduation) until the brown color disappeared. The amount consumed contains 1 equiv of the methyl magnesium chloride relative to iodine. The MeMgCl solution was titrated for 4 times.

Analysis of the nanoparticle

STEM (BF and HADDF) and EDX for Fe/ppm Pd nanocatalyst

Fe/ppm Pd nanocatalyst dry powder:

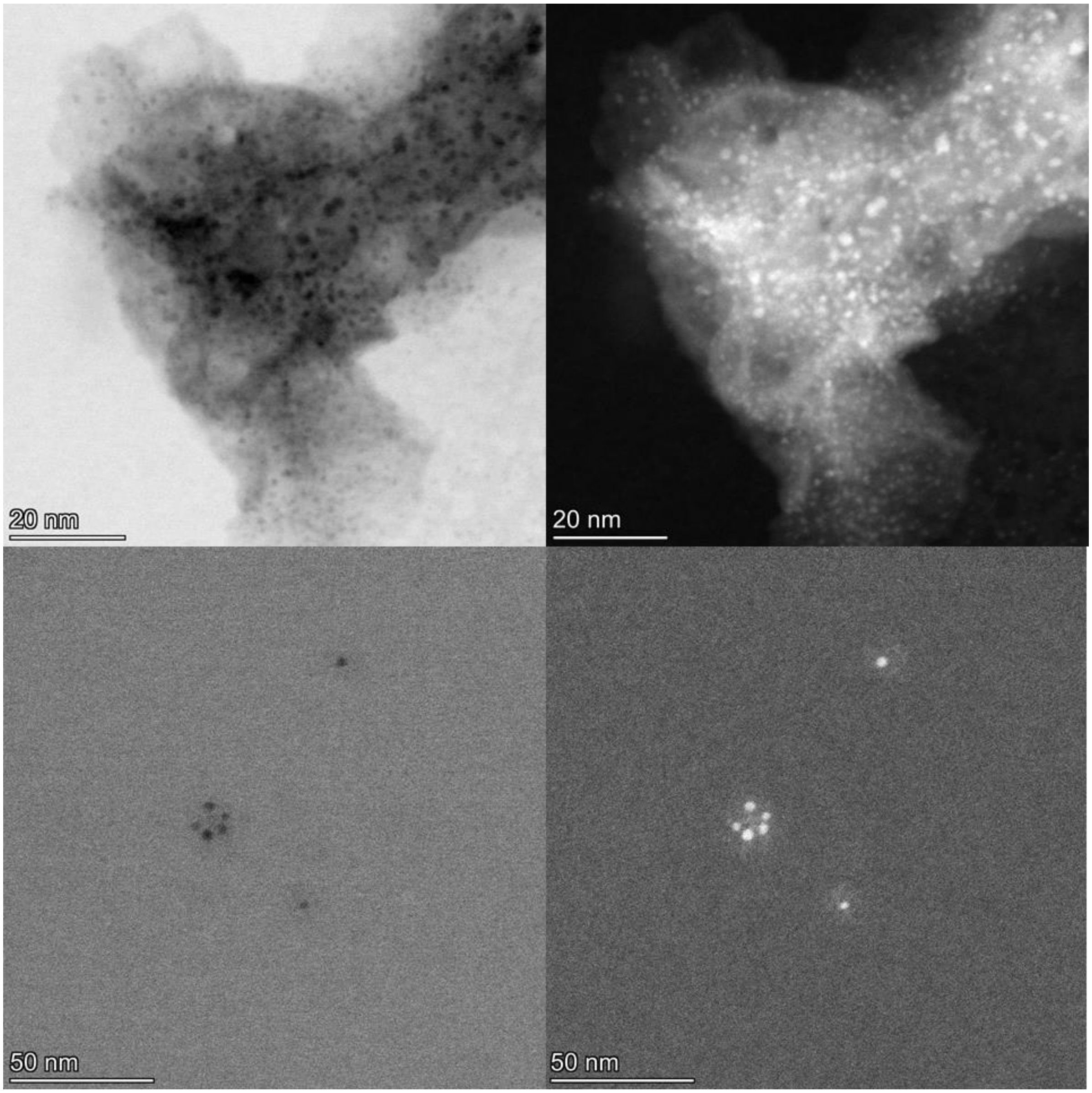
20 nm
20 nm
50 nm
50 nm

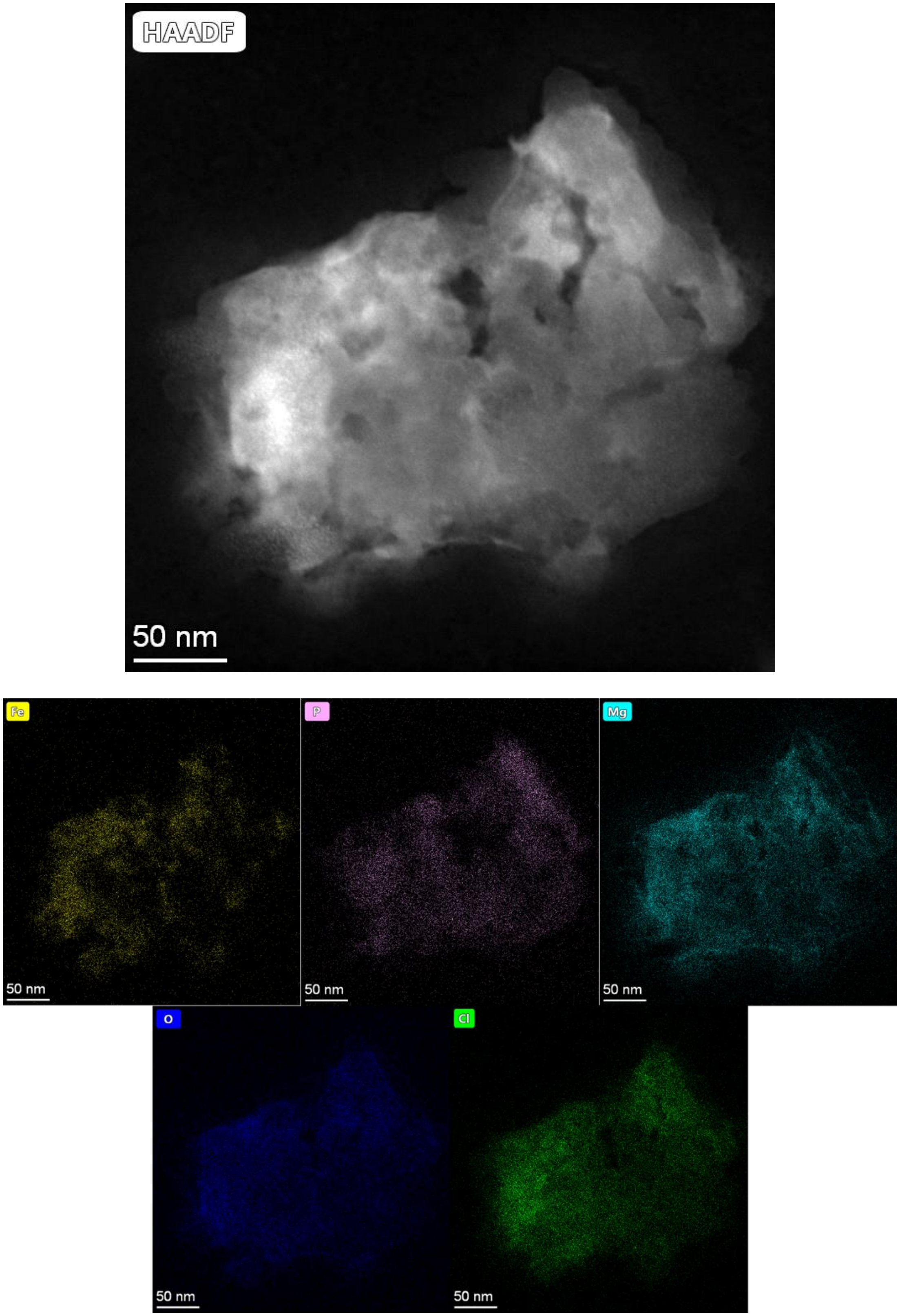
HAADF
50 nm
Fe
50 nm
P
50 nm
Mg
50 nm
O
50 nm
Cl
50 nm

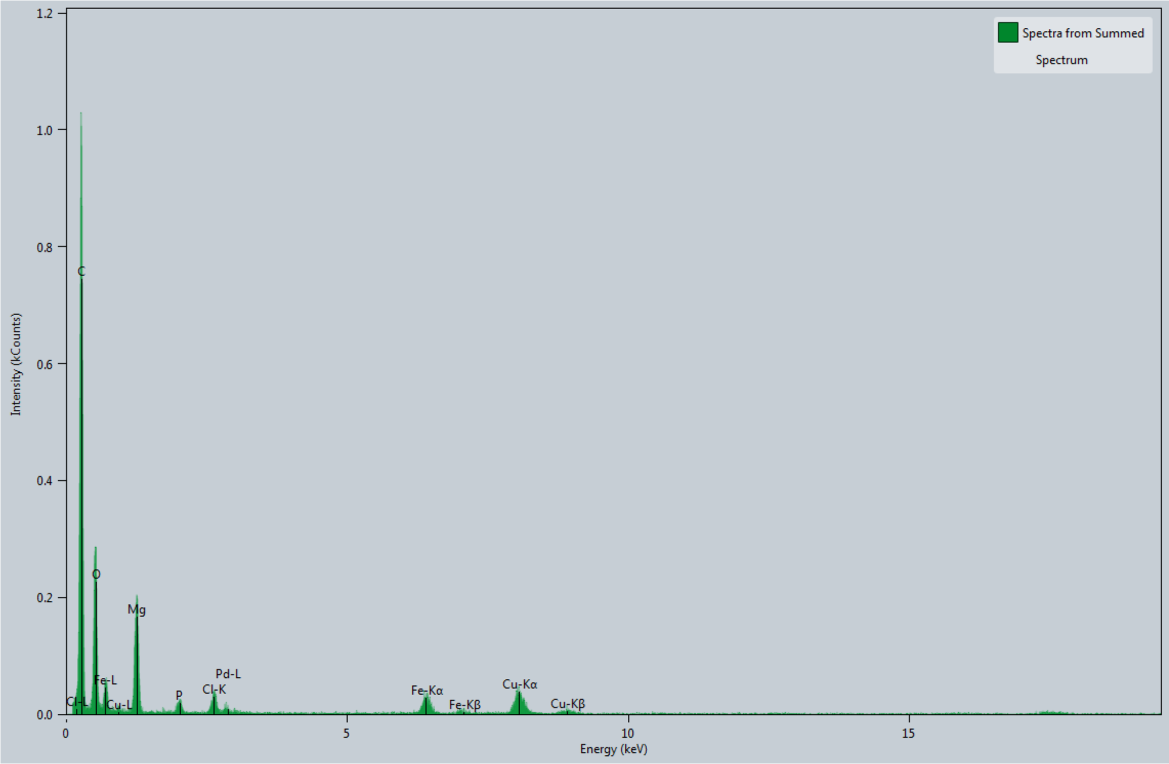

Element	Family	Atomic fraction (%)	Mass fraction (%)
C	K	76.5209	61.0421
O	K	13.0099	13.8248
Mg	K	6.0581	9.77942
P	K	0.628589	1.29313
Cl	K	0.986464	2.32282
Fe	K	1.04946	3.89252
(Cu)	K	1.58037	6.67004
Pd	L	0.166272	1.17523

Fe/ppm Pd nanoparticles in pure degassed H_2O before reaction:

The nanomaterial (2 mg) was added to a vial in the glove box, and the vial was covered with a septum. Pure degassed H_2O (2 mL) was inserted into the vial via syringe and the mixture was stirred for 1 h.

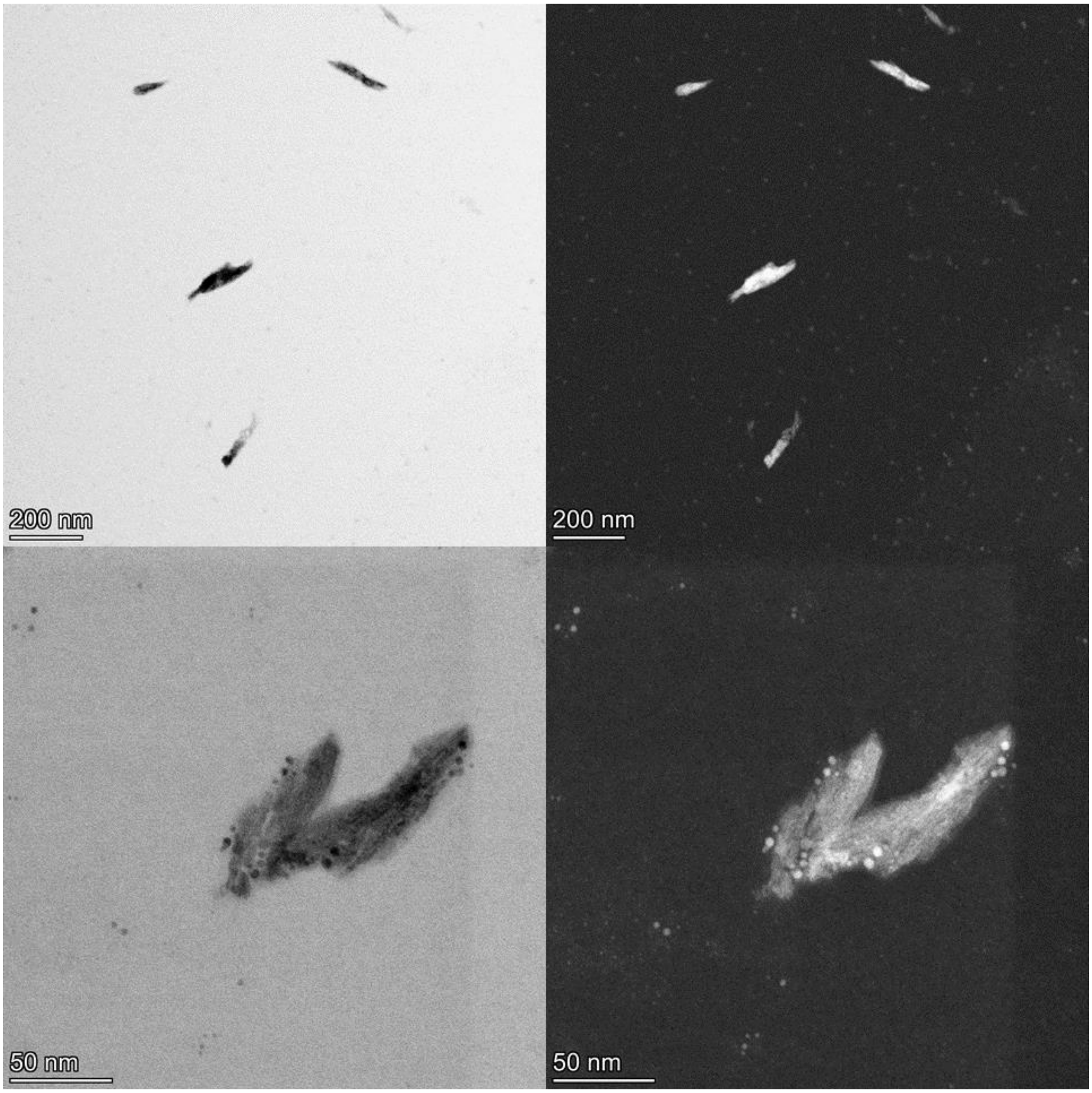

Fe/ppm Pd nanocatalyst in 2 wt % TPGS-750-M/H_2O before reaction:

The nanomaterial (2 mg) was added to a vial in the glove box, and the vial was covered with a septum. TPGS-750-M/H_2O (2 mL, 2 wt %) was inserted into the vial via syringe and the mixture was stirred for 1 h.

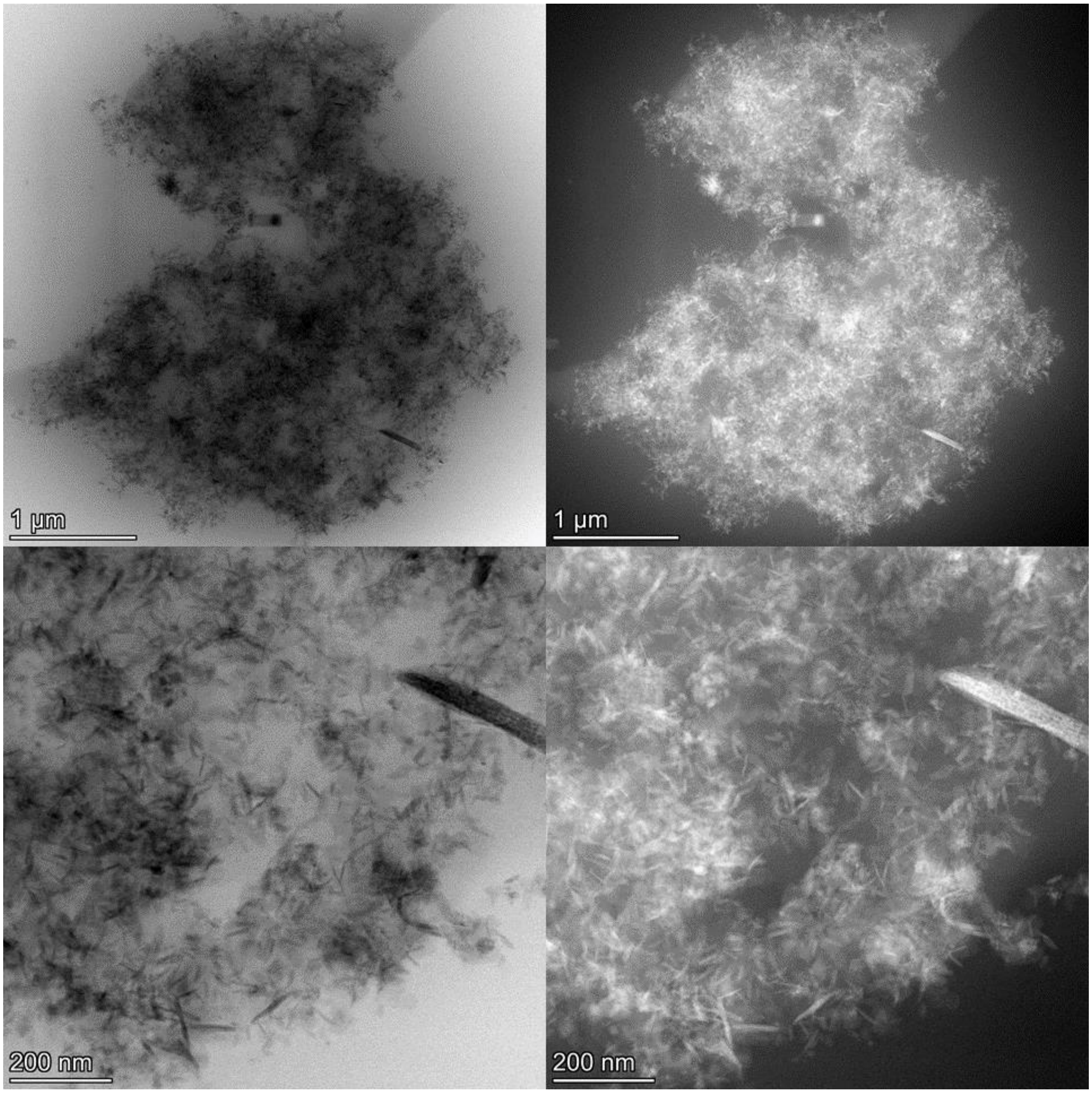
1 µm
1 µm
200 nm
200 nm

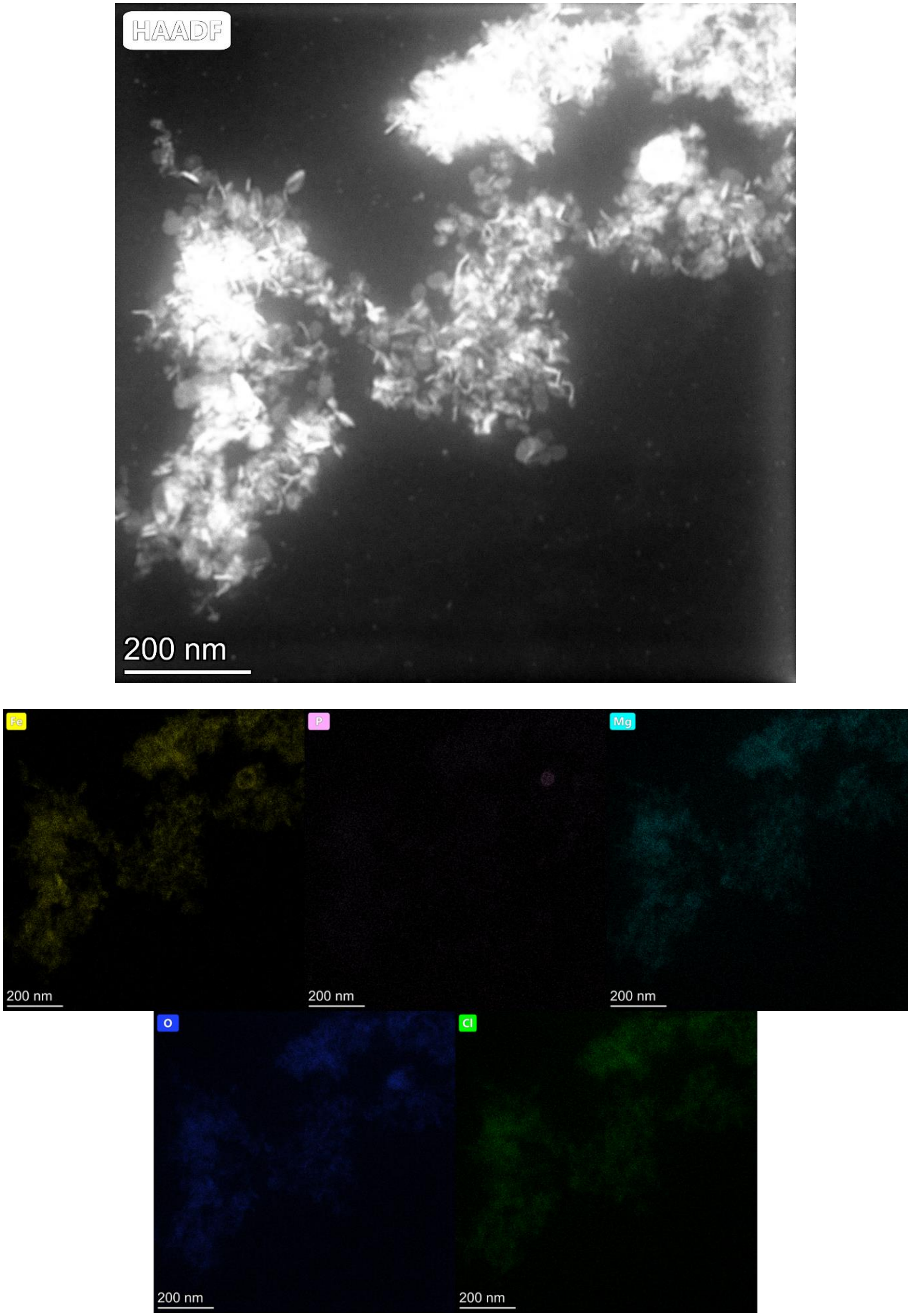
HAADF
200 nm
Fe
200 nm
P
200 nm
Mg
200 nm
O
200 nm
Cl
200 nm

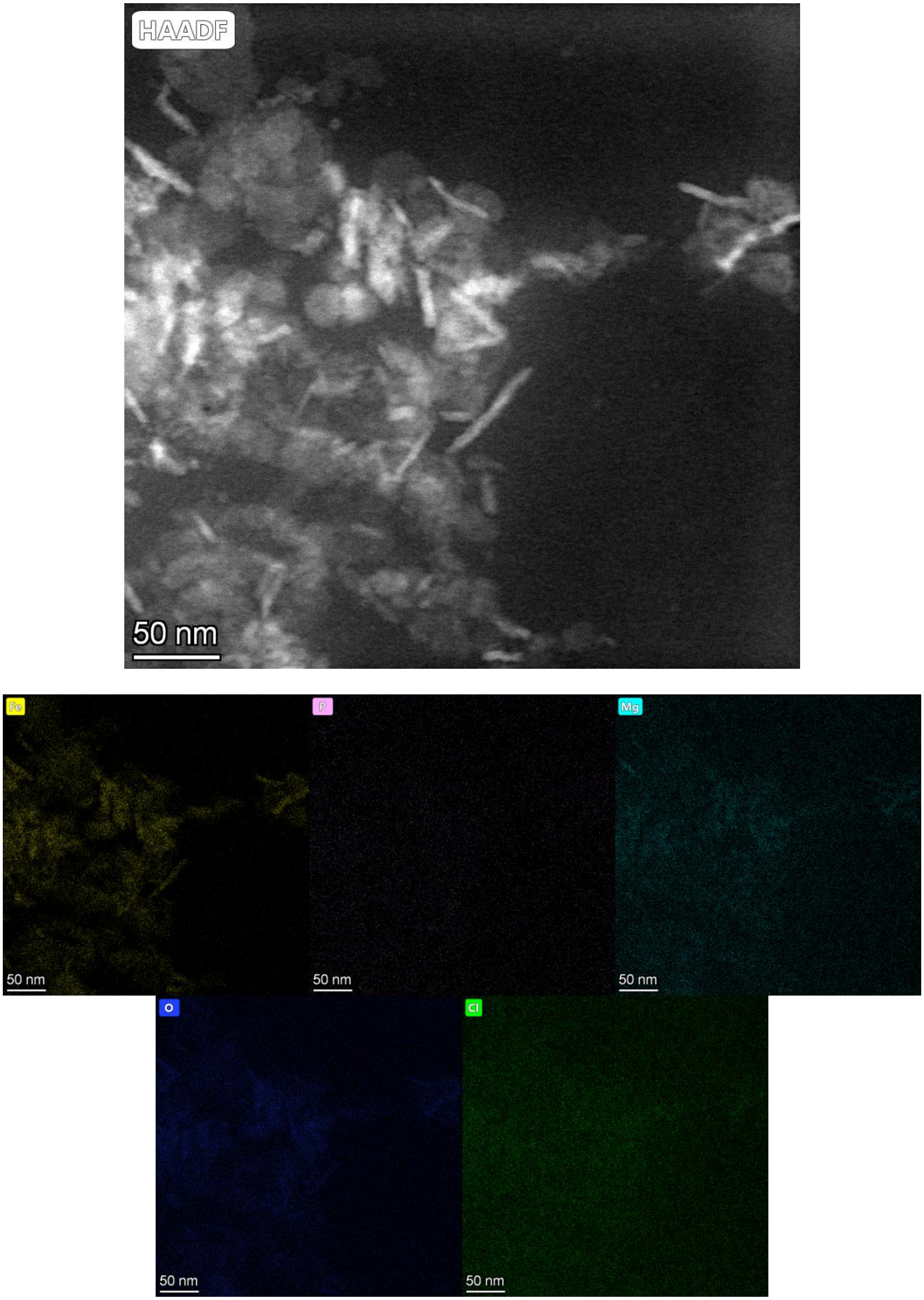
HAADF
50 nm
Fe
50 nm
P
50 nm
Mg
50 nm
O
50 nm
Cl
50 nm

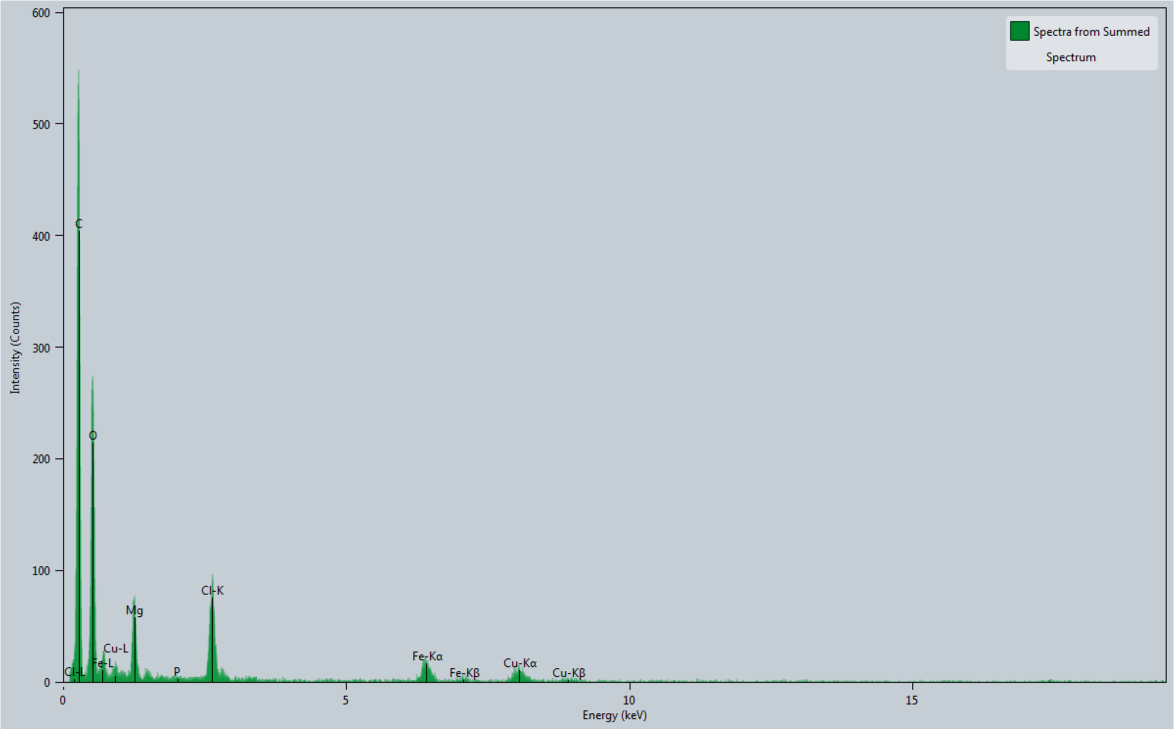

Fe/ppm Pd nanocatalyst in 2 wt % TPGS-750-M/H_2O after reaction:

To an oven dried 4 mL microwave vial, NaCl (70.2 mg, 1.2 mmol), K_3PO_4 (127.2 mg, 0.6 mmol), 1-iodo-4-methoxybenzene (46.8 mg, 0.2 mmol), *t*-butyl acrylate (51.3 mg, 0.4 mmol), and Fe/ppm Pd NPs (5 mg) were added in a glovebox. The vial was capped with a septum and removed from the glovebox. Through the septum, 0.4 mL aqueous solution of 2 wt % TPGS-750-M was added. The mixture was vigorously stirred at rt for 16 h. After complete consumption of starting material, the septum was removed. Minimal EtOAc was added, and the mixture was stirred *gently* for 1 min. Stirring was stopped and the organic layer was then allowed to separate, after which it was removed via pipette. After the extraction, the left-over mixture was diluted by 1.6 mL 2 wt % TPGS-750-M/H_2O and used as the sample for TEM analysis.

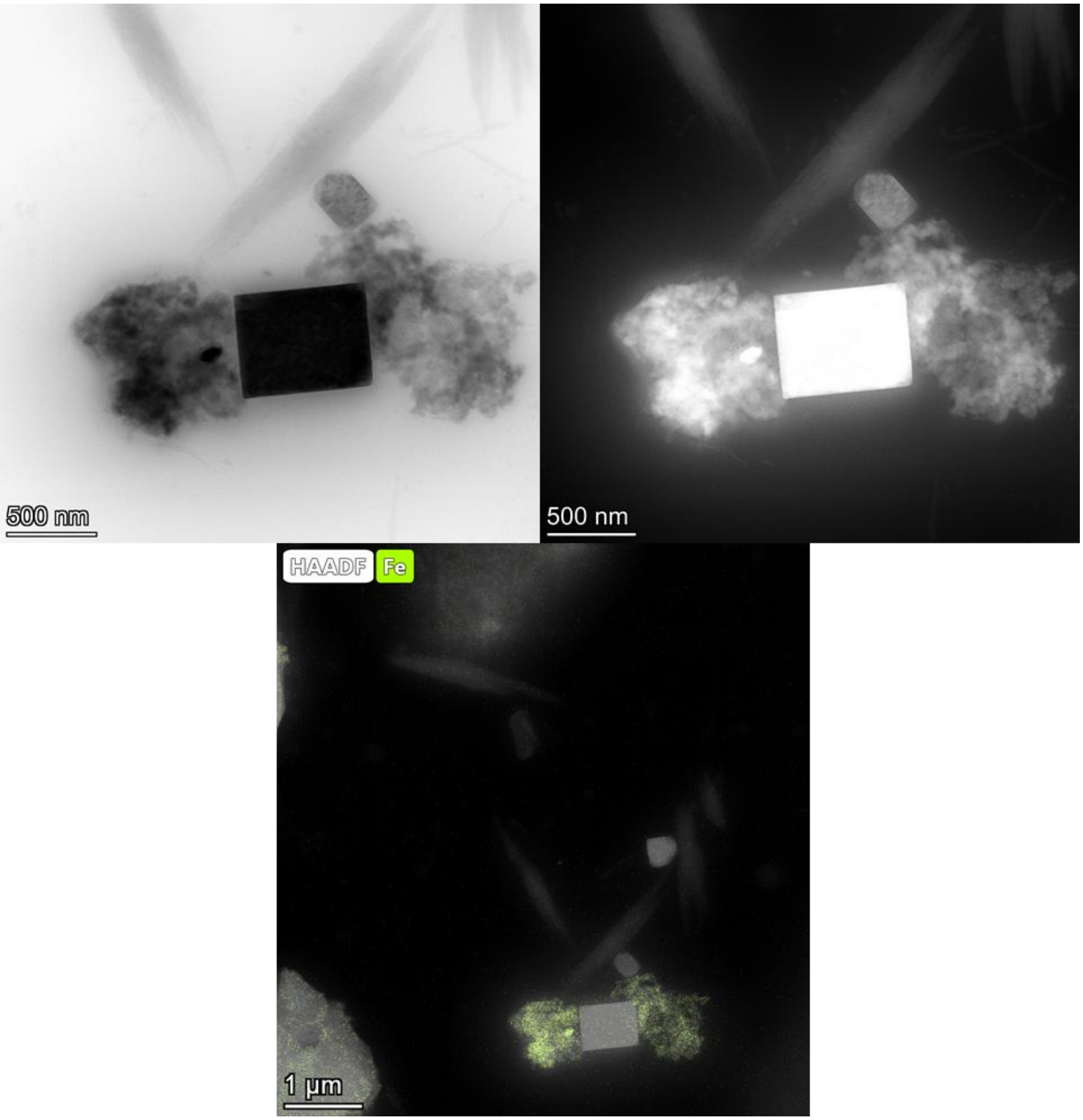

Cryo TEM analysis

Fe/ppm Pd nanocatalyst in 2 wt % TPGS-750-M/H_2O without DMF as cosolvent:

The nanomaterial (2 mg) was added to a vial in the glove box, and the vial was covered with a septum. TPGS-750-M/H_2O (0.1 mL 2 wt %) and 0.9 mL degassed HPLC water were inserted into the vial via syringe and the mixture was stirred for 1 h.

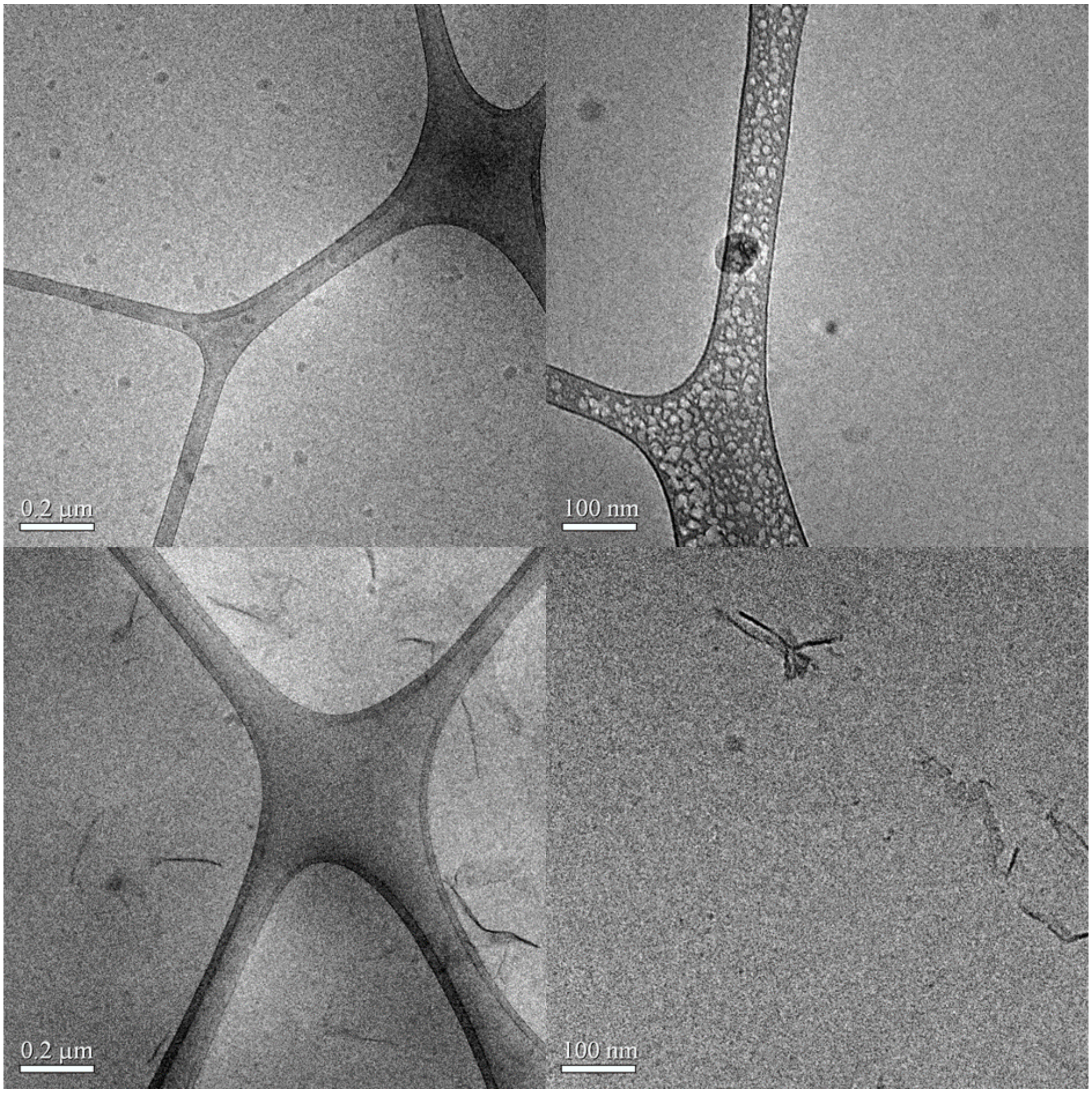
0.2 µm
100 nm
0.2 µm
100 nm

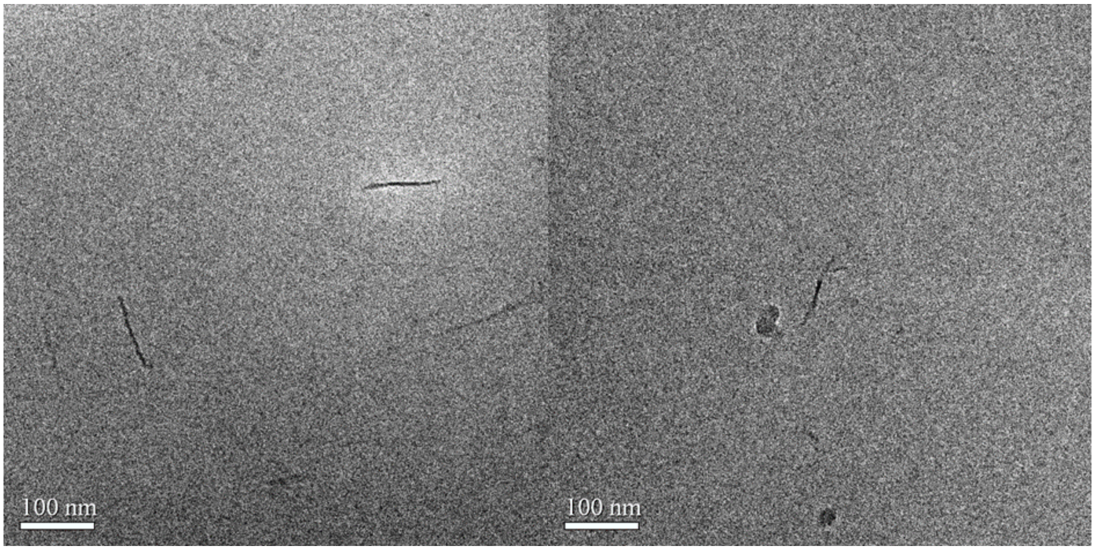
100 nm
100 nm

Fe/ppm Pd nanocatalyst in 2 wt % TPGS-750-M/H_2O with DMF as cosolvent:

The nanomaterial (2 mg) was added to a vial in the glove box, and the vial was covered with a septum. TPGS-750-M/H_2O (0.1 mL, 2 wt %), 10 µL DMF and 0.9 mL degassed HPLC water were inserted into the vial by a syringe and the mixture was stirred for 1 h.

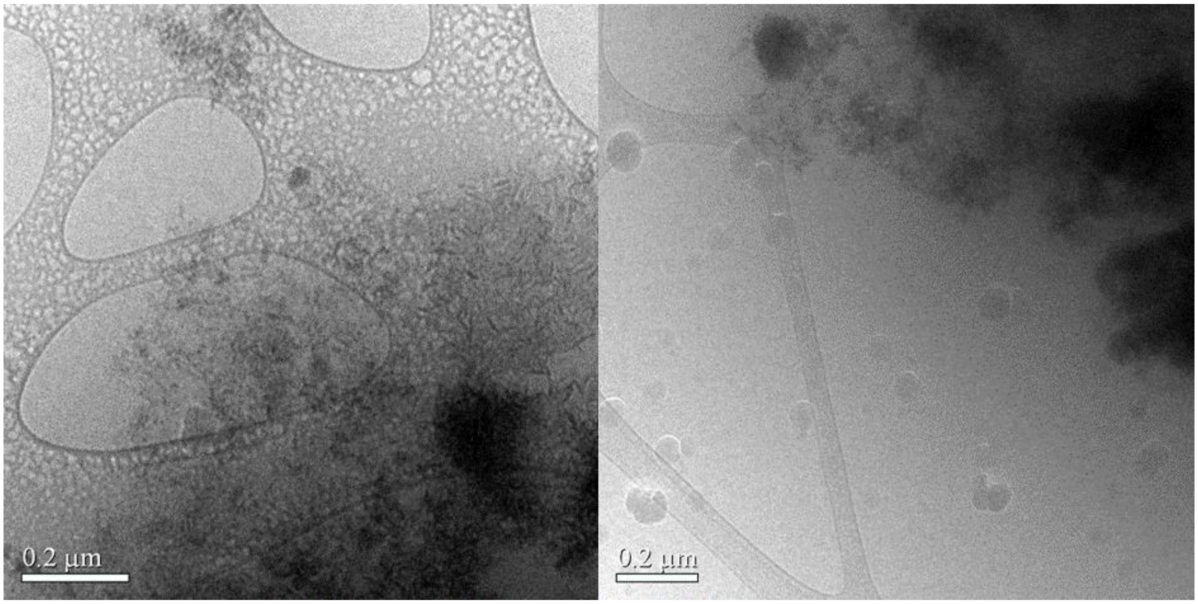

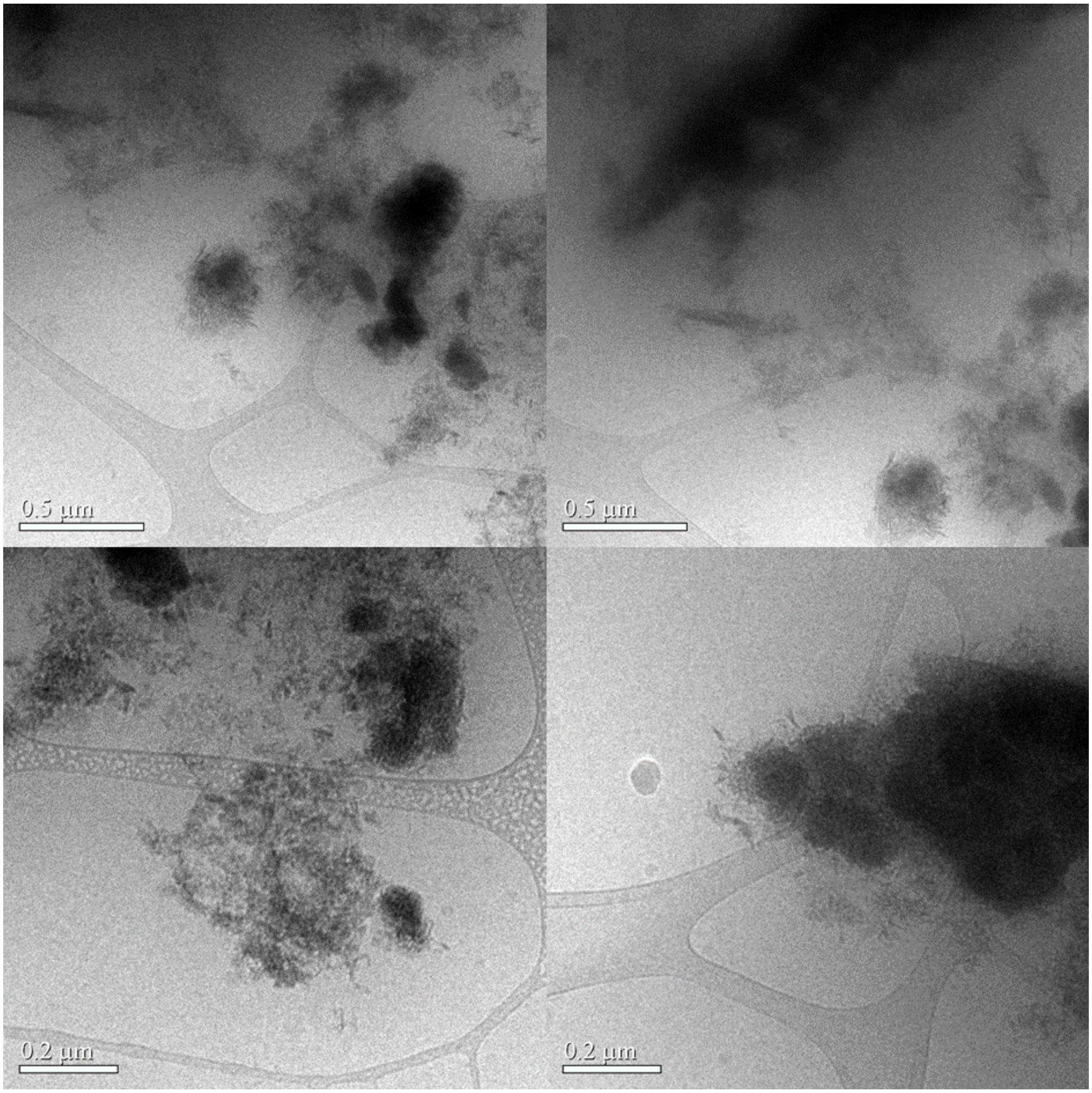

ICP-MS analysis

		Magnesium		Iron		Palladium	
		[µg/g]		[µg/g]		[µg/g]	
Sample #	Sample weight in analysis [mg]	Average*	stdev	Average*	stdev	Average*	stdev
HEK-1	4.80	98348.088	2208.333	62744.610	366.667	3898.620	117.083
HEK-2	0.62	73995.752	195.161	489347.343	4774.194	27912.762	454.839
Sample #	Sample weight in analysis [mL]	[µg/L]		[µg/L]		[µg/L]	
HEK-3	1.70	525853.765	3388.235	3010.462	36.353	103.040	3.682

**Each sample was done in triplicated measurements with background correction.*

n/a represents below detection limit.

	Dry powder (10 mg)	Leftover from water (1.2 mg)	Supernatant (1.7 mL)
Mg (mg)	0.983	0.089	0.894
Fe (mg)	0.627	0.587	0.051
Pd (mg)	0.039	0.033	0.0018

Sample preparation for ICP-MS

HEK-1: To an oven dried 4 mL microwave vial, Fe/ppm Pd NPs (10.0 mg) were added in the glovebox. The vial was capped with a septum and removed from the glovebox as HEK-1. Through the septum, 0.4 mL aqueous solution of 2 wt % TPGS-750-M was added followed by sequential addition of 0.04 mL DMF via syringe.

HEK-2 and HEK-3: To an oven dried 4 mL microwave vial, Fe/ppm Pd NPs (10.0 mg) were added in the glovebox. The vial was capped with a septum and removed from the glovebox. Through the septum, 1.8 mL degassed water was added via syringe. The mixture was stirred for 1 h and centrifuged for 2 min. The supernatant was transferred to a 4 mL microwave vial via syringe. The leftover was marked as HEK-2 and the supernatant was marked as HEK-3.

XPS analysis

Fe/ppm Pd nanocatalyst dry powder:

Full scan XPS:

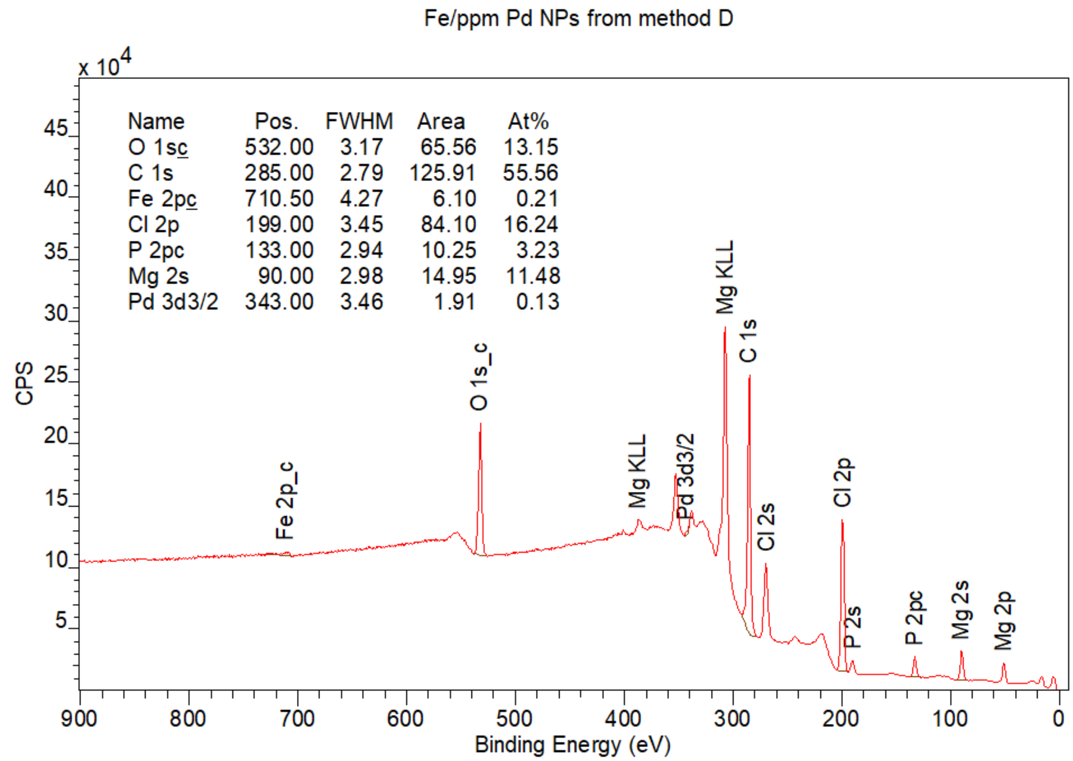

High resolution XPS:

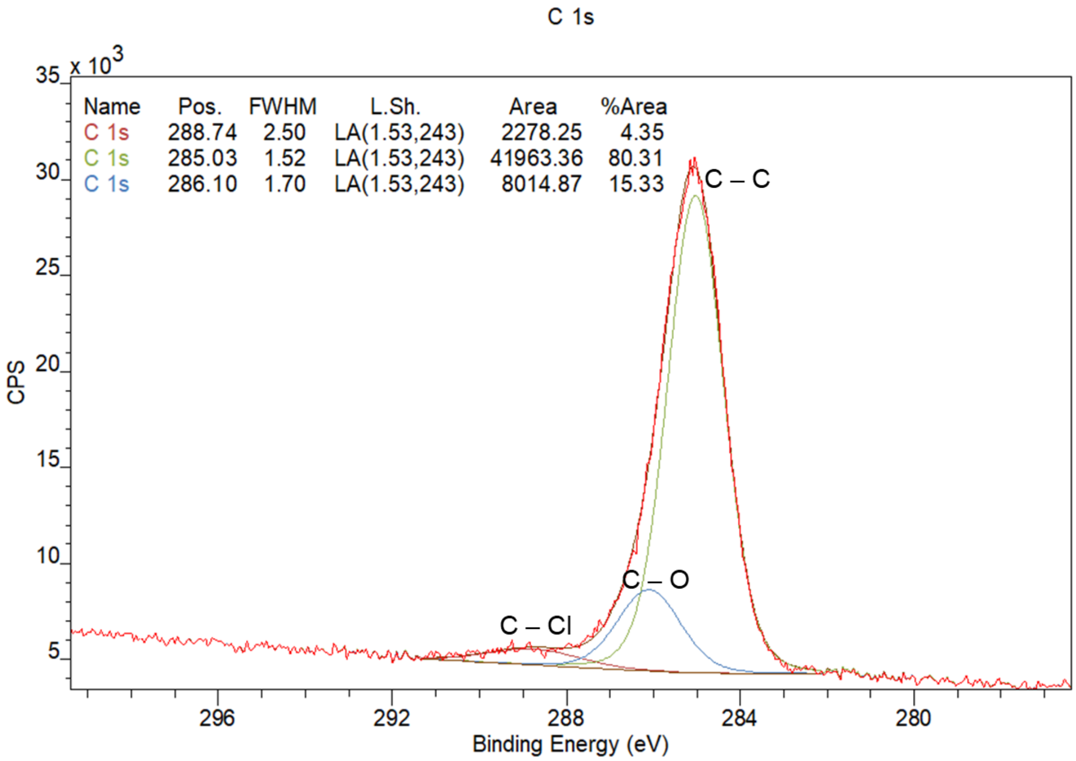

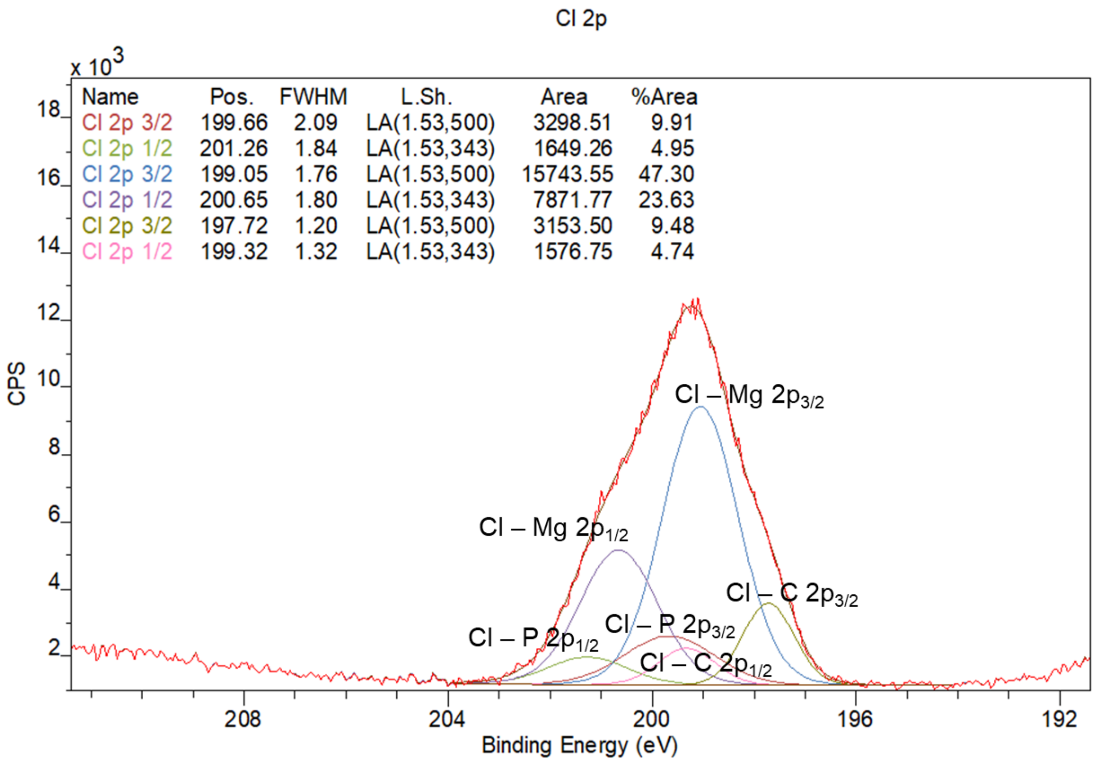
Cl 2p
x 10^3
Name Pos. FWHM L.Sh. Area %Area
Cl 2p 3/2 199.66 2.09 LA(1.53,500) 3298.51 9.91
Cl 2p 1/2 201.26 1.84 LA(1.53,343) 1649.26 4.95
Cl 2p 3/2 199.05 1.76 LA(1.53,500) 15743.55 47.30
Cl 2p 1/2 200.65 1.80 LA(1.53,343) 7871.77 23.63
Cl 2p 3/2 197.72 1.20 LA(1.53,500) 3153.50 9.48
Cl 2p 1/2 199.32 1.32 LA(1.53,343) 1576.75 4.74
Cl – Mg 2p3/2
Cl – Mg 2p1/2
Cl – C 2p3/2
Cl – P 2p3/2
Cl – P 2p1/2
Cl – C 2p1/2
CPS
18
16
14
12
10
8
6
4
2
208
204
200
196
192
Binding Energy (eV)

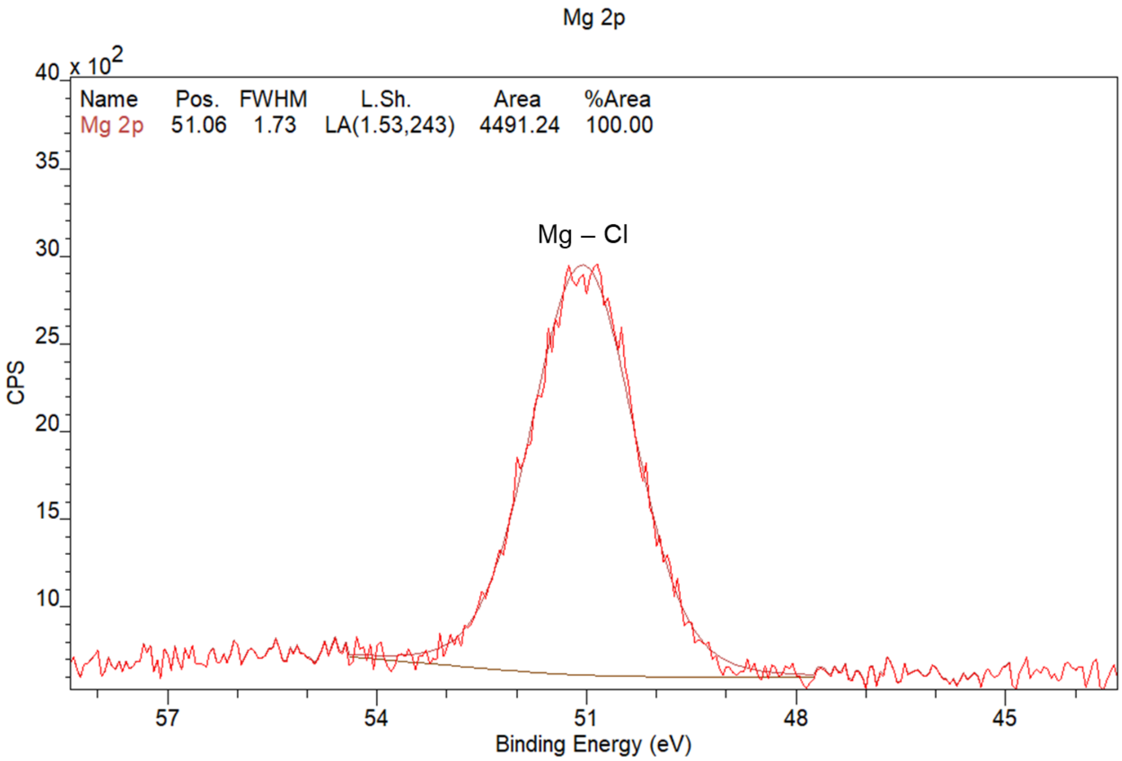
Mg 2p
x 10^2
Name Pos. FWHM L.Sh. Area %Area
Mg 2p 51.06 1.73 LA(1.53,243) 4491.24 100.00
Mg – Cl
CPS
40
35
30
25
20
15
10
57
54
51
48
45
Binding Energy (eV)

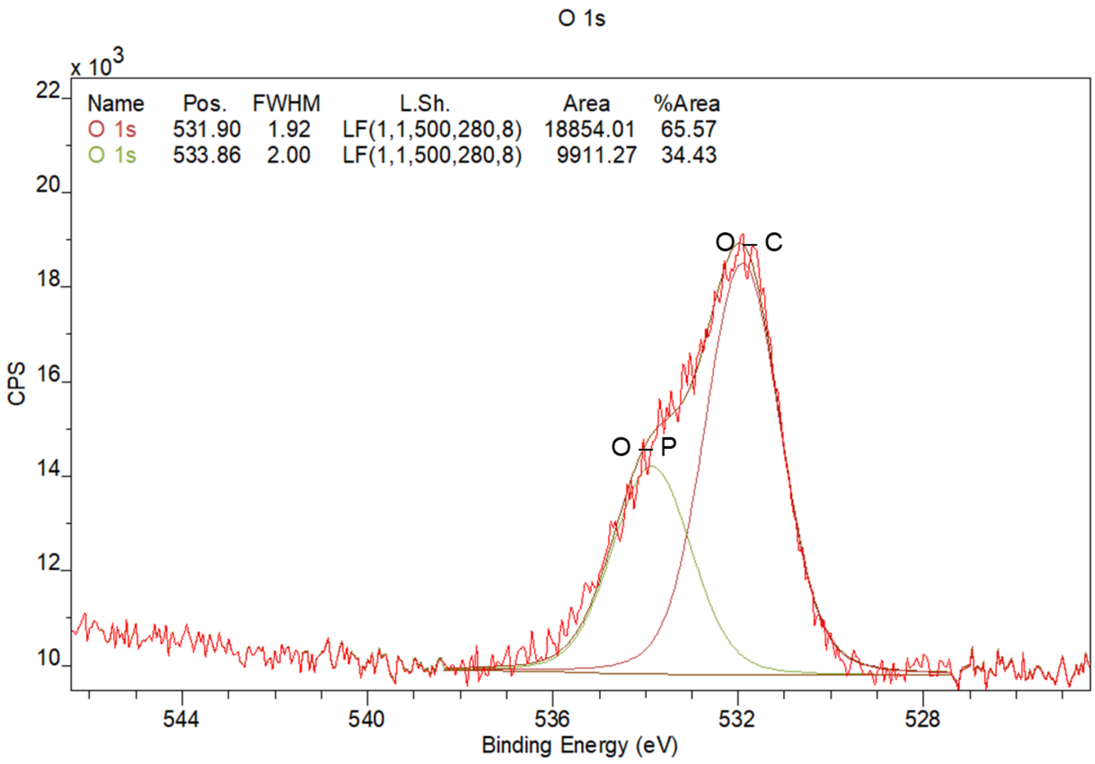
O 1s
x 10^3
Name Pos. FWHM L.Sh. Area %Area
O 1s 531.90 1.92 LF(1,1,500,280,8) 18854.01 65.57
O 1s 533.86 2.00 LF(1,1,500,280,8) 9911.27 34.43
O – C
O – P
CPS
22
20
18
16
14
12
10
544
540
536
532
528
Binding Energy (eV)

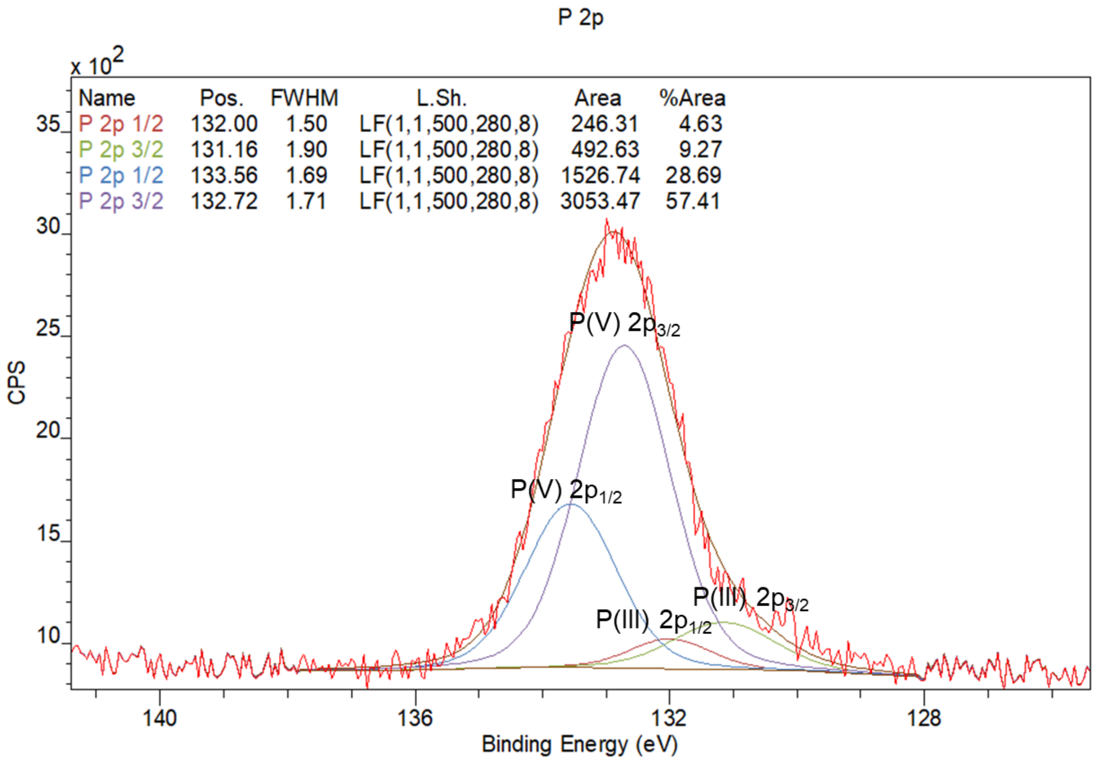
P 2p
x 10^2
Name Pos. FWHM L.Sh. Area %Area
P 2p 1/2 132.00 1.50 LF(1,1,500,280,8) 246.31 4.63
P 2p 3/2 131.16 1.90 LF(1,1,500,280,8) 492.63 9.27
P 2p 1/2 133.56 1.69 LF(1,1,500,280,8) 1526.74 28.69
P 2p 3/2 132.72 1.71 LF(1,1,500,280,8) 3053.47 57.41
P(V) 2p3/2
P(V) 2p1/2
P(III) 2p3/2
P(III) 2p1/2
CPS
35
30
25
20
15
10
140
136
132
128
Binding Energy (eV)

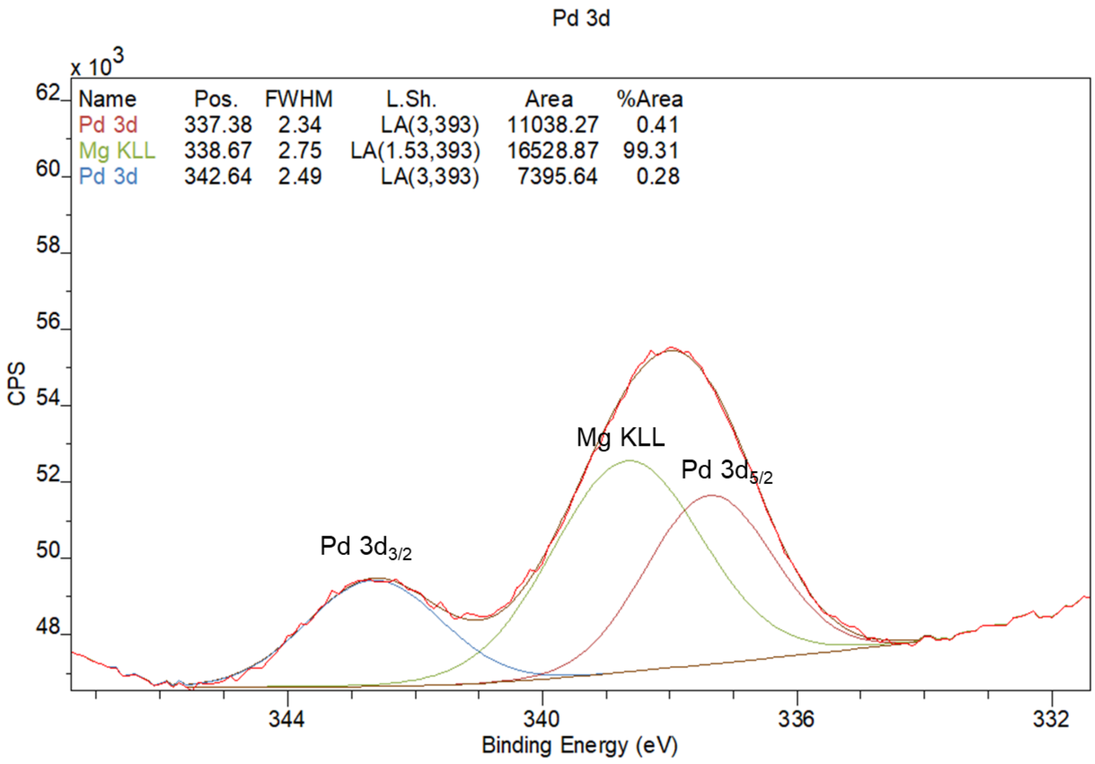
Pd 3d
x 10^3
Name Pos. FWHM L.Sh. Area %Area
Pd 3d 337.38 2.34 LA(3,393) 11038.27 0.41
Mg KLL 338.67 2.75 LA(1.53,393) 16528.87 99.31
Pd 3d 342.64 2.49 LA(3,393) 7395.64 0.28
Mg KLL
Pd 3d5/2
Pd 3d3/2
CPS
62
60
58
56
54
52
50
48
344
340
336
332
Binding Energy (eV)

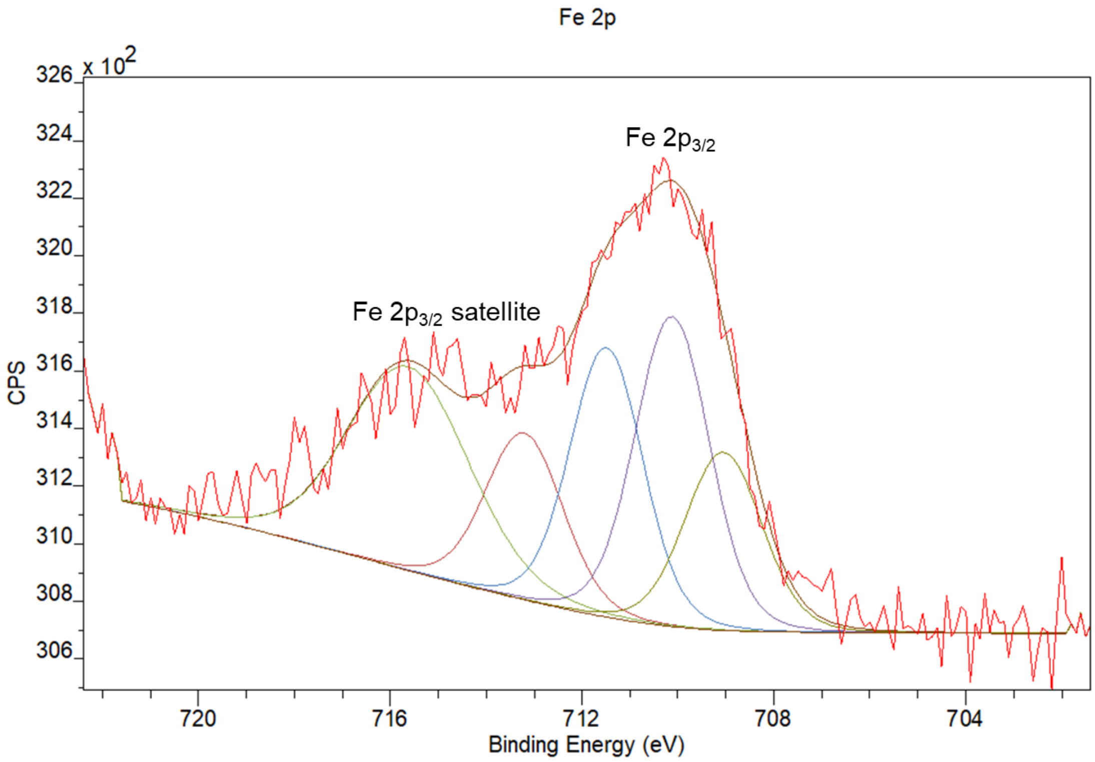
Fe 2p
x 10^2
Fe 2p3/2
Fe 2p3/2 satellite
CPS
326
324
322
320
318
316
314
312
310
308
306
720
716
712
708
704
Binding Energy (eV)

Fe/ppm Pd nanocatalyst dry powder after rinsing by water:

Full scan XPS:

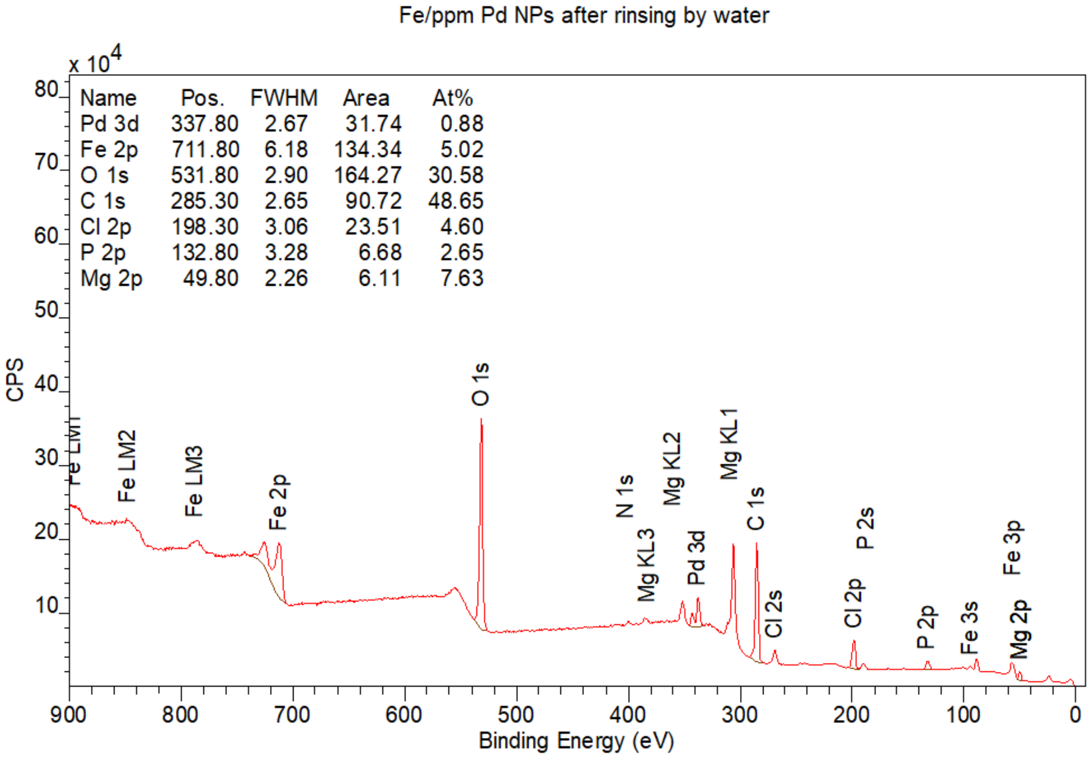

Name	Pos.	FWHM	Area	At%
Pd 3d	337.80	2.67	31.74	0.88
Fe 2p	711.80	6.18	134.34	5.02
O 1s	531.80	2.90	164.27	30.58
C 1s	285.30	2.65	90.72	48.65
Cl 2p	198.30	3.06	23.51	4.60
P 2p	132.80	3.28	6.68	2.65
Mg 2p	49.80	2.26	6.11	7.63

High resolution XPS:

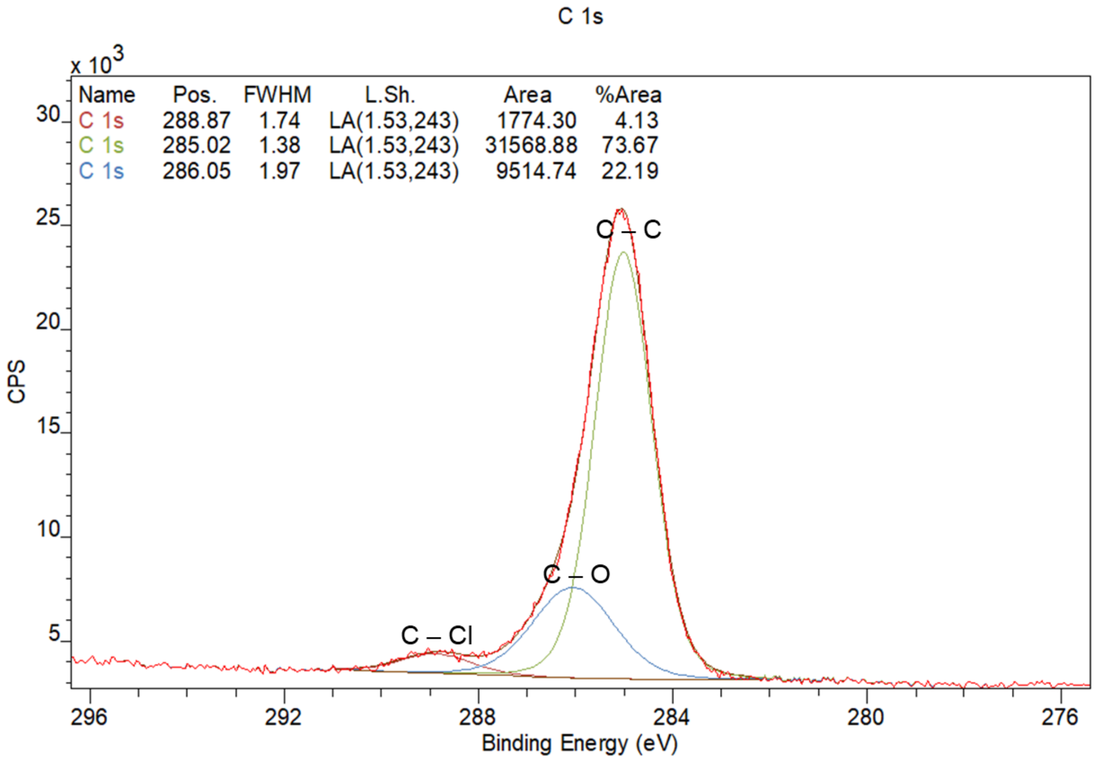
C 1s
x 10^3
Name Pos. FWHM L.Sh. Area %Area
C 1s 288.87 1.74 LA(1.53,243) 1774.30 4.13
C 1s 285.02 1.38 LA(1.53,243) 31568.88 73.67
C 1s 286.05 1.97 LA(1.53,243) 9514.74 22.19
C – C
C – O
C – Cl
CPS
30
25
20
15
10
5
296
292
288
284
280
276
Binding Energy (eV)

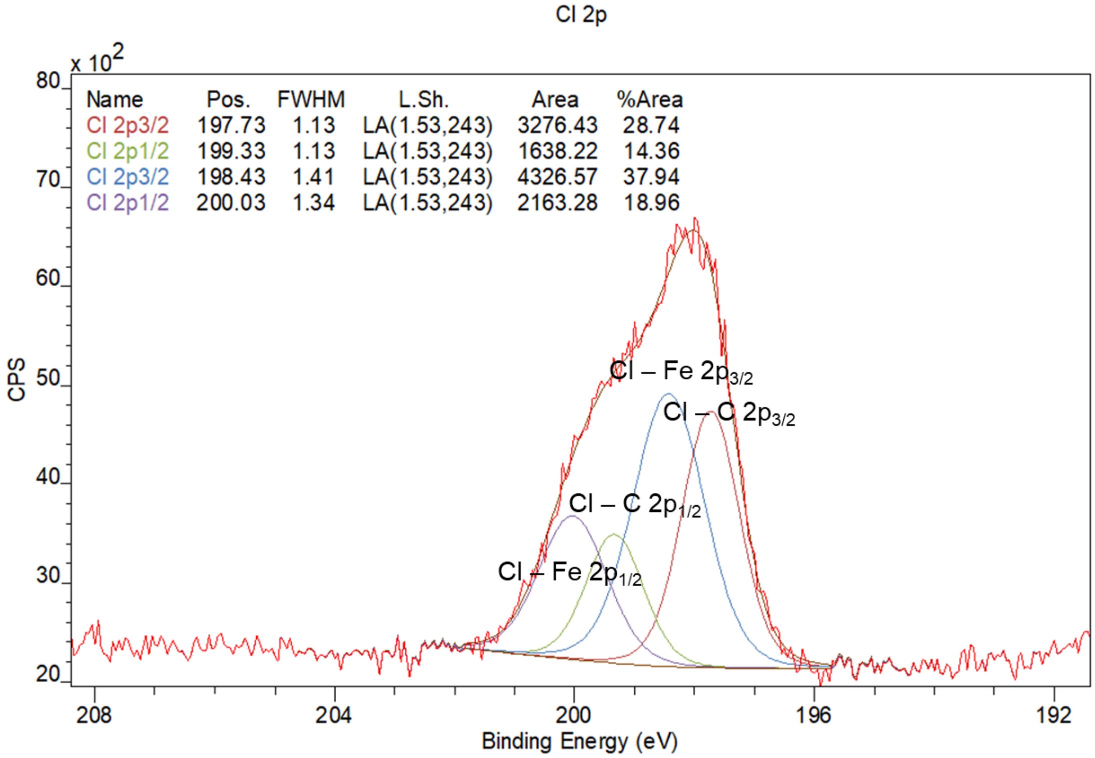
Cl 2p
x 10^2
Name Pos. FWHM L.Sh. Area %Area
Cl 2p3/2 197.73 1.13 LA(1.53,243) 3276.43 28.74
Cl 2p1/2 199.33 1.13 LA(1.53,243) 1638.22 14.36
Cl 2p3/2 198.43 1.41 LA(1.53,243) 4326.57 37.94
Cl 2p1/2 200.03 1.34 LA(1.53,243) 2163.28 18.96
Cl – Fe 2p3/2
Cl – C 2p3/2
Cl – C 2p1/2
Cl – Fe 2p1/2
CPS
80
70
60
50
40
30
20
208
204
200
196
192
Binding Energy (eV)

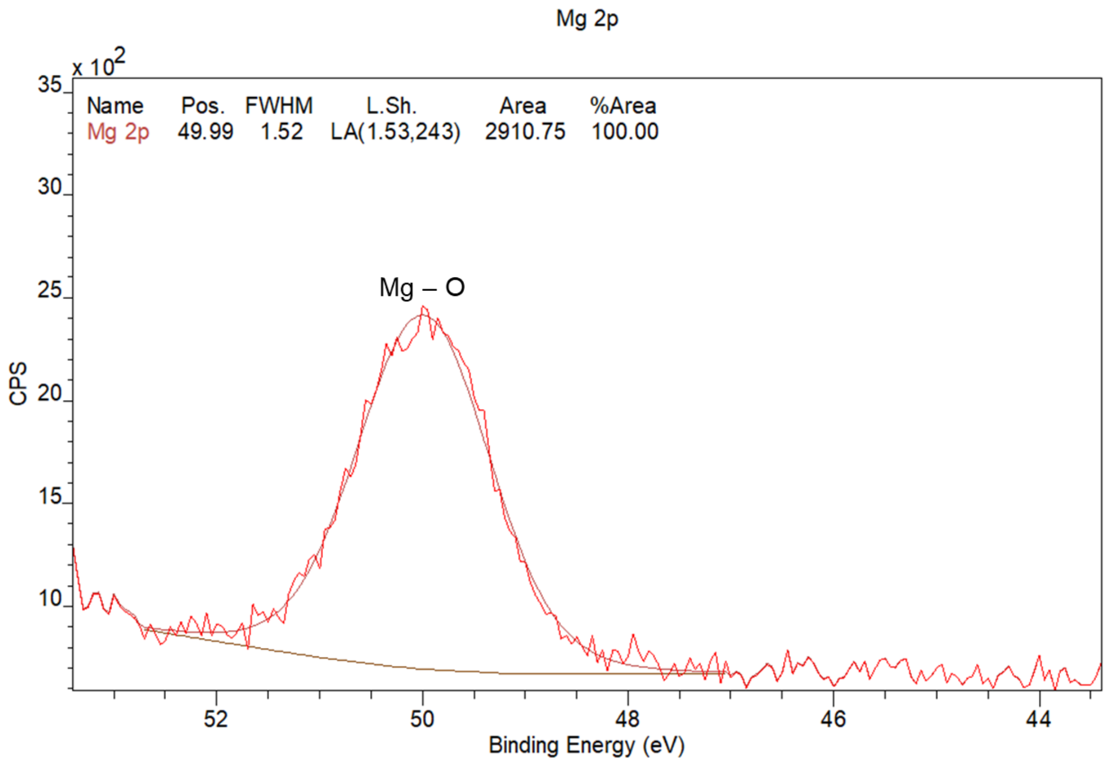
Mg 2p
x 10^2
Name Pos. FWHM L.Sh. Area %Area
Mg 2p 49.99 1.52 LA(1.53,243) 2910.75 100.00
Mg – O
CPS
35
30
25
20
15
10
52
50
48
46
44
Binding Energy (eV)

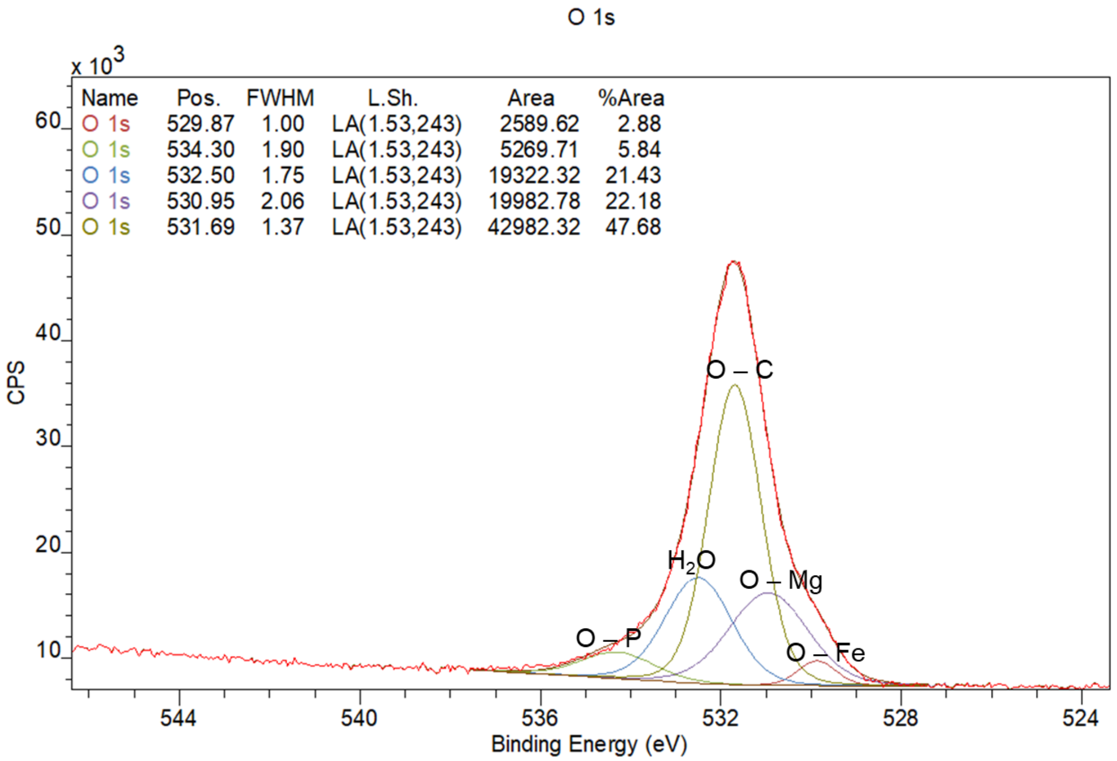
O 1s
x 10^3
Name Pos. FWHM L.Sh. Area %Area
O 1s 529.87 1.00 LA(1.53,243) 2589.62 2.88
O 1s 534.30 1.90 LA(1.53,243) 5269.71 5.84
O 1s 532.50 1.75 LA(1.53,243) 19322.32 21.43
O 1s 530.95 2.06 LA(1.53,243) 19982.78 22.18
O 1s 531.69 1.37 LA(1.53,243) 42982.32 47.68
O – C
H2O
O – Mg
O – P
O – Fe
CPS
60
50
40
30
20
10
544
540
536
532
528
524
Binding Energy (eV)

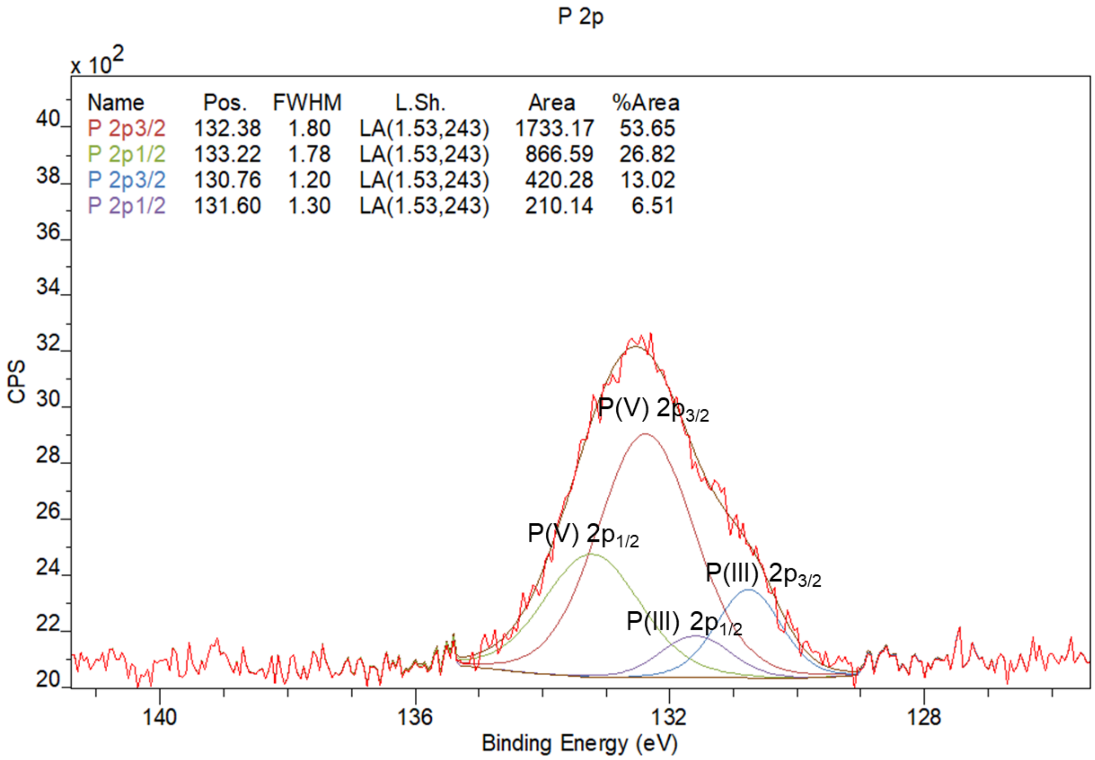
P 2p
x 10^2
Name Pos. FWHM L.Sh. Area %Area
P 2p3/2 132.38 1.80 LA(1.53,243) 1733.17 53.65
P 2p1/2 133.22 1.78 LA(1.53,243) 866.59 26.82
P 2p3/2 130.76 1.20 LA(1.53,243) 420.28 13.02
P 2p1/2 131.60 1.30 LA(1.53,243) 210.14 6.51
P(V) 2p3/2
P(V) 2p1/2
P(III) 2p3/2
P(III) 2p1/2
CPS
40
38
36
34
32
30
28
26
24
22
20
140
136
132
128
Binding Energy (eV)

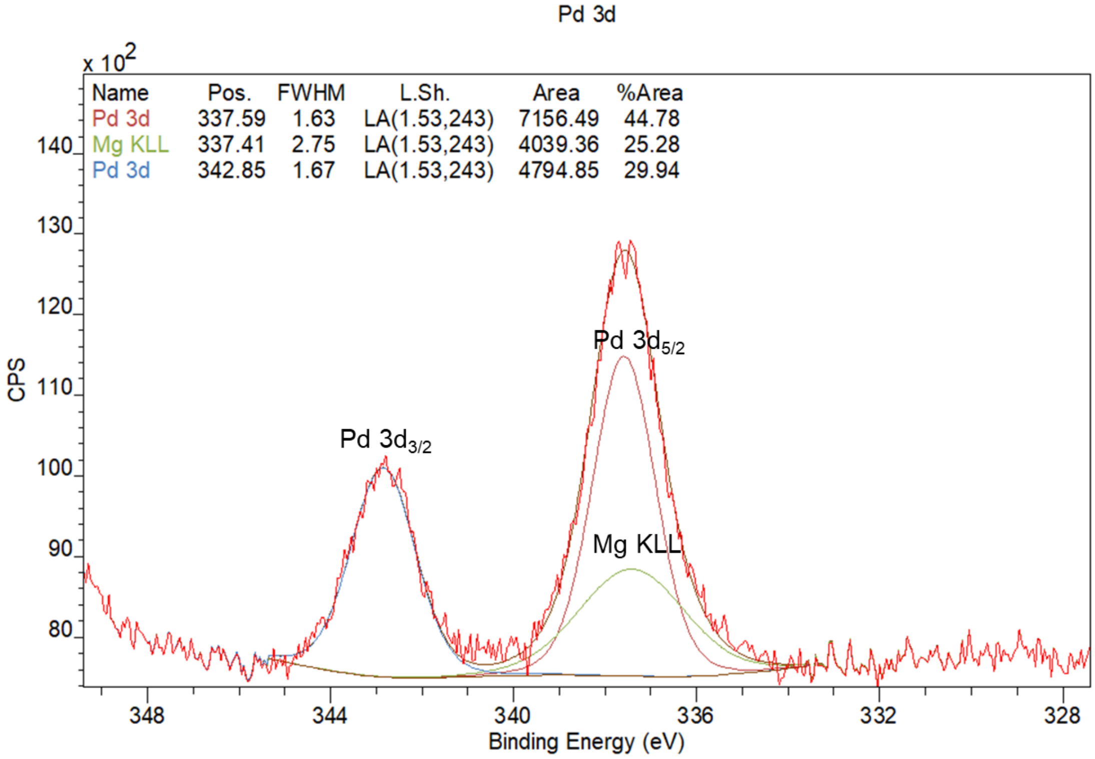
Pd 3d
x 10^2
Name Pos. FWHM L.Sh. Area %Area
Pd 3d 337.59 1.63 LA(1.53,243) 7156.49 44.78
Mg KLL 337.41 2.75 LA(1.53,243) 4039.36 25.28
Pd 3d 342.85 1.67 LA(1.53,243) 4794.85 29.94
Pd 3d5/2
Pd 3d3/2
Mg KLL
CPS
140
130
120
110
100
90
80
348
344
340
336
332
328
Binding Energy (eV)

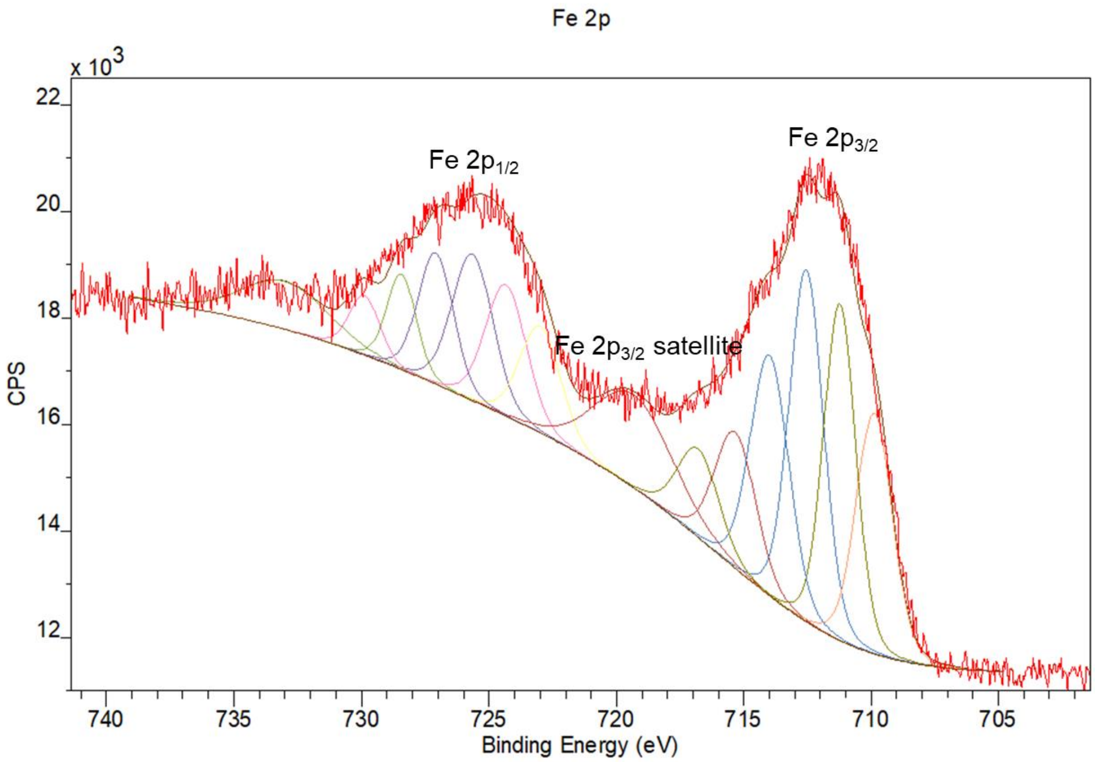

Synthesis and STEM of Fe/ppm Pd Nanoparticles with SPhos as ligand

Preparation

In an oven dried round-bottomed flask, $FeCl_3$ (81.1 mg, 0.5 mmol) was added under an atmosphere of dry argon. The flask was covered with a septum, and 2.5 mL dry THF was added by syringe. The reaction mixture was stirred for 20 min at rt. While maintaining a dry atmosphere at rt, a 1 M solution of MeMgCl in THF was very slowly (1 drop/2 sec) added to the reaction mixture (1 mL, 1 mmol). And then, the mixture was stirred for an additional 1 min at rt. After that time, 2.4 mL THF solution of 0.01 M $Pd(OAc)_2$ (0.025 mmol) and 0.25 M SPhos (0.6 mmol) were added to the reaction mixture. After addition, an additional 1 M solution of MeMgCl in THF was very slowly (1 drop/2 sec) added to the reaction mixture (0.75 mL, 1.75 mmol). After complete addition of the Grignard reagent, the mixture was stirred for an additional 30 min at rt. THF was then evaporated under reduced pressure at rt to provide black nanomaterial as a powder. The Fe nanoparticles obtained were dried under reduced pressure at rt for 3 h yielding 0.75 g Fe/ppm Pd NPs nanoparticles. The nanoparticles need to be stored under argon in glovebox. The material was used as such for subsequent reactions under micellar conditions.

STEM (BF and HADDF) for Fe/ppm Pd/SPhos nanoparticles

Fe/ppm Pd/SPhos nanoparticles dry powder

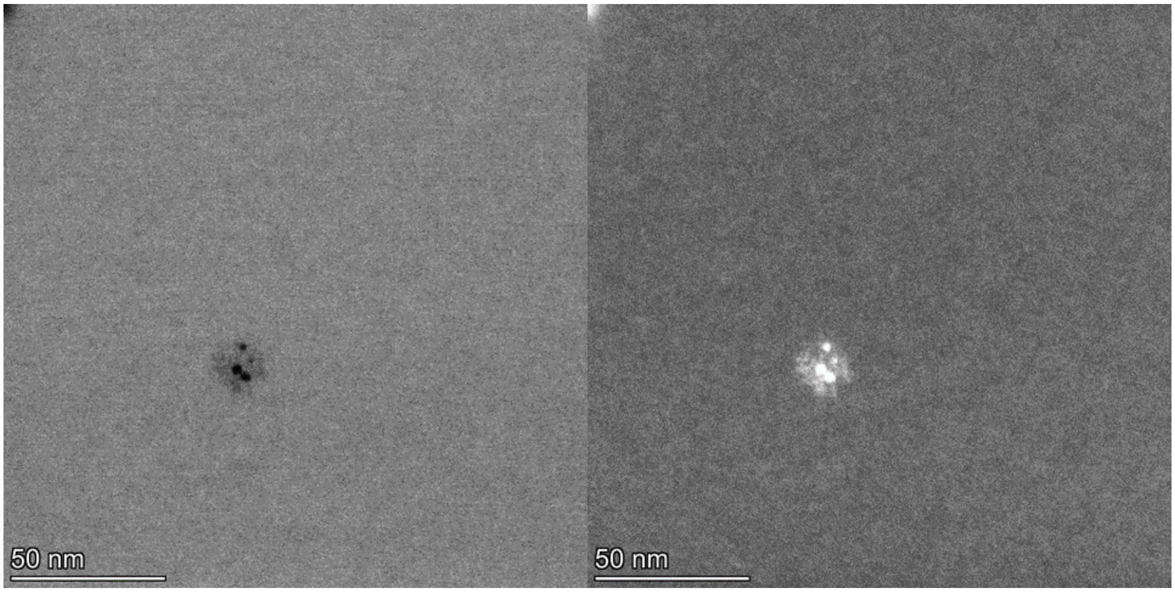

Fe/ppm Pd/SPhos nanoparticles in pure degassed H_2O:

The nanomaterial (2 mg) was added to a vial in the glove box, and the vial was covered with a septum. 2 mL pure degassed H_2O was inserted to the vial by a syringe and the mixture was stirred for 1 h.

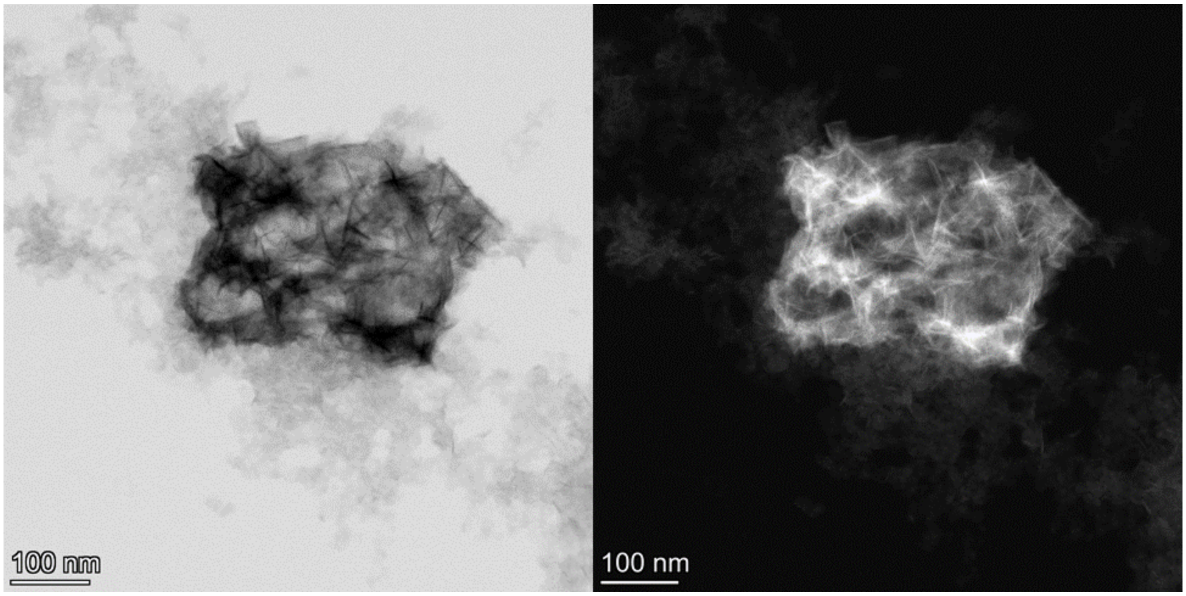

Fe/ppm Pd/SPhos nanoparticles in 2 wt % TPGS-750-M/H_2O before reaction:

The nanomaterial (2 mg) was added to a vial in the glove box, and the vial was covered with a septum. TPGS-750-M/H_2O (2 mL, 2 wt %) was inserted to the vial by a syringe and the mixture was stirred for 1 h.

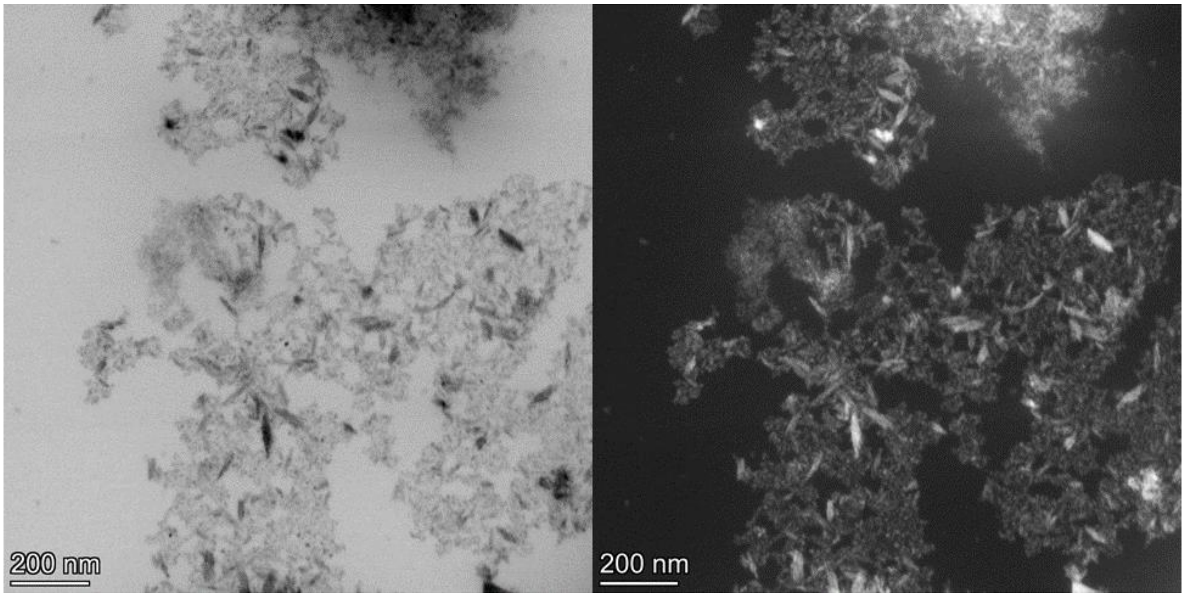

Synthesis and STEM of Fe/ppm Pd Nanoparticles with Cy-cBRIDP as ligand

Preparation

In an oven dried round-bottomed flask, $FeCl_3$ (81.1 mg, 0.5 mmol) was added under an atmosphere of dry argon. The flask was covered with a septum, and 2.5 mL dry THF was added by syringe. The reaction mixture was stirred for 20 min at rt. While maintaining a dry atmosphere at rt, a 1 M solution of MeMgCl in THF was very slowly (1 drop/2 sec) added to the reaction mixture (1 mL, 1 mmol). And then, the mixture was stirred for an additional 1 min at rt. After that time, 2.4 mL THF solution of 0.01 M $Pd(OAc)_2$ (0.025 mmol) and 0.25 M Cy-cBRIDP (0.6 mmol) were added to the reaction mixture. After addition, additional 1 M solution of MeMgCl in THF was very slowly (1 drop/2 sec) added to the reaction mixture (0.75 mL, 1.75 mmol). After complete addition of the Grignard reagent, the mixture was stirred for an additional 30 min at rt. THF was then evaporated under reduced pressure at rt to provide black nanomaterial as a powder. The Fe nanoparticles obtained were dried under reduced pressure at rt for 3 h yielding 0.75 g Fe/ppm Pd NPs nanoparticles. The nanoparticles need to be stored under argon in a glovebox. The material was used as such for subsequent reactions under micellar conditions.

STEM (BF and HADDF) for Fe/ppm Pd/Cy-cBRIDP nanoparticles

Fe/ppm Pd/Cy-cBRIDP nanoparticles dry powder

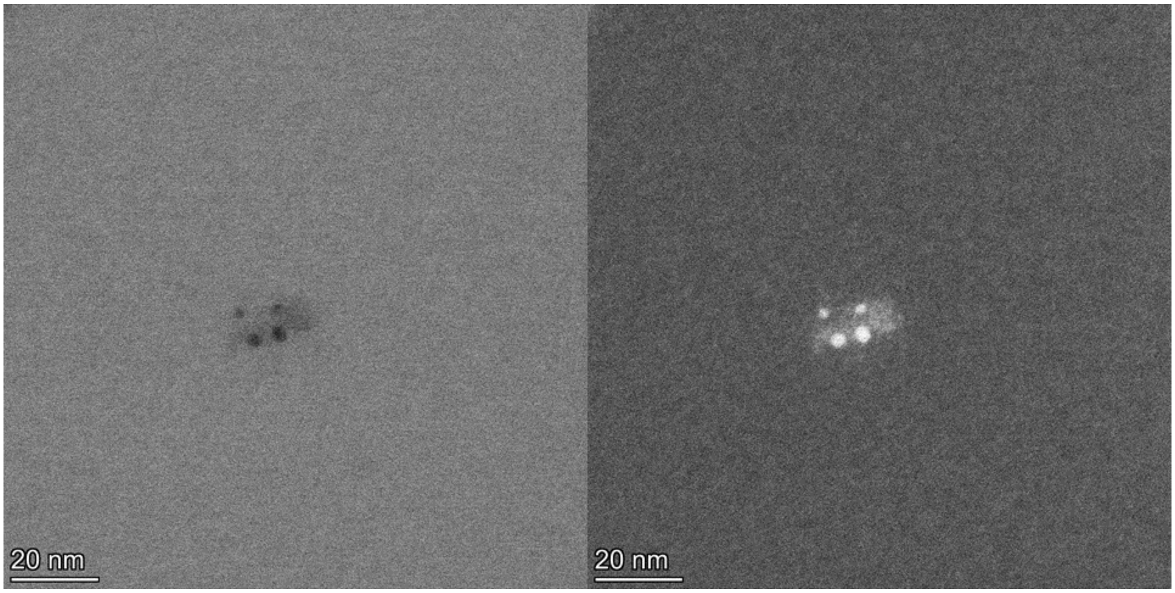

Fe/ppm Pd/Cy-cBRIDP nanoparticles in pure degassed H_2O before reaction

The nanomaterial (2 mg) was added to a vial in the glove box, and the vial was covered with a septum. 2 mL pure degassed H_2O was inserted to the vial by a syringe and the mixture was stirred for 1 h.

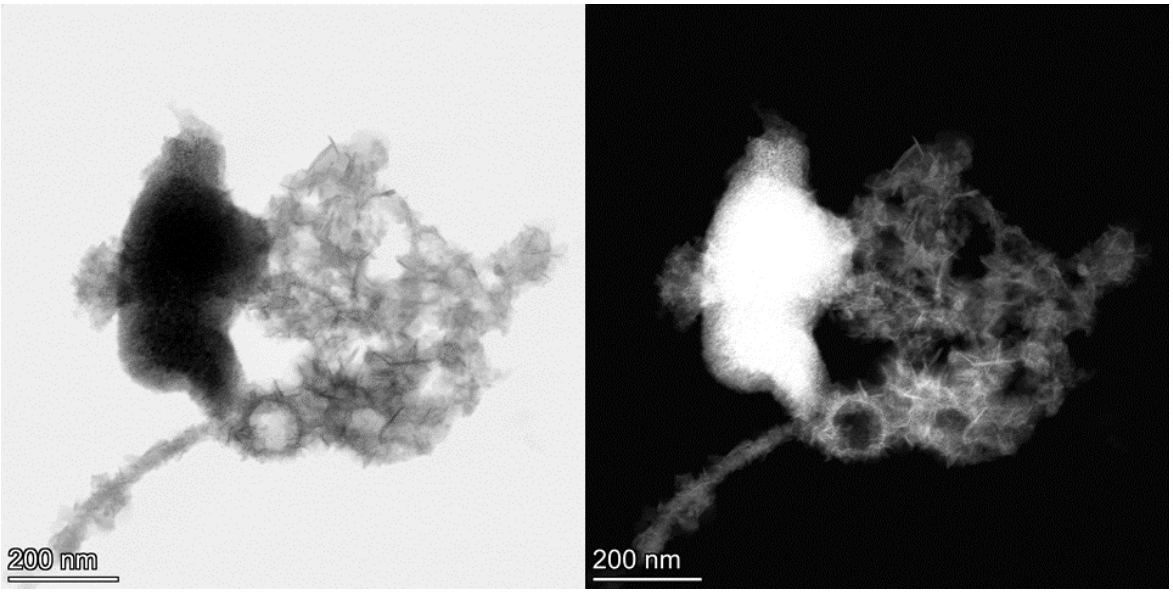

Fe/ppm Pd nanoparticles/Cy-cBRIDP in 2 wt % TPGS-750-M/H_2O before reaction

The nanomaterial (2 mg) was added to a vial in the glove box, and the vial was covered with a septum. TPGS-750-M/H_2O (2 mL, 2 wt %) was inserted to the vial by a syringe and the mixture was stirred for 1 h.

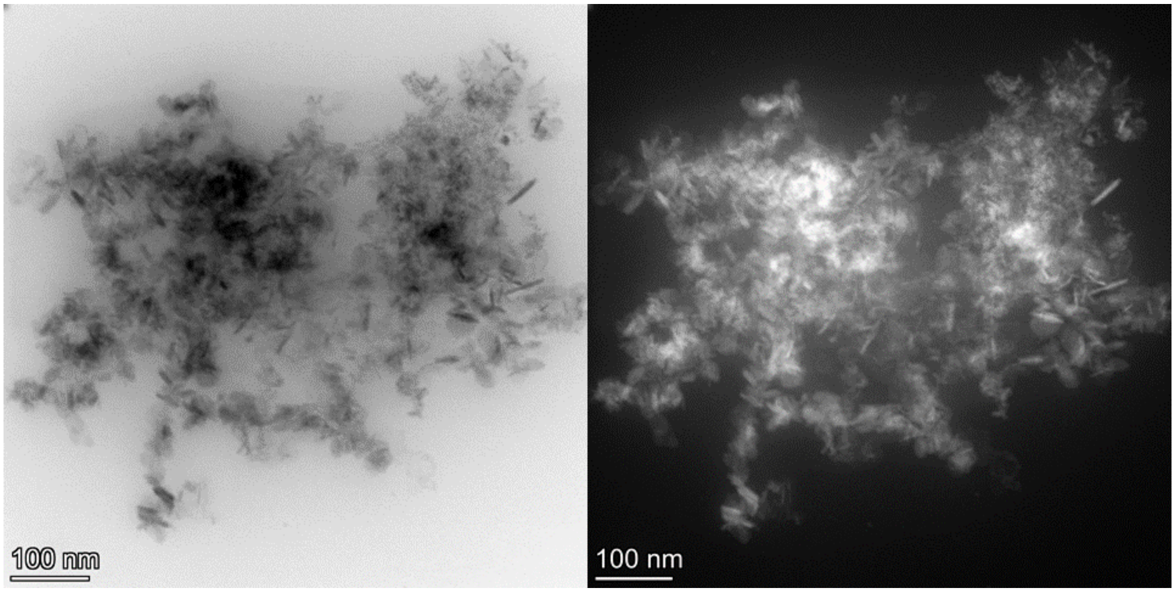

General Procedure for HM reaction

To an oven dried 4 mL microwave vial, NaCl (70.2 mg, 1.2 mmol), K_3PO_4 (127.2 mg, 0.6 mmol), iodide (0.2 mmol, 1 equivalent), alkene (0.4 mmol, 2 equivalents) and Fe/ppm Pd NPs (12.5 mg) were added in a glovebox. The vial was capped with a septum and removed from the glovebox. Through the septum, 0.4 mL aqueous solution of 2 wt % TPGS-750-M was added followed by sequential addition of 0.04 mL DMF via syringe. The mixture was vigorously stirred at 45 °C for 16 h. The progress of the reaction was monitored by TLC. After complete consumption of starting material, the septum was removed. Minimal EtOAc was added, and the mixture was stirred *gently* for 1 min. Stirring was stopped and the organic layer was then allowed to separate, after which it was removed via pipette. The same extraction procedure was repeated, and the combined organic extracts were dried over anhydrous Na_2SO_4. Volatiles were evaporated under reduced pressure and semi-pure product was purified by flash chromatography over silica gel.

Control experiments for Fe/ppm Pd NPs in HM reaction

Procedure for entry 1:

1-Iodo-4-methoxybenzene (46.8 mg, 0.2 mmol, 1 equivalent), K_3PO_4 (127.2 mg, 0.6 mmol), and NaCl (70.2 mg, 1.2 mmol) were added to the vial followed by sequential addition of optimized Fe/ppm NPs (5 mg) in a glovebox. The reaction vial was closed with a septum under an argon atmosphere. TPGS-750-M/H_2O (2 wt %, 0.4 mL) and *t*-butyl acrylate (51.3 mg, 0.4 mmol, 2 equiv) were added to the vial by syringe insertion and the mixture was stirred vigorously at rt for 16 hours, after which the mixture was extracted with EtOAc and purified by flash chromatography over silica gel yielding 46.4 mg (99%) of *t*-butyl (*E*)-3-(4-methoxyphenyl)acrylate.

Procedure for entry 2:

1-Iodo-4-methoxybenzene (46.8 mg, 0.2 mmol, 1 equiv), K_3PO_4 (127.2 mg, 0.6 mmol), and NaCl (70.2 mg, 1.2 mmol) were added to the vial followed by sequential addition of optimized Fe/ppm NPs (5 mg) in the glovebox. The reaction vial was covered with a septum under an argon atmosphere. THF (0.4 mL) and *t*-butyl acrylate (51.3 mg, 0.4 mmol, 2 equiv) were added to the vial by syringe insertion and the mixture was stirred vigorously at rt for 16 h, after which the mixture was extracted by EtOAc and purified by flash chromatography over silica gel only yielding 4.3 mg (9%) of *t*-butyl (*E*)-3-(4-methoxyphenyl)acrylate.

Procedure for entry 3:

1-Iodo-4-methoxybenzene (46.8 mg, 0.2 mmol, 1 equiv), K_3PO_4 (127.2 mg, 0.6 mmol), and NaCl (70.2 mg, 1.2 mmol) were added to the vial followed by sequential addition of optimized Fe/ppm NPs (5 mg) in the glovebox. The reaction vial was closed with a septum under an argon atmosphere. DMF (0.4 mL) and *t*-butyl acrylate (51.3 mg, 0.4 mmol, 2 equiv) was added to the vial by syringe insertion and the mixture was stirred vigorously at rt for 16 h, after which the mixture was extracted by EtOAc and purified by flash chromatography over silica gel yielding 19.2 mg (41%) of *t*-butyl (*E*)-3-(4-methoxyphenyl)acrylate.

Procedure for entry 4:

1-Iodo-4-methoxybenzene (46.8 mg, 0.2 mmol, 1 equivalent), K_3PO_4 (127.2 mg, 0.6 mmol), and NaCl (70.2 mg, 1.2 mmol) were added to the vial followed by sequential addition of optimized Fe/ppm NPs (5 mg) in the glovebox. The reaction vial was closed with a septum under an argon atmosphere. Pure water (0.4 mL) and *t*-butyl acrylate (51.3 mg, 0.4 mmol, 2 equiv) were added to the vial by syringe insertion and the mixture was stirred vigorously at rt for 16 h, after which the mixture was extracted by EtOAc and purified by flash chromatography over silica gel yielding 31.8 mg (68%) of *t*-butyl (*E*)-3-(4-methoxyphenyl)acrylate.

Procedure for entry 5:

The optimized Fe/ppm NPs (5 mg) was added to a vial in the glovebox. The vial was capped with a septum and removed from the glovebox. Through the septum, 0.4 mL pure degassed water was added and the medium was stirred for 1 h. The mixture was centrifuged and the reaction medium was withdrawn via syringe. 1-Iodo-4-methoxybenzene (46.8 mg, 0.2 mmol, 1 equiv), K_3PO_4 (127.2 mg, 0.6 mmol), and NaCl (70.2 mg, 1.2 mmol) were added to the vial and the vial was capped with a septum. The vial was evacuated and replaced with argon three times. TPGS-750-M/H_2O (2 wt %, 0.4 mL) and *t*-butyl acrylate (51.3 mg, 0.4 mmol, 2 equiv) were added to the vial by syringe and the mixture was stirred vigorously at rt for 16 h, after which the mixture was extracted by EtOAc and purified by flash chromatography over silica gel yielding 36.6 mg (78%) of *t*-butyl (*E*)-3-(4-methoxyphenyl)acrylate.

Procedure for entry 6:

The optimized Fe/ppm NPs (5 mg) was added to a vial in the glovebox. The vial was capped with a septum and removed from the glovebox. Through the septum, 0.4 mL pure degassed water was added and the medium was stirred for 1 h. The mixture was centrifuged and the reaction medium was withdrawn via syringe. 1-Iodo-4-methoxybenzene (46.8 mg, 0.2 mmol, 1 equiv), K_3PO_4 (127.2 mg, 0.6 mmol), and NaCl (70.2 mg, 1.2 mmol) were added to the vial and the vial was capped by septum. The vial was evacuated and replaced with argon three times. TPGS-750-M/H_2O (2 wt %, 0.4 mL), *t*-butyl acrylate (51.3 mg, 0.4 mmol, 2 equivalents) and *t*-Bu_3P THF solution (0.04 mL, 0.019 M) was added to the vial by syringe insertion and the mixture was stirred vigorously at rt for 16 h after which the mixture was extracted by EtOAc and purified by flash chromatography over silica gel yielding 44.5 mg (95%) of *t*-butyl (*E*)-3-(4-methoxyphenyl)acrylate.

Procedure for entry 7:

The optimized Fe/ppm NPs (5 mg) was added to a vial in the glovebox. The vial was capped with a septum and removed from the glovebox. Through the septum, 0.4 mL pure degassed water was added and the medium was stirred for 1 h. The mixture was centrifuged and the reaction medium was withdrawn via syringe. 1-Iodo-4-methoxybenzene (46.8 mg, 0.2 mmol, 1 equiv), K_3PO_4 (127.2 mg, 0.6 mmol), and NaCl (70.2 mg, 1.2 mmol) were added to the vial and the vial was capped with a septum. The vial was evacuated and replaced with argon three times. The reaction medium in the syringe was added back to the vial by syringe, followed by sequential addition of *t*-butyl acrylate (51.3 mg, 0.4 mmol, 2 equiv) and the mixture was stirred vigorously at rt for 16 h, after which the mixture was extracted by EtOAc and purified by flash chromatography over silica gel yielding 43.2 mg (92%) of *t*-butyl (*E*)-3-(4-methoxyphenyl)acrylate.

E Factor, residual palladium, and recycling reaction

E Factor

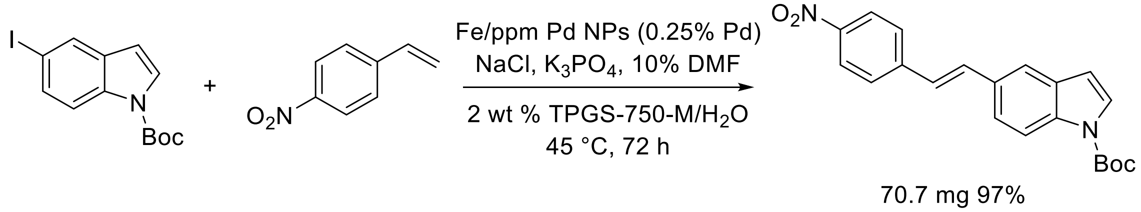

To an oven dried 4 mL microwave vial, NaCl (70.2 mg, 1.2 mmol), K_3PO_4 (127.2 mg, 0.6 mmol), *t*-butyl 5-iodo-1H-indole-1-carboxylate (68.6 mg, 0.2 mmol), 1-nitro-4-vinylbenzene (35.8 mg, 0.24 mmol) and Fe/ppm Pd NPs (12.5 mg) were added in a glovebox. The vial was capped with a septum and removed from the glovebox. Through the septum, 0.4 mL aqueous solution of 2 wt % TPGS-750-M was added followed by sequential addition of 0.04 mL DMF via syringe. The mixture was vigorously stirred at 45 °C for 72 h. The progress of the reaction was monitored by TLC. After complete consumption of starting material, the septum was removed and the reaction mixture was then transferred to a short pipette blocked with cotton. The solid in the pipette was washed with 1 mL DI water and air-dried to dryness to give 70.7 mg (97%) crude *t*-butyl (*E*)-5-(4-nitrostyryl)-1H-indole-1-carboxylate as a yellow solid.

^{1}H NMR (500 MHz, $CDCl_3$) δ 8.22 (d, *J* = 8.4 Hz, 2H), 8.16 (d, *J* = 8.5 Hz, 1H), 7.72 (s, 1H), 7.63 (d, *J* = 8.6 Hz, 3H), 7.54 (d, *J* = 8.5 Hz, 1H), 7.37 (d, *J* = 16.3 Hz, 1H), 7.15 (d, *J* = 16.2 Hz, 1H), 6.64 – 6.56 (m, 1H), 1.69 (s, 9H).

^{13}C NMR (126 MHz, $CDCl_3$) δ 149.66, 146.67, 144.39, 134.04, 131.21, 131.09, 127.00, 126.77, 125.19, 124.31, 123.27, 120.13, 115.69, 107.52, 84.19, 28.35.

HRMS(CI): Calcd. for $C_{16}H_{12}N_2O_2H$ $[M+H]^+$ 265.0977. Found: 265.0988.

E Factor calculation:

$$\text{E Factor (without water)} = \frac{\text{Mass of organic waste}}{\text{Mass of product}} = \frac{\text{Mass of DMF + Mass of excess styrene}}{\text{Mass of product}}$$

$$= \frac{0.04\ \text{mL} \times 944\ \text{mg/mL} + 0.04\ \text{mmol} \times 149.15\ \text{mg/mmol}}{70.7\ \text{mg}} = 0.62$$

$$\text{E Factor (with water)} = \frac{\text{Mass of organic waste + Mass of water}}{\text{Mass of product}}$$

$$= \frac{\text{Mass of DMF + Mass of excess styrene + Mass of water}}{\text{Mass of product}}$$

$$= \frac{0.04\ \text{mL} \times 944\ \text{mg/mL} + 0.04\ \text{mmol} \times 149.15\ \text{mg/mmol} + 0.4\ \text{mL} \times 1000\ \text{mg/mL}}{70.7\ \text{mg}} = 6.3$$

Density of DMF: 0.944 g/mL

Residual palladium as measured by ICP-MS

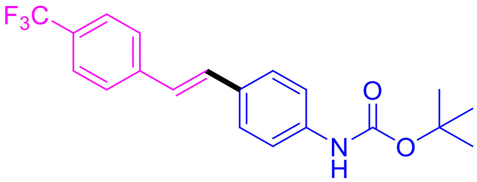

t-Butyl (4-iodophenyl)carbamate (63.8 mg, 0.2 mmol), K_3PO_4 (127.4 mg, 0.6 mmol) and NaCl (70.2 mg, 1.2 mmol) were added to a vial followed by sequential addition of optimized Fe/ppm NPs (12.5 mg, 0.25% Pd) in a glovebox. The reaction vial was covered with a septum under an argon atmosphere. An aqueous solution of 2 wt % TPGS-750-M (0.4 mL), 1-(trifluoromethyl)-4-vinylbenzene (68.9 mg, 0.4 mmol) and 0.04 mL DMF was added to the vial via syringe insertion and the mixture was stirred vigorously at 45 °C for 16 h. Subsequently, argon degassed MTBE (0.3 mL × 3) was injected to the vial by syringe to extract the resulting mixture. The organic layer was then separated (with the aid of a centrifuge) and combined, after which the volatiles were removed under reduced pressure and purified by flash chromatography with pre-packed 100-gram KP-Sil Biotage$^{\Theta}$ SNAP Cartridges on the Biotage$^{\Theta}$ Isolera Prime autocolumn to obtain *t*-butyl (*E*)-(4-(4-(trifluoromethyl)styryl)phenyl)carbamate (HP-HEK-289) (69.8 mg, 96%). The product was sealed in a 4 mL vial and sent to the UC Center for Environmental Implications of Nanotechnology at the University of California, Los Angeles, to get ICP-MS analyses.

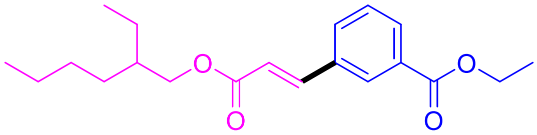

Ethyl 3-iodobenzoate (52.2 mg, 0.2 mmol), K_3PO_4 (127.4 mg, 0.6 mmol) and NaCl (70.2 mg, 1.2 mmol) were added to a vial followed by sequential addition of optimized Fe/ppm NPs (5 mg, 0.1% Pd) in the glovebox. The reaction vial was covered with a septum under an argon atmosphere. An aqueous solution of 2 wt % TPGS-750-M (0.4 mL), 2-ethylhexyl acrylate (73.7 mg, 0.4 mmol) and 0.04 mL DMF was added to the vial by syringe and the mixture was stirred vigorously at 45 °C for 16 h. Subsequently, argon degassed MTBE (0.3 mL × 3) was injected to the vial by syringe to extract the resulting mixture. The organic layer was then separated (with the aid of centrifuge) and combined, after which the volatiles were removed under reduced pressure and purified by flash chromatography with pre-packed 100-gram KP-Sil Biotage$^{\Theta}$ SNAP Cartridges on the Biotage$^{\Theta}$ Isolera Prime autocolumn to obtain ethyl (*E*)-3-(3-((2-ethylhexyl)oxy)-3-oxoprop-1-en-1-yl)benzoate (HP-HEK-291) (66.5 mg, 100%). The product was sealed in a 4 mL vial and sent to the UC Center for Environmental Implications of Nanotechnology at the University of California, Los Angeles, to get ICP-MS analyses.

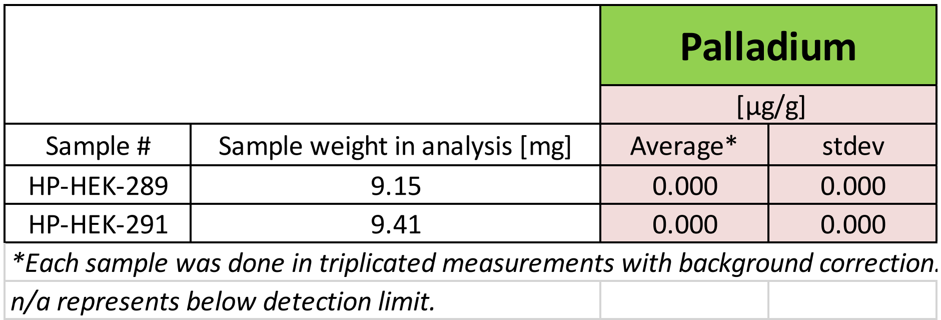

		Palladium	
		[μg/g]	
Sample #	Sample weight in analysis [mg]	Average*	stdev
HP-HEK-289	9.15	0.000	0.000
HP-HEK-291	9.41	0.000	0.000

**Each sample was done in triplicated measurements with background correction.*

n/a represents below detection limit.

Recycling reaction

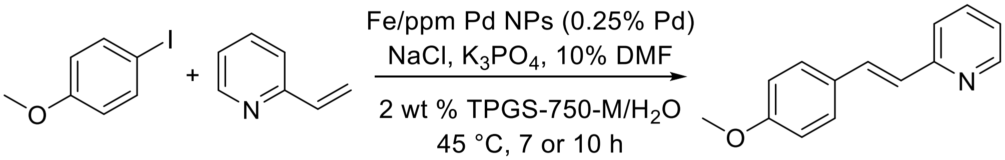

Initial reaction:

1-Iodo-4-methoxybenzene (46.8 mg, 0.2 mmol, 1 equiv), K_3PO_4 (63.6 g, 0.3 mmol) and NaCl (70.2 mg, 1.2 mmol) were added to the vial followed by sequential addition of optimized Fe/ppm NPs (12.5 mg, 0.25% Pd) in the glovebox. The reaction vial was covered with a septum under an argon atmosphere. An aqueous solution of 2 wt % TPGS-750-M (0.4 mL), 2-vinylpyridine (42 mg, 0.4 mmol) and 0.04 mL DMF was added to the vial via syringe and the mixture was stirred vigorously at 45 °C for 7 h. Subsequently, argon degassed MTBE (0.3 mL × 3) was injected to the vial by syringe to extract the resulting mixture. The organic layer was then separated (with the aid of centrifuge) and combined, after which the volatiles were removed under reduced pressure and purified by flash chromatography over silica gel with EtOAc/hexanes: 90/10 to obtain (*E*)-2-(4-methoxystyryl)pyridine. (39.3 mg, 0.186 mmol, 93%).

1st recycle:

To another vial was added 1-iodo-4-methoxybenzene (46.8 mg, 0.2 mmol, 1 equiv), K_3PO_4 (0.30 mmol, 1.5 equivalents) and nanoparticles (12.5 mg, 0.25% Pd) in a glovebox. The vial was covered with a septum under an argon atmosphere. To this was then added the prior 2 wt % TPGS-750-M by cannulation. 2-Vinylpyridine (42 mg, 0.4 mmol) and 0.04 mL DMF were added to the vial by syringe insertion and the mixture was stirred vigorously at 45 °C for 10 h. Subsequently, argon degassed MTBE (0.3 mL × 3) was injected to the vial by syringe to extract the resulting mixture. The organic layer was then separated (with the aid of centrifuge) and combined, after which the volatiles were removed under reduced pressure and purified by flash chromatography over silica gel with EtOAc/hexanes: 90/10 to obtain (*E*)-2-(4-methoxystyryl)pyridine. (38.9 mg, 0.184 mmol, 92%).

2nd recycle:

To another vial was added 1-iodo-4-methoxybenzene (46.8 mg, 0.2 mmol, 1 equiv), K_3PO_4 (0.30 mmol, 1.5 equivalents) and nanoparticles (12.5 mg, 0.25% Pd) in a glovebox. The vial was covered with a septum under an argon atmosphere. To this was added the prior 2 wt % TPGS-750-M by cannulation. 2-Vinylpyridine (42 mg, 0.4 mmol) and 0.04 mL DMF were added to the vial by syringe insertion and the mixture was stirred vigorously at 45 °C for 10 h. Subsequently, argon degassed MTBE (0.3 mL × 3) was injected to the vial by syringe to extract the resulting mixture. The organic layer was then separated (with the aid of centrifuge) and combined, after which the volatiles were removed under reduced pressure and purified by flash chromatography over silica gel with EtOAc/hexanes: 90/10 to obtain (*E*)-2-(4-methoxystyryl)pyridine. (39.7 mg, 0.188 mmol, 94%).

3rd recycle:

To another vial was added 1-iodo-4-methoxybenzene (46.8 mg, 0.2 mmol, 1 equiv), K_3PO_4 (0.30 mmol, 1.5 equivalents) and nanoparticles (12.5 mg, 0.25% Pd) in the glovebox. The vial was closed with a septum under an argon atmosphere. And then it was added the prior 2 wt % TPGS-750-M by cannulation. 2-Vinylpyridine (42 mg, 0.4 mmol) and 0.04 mL DMF were added to the vial by syringe insertion and the mixture was stirred vigorously at

45 °C for 10 h. Subsequently, argon degassed MTBE (0.3 mL × 3) was injected to the vial by syringe to extract the resulting mixture. The organic layer was then separated (with the aid of centrifuge) and combined, after which the volatiles were removed under reduced pressure and purified by flash chromatography over silica gel with EtOAc/hexanes: 90/10 to obtain (*E*)-2-(4-methoxystyryl)pyridine. (38.0 mg, 0.18 mmol, 90%).

Scale-up reaction

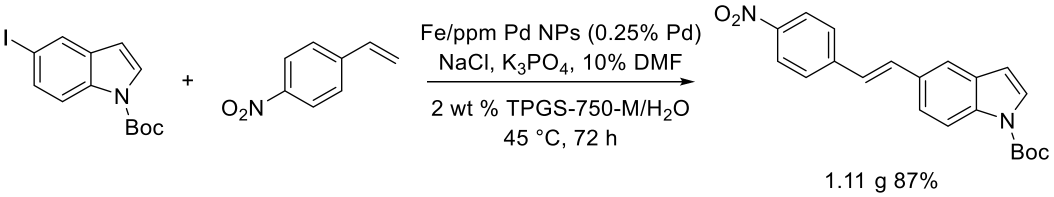

To an oven dried 25 mL round bottom flask, NaCl (1.23 mg, 21 mmol), K_3PO_4 (2.22 mg, 10.5 mmol), *t*-butyl 5-iodo-1H-indole-1-carboxylate (1.2 g, 3.5 mmol), 1-nitro-4-vinylbenzene (626.2 mg, 4.2 mmol) and Fe/ppm Pd NPs (219 mg) were added in a glovebox. The flask was capped with a septum and removed from the glovebox. Through the septum, 7 mL aqueous solution of 2 wt % TPGS-750-M was added followed by sequential addition of 0.7 mL DMF via syringe. The mixture was vigorously stirred at 45 °C for 72 h. The progress of the reaction was monitored by TLC. After complete consumption of starting material, the septum was removed and the reaction mixture was then filtered by a fritted filter. The solid in the filter was collected was purified by flash chromatography over silica gel yielding 1.11 g (87%) of *t*-butyl (*E*)-5-(4-nitrostyryl)-1H-indole-1-carboxylate as a yellow solid (hexane/EtOAc : 90/10).

1-Pot sequence of reactions

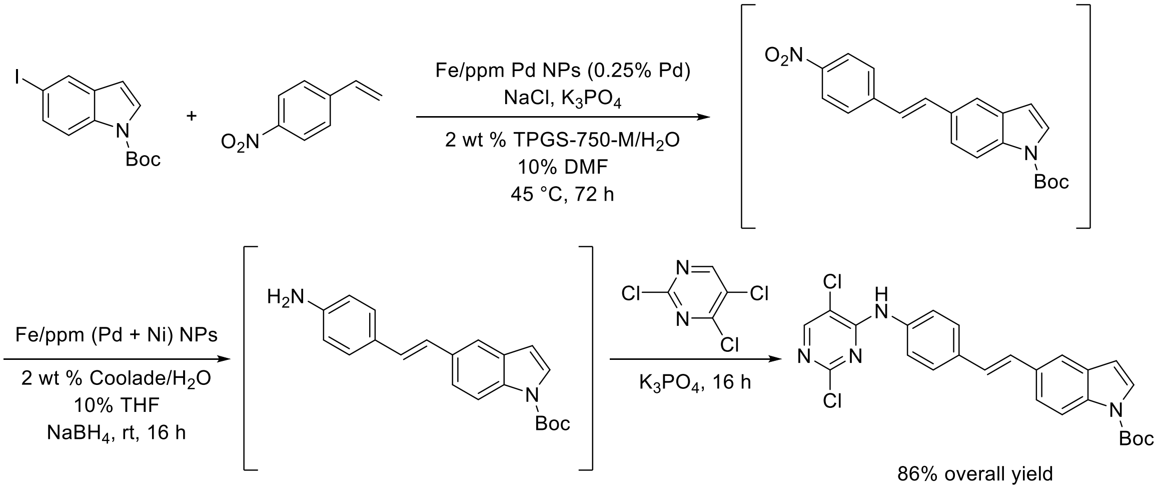

To an oven dried 4 mL microwave vial, NaCl (70.2 mg, 1.2 mmol), K_3PO_4 (127.2 mg, 0.6 mmol), *t*-butyl 5-iodo-1H-indole-1-carboxylate (68.6 mg, 0.2 mmol), 1-nitro-4-vinylbenzene (35.8 mg, 0.24 mmol) and Fe/ppm Pd NPs (12.5 mg) were added in the glovebox. The vial was capped with a septum and removed from the glovebox. Through the septum, 0.4 mL aqueous solution of 2 wt % TPGS-750-M was added followed by sequential addition of 0.04 mL DMF via syringe. The mixture was vigorously stirred at 45 °C for 72 h. The progress of the reaction was monitored by TLC.

After complete consumption of starting material, the septum was removed and $NaBH_4$ (45.2 mg, 1.2 mmol) and 0.1 mL THF were added. In another 4 mL microwave vial, Fe/ppm (Pd+Ni) NPs (6 mg), Coolade/H_2O (0.2 mL, 2 wt %), and 5 mg $NaBH_4$ were added. The black suspension was transferred to the reaction vial by pipette. Coolade/H_2O (2×0.2 mL, 2 wt %) was used to wash the vial and combine the suspension into the reaction vial. The reaction vial was capped and the mixture was vigorously stirred at rt for 16 h.

After 16 h, the cap was removed and concentrated HCl was used to neutralize the solution. After the pH reached 7, 2,4,5-trichloropyrimidine (55.1 mg, 0.3 mmol) and K_3PO_4 (51 mg, 0.24 mmol) were added to this reaction vial. The reaction vial was capped and the mixture was vigorously stirred at rt for 16 h. Then the cap was removed and minimal EtOAc was added, and the mixture was stirred *gently* for 1 min. Stirring was stopped and the organic layer was then allowed to separate, after which it was removed via pipette. The same extraction procedure was repeated, and the combined organic extracts were dried over anhydrous Na_2SO_4. Volatiles were evaporated under reduced pressure and semi-pure product was purified by flash chromatography over silica gel yielding *t*-butyl (*E*)-5-(4-((2,5-dichlorophenyl)amino)styryl)-1H-indole-1-carboxylate (82.7 mg, 86%) as a white solid (hexane/EtOAc : 80:20).

^{1}H NMR (500 MHz, $CDCl_3$) δ 8.18 (s, 1H), 8.12 (d, *J* = 7.2 Hz, 1H), 7.74 – 7.57 (m, 4H), 7.52 (dd, *J* = 15.0, 8.6 Hz, 3H), 7.27 (s, 1H), 7.17 (d, *J* = 16.3 Hz, 1H), 7.08 (d, *J* = 16.3 Hz, 1H), 6.57 (d, *J* = 3.6 Hz, 1H), 1.69 (s, 9H).

^{13}C NMR (126 MHz, $CDCl_3$) δ 158.35, 156.25, 154.65, 149.74, 135.96, 134.93, 134.69, 132.12, 131.13, 129.12, 127.14, 126.64, 126.60, 122.91, 121.25, 119.23, 115.44, 113.88, 107.52, 83.93, 28.33.

HRMS(ESI): Calcd. for $C_{25}H_{22}Cl_2N_4O_2Na$ $[M+Na]^+$ 503.1017. Found: 503.1024.

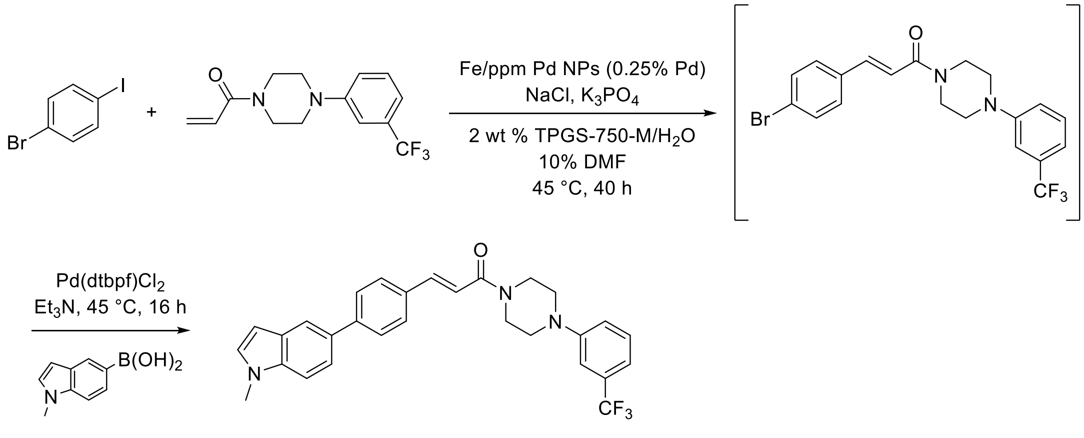

82% overall yield

To an oven dried 4 mL microwave vial, NaCl (70.2 mg, 1.2 mmol), K_3PO_4 (127.2 mg, 0.6 mmol), 1-bromo-4-iodobenzene (56.6 mg, 0.2 mmol), 1-(4-(3-

(trifluoromethyl)phenyl)piperazin-1-yl)prop-2-en-1-one (56.8 mg, 0.2 mmol) and Fe/ppm Pd NPs (12.5 mg) were added in a glovebox. The vial was capped with a septum and removed from the glovebox. Through the septum, 0.4 mL aqueous solution of 2 wt % TPGS-750-M was added followed by sequential addition of 0.04 mL DMF via syringe. The mixture was vigorously stirred at 45 °C for 40 h. Progress of the reaction was monitored by TLC.

After complete consumption of starting material, the septum was removed and concentrated HCl was used to neutralize the solution. After the pH reached 7, (1-methyl-1H-indol-5-yl)boronic acid (52.5 mg, 0.3 mmol), Pd(dtbpf)Cl_2 (3.9 mg, 0.006 mmol) and Et_3N (60.7 mg, 0.6 mmol) were added to this reaction vial. The reaction vial was capped and the mixture was vigorously stirred at 45 °C for 16 h. Then the cap was removed and minimal EtOAc was added, and the mixture was stirred *gently* for 1 min. Stirring was stopped and the organic layer was then allowed to separate, after which it was removed via pipette. The same extraction procedure was repeated, and the combined organic extracts were dried over anhydrous Na_2SO_4. Volatiles were evaporated under reduced pressure and semi-pure product was purified by flash chromatography over silica gel yielding (*E*)-3-(4-(1-methyl-1H-indol-5-yl)phenyl)-1-(4-(3-(trifluoromethyl)phenyl)piperazin-1-yl)prop-2-en-1-one (80.2 mg, 82%) as a white solid (hexane/EtOAc : 50:50).

^{1}H NMR (500 MHz, $CDCl_3$) δ 7.91 (s, 1H), 7.82 (d, *J* = 15.3 Hz, 1H), 7.71 (d, *J* = 8.1 Hz, 2H), 7.63 (d, *J* = 8.1 Hz, 2H), 7.52 (d, *J* = 8.5 Hz, 1H), 7.43 – 7.35 (m, 2H), 7.19 – 7.13 (m, 2H), 7.11 – 7.04 (m, 2H), 6.95 (d, *J* = 15.4 Hz, 1H), 6.57 (d, *J* = 2.6 Hz, 1H), 4.02 – 3.76 (m, 7H), 3.34 – 3.18 (m, 4H).

^{13}C NMR (126 MHz, $CDCl_3$) δ 165.68, 151.04, 144.07, 143.16, 136.54, 133.05, 131.70, 131.65 (q, $^1J_{(C\text{-}F)}$ = 31.5 Hz), 129.76, 129.06, 128.33, 127.56, 125.40 (q, $^1J_{(C\text{-}F)}$ = 273.4 Hz), 121.09, 119.37, 119.23, 116.55 (q, $^1J_{(C\text{-}F)}$ = 3.8 Hz), 115.85, 112.62 (q, $^1J_{(C\text{-}F)}$ = 3.8 Hz), 109.67, 101.50, 49.09, 48.86 (br), 45.49 (br), 41.89 (br), 32.92.

^{19}F NMR (376 MHz, $CDCl_3$) δ -62.52.

HRMS(ESI): Calcd. for $C_{29}H_{26}F_3N_3ONa$ $[M+Na]^+$ 512.1926. Found: 512.1929.

Analytical data for products

_t_-Butyl (_E_)-3-(4-methoxyphenyl)acrylate (1)

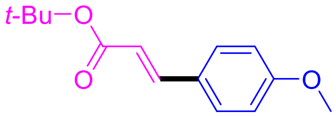

1-Iodo-4-methoxybenzene (46.8 mg, 0.2 mmol), *t*-butyl acrylate (51.3 mg, 0.4 mmol), NaCl (70.2 mg, 1.2 mmol), K_3PO_4 (127.4 mg, 0.6 mmol) and Fe/ppm Pd NPs (5 mg, 0.1% Pd), in 0.4 mL 2 wt % TPGS-750-M/H_2O were reacted at rt for 16 hours yielding 46.4 mg (99%) of *t*-butyl (*E*)-3-(4-methoxyphenyl)acrylate as a yellow oil (hexane/EtOAc : 90/10).

Spectral data matched to the reported in literature.[3] ^{1}H NMR (500 MHz, $CDCl_3$) δ 7.54 (d, *J* = 15.9 Hz, 1H), 7.45 (d, *J* = 8.7 Hz, 2H), 6.89 (d, *J* = 8.8 Hz, 2H), 6.24 (d, *J* = 15.9 Hz, 1H), 3.83 (s, 3H), 1.53 (s, 9H).

^{13}C NMR (126 MHz, $CDCl_3$) δ 166.80, 161.26, 143.32, 129.67, 127.56, 117.87, 114.39, 80.35, 55.48, 28.38.

GC-MS, *m/z*: 234 $[M^+]$.

Butyl (_E_)-3-(3-acetylphenyl)acrylate (2)

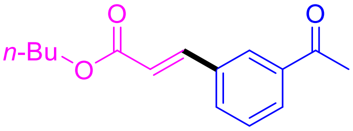

1-(3-Iodophenyl)ethan-1-one (49.2 mg, 0.2 mmol), *n*-butyl acrylate (51.3 mg, 0.4 mmol), NaCl (70.2 mg, 1.2 mmol), K_3PO_4 (127.4 mg, 0.6 mmol) and Fe/ppm Pd NPs (12.5 mg, 0.25% Pd), in 0.4 mL 2 wt % TPGS-750-M/H_2O were reacted at rt for 16 h yielding 46.3 mg (94%) of butyl (*E*)-3-(3-acetylphenyl)acrylate as a faint yellow oil (hexane/EtOAc : 90/10).

^{1}H NMR (500 MHz, $CDCl_3$) δ 8.07 (s, 1H), 7.92 (d, *J* = 7.8 Hz, 1H), 7.71 – 7.62 (m, 2H), 7.46 (t, *J* = 7.7 Hz, 1H), 6.49 (d, *J* = 16.1 Hz, 1H), 4.19 (t, *J* = 6.7 Hz, 2H), 2.60 (s, 3H), 1.67 (dt, *J* = 14.5, 6.7 Hz, 2H), 1.45 – 1.39 (m, 2H), 0.94 (t, *J* = 7.4 Hz, 3H).

^{13}C NMR (126 MHz, $CDCl_3$) δ 197.45, 166.72, 143.36, 137.75, 135.07, 132.22, 129.83, 129.27, 127.75, 119.81, 64.64, 30.82, 26.71, 19.26, 13.80.

HRMS(ESI): Calcd. for $C_{15}H_{18}O_3Na$ $[M+Na]^+$ 301.1416. Found: 301.1420.

(*E*)-2-(4-Methoxystyryl)pyridine (3)

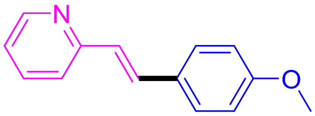

1-Iodo-4-methoxybenzene (46.8 mg, 0.2 mmol), 2-vinylpyridine (42 mg, 0.4 mmol), NaCl (70.2 mg, 1.2 mmol), K_3PO_4 (127.4 mg, 0.6 mmol) and Fe/ppm Pd NPs (12.5 mg, 0.25% Pd), in 0.4 mL 2 wt % TPGS-750-M/H_2O with DMF (0.04 mL) as co-solvent were reacted at 45 °C for 16 h yielding 41.8 mg (99%) of (*E*)-2-(4-methoxystyryl)pyridine as a yellow solid (hexane/EtOAc : 80/20).

Spectral data matched that reported in the literature.[4] ^{1}H NMR (500 MHz, $CDCl_3$) δ 8.57 (d, *J* = 4.2 Hz, 1H), 7.65 – 7.55 (m, 2H), 7.51 (d, *J* = 8.7 Hz, 2H), 7.32 (d, *J* = 7.9 Hz, 1H), 7.12 – 7.06 (m, 1H), 7.03 (d, *J* = 16.1 Hz, 1H), 6.90 (d, *J* = 8.7 Hz, 2H), 3.80 (s, 3H).

^{13}C NMR (126 MHz, $CDCl_3$) δ 159.93, 156.01, 149.63, 136.51, 132.33, 129.49, 128.49, 125.89, 121.82, 121.71, 114.25, 55.35.

GC-MS, *m/z*: 211 $[M^+]$.

Ethyl (*E*)-3-(3-((2-ethylhexyl)oxy)-3-oxoprop-1-en-1-yl)benzoate (4)

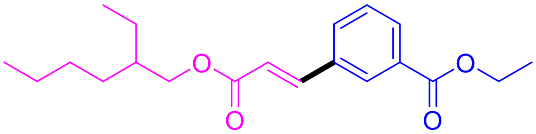

Ethyl 3-iodobenzoate (52.2 mg, 0.2 mmol), 2-ethylhexyl acrylate (73.7 mg, 0.4 mmol), NaCl (70.2 mg, 1.2 mmol), K_3PO_4 (127.4 mg, 0.6 mmol) and Fe/ppm Pd NPs (5 mg, 0.1% Pd), in 0.4 mL 2 wt % TPGS-750-M/H_2O with DMF (0.04 mL) as co-solvent were reacted at 45 °C for 16 h yielding 66.5 mg (100%) of ethyl (*E*)-3-(3-((2-ethylhexyl)oxy)-3-oxoprop-1-en-1-yl)benzoate as a colorless oil (hexane/EtOAc : 90/10).

^{1}H NMR (500 MHz, $CDCl_3$) δ 8.19 (s, 1H), 8.02 (d, *J* = 7.7 Hz, 1H), 7.73 – 7.63 (m, 2H), 7.44 (t, *J* = 7.8 Hz, 1H), 6.50 (d, *J* = 16.0 Hz, 1H), 4.38 (q, *J* = 7.1 Hz, 2H), 4.17 – 4.07 (m, 2H), 1.64 (p, *J* = 6.1 Hz, 1H), 1.42 – 1.27 (m, 11H), 0.93 – 0.87 (m, 6H).

^{13}C NMR (126 MHz, $CDCl_3$) δ 166.90, 166.03, 143.38, 134.87, 132.15, 131.34, 131.04, 129.01, 129.00, 119.69, 67.17, 61.32, 38.96, 30.55, 29.05, 23.93, 23.07, 14.40, 14.14, 11.11.

HRMS(ESI): Calcd. for $C_{20}H_{28}O_4Na$ $[M+Na]^+$ 387.2148. Found: 387.2145.

t-Butyl (E)-3-(3,4-dichlorophenyl)acrylate (5)

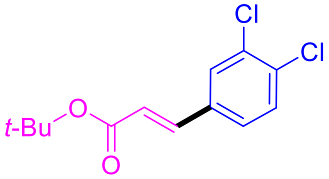

1,2-Dichloro-4-iodobenzene (54.6 mg, 0.2 mmol), *t*-butyl acrylate (51.3 mg, 0.4 mmol), NaCl (70.2 mg, 1.2 mmol), K_3PO_4 (127.4 mg, 0.6 mmol) and Fe/ppm Pd NPs (12.5 mg, 0.25% Pd), in 0.4 mL 2 wt % TPGS-750-M/H_2O were reacted at rt for 16 h yielding 47.5 mg (87%) of *t*-butyl (*E*)-3-(3,4-dichlorophenyl)acrylate as a yellow solid (hexane/EtOAc : 90/10).

Spectral data matched to the reported in literature.[5] ^{1}H NMR (500 MHz, $CDCl_3$) δ 7.57 (d, *J* = 1.9 Hz, 1H), 7.47 – 7.40 (m, 2H), 7.31 (dd, *J* = 8.3, 1.8 Hz, 1H), 6.34 (d, *J* = 16.0 Hz, 1H), 1.52 (s, 9H).

^{13}C NMR (126 MHz, $CDCl_3$) δ 165.71, 140.84, 134.86, 133.92, 133.26, 130.92, 129.59, 127.02, 122.25, 81.05, 28.28.

GC-MS, *m/z*: 272 [M^+].

(*E*)-1-Methoxy-4-styrylbenzene (6)

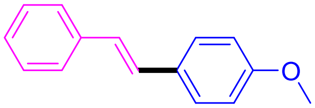

1-Iodo-4-methoxybenzene (46.8 mg, 0.2 mmol), styrene (46.7 mg, 0.4 mmol), NaCl (70.2 mg, 1.2 mmol), K_3PO_4 (127.4 mg, 0.6 mmol) and Fe/ppm Pd NPs (12.5 mg, 0.25% Pd), in 0.4 mL 2 wt % TPGS-750-M/H_2O with DMF (0.04 mL) as co-solvent were reacted at 45 °C for 40 h yielding 36.6 mg (87%) of (*E*)-1-methoxy-4-styrylbenzene as a white solid (hexane/EtOAc : 90/10).

Spectral data matched to the reported in literature.[3] ^{1}H NMR (500 MHz, $CDCl_3$) δ 7.50 (dd, *J* = 18.3, 8.1 Hz, 4H), 7.37 (t, *J* = 7.5 Hz, 2H), 7.26 (t, *J* = 7.1 Hz, 1H), 7.09 (d, *J* = 16.3 Hz, 1H), 7.00 (d, *J* = 16.3 Hz, 1H), 6.93 (d, *J* = 8.4 Hz, 2H), 3.85 (s, 3H).

^{13}C NMR (126 MHz, $CDCl_3$) δ 159.44, 137.78, 130.28, 128.76, 128.34, 127.84, 127.33, 126.74, 126.38, 114.27, 55.44.

GC-MS, *m/z*: 210 [M^+].

Ethyl (*E*)-3-(4-cyanostyryl)benzoate (7)

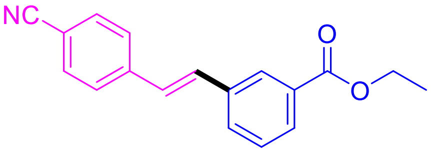

Ethyl 3-iodobenzoate (55.2 mg, 0.2 mmol), 4-vinylbenzonitrile (51.7 mg, 0.4 mmol), NaCl (70.2 mg, 1.2 mmol), K_3PO_4 (127.4 mg, 0.6 mmol) and Fe/ppm Pd NPs (12.5 mg, 0.25% Pd), in 0.4 mL 2 wt % TPGS-750-M/H_2O with DMF (0.04 mL) as co-solvent were reacted at 45 °C for 16 h yielding 55.5 mg (100%) of ethyl (*E*)-3-(4-cyanostyryl)benzoate as a white solid (hexane/EtOAc : 80/20).

^1H NMR (500 MHz, $CDCl_3$) δ 8.18 (s, 1H), 7.96 (d, *J* = 7.7 Hz, 1H), 7.67 (d, *J* = 7.8 Hz, 1H), 7.61 (d, *J* = 8.3 Hz, 2H), 7.56 (d, *J* = 8.3 Hz, 2H), 7.43 (t, *J* = 7.7 Hz, 1H), 7.20 (d, *J* = 16.4 Hz, 1H), 7.12 (d, *J* = 16.4 Hz, 1H), 4.39 (q, *J* = 7.1 Hz, 2H), 1.41 (t, *J* = 7.1 Hz, 3H).

^{13}C NMR (126 MHz, $CDCl_3$) δ 166.29, 141.43, 136.62, 132.53, 131.29, 131.18, 131.05, 129.45, 128.92, 127.88, 127.02, 118.95, 110.94, 61.24, 14.40.

HRMS(CI): Calcd. for $C_{18}H_{15}NO_2H$ $[M+H]^+$ 278.1181. Found: 278.1187.

2-Ethylhexyl (*E*)-3-(1-ethyl-1H-pyrazol-4-yl)acrylate (8)

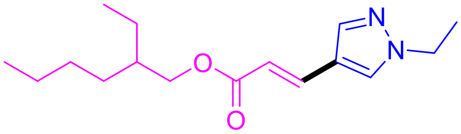

1-Ethyl-4-iodo-1H-pyrazole (44.4 mg, 0.2 mmol), 2-ethylhexyl acrylate (73.7 mg, 0.4 mmol), NaCl (70.2 mg, 1.2 mmol), K_3PO_4 (127.4 mg, 0.6 mmol) and Fe/ppm Pd NPs (12.5 mg, 0.25% Pd), in 0.4 mL 2 wt % TPGS-750-M/H_2O with DMF (0.04 mL) as co-solvent were reacted at 45 °C for 40 h yielding 55.5 mg (85%) of 2-ethylhexyl (*E*)-3-(1-ethyl-1H-pyrazol-4-yl)acrylate as a colorless oil (hexane/EtOAc : 90/10).

^1H NMR (500 MHz, $CDCl_3$) δ 7.68 (s, 1H), 7.60 – 7.48 (m, 2H), 6.15 (d, *J* = 15.9 Hz, 1H), 4.15 (q, *J* = 7.3 Hz, 2H), 4.07 (p, *J* = 5.0 Hz, 2H), 1.61 (dt, *J* = 12.0, 5.9 Hz, 1H), 1.48 (t, *J* = 7.3 Hz, 3H), 1.40 – 1.26 (m, 8H), 0.89 (q, *J* = 7.0, 6.4 Hz, 6H).

^{13}C NMR (126 MHz, $CDCl_3$) δ 167.62, 138.62, 135.09, 128.71, 118.27, 115.91, 66.80, 47.37, 38.98, 30.57, 29.06, 23.95, 23.08, 15.45, 14.15, 11.12.

HRMS(ESI): Calcd. for $C_{16}H_{26}N_2O_2Na$ $[M+Na]^+$ 301.1892. Found: 301.1884.

(*E*)-4-(4-(1H-Pyrrol-1-yl)styryl)benzonitrile (9)

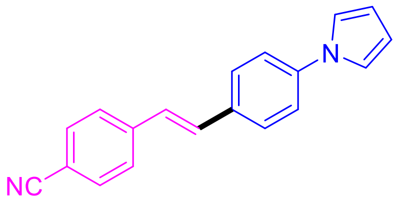

1-(4-Iodophenyl)-1H-pyrrole (53.8 mg, 0.2 mmol), 4-vinylbenzonitrile (51.7 mg, 0.4 mmol), NaCl (70.2 mg, 1.2 mmol), K_3PO_4 (127.4 mg, 0.6 mmol) and Fe/ppm Pd NPs (12.5 mg, 0.25% Pd), in 0.4 mL 2 wt % TPGS-750-M/H_2O with DMF (0.04 mL) as co-solvent were reacted at 45 °C for 16 h yielding 54.1 mg (100%) of (*E*)-4-(4-(1H-pyrrol-1-yl)styryl)benzonitrile as a yellow solid (hexane/EtOAc : 70/30).

^{1}H NMR (500 MHz, DMSO-d_6) δ 7.81 – 7.70 (m, 4H), 7.67 (d, *J* = 8.3 Hz, 2H), 7.58 (d, *J* = 8.3 Hz, 2H), 7.44 (d, *J* = 16.4 Hz, 1H), 7.38 (s, 2H), 7.29 (d, *J* = 16.4 Hz, 1H), 6.24 (s, 2H).

^{13}C NMR (126 MHz, DMSO- d_6) δ 142.41, 140.12, 133.76, 133.07, 131.83, 128.76, 127.51, 126.78, 119.72, 119.52, 119.31, 111.20, 109.82.

HRMS(CI): Calcd. for $C_{19}H_{14}N_2H$ $[M+H]^+$ 271.1235. Found: 271.1233.

(*E*)-3-(4-(Methylthio)phenyl)-1-(4-(3-(trifluoromethyl)phenyl)piperazin-1-yl)prop-2-en-1-one (10)

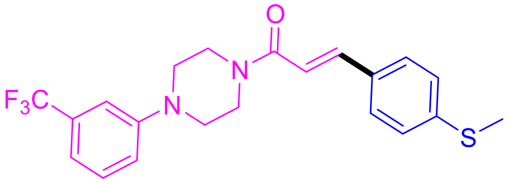

(4-Iodophenyl)(methyl)sulfane (50.0 mg, 0.2 mmol), 1-(4-(3-(trifluoromethyl)phenyl)piperazin-1-yl)prop-2-en-1-one (113.7 mg, 0.4 mmol), NaCl (70.2 mg, 1.2 mmol), K_3PO_4 (127.4 mg, 0.6 mmol) and Fe/ppm Pd NPs (12.5 mg, 0.25% Pd), in

0.4 mL 2 wt % TPGS-750-M/H_2O with DMF (0.04 mL) as co-solvent were reacted at 45 °C for 16 h yielding 81.3 mg (100%) of (*E*)-3-(4-(methylthio)phenyl)-1-(4-(3-(trifluoromethyl)phenyl)piperazin-1-yl)prop-2-en-1-one as a pale yellow solid (hexane/EtOAc : 70/30).

^{1}H NMR (500 MHz, $CDCl_3$) δ 7.66 (d, J = 15.3 Hz, 1H), 7.44 (d, J = 8.1 Hz, 2H), 7.36 (t, J = 8.0 Hz, 1H), 7.22 (d, J = 8.1 Hz, 2H), 7.16 – 7.09 (m, 2H), 7.06 (d, J = 8.3 Hz, 1H), 6.86 (d, J = 15.4 Hz, 1H), 3.85 (br, 4H), 3.26 (s, 4H), 2.49 (s, 3H).

^{13}C NMR (126 MHz, $CDCl_3$) δ 165.64, 151.09, 142.78, 141.23, 131.77, 131.75 (q, $^1J_{(C\text{-}F)}$ = 31.5 Hz), 129.80, 128.26, 126.18, 125.38 (q, $^1J_{(C\text{-}F)}$ = 273.4 Hz), 119.31, 116.69 (q, $^1J_{(C\text{-}F)}$ = 3.8 Hz), 115.69, 112.73 (q, $^1J_{(C\text{-}F)}$ = 3.8 Hz), 49.08 (br), 45.56 (br), 41.94 (br), 15.33.

^{19}F NMR (376 MHz, $CDCl_3$) δ -62.70.

HRMS(ESI): Calcd. for $C_{21}H_{21}F_3N_2OSNa$ $[M+Na]^+$ 429.1224. Found: 429.1222.

(*E*)-5-(4-Nitro-3-(trifluoromethyl)styryl)-2,3-dihydrobenzofuran (11)

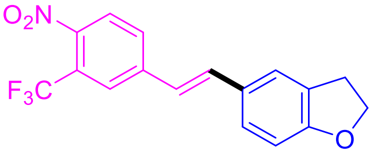

5-Iodo-2,3-dihydrobenzofuran (49.2 mg, 0.2 mmol), 1-nitro-2-(trifluoromethyl)-4-vinylbenzene (86.9 mg, 0.4 mmol), NaCl (70.2 mg, 1.2 mmol), K_3PO_4 (127.4 mg, 0.6 mmol) and Fe/ppm Pd NPs (12.5 mg, 0.25% Pd), in 0.4 mL 2 wt % TPGS-750-M/H_2O with DMF (0.04 mL) as co-solvent were reacted at 45 °C for 16 h yielding 65.7 mg (98%) of (*E*)-5-(4-nitro-3-(trifluoromethyl)styryl)-2,3-dihydrobenzofuran as an orange solid (hexane/EtOAc : 80/20).

^{1}H NMR (500 MHz, $CDCl_3$) δ 7.90 (d, J = 8.4 Hz, 1H), 7.84 (s, 1H), 7.70 (d, J = 8.3 Hz, 1H), 7.44 (s, 1H), 7.30 (d, J = 8.0 Hz, 1H), 7.21 (d, J = 16.2 Hz, 1H), 6.94 (d, J = 16.2 Hz, 1H), 6.80 (d, J = 8.2 Hz, 1H), 4.63 (t, J = 8.7 Hz, 2H), 3.24 (t, J = 8.6 Hz, 2H).

^{13}C NMR (126 MHz, $CDCl_3$) δ 161.50, 145.66, 143.21, 134.56, 129.27, 128.64, 128.41, 128.27, 126.17, 125.21 (q, $^1J_{(C\text{-}F)}$ = 5.1 Hz), 124.66 (q, $^1J_{(C\text{-}F)}$ = 34.0 Hz), 123.51, 123.29 (q, $^1J_{(C\text{-}F)}$ = 273.4 Hz), 122.03, 109.78, 71.85, 29.47.

^{19}F NMR (376 MHz, $CDCl_3$) δ -60.01.

HRMS(CI): Calcd. for $C_{17}H_{12}F_3NO_3H$ $[M+H]^+$ 336.0847. Found: 336.0858.

***t*-Butyl (*E*)-(4-(4-(trifluoromethyl)styryl)phenyl)carbamate (12)**

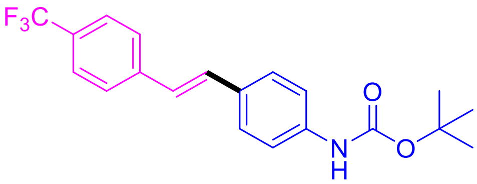

t-Butyl (4-iodophenyl)carbamate (63.8 mg, 0.2 mmol), 1-(trifluoromethyl)-4-vinylbenzene (68.9 mg, 0.4 mmol), NaCl (70.2 mg, 1.2 mmol), K_3PO_4 (127.4 mg, 0.6 mmol) and Fe/ppm Pd NPs (12.5 mg, 0.25% Pd), in 0.4 mL 2 wt % TPGS-750-M/H_2O with DMF (0.04 mL) as co-solvent were reacted at 45 °C for 16 h yielding 69.8 mg (96%) of *t*-butyl (*E*)-(4-(4-(trifluoromethyl)styryl)phenyl)carbamate as a white solid (hexane/EtOAc : 80/20).

^1H NMR (500 MHz, DMSO-d_6) δ 9.47 (s, 1H), 7.76 (d, J = 7.6 Hz, 2H), 7.69 (d, J = 7.7 Hz, 2H), 7.54 (d, J = 8.0 Hz, 2H), 7.50 (d, J = 7.8 Hz, 2H), 7.34 (d, J = 16.3 Hz, 1H), 7.20 (d, J = 16.4 Hz, 1H), 1.48 (s, 9H).

^{13}C NMR (126 MHz, DMSO-d_6) δ 152.66, 141.49, 139.75, 131.05, 130.30, 127.39, 127.24 (q, $^1J_{(C\text{-}F)}$ = 31.5 Hz), 126.63, 125.49 (q, $^1J_{(C\text{-}F)}$ = 3.8 Hz), 124.81, 123.30 (q, $^1J_{(C\text{-}F)}$ = 273.4 Hz), 118.14, 79.21, 28.09.

^{19}F NMR (376 MHz, DMSO-d_6) δ -60.89.

HRMS(ESI): Calcd. for $C_{20}H_{20}F_3NO_2Na$ $[M+Na]^+$ 386.1344. Found: 386.1347.

(*E*)-4-(2-(Benzo[d][1,3]dioxol-5-yl)vinyl)pyridine (13)

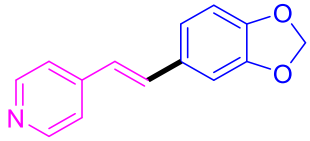

5-Iodobenzo[d][1,3]dioxole (49.6 mg, 0.2 mmol), 4-vinylpyridine (42 mg, 0.4 mmol), NaCl (70.2 mg, 1.2 mmol), K_3PO_4 (127.4 mg, 0.6 mmol) and Fe/ppm Pd NPs (12.5 mg, 0.25% Pd), in 0.4 mL 2 wt % TPGS-750-M/H_2O with DMF (0.04 mL) as co-solvent were reacted at 45 °C for 16 h yielding 43.7 mg (97%) of (*E*)-4-(2-(benzo[d][1,3]dioxol-5-yl)vinyl)pyridine as a pale yellow solid (hexane/EtOAc : 80/20).

Spectral data matched that reported in the literature.[6] ^{1}H NMR (500 MHz, $CDCl_3$) δ 8.52 (d, *J* = 4.5 Hz, 2H), 7.28 (d, *J* = 4.6 Hz, 2H), 7.16 (d, *J* = 16.2 Hz, 1H), 7.04 (s, 1H), 6.94 (d, *J* = 7.7 Hz, 1H), 6.86 – 6.71 (m, 2H), 5.96 (s, 2H).

^{13}C NMR (126 MHz, $CDCl_3$) δ 150.17, 148.36, 148.31, 144.74, 132.81, 130.68, 124.17, 122.58, 120.69, 108.55, 105.81, 101.40.

GC-MS, *m/z*: 225 [M^+].

(*E*)-3-(4-Nitro-3-(trifluoromethyl)styryl)thiophene (14)

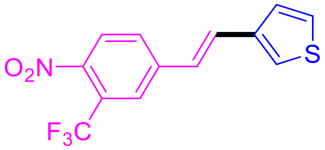

3-Iodothiophene (42 mg, 0.2 mmol), 1-nitro-2-(trifluoromethyl)-4-vinylbenzene (86.9 mg, 0.4 mmol), NaCl (70.2 mg, 1.2 mmol), K_3PO_4 (127.4 mg, 0.6 mmol) and Fe/ppm Pd NPs (12.5 mg, 0.25% Pd), in 0.4 mL 2 wt % TPGS-750-M/H_2O with DMF (0.04 mL) as co-solvent were reacted at 45 °C for 16 h yielding 58.7 mg (98%) of (*E*)-3-(4-nitro-3-(trifluoromethyl)styryl)thiophene as a yellow solid (hexane/EtOAc : 80/20).

^{1}H NMR (400 MHz, $CDCl_3$) δ 7.91 (d, *J* = 8.4 Hz, 1H), 7.86 (s, 1H), 7.73 (d, *J* = 8.3 Hz, 1H), 7.43 (s, 1H), 7.37 (s, 2H), 7.30 (d, *J* = 16.2 Hz, 1H), 6.96 (d, *J* = 16.2 Hz, 1H).

^{13}C NMR (126 MHz, $CDCl_3$) δ 146.06, 142.78, 138.78, 129.57, 128.40, 127.06, 126.13, 125.57, 125.37 (q, $^1J_{(C\text{-}F)}$ = 5 Hz), 124.80, 124.78, 124.68 (q, $^1J_{(C\text{-}F)}$ = 34 Hz), 123.23 (q, $^1J_{(C\text{-}F)}$ = 274.7 Hz).

^{19}F NMR (376 MHz, $CDCl_3$) δ -60.00.

HRMS(CI): Calcd. for $C_{13}H_8F_3NO_2SH$ $[M+H]^+$ 300.0306. Found: 300.0315.

(*E*)-3-(2-(Pyridin-2-yl)vinyl)-1-(tetrahydro-2H-pyran-2-yl)-1H-indazole (15)

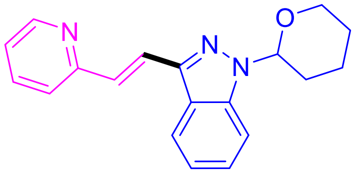

3-Iodo-1-(tetrahydro-2H-pyran-2-yl)-1H-indazole (65.6 mg, 0.2 mmol), 2-vinylpyridine (42 mg, 0.4 mmol), NaCl (70.2 mg, 1.2 mmol), K_3PO_4 (127.4 mg, 0.6 mmol) and Fe/ppm Pd NPs (12.5 mg, 0.25% Pd), in 0.4 mL 2 wt % TPGS-750-M/H_2O with DMF (0.04 mL) as co-solvent were reacted at 45 °C for 72 h yielding 55.0 mg (90%) of (*E*)-3-(2-(pyridin-2-yl)vinyl)-1-(tetrahydro-2H-pyran-2-yl)-1H-indazole as a white solid (hexane/EtOAc : 80/20).

Spectral data matched that reported in the literature.[7] ^{1}H NMR (500 MHz, $CDCl_3$) δ 8.64 (d, *J* = 4.2 Hz, 1H), 8.08 (d, *J* = 8.1 Hz, 1H), 7.93 (d, *J* = 16.4 Hz, 1H), 7.72 – 7.65 (m, 1H), 7.65 – 7.54 (m, 2H), 7.50 (d, *J* = 7.8 Hz, 1H), 7.43 (t, *J* = 7.6 Hz, 1H), 7.31 – 7.21 (m, 1H), 7.20 – 7.09 (m, 1H), 5.76 (dd, *J* = 9.3, 2.4 Hz, 1H), 4.06 (d, *J* = 10.0 Hz, 1H), 3.76 (dt, *J* = 11.0, 5.5 Hz, 1H), 2.69 – 2.49 (m, 1H), 2.25 – 2.14 (m, 1H), 2.13 – 2.04 (m, 1H), 1.87 – 1.59 (m, 3H).

^{13}C NMR (126 MHz, $CDCl_3$) δ 155.88, 149.75, 142.54, 140.90, 136.62, 130.39, 126.78, 124.06, 123.23, 122.21, 121.92, 121.76, 121.13, 110.48, 85.55, 67.63, 29.56, 25.22, 22.68.

GC-MS, *m/z*: 305 $[M^+]$.

(*E*)-3-(4-((2,5-Dichloropyrimidin-4-yl)amino)phenyl)-1-morpholinoprop-2-en-1-one (16)

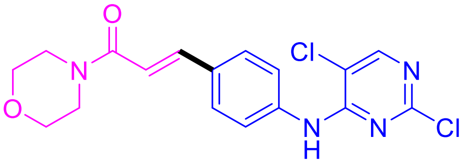

2,5-Dichloro-N-(4-iodophenyl)pyrimidin-4-amine (73.2 mg, 0.2 mmol), 1-morpholinoprop-2-en-1-one (56.5 mg, 0.4 mmol, NaCl (70.2 mg, 1.2 mmol), K_3PO_4 (127.4 mg, 0.6 mmol) and Fe/ppm Pd NPs (12.5 mg, 0.25% Pd), in 0.4 mL 2 wt % TPGS/H_2O with DMF (0.04 mL) as co-solvent were reacted at 45 °C for 40 h yielding 65.5 mg (86%) of (*E*)-3-(4-((2,5-dichloropyrimidin-4-yl)amino)phenyl)-1-morpholinoprop-2-en-1-one as a white solid (hexane/EtOAc : 30/70).

^{1}H NMR (600 MHz, $CDCl_3$) δ 8.15 (s, 1H), 7.60 (d, *J* = 8.7 Hz, 3H), 7.49 (d, *J* = 8.3 Hz, 2H), 7.18 (s, 1H), 6.74 (d, *J* = 15.4 Hz, 1H), 3.81 – 3.51 (m, 8H).

^{13}C NMR (126 MHz, $CDCl_3$) δ 165.66, 158.37, 156.25, 155.06, 142.37, 138.30, 131.93, 128.91, 121.08, 116.20, 114.09, 67.01, 46.45, 42.71.

HRMS(ESI): Calcd. for $C_{18}H_{20}Cl_2N_4O_3Na$ $[M+Na+CH_3OH]^+$ 433.0810. Found: 433.0816.

_t_-Butyl (_E_)-5-(2-(perfluorophenyl)vinyl)-1H-indole-1-carboxylate (17)

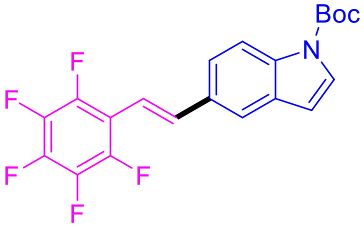

t-Butyl 5-iodo-1H-indole-1-carboxylate (68.6 mg, 0.2 mmol), 1,2,3,4,5-pentafluoro-6-vinylbenzene (77.6 mg, 0.4 mmol), NaCl (70.2 mg, 1.2 mmol), K_3PO_4 (127.4 mg, 0.6 mmol) and Fe/ppm Pd NPs (12.5 mg, 0.25% Pd), in 0.4 mL 2 wt % TPGS-750-M/H_2O with DMF (0.04 mL) as co-solvent were reacted at 45 °C for 40 h yielding 75.6 mg (92%) of *t*-butyl

(*E*)-5-(2-(perfluorophenyl)vinyl)-1H-indole-1-carboxylate as a white solid (hexane/EtOAc : 80/20).

^{1}H NMR (600 MHz, $CDCl_3$) δ 8.14 (d, *J* = 4.8 Hz, 1H), 7.69 (s, 1H), 7.61 (d, *J* = 2.4 Hz, 1H), 7.51 (dd, *J* = 13.4, 3.2 Hz, 2H), 6.96 (d, *J* = 16.8 Hz, 1H), 6.58 (d, *J* = 3.6 Hz, 1H), 1.69 (s, 9H).

^{13}C NMR (126 MHz, $CDCl_3$) δ 149.64, 145.96, 143.86, 138.90, 137.75, 135.63, 131.36, 131.14, 126.94, 123.04, 119.98, 115.57, 111.44, 107.49, 84.15, 28.29.

^{19}F NMR (376 MHz, $CDCl_3$) δ -141.74 – -144.21 (m), -157.45 (t, *J* = 20.8 Hz), -162.69 – -163.78 (m).

HRMS(ESI): Calcd. for $C_{16}H_8F_5N$ $[M-C_5H_9O_2+H]^+$ 309.0577. Found: 309.0592.

(*E*)-2-(4-(2-(Pyridin-2-yl)vinyl)phenoxy)-1-(pyrrolidin-1-yl)ethan-1-one (18)

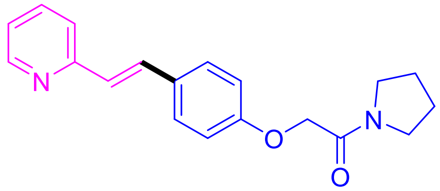

2-(4-Iodophenoxy)-1-(pyrrolidin-1-yl)ethan-1-one (66.2 mg, 0.2 mmol), 2-vinylpyridine(42.0 mg, 0.4 mmol), NaCl (70.2 mg, 1.2 mmol), K_3PO_4 (127.4 mg, 0.6 mmol) and Fe/ppm Pd NPs (12.5 mg, 0.25% Pd), in 0.4 mL 2 wt % TPGS-750-M/H_2O with DMF (0.04 mL) as co-solvent were reacted at 45 °C for 40 h yielding 54.9 mg (89%) of (*E*)-2-(4-(2-(pyridin-2-yl)vinyl)phenoxy)-1-(pyrrolidin-1-yl)ethan-1-one as a yellow solid (EtOAc).

^{1}H NMR (500 MHz, $CDCl_3$) δ 8.58 (d, *J* = 6.3 Hz 1H), 7.64 (t, *J* = 7.5 Hz, 1H), 7.57 (d, *J* = 16.1 Hz, 1H), 7.51 (d, *J* = 8.5 Hz, 2H), 7.35 (d, *J* = 7.8 Hz, 1H), 7.11 (t, *J* = 7.5 Hz, 1H), 7.04 (d, *J* = 16.1 Hz, 1H), 6.95 (d, *J* = 8.4 Hz, 2H), 4.64 (s, 2H), 3.52 (t, *J* = 6.8 Hz, 4H), 1.91 (dp, *J* = 56.9, 6.7 Hz, 4H).

^{13}C NMR (126 MHz, $CDCl_3$) δ 166.45, 158.42, 155.95, 149.68, 136.67, 132.26, 130.40, 128.63, 126.34, 121.90, 115.04, 68.20, 46.17, 26.39, 23.92.

HRMS(ESI): Calcd. for $C_{19}H_{20}N_2O_2H$ $[M+H]^+$ 309.1603. Found: 309.1600.

(1S,4S)-1,7,7-Trimethylbicyclo[2.2.1]heptan-2-yl (*E*)-3-(4-((3-methylbut-2-en-1-yl)oxy)phenyl)-acrylate (19)

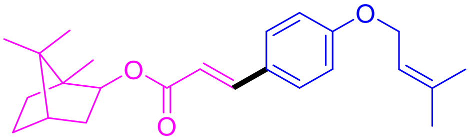

1-Iodo-4-((3-methylbut-2-en-1-yl)oxy)benzene (57.6 mg, 0.2 mmol), (1S,4S)-1,7,7-trimethyl-bicyclo[2.2.1]heptan-2-yl acrylate (83.3 mg, 0.4 mmol), NaCl (70.2 mg, 1.2 mmol), K_3PO_4 (127.4 mg, 0.6 mmol) and Fe/ppm Pd NPs (12.5 mg, 0.25% Pd), in 0.4 mL 2 wt % TPGS-750-M/H_2O with DMF (0.04 mL) as co-solvent were reacted at 45 °C for 40 h yielding 65.6 mg (89%) of (1S,4S)-1,7,7-trimethylbicyclo[2.2.1]heptan-2-yl (*E*)-3-(4-((3-methylbut-2-en-1-yl)oxy)phenyl)acrylate as a yellow solid (hexane/EtOAc : 90/10).

^1H NMR (400 MHz, $CDCl_3$) δ 7.58 (d, J = 16.0 Hz, 1H), 7.46 (d, J = 8.7 Hz, 2H), 6.90 (d, J = 8.7 Hz, 2H), 6.27 (d, J = 15.9 Hz, 1H), 5.48 (t, J = 6.7 Hz, 1H), 4.79 (dd, J = 7.2, 4.2 Hz, 1H), 4.53 (d, J = 6.7 Hz, 2H), 1.90 – 1.81 (m, 2H), 1.80 (s, 3H), 1.75 (s, 3H), 1.64 – 1.51 (m, 2H), 1.29 – 1.16 (m, 3H), 1.06 (s, 3H), 0.90 – 0.85 (m, 6H).

^{13}C NMR (101 MHz, $CDCl_3$) δ 167.06, 160.72, 144.05, 138.82, 129.79, 127.28, 119.34, 116.40, 115.08, 81.00, 65.02, 49.01, 47.12, 45.22, 39.02, 33.90, 29.84, 27.22, 25.97, 20.30, 20.15, 18.37, 11.65.

HRMS(ESI): Calcd. for $C_{24}H_{32}O_3Na$ $[M+Na]^+$ 391.2249. Found: 391.2259.

(Tetrahydrofuran-2-yl)methyl (*E*)-3-(3-formylphenyl) (20)

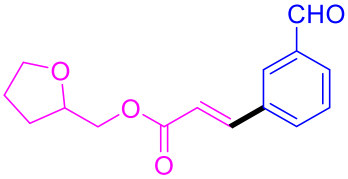

3-Iodobenzaldehyde (46.4 mg, 0.2 mmol), (tetrahydrofuran-2-yl)methyl acrylate (62.5 mg, 0.4 mmol), NaCl (70.2 mg, 1.2 mmol), K_3PO_4 (127.4 mg, 0.6 mmol) and Fe/ppm Pd NPs (12.5 mg, 0.25% Pd), in 0.4 mL 2 wt % TPGS-750-M/H_2O with DMF (0.04 mL) as co-solvent were reacted at 45 °C for 16 h yielding 42.7 mg (82%) of tetrahydrofuran-2-yl)methyl (*E*)-3-(3-formylphenyl)acrylate as a white solid (hexane/EtOAc : 80/20).

^{1}H NMR (400 MHz, $CDCl_3$) δ 10.02 (s, 1H), 8.00 (s, 1H), 7.87 (d, *J* = 7.5 Hz, 1H), 7.79 – 7.68 (m, 2H), 7.55 (t, *J* = 7.6 Hz, 1H), 6.57 (d, *J* = 16.0 Hz, 1H), 4.29 (dd, *J* = 10.9, 2.7 Hz, 1H), 4.24 – 4.09 (m, 2H), 3.86 (dq, *J* = 39.2, 7.4 Hz, 2H), 2.10 – 1.85 (m, 3H), 1.71 – 1.59 (m, 1H).

^{13}C NMR (101 MHz, $CDCl_3$) δ 191.72, 166.49, 143.41, 137.00, 135.48, 133.61, 131.14, 129.77, 129.06, 119.86, 76.62, 68.59, 66.88, 28.09, 25.79.

HRMS(ESI): Calcd. for $C_{15}H_{16}O_4Na$ $[M+Na]^+$ 283.0946. Found: 283.0954.

(*E*)-2,5-Dichloro-N-(4-(2-(3-methoxypyridin-2-yl)vinyl)phenyl)pyrimidin-4-amine (21)

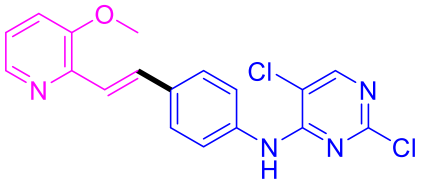

2,5-Dichloro-*N*-(4-iodophenyl)pyrimidin-4-amine (73.2 mg, 0.2 mmol), 3-methoxy-2-vinyl-pyridine (54.1 mg, 0.4 mmol), NaCl (70.2 mg, 1.2 mmol), K_3PO_4 (127.4 mg, 0.6 mmol) and Fe/ppm Pd NPs (12.5 mg, 0.25% Pd), in 0.4 mL 2 wt % TPGS-750-M/H_2O with DMF (0.04 mL) as co-solvent were reacted at 45 °C for 40 h yielding 62 mg (83%) of (*E*)-

2,5-dichloro-*N*-(4-(2-(3-methoxypyridin-2-yl)vinyl)phenyl)pyrimidin-4-amine as a yellow solid (hexane/EtOAc : 70/30).

^{1}H NMR (600 MHz, CDCl$_3$) δ 8.25 – 8.18 (m, 2H), 7.77 (d, *J* = 16.0 Hz, 1H), 7.69 – 7.63 (m, 4H), 7.57 (d, *J* = 16.0 Hz, 1H), 7.30 (s, 1H), 7.21 – 7.18 (m, 1H), 7.18 – 7.14 (m, 1H), 3.91 (s, 3H).

^{13}C NMR (126 MHz, CDCl$_3$) δ 158.44, 156.30, 154.81, 153.27, 145.37, 141.19, 136.72, 134.40, 132.02, 128.21, 122.90, 121.56, 121.12, 118.01, 113.98, 55.62.

HRMS(ESI): Calcd. for $C_{18}H_{14}Cl_2N_4OH$ [M+H]$^+$ 373.0623. Found: 373.0622.

_t_-Butyl (_E_)-5-(3-morpholino-3-oxoprop-1-en-1-yl)-1H-indole-1-carboxylate (22)

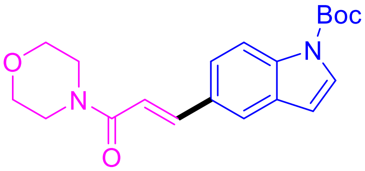

t-Butyl 5-iodo-1H-indole-1-carboxylate (68.6 mg, 0.2 mmol), 1-morpholinoprop-2-en-1-one(56.5 mg, 0.4 mmol), NaCl (70.2 mg, 1.2 mmol), K$_3$PO$_4$ (127.4 mg, 0.6 mmol) and Fe/ppm Pd NPs (12.5 mg, 0.25% Pd), in 0.4 mL 2 wt % TPGS-750-M/H$_2$O with DMF (0.04 mL) as co-solvent were reacted at 45 °C for 16 h yielding 68.5 mg (96%) of *t*-butyl (*E*)-5-(3-morpholino-3-oxoprop-1-en-1-yl)-1H-indole-1-carboxylate as a white solid. (hexane/EtOAc : 80/20).

^{1}H NMR (600 MHz, CDCl$_3$) δ 8.12 (d, *J* = 6.3 Hz, 1H), 7.80 (d, *J* = 15.3 Hz, 1H), 7.70 (s, 1H), 7.59 (d, *J* = 3.3 Hz, 1H), 7.50 (d, *J* = 8.5 Hz, 1H), 6.85 (d, *J* = 15.3 Hz, 1H), 6.56 (d, *J* = 3.3 Hz, 1H), 3.79 – 3.66 (m, 8H), 1.66 (s, 9H).

^{13}C NMR (126 MHz, CDCl$_3$) δ 165.94, 149.56, 143.99, 136.09, 131.04, 129.93, 126.98, 123.71, 121.29, 115.54, 115.15, 107.50, 84.19, 66.99, 46.38, 42.66, 28.26.

HRMS(ESI): Calcd. for $C_{20}H_{24}N_2O_4Na$ [M+Na]$^+$ 379.1634. Found: 379.1647.

(Tetrahydrofuran-2-yl)methyl (*E*)-3-(4-((trimethylsilyl)ethynyl)phenyl)acrylate (23)

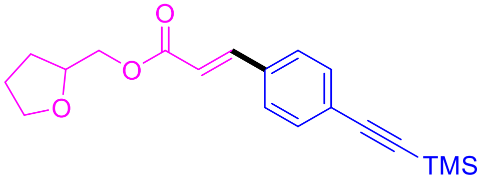

((4-Iodophenyl)ethynyl)trimethylsilane (60 mg, 0.2 mmol), (tetrahydrofuran-2-yl)methyl acrylate (62.5 mg, 0.4 mmol), NaCl (70.2 mg, 1.2 mmol), K_3PO_4 (127.4 mg, 0.6 mmol) and Fe/ppm Pd NPs (12.5 mg, 0.25% Pd), in 0.4 mL 2 wt % TPGS-750-M/H_2O with DMF (0.04 mL) as co-solvent were reacted at 45 °C for 40 h yielding 54.8 mg (83%) of (tetrahydrofuran-2-yl)methyl (*E*)-3-(4-((trimethylsilyl)ethynyl)-phenyl)acrylate as a yellow oil (hexane/EtOAc : 60/40).

^{1}H NMR (400 MHz, $CDCl_3$) δ 7.65 (d, *J* = 16.0 Hz, 1H), 7.48 – 7.41 (m, 4H), 6.47 (d, *J* = 16.0 Hz, 1H), 4.29 (dd, *J* = 11.1, 3.1 Hz, 1H), 4.23 – 4.06 (m, 2H), 3.96 – 3.76 (m, 2H), 2.09 – 1.97 (m, 1H), 1.97 – 1.83 (m, 2H), 1.69 – 1.57 (m, 1H), 0.24 (s, 9H).

^{13}C NMR (101 MHz, $CDCl_3$) δ 166.82, 144.19, 134.37, 132.48, 127.97, 125.07, 118.65, 104.55, 96.81, 76.66, 68.59, 66.77, 28.08, 25.79, 0.01.

HRMS(ESI): Calcd. for $C_{19}H_{24}O_3SiNa$ $[M+Na]^+$ 351.1393. Found: 351.1400.

(*E*)-Triisopropyl(4-(2-(perfluorophenyl)vinyl)phenoxy)silane (24)

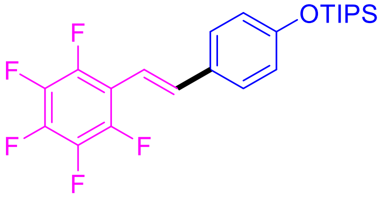

(4-Iodophenoxy)triisopropylsilane (75.3 mg, 0.2 mmol), 1,2,3,4,5-pentafluoro-6-vinylbenzene 77.6 mg, 0.4 mmol, NaCl (70.2 mg, 1.2 mmol), K_3PO_4 (127.4 mg, 0.6 mmol) and Fe/ppm Pd NPs (12.5 mg, 0.25% Pd), in 0.4 mL 2 wt % TPGS-750-M/H_2O with DMF (0.04 mL) as co-solvent were reacted at 45 °C for 40 h yielding 72.7 mg (82%) of (*E*)-

triisopropyl(4-(2-(perfluorophenyl)vinyl)phenoxy)silane as a white solid (hexane/EtOAc : 95/5).

^{1}H NMR (400 MHz, CDCl$_3$) δ 7.45 – 7.33 (m, 3H), 6.90 (d, *J* = 8.6 Hz, 2H), 6.83 (d, *J* = 16.7 Hz, 1H), 1.33 – 1.21 (m, 3H), 1.11 (d, *J* = 7.3 Hz, 18H).

^{13}C NMR (101 MHz, CDCl$_3$) δ 157.25, 146.06, 143.53, 136.96, 129.61, 128.37, 128.00, 120.45, 120.29, 110.50, 18.04, 12.81.

^{19}F NMR (376 MHz, CDCl$_3$) δ -143.19 – -143.32 (m), -157.56 (t, *J* = 20.7 Hz), -163.19 – -163.33 (m).

HRMS(ESI): Calcd. for $C_{23}H_{27}F_5OSi$ [M]$^+$ 442.1751. Found: 442.1740.

(1S,4S)-1,7,7-Trimethylbicyclo[2.2.1]heptan-2-yl (*E*)-3-(3-formylphenyl)acrylate (25)

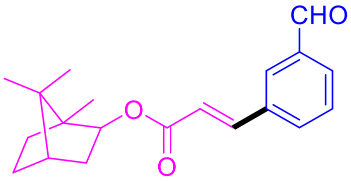

3-Iodobenzaldehyde (46.4 mg, 0.2 mmol), (1*S*,4*S*)-1,7,7-trimethylbicyclo[2.2.1]heptan-2-yl acrylate (83.3 mg, 0.4 mmol), NaCl (70.2 mg, 1.2 mmol), K_3PO_4 (127.4 mg, 0.6 mmol) and Fe/ppm Pd NPs (12.5 mg, 0.25% Pd), in 0.4 mL 2 wt % TPGS-750-M/H_2O with DMF (0.04 mL) as co-solvent were reacted at 45 °C for 40 h yielding 61.8 mg (99%) of (1S,4S)-1,7,7-trimethylbicyclo[2.2.1]heptan-2-yl (*E*)-3-(3-formylphenyl)acrylate as a yellow oil (hexane/EtOAc : 90/10).

^{1}H NMR (400 MHz, CDCl$_3$) δ 10.04 (s, 1H), 8.02 (s, 1H), 7.87 (d, *J* = 7.5 Hz, 1H), 7.76 (d, *J* = 7.6 Hz, 1H), 7.66 (d, *J* = 16.0 Hz, 1H), 7.56 (t, *J* = 7.6 Hz, 1H), 6.50 (d, *J* = 16.0 Hz, 1H), 4.80 (dd, *J* = 7.1, 4.2 Hz, 1H), 1.93 – 1.67 (m, 4H), 1.58 (td, *J* = 12.0, 11.5, 3.6 Hz, 1H), 1.25 – 1.02 (m, 5H), 0.87 (d, *J* = 11.9 Hz, 6H).

^{13}C NMR (101 MHz, $CDCl_3$) δ 191.83, 166.12, 142.57, 136.98, 135.66, 133.72, 131.17, 129.74, 128.79, 120.90, 81.51, 49.02, 47.11, 45.17, 38.95, 33.84, 27.16, 20.24, 11.62.

HRMS(ESI): Calcd. for $C_{22}H_{32}O_5$ Na $[M+Na+(CH_3OH)_2]^+$ 399.2148. Found: 399.2150.

(*E*)-2,5-Dichloro-N-(4-(2-(2-methylbenzo[d]oxazol-6-yl)vinyl)phenyl)pyrimidin-4-amine (26)

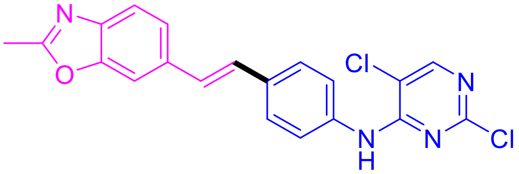

2,5-Dichloro-N-(4-iodophenyl)pyrimidin-4-amine (73.2 mg, 0.2 mmol), 2-methyl-6-vinyl-benzo[d]oxazole (63.7 mg, 0.4 mmol), NaCl (70.2 mg, 1.2 mmol), K_3PO_4 (127.4 mg, 0.6 mmol) and Fe/ppm Pd NPs(12.5 mg, 0.25% Pd), in 0.4 mL 2 wt % TPGS/H_2O with DMF (0.04 mL) as co-solvent were reacted at 45 °C for 40 h yielding 70.1 mg (88%) of (*E*)-2,5-dichloro-N-(4-(2-(2-methylbenzo[d]oxazol-6-yl)vinyl)phenyl)pyrimidin-4-amine as a yellow solid (hexane/EtOAc : 70/30).

^1H NMR (500 MHz, $CDCl_3$) δ 8.18 (s, 1H), 7.65 – 7.48 (m, 6H), 7.43 (d, J = 8.3 Hz, 1H), 7.22 (s, 1H), 7.10 (q, J = 16.3 Hz, 2H), 2.61 (s, 3H).

^{13}C NMR (126 MHz, $CDCl_3$) δ 164.57, 158.42, 156.32, 154.82, 151.80, 141.48, 136.39, 134.59, 134.23, 128.43, 128.03, 127.40, 123.37, 121.32, 119.49, 113.96, 107.78, 14.78.

HRMS(ESI): Calcd. for $C_{20}H_{14}Cl_2N_4OH$ $[M+H]^+$ 397.0623. Found: 397.0621.

References

1. Lipshutz, B. H.; Ghorai, S.; Abela, A. R.; Moser, R.; Nishikata, T.; Duplais, C.; Krasovskiy, A.; Gaston, R. D.; Gadwood, R. C. TPGS-750-M: A Second-Generation Amphiphile for Metal-Catalyzed Cross-Couplings in Water at Room Temperature. *J. Org. Chem.* **2011**, *76*, 4379.

2. Lee, N. R.; Cortes-Clerget, M.; Wood, A. B.; Lippincott, D. J.; Pang, H.; Moghadam, F. A.; Gallou, F.; Lipshutz, B. H. Coolade. A Low-Foaming Surfactant for Organic Synthesis in Water. *ChemSusChem* **2019**, *12*, 3159.

3. Zhu, M.-K.; Zhao, J.-F.; Loh, T.-P. Palladium-Catalyzed C–C Bond Formation of Arylhydrazines with Olefins via Carbon–Nitrogen Bond Cleavage. *Org. Lett.* **2011,** *13*, 6308.

4. Mao, D.; Hong, G.; Wu, S.; Liu, X.; Yu, J.; Wang, L. Lewis-Acid-Catalyzed Benzylic Reactions of 2-Methylazaarenes with Aldehydes. *Eur. J. Org. Chem.* **2014,** *2014*, 3009.

5. Wei, W.-T.; Yeh, J.-Y.; Kuo, T.-S.; Wu, H.-L. Highly Enantioselective Rhodium-Catalyzed Asymmetric 1,4-Addition Reactions of Arylboronic Acids to Acyclic α,β-Unsaturated Compounds: The Formal Synthesis of (−)-Indatraline. *Chem. Euro. J.* **2011,** *17*, 11405.

6. Liang, J.-H.; Yang, L.; Wu, S.; Liu, S.-S.; Cushman, M.; Tian, J.; Li, N.-M.; Yang, Q.-H.; Zhang, H.-A.; Qiu, Y.-J.; Xiang, L.; Ma, C.-X.; Li, X.-M.; Qing, H. Discovery of efficient stimulators for adult hippocampal neurogenesis based on scaffolds in dragon's blood. *Eur. J. Med. Chem.* **2017,** *136*, 382.

7. Yu, J.; Hong, Z.; Yang, X.; Jiang, Y.; Jiang, Z.; Su, W. Bromide-assisted chemoselective Heck reaction of 3-bromoindazoles under high-speed ball-milling conditions: synthesis of axitinib. *Beilstein J. Org. Chem.* **2018,** *14*, 786.

NMR spectra

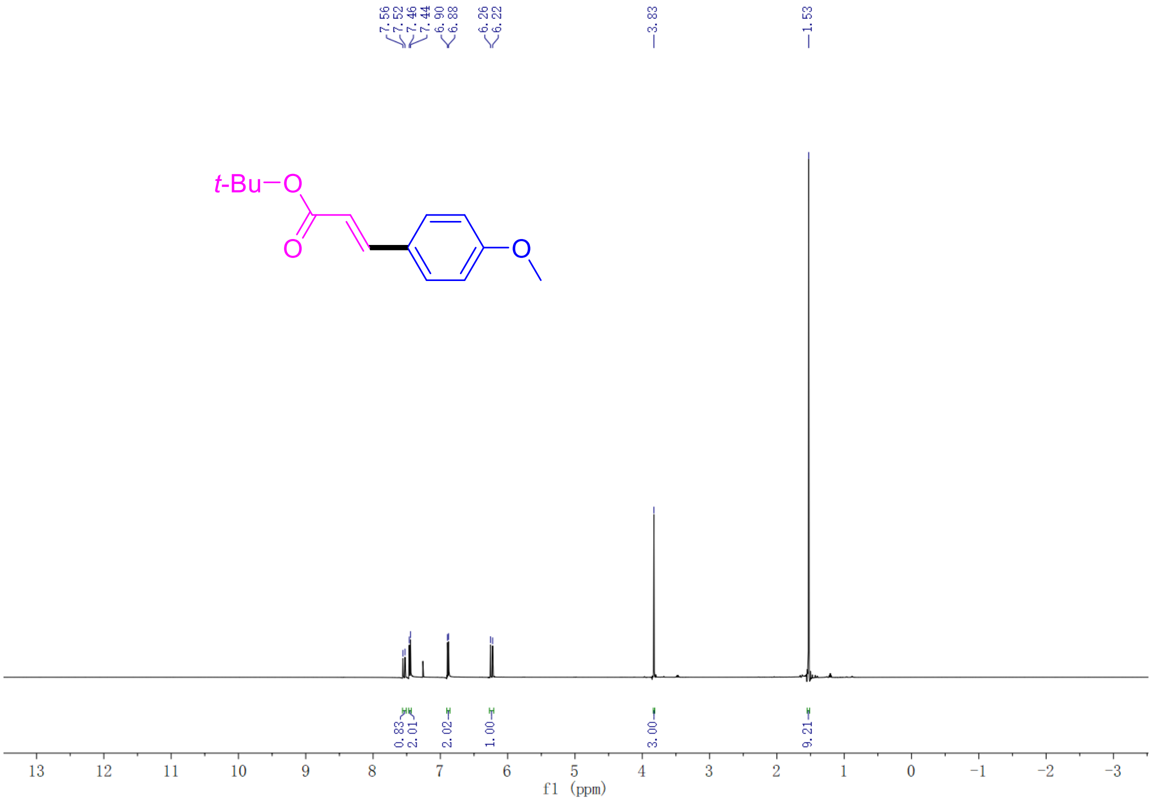
7.56
7.52
7.46
7.44
6.90
6.88
6.26
6.22
3.83
1.53
t-Bu–O
O
O
0.83
2.01
2.02
1.00
3.00
9.21
13
12
11
10
9
8
7
6
5
4
3
2
1
0
−1
−2
−3
f1 (ppm)

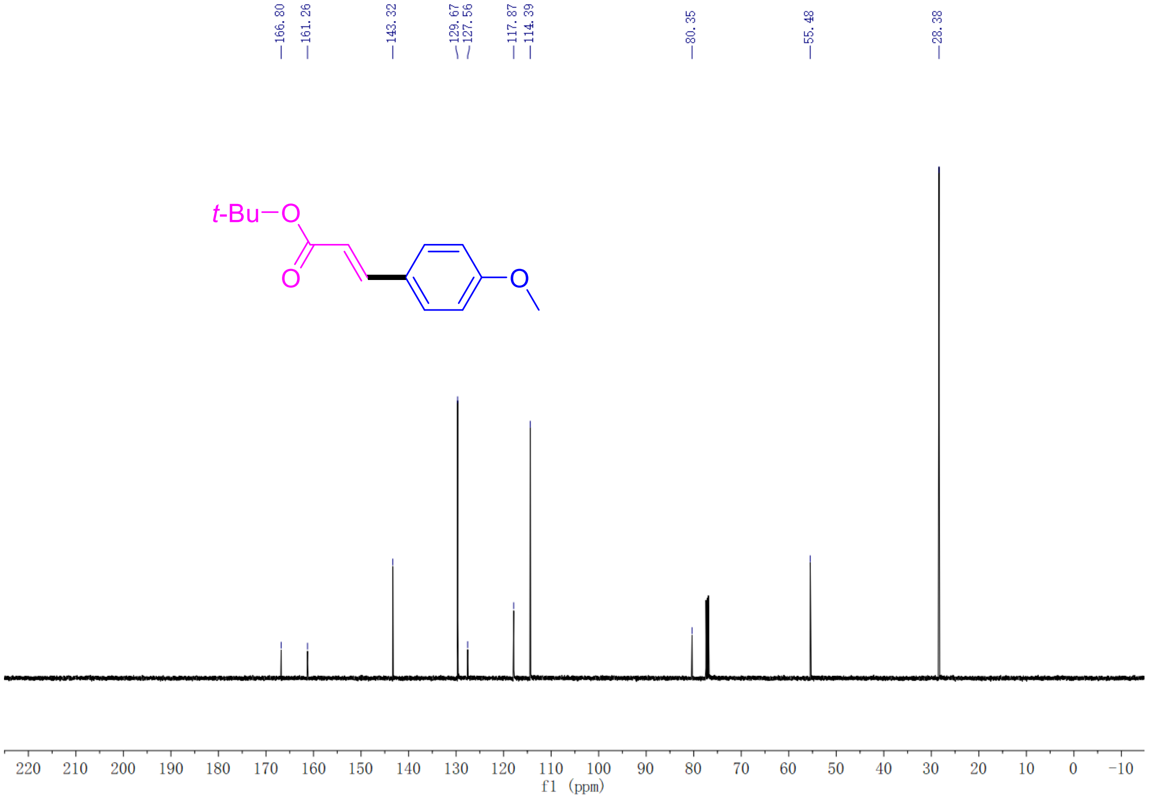
166.80
161.26
143.32
129.67
127.56
117.87
114.39
80.35
55.48
28.38
t-Bu–O
O
O
220
210
200
190
180
170
160
150
140
130
120
110
100
90
80
70
60
50
40
30
20
10
0
−10
f1 (ppm)

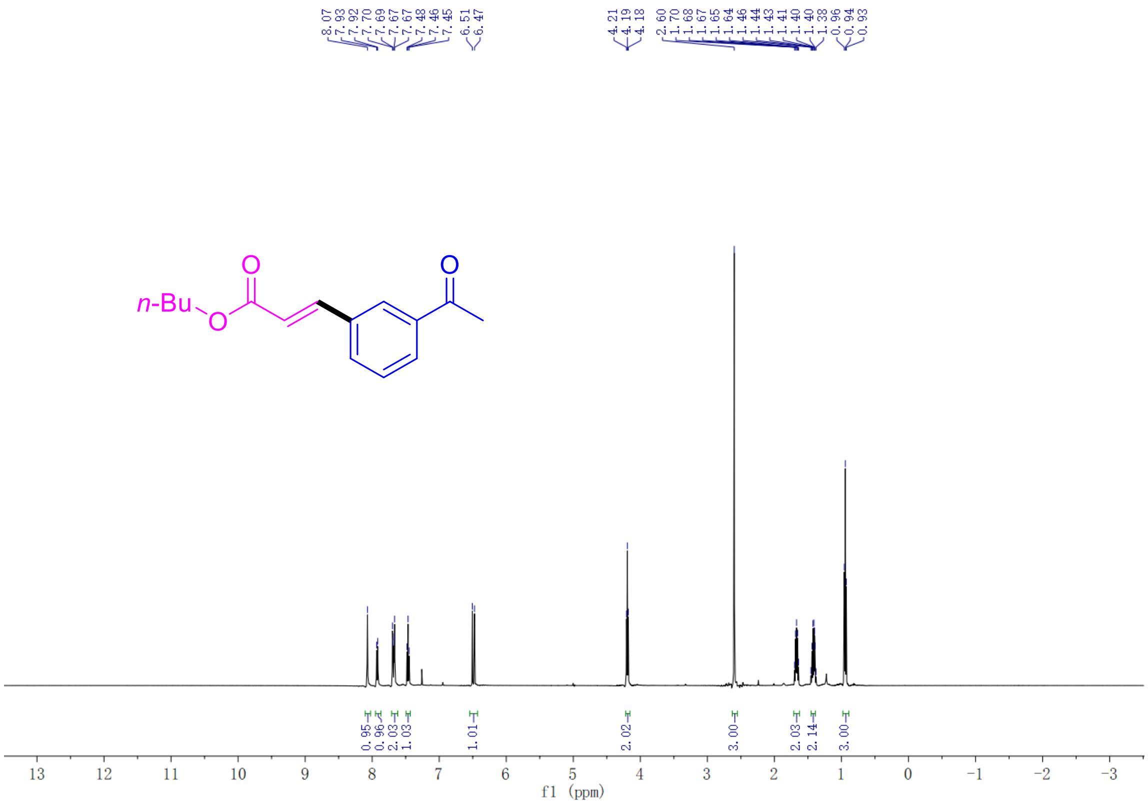
8.07
7.93
7.92
7.70
7.69
7.67
7.67
7.48
7.46
7.45
6.51
6.47
4.21
4.19
4.18
2.60
1.70
1.68
1.67
1.65
1.64
1.46
1.44
1.43
1.41
1.40
1.40
1.38
0.96
0.94
0.93
n-Bu
O
O
O
0.95
0.96
2.03
1.03
1.01
2.02
3.00
2.03
2.14
3.00
13
12
11
10
9
8
7
6
5
4
3
2
1
0
−1
−2
−3
f1 (ppm)

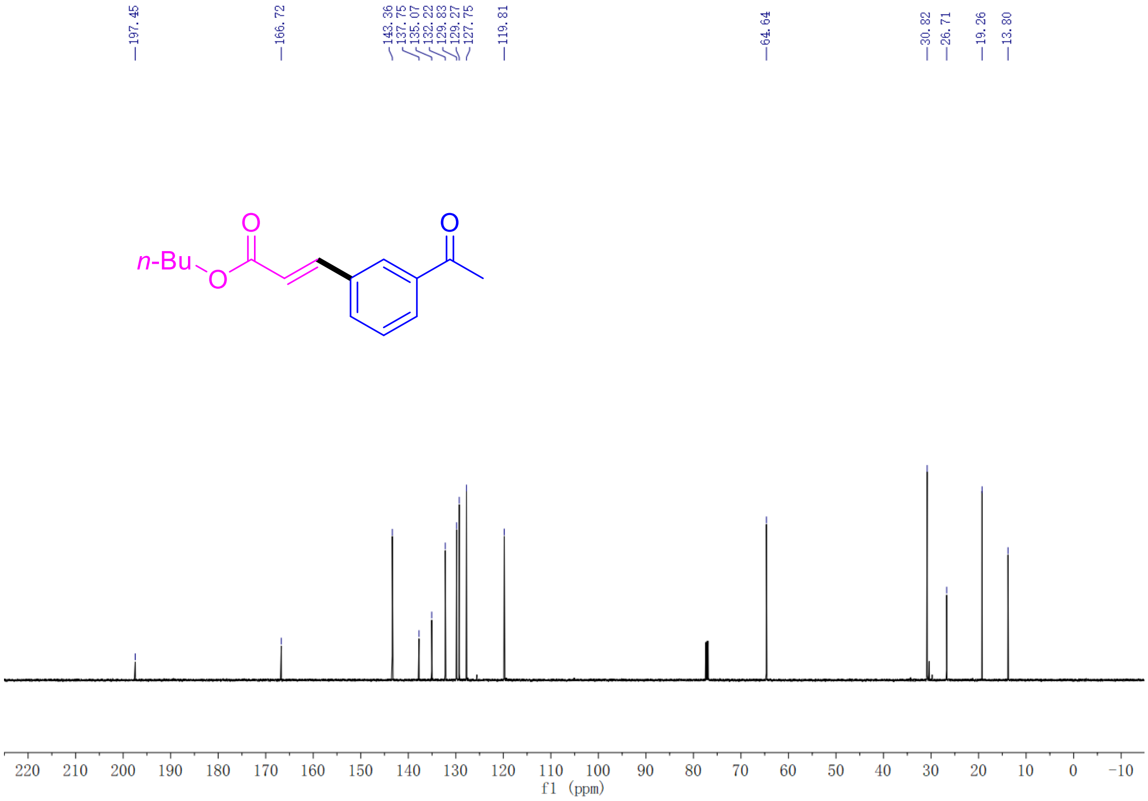
197.45
166.72
143.36
137.75
135.07
132.22
129.83
129.27
127.75
119.81
64.64
30.82
26.71
19.26
13.80
n-Bu
O
O
O
220
210
200
190
180
170
160
150
140
130
120
110
100
90
80
70
60
50
40
30
20
10
0
−10
f1 (ppm)

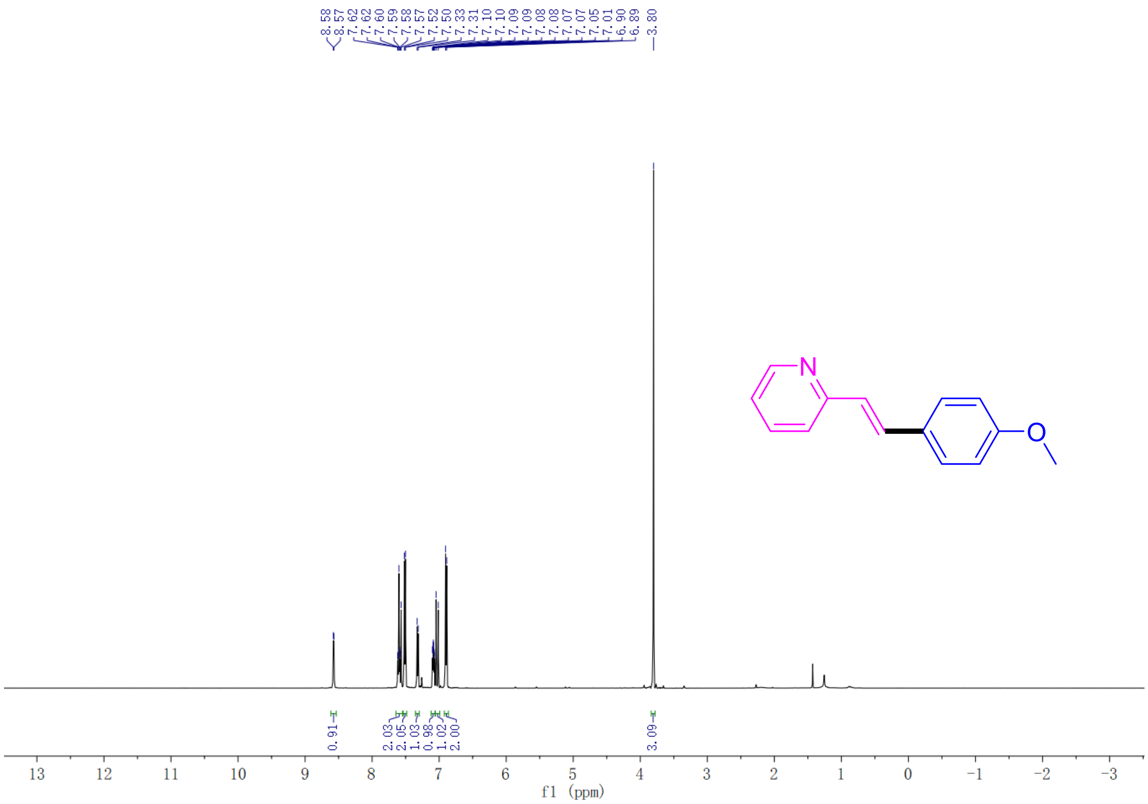
8.58
8.57
7.62
7.62
7.60
7.59
7.58
7.57
7.52
7.50
7.33
7.31
7.10
7.10
7.09
7.09
7.08
7.08
7.07
7.07
7.05
7.01
6.90
6.89
3.80
N
O
0.91
2.03
2.05
1.03
0.98
1.02
2.00
3.09
13 12 11 10 9 8 7 6 5 4 3 2 1 0 −1 −2 −3
f1 (ppm)

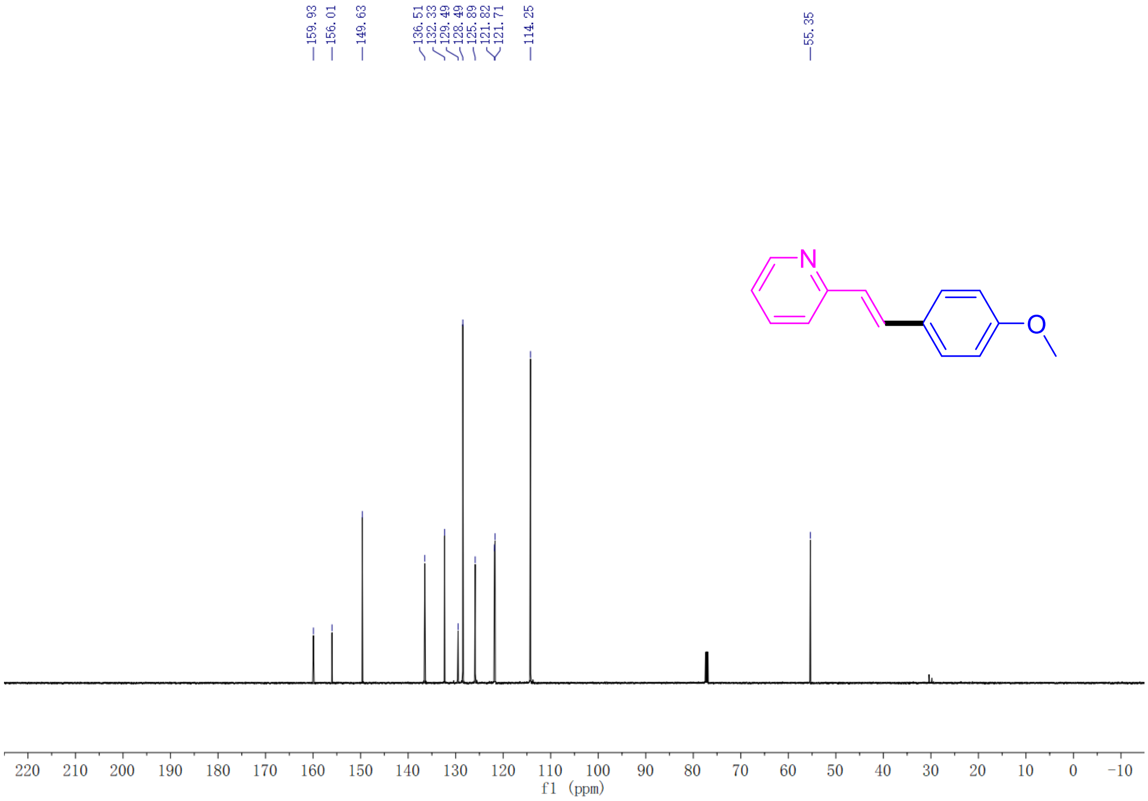
159.93
156.01
149.63
136.51
132.33
129.49
128.49
125.89
121.82
121.71
114.25
55.35
N
O
220 210 200 190 180 170 160 150 140 130 120 110 100 90 80 70 60 50 40 30 20 10 0 −10
f1 (ppm)

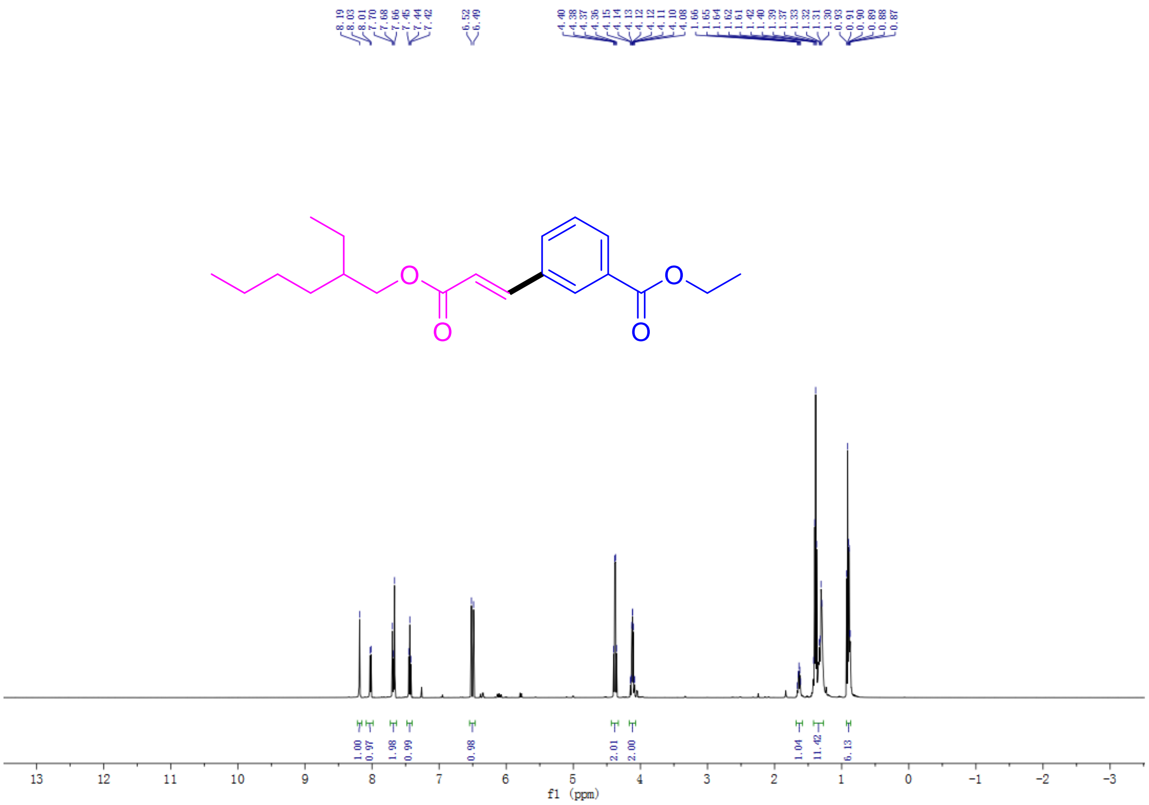
8.19
8.03
8.01
7.70
7.68
7.66
7.45
7.44
7.42
6.52
6.49
4.40
4.38
4.37
4.36
4.15
4.14
4.13
4.12
4.12
4.11
4.10
4.08
1.66
1.65
1.64
1.62
1.61
1.42
1.40
1.39
1.37
1.33
1.32
1.31
1.30
0.93
0.91
0.90
0.89
0.88
0.87
O
O
O
O
1.00
0.97
1.98
0.99
0.98
2.01
2.00
1.04
11.42
6.13
13
12
11
10
9
8
7
6
5
4
3
2
1
0
-1
-2
-3
f1 (ppm)

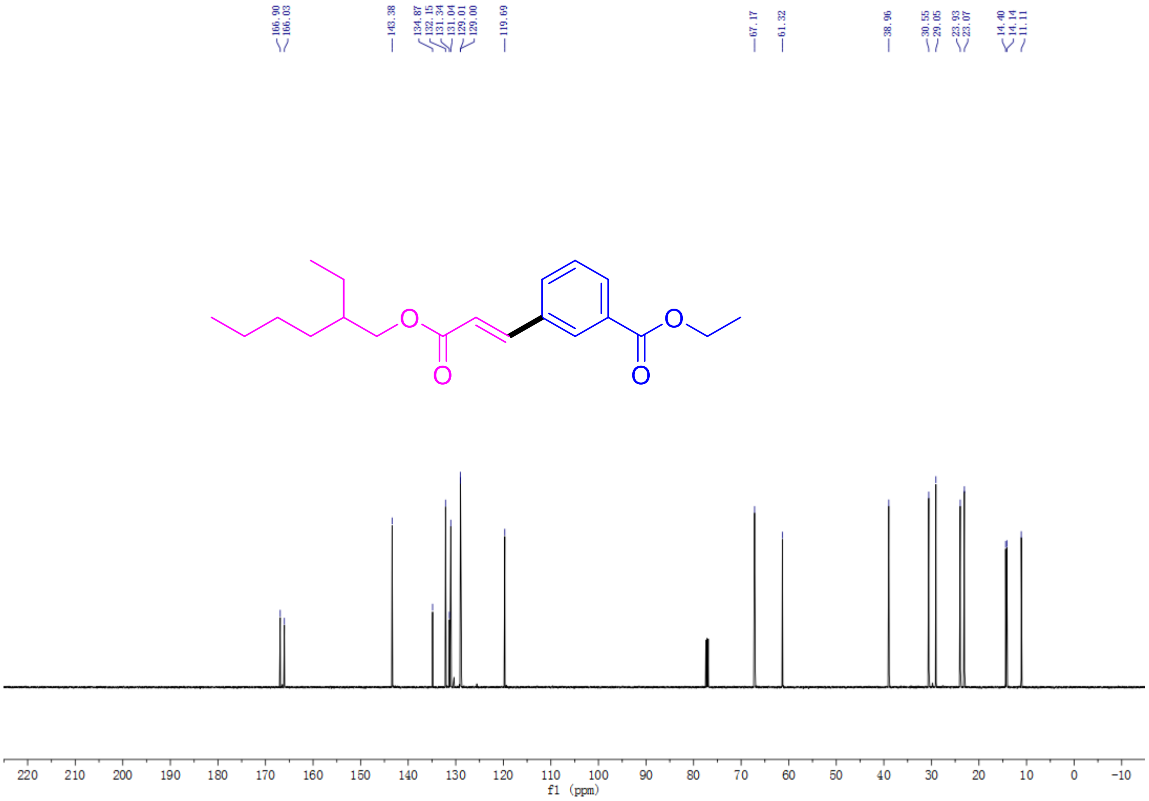
166.90
166.03
143.38
134.87
132.15
131.34
131.04
129.01
129.00
119.69
67.17
61.32
38.96
30.55
29.05
23.93
23.07
14.40
14.14
11.11
O
O
O
O
220
210
200
190
180
170
160
150
140
130
120
110
100
90
80
70
60
50
40
30
20
10
0
-10
f1 (ppm)

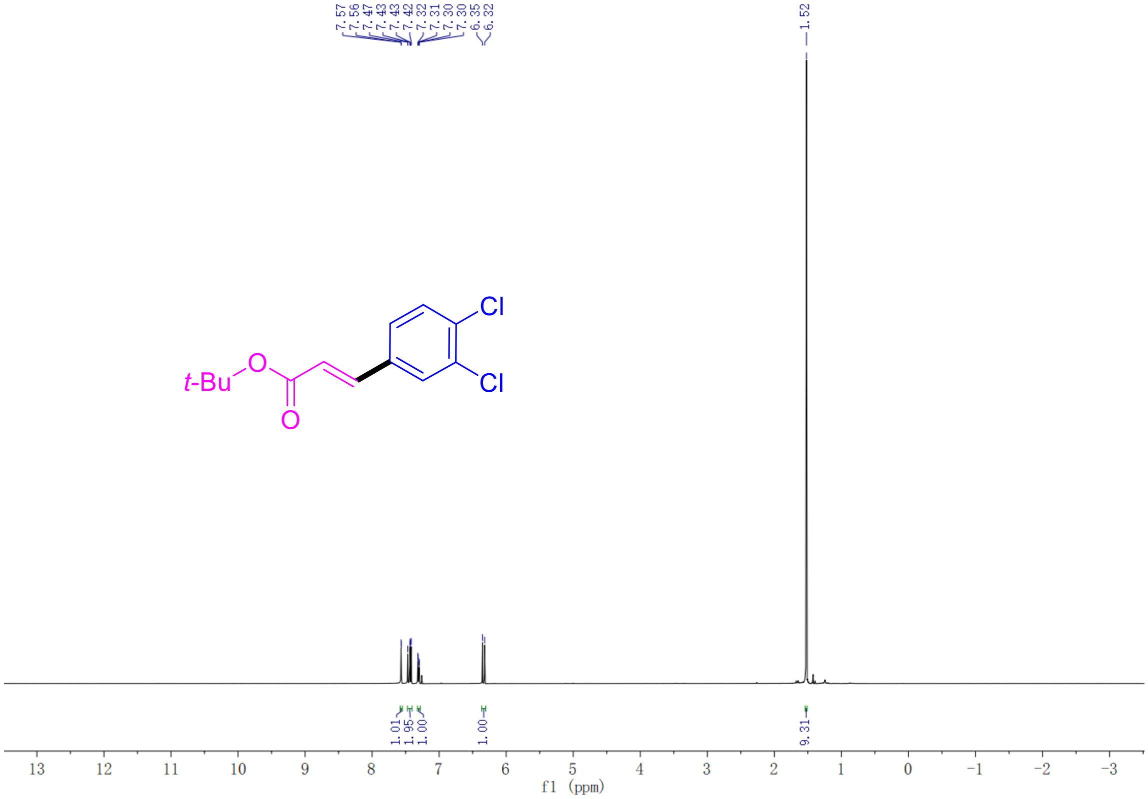
7.57
7.56
7.47
7.43
7.43
7.42
7.32
7.31
7.30
7.30
6.35
6.32
1.52
t-Bu
O
O
Cl
Cl
1.01
1.95
1.00
1.00
9.31
13
12
11
10
9
8
7
6
5
4
3
2
1
0
−1
−2
−3
f1 (ppm)

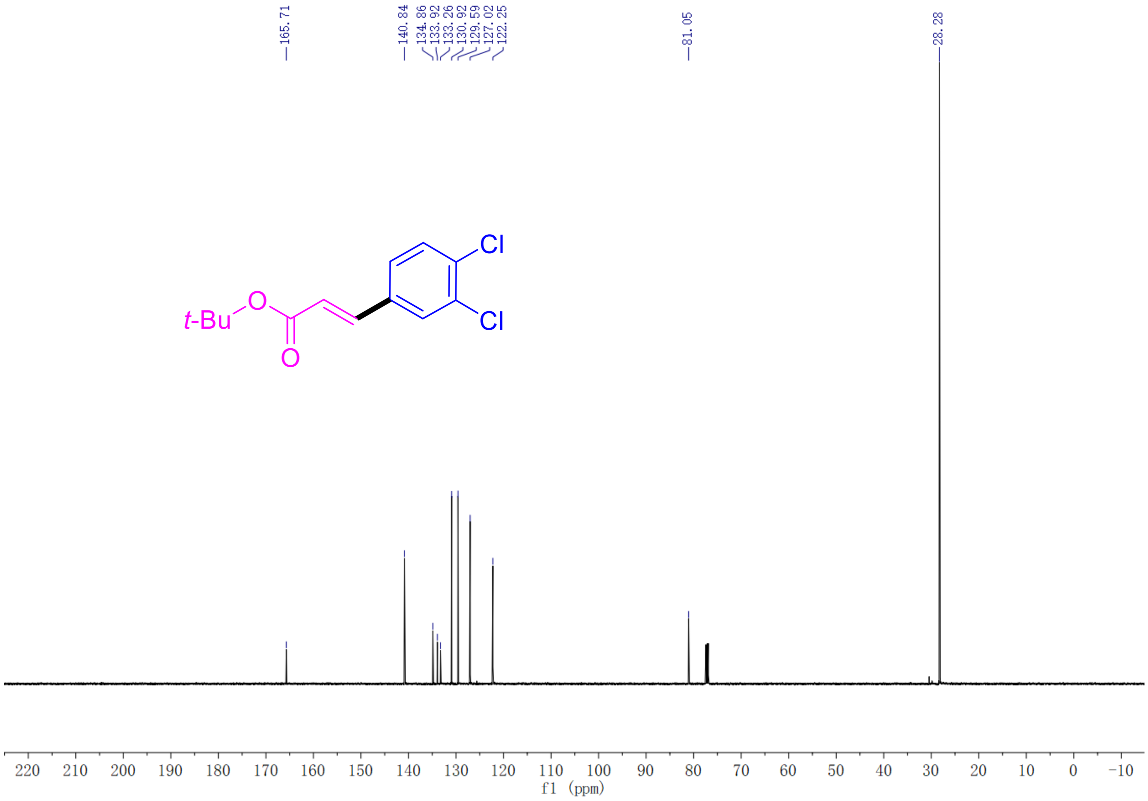
165.71
140.84
134.86
133.92
133.26
130.92
129.59
127.02
122.25
81.05
28.28
t-Bu
O
O
Cl
Cl
220
210
200
190
180
170
160
150
140
130
120
110
100
90
80
70
60
50
40
30
20
10
0
−10
f1 (ppm)

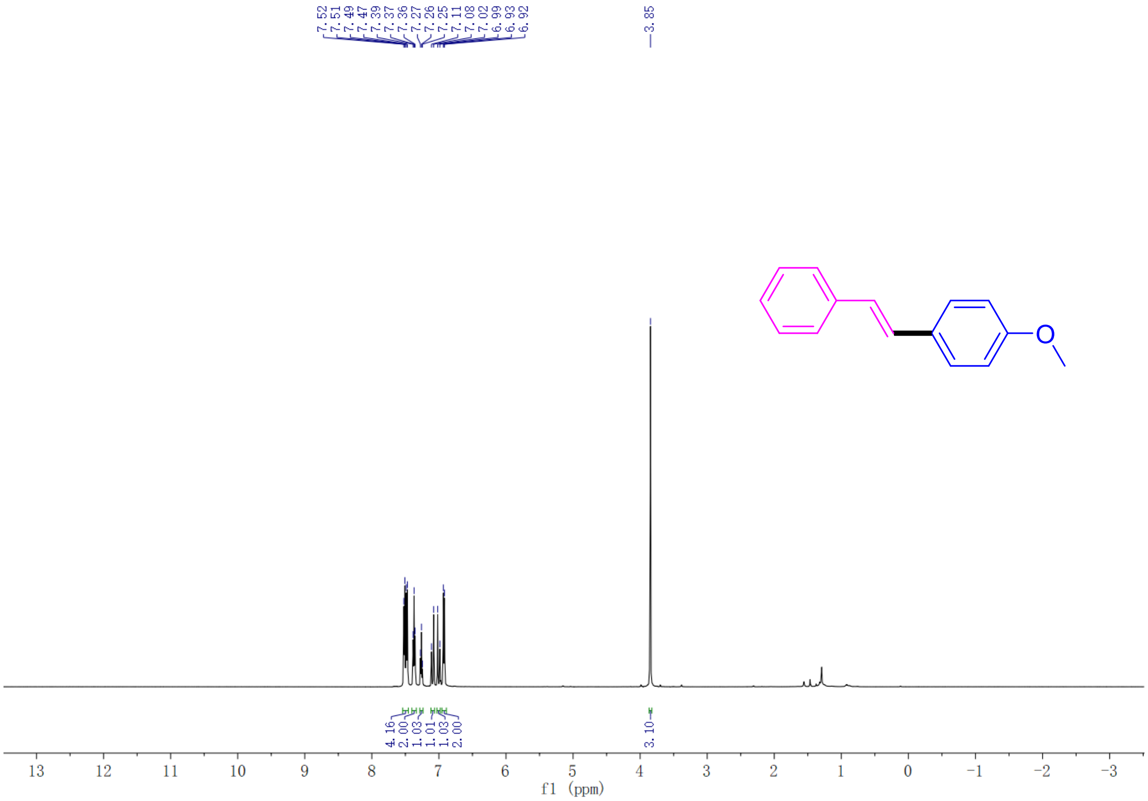
7.52
7.51
7.49
7.47
7.39
7.37
7.36
7.27
7.26
7.25
7.11
7.08
7.02
6.99
6.93
6.92
3.85
O
4.16
2.00
1.03
1.01
1.03
2.00
3.10
13
12
11
10
9
8
7
6
5
4
3
2
1
0
-1
-2
-3
f1 (ppm)

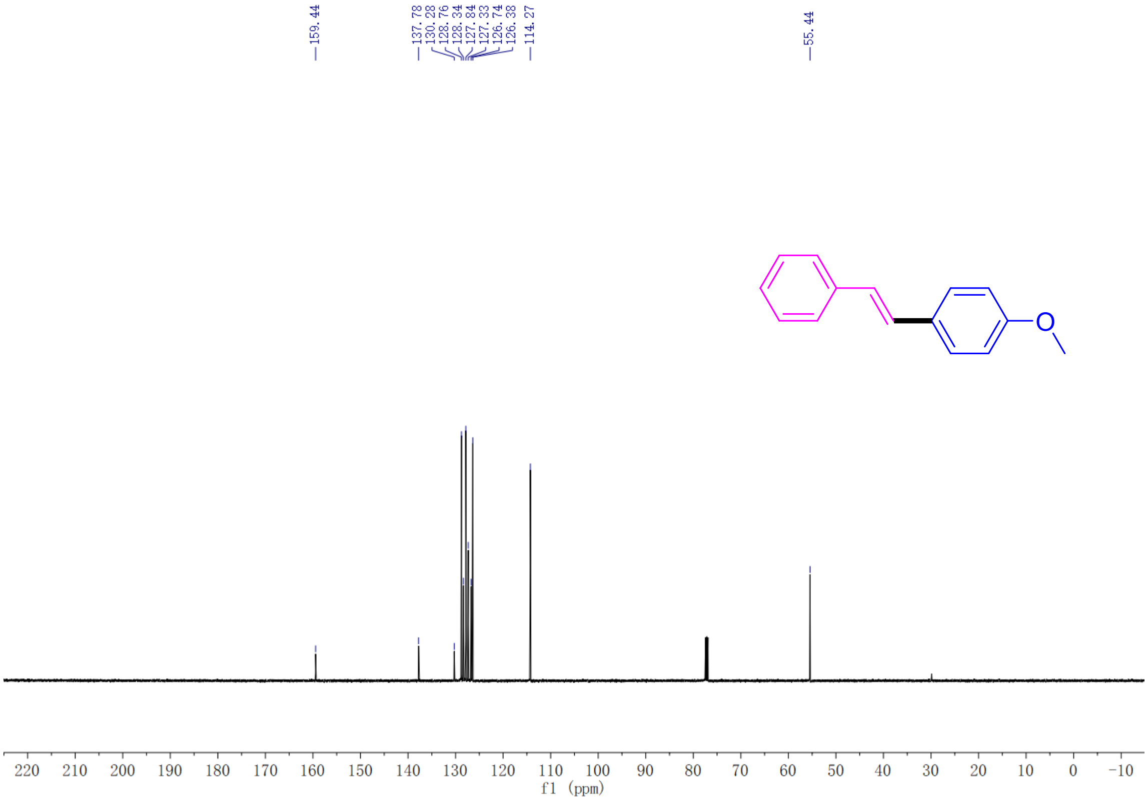
159.44
137.78
130.28
128.76
128.34
127.84
127.33
126.74
126.38
114.27
55.44
O
220
210
200
190
180
170
160
150
140
130
120
110
100
90
80
70
60
50
40
30
20
10
0
-10
f1 (ppm)

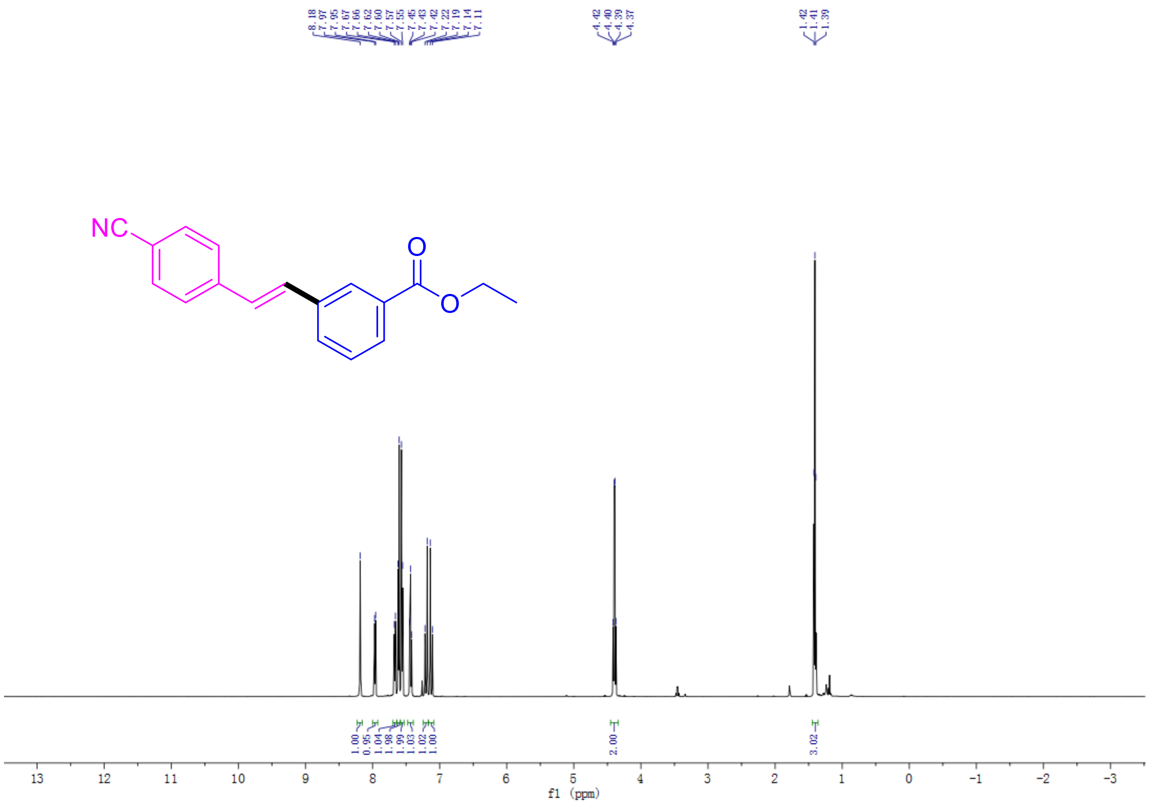
8.18
7.97
7.95
7.67
7.66
7.62
7.60
7.57
7.55
7.45
7.43
7.42
7.22
7.19
7.14
7.11
4.42
4.40
4.39
4.37
1.42
1.41
1.39
NC
O
O
1.00
0.95
1.04
1.98
1.99
1.03
1.02
1.00
2.00
3.02
13
12
11
10
9
8
7
6
5
4
3
2
1
0
-1
-2
-3
f1 (ppm)

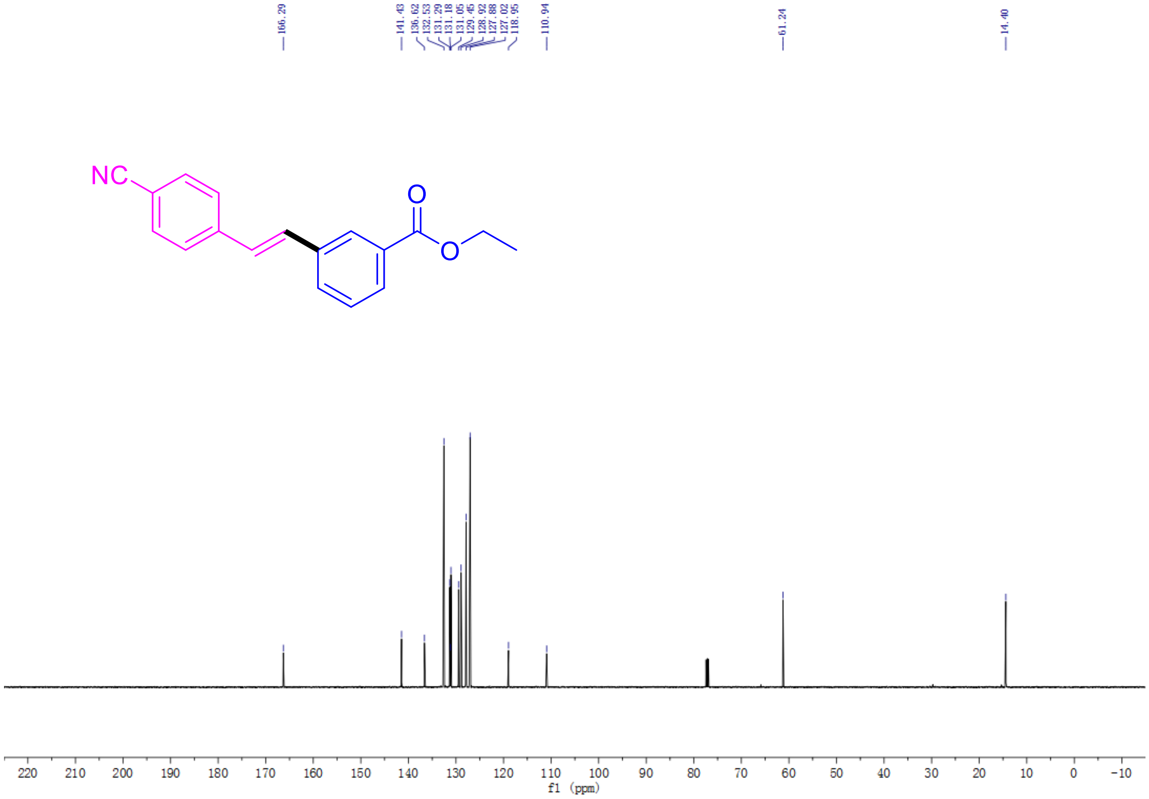
166.29
141.43
136.62
132.53
131.29
131.18
131.05
129.45
128.92
127.88
127.02
118.95
110.94
61.24
14.40
NC
O
O
220
210
200
190
180
170
160
150
140
130
120
110
100
90
80
70
60
50
40
30
20
10
0
-10
f1 (ppm)

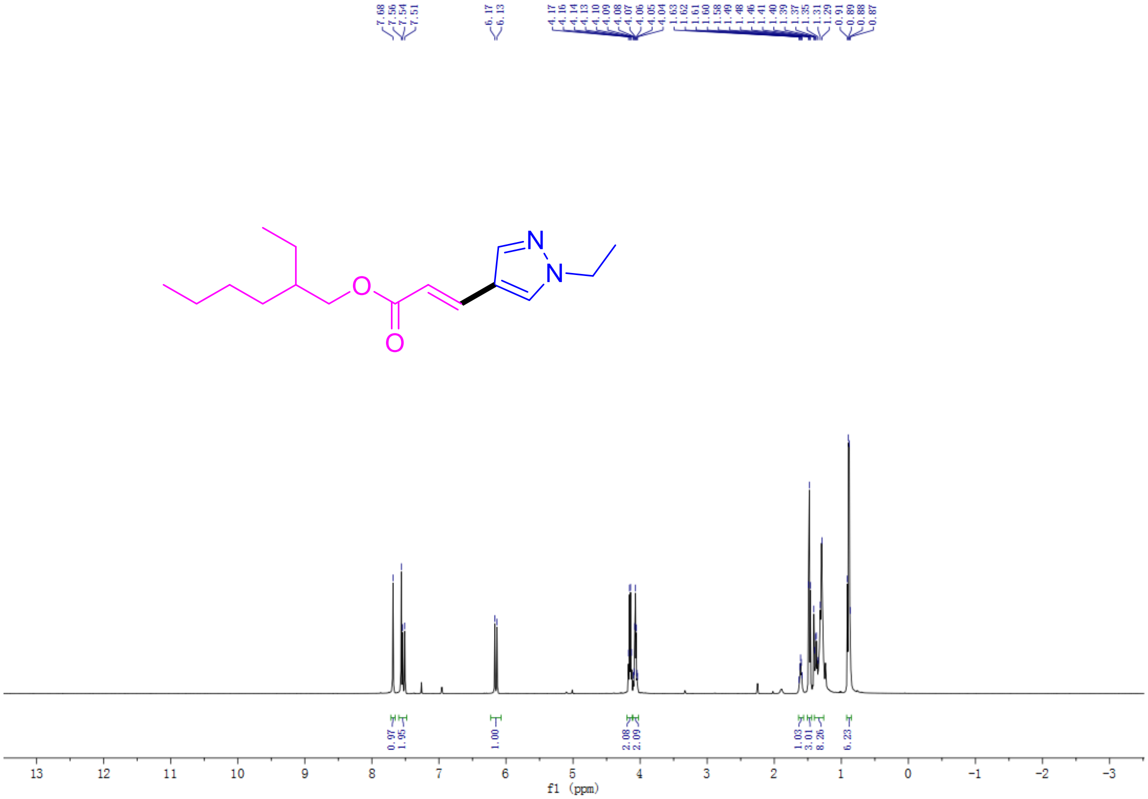
7.68
7.56
7.54
7.51
6.17
6.13
4.17
4.16
4.14
4.13
4.10
4.09
4.08
4.07
4.06
4.05
4.04
1.63
1.62
1.61
1.60
1.58
1.49
1.48
1.46
1.41
1.40
1.39
1.37
1.35
1.31
1.29
0.91
0.89
0.88
0.87
N
N
O
O
0.97
1.95
1.00
2.08
2.09
1.03
3.01
8.26
6.23
13
12
11
10
9
8
7
6
5
4
3
2
1
0
-1
-2
-3
f1 (ppm)

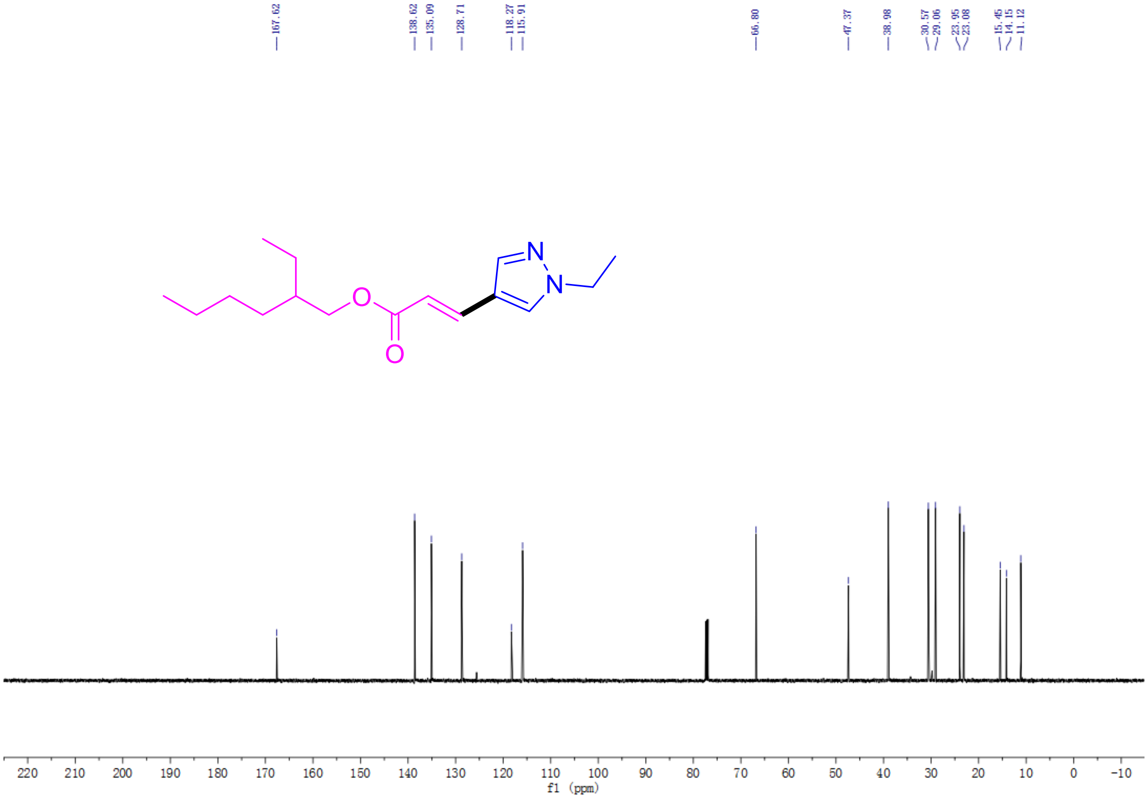
167.62
138.62
135.09
128.71
118.27
115.91
66.80
47.37
38.98
30.57
29.06
23.95
23.08
15.45
14.15
11.12
N
N
O
O
220
210
200
190
180
170
160
150
140
130
120
110
100
90
80
70
60
50
40
30
20
10
0
-10
f1 (ppm)

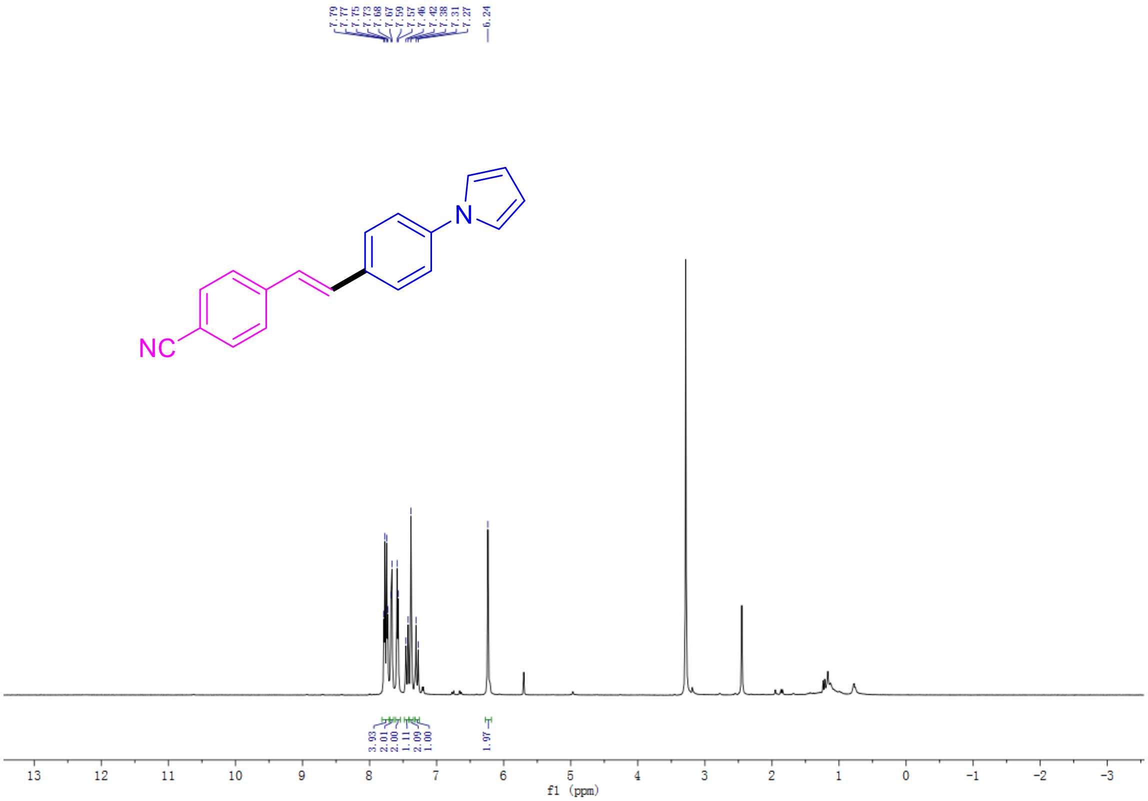
7.79
7.77
7.75
7.73
7.68
7.67
7.59
7.57
7.46
7.42
7.38
7.31
7.27
6.24
N
NC
3.93
2.01
2.00
1.11
2.09
1.00
1.97
13
12
11
10
9
8
7
6
5
4
3
2
1
0
-1
-2
-3
f1 (ppm)

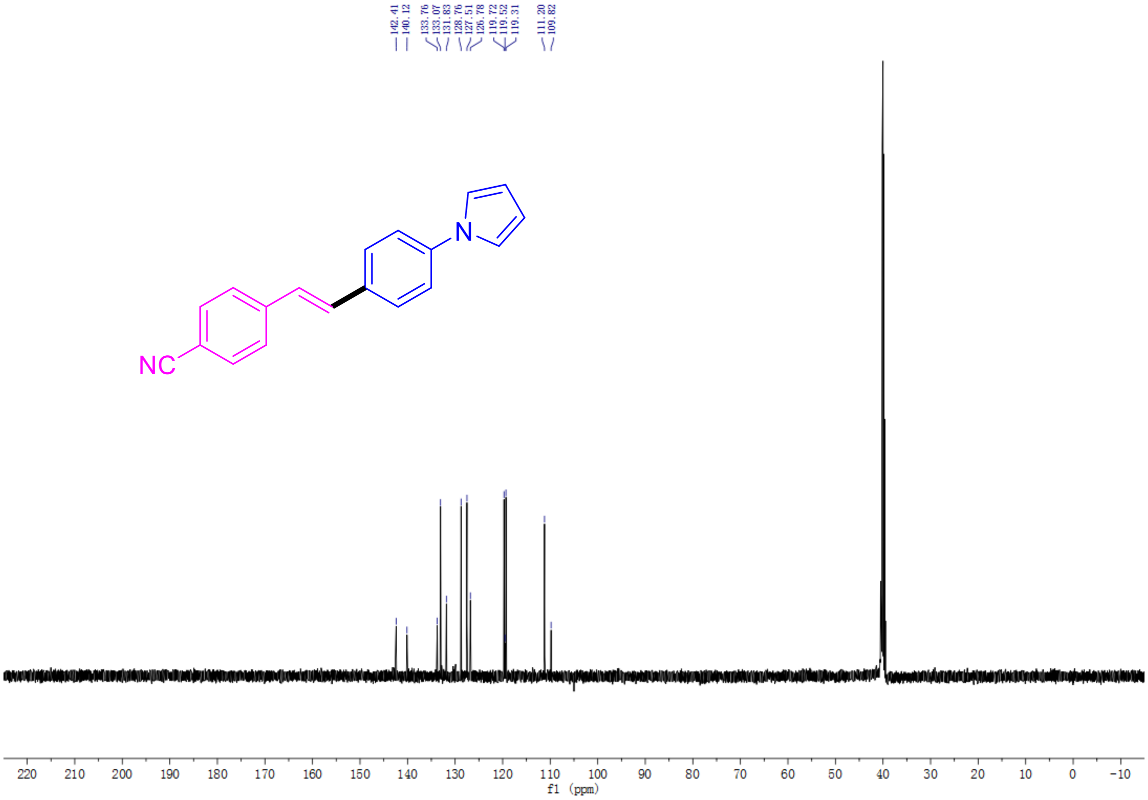
142.41
140.12
133.76
133.07
131.83
128.76
127.51
126.78
119.72
119.52
119.31
111.20
109.82
N
NC
220
210
200
190
180
170
160
150
140
130
120
110
100
90
80
70
60
50
40
30
20
10
0
-10
f1 (ppm)

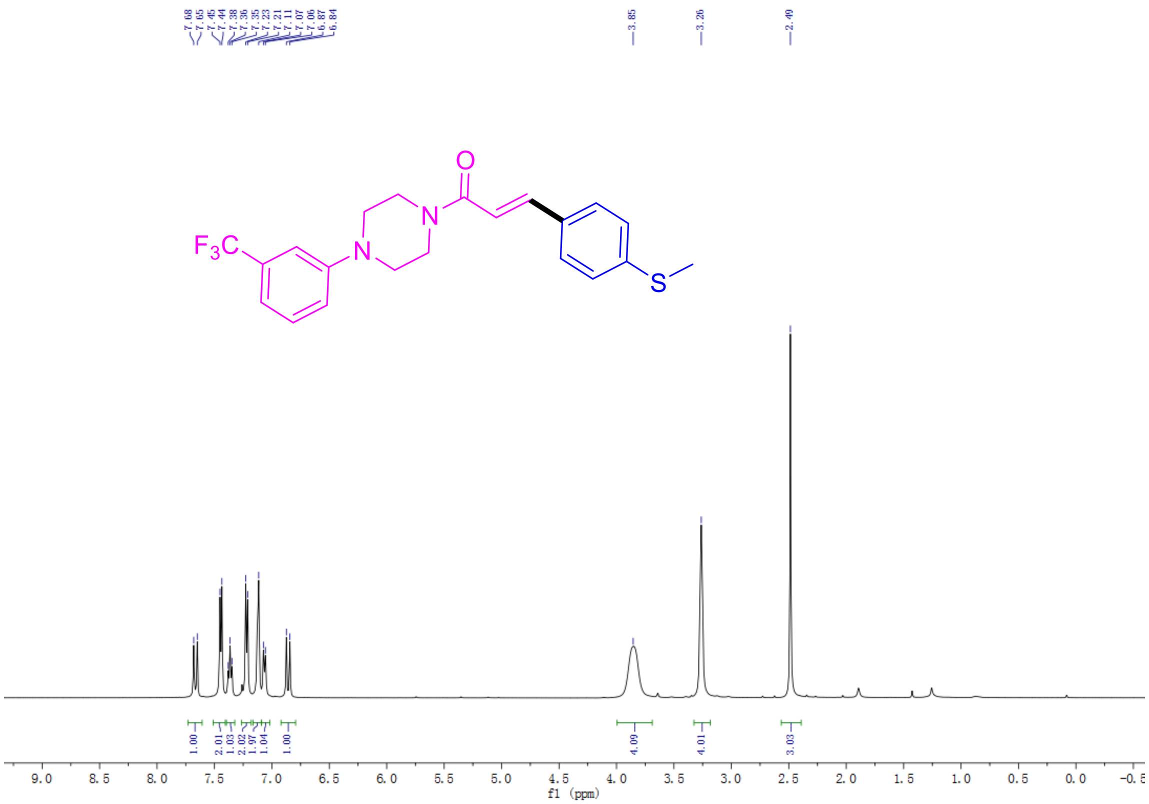
7.68
7.65
7.45
7.44
7.38
7.36
7.35
7.23
7.21
7.11
7.07
7.06
6.87
6.84
3.85
3.26
2.49
O
N
N
F3C
S
1.00
2.01
1.03
2.02
1.97
1.04
1.00
4.09
4.01
3.03
9.0
8.5
8.0
7.5
7.0
6.5
6.0
5.5
5.0
4.5
4.0
3.5
3.0
2.5
2.0
1.5
1.0
0.5
0.0
-0.5
f1 (ppm)

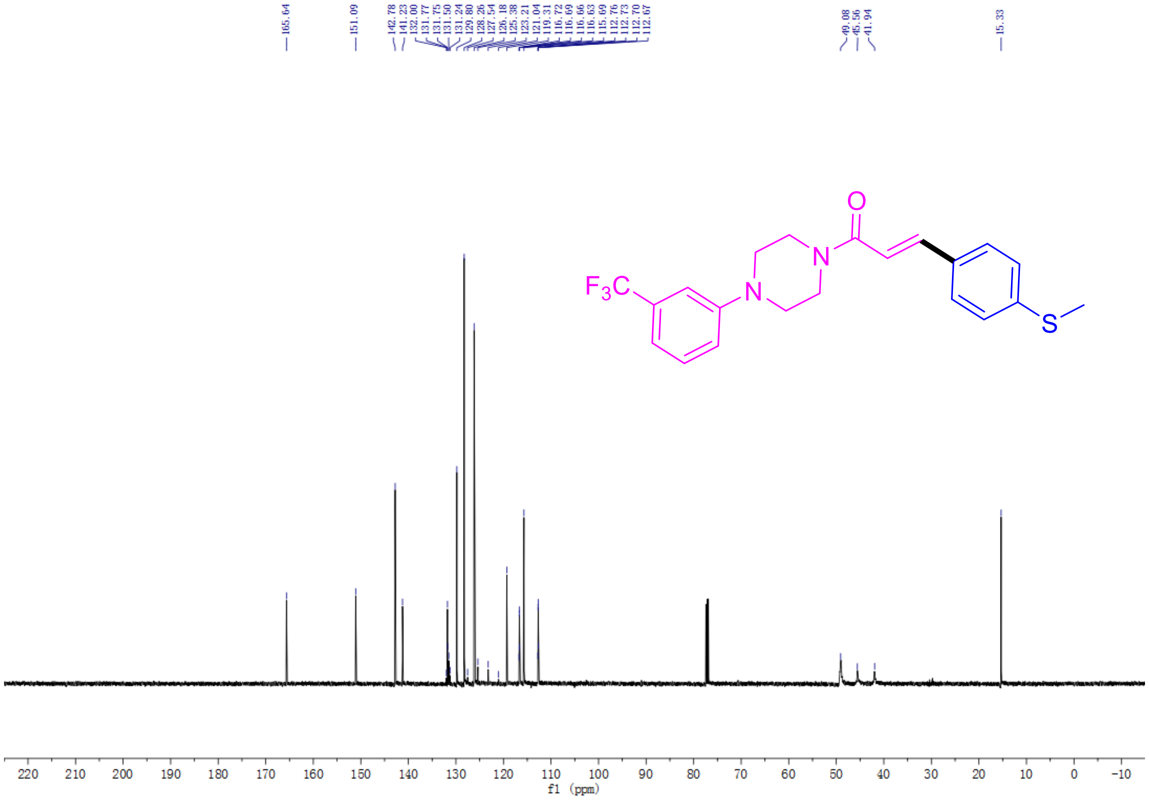
165.64
151.09
142.78
141.23
132.00
131.77
131.75
131.50
131.24
129.80
128.26
127.54
126.18
125.38
123.21
121.04
119.31
116.72
116.69
116.66
116.63
115.69
112.76
112.73
112.70
112.67
49.08
45.56
41.94
15.33
O
N
N
F3C
S
220
210
200
190
180
170
160
150
140
130
120
110
100
90
80
70
60
50
40
30
20
10
0
-10
f1 (ppm)

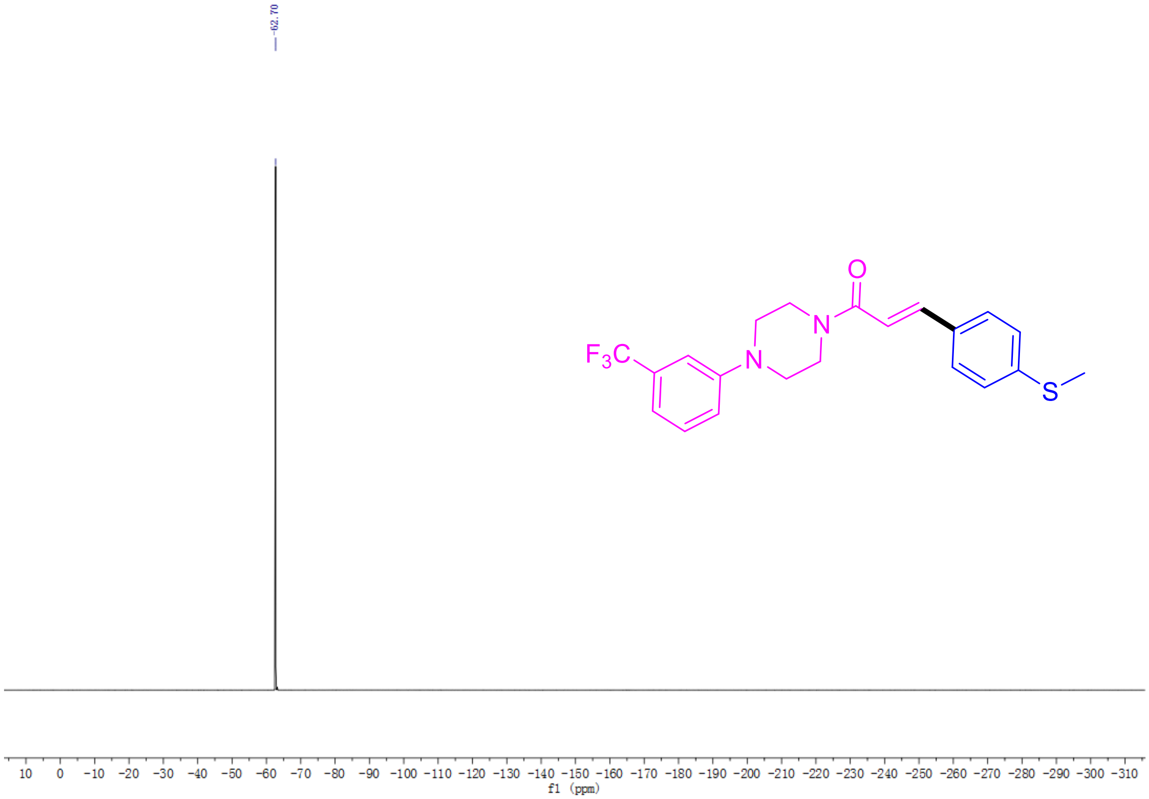
-62.70
F3C
N
N
O
S
10 0 -10 -20 -30 -40 -50 -60 -70 -80 -90 -100 -110 -120 -130 -140 -150 -160 -170 -180 -190 -200 -210 -220 -230 -240 -250 -260 -270 -280 -290 -300 -310
f1 (ppm)

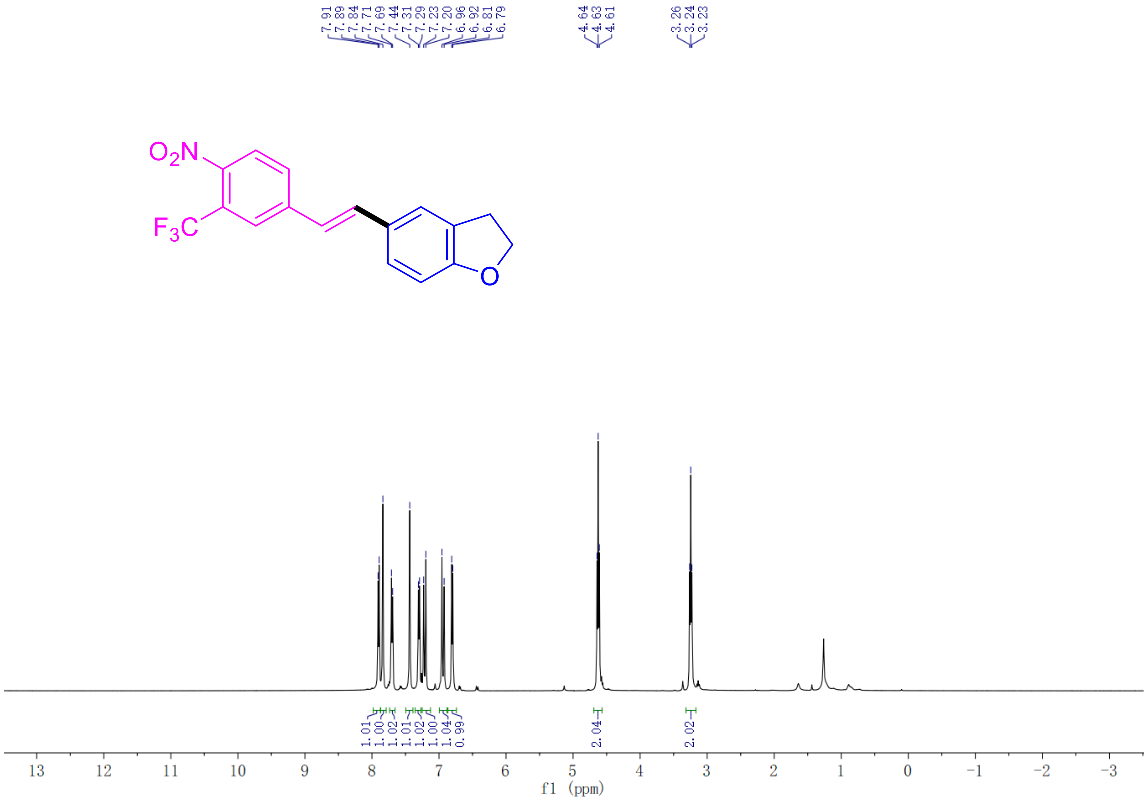
7.91
7.89
7.84
7.71
7.69
7.44
7.31
7.29
7.23
7.20
6.96
6.92
6.81
6.79
4.64
4.63
4.61
3.26
3.24
3.23
O2N
F3C
O
1.01
1.00
1.02
1.01
1.02
1.00
1.04
0.99
2.04
2.02
13 12 11 10 9 8 7 6 5 4 3 2 1 0 −1 −2 −3
f1 (ppm)

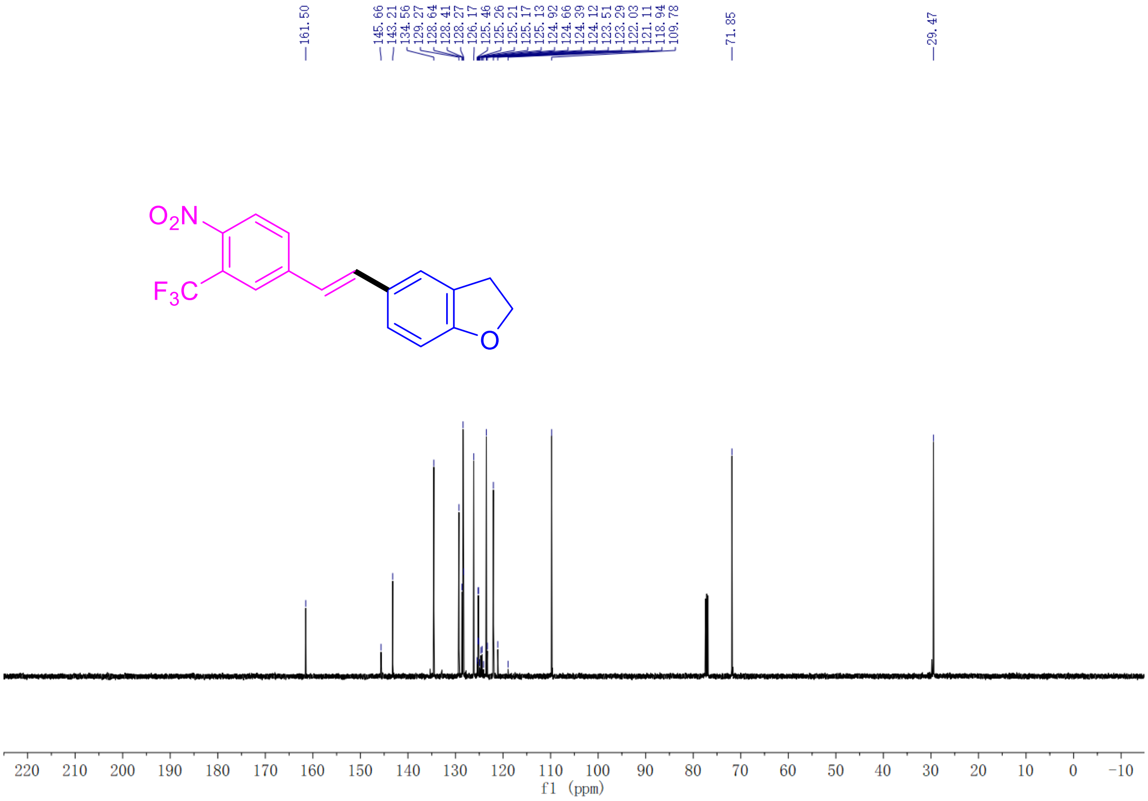
161.50
145.66
143.21
134.56
129.27
128.64
128.41
128.27
126.17
125.46
125.26
125.21
125.17
125.13
124.92
124.66
124.39
124.12
123.51
123.29
122.03
121.11
118.94
109.78
71.85
29.47
O2N
F3C
O
220 210 200 190 180 170 160 150 140 130 120 110 100 90 80 70 60 50 40 30 20 10 0 −10
f1 (ppm)

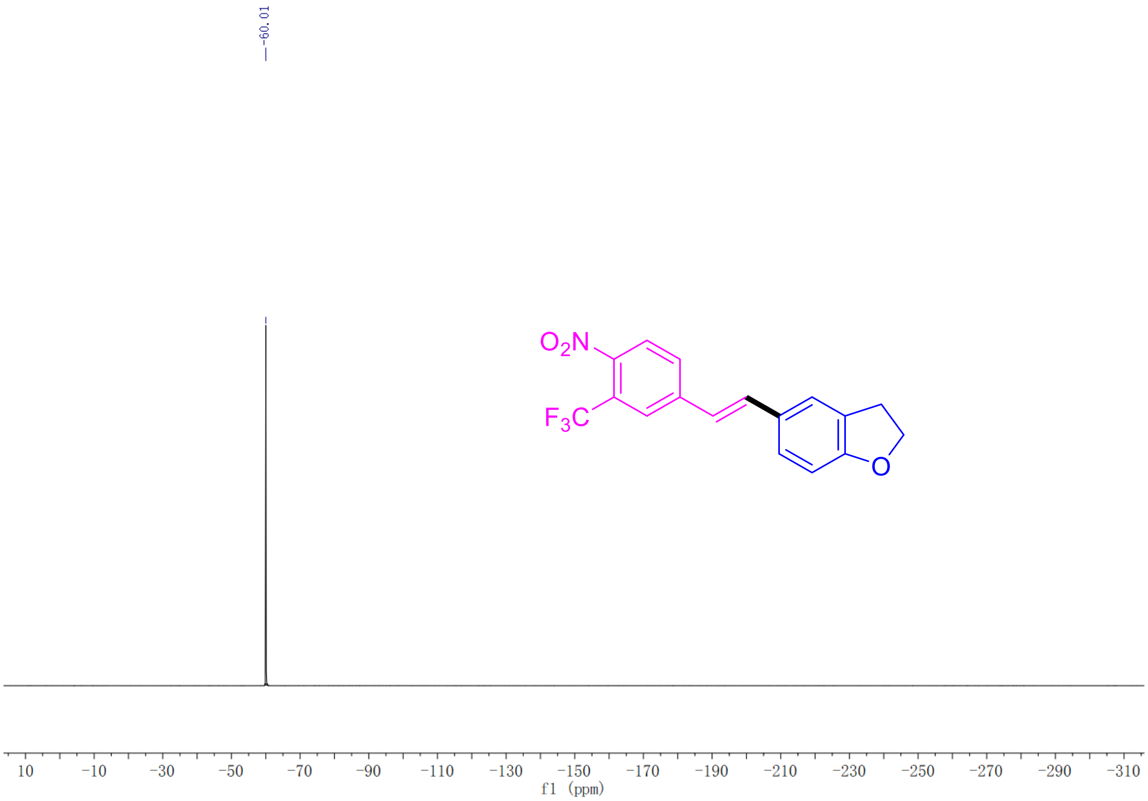
-60.01
O2N
F3C
O
10
-10
-30
-50
-70
-90
-110
-130
-150
-170
-190
-210
-230
-250
-270
-290
-310
f1 (ppm)

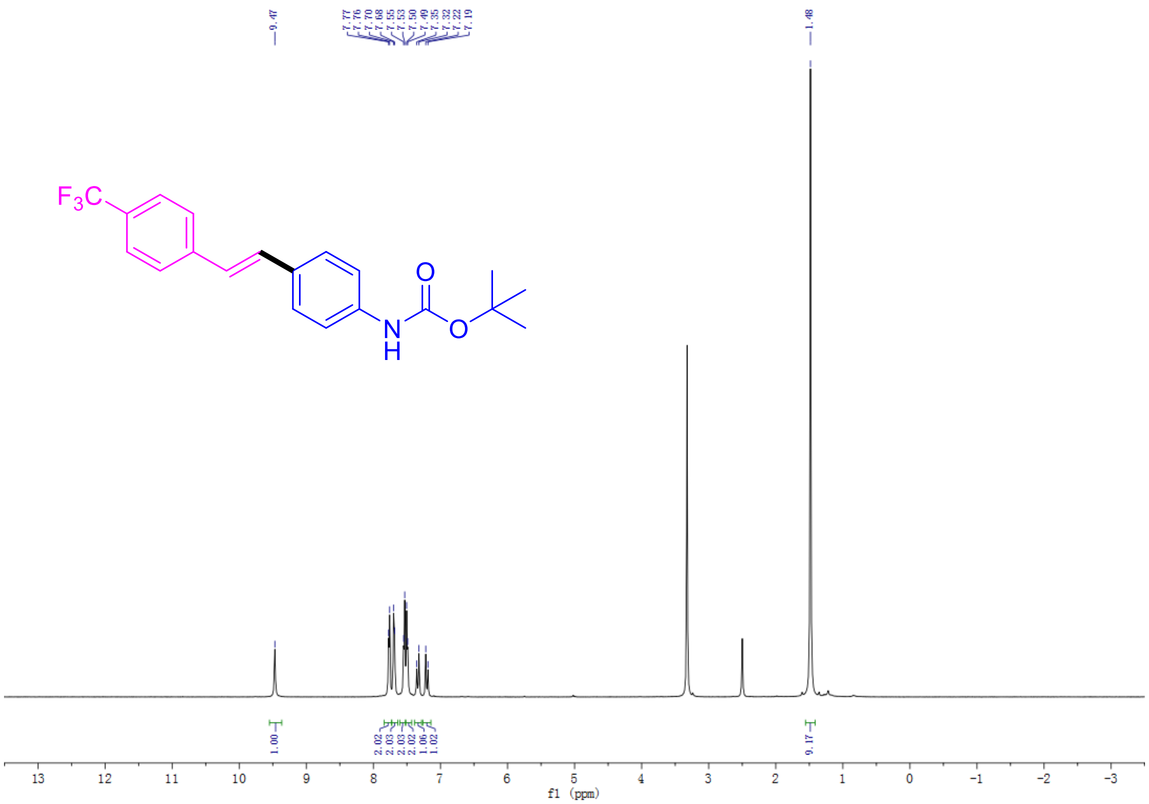

9.47
7.77
7.76
7.70
7.68
7.55
7.53
7.50
7.49
7.35
7.32
7.22
7.19
1.48
F3C
N
H
O
O
1.00
2.02
2.03
2.03
2.02
1.06
1.02
9.17
13
12
11
10
9
8
7
6
5
4
3
2
1
0
-1
-2
-3
f1 (ppm)

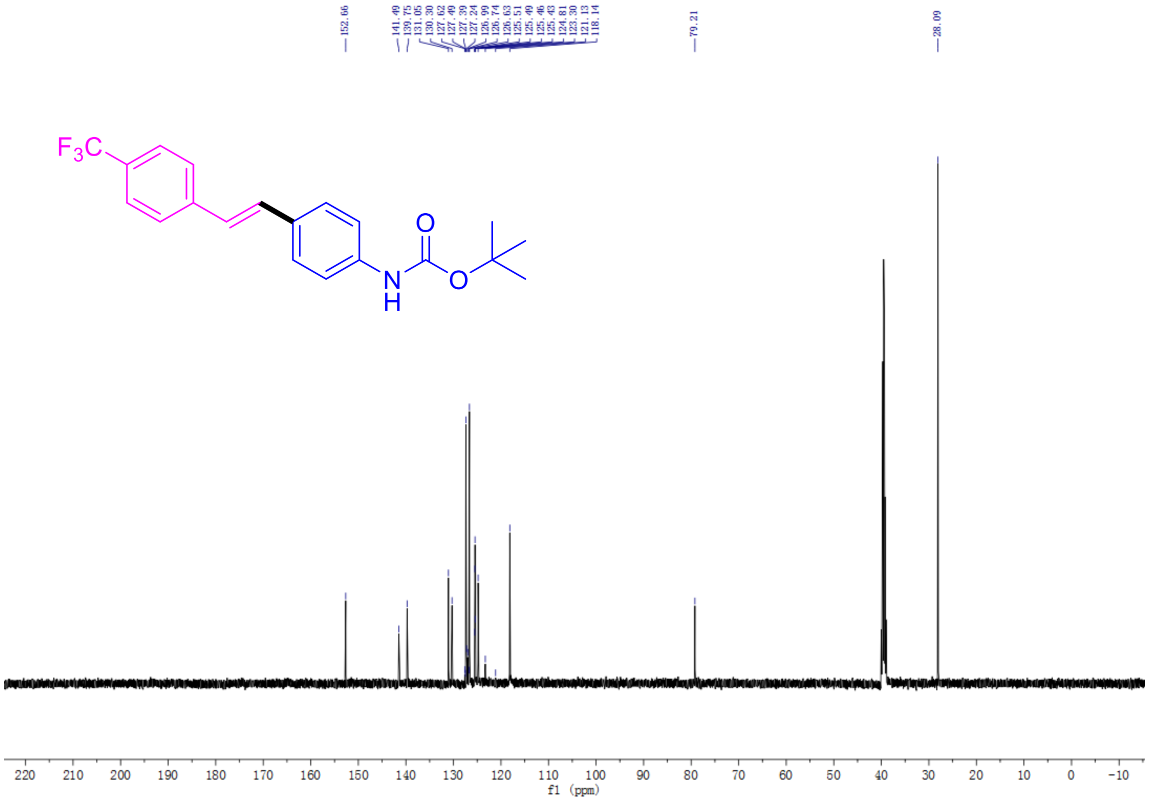

152.66
141.49
139.75
131.05
130.30
127.62
127.49
127.39
127.24
126.99
126.74
126.63
125.51
125.49
125.46
125.43
124.81
123.30
121.13
118.14
79.21
28.09
F3C
N
H
O
O
220
210
200
190
180
170
160
150
140
130
120
110
100
90
80
70
60
50
40
30
20
10
0
-10
f1 (ppm)

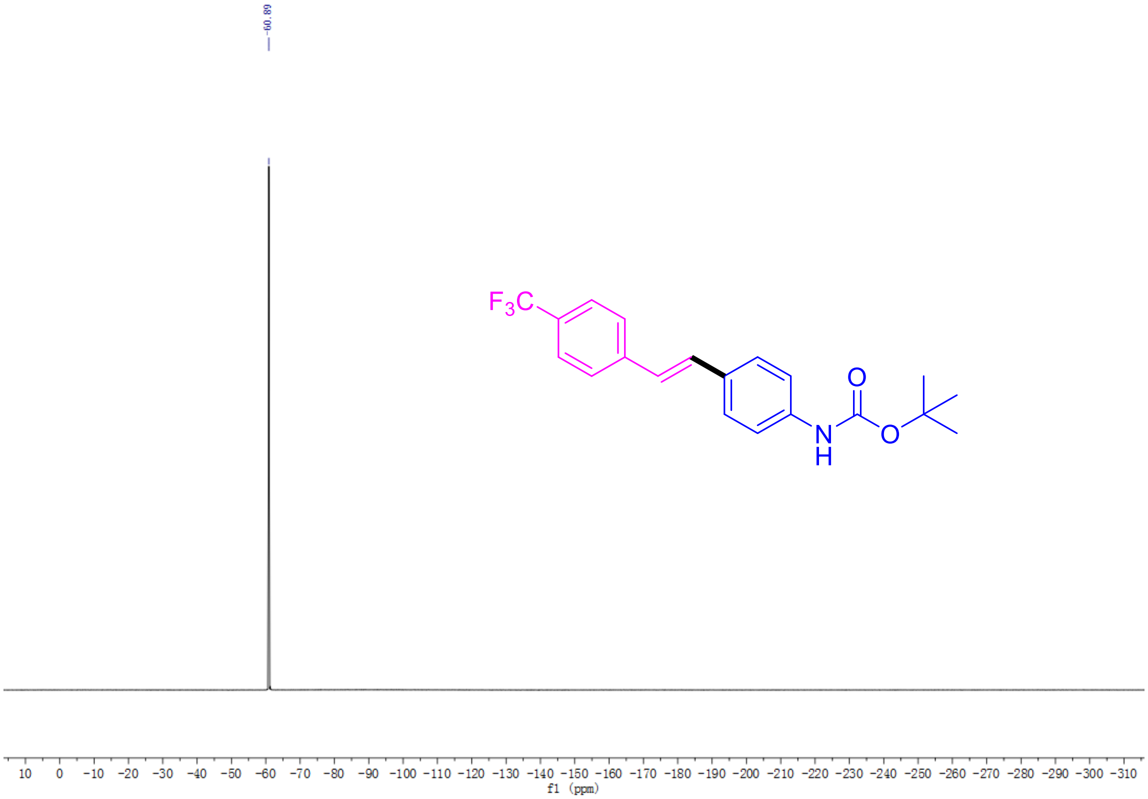
-60.89
F3C
O
N
H
O
10 0 -10 -20 -30 -40 -50 -60 -70 -80 -90 -100 -110 -120 -130 -140 -150 -160 -170 -180 -190 -200 -210 -220 -230 -240 -250 -260 -270 -280 -290 -300 -310
f1 (ppm)

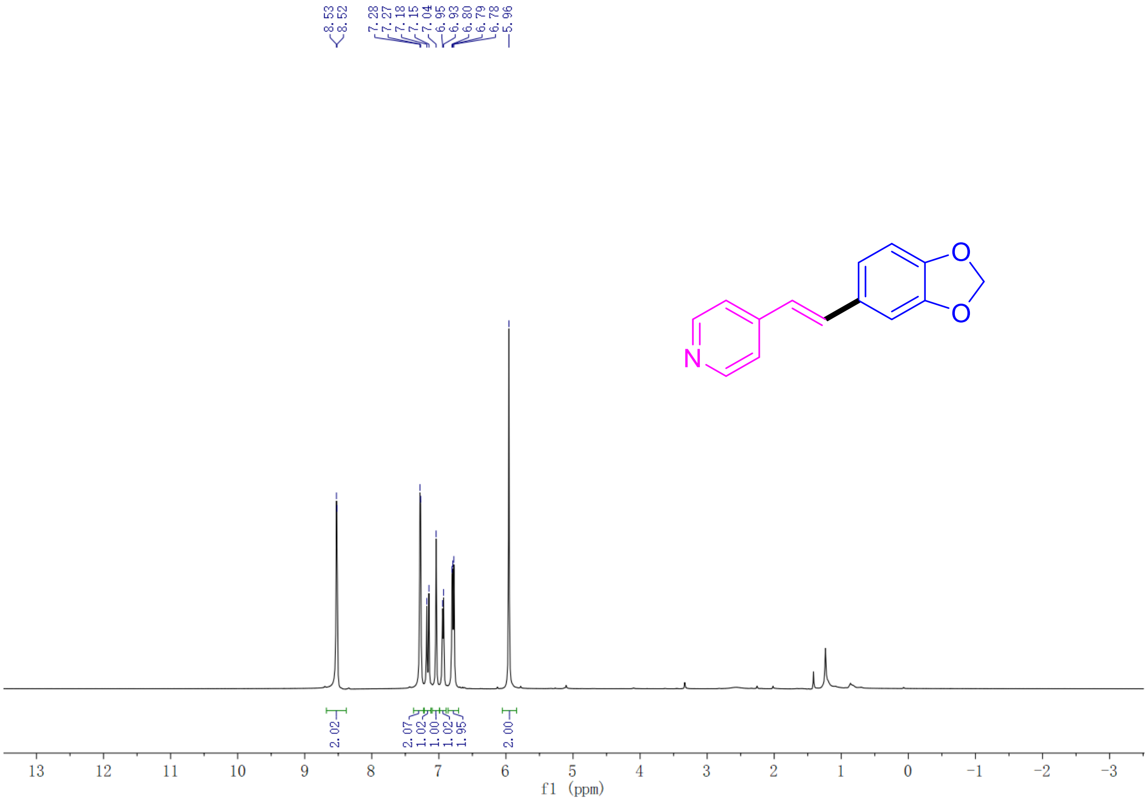
8.53
8.52
7.28
7.27
7.18
7.15
7.04
6.95
6.93
6.80
6.79
6.78
5.96
N
O
O
2.02
2.07
1.02
1.00
1.02
1.95
2.00
13
12
11
10
9
8
7
6
5
4
3
2
1
0
−1
−2
−3
f1 (ppm)

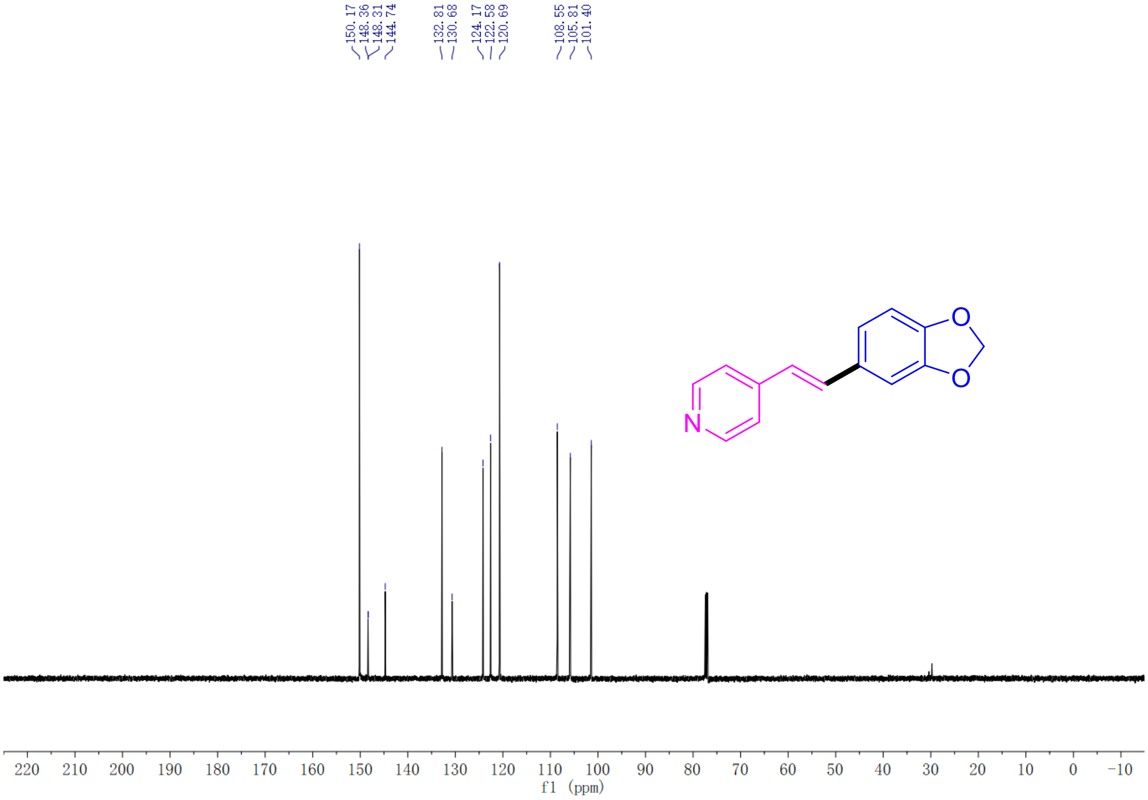
150.17
148.36
148.31
144.74
132.81
130.68
124.17
122.58
120.69
108.55
105.81
101.40
N
O
O
220
210
200
190
180
170
160
150
140
130
120
110
100
90
80
70
60
50
40
30
20
10
0
−10
f1 (ppm)

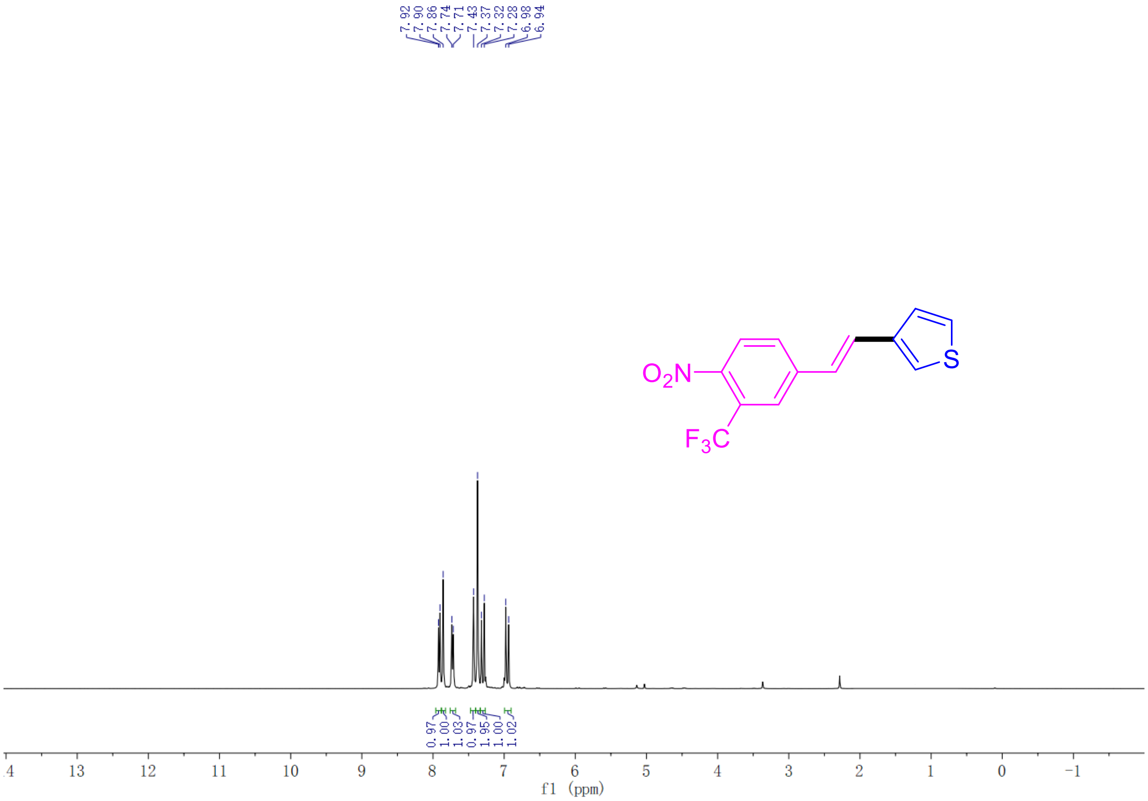
7.92
7.90
7.86
7.74
7.71
7.43
7.37
7.32
7.28
6.98
6.94
O_2N
F_3C
S
0.97
1.00
1.03
0.97
1.95
1.00
1.02
4
13
12
11
10
9
8
7
6
5
4
3
2
1
0
-1
f1 (ppm)

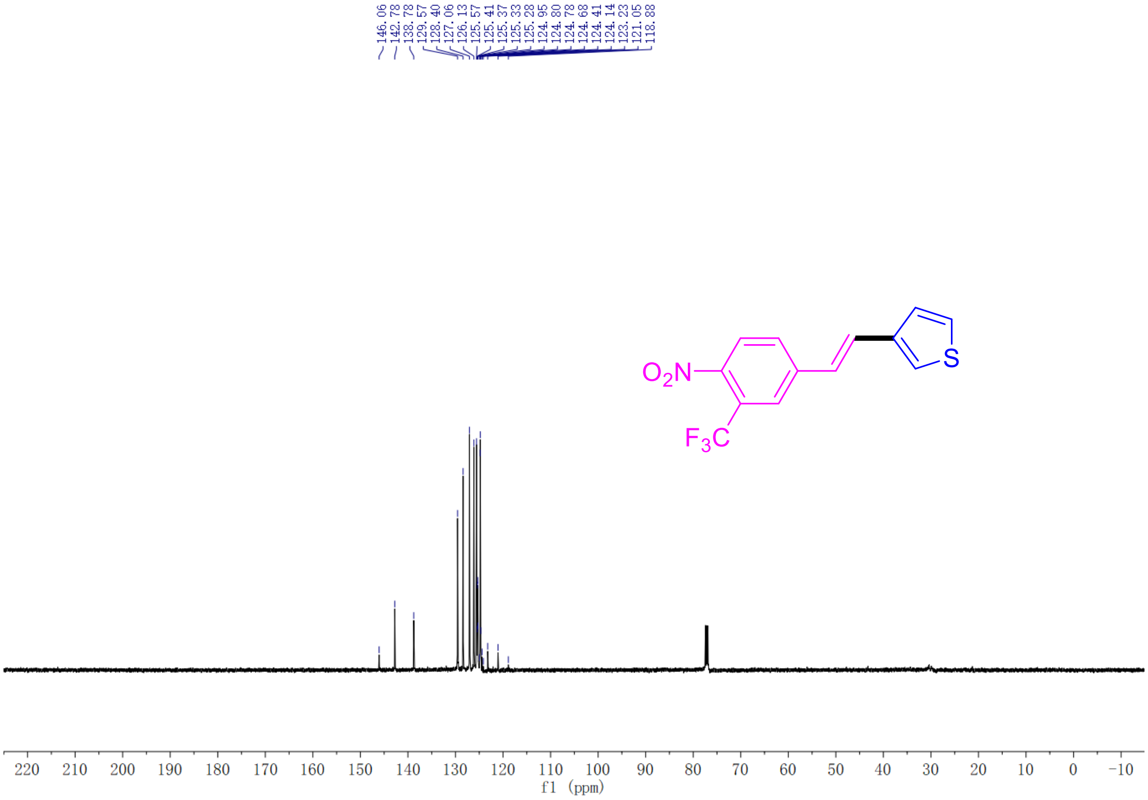
146.06
142.78
138.78
129.57
128.40
127.06
126.13
125.57
125.41
125.37
125.33
125.28
124.95
124.80
124.78
124.68
124.41
124.14
123.23
121.05
118.88
O_2N
F_3C
S
220
210
200
190
180
170
160
150
140
130
120
110
100
90
80
70
60
50
40
30
20
10
0
-10
f1 (ppm)

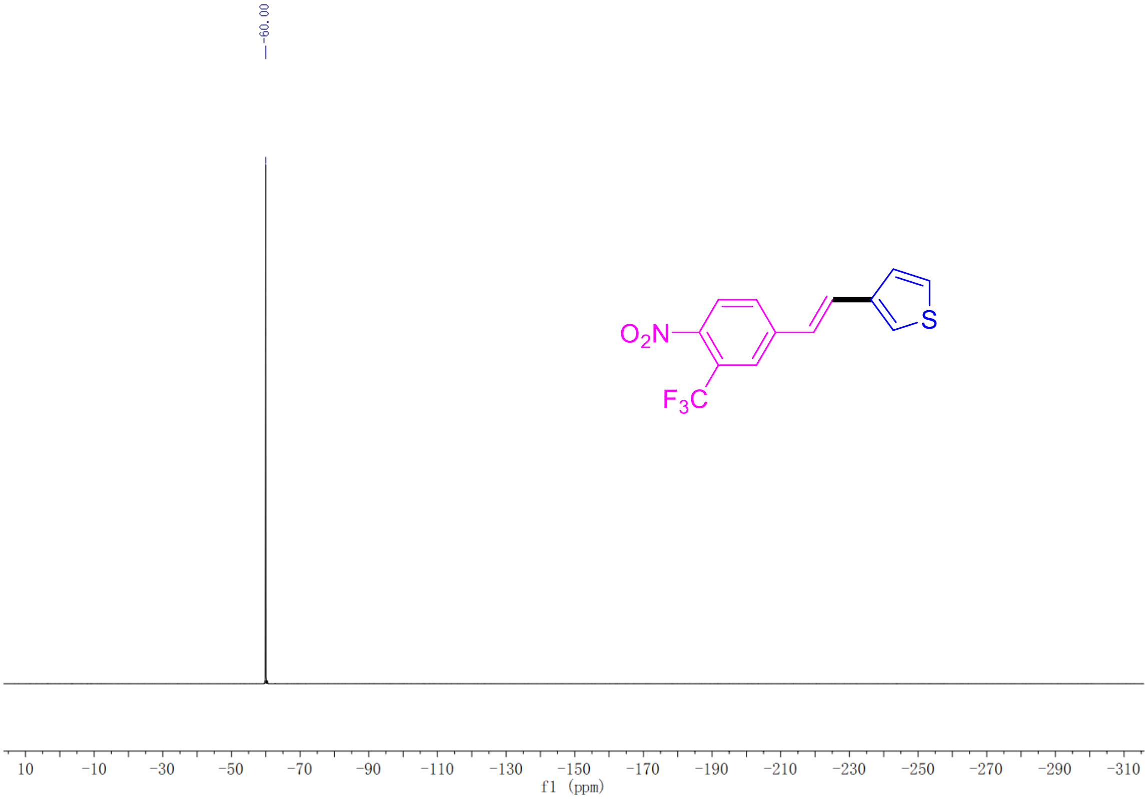
-60.00
O2N
F3C
S
10
-10
-30
-50
-70
-90
-110
-130
-150
-170
-190
-210
-230
-250
-270
-290
-310
f1 (ppm)

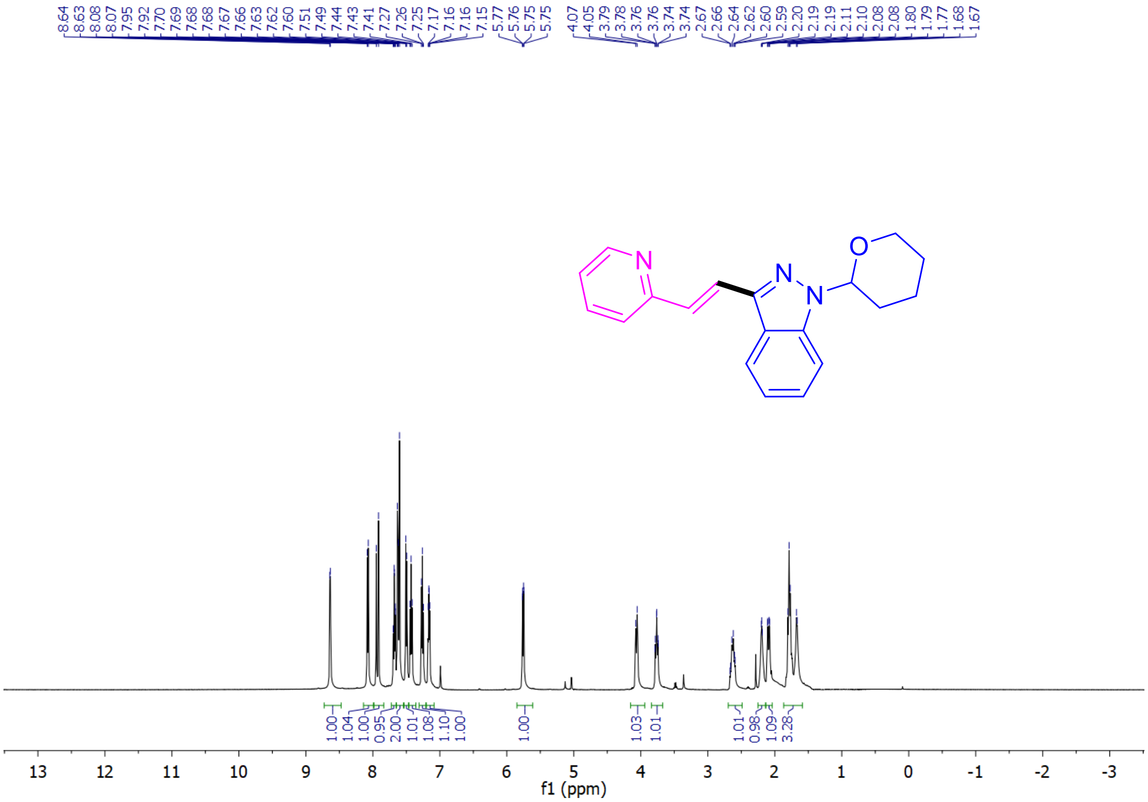
8.64
8.63
8.08
8.07
7.95
7.92
7.70
7.69
7.68
7.68
7.67
7.66
7.63
7.62
7.60
7.51
7.49
7.44
7.43
7.41
7.27
7.26
7.25
7.17
7.16
7.16
7.15
5.77
5.76
5.75
5.75
4.07
4.05
3.79
3.78
3.76
3.76
3.74
3.74
2.67
2.66
2.64
2.62
2.60
2.59
2.20
2.19
2.19
2.11
2.10
2.08
2.08
2.08
1.80
1.79
1.77
1.68
1.67
N
N
N
O
1.00
1.04
1.00
0.95
2.00
1.01
1.08
1.10
1.00
1.00
1.03
1.01
1.01
0.98
1.09
3.28
13
12
11
10
9
8
7
6
5
4
3
2
1
0
-1
-2
-3
f1 (ppm)

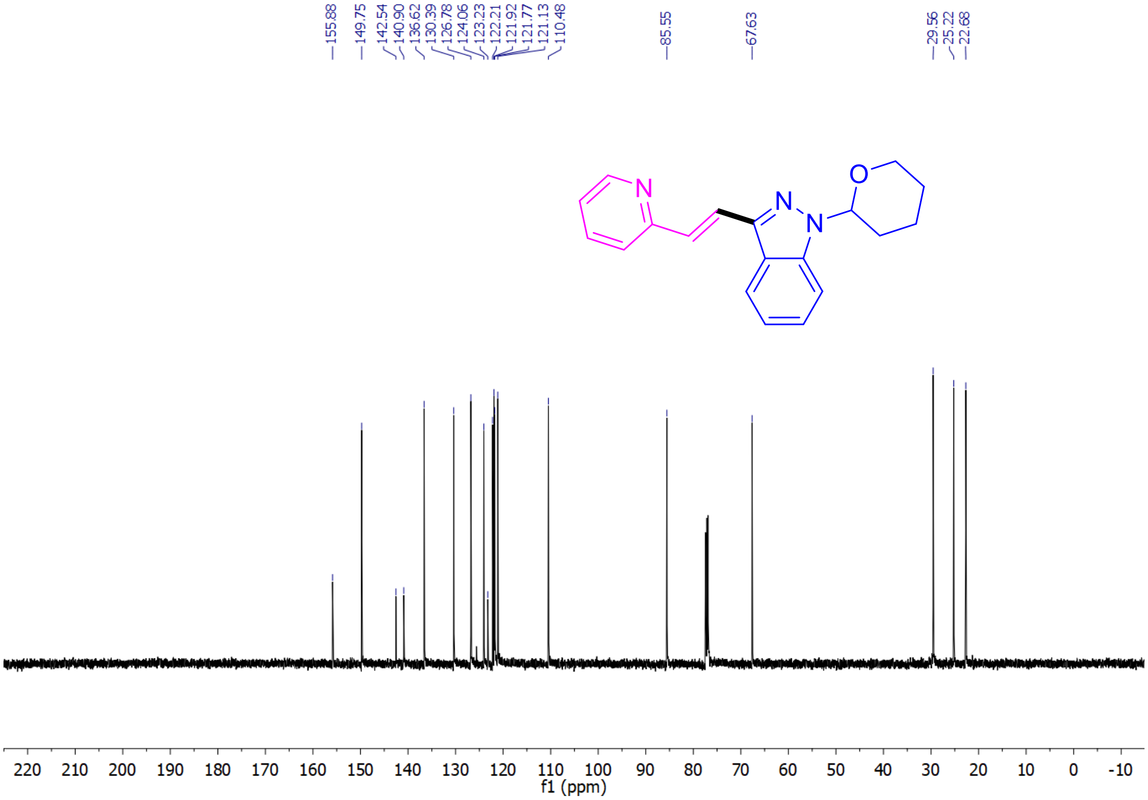
155.88
149.75
142.54
140.90
136.62
130.39
126.78
124.06
123.23
122.21
121.92
121.77
121.13
110.48
85.55
67.63
29.56
25.22
22.68
N
N
N
O
220
210
200
190
180
170
160
150
140
130
120
110
100
90
80
70
60
50
40
30
20
10
0
-10
f1 (ppm)

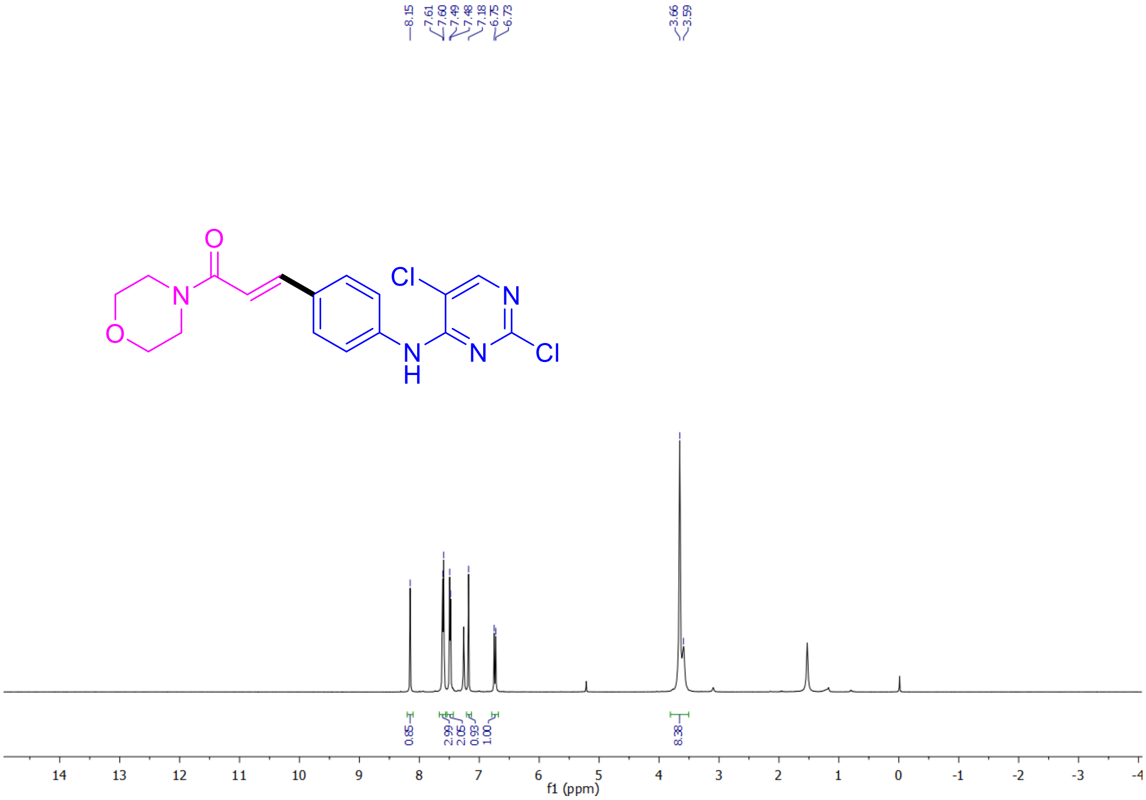
8.15
7.61
7.60
7.49
7.48
7.18
6.75
6.73
3.66
3.59
O
N
O
Cl
N
N
Cl
N
H
0.85
2.99
2.05
0.93
1.00
8.38
14
13
12
11
10
9
8
7
6
5
4
3
2
1
0
-1
-2
-3
-4
f1 (ppm)

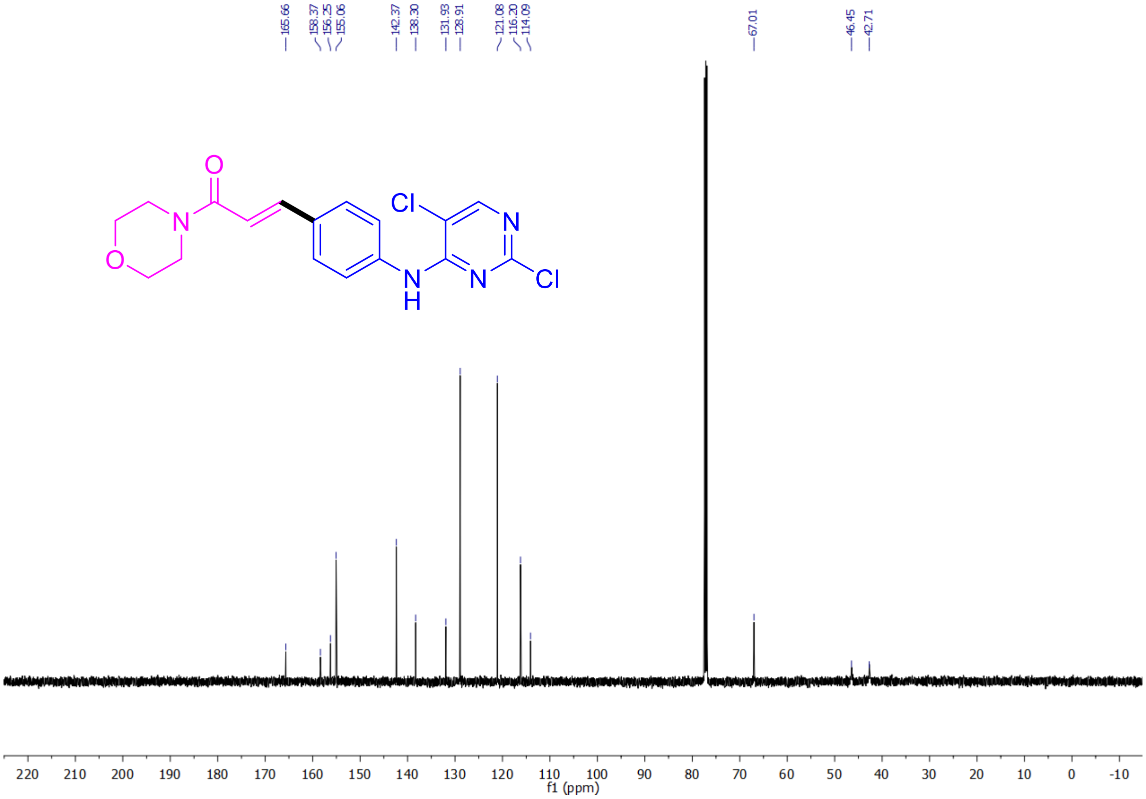
165.66
158.37
156.25
155.06
142.37
138.30
131.93
128.91
121.08
116.20
114.09
67.01
46.45
42.71
O
N
O
Cl
N
N
Cl
N
H
220
210
200
190
180
170
160
150
140
130
120
110
100
90
80
70
60
50
40
30
20
10
0
-10
f1 (ppm)

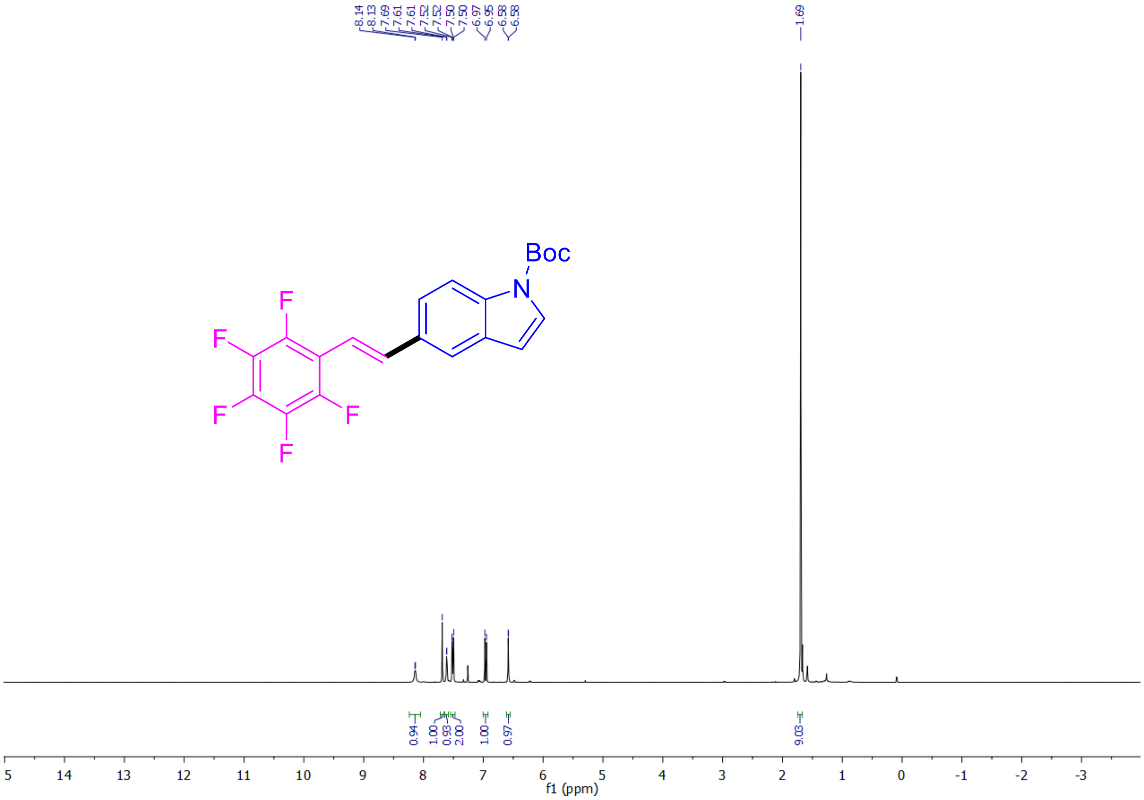
8.14
8.13
7.69
7.61
7.61
7.52
7.52
7.50
7.50
6.97
6.95
6.58
6.58
1.69
Boc
N
F
F
F
F
F
0.94
1.00
0.93
2.00
1.00
0.97
9.03
5
14
13
12
11
10
9
8
7
6
5
4
3
2
1
0
-1
-2
-3
f1 (ppm)

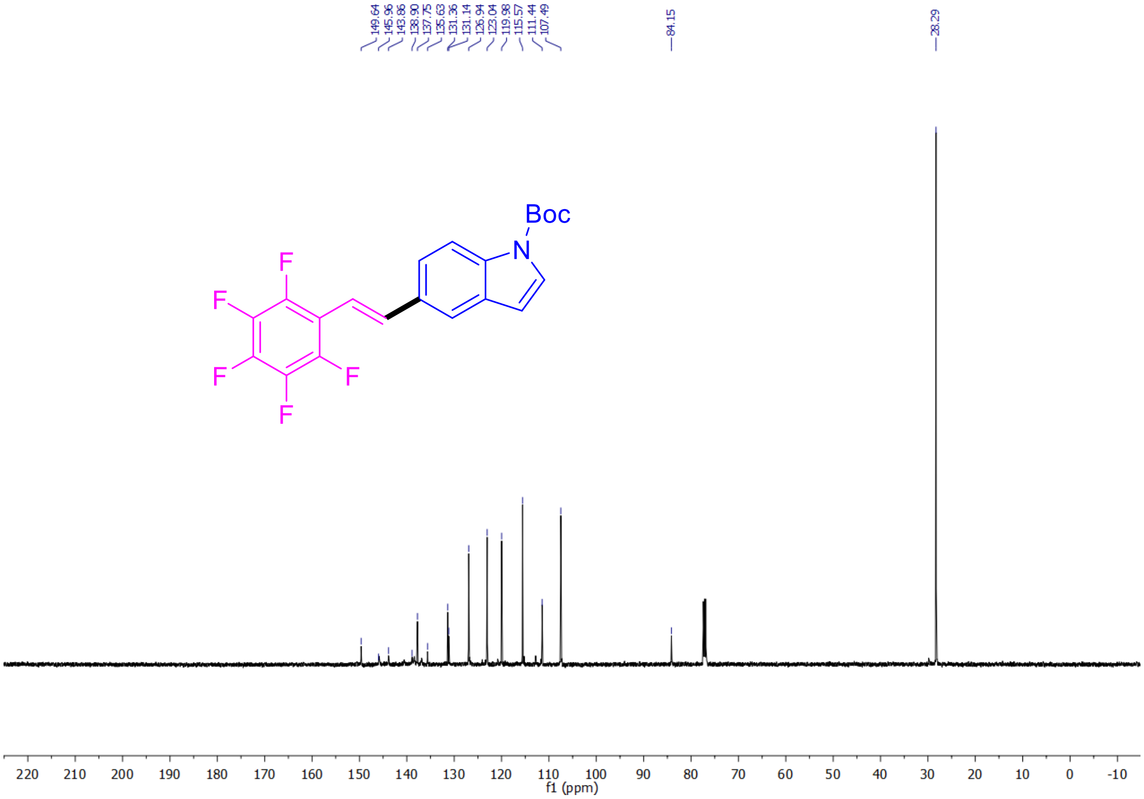
149.64
145.96
143.86
138.90
137.75
135.63
131.36
131.14
126.94
123.04
119.98
115.57
111.44
107.49
84.15
28.29
Boc
N
F
F
F
F
F
220
210
200
190
180
170
160
150
140
130
120
110
100
90
80
70
60
50
40
30
20
10
0
-10
f1 (ppm)

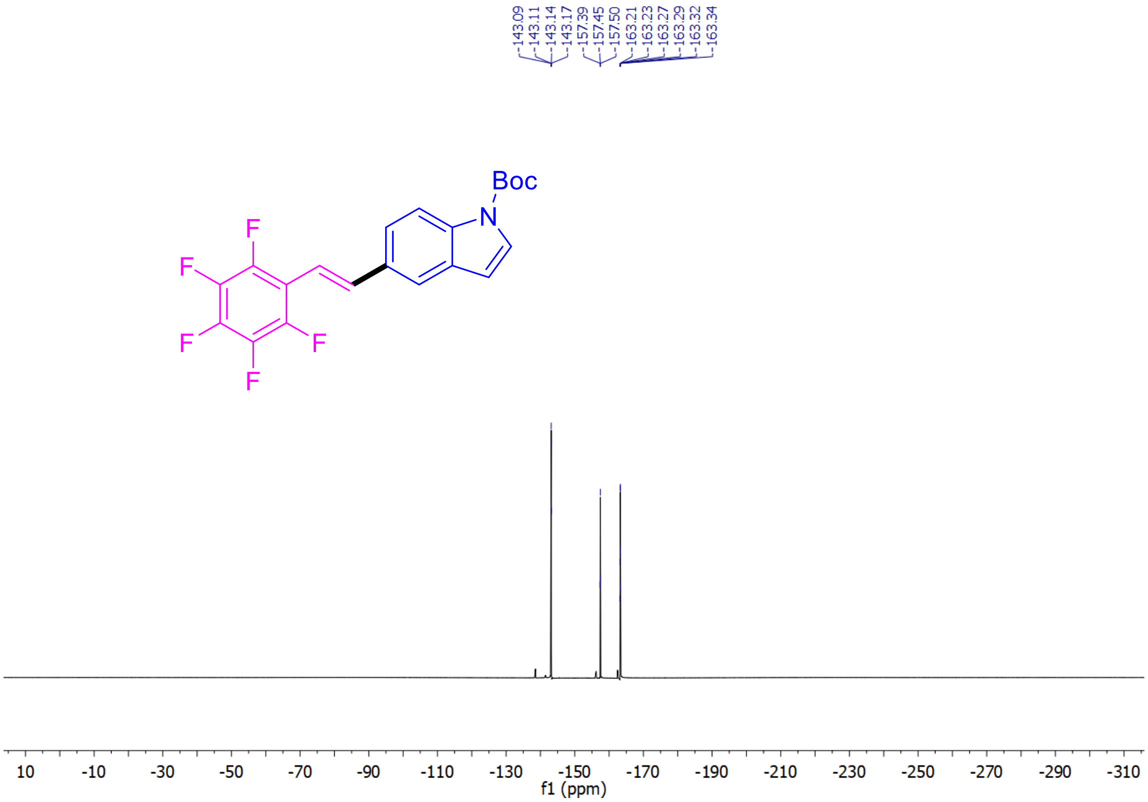
-143.09
-143.11
-143.14
-143.17
-157.39
-157.45
-157.50
-163.21
-163.23
-163.27
-163.29
-163.32
-163.34
Boc
N
F
F
F
F
F
10
-10
-30
-50
-70
-90
-110
-130
-150
-170
-190
-210
-230
-250
-270
-290
-310
f1 (ppm)

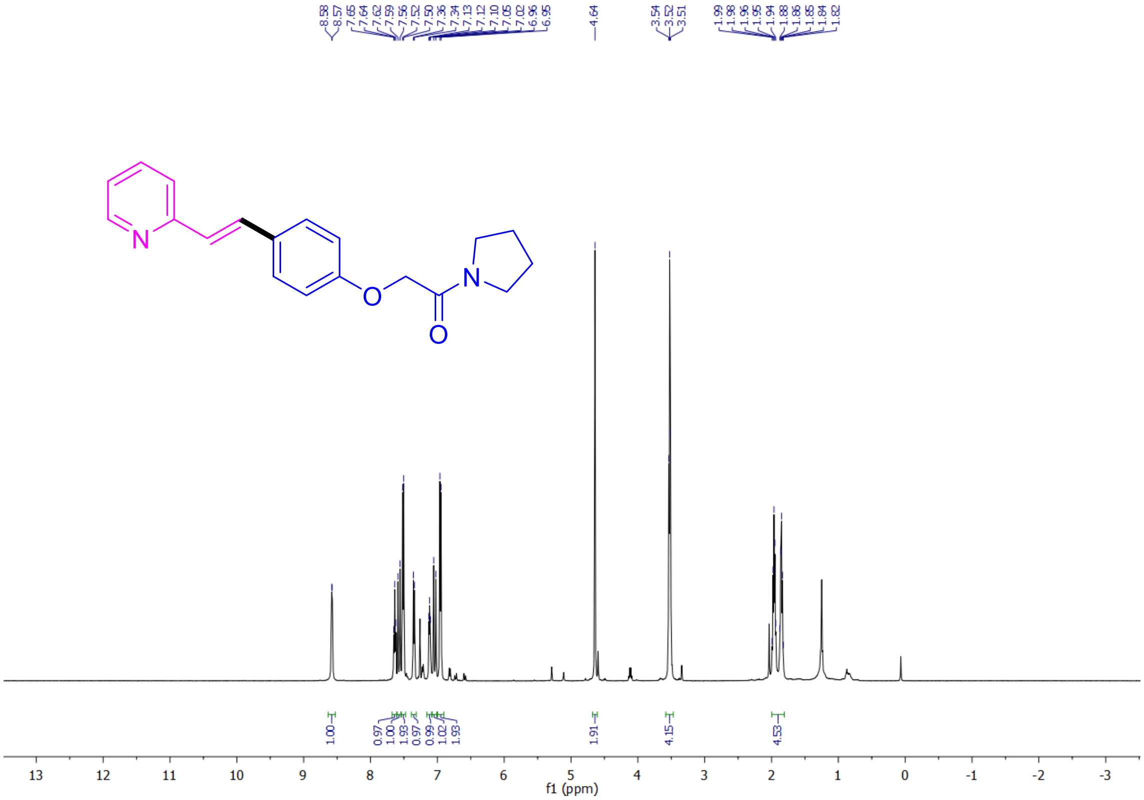

8.58
8.57
7.65
7.64
7.62
7.59
7.56
7.52
7.50
7.36
7.34
7.13
7.12
7.10
7.05
7.02
6.96
6.95
4.64
3.54
3.52
3.51
1.99
1.98
1.96
1.95
1.94
1.88
1.86
1.85
1.84
1.82
N
O
N
O
1.00
0.97
1.00
1.93
0.97
0.99
1.02
1.93
1.91
4.15
4.53
13
12
11
10
9
8
7
6
5
4
3
2
1
0
-1
-2
-3
f1 (ppm)

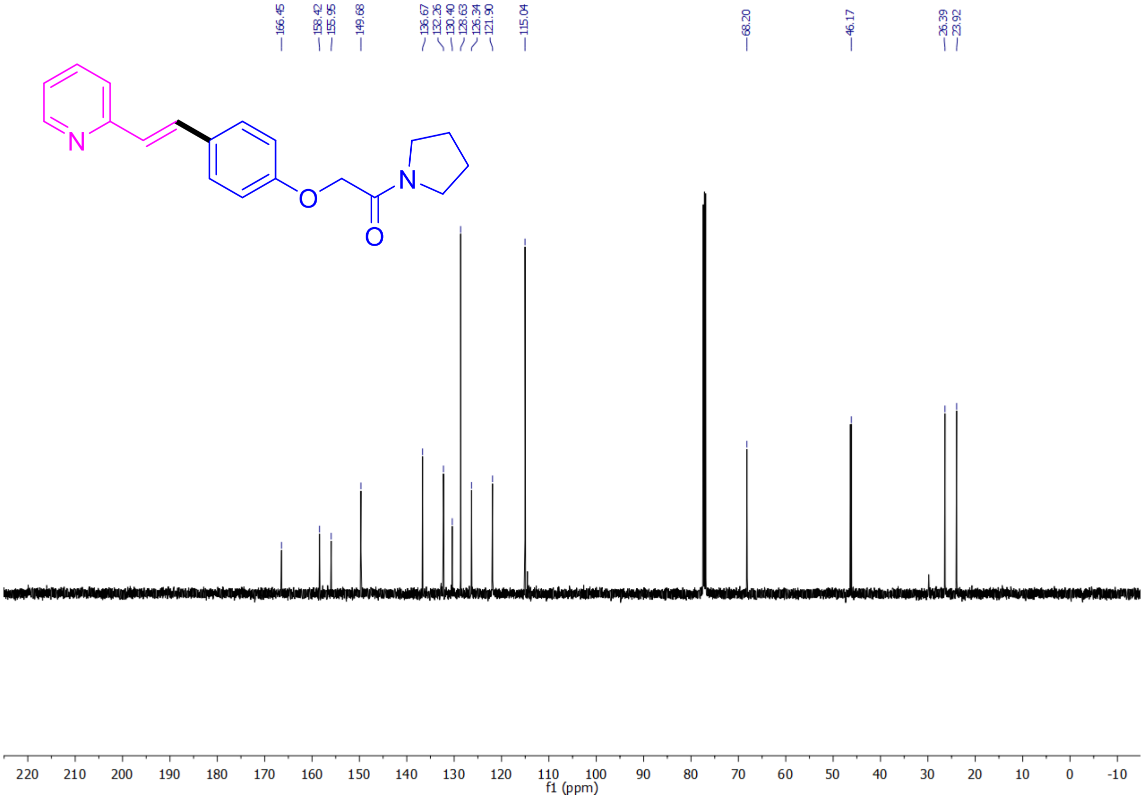

166.45
158.42
155.95
149.68
136.67
132.26
130.40
128.63
126.34
121.90
115.04
68.20
46.17
26.39
23.92
N
O
N
O
220
210
200
190
180
170
160
150
140
130
120
110
100
90
80
70
60
50
40
30
20
10
0
-10
f1 (ppm)

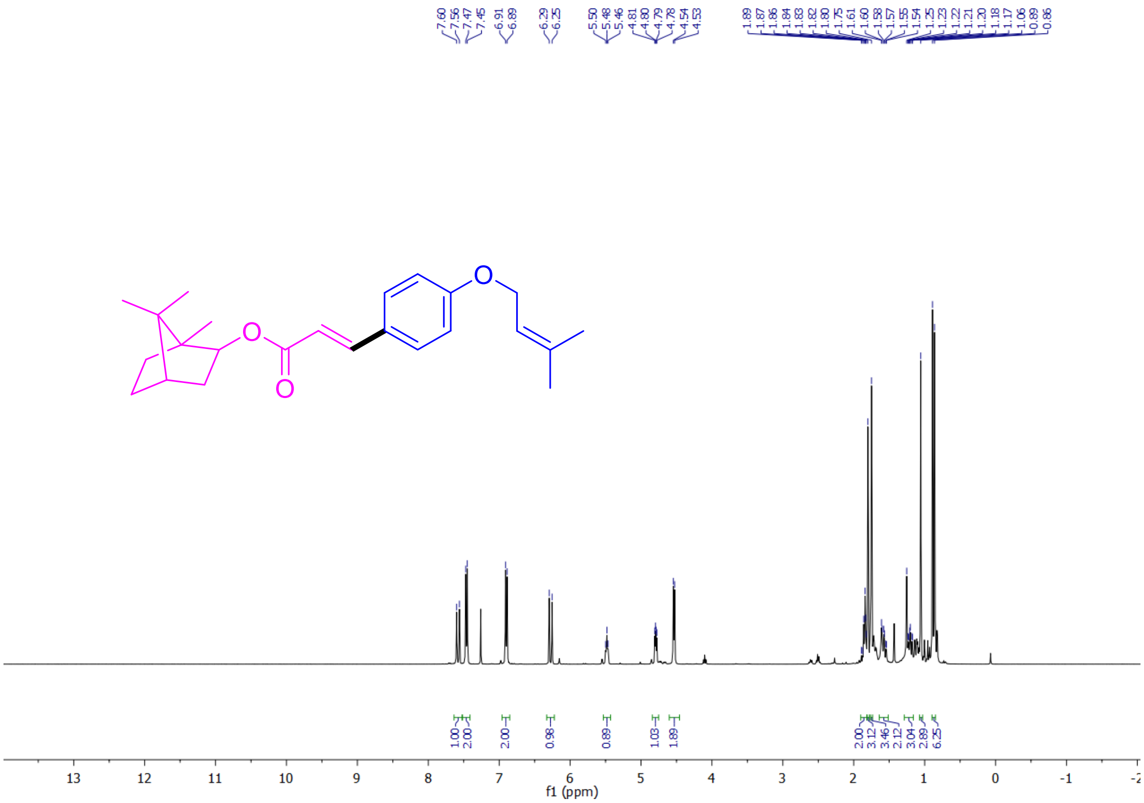
7.60
7.56
7.47
7.45
6.91
6.89
6.29
6.25
5.50
5.48
5.46
4.81
4.80
4.79
4.78
4.54
4.53
1.89
1.87
1.86
1.84
1.83
1.82
1.80
1.75
1.61
1.60
1.58
1.57
1.55
1.54
1.25
1.23
1.22
1.21
1.20
1.18
1.17
1.06
0.89
0.86
O
O
O
1.00
2.00
2.00
0.98
0.89
1.03
1.89
2.00
3.12
3.46
2.12
3.04
2.89
6.25
13
12
11
10
9
8
7
6
5
4
3
2
1
0
-1
-2
f1 (ppm)

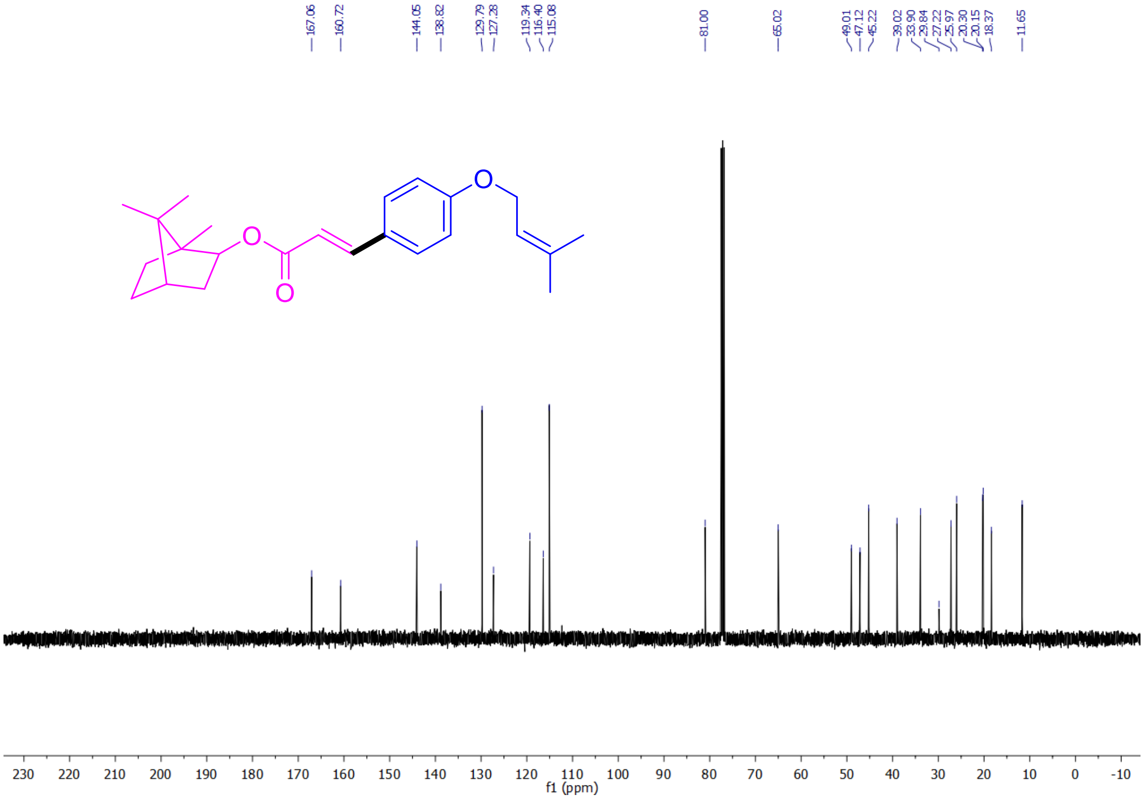
167.06
160.72
144.05
138.82
129.79
127.28
119.34
116.40
115.08
81.00
65.02
49.01
47.12
45.22
39.02
33.90
29.84
27.22
25.97
20.30
20.15
18.37
11.65
O
O
O
230
220
210
200
190
180
170
160
150
140
130
120
110
100
90
80
70
60
50
40
30
20
10
0
-10
f1 (ppm)

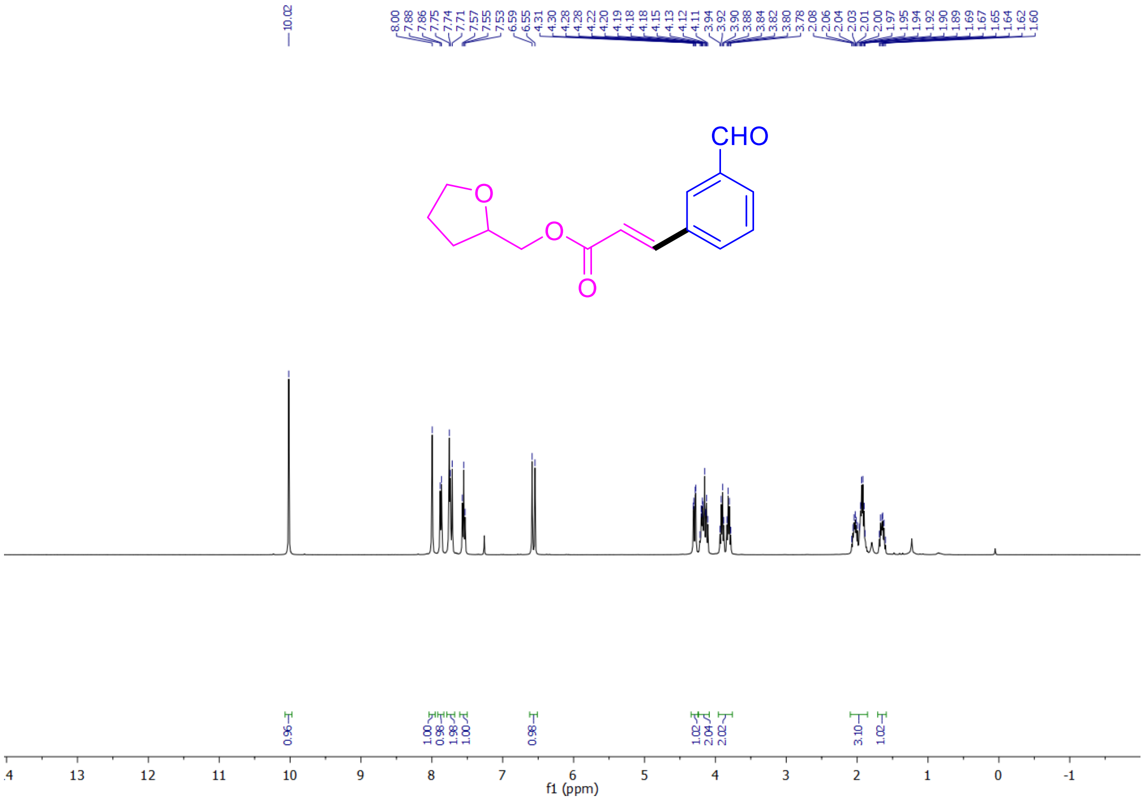
10.02
8.00
7.88
7.86
7.75
7.74
7.71
7.57
7.55
7.53
6.59
6.55
4.31
4.30
4.28
4.28
4.22
4.20
4.19
4.18
4.18
4.15
4.13
4.12
4.11
3.94
3.92
3.90
3.88
3.84
3.82
3.80
3.78
2.08
2.06
2.04
2.03
2.01
2.00
1.97
1.95
1.94
1.92
1.90
1.89
1.69
1.67
1.65
1.64
1.62
1.60
CHO
O
O
O
0.96
1.00
0.98
1.98
1.00
0.98
1.02
2.04
2.02
3.10
1.02
14
13
12
11
10
9
8
7
6
5
4
3
2
1
0
-1
f1 (ppm)

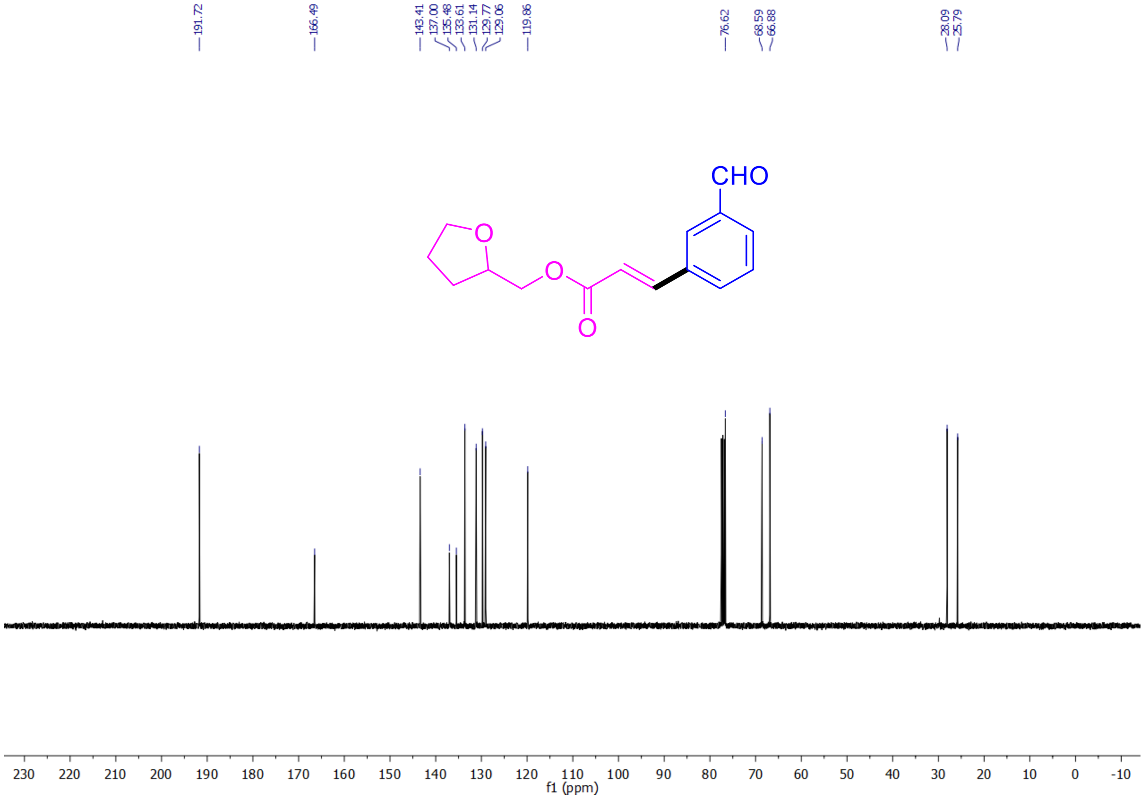
191.72
166.49
143.41
137.00
135.48
133.61
131.14
129.77
129.06
119.86
76.62
68.59
66.88
28.09
25.79
CHO
O
O
O
230
220
210
200
190
180
170
160
150
140
130
120
110
100
90
80
70
60
50
40
30
20
10
0
-10
f1 (ppm)

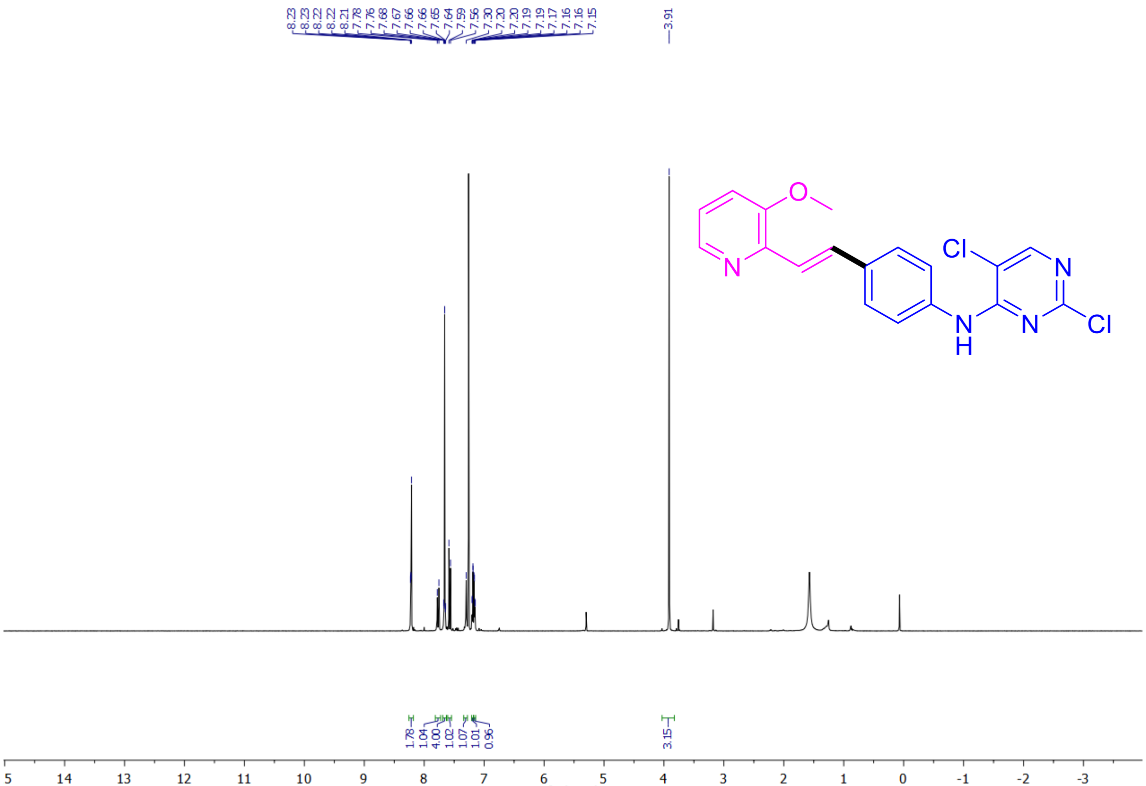
8.23
8.23
8.22
8.21
7.78
7.76
7.68
7.67
7.66
7.66
7.65
7.64
7.59
7.56
7.30
7.20
7.20
7.19
7.17
7.16
7.16
7.15
3.91
O
N
Cl
N
N
Cl
N
H
1.78
1.04
4.00
1.02
1.07
1.01
0.96
3.15
5
14
13
12
11
10
9
8
7
6
5
4
3
2
1
0
-1
-2
-3
f1 (ppm)

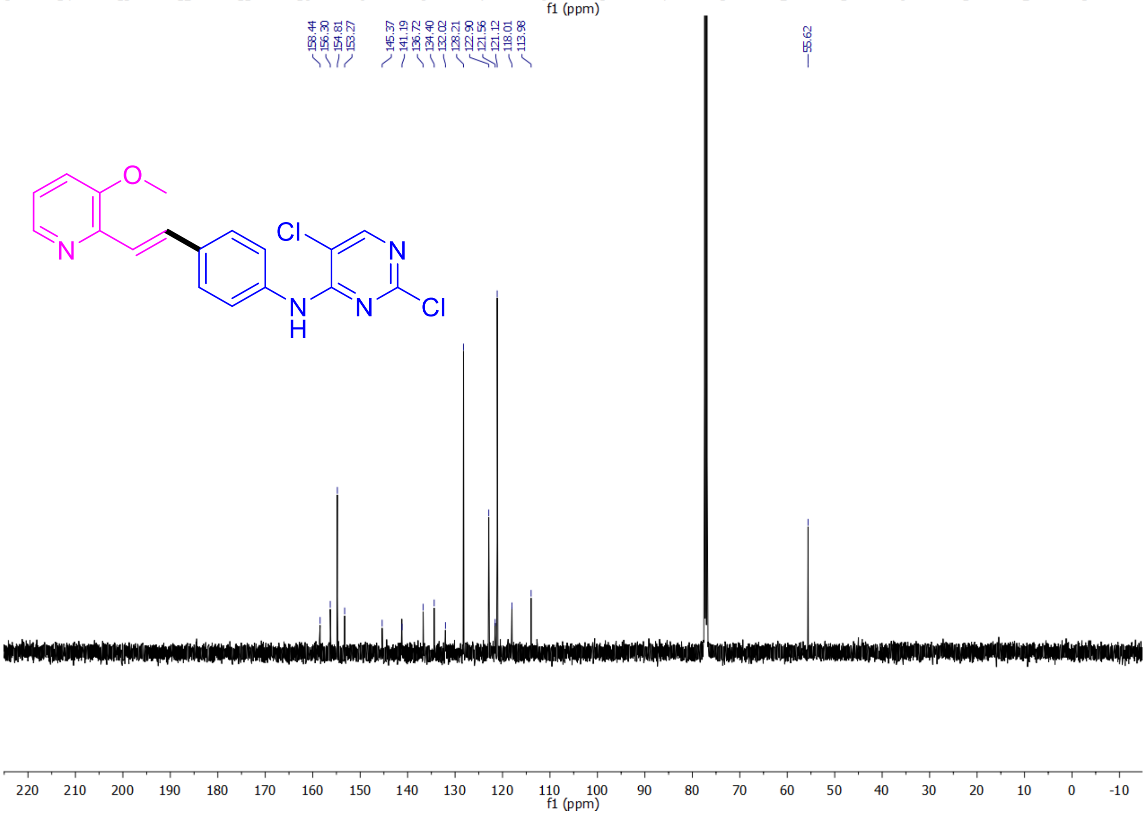
158.44
156.30
154.81
153.27
145.37
141.19
136.72
134.40
132.02
128.21
122.90
121.56
121.12
118.01
113.98
55.62
O
N
Cl
N
N
Cl
N
H
220
210
200
190
180
170
160
150
140
130
120
110
100
90
80
70
60
50
40
30
20
10
0
-10
f1 (ppm)

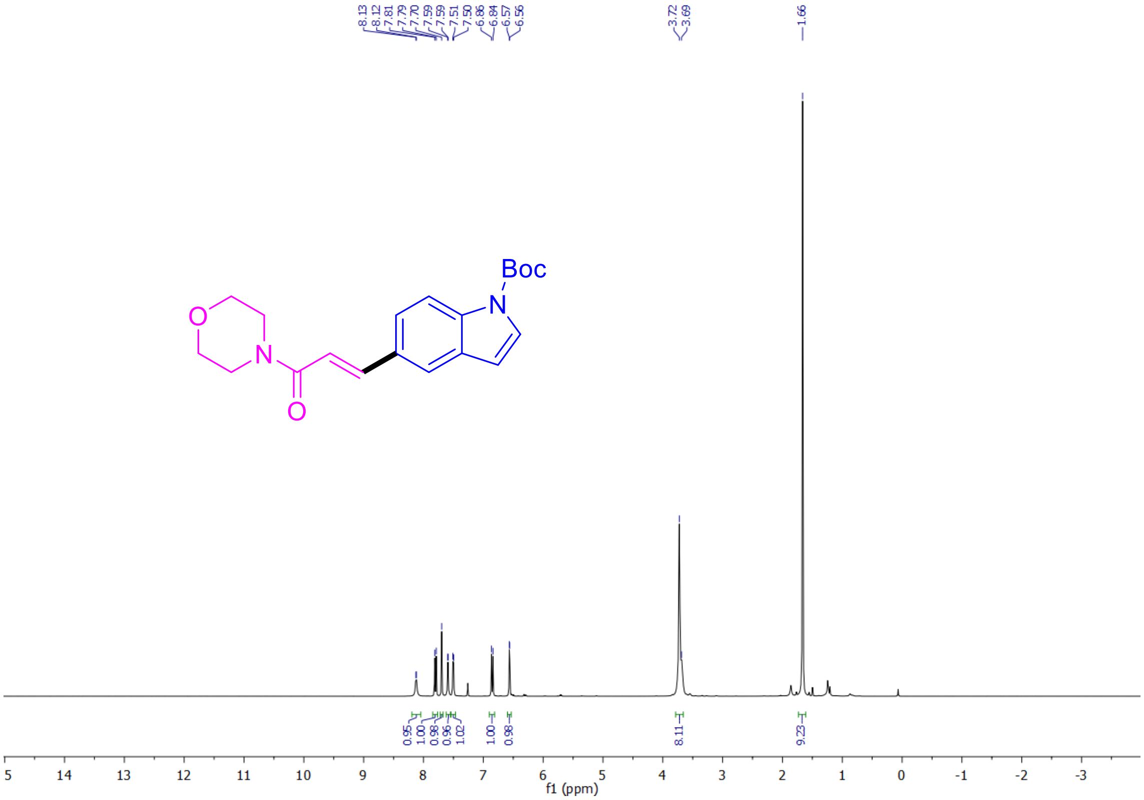

8.13
8.12
7.81
7.79
7.70
7.59
7.59
7.51
7.50
6.86
6.84
6.57
6.56
3.72
3.69
1.66
Boc
N
O
N
O
0.95
1.00
0.98
0.96
1.02
1.00
0.98
8.11
9.23
5
14
13
12
11
10
9
8
7
6
5
4
3
2
1
0
-1
-2
-3
f1 (ppm)

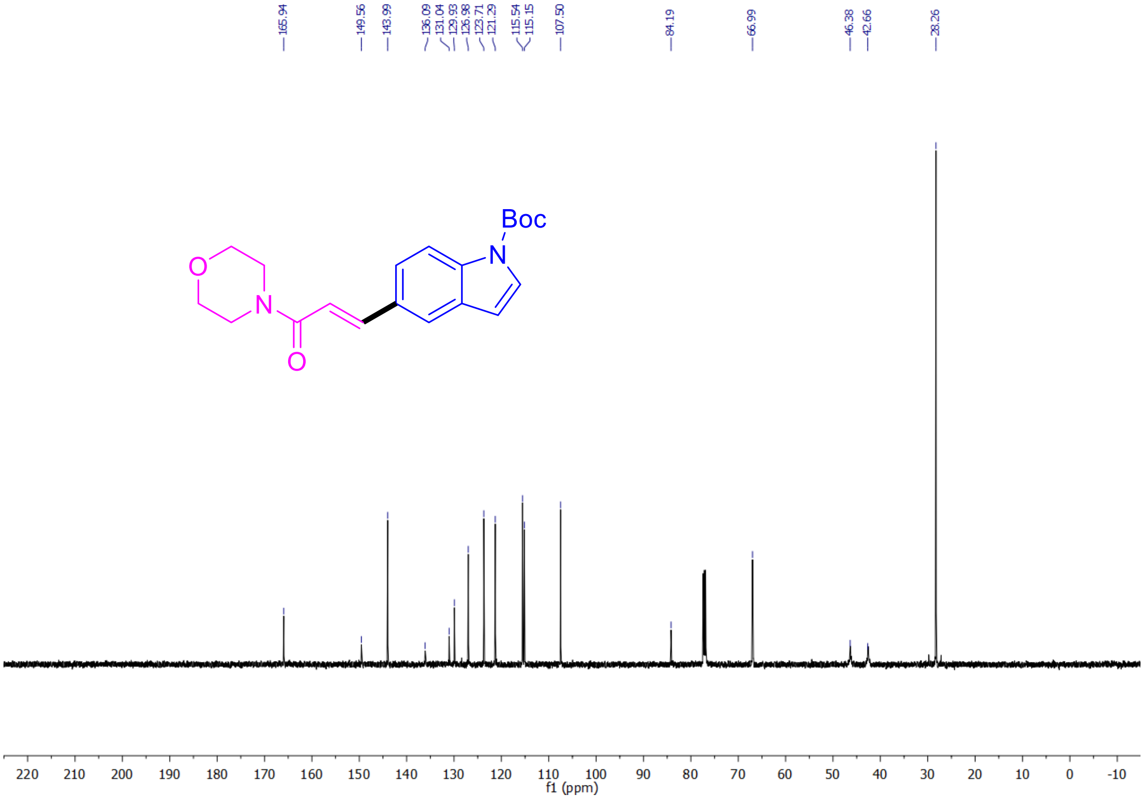

165.94
149.56
143.99
136.09
131.04
129.93
126.98
123.71
121.29
115.54
115.15
107.50
84.19
66.99
46.38
42.66
28.26
Boc
N
O
N
O
220
210
200
190
180
170
160
150
140
130
120
110
100
90
80
70
60
50
40
30
20
10
0
-10
f1 (ppm)

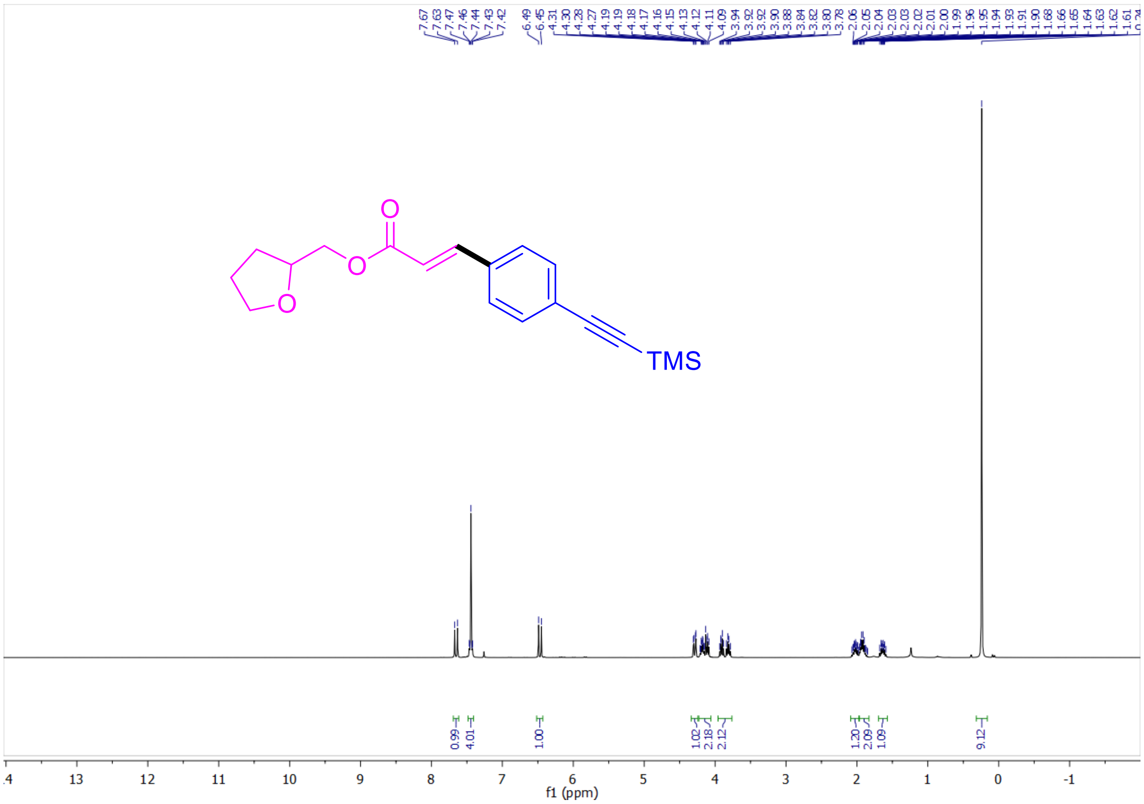
7.67
7.63
7.47
7.46
7.44
7.43
7.42
6.49
6.45
4.31
4.30
4.28
4.27
4.19
4.19
4.18
4.17
4.16
4.15
4.13
4.12
4.11
4.09
3.94
3.92
3.92
3.90
3.88
3.84
3.82
3.80
3.78
2.06
2.05
2.04
2.03
2.03
2.02
2.01
2.00
1.99
1.96
1.95
1.94
1.93
1.91
1.90
1.68
1.66
1.65
1.64
1.63
1.62
1.61
0.2
O
O
O
TMS
0.99
4.01
1.00
1.02
2.18
2.12
1.20
2.09
1.09
9.12
4
13
12
11
10
9
8
7
6
5
4
3
2
1
0
-1
f1 (ppm)

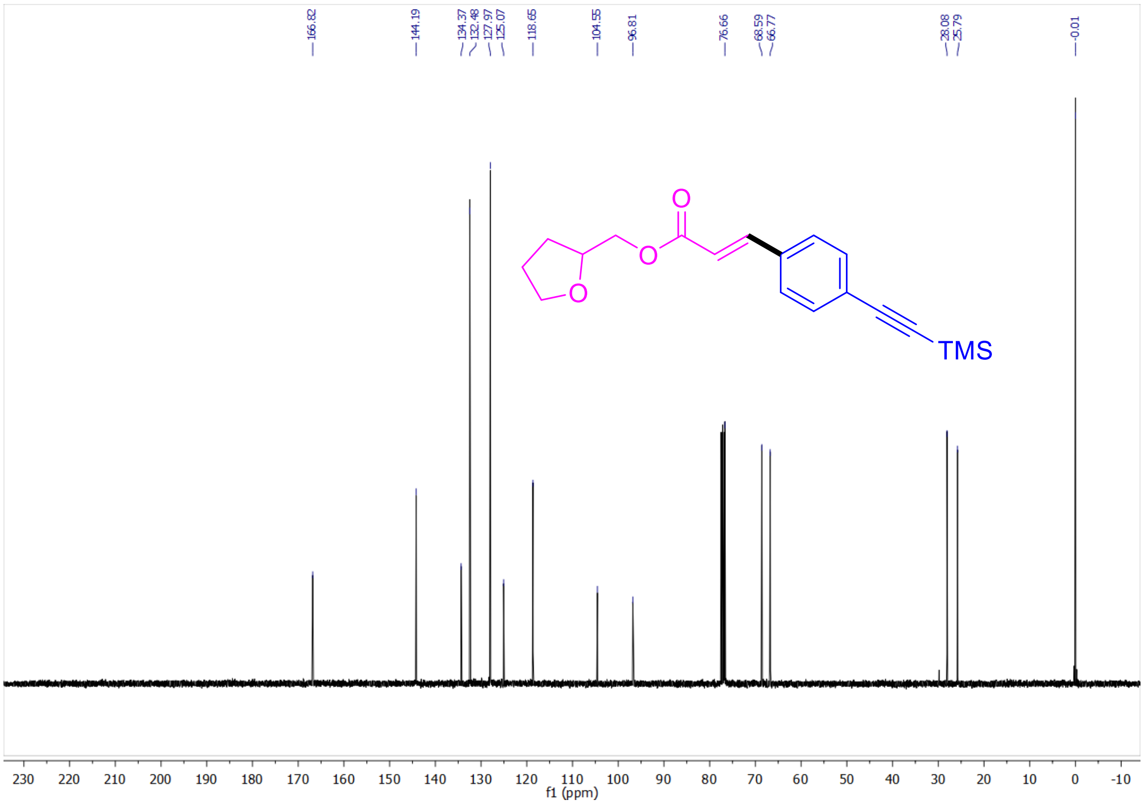
166.82
144.19
134.37
132.48
127.97
125.07
118.65
104.55
96.81
76.66
68.59
66.77
28.08
25.79
-0.01
O
O
O
TMS
230
220
210
200
190
180
170
160
150
140
130
120
110
100
90
80
70
60
50
40
30
20
10
0
-10
f1 (ppm)

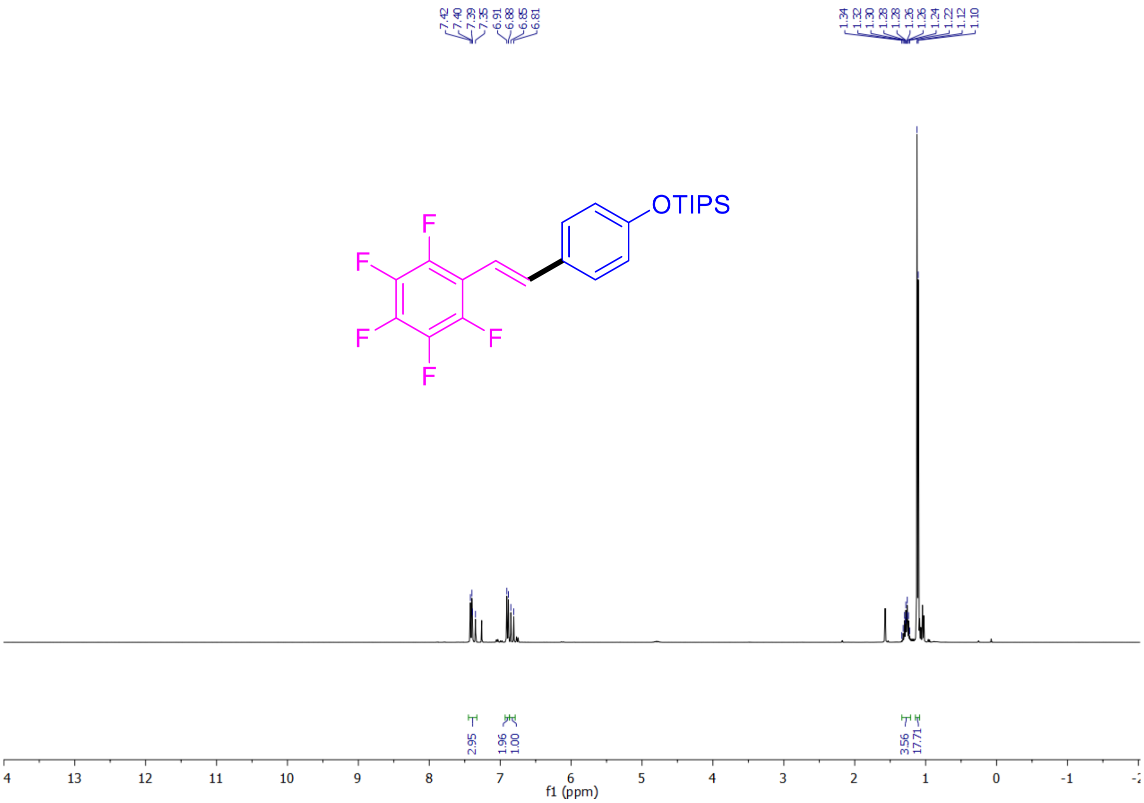
7.42
7.40
7.39
7.35
6.91
6.88
6.85
6.81
1.34
1.32
1.30
1.28
1.28
1.26
1.26
1.24
1.22
1.12
1.10
OTIPS
F
F
F
F
F
2.95
1.96
1.00
3.56
17.71
4
13
12
11
10
9
8
7
6
5
4
3
2
1
0
-1
-2
f1 (ppm)

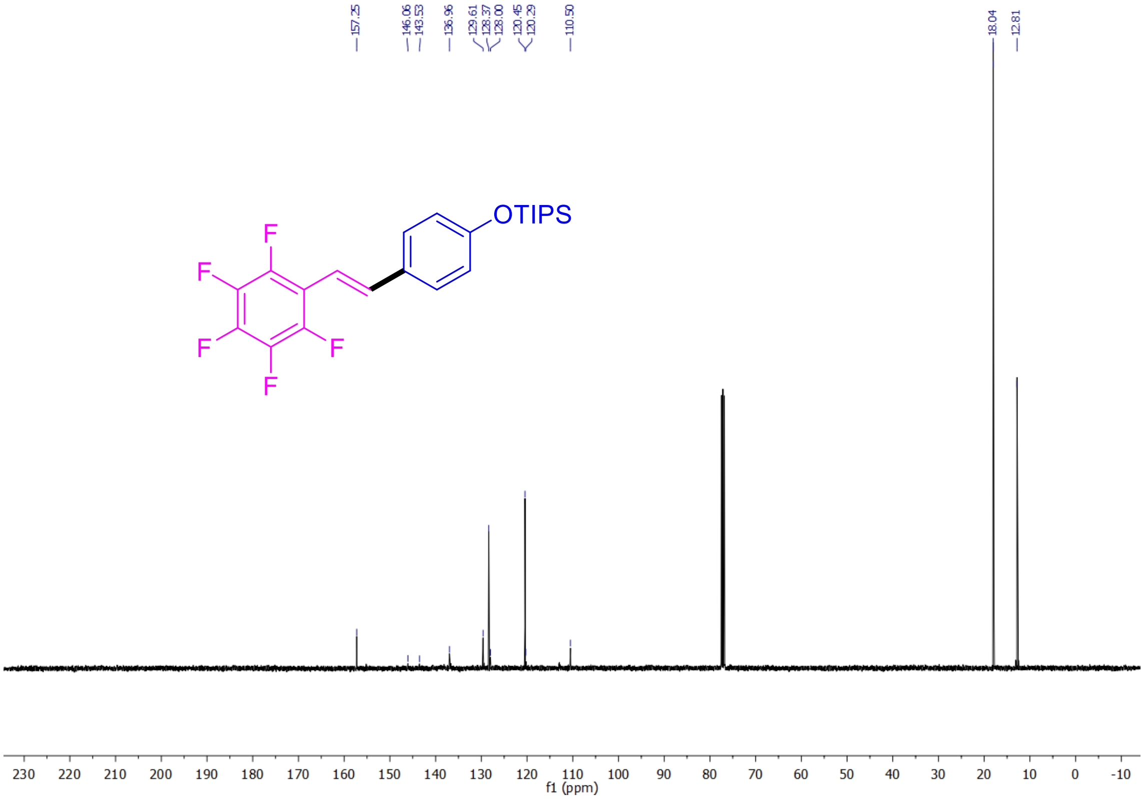
157.25
146.06
143.53
136.96
129.61
128.37
128.00
120.45
120.29
110.50
18.04
12.81
OTIPS
F
F
F
F
F
230
220
210
200
190
180
170
160
150
140
130
120
110
100
90
80
70
60
50
40
30
20
10
0
-10
f1 (ppm)

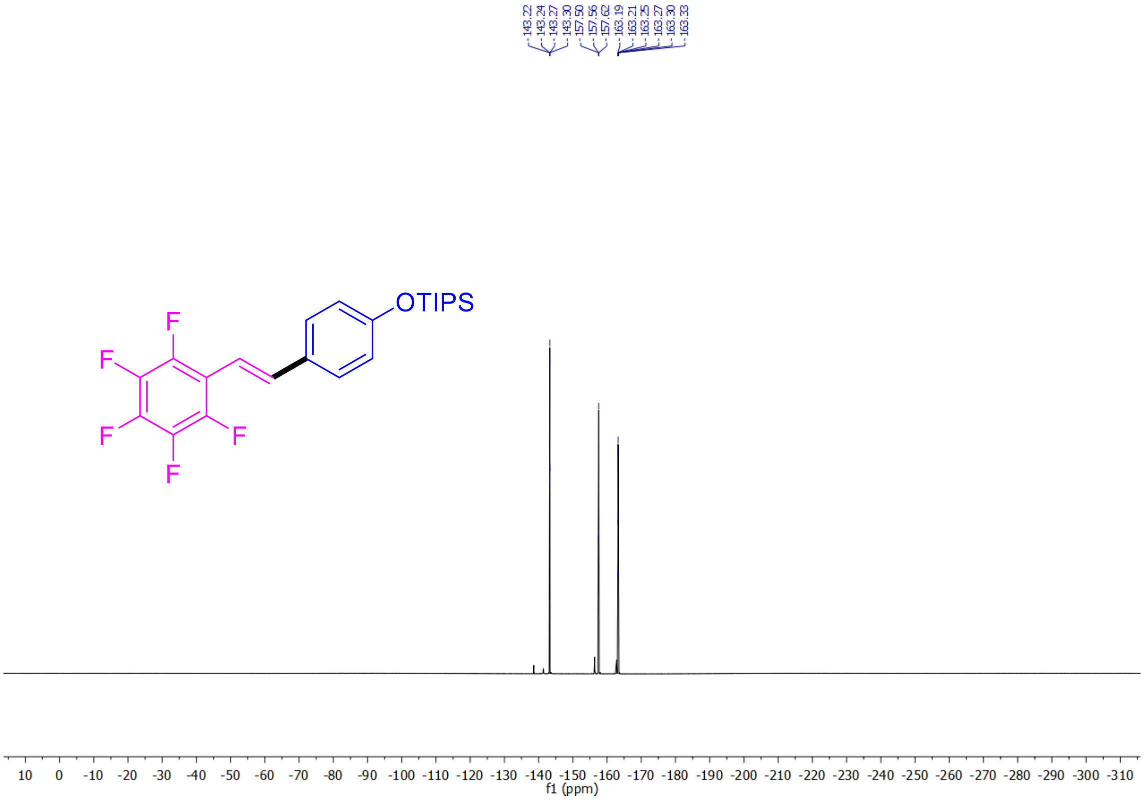
143.22
143.24
143.27
143.30
157.50
157.56
157.62
163.19
163.21
163.25
163.27
163.30
163.33
F
F
F
F
F
OTIPS
10
0
-10
-20
-30
-40
-50
-60
-70
-80
-90
-100
-110
-120
-130
-140
-150
-160
-170
-180
-190
-200
-210
-220
-230
-240
-250
-260
-270
-280
-290
-300
-310
f1 (ppm)

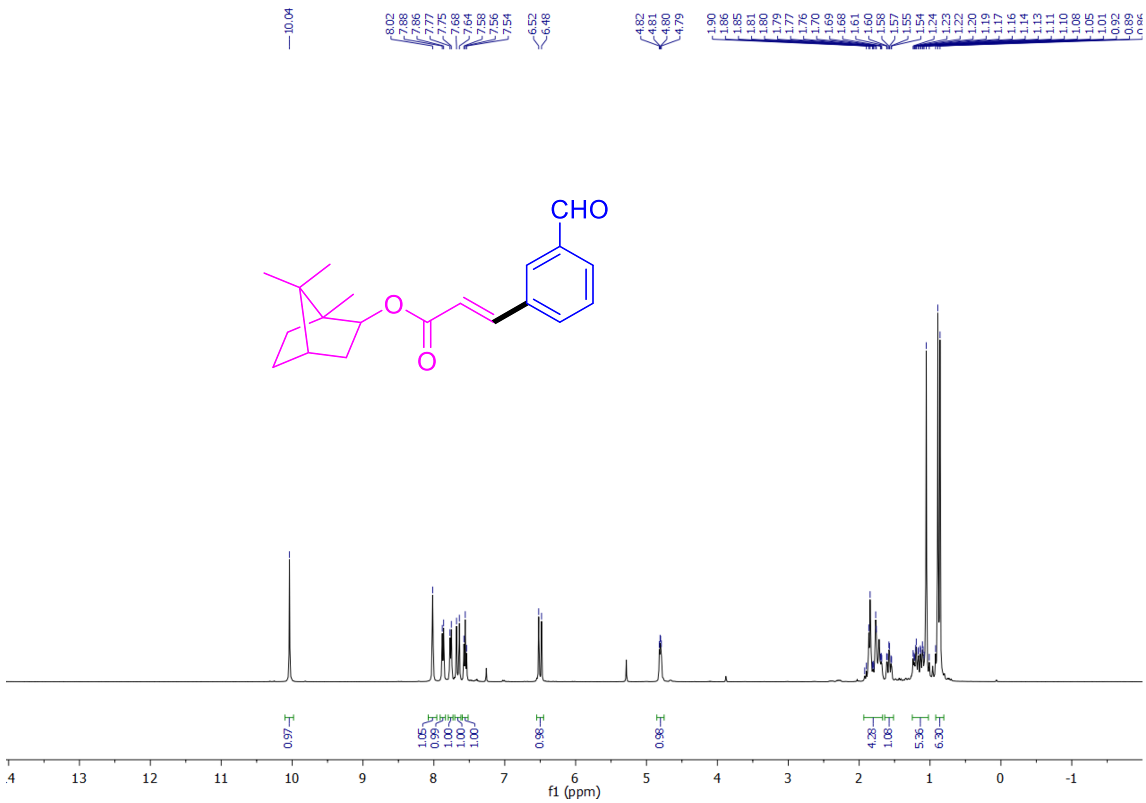
10.04
8.02 7.88 7.86 7.77 7.75 7.68 7.64 7.58 7.56 7.54
6.52 6.48
4.82 4.81 4.80 4.79
1.90 1.86 1.85 1.81 1.80 1.79 1.77 1.76 1.70 1.69 1.68 1.61 1.60 1.58 1.57 1.55 1.54 1.24 1.23 1.22 1.20 1.19 1.17 1.16 1.14 1.13 1.11 1.10 1.08 1.05 1.01 0.92 0.89
CHO
O
O
0.97
1.05 0.99 1.00 1.00 1.00
0.98
0.98
4.28 1.08
5.36 6.30
14 13 12 11 10 9 8 7 6 5 4 3 2 1 0 -1
f1 (ppm)

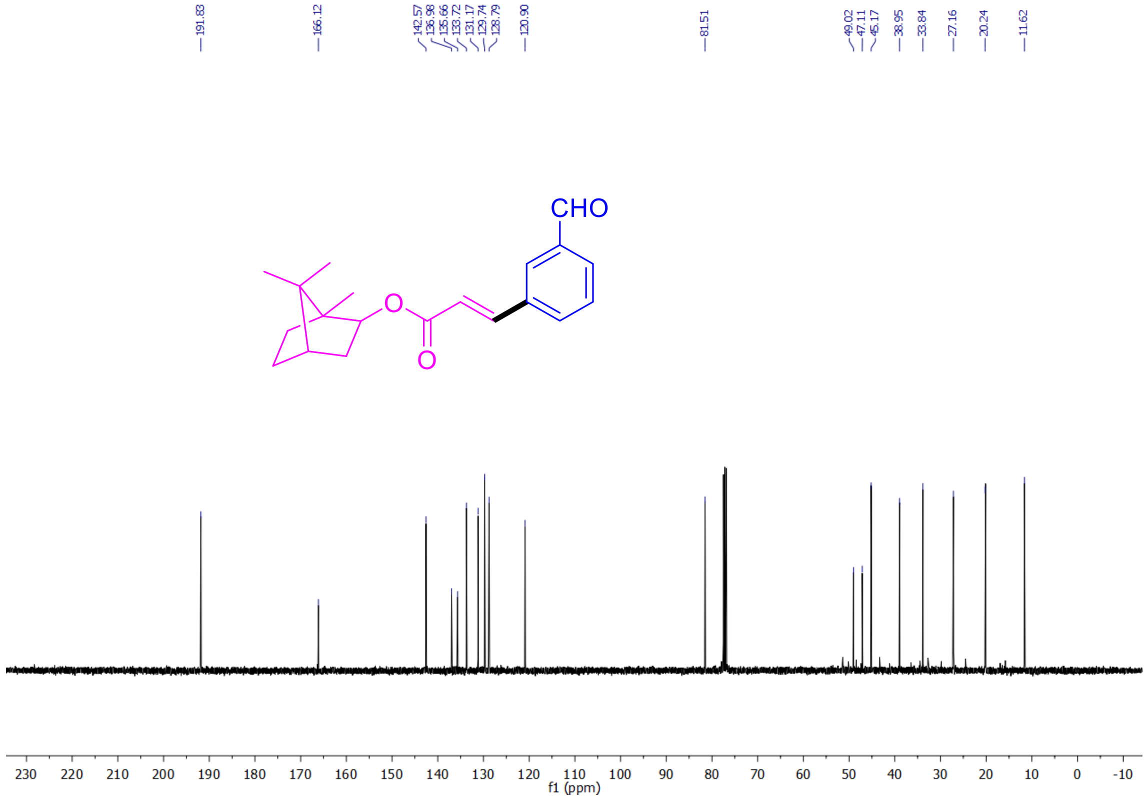
191.83
166.12
142.57 136.98 135.66 133.72 131.17 129.74 128.79
120.90
81.51
49.02 47.11 45.17
38.95
33.84
27.16
20.24
11.62
CHO
O
O
230 220 210 200 190 180 170 160 150 140 130 120 110 100 90 80 70 60 50 40 30 20 10 0 -10
f1 (ppm)

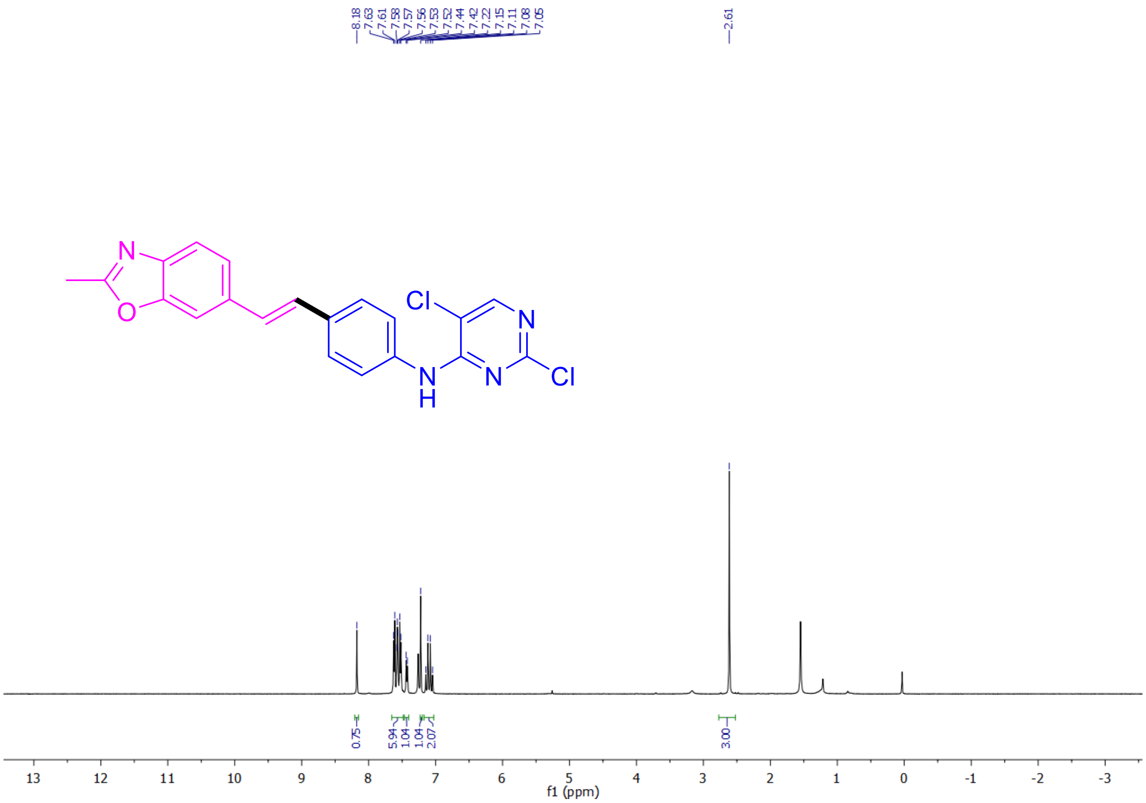
8.18
7.63
7.61
7.58
7.57
7.56
7.53
7.52
7.44
7.42
7.22
7.15
7.11
7.08
7.05
2.61
N
O
Cl
N
N
Cl
N
H
0.75
5.94
1.04
1.04
2.07
3.00
13
12
11
10
9
8
7
6
5
4
3
2
1
0
-1
-2
-3
f1 (ppm)

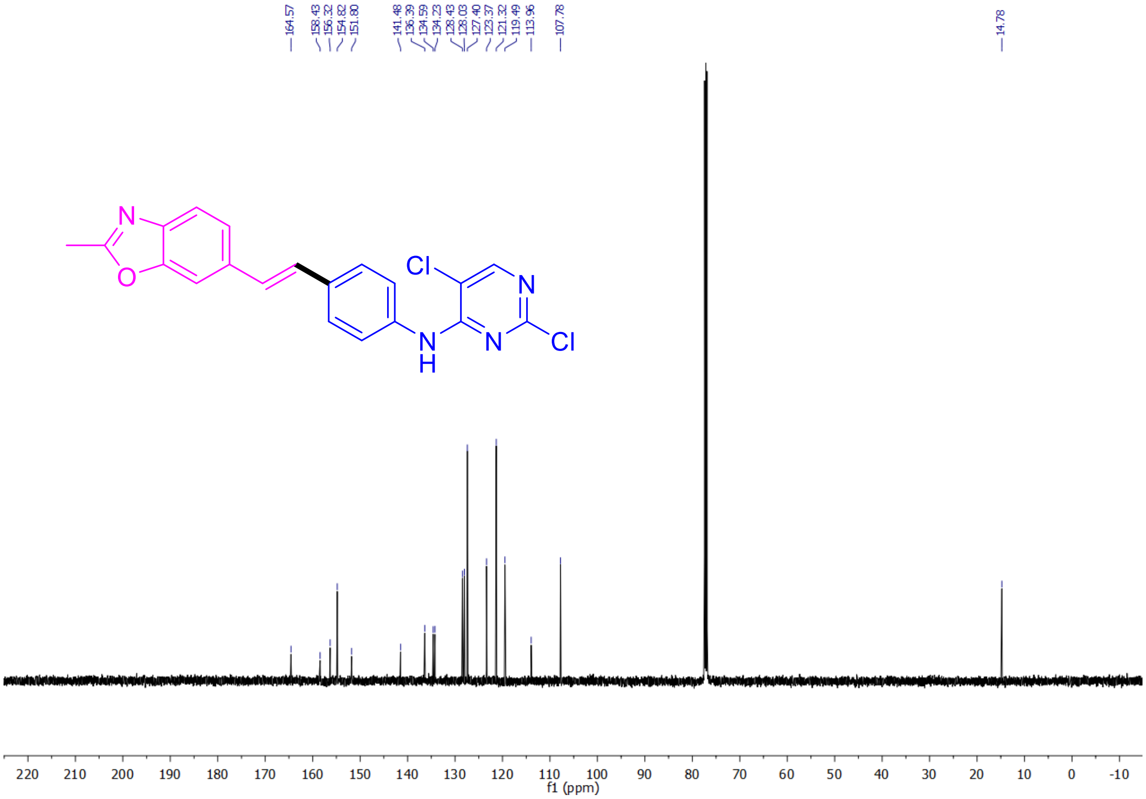
164.57
158.43
156.32
154.82
151.80
141.48
136.39
134.59
134.23
128.43
128.03
127.40
123.37
121.32
119.49
113.96
107.78
14.78
N
O
Cl
N
N
Cl
N
H
220
210
200
190
180
170
160
150
140
130
120
110
100
90
80
70
60
50
40
30
20
10
0
-10
f1 (ppm)

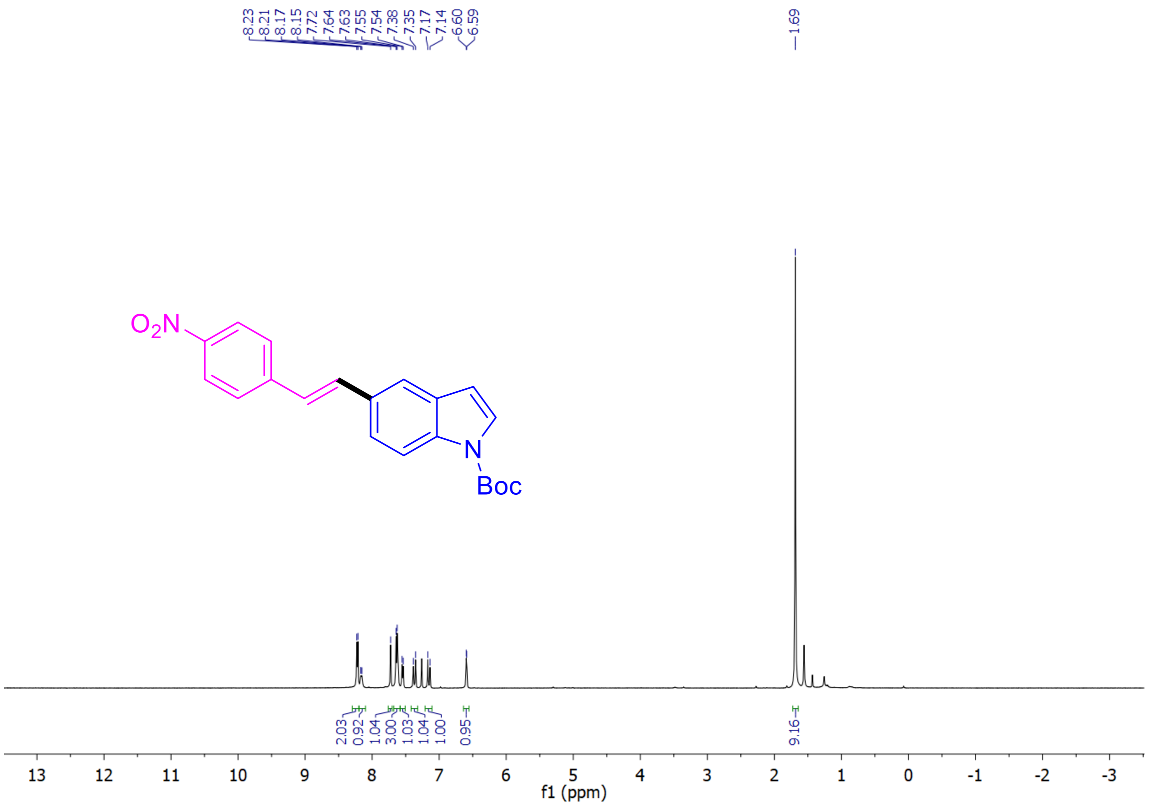
8.23
8.21
8.17
8.15
7.72
7.64
7.63
7.55
7.54
7.38
7.35
7.17
7.14
6.60
6.59
1.69
O_2N
N
Boc
2.03
0.92
1.04
3.00
1.03
1.04
1.00
0.95
9.16
13
12
11
10
9
8
7
6
5
4
3
2
1
0
-1
-2
-3
f1 (ppm)

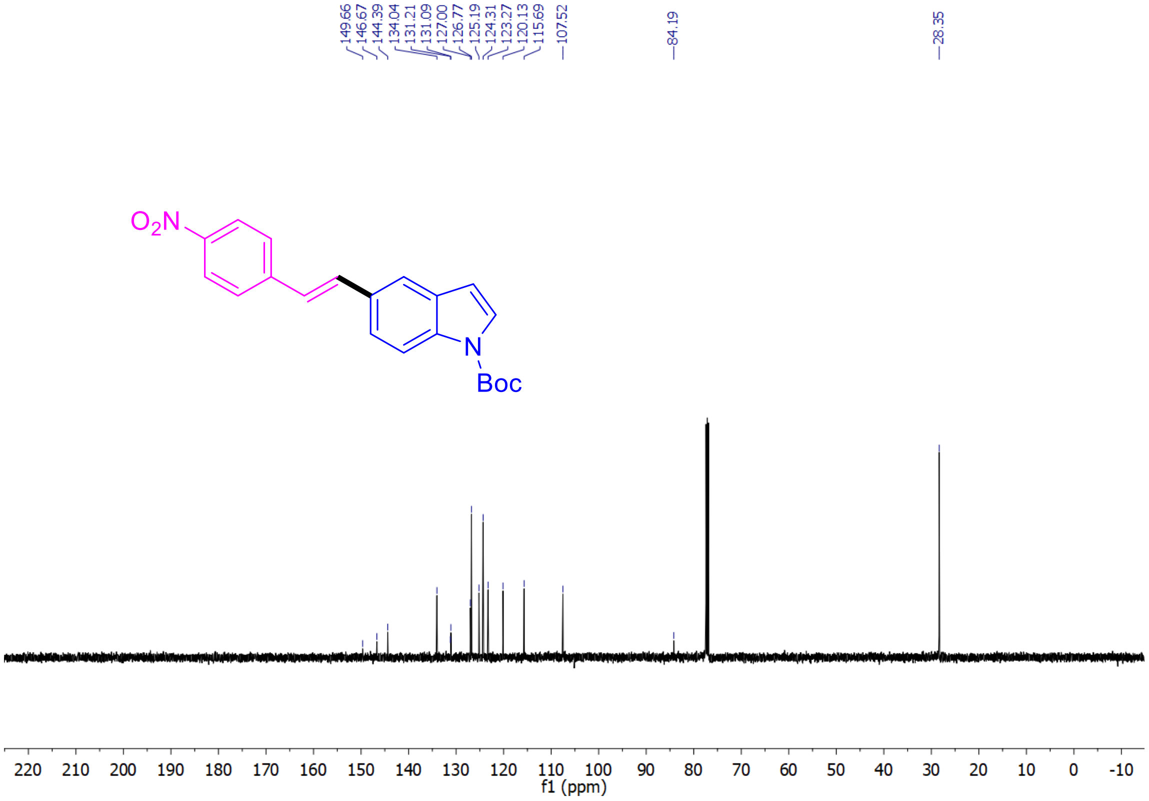
149.66
146.67
144.39
134.04
131.21
131.09
127.00
126.77
125.19
124.31
123.27
120.13
115.69
107.52
84.19
28.35
O_2N
N
Boc
220
210
200
190
180
170
160
150
140
130
120
110
100
90
80
70
60
50
40
30
20
10
0
-10
f1 (ppm)

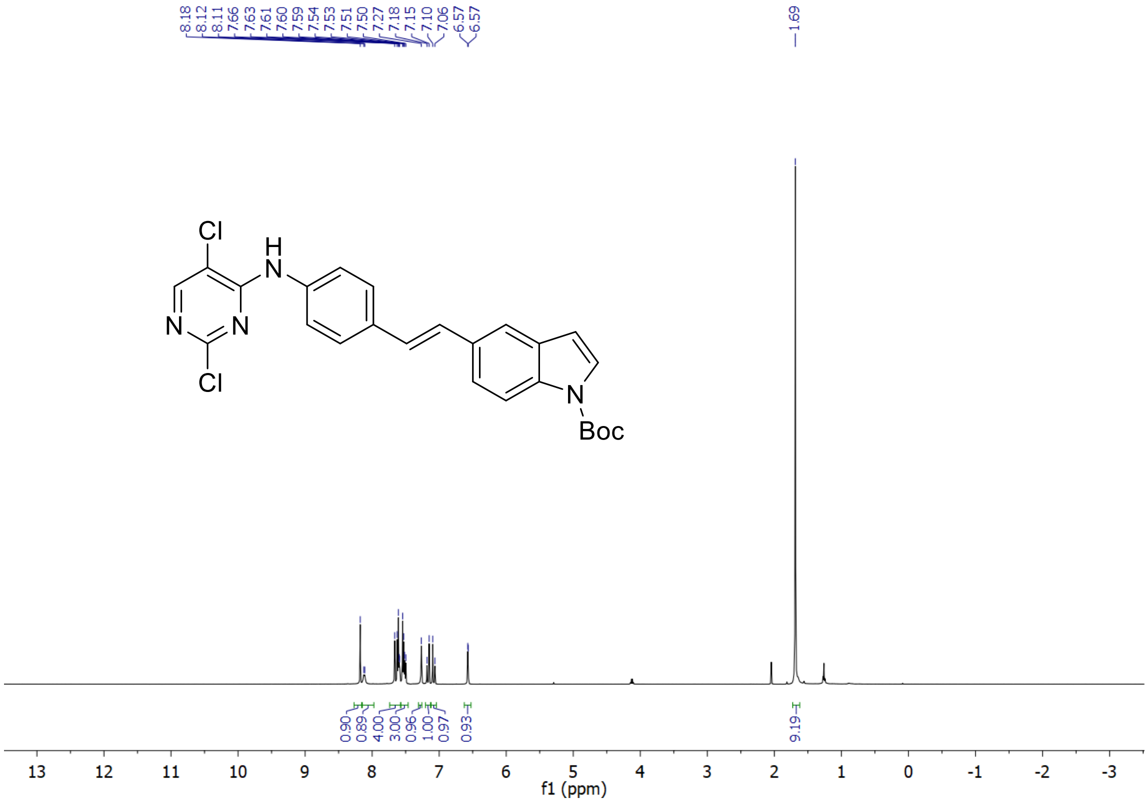
8.18
8.12
8.11
7.66
7.63
7.61
7.60
7.59
7.54
7.53
7.51
7.50
7.27
7.18
7.15
7.10
7.06
6.57
6.57
1.69
Cl
H
N
N
N
Cl
N
Boc
0.90
0.89
4.00
3.00
0.96
1.00
0.97
0.93
9.19
13
12
11
10
9
8
7
6
5
4
3
2
1
0
-1
-2
-3
f1 (ppm)

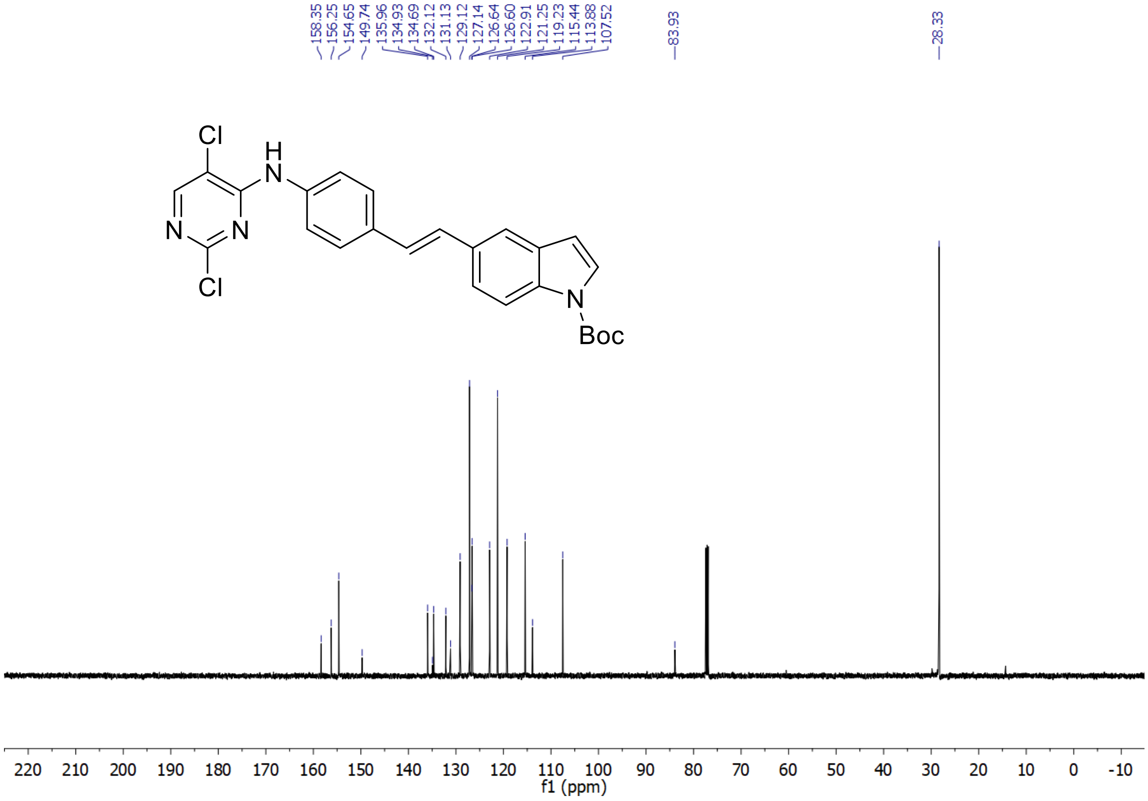
158.35
156.25
154.65
149.74
135.96
134.93
134.69
132.12
131.13
129.12
127.14
126.64
126.60
122.91
121.25
119.23
115.44
113.88
107.52
83.93
28.33
Cl
H
N
N
N
Cl
N
Boc
220
210
200
190
180
170
160
150
140
130
120
110
100
90
80
70
60
50
40
30
20
10
0
-10
f1 (ppm)

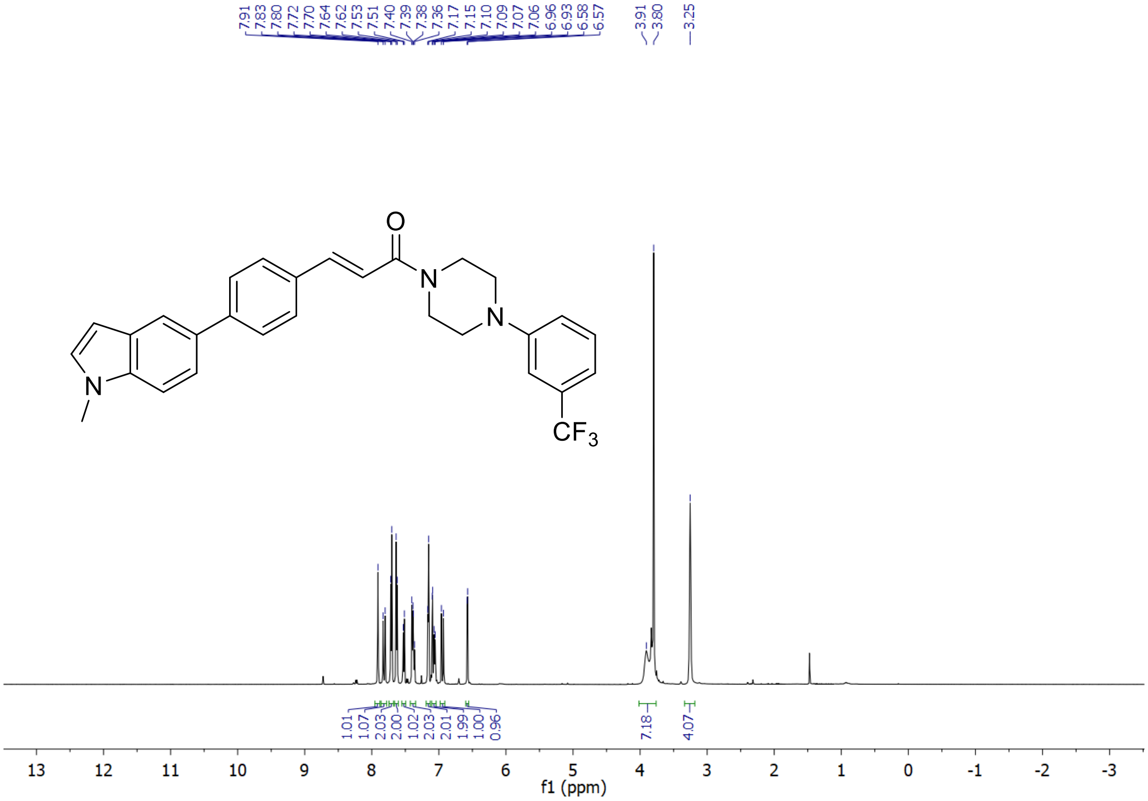
7.91
7.83
7.80
7.72
7.70
7.64
7.62
7.53
7.51
7.40
7.39
7.38
7.36
7.17
7.15
7.10
7.09
7.07
7.06
6.96
6.93
6.58
6.57
3.91
3.80
3.25
O
N
N
N
CF3
1.01
1.07
2.03
2.00
1.02
2.03
2.01
1.99
1.00
0.96
7.18
4.07
13
12
11
10
9
8
7
6
5
4
3
2
1
0
-1
-2
-3
f1 (ppm)

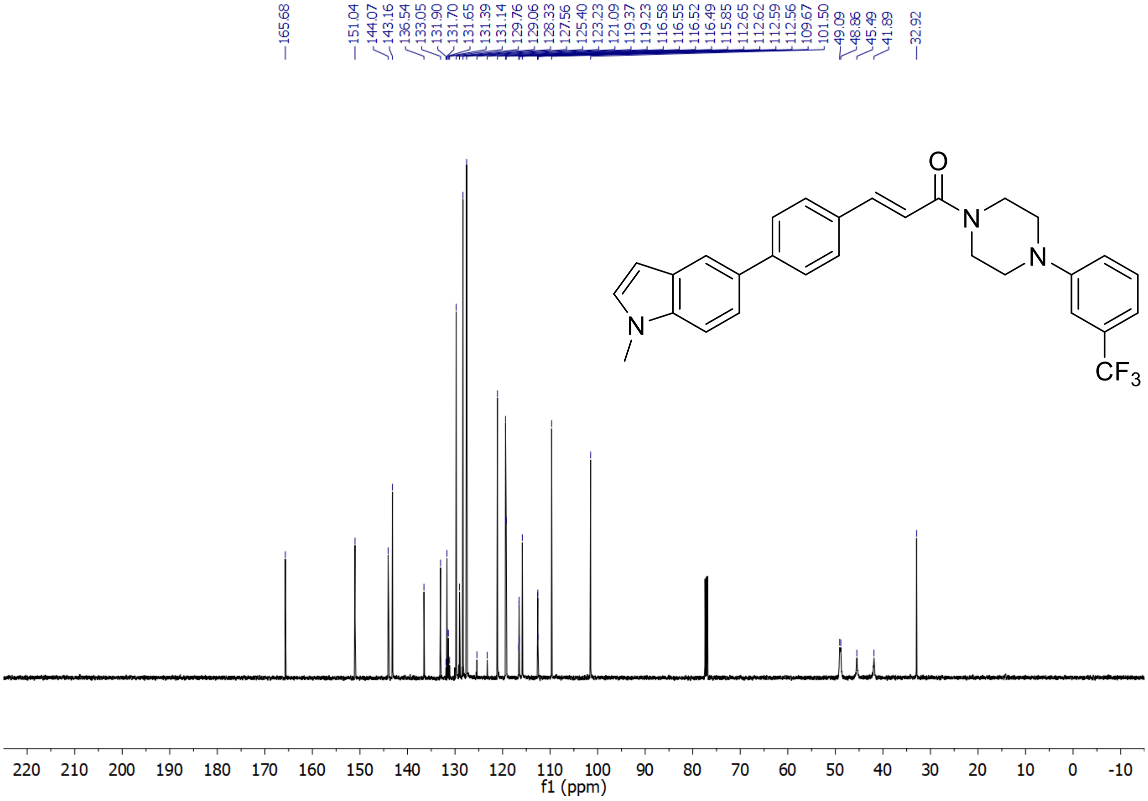
165.68
151.04
144.07
143.16
136.54
133.05
131.90
131.70
131.65
131.39
131.14
129.76
129.06
128.33
127.56
125.40
123.23
121.09
119.37
119.23
116.58
116.55
116.52
116.49
115.85
112.65
112.62
112.59
112.56
109.67
101.50
49.09
48.86
45.49
41.89
32.92
O
N
N
N
CF3
220
210
200
190
180
170
160
150
140
130
120
110
100
90
80
70
60
50
40
30
20
10
0
-10
f1 (ppm)

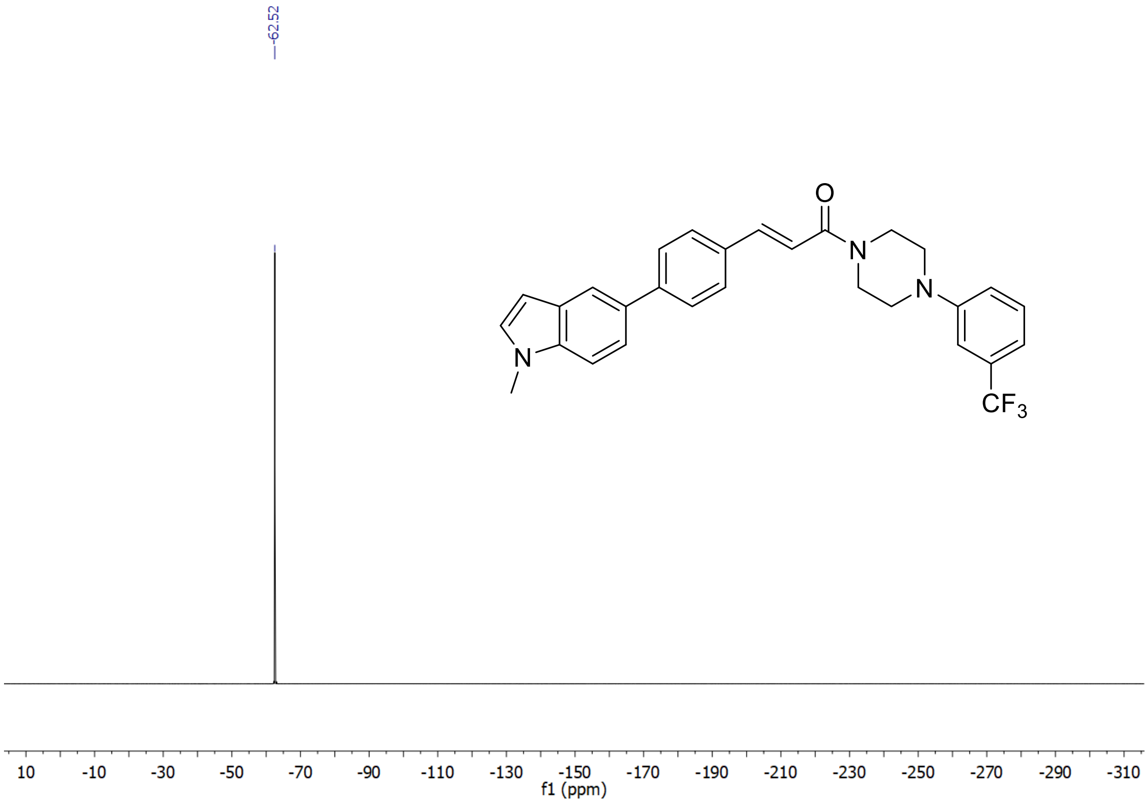
-62.52
CF3
10
-10
-30
-50
-70
-90
-110
-130
-150
-170
-190
-210
-230
-250
-270
-290
-310
f1 (ppm)